

THE TAYLOR CREEK DISTRICT, NEW MEXICO:  
GEOLOGY, PETROLOGY, AND TIN DEPOSITS

by

Ted L. Eggleston

Submitted in Partial Fulfillment of  
the Requirements for the Degree of  
Doctor of Philosophy

NEW MEXICO INSTITUTE OF MINING AND TECHNOLOGY

Socorro, New Mexico

May 1987

## DISCLAIMER

The format of this dissertation is unique at the New Mexico Institute of Mining and Technology. This dissertation is written as a series of 4 coauthored manuscripts, each of which deals with a separate aspect of the geology, geochemistry, or ore deposits in the Taylor Creek District in the Black Range of southwestern New Mexico. Each manuscript will be published separately. With the exception of strontium isotope data, all of the data collection has been done by me and interpretations of the data presented here are exclusively mine. Although each chapter has one or more coauthors, the entire dissertation was written by me. The responsibilities of the coauthors are: David I. Norman collected the strontium isotope data on samples provided by me and advised this thesis; Samuel M. Savin provided the laboratory facilities where I collected the oxygen isotope data.

Ted L. Eggleston  
21 MAY 1987



## TABLE OF CONTENTS

Title Page .....	1
Disclaimer.....	2
Table of Contents.....	3
Abstract.....	11
Format for This Dissertation.....	17
Acknowledgements.....	19
<u>Chapter 1</u> GEOLOGY OF THE TAYLOR CREEK DISTRICT: BLACK RANGE, NEW MEXICO.....	21
Abstract.....	22
Introduction.....	24
Analytical Methods.....	27
Regional Geology.....	29
Correlation.....	32
Stratigraphy.....	32
Tertiary bedded deposits.....	33
Rubio Peak Formation.....	33
Kneeling Nun Tuff.....	34
tuff of Koko Well.....	35
basaltic andesite of Poverty Creek.....	36
tuff of Stiver Canyon.....	37
tuff of Lookout Mountain.....	39
rhyolite of Sawmill Peak.....	39
tuff of Kline Mountain.....	40
rhyolite of Dolan Peak.....	41
La Jencia Tuff.....	43
rhyolite of Whitetail Canyon.....	43
rhyolite of Hoyt Creek.....	44
rhyolite of Keith Tank.....	45
unnamed tuff.....	46
Taylor Creek Rhyolite.....	46
unnamed pyroclastic rocks.....	52
tuff of Garcia Camp.....	55
sandstone of Inman Ranch.....	57
Bloodgood Canyon Tuff.....	58
Bearwallow Mountain Formation.....	59
Gila Conglomerate.....	59
Quaternary Deposits.....	60
Tertiary Intrusive Rocks.....	61
rhyolite of Franks Mountain.....	61
Structural Geology.....	63
Geomorphology.....	64
Hydrothermal Alteration.....	65
Kline Mountain intrusive.....	65
Alteration associated with the Taylor Creek Rhyolite.....	68
Vapor-Phase Crystallization.....	69
Tin Mineralization.....	71
Sierra Cuchillo.....	73
Discussion of Geologic History.....	77

Acknowledgements.....	84
Bibliography.....	85

### Tables

1 Geochemistry of selected samples from the Taylor Creek district.....	97
2 Point count data for various units in the Black Range.....	101
3 Isotopic dates for the Taylor Creek Rhyolite.....	102
4 Geochemistry of selected samples in the Sierra Cuchillo.....	103
5 Point count data for units in the Sierra Cuchillo....	105

### Figures

1 Generalized geologic map of the Taylor Creek district.....	106
2 Stratigraphic correlation chart for the Taylor Creek district.....	108
3 Stratigraphic column for the Taylor Creek district.....	110
4 SiO <sub>2</sub> -total alkali classification diagram of LeMaitre (1984).....	112
5 Exposures of Rubio Peak Formation in Poverty Creek...	114
6 Outcrops of Kneeling Nun Tuff in Poverty Creek.....	115
7 Stratigraphic section at Mud Hole.....	116
8 Felty texture in groundmass of rhyolite of Sawmill Peak.....	117
9 Typical exposures of tuff of Kline Mountain.....	118
10 Exploration excavations in the advanced argillic alteration at the "clay" pits.....	119
11 La Jencia Tuff in Scales Canyon.....	120
12 Photomicrograph of rhyolite of Whitetail Canyon.....	121
13 Flowbanded Taylor Creek Rhyolite near Wall Lake.....	122
14 Glomeroporphyritic sanidine in the Taylor Creek Rhyolite.....	123
15 Granophyric texture in the Taylor Creek Rhyolite.....	124
16 Relict spherulites in Taylor Creek Rhyolite.....	125
17 Taylor Creek Rhyolite near Wall Lake.....	126
18 Enrichment-depletion diagram for typical Taylor Creek Rhyolite compared to average rhyolite and granite.....	127
19 Pyroclastic rocks associated with the Taylor Creek Rhyolite.....	129
A) Pyroclastic rocks in Scales Canyon.....	130
B) Pyroclastic flow deposits from the base of section in A.....	130
C) Pyroclastic fall deposits near the top of the section in A.....	131
D) Pyroclastic breccia at the top of the section in A.....	131
20 Type section of sandstone of Inman Ranch in Stiver Canyon.....	132

21	Angular unconformity between sandstone of Inman Ranch and the Gila Conglomerate.....	133
22	Massive, poorly sorted sandstone in the sandstone of Inman Ranch.....	134
23	Gila Conglomerate at Wall Lake.....	135
24	View of the west flank of the Black Range showing the regional erosion surface.....	136
25	General geology and alteration of the rhyolite porphyry of Kline Mountain.....	137
26	Generalized geology of the Monticello Cutoff area in the Sierra Cuchillo.....	139
27	Photograph of the southwest side of Burro Ridge in the Sierra Cuchillo.....	141

Chapter 2 INTENSE VAPOR-PHASE CRYSTALLIZATION:  
MINERALOGICAL AND CHEMICAL EFFECTS IN  
HIGH-SILICA RHYOLITE LAVAS..... 142

Abstract.....	143
Introduction.....	145
Geology.....	147
Analytical Procedures.....	149
Vapor-Phase Crystallization.....	150
Physical and Mineralogical Changes.....	150
Chemical Changes.....	153
Oxygen Isotope Changes.....	155
Fluid Inclusions.....	157
Discussion.....	160
Model.....	163
Conclusions.....	164
Acknowledgements.....	165
Bibliography.....	166

Tables

1	Selected geochemical analyses of mildly and intensely vapor-phase crystallized samples from the Taylor Creek Rhyolite.....	172
2	Oxygen isotopic analyses of mildly and intensely vapor phase crystallized rhyolite.....	173
3	Fluid inclusion microthermometric data for various vapor phase minerals.....	174

Figures

1	Location map for zones of intense vapor phase crystallization discussed in the text.....	175
2	Schematic cross section of a typical Taylor Creek Rhyolite dome.....	177
3	A) Photograph of quartz phenocryst with overgrowth... B) photograph of multisolid-vapor inclusion in overgrowth.....	179

4	Typical zone of intense VPC and the overlying lithophysal rhyolite at Paramount Canyon.....	180
5	Lithophysae near the right skyline in Figure 4.....	151
6	Enrichment-depletion diagrams comparing mild and intense VPC From several Taylor Creek Rhyolite domes.....	182
	A) Nugget Gulch dome.....	183
	B) Paramount Canyon area of the Boiler Peak Dome.....	184
	C) Indian Peaks dome.....	185
7	Chondrite normalized rare earth element plots.....	186
	A) for Nugget Gulch.....	187
	B) Paramount Canyon area of the Boiler Peak Dome.....	188
	b) Indian Peaks dome.....	189
8	Enrichment-depletion diagram comparing zones of intense VPC from the three domes discussed in the text.....	190
9	Large type 2 inclusion with daughter minerals	
	A) 25 <sup>o</sup> C.....	192
	B) 400 <sup>o</sup> C.....	192
10	Schematic diagram showing enrichments, depletions, and inconsistent chemical trends due to VPC.....	193

CHAPTER 3 PETROLOGY OF TIN-BEARING RHYOLITES,  
NORTHERN BLACK RANGE AND SIERRA CUCHILLO,  
NEW MEXICO..... 195

Abstract.....	196
Introduction.....	198
Regional Geologic and Tectonic Setting.....	200
Regional Geologic Setting.....	200
Tectonic Setting.....	201
Local Geology.....	202
Analytical Procedures.....	205
Petrography and Mineralogy.....	206
Tin-bearing rhyolites.....	206
Rhyolite of Sawmill Peak.....	207
Older rhyolites.....	207
Trachytes.....	208
Mafic rocks.....	208
Petrochemistry.....	209
Samples.....	209
Major elements.....	209
Trace elements.....	211
Rare-earth elements.....	212
Strontium Isotopes.....	213
Oxygen Isotopes.....	215
Discussion.....	218
Petrologic affinities of the tin-bearing rhyolites..	218
Constraints on the origin of tin-bearing rhyolites..	218
The role of fluorine.....	222
Source region constraints.....	223
Composition of the parent magma.....	225
Source rocks for the parent magma.....	227
Petrogenesis of tin-bearing rhyolites.....	228



Conclusions.....	229
Acknowledgements.....	230
Bibliography.....	232

#### Tables

1	Geochemical analyses of selected samples of various units in the northern Black Range.....	246
2	Characteristics of tin-bearing rhyolite groups.....	251
3	Initial $^{87}\text{Sr}/^{86}\text{Sr}$ ratios for various units in the northern Black Range.....	252
4	a) Oxygen isotope analyses for the tin-bearing rhyolites. ....	253
	b) Temperatures calculated from oxygen isotope determinations of mineral pairs. ....	253
5	Comparison of I-, S-, and A-type granitoids with the tin-bearing rhyolites.....	254
6	Ranges of crystal-liquid partition coefficients for high-silica rhyolites.....	255
7	Trace element crystal-liquid fractionation models for fractionation of Group B rhyolites to Group A rhyolites.....	256
8	Trace element crystal-liquid fractionation models for fractionation of Group C rhyolites to Group D rhyolites.....	257
9	a) Trace element crystal-liquid fractionation model for fractionation of the basaltic andesite of Poverty Creek to Group B rhyolites.....	258
	b) Major element mixing model to produce Group B rhyolites from the basaltic andesite of Poverty Creek.....	258
10	Trace element crystal-liquid fractionation models for fractionation of older rhyolites in the Black Range to Group B rhyolites.....	259
11	a) Trace element crystal-liquid fractionation model for fractionation of the rhyolite of Sawmill Peak to Group B rhyolites.....	260
	b) Major element mixing model for the rhyolite of Sawmill Peak and Group B rhyolites.....	260
12	Major element mixing model for A-type granites and Group B rhyolites.....	261
13	Trace element crystal-liquid fractionation model for fractionation of A-type granites to Group B rhyolites.....	262

#### Figures

1	Location map of the Taylor Creek district superimposed on the Rio Grande rift.....	263
2	General geologic map of northern Black Range.....	265
3	Major element variation diagrams for volcanic units in the northern Black Range.....	267
4	Enrichment-depletion diagram for Taylor Creek Rhyolite comparing it to average rhyolite and average granite.....	275

5	Ternary $Al_2O_3$ - $CaO$ - $Na_2O+K_2O$ diagram for the felsic units <sup>3</sup> in the northern Black Range.....	277
6	Q-Or-Ab ternary diagram with granite minima of Tuttle and Bowen (1958).....	279
7	Alkali- $SiO_2$ classification diagram of Le Maitre (1984) with the alkaline-subalkaline fields of Irvine and Baragar (1971).....	281
8	Trace element variation diagrams.....	283
9	Chondrite normalized rare earth element diagrams for the units in the Black Range and Sierra Cuchillo.....	291
10	Isochron diagrams for various Taylor Creek Rhyolite domes.....	296
11	Strontium evolution diagrams for the Taylor Creek Rhyolite domes in Figure 10.....	298
12	Strontium mixing models for the Taylor Creek Rhyolite domes in Figure 10.....	300
	<u>Chapter 4</u> ORIGIN OF TIN MINERALIZATION ASSOCIATED WITH HIGH-SILICA, TOPAZ RHYOLITES, BLACK RANGE, NEW MEXICO.....	302
	Abstract.....	303
	Introduction.....	306
	Regional Geologic Setting.....	307
	Analytical Procedures.....	309
	Local Geology.....	311
	Tin-bearing rhyolites.....	311
	Lithology and geometry.....	311
	Geochemistry.....	312
	Vapor-phase crystallization.....	313
	Comparison with tin granites.....	314
	Tin Deposits.....	315
	Types of deposits.....	315
	Paragenesis.....	317
	Hydrothermal alteration.....	319
	Chemistry of the cassiterite and hematite.....	320
	Fluid Inclusions.....	321
	Petrography.....	321
	Microthermometric studies.....	323
	Pressure estimates.....	326
	Fluid inclusion gas analyses.....	328
	Oxygen Isotope Data.....	330
	Discussion.....	332
	$f_{O_2}$ of the mineralizing fluids.....	332
	Origin of mineralizing fluids.....	333
	Origin of tin in the rhyolites.....	336
	Origin of tin-bearing rhyolites.....	337
	Transport of Tin.....	338
	The Wood Tin Problem.....	339
	Model.....	341
	Implications For Other Deposit Types.....	343
	Sn-bearing and Sn-Barren High-Silica Rhyolites.....	344
	Conclusions.....	345

Acknowledgements.....	346
Bibliography.....	348
Tables	
1 Geochemistry of the tin-bearing rhyolites in New Mexico and other tin-bearing granitoids.....	364
2 Geochemistry of hematite and cassiterite the tin-bearing veinlets in New Mexico.....	365
3 Summary of characteristics of fluid inclusion types.....	366
4 Summary of Tm and Th of Type 2 inclusions.....	367
5 Summary of Th and salinities of Type 4 and 5 inclusions.....	368
6 Fluid inclusion gas analyses.....	370
7 Oxygen isotope data.....	371
Figures	
1 Location map and general geology of the Taylor Creek district, New Mexico.....	372
2 Typical exposures of the Taylor Creek Rhyolite in the Taylor Creek district.....	374
3 Schematic cross section of a typical tin-bearing rhyolite dome.....	375
4 Chondrite normalized rare earth element patterns for the Taylor Creek Rhyolite and other tin-bearing granitoids.....	377
5 Comparison of various tin-bearing granitoids with the Taylor Creek Rhyolite.....	379
6 Typical zone of intense vapor-phase crystallization..	382
7 Wood tin nuggets recovered from the placer deposits in Nugget Gulch.....	383
8 Hematite-cassiterite-wood tin veinlets.....	384
9 Paragenesis of the tin mineralization in the deposits hosted by high-silica rhyolites in New Mexico.....	385
10 Interbanded hematite and cassiterite.....	387
11 Interbanded cassiterite and wood tin.....	388
12 Photographs of fluid inclusions.....	389
A) Overgrowth on quartz phenocryst in the zone of intense vapor-phase crystallization in Paramount Canyon.....	390
B) Type 2 inclusions in the overgrowth in Figure 12 A.....	390
C) Type 1 inclusion in quartz.....	390
D) Type 2 inclusion in Topaz.....	390
E) Type 5 inclusions in calcite.....	391
F) Type 1 and Type 2 inclusions in the same plane.....	391
G) Type 2 inclusions at 25° C.....	391
H) Type 2 inclusions at 370° C.....	391
I) Type 2 inclusion after quenching.....	392
J) Type 2 inclusion at 400° C.....	392
K) Type 6 magmatic inclusions in quartz phenocryst in Figure 12 A.....	392

L)	Brecciated cassiterite in veinlet.....	392
M)	Naturally decrepitated inclusion in quartz.....	393
13	Histogram of Th for Type 4 and Type 5 inclusions.....	395
14	Plot of CO <sub>2</sub> vs. N <sub>2</sub> gases in fluid inclusions.....	396
15	Ternary CO <sub>2</sub> -N <sub>2</sub> -CNHN plot for gases in fluid inclusions.....	398
16	f <sub>O<sub>2</sub></sub> -f <sub>S<sub>2</sub></sub> diagram at 627° C.....	400
17	f <sub>O<sub>2</sub></sub> controls on solubility of Sn after Wilson and Eugster (1984).....	402
18	Model for the formation of the Taylor Creek tin deposits.....	404

#### APPENDICES

1	A) detection X-ray fluorescence spectrometry and sample preparation.....	406
	B) Geochemical analyses of samples from the Black Range and Sierra Cuchillo.....	407
	C) Oxygen isotope analyses of samples from the Black Range and Sierra Cuchillo.....	432
	D) Strontium isotope analyses of samples from the Black Range and Sierra Cuchillo.....	433
2	A) Sample descriptions of samples from the Black Range and Sierra Cuchillo.....	435
	B) Point count data of samples from the Black Range and Sierra Cuchillo.....	459
3	Instrumental settings and analytical parameters for X-ray fluorescence spectrometry and instrumental neutron activation analysis.....	461
4	Precision of analyses.....	464
	A) Major element precision for TTC internal standard.....	466
	B) Major element precision for NMR internal standard.....	467
	C) Major element precision for CZB internal standard.....	467
	D) Loss on ignition precision.....	468
	E) Trace element precision for TTC internal standard.....	469
	F) Trace element precision for CZB internal standard.....	471
	G) Estimates of precision of instrumental neutron activation analyses.....	472
	H) Representative analyses of U.S. Geological Survey reference samples G-2 and BCR-1 to estimate accuracy of instrumental neutron activation analyses.....	473
	Plate 1 .....	In pocket



## ABSTRACT

The Taylor Creek district is located in the northern Black Range of southwestern New Mexico and has produced about 70 tons of tin concentrate that averaged 40 to 50% Sn. Tin deposits similar to those in the Taylor Creek district occur in the Sierra Cuchillo; 20 to 30 km east of the Taylor Creek district. The tin deposits occur in high-silica rhyolite lavas, three of which are presently known; the Taylor Creek Rhyolite and rhyolite of Dolan Peak in the Black Range and the rhyolite of Willow Springs Draw in the Sierra Cuchillo. These lavas occur near the top of the Tertiary volcanic plateau known as the Mogollon-Datil volcanic field. In the Black Range and Sierra Cuchillo, the Mogollon-Datil volcanic field can be divided into two age groups. The older group (44 to 35 Ma) consists of intermediate to mafic lava flows, locally derived volcanoclastic sedimentary rocks, and felsic pyroclastic rocks. The bulk of the group is included in the Rubio Peak Formation. The top of the group is the 35 Ma Kneeling Nun Tuff.

A hiatus in volcanism of perhaps 5 to 6 Ma occurred after the Kneeling Nun Tuff was erupted and appears to have occurred over the entire Mogollon-Datil volcanic field; however, a few volcanic units were erupted during this time. The basaltic andesite of Poverty Creek was erupted after the hiatus and is in turn overlain by a thick sequence of high-silica rhyolite lavas and pyroclastic rocks that includes the tin-bearing rhyolite lavas. The high-silica rhyolites were

erupted about 29 to 28 Ma.

The high-silica rhyolites were quickly covered by the sandstone of Inman Ranch that was in turn covered by the Gila Conglomerate and the andesites of the Bearwallow Mountain Formation, the youngest volcanic unit in the Taylor Creek district. After eruption of the Bearwallow Formation, a regional erosion surface that sloped gently to the west formed. Epeirogenic uplift about 5 Ma ago caused streams in the area to incise and created the plateaus and deep canyons that are typical of the present topography.

Vapor-phase crystallization (VPC) is widespread in the high-silica rhyolite domes of the tin-bearing rhyolites and is intimately associated with the tin mineralization. Three intensities of VPC are recognized: mild, moderate and intense. Mild VPC is pervasive and is characterized by mild bleaching of the rhyolite and deposition of quartz and sanidine in open space along flowbanding. Moderate VPC is restricted to thin zones around areas of intense VPC. The zones of moderate VPC are intensely bleached and quartz, sanidine, hematite, pseudobrookite, bixbyite, topaz, beryl, and cassiterite are deposited in lithophysae. Selvages on lithophysae have undergone intense VPC. Small zones of intense VPC typically several tens of meters across are distinct and consist of "punky", flowbanded rhyolite lava. Overgrowths on quartz and sanidine phenocrysts, dramatically increased groundmass crystallite size, and recrystallization of spherulites to granophyre are typical mineralogical changes. Intense VPC occurs within a few tens of meters of

the paleosurface of the affected domes.

Most elements were mobilized by the fluids responsible for VPC. Ba, Cs, Y, and the rare earth elements (REE) are dramatically enriched in the zones of intense VPC relative to mildly vapor-phase crystallized rhyolite; Ti, Nb, Pb, Sb, U, and Sn are depleted; As, Cl, F, Sc, Sr, and Zn exhibit both enrichments and depletions. Enrichments and depletions in zones of moderate VPC are similar to those in zones of intense VPC, except that F, Mn, Mg, Se, and Sr are enriched in these zones. Sn, Fe<sub>2</sub>O<sub>3</sub>, As, Sb, Pb, W, U, Sc, Ta, Cs, Co, and Cr are enriched in the tin deposits that occur in and above the zone of moderate VPC (lithophysal zone). Ga, Hf, Zr, and Th are apparently immobile. Oxygen-isotope composition of quartz from lithophysae (+7.5<sup>o</sup>/oo) suggests that the fluids responsible for VPC were magmatic. Fluid inclusion homogenization temperatures in quartz overgrowths and quartz from lithophysae are >720<sup>o</sup> C, also suggesting that the fluids responsible for VPC were of magmatic origin.

The tin-bearing rhyolite lavas are enriched in SiO<sub>2</sub>, K<sub>2</sub>O, Rb, Nb, Th, and U and depleted in CaO, Sr, and Ba compared to average rhyolite and granite. The major element compositions of the lavas are virtually identical with the exception of TiO<sub>2</sub>, which decreases with increasing Rb. Nb, Ta, and Th increase with increasing Rb and Ba, Sc, and Sr decrease with increasing Rb in the magmas. Rare-earth element patterns are flat with large negative Eu anomalies. The middle rare-earth elements exhibit a distinct sag relative to the light and heavy rare earth elements.

Initial  $^{87}\text{Sr}/^{86}\text{Sr}$  ratios for the tin-bearing rhyolites are between 0.708 and 0.713. The oxygen-isotopic composition of quartz phenocryst separates from the rhyolites are between 7.5 and 7.8 ‰.

Crystal-liquid fractionation models suggest that crystallization of plagioclase, K-feldspar, and quartz in a shallow magma chamber produced trace element covariations observed in the rhyolites and controlled the major element concentrations in the rhyolite magmas. The rare earth concentrations were controlled by plagioclase, allanite, and sphene crystallization. Variable contamination of the rhyolite magmas produced the variations of initial  $^{87}\text{Sr}/^{86}\text{Sr}$  ratios. Major and trace element modeling with the mode present in the rocks will not produce the trace element covariations observed in the rocks; however, modeling with the same minerals in different ratios will produce most of the trace element covariations observed.

The lack of intermediate composition volcanic rocks associated with the tin-bearing rhyolites argues against fractionation of an upper mantle-derived parent for the tin-bearing rhyolite magmas because of the large amounts of crystal-liquid fractionation required to produce the tin-bearing rhyolites from mantle derived, alkali basalts. Partial melting of lower to mid-crustal, felsic granulites can produce magmas very similar to A-type granites in composition. Crystallization of plagioclase and amphibole from the A-type granite composition melts produced the most mafic of the tin-bearing rhyolite magmas.

Lode tin mineralization consists of hematite-cassiterite-wood tin veinlets located near the paleosurface of the rhyolite domes. Very small amounts of quartz-calcite-fluorite mineralization fills open space that remained after tin deposition was complete. The tin mineralization is intimately associated with small zones of intense vapor phase crystallization of the host rhyolite.

Fluid inclusion homogenization temperatures ( $T_h$ ) in cassiterite, quartz and topaz in the tin mineralization are  $>650^\circ$  C. Overgrowths on quartz phenocrysts in zones of intense vapor phase crystallization contain inclusions with  $T_h$  of  $730^\circ$  C. Fluid inclusion  $T_h$  in quartz-calcite-fluorite mineralization are between 380 to  $130^\circ$  C. The oxygen isotope composition of quartz associated with the tin mineralization is about  $7.5^\circ$ /oo. Quartz in the quartz-calcite-fluorite has  $\delta^{18}O$  compositions of 5 to  $11^\circ$ /oo. Whole rock rhyolite samples near the tin mineralization has  $\delta^{18}O$  values of 6.1 to 9.9. Estimated magmatic values for the whole rock samples are 6.5 to  $6.8^\circ$ /oo suggesting that the whole rock samples were enriched with  $^{18}O$ . Fluid inclusion gases in the tin minerals are similar to recently active volcanic fumaroles. Calculated  $f_{O_2}$  of fluid inclusion gases in wood tin and cassiterite indicate that the  $f_{O_2}$  of the fluids ranged from  $10^{-20}$  to  $10^{-10}$  at  $627^\circ$  C. The higher  $f_{O_2}$  values were for tin mineralization very near the paleosurface. The  $f_{O_2}$  of the fluid inclusion gases in tin minerals decreased with depth of the host mineral. Fluid inclusion gases in the quartz-calcite-fluorite mineralization are organic-rich fluids

similar to fluid inclusion gases in many epithermal deposits.

The data strongly suggest that the fluids responsible for the tin mineralization were magmatic fluids derived from the host rhyolite and that the tin was deposited as fumarolic incrustations. Fluids responsible for quartz-calcite-fluorite mineralization were meteoric water, but had an undetermined magmatic water component. The small volume of the quartz-calcite-fluorite mineralization and the lack of  $\delta^{18}\text{O}$  depletion in the host rhyolite indicate that the meteoric water dominated hydrothermal system that deposited the quartz-calcite-fluorite mineralization was short lived.

The host rhyolites probably originated as partial melts of lower crustal, biotite-bearing granulites with a small, but undetermined upper mantle component. The parent liquids were probably similar to A-type granites and crystallization of plagioclase, K-feldspar, and quartz in a high level magma chamber enriched Rb, Nb, Ta, Th, and Sn and depleted Sr and Ba in the tin-bearing rhyolites. Tin was transported as  $\text{SnCl}^+$  in magmatic, supercritical fluids and was deposited as near surface, fumarole incrustations by decreasing temperatures and increasing  $f_{\text{O}_2}$ . Fluid flow rates determined the texture of the resulting tin mineralization. Tin was enriched in the magma by crystal-liquid fractionation.

Economic potential for the rhyolite-hosted tin mineralization is low. Potential for tin- and tungsten-bearing skarn mineralization and lode deposits at depth is very good, but depth to the deposits may be prohibitive.



## FORMAT OF THIS DISSERTATION

This dissertation is written as a series of 4 manuscripts (see DISCLAIMER on page 2). Each chapter thus has an abstract, introduction, a section on regional and local geology, and a reference list. This format leads to some duplication in the regional and local geology sections and in the reference lists; however, duplication of data has been minimized by referencing each chapter as a separate paper. The chapters are as follows:

Chapter 1 describes the stratigraphy and discusses the geologic history of the Taylor Creek district and the volcanic section in the Sierra Cuchillo. It will appear in print as a New Mexico Bureau of Mines and Mineral Resources Bulletin coauthored by Ted L. Eggleston and David I. Norman. In this dissertation, it is referred to as Eggleston and Norman (1987; in prep.).

Chapter 2 describes and discusses the mineralogical and chemical effects of intense vapor phase crystallization on high-silica rhyolite lavas. It is coauthored by Ted L. Eggleston, David I. Norman and Samuel M. Savin and will be referred to as Eggleston and others (1987; in prep.) with a letter designator appropriate for the chapter in which the reference appears. This chapter will be submitted to the Journal of Volcanology and Geothermal Research.

Chapter 3 discusses the petrochemistry and petrology of the tin-bearing rhyolites. It will be coauthored by Ted L.

Eggleston, David I. Norman, and Samuel M. Savin and will be referred to as Eggleston and others (1987; in prep.) with a letter designator appropriate for the chapter in which the reference appears. This manuscript will be submitted to Contributions to Mineralogy and Petrology.

Chapter 4 describes the tin mineralization and discusses the possible origin for the mineralization. It will also be coauthored by Ted L. Eggleston, David I. Norman, and Samuel M. Savin and will be referred to as Eggleston and others (1987; in prep.) with a letter designator appropriate for the chapter for which the reference appears. This chapter will be submitted to Economic Geology.

The appendices at the end of the manuscript will be included with Chapter 1 in the New Mexico Bureau of Mines and Mineral Resources Bulletin.



## ACKNOWLEDGEMENTS

Although I am responsible for the interpretations as well as the misinterpretations that follow, numerous people have contributed to the completion of this project. David Norman advised and guided this study and is thanked for his support and guidance. I especially thank Don Richter of the U.S. Geological Survey for his hospitality and for many hours of stimulating discussion on the stratigraphy and structure of the region as well as for editing various versions of the manuscript and Plate 1. Special thanks also to Philip Kyle who taught me the care and feeding of both X-ray fluorescence and gamma ray spectrometers. W.E. Elston, Charles Maxwell, G.R. Osburn, Richard Harrison, James Ratte', Charles Chapin, Bill McIntosh, Wendell Duffield, and Tom Woodard have contributed significantly to my understanding of the geology of the region. Samuel Savin, Mingchow Lee, and Linda Abel of Case Western Reserve University patiently guided me through the procedures necessary for oxygen-isotopic analyses. Kent Condie and George Griswold edited early versions of the manuscripts and served on the examination committee and they are thanked for their help. I also thank Anne Wright, who shared an office with me, for patiently ignoring the many messes that I created there.

Bob Kerr kindly permitted access to his claims in the area. Danny Fowler and the Ladder Ranch permitted access to their ranch properties. FRM Minerals, the Geological Society

of America, the New Mexico Geological Society, the Rocky Mountain Federation of Mineralogical Societies, the National Science Foundation (Grants EAR 8319913 and EAR 8410481 to David I. Norman) and the U.S. Department of the Interior's Mineral Institutes Program administered by the U.S. Bureau of Mines (allotment grant G1164135 to David I. Norman) funded various aspects of the field and laboratory work. The New Mexico Bureau of Mines and Mineral Resources, Frank Kottlowski, Director, supported this work in the form of a graduate assistantship as well as funds for thin section preparation. Lynn Brandvold, chemist, New Mexico Bureau of Mines and Mineral Resources provided the F and Cl analyses. Finally I thank my wife, Roberta, and my children, Beth and Will, for support during the course of the study.

CHAPTER 1

The data collection and interpretation in this chapter is the responsibility of Ted L. Eggleston. David I. Norman advised this thesis.

GEOLOGY OF THE TAYLOR CREEK DISTRICT,  
BLACK RANGE, NEW MEXICO

Ted L. Eggleston and David I. Norman  
New Mexico Institute of Mining and Technology  
Socorro, New Mexico 87801

ABSTRACT

The Taylor Creek district is located in the northern Black Range of southwestern New Mexico and has produced about 70 tons of tin concentrate that averaged 40 to 50% Sn. Tin deposits similar to those in the Taylor Creek district occur in the Sierra Cuchillo; 20 to 30 km east of the Taylor Creek district. The tin deposits occur in high-silica rhyolite lavas. Three tin-bearing rhyolites are presently known; the Taylor Creek Rhyolite and rhyolite of Dolan Peak in the Black Range and the rhyolite of Willow Springs Draw in the Sierra Cuchillo. These lavas occur near the top of the Tertiary volcanic plateau known as the Mogollon-Datil volcanic field. In the Black Range and Sierra Cuchillo, the

Mogollon-Datil volcanic field can be divided into two age groups. The older group (44 to 35 Ma) consists of intermediate to mafic lava flows, locally derived volcaniclastic sedimentary rocks, and felsic pyroclastic rocks. The bulk of the unit is included in the Rubio Peak Formation. The top of the group is the 35 Ma Kneeling Nun Tuff.

A hiatus in volcanism of perhaps 5 to 6 Ma occurred after the Kneeling Nun was erupted. That hiatus appears to have occurred over the entire Mogolon-Datil volcanic field; however, a few volcanic units were erupted during this time. The basaltic andesite of Poverty Creek was erupted after the hiatus and is in turn overlain by a thick sequence of high-silica rhyolite lavas and pyroclastic rocks that includes the tin-bearing rhyolites. The high-silica rhyolites were erupted about 29 to 28 Ma.

The high-silica rhyolites were quickly covered by the sandstone of Inman Ranch that was in turn covered by the Gila Conglomerate and the basaltic andesites of the Bearwallow Mountain Formation, the youngest volcanic unit in the Taylor Creek district. After eruption of the Bearwallow Formation, a regional erosion surface formed in the region. Pediments formed to the crest of the Black Range and were graded to the west. Epeirogenic uplift about 5 Ma ago caused streams in the area to incise and created the plateaus and deep canyons that are typical of the present topography.

## INTRODUCTION

Tin mineralization in the Black Range of New Mexico was rediscovered by J.N. Welch in 1918 while he was prospecting for gold (Hill, 1921). Prior to that time, wood tin (a microcrystalline, botryoidal form of cassiterite) nuggets had been used by cliff-dwelling Indians as ornamental stones (Harrington, 1943). After Welch's discovery in 1918, the region experienced a short-lived boom and most of the tin occurrences known today were located. Tin was found in placers as both wood tin and as coarsely crystalline cassiterite. Lode deposits consisting of hematite-cassiterite-bearing veinlets were also located. Since little tin was discovered, the boom soon fizzled and interest in the area dwindled. During the Second World War, the region was again the center of interest because the United States' major supplier of tin, Southeast Asia, was cut off from the rest of the World (Harrington, 1943a; 1943b). An experimental mill was erected on Taylor Creek and a small amount of ore was processed by grinding, gravity separation and finally, magnetic separation. The ore, however, was not of sufficient grade and tonnage to sustain the mill. Placer production was small. The lack of water and small size of the placers are problems even today. Since World War II placer deposits have contributed all of the production in the district, which amounts to a few tens of tons of cassiterite concentrate. None of the tin properties in the Black Range are currently

operating, although sporadic exploration continues.

The Taylor Creek district was named by Hill (1921) and includes all or parts of T. 8, 9, 10, 11, 12 S., R. 10, 11, 12 W. Although several names including Black Range tin district (Fries and Butler, 1943; Maxwell and others, 1985), and the Black Range district (File and Northrup, 1966) have been used for this district, we retain Hill's (1921) nomenclature to avoid ambiguity because what is now the Chloride district (File and Northrup, 1966) has also been known as the Black Range district.

During the course of a study of the tin mineralization in the Taylor Creek district (Fig. 1), it became evident that the regional geologic setting of the district was poorly understood. Also, the spatial and temporal relationships of the tin mineralization and the rhyolites that host them were likewise poorly understood. With the exception of the regional mapping of Fries and Butler (1943), studies of the geology of the tin district were restricted to the immediate vicinity of tin occurrences (Fries, 1940; Volin and others, 1947; Lufkin, 1972; Correa, 1981; Goerold, 1981; Harvey, 1985). Coney (1976) and W.E. Elston (unpublished mapping) defined much of the regional stratigraphy, but those studies were reconnaissance in nature and did not specifically address the tin district. The U.S. Geological Survey has recently published a few geologic quadrangle maps that cover parts of the district (Richter, 1978; Lawrence and Richter, 1986; Richter and others, 1986), but those studies cover geology on the fringes of the main tin district (see index

map on Plate 1). Other studies by Harley (1934), Erickson and others, (1970), Woodard (1982), and Fodor (1976) have included geology near the district. The mineralogic studies of Fries and others (1942), Lufkin, (1976; 1977), Kimbler and Haynes (1980), Narsavage (1981), and Foord and others (1985) have described, in detail, the mineralogy of the tin deposits and associated gangue.

In order to define the detailed geologic history of the region as well as the spatial and temporal relationships of tin mineralization to domes that host the mineralization, the region was mapped at a scale of 1:24,000 and then reduced to 1:50,000 (Plate 1). The index map on Plate 1 indicates where prior mapping is available. Prior mapping was compiled, field checked, and the nomenclature adjusted to conform to that of this study. Stratigraphic nomenclature described in this report supercedes the nomenclature of Eggleston and Norman (1983).

Each unit was sampled for geochemical analysis. The samples were chosen to accurately represent the unit in question. In most units, multiple samples were taken. Since non-hydrated vitrophyres are not present in these rocks, dense, lithoidal rhyolite was the first choice for representative analyses. When poorly welded ignimbrites were sampled, pumice fragments were chosen. To evaluate the importance of chemical zonation in these ignimbrites, multiple samples were collected from vertical sections of the unit in question. With rare exception, geochemical samples were collected from the cores of boulders to minimize the



effects of weathering. Some units such as the basaltic andesite of Poverty Creek are intensely fractured and large boulders are rare. In those cases, sampling was accomplished by searching for fresh outcrops and carefully trimming the largest fragments available. Appendix 1 is a complete tabulation of all geochemical analyses obtained during this study. Appendix 2 consists of brief sample descriptions with locations of each sample. Additional geochemical analyses of the Taylor Creek Rhyolite are found in Lufkin (1972), Bornhorst (1980), Correa (1981), Goerold (1981), and Maxwell and others (1986).

Multiple samples of each of the various domes of Taylor Creek Rhyolite were collected to investigate the effects of vapor phase crystallization. Samples were collected to evaluate the process from its incipient to most intense stages.

#### ANALYTICAL METHODS

Major and some trace element analyses were performed on a Rigaku six-position, computer-controlled x-ray fluorescence spectrometer (XRF) at the New Mexico Bureau of Mines and Mineral Resources. The spectrometer utilizes a Rhodium x-ray tube. A fusion disk technique similar to that described by Norrish and Hutton (1969) was used for major elements. Loss on ignition was determined gravimetrically after fusing a sample for 2 hours at 1010<sup>0</sup> C. in a muffle furnace. Instrumental settings for major and trace element analyses

are found in Appendix 3.

Rb, Sr, Y, Nb, Zr, Th, U, Pb, Cu, Ni, Zn, Ga, and Sn were determined by XRF using pressed pellets. Mass absorption corrections were applied using the rhodium K-alpha Compton peak. The pellets were pressed under 10 tons of pressure with 2% polyvinyl alcohol as a binder. Cr, V, and Ba were determined on the same pellets using mass absorption coefficients calculated from the major element analyses.

Instrumental neutron activation analysis (INAA) was used for analysis of the rare earth elements (REE) and a number of trace elements (Table 1). The samples were sealed in high-purity quartz tubes (Jacobs and others, 1977) and irradiated at the reactor at the University of Missouri, Columbia. The samples were then counted at the New Mexico Institute of Mining and Technology. Data reduction was accomplished using software supplied by Nuclear Data, the system manufacturer, or by a software package called TEABAGS (Lindstrom and Korotev, 1982).

FeO was determined by titration (Reichen and Fahey, 1962). F was determined by specific-ion electrode after fusing the sample in lithium metaborate following the procedure of Bodkin (1977). Cl analyses by mercuric nitrate titration were kindly provided by Lynn Brandvold, Chemist, New Mexico Bureau of Mines and Mineral Resources.

Precision of the analyses of all the elements was estimated by analyzing multiple aliquots of internal standards (Appendix 4). Three materials were used for this purpose: 1) a sample of the Taylor Creek Rhyolite (TTC); a

sample of a normal rhyolite from the Socorro area (NMRI), and 3) a sample of basalt from the young basalt flows near Carrizozo, New Mexico (CZB).

Oxygen isotopic analyses were performed by the author at the Laboratory of S. Savin, Case Western Reserve University, Cleveland, Ohio. Oxygen was liberated from silicate materials using the bromine pentafluoride technique of Clayton and Mayeda (1963) and analyzed on a Nuclide 6-inch, 60°-sector, ratio mass spectrometer. Sr-isotopic analyses were performed by Dr. David Norman at the Mineralogisk-Geologisk Museum, Oslo, Norway. Rb and Sr in most of the samples were determined by isotope dilution.

Thin sections of each geochemical sample were stained using a modification of the technique of Wilson and Sedora (1979). Point counts of selected thin sections were performed to accurately determine the quartz-sanidine ratios.

#### REGIONAL GEOLOGY

The Taylor Creek district is located near the center of the Mogollon-Datil volcanic field west of Winston, New Mexico (Fig. 1). This volcanic field is a mid-Tertiary volcanic plateau consisting of mafic to felsic lavas, pyroclastic rocks, and volcanoclastic sedimentary rocks that rest unconformably on Precambrian to early Tertiary rocks. In the Taylor Creek region, the volcanic rocks can be divided into two broad groups, a lower, generally mafic to intermediate group and an upper, bimodal group.

The lower group consists of the Rubio Peak Formation, which is a thick sequence of mafic to intermediate lavas, volcanoclastic sedimentary rocks, and mudflow deposits. Near the top of the formation, thin felsic tuffs are common (R. Harrison, 1986). This formation is broadly similar to the Datil Group to the north (Osburn and Chapin, 1983). The age of the Rubio Peak Formation is between about 40 Ma and 35 Ma. The lower boundary is not clearly defined and some Rubio Peak Formation rocks may be older than 40 Ma in the Hillsboro area (Seager and others, 1984). The upper limit of the Rubio Peak is the base of the Kneeling Nun Tuff,  $^{40}\text{Ar}/^{39}\text{Ar}$  dated at  $35.28 \pm 0.15$  Ma (McIntosh and others, 1986).

Overlying the Kneeling Nun Tuff is an unnamed bimodal sequence that consists of basaltic andesite lavas and high-silica rhyolite lavas and pyroclastic material. The mafic portion of this sequence is the basaltic andesite of Poverty Creek, the felsic portion is the high-silica rhyolites comprising the Taylor Creek Rhyolite, rhyolite of Dolan Peak, and pyroclastic rocks associated with these units. The Taylor Creek Rhyolite overlies the La Jencia Tuff, which is a regional ignimbrite erupted from the Sawmill Canyon and Mogollon cauldrons in the Magdalena Mountains near Socorro New Mexico. The La Jencia Tuff has been dated by McIntosh and others (1986) by  $^{40}\text{Ar}/^{39}\text{Ar}$  at  $28.78 \pm 0.15$  Ma. A sample of the La Jencia Tuff collected from exposures in Scales Canyon in the study area yielded a  $^{40}\text{Ar}/^{39}\text{Ar}$  date of  $28.8 \pm 0.15$  Ma (McIntosh, 1986, oral communication).

In other parts of the Mogollon-Datil volcanic field, the

period between 29 and 27 Ma was a time of cauldron formation and eruption of regional ignimbrites (Osburn and Chapin, 1983; Ratte' and others, 1984; Elston and others, 1984). In the Socorro area, cauldrons erupted several thousand km<sup>3</sup> of ignimbrites (Osburn and Chapin, 1983; McIntosh and others, 1986). Similarly, cauldrons in the Mogollon Mountains near Mogollon erupted large volumes of ignimbrites (Ratte and others, 1984). The Bloodgood Canyon Tuff from the Bursum caldera near Mogollon overlies the Taylor Creek Rhyolite near Wall Lake. McIntosh and others (1986) report a <sup>40</sup>Ar/<sup>39</sup>Ar date of 28.23 ± 0.15 Ma for the Bloodgood Canyon Tuff.

The Bearwallow Mountain Formation is the youngest volcanic unit within the study area. Dates for this unit range from about 20 to about 26 Ma. (Elston, 1976). Within the study area, the Bearwallow Mountain Formation overlies the sandstone of Inman Ranch, which has been dated at upper Oligocene to lower Miocene by vertebrate fossils (Tedford, 1981; 1986, written communication). Relations between the Bearwallow Mountain Formation and the older units in the area are uncertain.

The Gila Conglomerate caps the Tertiary volcanic section in the Black Range. Numerous basalt flows intercalated within the Gila Conglomerate have been dated by conventional K-Ar methods and typically fall between 0.9 and 20.6 Ma (Elston, 1976). The Gila Conglomerate is broadly correlative with the Santa Fe Group in the Rio Grande Valley. The boundary between the two units has arbitrarily placed at the continental divide (Elston and Netelbeek, 1965; Elston, 1976).

## CORRELATION

Figure 2 outlines the various published and unpublished stratigraphic sections in the study area and the proposed correlations between the various sections. As can be seen from the diagram, the nomenclature for the region has developed since the pioneering work of Fries (1940). Coney's (1976) nomenclature was the basis for this study and was revised as necessary. See the notes in the caption for Figure 2 for descriptions of detailed problems with correlations.

## STRATIGRAPHY

The following section includes brief descriptions of the lithology and geochemistry of the stratigraphic section in the Taylor Creek district. Figure 3 is a schematic stratigraphic column of the Taylor Creek district. In addition to the lithologic descriptions of each unit, representative geochemical analyses are included (Table 1) as an aid to classifying the rocks. Appendix 1 is a tabulation of analyses for rocks analyzed during this study. Appendix 2a is a listing of the samples including sample locations and descriptions for each sample. Appendix 2b is a tabulation of point-count data for various units in the stratigraphic section. Figure 4 is the total alkali-SiO<sub>2</sub> diagram that is the basis for the IUGS classification for volcanic rocks (Le

Maitre, 1984) and is used by this study for classification of the volcanic rocks. Table 2 lists thin section point counts for various units in the Taylor Creek district.

Most of the deposits in the Taylor Creek district are Oligocene age. Exceptions are the lower Rubio Peak Formation which is late Eocene (Seager and others, 1982); the Bearwallow Mountain Formation that may be in part, lower Miocene (Elston, 1976); and the Gila Conglomerate. The age of Gila Conglomerate in this area is not known; however, isotopic dates on basalts intercalated within the Gila Conglomerate elsewhere range from 0.9 to about 21 Ma (Elston, 1976).

#### TERTIARY VOLCANIC AND VOLCANICLASTIC DEPOSITS

##### Rubio Peak Formation

Within the study area, the Rubio Peak Formation (Jicha, 1954) consists entirely of basaltic andesite lava flows and intercalated volcanoclastic sedimentary rocks (Fig. 5). The base of the unit is not exposed, thus no estimate of the total thickness can be made. Harrison (1986) has mapped felsic ignimbrites near the top of the Rubio Peak Formation immediately east of the area of Plate 1. No source for these ignimbrites has yet been recognized.



## Kneeling Nun Tuff

The Kneeling Nun Tuff (Jicha, 1954) consists of as much as 200 m of rhyolite ignimbrite in a normally zoned, multiple flow unit (Bornhorst, 1980). At Poverty Creek, it is densely welded, crystal-rich, and white to buff in color with variable proportions of pumice and lithic fragments (Fig. 6). The rock contains about 35% total phenocrysts consisting of sanidine (15%), quartz (12%), plagioclase (5%), biotite (2%) and traces each of zircon and opaque minerals. The phenocrysts are generally broken and the quartz is embayed. Sanidine and quartz phenocrysts may be as much as 3 mm in diameter. Pumice is generally axiolitic and the groundmass is vitroclastic. The major element chemistry of a single sample indicates that the Kneeling Nun is rhyolite (Fig. 4). Data from Bornhorst (1980) suggests that the Kneeling Nun Tuff is normally zoned, that is, it is more felsic near the base than at the top of the unit.

Coney (1976) and Woodard (1982) tentatively correlated these exposures with the Hells Mesa Tuff to the north, but the age and apparent normal zoning of the exposures in Poverty Creek precludes that correlation (Eggleston and others, 1983; Bornhorst, 1980). McIntosh and others (1986) determined a  $^{40}\text{Ar}/^{39}\text{Ar}$  plateau date for the Kneeling Nun in Poverty Creek of  $35.28 \pm 0.15$  Ma that also precludes correlation with the Hells Mesa Tuff because the Hells Mesa has been dated at  $32.04 \pm 0.15$  Ma ( $^{40}\text{Ar}/^{39}\text{Ar}$ ,



McIntosh and others, 1986). Woodard (1982) mapped the Kneeling Nun Tuff as two members, but such a division was not possible within this study area. The source of the Kneeling Nun Tuff is believed to be the Emory cauldron, several kilometers south of the study area (Elston, 1976).

#### Tuff of Koko Well

The tuff of Koko Well (informal name) is a thick, poorly welded ignimbrite that overlies the Kneeling Nun Tuff. The base of the Koko Well is thinly bedded and crystal-poor with only about 3% feldspar and a trace each of quartz and biotite. The bulk of the unit has the same mineralogy, but is massively bedded. Pumice is common and locally defines a foliation; lithic content is variable. The unit is as much as 60 m thick and is locally eroded leaving the overlying basaltic andesite of Poverty Creek in contact with the Kneeling Nun Tuff. At the base of the tuff of Koko Well is a discontinuous, moderately to densely welded ignimbrite that contains about 6% sanidine, 3% plagioclase, 1% biotite and a trace of amphibole and opaque minerals. The unit is rhyolitic and as much as 10 m thick. This basal ignimbrite is an alkali-rich rhyolite (Fig. 4). Sources for both these tuffs are unknown.

The unit is named for exposures along the south side of Poverty Creek at Koko Well (SW1/4, S. 6, T.10 S., R.9 W.). A complete section of the tuff of Koko Well is not known at this time. The unconformity at the base of the Poverty Creek

is regional in extent and has eroded through the tuff of Koko Well into the underlying Kneeling Nun Tuff (R. Harrison, 1986, oral communication).

#### Basaltic andesite of Poverty Creek

The basaltic andesite of Poverty Creek (Coney, 1976) consists of as much as 200 m of basaltic andesite to dacite lava flows (Fig. 4) with minor interbedded volcanoclastic sedimentary rocks (Fig. 7). Woodard (1982) reports a conventional K-Ar date of  $28.3 \pm 0.6$  Ma for the basaltic andesite of Poverty Creek. The basaltic andesite is fine-grained, nearly aphyric rock with 1 to 2 mm phenocrysts in a trachytic groundmass. The sparse phenocrysts consist of clinopyroxene and plagioclase. As much as 10% iddingsite and bowlingite are present and are probably alteration products after olivine. A few grains of amphibole are present in some flows. Thickness of the individual flows is difficult to establish because of poor exposures in the low, rolling topography that typically occurs on this unit.

The sedimentary rocks intercalated between the flows are typically green sandstones and siltstones that rarely exceed a thickness of 2 m. The detritus is all andesitic and suggests that the detritus was locally derived.

The  $\text{SiO}_2$  content of the basaltic andesite of Poverty Creek ranges from about 53% to 63% indicating that the unit consists of both basaltic andesite and andesite (Fig. 4). The basaltic andesite of Poverty Creek is more felsic at the

top than at the base (Table 1, Fig. 4). This change is noticeable in thin section because the upper flows contain more plagioclase than do the flows near the base. Near the continental divide, flows near the top of the unit have been mildly propylitized; the center of alteration is south of Kline Mountain.

Thickness of the basaltic andesite of Poverty Creek is controlled by paleotopography on the unconformity at the base of the unit. As much as 100 m of relief is apparent on that unconformity. The top of the Poverty Creek has as much as 30 m of relief, thus the thickness of the unit is between 40 and 200 m.

#### Tuff of Stiver Canyon

The tuff of Stiver Canyon is a crystal-poor to moderately crystal-rich, high-silica rhyolite-ignimbrite (Fig. 4) named for exposures in Stiver Canyon (Woodard, 1982). North of Kline Mountain, this cliff-forming ignimbrite consists of phenocrysts of sanidine (2%), quartz (1%) and biotite (trace) in a vitroclastic groundmass (Fig. 7). Lithic fragments comprise as much as 5% of the rock and consist of flow banded rhyolite and andesite. Several individual flow units have been recognized and a fluvial interval is locally present near the base of the unit. The fluvial interval consists of 1 to 2 m of sandstone and conglomerate with pebble to cobble size clasts.

South of Kline Mountain, the unit is moderately crystal-

rich and consists of sanidine (10%), quartz (5%), and biotite (trace) phenocrysts in a vitroclastic groundmass. This assemblage is present in the type section (Woodard, 1982), however, B. McIntosh (1986, oral communication) reports that the paleomagnetic inclination and declination is different for the two areas.

The differences in crystal content and paleomagnetism of the tuff north and south of Kline Mountain is problematic. Because the unit occurs at the same stratigraphic interval, the difference in crystal content may be due to zonation in the unit or may be due to miscorrelation. The paleomagnetic data suggests that the tuff in the two areas was erupted at different times and that the tuff that immediately overlies the basaltic andesite of Poverty Creek north of Kline Mountain is probably not correlative with the tuff south of Kline Mountain, but that controversy will only be settled by detailed mapping north and south of this study area.

Woodard (1982) reported 170 m of Stiver Canyon near Lookout Mountain, south of the area of Plate 1. Within the area of Plate 1, the Stiver Canyon is a maximum of 40 m thick. The source of the tuff of Stiver Canyon is unknown.

## Tuff of Lookout Mountain

The tuff of Lookout Mountain (Woodard, 1982) is a moderately welded, crystal-rich ignimbrite. Woodard (1982) reports that the unit consists of phenocrysts of quartz (10%), sanidine (15%), amphibole (tr), and opaque minerals (tr) in a vitroclastic groundmass. The unit is exposed only along the southeastern border of Plate 1 thus little is known about its regional extent. The source vent for this ignimbrite is not known at this time.

## Rhyolite of Sawmill Peak

The rhyolite of Sawmill Peak (new, informal name) is a sequence of dark, red-brown, rhyolite lavas found on Sawmill Peak and on the north rim of Poverty Creek (Fig. 7). It is named for the section on Sawmill Peak (sec.7, T.10 S., R.9 W.). The color of these lavas is distinctive as are the 7 to 10% large sanidine phenocrysts that commonly exceed 7 mm in length. Only trace amounts of quartz and biotite are present as phenocrysts and plagioclase is notably absent. The groundmass is microtrachytic and flowbanded (Fig. 8). The rhyolite of Sawmill Peak is markedly flow-banded and a breccia commonly marks the top and bottom of individual flows. At least two flows are present on Sawmill Peak. One flow overlies the tuff of Stiver Canyon, the other flow is intercalated in the tuff of Stiver Canyon. On the north rim of Poverty Creek, two flows overlie the tuff of Stiver Canyon

that rests directly on the basaltic andesite of Poverty Creek. These flows are typically 20 to 30 m thick, indicating that they were much less viscous than the nearby high-silica rhyolites which form flows hundreds of meters thick. Coney (1976) included these lavas with the rhyolite of Dolan Peak. The chemistry of the rhyolite of Sawmill Peak is unique for this area (#6, Fig. 4) in that its agpaite index is about 1, suggesting a peralkaline affinity for these lavas.

#### Tuff of Kline Mountain

A sequence of nonwelded, thinly bedded, moderately crystal-rich, high-silica rhyolite (#7, Fig. 4) ignimbrites exposed on the north flank of Kline Mountain (sec.22, T.10 S., R.10 W.) has been informally named the tuff of Kline Mountain (Fig. 9). This ignimbrite comprises numerous 1 to 3 m thick flow units that contain as much as 50% pumice fragments. Crystal content varies from flow unit to flow unit, but averages about 12%. The phenocryst ratios also vary, but sanidine is always more abundant than quartz. Plagioclase is a trace constituent, as is biotite, zircon, and opaque minerals. Locally, near the top of the unit, vitric lithic fragments identical to the overlying rhyolite of Dolan Peak are common. The tuff of Kline Mountain may be an ignimbrite apron related to emplacement of the rhyolite of Dolan Peak domes and flows. Geometry of the tuff of Kline Mountain suggests that it fills a broad, shallow paleovalley

with as much as 200 m of relief.

Argillic and advanced argillic alteration associated with intrusion of a rhyolite porphyry south of Kline Mountain has converted much of the tuff of Kline Mountain to an assemblage of kaolinite-alunite-chalcedony (Fig. 10). Alteration minerals are present in variable proportions, but alunite generally increases as the intrusive is approached, kaolinite increases away from the intrusive and then declines dramatically toward the edge of the argillic alteration. Chalcedony occurs as disseminations in the tuff and as large replacement bodies above kaolinite-alunite bodies. Intensity of the alteration decreases rapidly north of NM-59 along the continental divide. Prospect pits immediately south of NM 59 on the continental divide are excavated in the tuff of Kline Mountain. Kaolinite is the dominant mineral and was the mineral of interest when the prospects were developed.

#### Rhyolite of Dolan Peak

Coney (1976) named all the rhyolite lavas and ignimbrites between the top of the basaltic andesite of Poverty Creek and the base of the Taylor Creek Rhyolite the rhyolite of Dolan Peak. The rhyolite of Dolan Peak is here restricted to the high-silica rhyolite flows and associated ignimbrites between the top of the rhyolite of Sawmill Peak and the base of the La Jencia Tuff, which Coney (1976) also included in the rhyolite of Dolan Peak (Fig. 2). The Dolan Peak consists of more than 200 m of high-silica rhyolite



lavas and ignimbrites that contain between 8 and 20% phenocrysts of sanidine and quartz. The quartz/sanidine ratio is 0.1 to 0.3 and distinctive from the quartz/sanidine ratio of about 1 in the very similar appearing Taylor Creek Rhyolite (Table 2). On the basis of the quartz/sanidine ratios, Woodard's (1982) Taylor Creek Rhyolite is here correlated with the rhyolite of Dolan Peak. Spherulitic devitrification is common in the rhyolite of Dolan Peak and uncommon in the Taylor Creek Rhyolite.

The  $\text{SiO}_2$  content of the rhyolite of Dolan Peak is typically >75% (Fig. 4, Table 1). The major element concentrations in the rhyolite of Dolan Peak are indistinguishable from those of the Taylor Creek Rhyolite.

The rhyolite of Dolan Peak consists of both rhyolite domes and lava flows. Many of the flows are less than 100 m thick. The domes are more than 200 m thick and locally exhibit intense vapor phase crystallization. Tin mineralization, similar to that found in the younger Taylor Creek Rhyolite, is associated with intense vapor-phase crystallization in domes south of the area studied (Foord and others, 1984).

Ignimbrites included with the Dolan Peak have the same mineralogy and similar quartz/sanidine ratios as the lavas. The geometry of many of these ignimbrites suggest that they were deposited in cusps between coalescing domes.



### La Jencia Tuff

The La Jencia Tuff (Osburn and Chapin, 1983) is a crystal-poor, densely welded, foliated and locally lineated rhyolite ignimbrite (Fig. 11). Within the study area, the La Jencia Tuff is exposed along the continental divide north of NM 59 and west of Kline Mountain, and pinches out immediately south of Stiver Canyon. Where fresh, the La Jencia Tuff is light to dark gray in color with about 7% sanidine and a traces of quartz, plagioclase, biotite, zircon, and pyroxene as phenocrysts in a vitroclastic groundmass. Thin, discontinuous vitrophyres are found in Scales Canyon. The  $\text{SiO}_2$  content of the La Jencia is typically about 73% (Fig. 4).

McIntosh and others (1986) report a  $^{40}\text{Ar}/^{39}\text{Ar}$  plateau date of  $28.76 \pm 0.15$  Ma on samples of the La Jencia Tuff. The source of the La Jencia Tuff is believed to be the Sawmill Canyon-Magdalena cauldrons in the Magdalena Mountains near Socorro (Osburn and Chapin, 1983).

### Rhyolite of Whitetail Canyon

The rhyolite of Whitetail Canyon (Richter and others, 1986) is a crystal-poor, gray, finely flow-banded rhyolite lava (Fig. 4). The rock contains plagioclase (5%), pyroxene (1%), biotite (0.25%), and traces of amphibole, and opaque oxides set in a microtrachytic groundmass of feldspar

microlites (Fig. 12). Perlitic cracks crosscut the microtrachytic groundmass where interstitial glass is abundant. Most of the phenocrysts exhibit incipient alteration around the edges. Vapor-phase crystallization is pervasively mild; it imparts a mildly bleached appearance to the rock.

The rhyolite of Whitetail Canyon is spatially associated with the rhyolite of Hoyt Creek and both units are chemically and texturally similar. The rhyolite of Whitetail Canyon probably immediately postdates the rhyolite of Hoyt Creek, but the relationships are equivocal. Those similarities and the apparent age relationships suggest that the rhyolite of Whitetail Canyon is a late effusive phase of the rhyolite of Hoyt Creek.

#### Rhyolite of Hoyt Creek

The rhyolite of Hoyt Creek (Richter and others, 1986) is a finely flow-banded, virtually aphyric high-silica rhyolite lava (Fig. 4). Morphology of the lavas suggest that the rhyolite of Hoyt Creek is a dome-flow complex with the effusive center near Whitetail Canyon and a short, stubby flow extending south to Hoyt Creek. The rock contains a trace to 0.5% plagioclase and biotite and a trace each of pyroxene, amphibole, and zircon as phenocrysts in a microtrachytic groundmass composed of feldspar microlites. The microlites do not stain for potassium indicating that they are albitic.

The ages of the rhyolite of Whitetail Canyon and the rhyolite of Hoyt Creek are unknown. They underlie the Taylor Creek Rhyolite and thus are older than about 28.2 Ma. In Hoyt and Diamond Creeks, south of the study area, the rhyolite of Hoyt Creek overlies a sequence of basaltic andesite that may correlate with the basaltic andesite of Poverty Creek (Richter and others, 1986).

#### Rhyolite of Keith Tank

The rhyolite of Keith Tank (informal name for a single exposure in sec. 3, T. 11 S., R. 11 W.) consists of a vitric, flow-banded, rhyolite lava that contains quartz (1%), plagioclase (0.8%), sanidine (0.2%), biotite (0.4%), lithic fragments (12%), and traces of green hornblende, pyroxene, zircon, and opaque minerals. Phenocrysts are all small, generally less than 0.5 mm in diameter. The lithic fragments are <1 cm in diameter and consist of flow-banded rhyolite and coarsely crystalline gabbro (?), and basalt. The amphibole and pyroxene in the rhyolite may in part be xenocrysts derived from these lithic fragments. A single sample of the unit (#10, Fig. 4 and Table 1) suggests that the unit is a high-silica rhyolite.

Because this unit is represented by only one isolated exposure, little is known about its age relative to other units in the area. It underlies the Gila Conglomerate and the sandstone of Inman Ranch and is chemically similar (Table 2) to the rhyolites of Hoyt Creek and Whitetail Canyon.

This suggests that the rhyolite of Keith Tank is older than the Taylor Creek Rhyolite, but no stratigraphic relationship with either the rhyolite of Hoyt Creek or rhyolite of Whitetail Canyon has been established.

#### Unnamed tuff

A multiple-flow, nonwelded ignimbrite occurs immediately below the Taylor Creek Rhyolite in a small tributary to Scales Canyon (sec. 30, T.10 S., R.10 W.) and along the western edge of Burnt Cabin Flats. The ignimbrite is as much as 30 m thick with no exposed base. The unit consists of a 10-m-thick, massive pyroclastic flow unit overlain by numerous thin pyroclastic flow units. The ignimbrite is crystal-poor and moderately pumice-rich. About 5% sanidine and a trace of plagioclase are present as phenocrysts. The pumice is dark-gray to black in a tan to light-gray groundmass. The exposure is restricted to a few hundred m<sup>2</sup>, thus precluding correlation with other units in the area. The unit is chemically similar to, and in the same stratigraphic position as the La Jencia Tuff, and may correlate with it, but the close proximity of densely welded La Jencia Tuff to this non-welded unit is problematic.

#### Taylor Creek Rhyolite

Named for exposures in Taylor Creek, (Elston, 1968) east of Wall Lake (S1/2, sec. 2, T.11 S., R.12 W.), the Taylor

Creek Rhyolite is a group of roughly time equivalent, chemically similar, high-silica rhyolite lavas located on the western flank of the northern Black Range (Elston, 1968; Table 1 and Appendix 1B). Figure 1 shows the distribution of the Taylor Creek Rhyolite and the various geographic localities described in the following section. As is obvious from Figure 1, the Taylor Creek is not a continuous unit, but a group of discrete, widely separated eruptive centers. All of these eruptive centers have been included in the Taylor Creek Rhyolite because of time equivalence and similarities of lithology and geochemistry (Plate 1).

In general, the Taylor Creek Rhyolite is moderately crystal-rich to crystal-rich, flow-banded, white-to-buff rhyolite lava (Fig. 13). The absolute concentration of phenocrysts in each eruptive center is distinctive and will be detailed below. The quartz/sanidine ratio of the Taylor Creek is about 0.6 to 1.2 and distinguishes it from the rhyolite of Dolan Peak that has quartz/sanidine ratios of 0.1 to 0.3 (Table 2). Both quartz and sanidine are euhedral to subhedral. Quartz is rounded and locally deeply embayed. Sanidine crystals are also embayed giving them a "wormy" appearance. Plagioclase is always rounded and generally rimmed by sanidine. Cores of plagioclase phenocrysts are typically "wormy" and both sanidine and plagioclase are typically glomeroporphyritic (Fig. 14). All accessory minerals occur as euhedra except zircon which is typically enclosed by biotite. The groundmass texture is granophyric with rare spherulitic zones (Fig. 15). The size of the

groundmass crystallites is correlative with intensity of vapor-phase crystallization. In mildly vapor-phase crystallized zones, the groundmass crystallite size is about 0.05 to 0.1 mm and exceeds 0.5 mm in intensely vapor-phase crystallized zones. A complete description of the textural and chemical effects of vapor-phase crystallization is presented in Eggleston and others (1987a). The rare vitric material, found only in the carapace breccias, contains a few percent of spherulites (Fig. 16) and is always hydrated.

The  $\text{SiO}_2$  content of the Taylor Creek Rhyolite is typically between 76 and 78%. No major element variations occur between the various Taylor Creek Rhyolite domes (Fig. 4).

The geometry of the Taylor Creek Rhyolite bodies suggest that the Taylor Creek Rhyolite consists of rhyolite domes and short, stubby flows. Domes near Boiler Peak and Wall Lake have coalesced to form eruptive centers comprising 4 or more domes each. Carapace breccia, flow banding, ramp structures, and pyroclastic material are associated with each rhyolite dome and mark the boundaries between individual domes.

With the exception of the Taylor Creek eruptive center near Wall Lake, the Taylor Creek Rhyolite consists of about 15 to 20% of 1 to 2 mm phenocrysts of sanidine and quartz in subequal proportions. Plagioclase, biotite, and zircon occur as trace minerals. In the Taylor Creek eruptive center, the rhyolite consists of about 35% phenocrysts of 5 to 8 mm phenocrysts of quartz and sanidine in subequal proportions

(Fig. 17). The accessory minerals are similar with the exception of sphene that is abundant in the Taylor Creek eruptive center and rare in the other domes and eruptive centers. The biotite, pyroxenes and amphiboles are altered to opaque minerals, presumably during vapor-phase crystallization.

Within the area of Plate 1, only the Nugget Gulch dome is an isolated, single rhyolite dome. The Boiler Peak dome is located near the middle of an effusive center that consists of that dome as well as the Alexander Cienega, North Paramount Canyon, and Sawmill Canyon domes. The Taylor Creek dome, in the lower reaches of Whitewater Canyon, is the southeastern edge of an eruptive center comprising that dome as well as the Indian Creek, Kemp Mesa, and the North Taylor Creek domes. The geometry of the Indian Creek and North Taylor Creek domes is speculative because contacts are covered by younger rocks. The geometry of the rhyolite at Squaw Creek suggests that the vent is north of Squaw Creek, near Corduroy Canyon, where more than one dome may be present (W. Duffield, 1985, oral communication). Other exposures of Taylor Creek Rhyolite in the region (Fig. 1) are at Indian Peaks (north of the area of Plate 1) and Round Mountain (south of Plate 1). The rhyolite lava at Round Mountain appears to consist of a single dome, but little is known about the area. Lawrence and Richter (1986) and Richter and others (1986) have mapped the Indian Peaks area and suggest the possibility that 2 domes are present and that these domes produced short lava flows.



Age relations between the domes that comprise the various eruptive centers are difficult to establish. Contacts between the various domes are frequently marked by carapace breccia and/or pyroclastic rocks. In the Boiler Peak eruptive center, the Boiler Peak dome is the oldest. It is overlain by the Alexander Cienega, the north Paramount Canyon, and the Sawmill Canyon domes. Age relations between these three overlying domes are not clear. Similarly, the Taylor Creek dome is overlain by the Indian Creek, north Taylor Creek, and the Kemp Mesa domes. The relations between these younger domes is also unknown. No vent areas have been documented as yet.

The total thickness of the individual domes is difficult to ascertain. Exposures in lower Whitewater Canyon indicate that the Taylor Creek dome is more than 250 m thick. Similar exposures in Paramount Canyon suggest that the Boiler Peak dome is over 200 m thick. The tops of the domes are rarely preserved and the bases are not exposed. Individual domes are typically 2 to 5 km in diameter. Assuming a maximum thickness of 300 m, the total volume of the Taylor Creek Rhyolite is more than 80 km<sup>3</sup>.

Figure 18 is a comparison of a representative sample of the Taylor Creek Rhyolite and an average rhyolite (major elements after Le Maitre, 1976; trace elements after Turekian and Wedepohl, 1963). This diagram shows the enrichment of SiO<sub>2</sub>, Rb, and other lithophile elements and the marked depletion of CaO, Fe<sub>2</sub>O<sub>3</sub>, Sr, and Ba. This pattern is characteristic of all the Taylor Creek Rhyolite. Eggleston



and others (1987b) discuss the petrology of the Taylor Creek Rhyolite.

The age of the Taylor Creek Rhyolite has been disputed for many years (Table 3). Elston (1973) published a conventional K-Ar date of  $24.6 \pm 0.5$  Ma (new constants) on sanidine. Ratte and others (1984) published a conventional K-Ar date of  $27.7 \pm 0.9$  Ma, also using sanidine. A sample collected during the course of this study yielded a conventional K-Ar date of  $27.2 \pm 1.1$  Ma on sanidine ( $\text{Ar}^{40*} = 0.07682$  ppm;  $\text{Ar}^{40*}/\text{Total Ar}^{40} = 0.547$ ;  $K = 3.872\%$ ;  $K^{40} = 4.723$  ppm). Maxwell and others (1986) published a number of dates that range from about 21 to 27 Ma.

McIntosh and others (1986) reported a  $^{40}\text{Ar}/^{39}\text{Ar}$  plateau date on the La Jencia Tuff that underlies the Taylor Creek Rhyolite of  $28.76 \pm 0.15$  Ma. This constrains the maximum age of all the Taylor Creek Rhyolite in Plate 1 with the exception of the Taylor Creek eruptive center. The relationship of the La Jencia tuff to the Taylor Creek eruptive center is not known so its stratigraphic position above the La Jencia is only inferred. McIntosh and others (1986) also report a  $^{40}\text{Ar}/^{39}\text{Ar}$  plateau date of  $28.52 \pm 0.15$  Ma for the Shelley Peak Tuff that overlies the Taylor Creek Rhyolite northwest of Indian Peaks. On the rim of Whitewater Canyon, near Wall Lake, the Bloodgood Canyon Tuff overlies the Taylor Creek Rhyolite. The Bloodgood Canyon Tuff has been dated at  $28.2 \pm 0.15$  Ma by McIntosh and others (1986). These stratigraphic brackets thus place the age of the Taylor Creek Rhyolites between about 28.8 and 28.2 Ma with the

additional constraint that the domes near Indian Peaks may fall between 28.8 and 28.5 Ma. All the Taylor Creek Rhyolite is believed to fall between these limits. A single  $^{40}\text{Ar}/^{39}\text{Ar}$  date of  $28.18 \pm 0.15$  Ma has been obtained by McIntosh (1986, oral communication) on the Nugget Gulch dome. That date is statistically indistinguishable from the date on the overlying Bloodgood Canyon Tuff.

#### Unnamed pyroclastic rocks

Pyroclastic rocks associated with the Taylor Creek Rhyolite are widespread, but not voluminous. These deposits consist of high-silica rhyolite pyroclastic flow, fall, and surge deposits in variable proportions. Because these deposits are found in widely separated, isolated exposures, no name was assigned to them. On Plate 1, the number that accompanies the Tt symbol is intended to suggest possible correlations of the pyroclastic deposits with a source rhyolite dome. These correlations are tenuous and not accepted by all workers in the region (W. Duffield, 1986, oral communication).

Ignimbrites are the most common as well as the most voluminous deposits. These deposits mantle most of the rhyolite domes in the region and consist of individual 0.5- to-2 m thick flow units stacked to a thickness of as much as 80 m. Kyle and others (1986) describe five measured sections in Scales Canyon on the eastern flanks of the Boiler Peak dome. The pyroclastic deposits in Scales Canyon are

particularly well exposed and three types of deposits have been recognized (Fig. 19a). The lower part of the section consists of as much as 45 m of 0.5 to 2-m-thick ignimbrites (Fig. 19b). Included in this sequence are numerous 1 to 20-cm-thick pyroclastic fall deposits as well as aeolian sandstone that fills topography on two unconformities within the section. Many of the ignimbrites exhibit vertical zoning similar to that described by Sparks and others (1983) and Fisher and Schminke (1984). Sparks and others' (1973) layers 1 and 3 are rarely preserved. Layer 2a is generally very thin and difficult to recognize. Layer 2b is well developed and consists of a thin basal zone of normally graded lithic fragments, an internal zone of massive to plane parallel bedding, and an upper zone of inversely graded pumice. Layer 3 deposits were not recognized.

Pyroclastic surge deposits were not positively identified in this section; however, surge deposits were observed in other areas. These deposits consist of thinly bedded, moderately well-sorted, fine-to-coarse ash deposits that rarely exceed a few cm thick. Crossbedding is common in these deposits.

The second type of deposit found in Scales Canyon consists of coarse-to-fine pyroclastic fall deposits (Fig. 19c). In the measured sections, about 3 m of continuous fall deposits were recognized (Kyle and others, 1986). The lower 2 m consist of normally graded, well-sorted pumice as much as 7 cm in diameter near the base. Near the top, the maximum pumice is less than 1 cm in diameter. This deposit is

believed to be the result of a plinian or sub-plinian eruption. The remaining meter consists of thinly bedded, well-sorted, coarse ash with sparse vitric clasts.

Pyroclastic fall deposits are rarely exposed in other outcrops of this unit. A thin, well-sorted deposit on the east flank of the Boiler Peak dome about 2 km south of NM-59 consists of very well sorted 2 to 5 mm pumice. This deposit is likely a Plinian or sub-Plinian deposit.

The top of the deposits in Scales Canyon consists of a coarse breccia believed to have been emplaced as a hot pyroclastic flow (Fig. 19d). The deposit consists of clast supported blocks of vesiculated Taylor Creek-like rhyolite lava. The blocks are generally 0.1 to 0.5 m in diameter, but blocks in excess of 3 m were found during this study. Kyle and others (1986) report that many of the clasts in the deposit were emplaced above the Curie temperature, indicating that the deposits were emplaced as a hot (>500 deg. C.) pyroclastic flow, possibly the result of collapse of a spire or dome on the nearby Boiler Peak dome. No similar deposits have been found elsewhere in the region.

A particularly problematic type of pyroclastic deposit is exposed north of Nugget Gulch and in the northwest wall of Paramount Canyon. These deposits consist of large flattened, vitric and devitrified clasts in a coarse ash matrix. The clasts appear to be nonvesiculated juvenile magma that was emplaced hot enough to flatten. Many clasts have length to thickness ratios larger than 5. These deposits are everywhere welded and locally welding is dense enough to give

a rheomorphic aspect to the material. Similar deposits in Italy, called piperno, are believed to be agglutinates from felsic fire fountain eruptions (Fisher and Schminke, 1984). A mode of eruption and emplacement similar to that which formed piperno is envisioned for these deposits.

#### Tuff of Garcia Camp

The tuff of Garcia Camp (Lawrence and Richter, 1986) consists of as much as 20 m of cliff-forming, high-silica rhyolite ignimbrite (#20, Fig. 4). About 10% quartz, 6% sanidine, 1% biotite, and a trace each of plagioclase, amphibole, zircon, and opaque minerals are present as phenocrysts in a vitroclastic groundmass. Pumice is abundant and locally imbricated. This ignimbrite underlies the Taylor Creek Rhyolite at Indian Peaks (Lawrence and Richter, 1986) and a correlative exposure overlies the Taylor Creek Rhyolite of the Boiler Peak eruptive center. Intense vapor-phase crystallization has locally produced a granophyric groundmass texture with overgrowths on quartz and sanidine phenocrysts.

W. Duffield (1986, oral communication) and C. Maxwell (1986, oral communication) suggest that even though the rocks correlated with the Garcia Camp on Plate 1 are lithologically similar to the type Garcia Camp, these rocks may be of more local derivation. They suggest that the source of these deposits may be the Tin Mountain dome north of Nugget Gulch. The Tin Mountain dome is another high-silica rhyolite dome included with the Taylor Creek Rhyolite.

San

pr

an

t

up

on

To

fo

ve

an

of

the

of

the

of

of

of

of

of

of

of

of

of

of

of

of

of

of

of

of



## Sandstone of Inman Ranch

Sandstone of Inman Ranch is a new, informal name proposed for exposures of tuffaceous siltstone, sandstone, and conglomerate near Inman Ranch in Stiver Canyon (sec 31, T.10 S., R. 10 W.) (Fig. 20). The sandstone of Inman Ranch unconformably overlies the Taylor Creek Rhyolite and is unconformably overlain by the Gila Conglomerate (Fig. 21). The sandstones and siltstones are poorly sorted, moderately indurated, and thinly bedded. High-angle crossbedding in well-sorted sandstones near the base of the unit suggest aeolian deposition. Most of the unit is fluvial, however, and consists of thin beds with scour-and-fill features at the base of the units. Many of the paleochannels have pebble-to-cobble-sized material lining the channel bottoms. Clast lithologies reflect the local bedrock and in the lower portions of the unit, clasts of Taylor Creek Rhyolite are the dominant lithology. Higher in the section, clasts of the La Jencia Tuff are dominant. These observations indicate a local source for the sandstone of Inman Ranch.

Massive, poorly sorted sandstones with no obvious internal structures (Fig. 22) occur in the upper part of this unit. These deposits are 0.5- to 2-m-thick and contain abundant 2- to 5-cm-diameter exotic clasts of various lithologies. Thin, very discontinuous pebble and cobble conglomerate occur with the sandstones. S. Cather (1986, oral communication) interprets this deposit to be the product of braided stream deposition.

Intercalated near the top of the sandstone of Inman Ranch, in Scales and Stiver Canyons is a 2- to 8-m-thick, nonwelded ignimbrite that consists of poorly sorted fine-to-coarse ash, pumice, and lithic fragments. This tuff may be the distal end of a major, regional ignimbrite. W. McIntosh (1986, oral communication) suggested that this tuff may be the distal end of the South Canyon Tuff (Osburn and Chapin, 1983) because of the similarities of paleomagnetic declination and inclination.

The sandstone of Inman Ranch contains vertebrate fossils dated by R. Tedford (1981; 1986, written communication) at upper Oligocene to lower Miocene.

#### Bloodgood Canyon Tuff

The Bloodgood Canyon Tuff (Elston, 1968) is a moderately crystal-rich, regional, high-silica rhyolite ignimbrite (Fig. 4) probably erupted from the Bursum cauldron near the town of Mogollon (Ratte' and others, 1984). The Bloodgood Canyon Tuff is as much as 50 m thick and contains quartz (3%), sanidine (7%), and a traces of plagioclase, biotite, sphene, zircon, and opaque minerals as phenocrysts in a vitroclastic groundmass. Lithic fragments are uncommon. Within the study area, multiple-flow, poorly to moderately welded Bloodgood Canyon Tuff is restricted to cusps between coalescing rhyolite domes. McIntosh and others (1986) report an  $^{40}\text{Ar}/^{39}\text{Ar}$  plateau date of  $28.36 \pm 0.15$  Ma for a sample of Bloodgood Canyon from Railroad Canyon, about 15 km northwest

of this study area.

#### Bearwallow Mountain Formation

The Bearwallow Mountain Formation (Elston, 1968) consists of numerous andesite and latite lava flows (Fig 4). These deposits are exposed on the west side of the study area. Elston (1968) mapped the Wall Lake Andesite as a separate member of the Bearwallow Mountain Formation; however, in this report, the Wall Lake Andesite has not been separated from the Bearwallow Mountain Formation.

Along Beaver Creek, at the west edge of the study area, the Bearwallow Mountain Formation consists of numerous flows with brecciated bases and tops. Breccias in Indian Creek have been interpreted by Richter (1978) as vent breccias. Isolated exposures of an aphyric andesite near Keith Tank, in the southern part of the study area, is probably correlative with the Bearwallow Mountain. The age of the Bearwallow Mountain Formation in the Black Range is poorly constrained. It overlies the sandstone of Inman Ranch and is thus younger than lower Miocene. This places a lower limit on the age of the Bearwallow Mountain Formation which is as much as 150 m thick in the map area.

#### Gila Conglomerate

In this portion of the Black Range, the Gila Conglomerate (Gilbert, 1875) consists of as much as 100 m of

nearly flat-lying conglomerate and coarse sandstone unconformably overlying all older rocks in the region. Clast lithologies reflect the local bedrock and are dominated by the Taylor Creek Rhyolite. Much of the conglomerate is clast supported with a coarse sand matrix. Induration is generally poor to moderate; however, the unit is locally a cliff former (Fig. 23). Within the area of Plate 1, the Gila Conglomerate overlies the volcanic section. No other constraints on the age are known in this area. Elston (1976) suggests that the Gila Conglomerate spans time from about 21 Ma to about 0.9 Ma.

The Gila Conglomerate is roughly time equivalent with the Santa Fe Group in the Rio Grande drainage. The contact between the two units has been arbitrarily placed along the continental divide (Elston and Netelbeek, 1965; Elston, 1976). Both units were deposited in basins formed in response to extension within the Rio Grande rift and Basin and Range Province.

#### QUATERNARY DEPOSITS

Quaternary deposits in the study area consist of alluvium in the larger, active stream channels and colluvium on gentle hillslopes and in small stream channels. Piedmont slope deposits cover much of the Gila Conglomerate. Isolated exposures of piedmont slope deposits are found on the Taylor Creek Rhyolite, suggesting that the entire area was graded at some point. All of the deposits consist of

fine-to-coarse sedimentary material and are poorly indurated. The alluvial deposits in stream channels that drain areas of exposed Taylor Creek Rhyolite locally contain abundant wood tin and cassiterite and are potential tin resources.

#### TERTIARY INTRUSIVE ROCKS

##### Rhyolite of Franks Mountain

The rhyolite of Franks Mountain (informal name; Woodard, 1982) consists of a group of high-silica rhyolite intrusives (#24, Fig. 4) that forms a north-south trending belt that extends from Kline Mountain on the north to Diamond Creek on the south (Woodard, 1982). The belt may extend farther south, but the geology farther south is poorly known. No northward extension is known. The name "rhyolite porphyry of Kline Mountain" that appears throughout this bulletin refers only to the intrusive mass exposed immediately south of Kline Mountain and does not supercede Woodard's regional nomenclature. This nomenclature is adopted so that individual intrusive masses of the rhyolite of Franks Mountain can be referenced.

The rocks contain about 15% total phenocrysts consisting of quartz (5%) and sanidine (10%) in a granophyric groundmass. Biotite and possibly amphiboles are trace constituents that are rarely preserved. Flowbanding and granophyric groundmass, as well as the fact that these

rhyolites intrude the youngest rocks in the area, indicate that these intrusives were subvolcanic. Alteration associated with the rhyolite porphyry of Kline Mountain is responsible for the advanced argillic alteration north of the intrusive. Most of this intrusive has been silicified and much of it has undergone argillic alteration. Near the north end of the intrusive body, quartz-pyrite stockworks are common. The alteration associated with this intrusive is described in a later section. Woodard (1982) describes similar alteration associated with many of the Franks Mountain intrusives south of this study area.

The rhyolite porphyry of Kline Mountain intrudes the rhyolite of Dolan Peak. The La Jencia Tuff that overlies the rhyolite of Dolan Peak curves around the intrusive, suggesting that the La Jencia Tuff was emplaced prior to intrusion of the rhyolite porphyry of Kline Mountain. Change in strike of beds above the La Jencia Tuff is not certain, but non-welded pyroclastic rocks associated with the Taylor Creek Rhyolite are possibly warped in a manner similar to the La Jencia Tuff.

A conventional K-Ar date of  $28.4 \pm 1.2$  Ma was determined on alunite from the advanced argillic assemblage near the summit of Kline Mountain (Eggleston and Norman, 1987). The sample was probably collected from the tuff of Kline Mountain, but alteration was too intense to positively correlate the unit. The association of the alteration with this particular intrusive suggests a genetic relationship, thus the age of the alteration is probably the age of the



intrusive. This suggests that the Kline Mountain intrusive is younger than the Taylor Creek Rhyolite; a contention supported by the structural geology.

#### STRUCTURAL GEOLOGY

The structural geology of the Taylor Creek district is remarkably simple (Plate 1). The strata dip gently to the west at about 8 to 10 degrees. The tuff of Garcia Camp dips about 4 degrees to the west suggesting that 4 to 6 degrees of tilting occurred between the time of deposition of the tuff of Stiver Canyon and the tuff of Garcia Camp. In the Alexander Canyon area, the Gila Conglomerate is flat-lying.

The paucity of faults in the region is remarkable. Few faults were mapped in the entire study area. The largest of the mapped faults is located near the mouth of Whitewater Canyon and has about 100 m of down-to-the-west displacement. Small faults were mapped in the vicinity of Burnt Cabin Flat and have down-to-the-west displacements on the order of a few meters. On Sawmill Peak, near the eastern edge of the map area, two faults with down-to-the-east displacements were mapped. These faults, which have only a few meters of displacement, are related to the Winston graben, the westernmost basin of the Rio Grande rift in the region. The westerly dip of the rocks in the northern Black Range may be due to uplift related to the Rio Grande rift.

The only other structural feature worthy of note is a change in strike of the volcanic rocks just north of Poverty

Creek. The strike changes from north-south to N 30 E and then changes back to north-south immediately west of Kline Mountain. This change in strike affects rocks as young as the Taylor Creek Rhyolite and is possibly due to intrusion of the rhyolite porphyry of Kline Mountain. Intrusion of the rhyolite of Franks Mountain may also be responsible for formation of the small sedimentary basin between the eastern front of the Taylor Creek Rhyolite and Franks Mountain. That basin is now filled with the sandstone of Inman Ranch.

#### GEOMORPHOLOGY

Plateaus and deep canyons dominate the landforms in the map area west of the continental divide (Fig. 24). Plateaus slope gently to the west from the crest of the Black Range. Near the crest, elevations are about 2440 m.; on Kemp Mesa, 25 km west of the crest, elevations are about 2290 m for an average slope of only 6 m/km. This regional erosion surface is cut by westerly flowing canyons as much as 300 m deep. Numerous low rounded hills that may be paleoinselbergs are scattered on the plateau surface. Boiler Peak, Alexander Peak, and Round Mountain (south of the map area) are examples.

West of the map area, Black Mountain also rises above this slope. Significance of this break in the regional erosion surface is not obvious. Because the age of the regional erosion surface relative to the formation of Black Mountain is unknown, two possibilities for the break are

offered. First, the bulk of Black Mountain, a mafic volcanic center (Coney, 1976) may have been erupted onto the regional erosion surface. This possibility is unlikely because basalts that may have been erupted from the area of Black Mountain have been graded. Second, Black Mountain may have formed a high mountain mass during this period of erosion and was too massive to be completely removed by erosion during the time interval within which the regional erosion surface formed. The aerial extent of this regional erosion surface suggests that the region was tectonically stable for a long period of time. Leopoldt (1981) suggests that rejuvenation of the streams and incision of the deep canyons on the western Mogollon Plateau may have begun before 5 Ma.

East of the crest of the Black Range, the topography is mountainous with deep canyons draining into the Winston Graben and thus into the Rio Grande. This topographic relief results from differential vertical movements between the Winston graben and the Black Range, which is the uplifted and outward-tilted west flank of the Rio Grande rift.

#### HYDROTHERMAL ALTERATION

##### Kline Mountain Intrusive

Hydrothermal alteration is limited to a halo of propylitic, argillic and advanced argillic alteration of

felsic and mafic volcanic rocks surrounding the rhyolite porphyry of Kline Mountain (Fig. 25). The propylitic assemblage consists of epidote, calcite, and possibly chlorite along fracture surfaces in the basaltic andesite of Poverty Creek. Pervasive propylitic alteration was not observed in the area. All of the basaltic andesite of Poverty Creek in the area of Figure 25 is mildly propylitized and the intensity of alteration decreases rapidly immediately northwest of the area.

Argillic alteration is characterized by a kaolinite-chalcedony assemblage that has replaced the groundmass and locally replaced alkali-feldspars in high-silica rhyolite ignimbrites. The argillic assemblage begins about 2 km northeast of where NM Highway 59 crosses the continental divide and increases in intensity southward. Near the northern extremity of the argillic alteration, plagioclase feldspar is altered to clay minerals, ferromagnesian minerals are altered to various opaque oxides, manganese oxides coat fractures, and hematite is disseminated throughout the tuff. With increasing intensity of alteration, the groundmass was converted to clay minerals and alkali-feldspars were locally converted to clay minerals. The end stage of argillic alteration is marked by conversion of the groundmass of the tuffs to clay minerals, conversion of all alkali-feldspars to clay minerals, and deposition of veinlets of chalcedonic quartz in the tuff host rock. The transition from argillic to advanced argillic alteration occurs in a zone about 1 km wide and is characterized by the first occurrence of alunite.

The advanced argillic assemblage is found in proximity to the rhyolite porphyry of Kline Mountain and is restricted to a north-trending zone north of the intrusive. The controls of this north-south zone are not obvious but may be related to as yet unrecognized faults. Variable proportions of kaolinite, alunite, and chalcedonic quartz are characteristic of this assemblage. Near the contact with the intrusive, the tuff of Kline Mountain is a mixture of alunite (70%), kaolinite (20%), and chalcedony (10%). The proportion of kaolinite increased northward until nearly pure kaolinite is encountered near NM Highway 59. Large chalcedonic silica bodies are locally present in this assemblage. Subhedral to euhedral quartz crystals within the chalcedony are interpreted to be relict phenocrysts and lead to the interpretation of these bodies as chalcedony replacements of an ignimbrite protolith.

The primary textures of the rocks affected by advanced argillic alteration are obscured by the alteration. For this reason, the north and west contacts of the rhyolite porphyry of Kline Mountain and the surrounding rocks is only approximated on Plate 1.

Silicification of the rhyolite porphyry of Kline Mountain is incipient to intense. The most intense silicification is in the northern part of the intrusive, 1 or 2 km south of the northern contact. In this area, the silicified intrusive is locally crosscut by quartz-pyrite stockworks. These stockworks resemble those in porphyry molybdenum deposits, but no economic mineralization was noted

and the molybdenum content of the area is similar to that of the surrounding rocks (Table 1). The least silicified part of the intrusive is in the southeast quadrant of the intrusive where local pods of non-silicified intrusive can be found.

Bright-red hematitic alteration is locally present. The controls of this alteration are not obvious. Float samples of banded hematite vein material and hematite-cemented breccia are common around the intrusive and most common in the advanced argillic assemblage. No outcrops of this material were discovered, thus controls on this type of mineralization are not known.

#### Alteration Associated With The Taylor Creek Rhyolite

In the Nugget Gulch area, a small zone on the carapace of the Nugget Gulch dome contains numerous pods of silicified Taylor Creek Rhyolite lava. These pods are typically only a few meters in diameter and consist of chalcedonic quartz with relict quartz phenocrysts, suggesting local replacement of the lavas by silica. Zones of clay alteration of the rhyolite lava, 1 to 5 m in diameter, are associated with these pods of silicification. Silicified selvages of the host rhyolite lava as much as 10 cm wide locally enclose hematite-cassiterite-wood tin veinlets. At both the Nugget Gulch and Boiler Peak tin occurrences, fractures and flow planes commonly exhibit minor hematitic alteration.

All of the alteration found in the Taylor Creek Rhyolite



is restricted to within a few meters of the carapace of the domes and where units overlie the domes, those units are not altered. This observation suggests that the alteration occurs while the dome is cooling, possibly due to fumarolic processes. Condensation of fumarole gasses may provide both acids to attack the rhyolite and produce clay minerals as well as silica for replacement of the lavas.

Many authors, including Lufkin (1972), Goerold (1981), and Eggleston and Norman (1983) have mistaken zones of intense vapor-phase crystallization for zones of argillic alteration. Clay minerals and quartz typical of argillic alteration are generally absent. The very small amounts of clay minerals found in these zones may be due to weathering processes.

#### VAPOR-PHASE CRYSTALLIZATION

Vapor-phase crystallization (hereafter abbreviated VPC) is a post-emplacement process common in ignimbrites and certain high-silica rhyolite lavas (Smith, 1960). The most common effect of VPC is bleaching of the affected rock body. Other effects include deposition of secondary quartz, sanidine, pseudobrookite, and rarely, bixbyite in open spaces; deposition of overgrowths on quartz and sanidine; and in extreme cases, destruction of the groundmass. The fluids responsible for VPC are believed to be derived from the affected rock body during cooling and crystallization (Smith, 1960).

Most of the Taylor Creek Rhyolite has undergone



pervasive, mild VPC. VPC is characterized by bleaching of the rock and growth of K-feldspar and various silica minerals in available pore space. The speciation of the silica minerals was not investigated during this study, but Smith (1960) reports that tridymite and cristobalite are the most common forms. Locally, pseudobrookite and bixbyite were deposited in vugs. With the exception of the carapace breccias on the domes, mild VPC has affected all of the exposures mapped as Taylor Creek Rhyolite.

Locally, zones of intense VPC are found within the individual domes. These zones are characterized by intense bleaching of the rhyolite, dramatic increases in the groundmass crystallite size, deposition of overgrowths on quartz and sanidine phenocrysts, deposition of abundant hematite, pseudobrookite, bixbyite and sparse topaz, cassiterite and beryl in available pore space, and recrystallization of pre-existing spherulites. The rock is "punky", suggesting that a portion of the groundmass has been removed. The borders of these zones are gradational over a few meters with the mildly vapor-phase recrystallized material. A zone of dense rhyolite, usually containing abundant lithophysae is found above most of these zones. The lithophysae exhibit a reverse size gradation upward. This zone is in turn capped by carapace breccia. The distance from the top of the intense VPC zone to the margin of the dome is typically a few tens of meters. Chemical changes include enrichment of Sr and the rare earth elements and depletion of Rb, Th, and Ta. These changes are detailed in

Eggleston and others (1987a).

#### TIN MINERALIZATION

Placer and lode tin deposits are associated with the Taylor Creek Rhyolite. The only productive deposits are the placer deposits. The placers can be subdivided into alluvial and colluvial types. The alluvial placers are as much as a few tens of meters wide, 2 to 3 m thick, and 2 km long and consist of recent alluvium in valley bottoms that drain tin-bearing rhyolite domes. Colluvial placers consisting of 1 to 2 meters of recent eluvium occur over tin-bearing rhyolite domes and are responsible for much of the production. Nugget Gulch and Boiler Peak are examples of productive colluvial placer deposits. Examination of trenches in the colluvial placers at the Juniper prospect near Indian Peaks (north of the study area) indicates that the colluvial placers can be very rich. No assays of the placers were performed. Estimates of tin content are in pounds Sn/yd<sup>3</sup> based on visual estimates of the wood tin content of the eluvium, however, tonnage is severely limited. The most common tin mineral in the placer deposits is wood tin. Nuggets as large as 10 X 10 X 5 cm are known from placers, however the wood tin nuggets are typically 0.1 to 1.0 cm in diameter. Coarse cassiterite is present, but is volumetrically insignificant. The Taylor Creek district has produced less than 150,000 lbs of tin concentrates from placer deposits since the district was discovered. The concentrates averaged 40 to 50% Sn (Maxwell

and others, 1986).

Lode tin occurrences are common, but no production has been reported from any of the deposits. Tin deposits visited during this study are indicated on Plate 1 and Figure 1. The typical tin lode consists of hematite-cassiterite-wood tin veinlets a few meters in vertical and horizontal dimension and as much as 5 cm thick. Cassiterite and hematite occur in variable proportions. Individual veinlets locally contain as much as 50% Sn, but those grades are restricted to a few hundred kilograms of vein material. Cassiterite is typically disseminated in the vein wallrocks. The cassiterite-bearing wallrocks contain only a few hundred ppm Sn, but the tin content typically drops to background values in less than 1 m. Fries and others (1942), Lufkin (1976; 1977), Kimbler and Haynes (1980, Narsavage (1981), Foord and others (1984), and Maxwell and others (1986) have described the mineralogy of the tin deposits in detail.

Eggleston and others (1987c) discuss the genesis of the deposits. On the basis of fluid inclusion, oxygen isotopic, and field studies, they concluded that the tin mineralization consists of fumarolic incrustations deposited from high temperature ( $>650^{\circ}$  C), magmatic fluids. The tin mineralization was followed by very short lived epithermal systems that deposited quartz, calcite, and fluorite in the veinlets from meteoric water dominated fluids at temperatures between  $340$  and  $130^{\circ}$  C.

## SIERRA CUCHILLO

Tin occurrences similar to those in the northern Black Range are found in the Sierra Cuchillo, about 20 km east of the Black Range (Fig. 26). Those deposits and the stratigraphy of the area were briefly studied in order to compare the tin deposits and the geology with the Black Range. Figure 26 exhibits a simplified stratigraphic section of the volcanic rocks in the Sierra Cuchillo that is remarkably similar to that of the Black Range. Table 4 and Appendix 1 contain representative geochemical analyses of samples of most of the units in Figure 26. Appendix 2 contains descriptions and locations for those samples. Table 5 contains point-count data from thin sections of many of the units in the area.

The upper part of the section consists of high-silica rhyolite lavas chemically identical to parts of the Taylor Creek Rhyolite. These lavas have been informally named the rhyolite of HOK Ranch and the rhyolite of Willow Springs Draw. The top of the volcanic section is the rhyolite of Willow Springs Draw, a high-silica, mildly to intensely vapor-phase-crystallized rhyolite found on the east flank of the Sierra Cuchillo, north of NM Highway 59. This unit consists of phenocrysts of rounded and embayed quartz (15%), euhedral to subhedral sanidine (18%), biotite (0.3%), plagioclase (0.2%), zircon (tr.) and opaque oxides (tr.) in a granophyric groundmass. Intense vapor-phase crystallization

has locally produced bleached, punky rock from a normally dense rhyolite lava. Heyl and others (1983) report a fission-track date of  $27.8 \pm 1$  Ma on zircon and apatite on the rhyolite of Willow Springs Draw. Minimum thickness of the rhyolite of Willow Springs Draw is greater than 200 m; however, the top of the unit is not exposed.

In the southern part of the mapped area in Figure 26, two mineralogically distinct trachytes separate the rhyolite of Willow Springs Draw from the rhyolite of HOK Ranch. These trachytes consist of thick flows that may in fact be domes of crystal-poor trachyte lava. One of the lavas is nearly aphyric, containing plagioclase (1%), biotite (tr), zircon (tr), clinopyroxene (tr), and euhedral apatite (tr) in a pilotaxitic to granophyric groundmass. The other lava contains plagioclase (5%), biotite (1%), sanidine (1%), pyroxene (tr), and zircon (tr) in a trachytic groundmass.

The rhyolite of HOK Ranch underlies the rhyolite of Willow Spring Draw and is named for exposures near HOK Ranch on the east flank of the Sierra Cuchillo (Fig. 27). This unit is a cliff-forming rhyolite lava containing phenocrysts of quartz (9%), sanidine (6%), plagioclase (3%), biotite (2%), and a trace each of zircon and opaque oxides in a granophyric groundmass. Quartz phenocrysts are rounded and embayed. Sanidine phenocrysts are euhedral to subhedral. Vapor-phase crystallization is minimal. The rhyolite of HOK Ranch and the rhyolite of Willow Springs Draw are distinguished by the abundance of plagioclase and the paucity of vapor-phase crystallization in the HOK Ranch. Known tin

mineralization is restricted to the rhyolite of Willow Springs Draw. The thickness of the rhyolite of HOK Ranch is estimated to be in excess of 100 m.

Immediately below the rhyolite of HOK Ranch is 20 to 30 m of Vicks Peak Tuff (Deal and Rhodes, 1976), a very crystal-poor, moderately to densely welded, high-silica rhyolite ignimbrite erupted from the Nogal Canyon cauldron in the southern San Mateo Mountains about 20 km northeast of the Sierra Cuchillo (Osburn and Chapin, 1983). McIntosh and others (1986) report a  $^{40}\text{Ar}/^{39}\text{Ar}$  plateau date of  $28.46 \pm 0.15$  Ma for the Vicks Peak Tuff. The Vicks Peak Tuff contains less than 5% sanidine and a trace of quartz as phenocrysts in a vitroclastic groundmass. Granular textures in collapsed pumice are distinctive of this unit.

A thick sequence of basaltic andesite lavas that are tentatively correlated with the basaltic andesite of Poverty Creek (Coney, 1976) are immediately beneath the Vicks Peak Tuff. These lavas are as much as 200 m thick and consist of phenocryst-poor, fine-grained flows. On Carrizo Peak, about 5 km north of NM Highway 52, this sequence of lavas contains more plagioclase at the top than at the bottom, suggesting that the lavas became more felsic with time. Similar features are seen in the basaltic andesite of Poverty Creek in the Black Range.

As much as 30 m of Kneeling Nun Tuff (Jicha, 1954) underlie the basaltic andesite lavas. The Kneeling Nun Tuff is a crystal-rich, rhyolitic ignimbrite erupted from the Emory cauldron in the Black Range (Elston, 1976) and contains



phenocrysts of sanidine (15%), quartz (12%), plagioclase (5%), and biotite (2%) in a vitroclastic groundmass. Zircon and opaque oxides are common accessory minerals. In the vicinity of HOK Ranch, "chalky" feldspars suggest that the Kneeling Nun Tuff has been affected by a potassium metasomatic event similar to the potassium metasomatism described by D'Andrea-Dinkleman and others (1983) in the Socorro area.

Mafic lava flows, felsic ignimbrites and volcaniclastic sedimentary rocks of the Rubio Peak Formation (Jicha, 1954) underlie the Kneeling Nun Tuff in the Sierra Cuchillo. These rocks were mapped in reconnaissance fashion only, thus little is known about them.

A pinkish, aplitic granite in the northern Sierra Cuchillo, here informally named the granite of Iron Mountain, was investigated because of its age. Chapin and others (1978) report a conventional K-Ar date on biotite of  $30.0 \pm 1.1$  Ma. The granite consists mainly of K-feldspar and quartz with subordinate plagioclase. Exsolution textures between the K-feldspar and plagioclase are common. Locally the granite is crosscut by numerous quartz-fluorite veinlets. The chemistry of this granite is broadly similar to the chemistry of the Taylor Creek Rhyolite in the Black Range and the rhyolite of Willow Springs Draw farther south in the Sierra Cuchillo (Table 4). The similar age and chemistry of the granite and the high-silica rhyolite lavas suggests that the granite may be a subvolcanic equivalent of the rhyolites.



## DISCUSSION OF GEOLOGIC HISTORY

The following is a brief discussion of the geologic history of the region around the Taylor Creek district. The geologic history of the region begins with eruption of the Rubio Peak Formation. The lavas in the Rubio Peak are possibly derived from as yet unrecognized stratovolcanos and the sedimentary rocks are probably derived by degradation of those volcanos. Numerous felsic ignimbrites that occur in this part of the section may be products of caldera collapse, but those calderas have not yet been defined. Many of these ignimbrites are similar to ignimbrites in the Datil, New Mexico area and may have been derived from that area (R. Harrison, 1986, oral communication).

Eruption of the Kneeling Nun Tuff (35.3 Ma) marked the end of Rubio Peak volcanism. The Kneeling Nun Tuff erupted during collapse of the Emory cauldron several kilometers south of the Taylor Creek district (Elston and others, 1975). Cather (1986) suggests that eruption of the tuff of Datil Well (35.5 Ma) marks the beginning of extension in the Rio Grande rift. These regional tuffs also mark the base of bimodal volcanism in the Mogollon-Datil volcanic field (Cather, 1986). The Kneeling Nun Tuff may likewise mark the beginning of extension in the Black Range. R. Harrison (1986, oral communication) reports strike-slip faulting cutting the lower Rubio Peak Formation suggesting a compressional stress regime as late as 38 to 36 Ma. These

observations suggest that extension was indeed active as early as 35 Ma; however, no large extension-related basins are known from that period.

The tuff of Koko Well was erupted after the Kneeling Nun Tuff, but the age and aerial distribution of the Koko Well is not known. It is locally as much as 150 m thick, but the unit is severely eroded, leaving only isolated remnants. No source can be postulated from exposures in this study area. R. Harrison (1986, oral communication) suggests that the tuff of Koko Well may be correlative with the Rock House Canyon Tuff in the Datil, New Mexico, area. The marked unconformity on top of the tuff of Koko Well suggests an extended period of erosion after the tuff of Koko Well and prior to eruption of the basaltic andesite of Poverty Creek.

Following eruption of the tuff of Koko Well, a hiatus in ignimbrite volcanism of perhaps 3 to 6 Ma occurred (McIntosh and others, 1986). Only two regional ignimbrites are known to have erupted during this hiatus, the Hells Mesa Tuff (32.04 Ma; McIntosh and others, 1986) in the Socorro area and the Caballo Blanco Tuff (31.6 Ma; McIntosh, 1986, oral communication) in the central and southern Black Range. Mafic volcanism is likewise rare in this interval. This hiatus may be represented by the unconformity below the basaltic andesite of Poverty Creek and may, in part, correlate with a regional unconformity between the Hells Mesa Tuff (32.2 Ma) and the La Jencia Tuff (28.8 Ma) in the northeastern portion of the Mogollon-Datil volcanic field. The hiatus in volcanism and extended erosional episode

suggests an anorogenic period concomitant with the hiatus.

The basaltic andesite of Poverty Creek was erupted as lava flows, but no source vents have been located within the study area. R. Harrison (1986, oral communication) believes that a number of mafic dikes found in the Black Range, south of this study area may be local feeders for the Poverty Creek. The presence of dikes indicates an extensional stress regime and suggests a recurrence of extension beginning about 30 Ma, although the age of the basaltic andesite of Poverty Creek is not well constrained. Eruption of several hundred meters of high-silica rhyolite lavas and ignimbrites immediately followed eruption of the basaltic andesite of Poverty Creek. Bimodal assemblages are typical of the extensional environments in the western United States (Christiansen and Lipman, 1972). This bimodal, basaltic andesite-high-silica rhyolite assemblage marks the early development of rifting and extensional basins began to form shortly after the high-silica rhyolite eruptions began (Chamberlin, 1978; Chapin and Seager, 1978).

Most of the ignimbrites in the Taylor Creek district are probably locally derived and their geometry suggests that they fill the cusps between domes and other paleovalley features; however, several thousand km<sup>3</sup> of major ignimbrites were erupted from other parts of the Mogollon-Datil volcanic field (McIntosh and others, 1986). These major ignimbrites are typically high-silica rhyolites and are intercalated with basaltic andesite lavas. Major ignimbrite eruptions abruptly ceased about 27 Ma.

The Taylor Creek Rhyolite and associated pyroclastic rocks were erupted during this volcanic outbreak and produced numerous domes and short flows. The domes are as much as 250 m thick, but the tops of all the exposed domes are eroded indicating that the original domes were thicker than the present exposures indicate. These domes were erupted in a very short time, possibly in as little as 0.3 Ma. The Bloodgood Canyon Tuff was erupted from the Bursum cauldron in the Mogollon Mountains following eruption of the Taylor Creek Rhyolite domes in the Wall Lake region. This observation precludes the interpretation that the Taylor Creek Rhyolite is the product of post-collapse ring-fracture volcanism that followed eruption of the Bloodgood Canyon Tuff (Rhodes, 1976).

Carapace breccias that mantle the domes and fossil fumaroles are preserved on the flanks and near the tops of the domes suggesting that no prolonged period of erosion followed emplacement of the domes. This observation implies that the lower part of the sandstone of Inman Ranch was deposited very soon after the rhyolites were emplaced, covering the domes and protecting the carapace breccia. This protection was necessary to preserve the lode tin deposits that were deposited as fumarolic incrustations within a few tens of meters of the outside of the domes.

The sandstone of Inman Ranch covers parts of most of the Taylor Creek Rhyolite domes and fills a shallow basin between the easternmost margin of the Taylor Creek Rhyolite and the crest of the Black Range where the rhyolite of Franks

Mountain crops out. A date on the alteration associated with the intrusive at Kline Mountain (28.4 Ma) suggests that it was emplaced at about the same time as the Taylor Creek Rhyolite; however, structural evidence suggests that the rhyolite of Franks Mountain postdated the Taylor Creek Rhyolite. The rhyolite of Franks Mountain forms a north-northeast-trending belt of intrusives that parallels the eastern margin of the basin filled with the sandstone of Inman Ranch.

The sandstone of Inman Ranch consists of coarse conglomerates and fluvial and aeolian sandstones near its base. Fluvial sandstones interpreted as braided-stream deposits dominate higher in the section. The rapid deposition of the lower part of the unit and the presence of clasts of La Jencia Tuff suggest that the source of the unit was a highland to the east of the present outcrop belt. That highland may have been due to intrusion of the rhyolite of Franks Mountain or to uplift due to extension that was occurring along the Rio Grande rift or to a combination of both processes. Alternatively, the basin could be a graben formed by extensional faulting related to extension along the Rio Grande rift, but no such faults were recognized during study.

The presence of the sandstone of Inman Ranch near Beaver Creek at the western edge of Plate 1 suggests a source of detritus to the west of Beaver Creek. Potential source regions are covered by younger volcanic and sedimentary rocks. Deposition of the sandstone of Inman Ranch continued

into the lower Miocene as evidenced by the vertebrate fossils described by Tedford (1981; 1986, written communication).

Overlying the high-silica rhyolite portion of the section and the sandstone of Inman Ranch in the western part of the study area is a thick sequence of andesites known as the Bearwallow Mountain Formation. These rocks were erupted from several stratovolcanos such as Black Mountain and O Bar O Mountain that form prominent topographic features on the Mogollon Plateau. Recent dating by J. Ratte (1986, oral communication) suggests that much of the Bearwallow Mountain Formation is 28 to 24 Ma, and may thus be a continuation of the bimodal sequence begun when the basaltic andesite of Poverty Creek was erupted.

Within the study area, volcanism ceased after eruption of the Bearwallow Mountain Formation and deposition of the Gila Conglomerate began. Fanglomerates and coarse conglomerates and sandstones are typical of the Gila Conglomerate and no lacustrine or playa deposits were found within the study area. The Gila Conglomerate unconformably overlies the sandstone of Inman Ranch and fills topography created by effusive domes of the Taylor Creek Rhyolite and other volcanic units in the region. No faults were recognized that suggest that the area was an extensional basin. These observations suggest that the Gila Conglomerate may have been deposited as piedmont accumulations of detritus derived from uplifts surrounding the Mogollon Plateau rather than as basin-fill deposits. Highlands on the east and west sides of the Mogollon Plateau may have been epeirogenic



uplift related to extension when the Winston and Mangas grabens were formed. An alternative explanation for the distribution of the Gila Conglomerate is that the central part of the Mogollon Plateau was downdropped, but that process is difficult to distinguish from uplift along the edges of the Mogollon Plateau. The region is believed to be underlain by a batholith (Rhodes, 1976), thus downdropping of the center of the Mogollon Plateau is improbable.

After a period of prolonged erosion and filling of topographic lows with the Gila Conglomerate, the region was graded. Pediments occur on the Taylor Creek Rhyolite, Bearwallow Mountain Formation, and on the Gila Conglomerate. Concordant surfaces can be found throughout the Mogollon Plateau. More recent uplift rejuvenated and incised streams on the Mogollon Plateau. Canyons are now as much as 300 m deep with very steep sides. The age of this rejuvenation is unknown. Leopoldt (1981) suggests that uplift of the Mogollon Plateau occurred between 8 and 4 Ma and was contemporaneous with epeirogenic uplift elsewhere in the Rio Grande rift (7 to 4 Ma; Chapin, 1979) and in Colorado (Pliocene; Scott, 1975) which has continued to the present at a lesser rate.

A similar history is envisioned for the Sierra Cuchillo, however, the entire mountain range has been rotated so that dips are 20 to 40° to the east. The Sierra Cuchillo is part of an extensive domain of east-tilted, intrarift blocks extending southward from the Socorro area (Stewart, 1980). This rotation is believed to be related to extension along



the Rio Grande rift. Basins on either side of the Sierra Cuchillo, the Winston graben on the west and the Palomas basin on the east (Kelley, 1979) are filled with fluvial sedimentary rocks of the Santa Fe Group.

#### ACKNOWLEDGEMENTS

Numerous people contributed to the our understanding of the geology of the Taylor Creek district. We especially thank Don Richter of the U.S. Geological Survey for his many hours of stimulating discussion on the stratigraphy and structure of the region as well as for editing various versions of Plate 1. Philip Kyle, Kent Condie, and George Griswold suggested improvements of early versions of this manuscript. W.E. Elston, Charles Maxwell, G.R. Osburn, Richard Harrison, James Ratte', Charles Chapin, Bill McIntosh, Wendell Duffield, and Tom Woodard have contributed significantly to our understanding of the geology of the region. Bob Kerr kindly permitted access to his claims in the area. Danny Fowler and the Ladder Ranch permitted access to their ranch properties. Funding for this research was provided by FRM Minerals, The Geological Society of America, the New Mexico Geological Society, and the Rocky Mountain Federation of Mineralogical Societies. The New Mexico Bureau of Mines and Mineral Resources, Frank Kottowski, Director, supported this work in the form of a graduate assistantship as well as funds for thin section preparation.

## BIBLIOGRAPHY

- Abbey, S., 1983, Studies in "standard samples" of silicate rocks and minerals 1969-1982: Geological Survey of Canada Paper 83-15, 101p.
- Bodkin, J.B., 1977, Determination of fluorine in silicates by use of an ion-selective electrode following fusion with lithium metaborate: *Analyst*, v. 102, p. 409-413.
- Bornhorst, T.J., 1980, Major- and trace-element geochemistry and mineralogy of upper Eocene to Quaternary volcanic rocks of the Mogollon-Datil volcanic field, southwestern New Mexico: Ph.D. dissertation, The University of New Mexico, Albuquerque, 1108 p.
- Chamberlin, R.M., 1978, Structural development of the Lemitar Mountains, an intrarift tilted fault-block uplift, central New Mexico: Los Alamos Scientific Laboratory, University of California, p. 22-24.
- Chapin, C.E., 1979, Evolution of the Rio Grande rift—a summary: in Reiker, R.E., ed., Rio Grande rift: tectonics and magmatism: American Geophysical Union, Washington, D.C., p. 1-5.
- Chapin, C.E., Jahns, R.H., Chamberlin, R.M., and Osburn, G.R., 1978, First day road log from Socorro to Truth or Consequences via Magdalena and Winston: in Chapin, C.E., and Elston, W.E., eds., Field guide to selected cauldrons and mining districts of the Datil-Mogollon volcanic field, New Mexico: New Mexico Geological Society Special Publication No. 7, p. 1-31.

- Christiansen, R.L. and Lipman, P.W., 1972, Cenozoic volcanism and plate-tectonic evolution of the western United States. II. Late Cenozoic: *Philosophical Transactions of the Royal Society of London*, v. 271, p. 249-284.
- Coney, P.J., 1976, Structure, volcanic stratigraphy, and gravity across the Mogollon Plateau, New Mexico: in Elston, W. E., and Northrup, S. A., eds., *Cenozoic volcanism in southwester New Mexico*: New Mexico Geological Society Special Publication No. 5, p. 29-41.
- Correa, B.P., 1981, The Taylor Creek Rhyolite and associated tin deposits, southwestern New Mexico: M.S. Thesis, Arizona State University, Tempe, 105 p.
- D'Andrea-Dinkleman, J.F., Lindley, J.I., Chapin, C.E., and Osburn, G.R., 1983, The Socorro  $K_2O$  anomaly: a fossil geothermal system in the Rio Grande Rift: *New Mexico Geological Society Guidebook 34*, p. 76-77.
- Deal, E.G. and Rhodes, R.C., 1976, Volcano-tectonic structures in the San Mateo Mountains, Socorro County, New Mexico: in Elston, W.E. and Northrup, S.A., eds., *Cenozoic volcanism in southwestern New Mexico*: New Mexico Geological Society Special Publication 5, p. 51-56.
- Di Girolamo, P., 1984, Magmatic character and geotectonic setting of some Tertiary-Quaternary Italian volcanic rocks: orogenic, anorogenic, and <<transitional>> associations: a review: *Bulletin Volcanologique*, v. 47, p. 421-432.

- Eggleston, T.L. and Norman, D.I., 1983, Taylor Creek tin district-stratigraphy, structure, and timing of mineralization: *New Mexico Geology*, v. 5, p. 1-4.
- Eggleston, T.L., Norman, D.I., and Savin, S.M., 1987a, Intense vapor phase crystallization: mineralogical and chemical effects in high-silica rhyolite lavas: in prep.
- Eggleston, T.L., Norman, D.I., and Savin, 1987b, Petrology of tin-bearing rhyolites, northern Black Range and Sierra Cuchillo, New Mexico: in prep.
- Eggleston, T.L., Norman, D.I., and Savin, S.M., 1987c, Origin of tin mineralization associated with high-silica, topaz rhyolites, Black Range and Sierra Cuchillo, New Mexico: in prrp.
- Eggleston, T.L., Osburn, G.R., and Chapin, C.E., 1983, Reversely zoned Hells Mesa Tuff and Socorro cauldron: *EOS*, v. 64, p. 884.
- Elston, W.E., 1957, Geology and mineral resources of the Dwyer quadrangle-Grant, Luna, and Sierra Counties, New Mexico: *New Mexico Bureau of Mines and Mineral Resources Bulletin*, 38, 86 p.
- Elston, W.E., 1968, Terminology and distribution of ash-flows of the Mogollon-Silver City-Lordsburg region, New Mexico: *Arizona Geological Society Guidebook III to southern Arizona*, p. 231-240.

- Elston, W.E., 1976, Glossary of stratigraphic terms of the Mogollon-Datil volcanic province, New Mexico: in Elston, W.E., and Northrup, S.A., eds., Cenozoic volcanism in southwestern New Mexico: New Mexico Geological Society, Special Publication 5, p. 131-144.
- Elston, W.E., 1984, Mid-Tertiary ash flow tuff cauldrons, southwestern New Mexico: Journal of Geophysical Research v. 89, p. 8733-8750.
- Elston, W.E. and Netelbeek, T.A., 1965, Roadlog from Mimbres Valley to Silver City: New Mexico Geological Society Guidebook 16, p. 167-174.
- Ericksen, G.E., Wedow, H., Jr., Eaton, G.P., and Leland, G.R., 1970, Mineral resources of the Black Range Primitive Area, Grant, Sierra, and Catron Counties, New Mexico: U. S. Geological Survey, Bulletin 1319-E, 162 p.
- Ewart, A., 1979, A review of the mineralogy and chemistry of Tertiary-Recent dacitic, latitic, and rhyolitic and related salic volcanic rocks: in Barker, F., ed., Trondhjemites, dacites, and related rocks: Amsterdam, Elsevier, p. 13-121.
- Fisher, R.V. and Schminke, H.-U., 1984, Pyroclastic rocks: Berlin, Springer-Verlag, 472 p.
- Fodor, R.V., 1976, Volcanic geology of the northern Black Range, New Mexico: in Elston, W. E., and Northrup, S. A., eds., Cenozoic volcanism in southwestern New Mexico: New Mexico Geological Society, Special Publication 5, p. 68-70.

- Foord, E.E., Oakman, M.R., and Maxwell, C.H., 1985, Durangite from the Black Range, New Mexico, and new data on durangite from Durango and Cornwall: *Canadian Mineralogist*, v. 23, p. 241-246.
- Fries, C. Jr., 1940, Tin deposits of the Black Range, Catron and Sierra Counties, New Mexico: U. S. Geological Survey Bulletin 922-m, p. 355-370.
- Fries, C. Jr. and Butler, A.P., 1943, Geologic Map of the Black Range tin district, New Mexico: U. S., Geological Survey Open-File Map.
- Fries, C., Jr., Schaller, W.T., and Glass, J.J., 1942, Bixbyite and pseudobrookite from the tin-bearing rhyolite of the Black Range, New Mexico: *American Mineralogist*, v. 27, p. 305-323.
- Gilbert, G.K., 1875, Report on the geology of portions of New Mexico and Arizona examined in 1873: U. S. Geographical and Geological Surveys west 100th Mer. (Wheeler), v. 3, pt. 5, p. 505-567.
- Goerold, W.T., 1981, Geology and geochemistry of tin occurrences in southwestern New Mexico: M. S. Thesis, The Pennsylvania State University, 131 p.
- Govindaraju, K., 1984, Compilation of working values and sample descriptions for 170 international reference samples of mainly silicate rocks and minerals: *Geostandards Newsletter*, v.8, 16 p. and appendices.
- Harley, G.T., 1934, The geology and ore deposits of Sierra County, New Mexico: New Mexico Bureau of Mines and Mineral Resources Bulletin 10, 232 p.

- Harrington, E.R., 1943, Tin in New Mexico: Mines Magazine, v. 23, p. 123 and 130.
- Harrington, E.R., 1943, Here's your tin (in Catron and Sierra Cos.): New Mexico Magazine, v. 21, p. 7-9.
- Harvey, D.B., 1985, Cassiterite mineralization in the Black Range tin district, Sierra and Catron Counties, New Mexico: M. S. Thesis, The University of Texas at El Paso, El Paso, 147 p.
- Heyl, A.V., Maxwell, C.H., and Davis, L.L., 1983, Geology and mineral deposits of the Priest Tank Quadrangle, Sierra County, New Mexico: U.S. Geological Survey Miscellaneous Field Studies Map MF-1665.
- Hildreth, W., 1979, The Bishop Tuff: evidence for the origin of compositional zonation in silicic magma chambers: in Chapin, C. E., and Elston, W. E., eds., Ash-flow Tuffs: Geological Society of America, Special Paper 180, p. 43-75.
- Hill, J.M., 1921, The Taylor Creek tin deposits, New Mexico: in, Ransome, F. L., and Burchard, E. F., eds., Contributions to economic geology-1921: U. S. Geological Survey, Bulletin 725, p. 347-359.
- Ingalls, W.R., 1896, The tin deposits of Durango, Mexico: American Institute of Mining Engineers Transactions, v. 25, p. 146-163.



- Jacobs, J.W., Korotev, R.L., Blanchare, D.P., and Haskin, L.A., 1977, A well-tested procedure for instrumental neutron activation analysis of silicate rocks and minerals: *Journal of Radioanalytical Chemistry*, v. 40, p. 93-114.
- Jicha, H.L., 1954, Geology and mineral deposits of Lake Valley quadrangle-Grant, Luna, and Sierra counties, New Mexico: New Mexico Bureau of Mines and Mineral Resources, Bulletin 37, 93 p.
- Kimbler, F.S. and Haynes, P.E., 1980, An occurrence of red beryl in the Black Range, New Mexico: *New Mexico Geology*, v. 2, p. 15-16.
- Kyle, P.R., Eggleston, T.L., McIntosh, B., Dunbar, N., Hammond, C.M., Johnson, W.D., Knoper, M., and Moore, J., 1986, Pyroclastic rocks associated with the Taylor Creek Rhyolite, Scales Canyon, New Mexico: *New Mexico Geological Society Guidebook 37*, p. 197-201.
- Lawrence, V. and Richter, D.H., 1986, Geologic map of the Indian Peaks West quadrangle, Catron County, New Mexico: U. S. Geological Survey, Miscellaneous Field Studies Map.
- Le Maitre, R.W., 1976, The chemical variability of some common igneous rocks: *Journal of Petrology*, v. 17, p. 589-637.

- Le Maitre, R.W., 1984, A proposal by the IUGS subcommission on the systematics of igneous rocks for a chemical classification of volcanic rocks based on the total alkali-silica (TAS) diagram: Australian Journal of Earth Sciences, v. 31, p. 243-255.
- Leopoldt, W., 1981, Neogene geology of the central Mangas graben, Cliff-Gila area, Grant County, New Mexico: M.S. Thesis, The University of New Mexico, Albuquerque, 166p.
- Lindstrom, D.J., and Korotev, R.L., 1982, TEABAGS: a computer program for instrumental neutron activation analysis: Journal of Radioanalytical Chemistry, v. 70, p. 439-458.
- Lufkin, J.L., 1972, Tin mineralization within rhyolite flow-domes, Black Range, New Mexico: Ph.D dissertation, Stanford University, Stanford, 149 p. (available as New Mexico Bureau of Mines and Mineral Resources Open-File Report 57).
- Lufkin, J.L., 1976, Oxide minerals in miarolitic rhyolite, Black Range, New Mexico: American Mineralogist, v. 61, p. 425-430.
- Lufkin, J.L., 1977, Chemistry and mineralogy of wood-tin, Black Range, New Mexico: American Mineralogist, v. 62, p. 100-106.
- Maxwell, C.H., Foord, E.E., Oakman, M.R., and Harvey, D.D., 1986, Tin deposits in the Black Range tin district: New Mexico Geological Society Guidebook 37, p. 273-281.

- McIntosh, W.C., Sutter, J.L., Chapin, C.E., Osburn, G.R., and Ratte', J.C., 1986, A stratigraphic framework for the eastern Mogollon-Datil volcanic field based on paleomagnetism and high-precision  $^{40}\text{Ar}/^{39}\text{Ar}$  dating of ignimbrites--a progress report: New Mexico Geological Society Guidebook 37, p. 183-195.
- Narsavage, R.J., 1981, Cassiterite at Taylor Creek, Sierra County: New Mexico Geology, v, 3, p. 16.
- Norrish, K. and Chappell, B.W., 1977, X-ray fluorescence spectrometry: in Zussman, J., ed., Physical methods in determinative mineralogy: Academic Press, p. 201-272.
- Norrish, K. and Hutton, J.T., 1969, An accurate x-ray spectrographic method for the analysis of a wide range of geologic samples: Geochimica et Cosmochimica Acta, v. 33, p. 431-453.
- Osburn, G.R. and Chapin, C.E., 1983, Nomenclature for Cenozoic rocks of northeast Mogollon-Datil volcanic field, New Mexico: New Mexico Bureau of Mines and Mineral Resources Stratigraphic Chart 1.
- Pan, Y.-S., 1974, The genesis of the Mexican type tin deposits in acidic rocks: Ph. D. Dissertation, Columbia University, New York, 286 p.
- Peccerillo, A. and Taylor, S.R., 1976, Geochemistry of Eocene calc-alkaline volcanic rocks from the Kastamonu area, northern Turkey: Contributions to Mineralogy and Petrology, v. 58, p. 63-81.

- Ratte', J.C., Marvin, R.F., and Naeser, C.W., 1984, Calderas and ash flow tuffs of the Mogollon Mountains, southwestern New Mexico: *Journal of Geophysical Research*, v. 89, p. 8713-8732.
- Reichen, L.E. and Fahey, J.J., 1962, an improved method for the determination of FeO in rocks and minerals including garnet: U. S. Geological Survey, Bulletin 1144-B, 5 p.
- Rhodes, R.C., 1976, Petrologic framework of the Mogollon Plateau volcanic ring complex, New Mexico—Surface expression of a major batholith: in Elston, W.E. and Northrup, S.A., eds. Cenozoic volcanism in southwestern New Mexico: New Mexico Geological Society Special Publication 5, p. 103-112.
- Richter, D.H., 1978, Geologic map of the Spring Canyon quadrangle, Catron County, New Mexico: U. S. Geological Survey, Map MF-966.
- Richter, D.H., Eggleston, T.L., and Duffield, W., 1986, Geologic map of the Wall Lake quadrangle, Catron County, New Mexico: U. S. Geological Survey Miscellaneous Field Studies Map Mf-1909.
- Richter, D.H., Lawrence, V., and Duffield, W.A., 1986, Geologic map of the Indian Peaks East quadrangle, Catron County, New Mexico: U. S. Geological Survey, Miscellaneous Field Studies Map.

- Scott, G.R., 1975, Cenozoic surfaces and deposits in the southern Rocky Mountains: Geological Society of America Memoir 144, p. 227-248.
- Seager, W.R., Shafiquallah, M., Hawley, J.W., and Marvin, R.F., 1984, New K-Ar dates from basalts and the evolution of the Rio Grande Rift: Geological Society of America Bulletin, v. 95, p. 87-99.
- Sparks, R.S.J., Self, S., and Walker, G. P. L., 1973, Products of ignimbrite eruptions: Geology, v. 1., p. 115-118.
- Steiger, R.H., and Jaeger, E., 1977, Subcommittee on geochronology: constants in geo- and cosmochronology: Earth and Planetary Science Letters, v. 36, p. 359-362.
- Stewart, J.H., 1980, Regional tilt patterns of late Cenozoic basin-range fault blocks, western United States: Geological Society of America Bulletin, v. 91, p. 460-464.
- Tedford, R.H., 1981, Mammalian biochronology of the late Cenozoic basins of New Mexico: Geological Society of America Bulletin, v. 92, p. 1008-1022.
- Turekian, K.K., and Wedepohl, K.H., 1961, Distribution of the elements in some major units of the Earth's crust: Geological Society of America Bulletin, v. 72, p. 175-192.
- Volin, M.E., Russell, P.L., Price, F.L.C., and Mullen, D.H., 1947, Catron and Sierra Counties tin deposits, New Mexico: U. S. Bureau of Mines, RI 4068, 60 p.

- Williams, H., 1932, The history and character of volcanic domes: University of California Publications, Bulletin of the Department of Geological Sciences, v. 21, p. 51-146.
- Wilson, M.D. and Sedora, S.S., 1979, An improved thin section stain for potash feldspar: Journal of Sedimentary Petrology, v. 49, p. 637-638.
- Woodard, T.W., 1982, Geology of the Lookout Mountain area, Northern Black Range, Sierra County, New Mexico: M.S. Thesis, The University of New Mexico, Albuquerque, 95 p.
- York, D., 1969, Least squares fitting of a straight line with correlated errors: Earth and Planetary Science Letters, v. 5., p. 320-324.

Table 1. Geochemistry of selected samples from the Taylor Creek district. Complete sample descriptions are in Appendix 2, analytical techniques are in text. Tkn-Kneeling Nun Tuff; Tkw-tuff of Koko Well, lower 10 m.; Tpc-1-lower part of basaltic andesite of Poverty Creek; Tpc-2-upper part of basaltic andesite of Poverty Creek; Tsc-tuff of Stiver Canyon; Tkm-tuff of Kline Mountain; Tdp-rhyolite of Dolan Peak; Tlj-La Jencia Tuff; Tkt-rhyolite of Kieth Tank; Thc-rhyolite of Hoyt Creek; Twh-rhyolite of Whitetail Canyon; Ttc-2-Taylor Creek rhyolite, Nugget Gulch dome; Ttc-4-Taylor Creek Rhyolite, North Paramount Canyon dome; Ttc-5-Taylor Creek Rhyolite, Boiler Peak dome; Ttc-6-Taylor Creek Rhyolite, Alexander Cienega dome; Ttc-7-Taylor Creek Rhyolite, Taylor Creek dome; Ttc-8-Taylor Creek Rhyolite, Indian Creek dome; Ttc-9-Taylor Creek Rhyolite, Kemp Mesa dome; Tgc-tuff of Garcia Camp; Tbc-Bloodgood Canyon Tuff; Tbm-1-Bearwallow Mountain Formation; Tbm-2-Bearwallow Mountain Formation; Tkmp-rhyolite porphyry of Kline Mountain.

Ba

Be

Cl(2)

Cr

Ca

Fe(2)

Fe

HF

Hr

Hb

Hl

Hs

Ht

Hv

Hw

Hx

Hy

Hz

Ia

Ib

Ic

Id

Ie

If

Ig

Ih

Ii

Ij

Ik

Il

Im

In

Io

Ip

Iq

Ir

Is

It

Iu

Iv

Iw

Ix

Iy

Iz



Ref. #	1	2	3	4	5	6	7	8	9	10
UNIT	Tkn	Tkw	Tpc-1	Tpc-2	Tsc	Tsp	Tkm	Tdp	Tlj	Tkt
SAMPLE	19	123	41	39	23	22	57	55	177	218
SiO <sub>2</sub>	72.60	69.80	52.23	61.77	75.40	71.45	73.33	76.41	72.42	73.71
TiO <sub>2</sub>	0.27	0.45	1.11	1.05	0.16	0.48	0.14	0.18	0.35	0.19
Al <sub>2</sub> O <sub>3</sub>	13.94	15.09	16.34	17.50	11.96	14.24	11.96	12.09	13.51	12.58
Fe <sub>2</sub> O <sub>3</sub>	1.77	2.15	9.04	5.63	1.10	2.03	1.62	1.65	1.87	1.26
MnO	0.02	0.01	0.14	0.01	0.04	0.02	0.03	0.03	0.07	0.06
MgO	0.57	0.42	6.29	0.75	0.28	0.27	0.71	0.16	0.11	0.55
CaO	0.99	0.28	8.44	3.85	0.38	0.33	0.62	0.23	0.61	0.84
Na <sub>2</sub> O	2.90	3.12	3.50	4.30	2.85	5.11	1.86	3.64	4.34	3.28
K <sub>2</sub> O	4.93	6.44	1.32	3.09	5.58	6.13	4.96	5.27	5.41	4.91
P <sub>2</sub> O <sub>5</sub>	0.06	0.08	0.25	0.53	0.03	0.07	0.01	0.02	0.06	0.03
LOI	1.04	1.27	1.39	1.82	1.26	0.45	4.96	.58	0.66	3.25
Total	99.09	99.11	100.05	100.30	99.04	100.58	100.20	100.26	99.41	100.66
As	---	---	<1.0	---	2.5	<0.2	1.1	1.3	---	3.8
Ba	599	1757	526	1328	82	81	28	<16	109	106
Br	---	---	<1.0	---	<1.0	<1.0	2.2	<0.5	---	0.5
CL(%)	---	---	---	---	---	---	---	---	---	---
Cr	13	<10	272	52	3	<10	<10	6	<10	<10
Cs	---	---	1.3	---	2.6	2.8	14.6	2.5	---	6.4
F(%)	---	---	---	---	---	---	---	---	---	---
Ga	16	13	19	21	16	21	19	19	20	18
Hf	---	---	4.3	---	7.0	19.0	11.0	12.2	---	6.4
Mo	<1	---	2	1	1	2	3	2	---	3
Nb	18	18	6	13	23	27	36	32	26	21
Ni	<5	<5	122	41	<5	<5	<5	<5	6	0
Pb	21	21	7	12	20	23	29	30	25	30
Rb	182	232	23	59	202	171	329	223	138	236
Sb	---	---	0.2	---	0.2	0.1	0.2	0.1	---	0.5
Sc	---	---	20.9	---	3.7	10.0	3.5	4.8	---	3.0
Se	---	---	<1.0	---	<1.0	0.1	0.1	<1.5	---	---
Sn	<6	<6	<6	25	<6	6	10	7	<6	---
Sr	151	127	581	906	18	3	28	4	33	67
Ta	---	---	0.4	---	1.8	2.1	2.8	2.5	---	1.7
Th	28	27	<3	<3	23	18	27	25	26	27
U	<3	<3	<3	<3	4	5	7	6	3	6
V	17	30	183	124	<3	<3	<3	<3	8	<3
Y	29	60	20	18	45	89	126	124	59	38
Zn	30	38	87	82	40	94	100	73	64	36
Zr	134	478	153	275	172	763	290	256	504	175
La	---	---	17	---	31	68	58	122	---	40
Ce	---	---	41	---	59	153	123	213	---	76
Nd	---	---	26	---	22	78	55	115	---	21
Sm	---	---	5.0	---	5.7	15.7	12.9	21.9	---	3.5
Eu	---	---	1.46	---	0.32	3.37	0.49	0.96	---	0.31
Tb	---	---	0.6	---	1.0	2.5	2.6	3.4	---	0.6
Yb	---	---	1.7	---	4.1	8.2	11.0	10.0	---	3.6
Lu	---	---	0.27	---	0.65	1.30	1.82	1.49	---	0.63

REF. #	11	12	13	14	15	16	17	18	19	20
UNIT	Thc	Twh	Ttc-2	Ttc-4	Ttc-5	Ttc-6	Ttc-7	Ttc-8	Ttc-9	Tgc
SAMPLE	259	260	142	223	149	215	9	8	1	209
SiO <sub>2</sub>	73.83	69.20	77.05	76.53	74.54	76.71	76.82	77.22	77.84	77.20
TiO <sub>2</sub>	0.12	0.35	0.12	0.11	0.09	0.11	0.16	0.16	0.14	0.16
Al <sub>2</sub> O <sub>3</sub>	12.34	14.23	11.72	12.33	12.05	11.94	11.37	11.84	11.71	11.37
Fe <sub>2</sub> O <sub>3</sub>	0.94	2.00	1.10	1.17	1.13	1.08	1.03	1.10	1.06	1.27
MnO	0.04	0.07	0.05	0.05	0.06	0.05	0.06	0.05	0.05	0.06
MgO	0.29	0.71	0.28	<0.01	0.13	0.24	0.34	0.22	0.20	0.12
CaO	0.86	1.62	0.46	0.18	0.40	0.23	0.46	0.30	0.26	0.23
Na <sub>2</sub> O	3.44	4.10	3.16	3.55	3.74	3.53	3.64	3.64	3.42	3.48
K <sub>2</sub> O	4.28	4.32	4.71	4.82	4.69	5.04	4.80	4.94	5.14	5.01
P <sub>2</sub> O <sub>5</sub>	0.02	0.10	0.02	0.02	0.01	0.02	0.02	0.01	0.01	0.02
LOI <sup>5</sup>	4.46	3.74	0.84	0.69	2.36	0.56	0.48	0.31	0.15	0.31
Total	100.62	100.44	99.51	99.46	99.20	99.51	99.18	99.79	99.98	99.23
As	0.6	0.5	10.0	1.9	2.4	8.1	--	--	7.0	2.2
Ba	685	900	33	44	19	55	67	55	69	83
Br	2.8	2.9	--	<0.3	--	0.3	--	--	--	--
Cl(%)	--	--	0.005	--	0.003	--	--	--	--	--
Cr	<10	<10	12	<1	14	<1	<6	<10	<10	<1
Cs	5.1	2.8	5.0	8.2	10.3	5.0	6.8	--	4.5	4.2
F(%)	--	--	0.17	--	0.20	--	0.15	--	--	--
Ga	--	--	19	22	22	21	19	19	20	19
Hf	3.3	7.4	7.1	8.2	7.9	8.0	6.7	--	7.2	8.5
Mo	2	2	3	--	5	--	--	--	3	--
Nb	15	17	33	49	47	47	36	37	44	33
Ni	<33	<15	<5	<5	<5	<5	<5	<5	<5	6
Pb	27	23	26	26	36	29	22	26	27	24
Rb	222	141	288	375	360	349	247	257	294	289
Sb	0.2	0.1	0.4	0.1	0.4	0.4	<0.1	--	0.3	0.1
Sc	2.3	2.8	2.6	2.1	2.4	2.0	3.2	--	3.2	2.5
Se	--	<0.4	0.4	<0.1	0.6	10.4	0.7	--	0.6	<0.5
Sn	<6	<6	6	<6	12	<6	<6	<6	6	<6
Sr	73	250	9	5	2	4	55	11	110	6
Ta	1.6	1.4	3.7	4.4	4.8	4.3	5.4	--	--	3.4
Th	24	16	30	34	41	32	30	30	34	29
U	6	4	7	5	14	8	9	<3	10	9
V	<3	--	16	--	<3	--	<3	6	44	--
Y	39	39	94	69	131	112	101	77	114	94
Zn	--	--	42	37	73	45	37	42	42	33
Zr	116	282	160	177	168	175	151	156	162	209
La	40	46	48	26	40	37	45	--	41	50
Ce	80	96	110	122	98	91	106	--	103	120
Nd	27	37	40	25	37	41	41	--	47	50
Sm	5.1	6.3	10.3	7.1	11.6	10.4	10.1	--	10.3	11.2
Eu	0.62	1.15	0.33	0.21	0.17	0.22	0.40	--	0.33	0.37
Tb	0.9	0.9	1.8	1.7	23	2.4	1.9	--	2.2	2.3
Yb	3.4	3.5	10.8	8.6	13.8	11.2	10.3	--	11.9	9.9
Lu	0.55	0.58	1.57	1.34	1.94	1.77	1.32	--	1.52	1.61

REF. #	21	22	23	24
UNIT	Tbc	Tbm-1	Tbm-2	Tkmrp
SAMPLE	203	217	256	125
SiO <sub>2</sub>	77.09	58.55	59.55	76.25
TiO <sub>2</sub>	0.19	1.46	1.04	0.15
Al <sub>2</sub> O <sub>3</sub>	12.11	14.78	16.10	12.07
Fe <sub>2</sub> O <sub>3</sub>	1.14	7.24	6.61	1.59
MnO	0.08	0.10	0.10	<0.01
MgO	0.19	2.15	3.44	0.18
CaO	0.43	4.24	5.57	0.24
Na <sub>2</sub> O	4.07	5.77	3.45	2.52
K <sub>2</sub> O	4.99	3.86	2.58	5.56
P <sub>2</sub> O <sub>5</sub>	0.14	0.74	0.34	0.01
LOI	0.47	1.62	2.25	1.24
Total	100.90	100.51	101.03	99.81
As	--	<1.4	<0.7	<1.6
Ba	51	1550	1070	<16
Br	--	<0.7	0.9	--
Cl(%)	--	--	--	0.005
Cr	<10	<10	47	<10
Cs	--	2.1	0.9	4.3
F(%)	--	--	--	0.20
Ga	21	21	--	19
Hf	--	11.7	7.6	11.5
Mo	--	--	--	1
Nb	37	22	16	33
Ni	6	6	<38	<5
Pb	--	12	15	22
Rb	278	113	90	274
Sb	--	<0.1	<0.1	0.3
Sc	--	12.5	13.9	4.5
Se	--	<0.9	<0.8	0.4
Sn	--	--	--	<6
Sr	26	744	570	15
Ta	--	1.3	0.9	2.9
Th	--	10	8	28
U	--	2	1	6
V	5	--	--	<3
Y	75	63	40	114
Zn	61	103	--	108
Zr	194	475	304	348
La	--	73	49	89
Ce	--	168	101	180
Nd	--	89	48	86
Sm	--	15.6	9.0	17.7
Eu	--	3.51	1.81	0.87
Tb	--	1.9	1.1	2.9
Yb	--	5.4	3.3	10.8
Lu	--	0.82	0.51	1.52

Table 2. Point count data (in volume %) for selected samples of various units in the Taylor Creek district. See text and Plate 1 for unit descriptions. Complete sample descriptions are in Appendix 2. Q/S is the quartz/sanidine ratio. Tsp-rhyolite of Sawmill Peak; Tdp-rhyolite of Dolan Peak; Tkt-rhyolite of Kieth Tank; Twh-rhyolite of Whitetail Canyon; Ttc1-Taylor Creek Rhyolite, Squaw Creek dome; Ttc2-Taylor Creek Rhyolite, Nugget Gulch dome; Ttc5-Taylor Creek Rhyolite, Boiler Peak dome; Ttc6-Taylor Creek Rhyolite, Alexander Cienega dome; Ttc7-Taylor Creek Rhyolite, Taylor Creek dome; Ttc9-Taylor Creek Rhyolite, Kemp Mesa dome; Tgc-tuff of Garcia Camp.

Unit	Tsp	Tdp	Tdp	Tkt	Twh	Ttc1	Ttc2	Ttc2	Ttc4
Sample	21	56	220	218	232	124	136	140	153
points	2000	1787	500	500	500	2000	2000	2000	2000
quartz	tr	1.1	5.2	1.0	---	9.6	8.4	10.4	6.5
sanidine	5.3	5.4	15.2	0.2	---	11.5	8.9	14.0	9.3
plagioclase	---	---	---	0.8	5.2	---	---	---	---
biotite	0.3	---	0.4	0.4	0.2	0.1	0.2	0.4	0.1
amphibole	---	0.1	---	tr	tr	---	---	---	---
pyroxene	---	---	---	tr	1.0	---	---	---	---
opaques	tr	tr	tr	tr	tr	tr	tr	tr	tr
zircon	tr	tr	tr	tr	tr	tr	tr	tr	tr
sphene	---	---	---	---	---	---	---	---	---
lithics	---	---	---	12.4	---	---	---	---	---
total phenocrysts	5.6	6.6	20.8	2.4	5.4	21.2	17.5	24.8	15.9
Q/S	---	0.2	0.3	5.0	---	0.8	0.9	0.7	0.7

Unit	Ttc5	Ttc5	Ttc6	Ttc7	Ttc7	Ttc9	Ttc9	Tgc
Sample	221	149	213	10	155	1	167	209
Points	1000	2000	2000	2000	2000	2000	2000	500
quartz	7.2	7.2	8.0	11.8	17.3	15.5	18.9	10.0
sanidine	6.6	8.0	13.0	14.8	13.9	14.7	16.0	6.2
plagioclase	0.2	0.8	0.1	1.7	0.8	0.9	0.7	---
biotite	0.2	0.2	0.2	0.6	1.0	0.3	0.5	0.6
amphibole	tr	tr	---	---	---	---	---	---
pyroxene	---	---	---	---	---	---	---	tr
opaques	tr	tr	0.2	tr	tr	tr	tr	tr
zircon	tr	tr	tr	tr	0.2	tr	tr	tr
sphene	---	---	---	tr	tr	tr	tr	---
lithics	---	---	---	---	---	---	---	---
Total phenocrysts	14.2	16.2	21.5	28.9	33.2	21.4	36.1	16.8
Q/S	1.1	0.9	0.6	0.8	1.2	1.1	1.2	1.6

Table 3. Isotopic dates for the Taylor Creek Rhyolite. All conventional K-Ar dates are corrected to the constants of Steiger and Jaeger (1977). All dates are on sanidine.

Date (Ma)	Type	Source
24.6 $\pm$ 1.5	K/Ar	Elston and others, 1973
27.7 $\pm$ 0.9	K/Ar	Ratte' and others, 1984
26.3 $\pm$ 1.7	K/Ar	Maxwell and others, 1986
25.9 $\pm$ 0.9	K/Ar	Maxwell and others, 1986
25.7 $\pm$ 0.9	K/Ar	Maxwell and others, 1986
25.9 $\pm$ 2.1	K/Ar	Maxwell and others, 1986
25.0 $\pm$ 0.9	K/Ar	Maxwell and others, 1986
25.9 $\pm$ 0.9	K/Ar	Maxwell and others, 1986
26.6 $\pm$ 1.0	K/Ar	Maxwell and others, 1986
27.3 $\pm$ 1.0	K/Ar	Maxwell and others, 1986
27.0 $\pm$ 1.0	K/Ar	this study
28.18 $\pm$ 0.15	$^{40}\text{Ar}/^{39}\text{Ar}$	W. McIntosh, 1986, oral comm.

Table 4. Geochemical analyses of selected samples from the Monticello Cutoff area. See text for analytical methods and Appendix 2 for complete sample descriptions. Trp-Rubio Peak Formation andesite; Trpt1-Rubio Peak Formation ignimbrite; Trpt2-Rubio Peak Formation ignimbrite; Tkn-Kneeling Nun Tuff; Ttr1-Unnamed trachyte lava; Ttr2-Unnamed trachyte lava; Thok-rhyolite of HOK Ranch; Twd-rhyolite of Willow Springs Draw.

H<sub>2</sub>O  
H<sub>2</sub>O  
CaO  
Na<sub>2</sub>O  
K<sub>2</sub>O  
SiO<sub>2</sub>  
LOI  
TOT

As  
Ba  
Br  
Cl  
Cr  
Cu  
Fe  
Ga  
Hf  
Hg  
In  
K  
Li  
Mn  
Mo  
Ni  
P  
Pb  
Rb  
S  
Se  
Sr  
Tl  
U  
V  
Zn

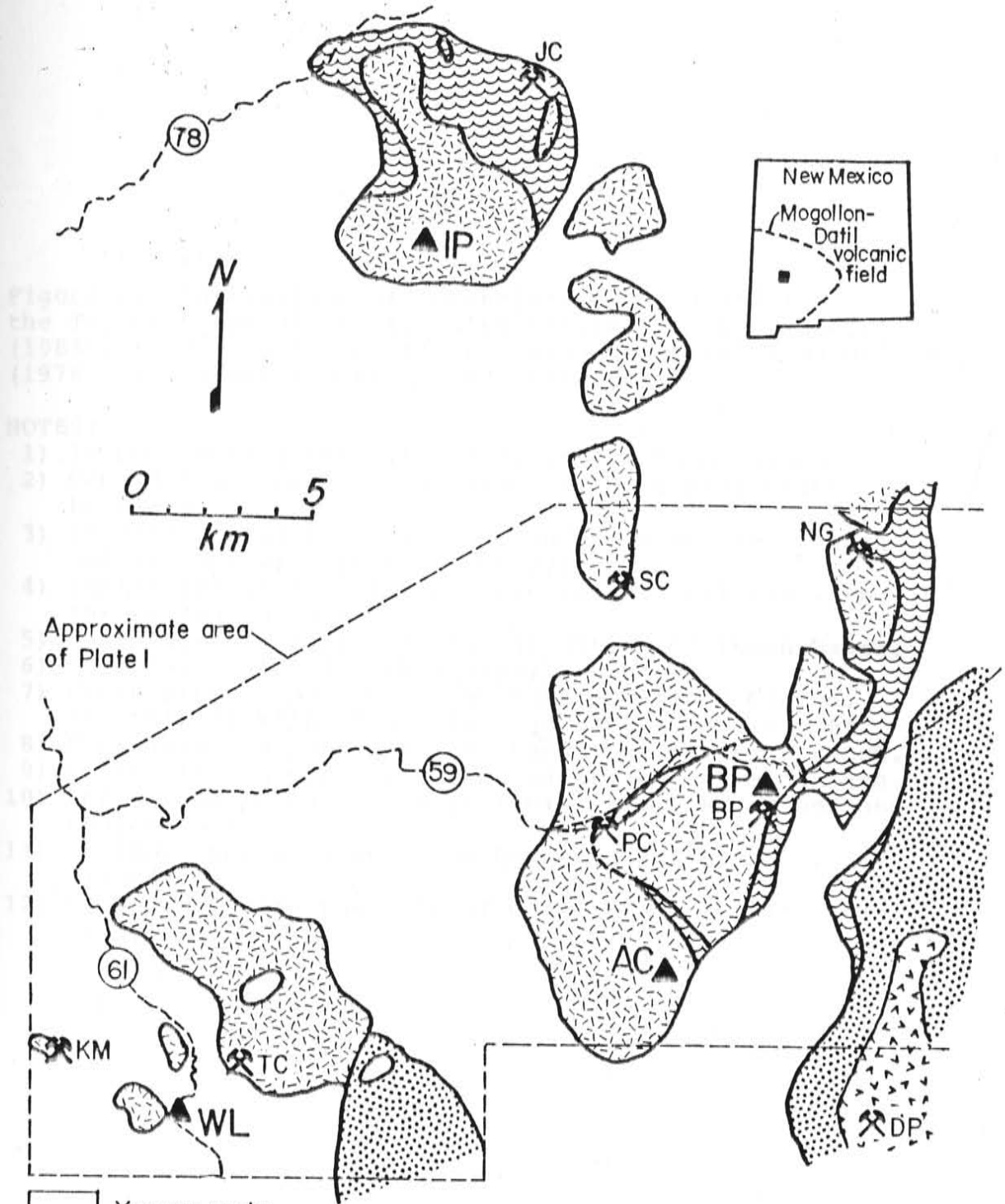
UNIT (1) SAMPLE #	Trp 245	Trpt1 244	Trpt2 246	Tkn 243	Ttr1 237	Ttr2 239	Thok 180	Twd 115
SiO <sub>2</sub>	61.73	69.73	74.08	69.83	65.19	66.11	76.47	76.47
TiO <sub>2</sub>	0.54	0.50	0.29	0.43	0.44	0.44	0.16	0.15
Al <sub>2</sub> O <sub>3</sub>	17.34	15.70	13.22	15.03	17.15	16.36	11.98	12.28
Fe <sub>2</sub> O <sub>3</sub>	4.60	2.23	1.65	2.57	3.07	2.93	1.61	1.12
MnO	0.07	0.02	0.02	0.02	0.12	0.17	0.04	0.06
MgO	2.28	0.33	0.45	0.34	0.52	0.49	0.28	0.21
CaO	1.58	0.55	0.64	1.47	1.14	1.00	0.41	0.31
Na <sub>2</sub> O	4.60	2.99	3.78	3.44	6.09	5.86	3.11	3.45
K <sub>2</sub> O	4.79	6.76	5.38	5.79	5.56	5.66	4.96	5.16
P <sub>2</sub> O <sub>5</sub>	0.27	0.07	0.05	0.16	0.17	0.16	0.03	0.02
LOI	3.30	0.49	1.18	0.51	0.46	0.64	0.87	0.51
TOTAL	101.10	99.37	100.74	99.59	99.90	99.82	99.92	99.74
As	---	---	---	---	<0.3	1.4	1	36
Ba	1484	1168	1338	919	2124	1291	355	85
Br	---	---	---	---	---	0.8	1.1	---
Cl (%)	---	---	---	---	---	---	---	0.004
Cr	<10	<10	25	10	<1	<1	<1	<9
Cs	---	---	---	---	0.5	0.7	5.2	4.2
F (%)	---	---	---	---	---	---	---	0.19
Ga	---	---	---	---	---	---	21	19
Hf	---	---	---	---	13.4	15.5	8.4	7.6
Mo	---	---	---	---	---	---	---	1
Nb	8	23	21	16	55	63	39	36
Ni	---	---	---	---	---	<12	<5	8
Pb	14	25	47	23	20	23	28	21
Rb	100	236	160	227	109	119	313	259
Sb	---	---	---	---	<0.1	<0.1	0.3	9
Sc	---	---	---	---	6.6	6.6	4.0	3.3
Se	---	---	---	---	<0.8	<0.2	<1.0	0.4
Sn	<5	<5	<5	<5	<5	<5	11	25
Sr	635	110	140	242	97	60	92	16
Ta	---	---	---	---	3	3.5	3.7	3.5
Th	<3	30	31	22	16	18	41	29
U	<3	3	3	<3	3	3	9	8
V	19	28	8	29	14	9	3	<3
Y	19	47	62	34	46	56	103	116
Zn	---	---	---	---	---	---	51	57
Zr	155	526	311	185	601	706	200	187
La	---	---	---	---	85	99	55	59
Ce	---	---	---	---	168	187	140	132
Nd	---	---	---	---	66	77	59	61
Sm	---	---	---	---	10.6	12.0	12.3	12.9
Eu	---	---	---	---	2.9	2.7	0.65	0.51
Tb	---	---	---	---	1.4	1.6	2.2	2.2
Yb	---	---	---	---	4.4	5.5	11.1	10.6
Lu	---	---	---	---	0.73	0.89	1.75	1.42



Table 5. Point count data for various units in the Monticello Cutoff area (in volume %). Points is the total number of points counted on the thin section. See Appendix 2 for complete sample descriptions. Ttrl-unnamed trachyte lava; Tkn-Kneeling Nun Tuff; Thok-rhyolite of HOK Ranch; Twd-rhyolite of Willow Springs Draw.

UNIT	Ttrl	Tkn	Thok	Twd	Twd
SAMPLE #	244	243	248	115	116
POINTS	500	500	2000	500	500
-----	-----	-----	-----	-----	-----
QUARTZ	6.8	4.2	8.6	10.6	14.6
SANIDINE	6.4	5.2	6.1	18.0	17.4
PLAGIOCLASE	2.0	11.8	2.8	0.2	0.2
BIOTITE	1.8	3.8	2.4	0.2	0.4
OPAQUES	tr	tr	tr	tr	tr
ZIRCON	tr	tr	tr	tr	tr
-----	-----	-----	-----	-----	-----
TOTAL					
PHENOCRYSTS	17.0	25.0	19.9	29.0	32.6
GROUNDMASS	83.0	75.0	80.1	71.0	67.4

Figure 1. Generalized geologic and location map for the Taylor Creek district. Geography (triangles): IP--Indian Peaks; BP--Boiler Peak; AC--Alexander Cienega; WL--Wall Lake; RM--Round Mountain. Lode tin occurrences (hammer and shovel): JC--Juniper Claims; SC--Squaw Creek; NG--Nugget Gulch; PC--Paramount Canyon; BP--Boiler Peak; KM--Kemp Mesa; TC--Taylor Creek.



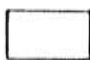


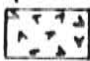

-  Younger rocks
-  Pyroclastic rocks associated with the Taylor Creek Rhyolite
-  Taylor Creek Rhyolite
-  Rhyolite of Dolan Peak
-  Older rocks

Figure 2. Correlation of nomenclature for units in the Taylor Creek district. With the exception of Harvey (1985), the nomenclature for the area has been based on Coney (1976) with minor additions and revisions.

## NOTES:

- 1) In part correlates with sandstone of Inman Ranch.
- 2) Considered here to be a phase of the Taylor Creek Rhyolite.
- 3) In part correlates with the sandstone of Inman Ranch and in part with Tt (this study).
- 4) Ignimbrite at top of the Dolan Peak correlates with the La Jencia Tuff.
- 5) Correlates in part with the sandstone of Inman Ranch.
- 6) Correlates with Tt (this study).
- 7) Correlates in part with the tuff of Stiver Canyon, the tuff of Kline Mountain, and the La Jencia Tuff.
- 8) Correlates in part with the sandstone of Inman Ranch.
- 9) Correlates in part with the sandstone of Inman Ranch.
- 10) Correlates in part with Tt (this study) and Bloodgood Canyon Tuff.
- 11) Includes nomenclature from Lawrence and Richter, (1986).
- 12) Correlates with the tuff of Garcia Camp and Tt (this study)

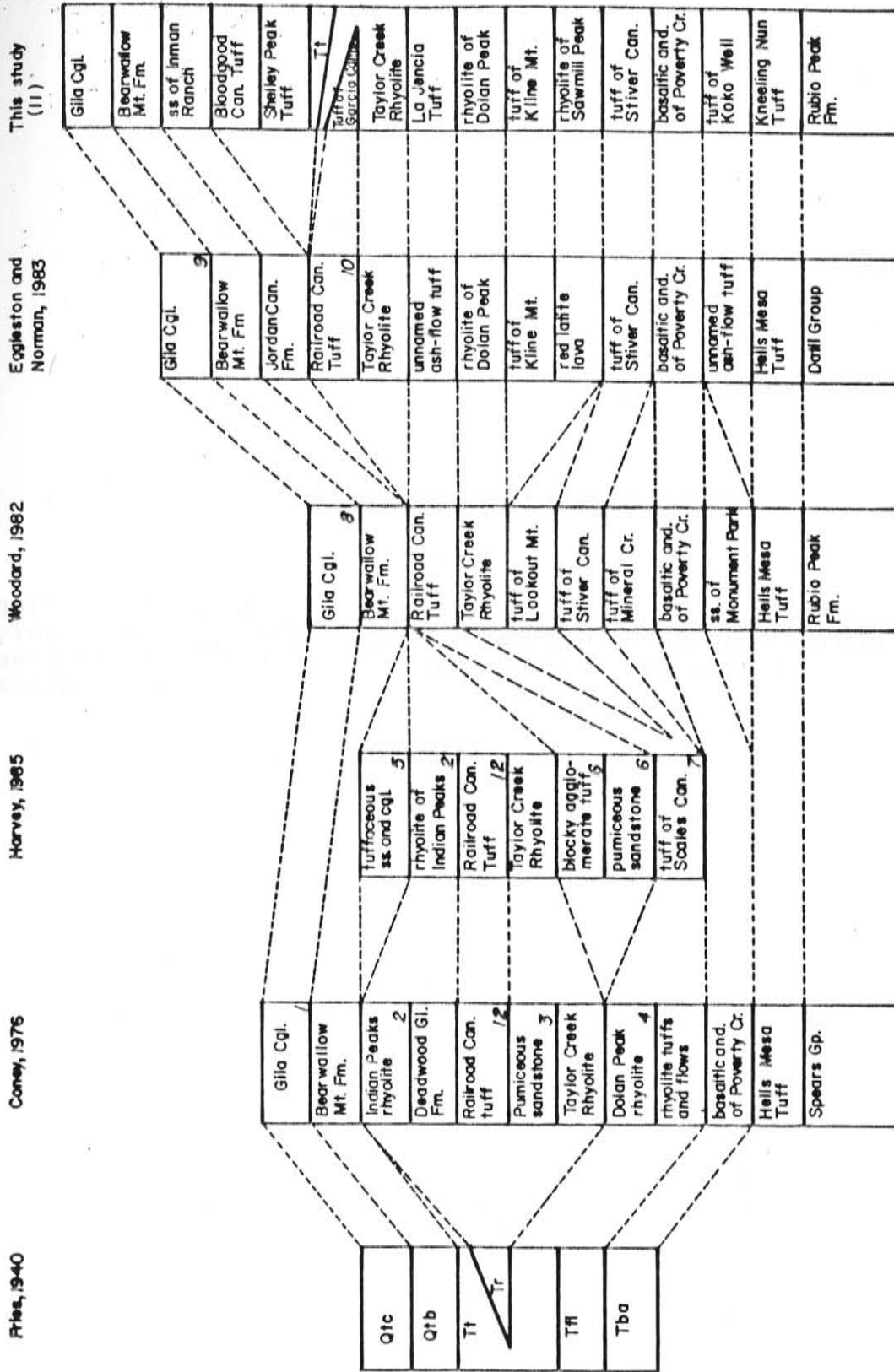
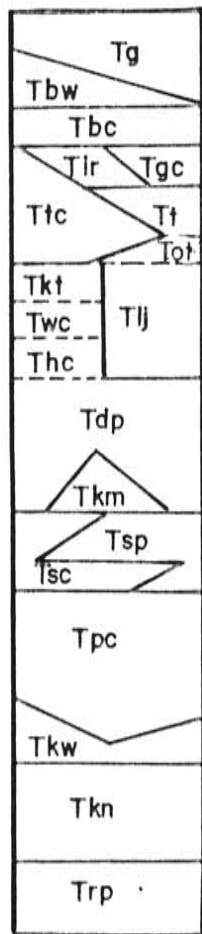


Figure 3. Stratigraphic section of bedded rocks in the Taylor Creek district. Age information based on McIntosh and others (1986)  $^{40}\text{Ar}/^{39}\text{Ar}$  dates. See text for unit descriptions.



- Tg-- Gila Conglomerate
- Tbw--Bearwallow Mountain Fm
- Tbc--Bloodgood Canyon Tuff
- Tir-- sandstone of Inman Ranch
- Tgc-- tuff of Garcia Camp
- Ttc--Taylor Creek Rhyolite
- Tt--unnamed pyroclastic deposits
- Tot--unnamed ignimbrite
- Tlj--La Jencia Tuff
- Tkt--rhyolite of Kieth Tank
- Twc--rhyolite of Whitetail Canyon
- Thc--rhyolite of Hoyt Creek
- Tdp--rhyolite of Dolan Peak
- Tkm-- tuff of Kline Mountain
- Tsp-- rhyolite of Sawmill Peak
- Tsc-- tuff of Stiver Canyon
- Tpc-- basaltic andesite of Poverty Creek
- Tkw--tuff of Koko Well
- Tkn--Kneeling Nun Tuff
- Trp-- Rubio Peak Fm



Figure 4.  $\text{SiO}_2$ -total alkali classification diagram based on the IUGS suggested classification proposed by Le Maitre (1984). Numbers refer to the headings in Table 1.

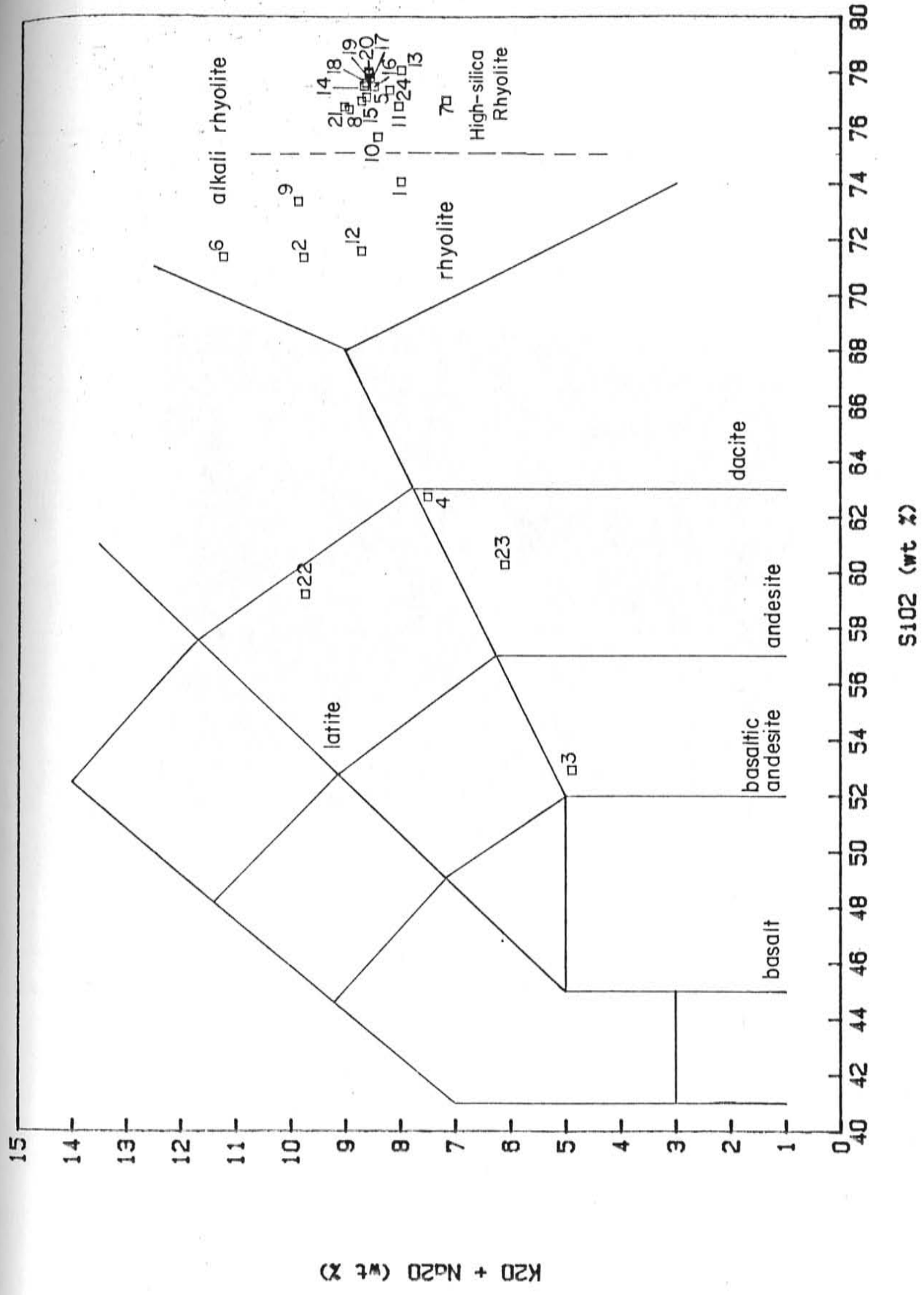




Figure 5. Typical exposures of the andesitic lava flows of the Rubio Peak Formation in Poverty Creek, about 1 km from Poverty Creek Store at the east edge of Plate 1.

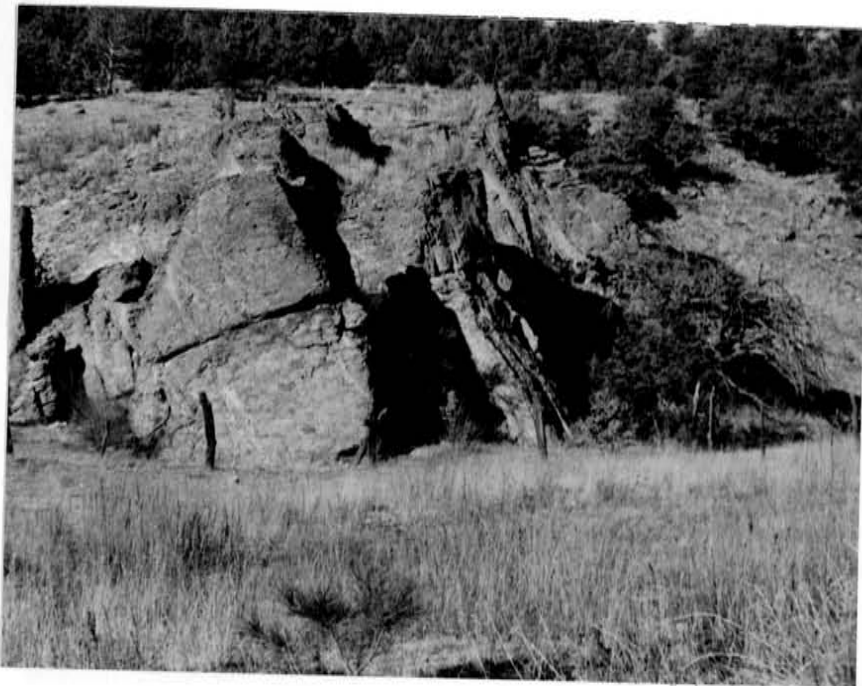


Figure 6. Exposure of the Kneeling Nun Tuff immediately east of Mud Hole. Dip is to the left (west) and defined by flattened pumice. Joints are subparallel with dip.

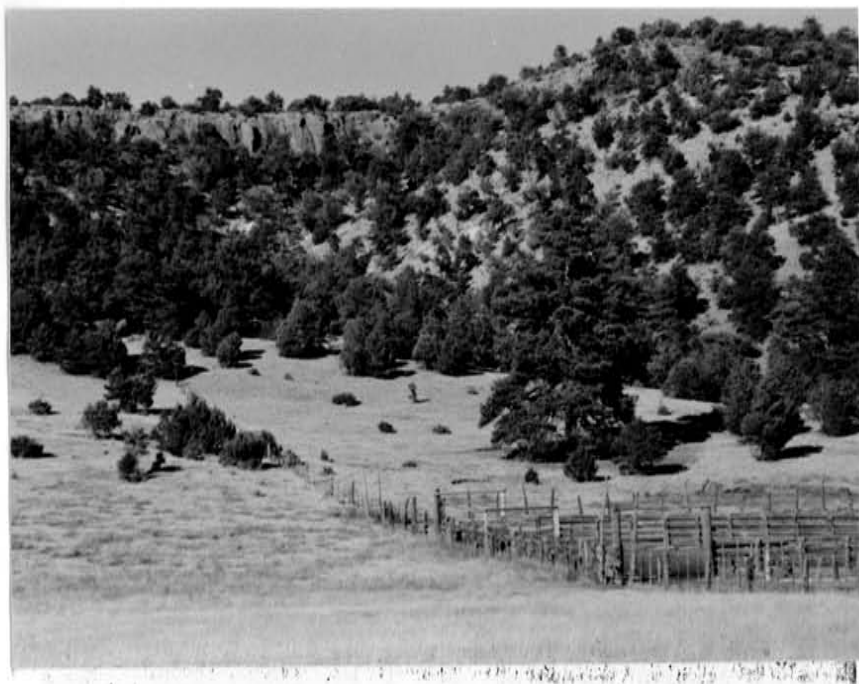


Figure 7. View looking north at the stratigraphic section at Mud Hole. The foreground consists of the basaltic andesite of Poverty Creek. The light colored middle portion of the hill is the tuff of Stiver Canyon. The cliff forming unit at the top of the ridge is the rhyolite of Sawmill Peak.

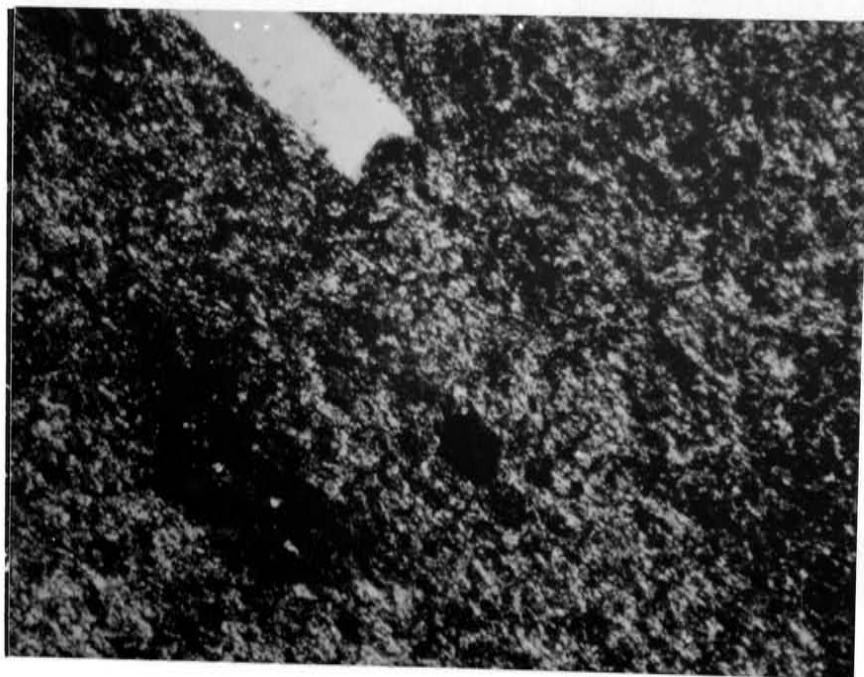


Figure 8. Typical "felty" texture in the groundmass of the rhyolite of Sawmill Peak. The phenocryst at the top of the photograph is sanidine. Field of view is 2.5 mm.

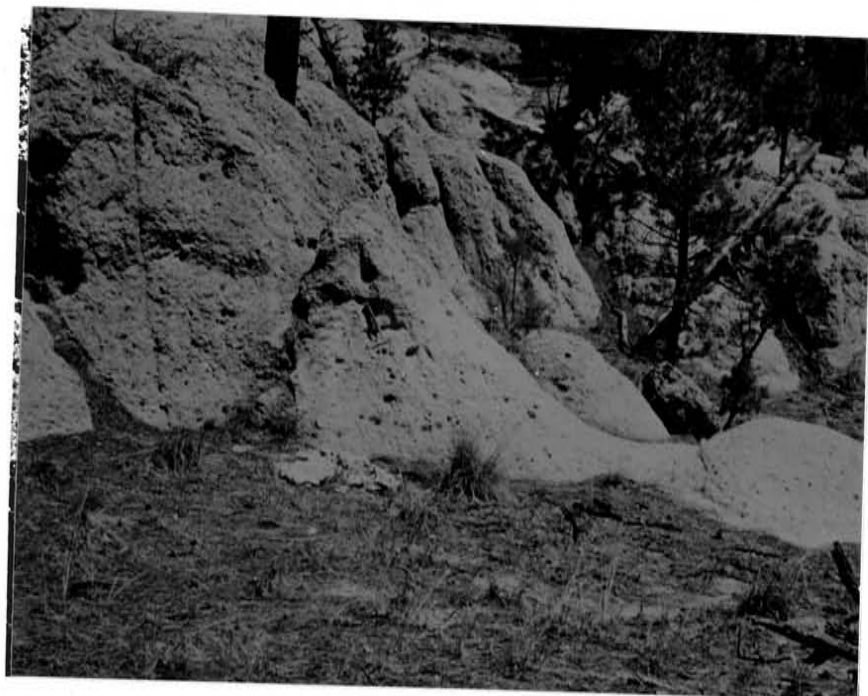


Figure 9. Typical exposures of the tuff of Kline Mountain. At this locality, the tuff has a pink tint, possibly due to alteration related to a nearby rhyolite intrusive. At other localities, this tuff is white.



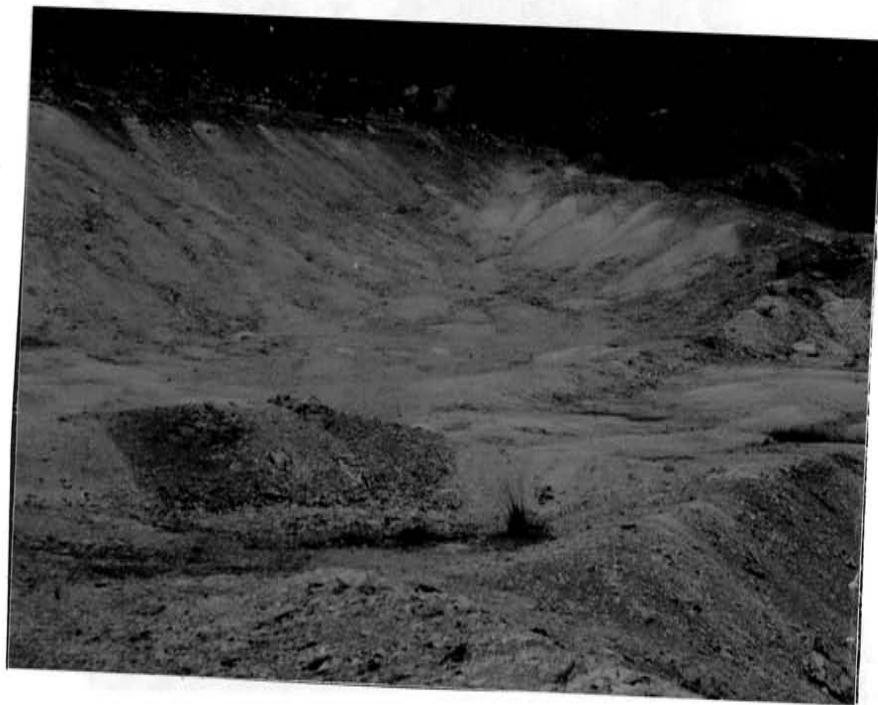


Figure 10. Exploration excavations at the kaolinite prospects locally known as the "clay pits". The alteration is an advanced argillic assemblage consisting of kaolinite and minor alunite. The darker gray material in the center of the photograph is chalcidonic quartz believed to be the product of silica replacement of the tuff of Kline Mountain.



Figure 11. Exposures of the La Jencia Tuff on the north bank of Scales Canyon. The tuff is densely welded and crystal-poor. The prominent ledge at the top of the exposure is about 1 m high. The slope below the top ledge is due to a vitric zone in the tuff. The differences in texture indicate that the unit consists of multiple pyroclastic-flow deposits.

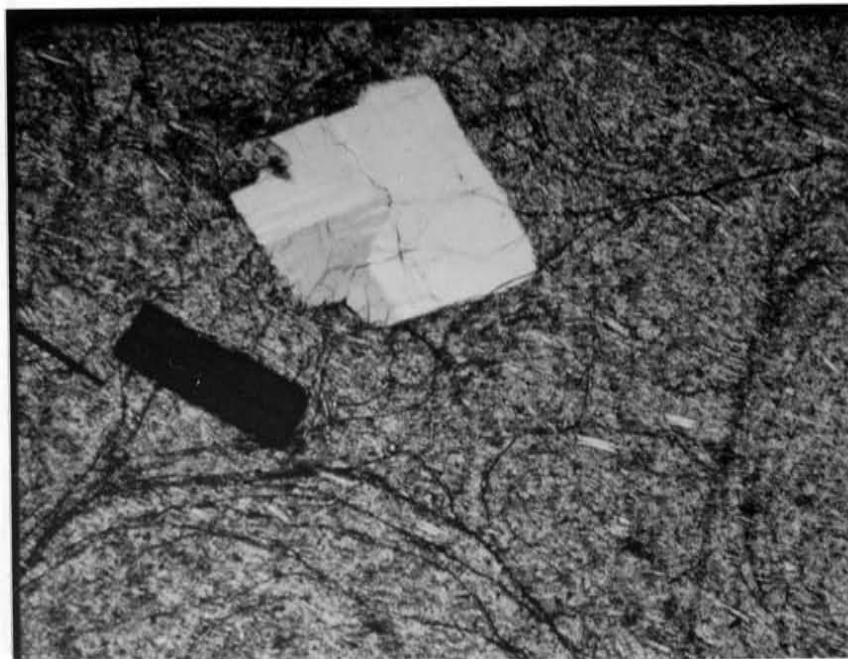


Figure 12. Photomicrograph of the rhyolite of Whitetail Canyon. The phenocrysts of plagioclase (white) and biotite (dark) are set in a microtrachytic groundmass with perlitic cracks. Field of view is about 2.5 mm.



Figure 13. Flowbanded Taylor Creek Rhyolite below Wall Lake. The fan-like geometry of the flowbanding may indicate an underlying vent area but is probably due to ramping of a moving lava lobe over a previously erupted lobe.

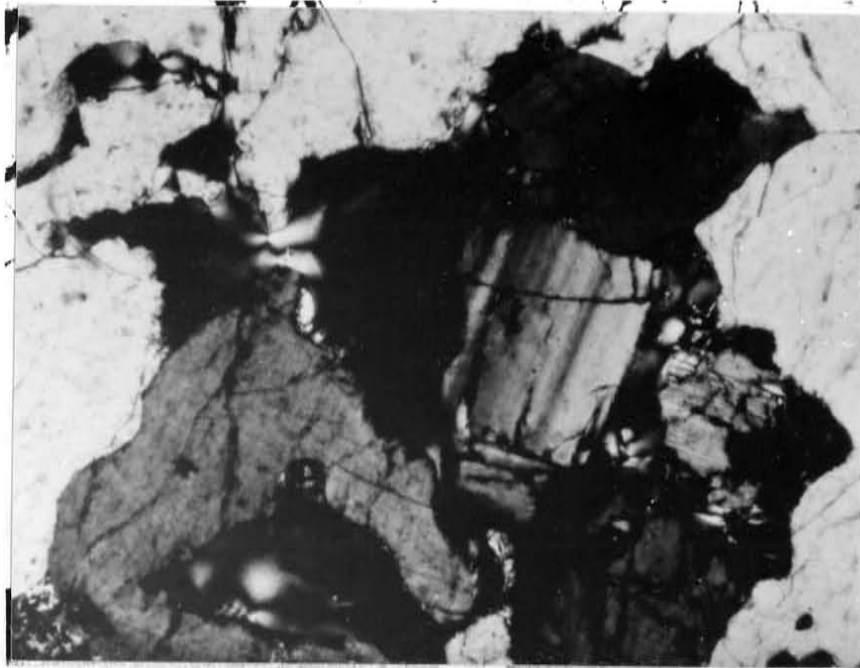


Figure 14. Glomeroporphyritic sanidine with a core of plagioclase in the Taylor Creek Rhyolite. With the exception of the plagioclase in the center, the entire view is filled with sanidine. The field of view is about 2.5 mm.

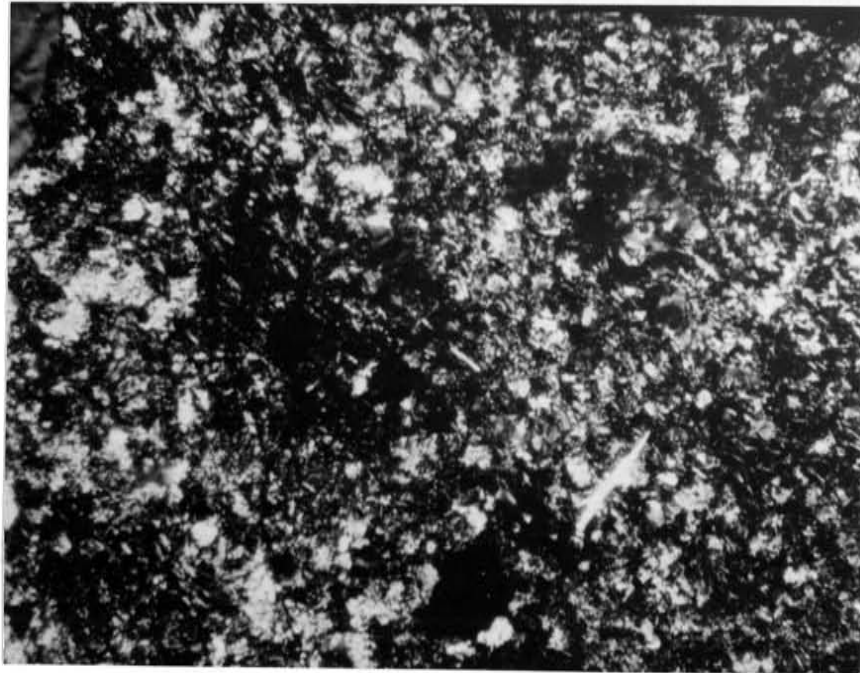


Figure 15. Granophyric texture typical of the Taylor Creek Rhyolite. The field of view is about 2.5 mm.

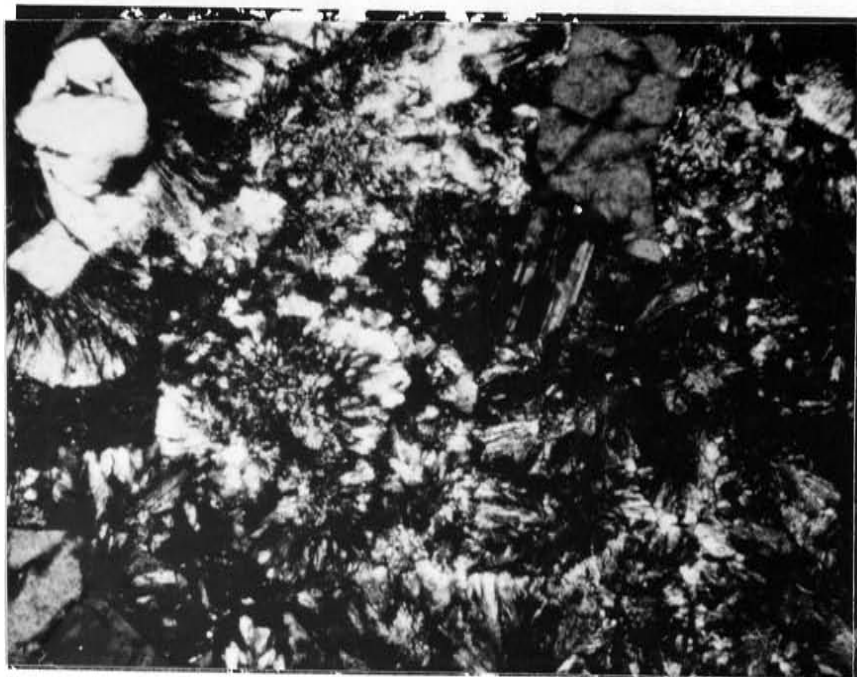


Figure 16. Relict spherulites in the Taylor Creek Rhyolite. The radial texture is outlined by opaque oxides. The original, fine-grained, radial quartz and sanidine have been recrystallized to coarse granophyric quartz and sanidine. Field of view is about 2.5 mm.



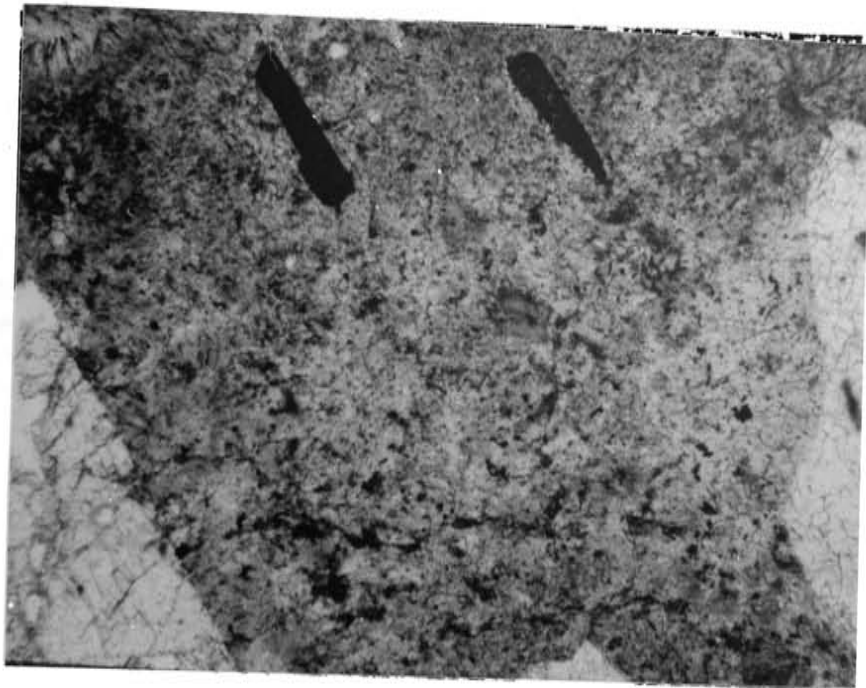


Figure 17. Photomicrograph of a thin section from the Taylor Creek dome near Wall Lake. The groundmass is granophyric. Mineralogy: Q-quartz, S-sanidine, B-biotite, Sp-sphene. Field of view is about 2.5 mm.




Figure 18. Enrichment-depletion diagram for typical Taylor Creek Rhyolite. The major elements are compared to the average rhyolite of Le Maitre (1976); trace elements are compared to Turekian and Wedepohl's (1961) average low-Ca granite.

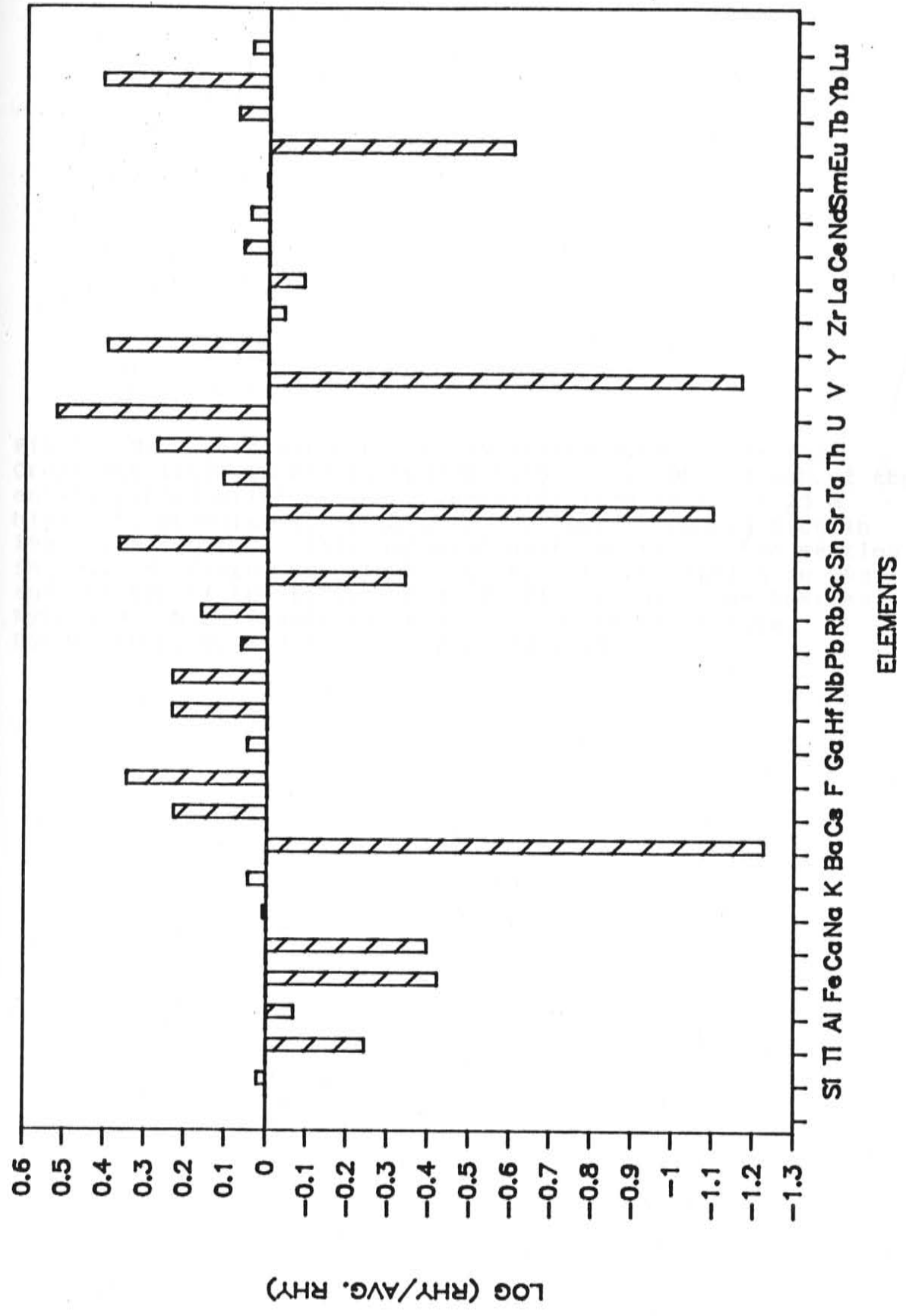


Figure 19. Pyroclastic rocks associated with the Taylor Creek Rhyolite exposed in Scales Canyon. a. Photograph of the entire pyroclastic section. The cliff face is about 25 m high. b. Pyroclastic flows near the base of the section in 19a. c. pyroclastic fall deposits near the top of the section in 19a. d. Coarse breccia at the top of the section in 19a and the top of the fallout unit in Figure 19c. See text and Kyle and others (1986) for a more complete discussion. Hammer in b, c, and d is about 75 cm long.

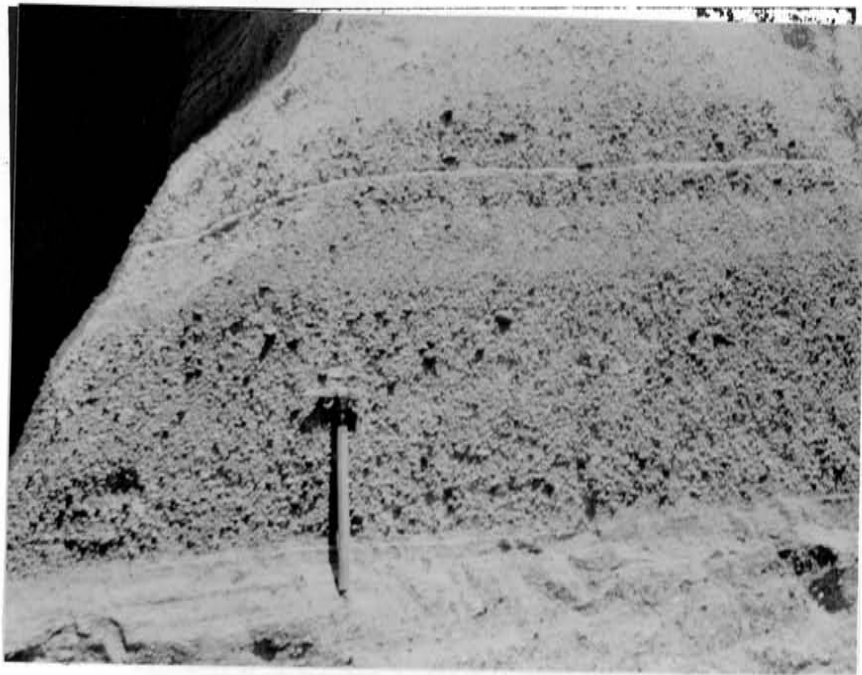
(130)



a



b



c



d



Figure 20. Type section of the sandstone of Inman Ranch in Stiver Canyon (looking north). Inman Ranch is about 1 km to the right of the photograph. The cliff-forming unit near the top of the hill is a tuff, possibly correlative with the South Canyon Tuff.



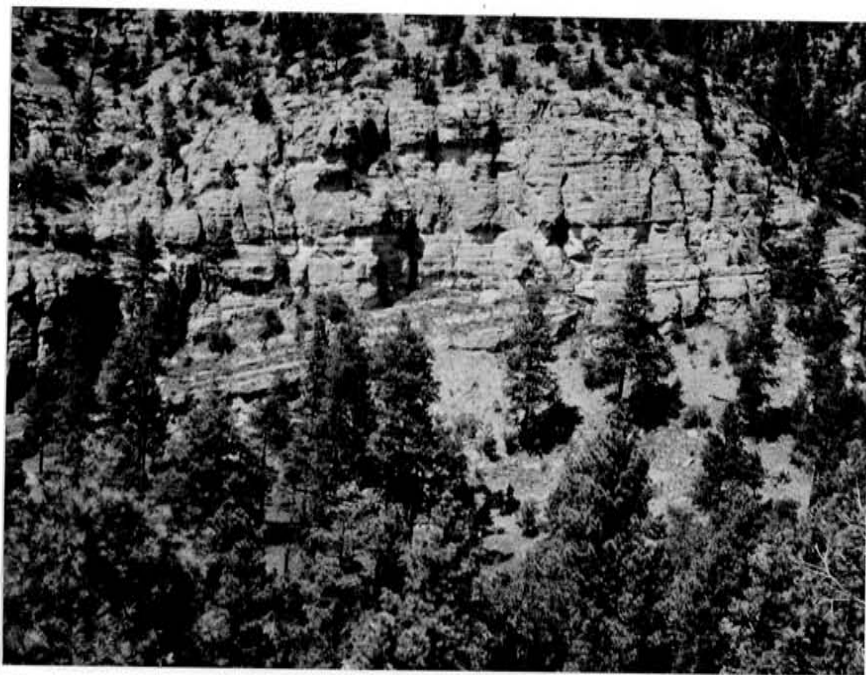


Figure 21. Angular unconformity of  $15^{\circ}$  between the sandstone of Inman Ranch (lower) and the Gila Conglomerate (upper) in Whitewater Canyon.

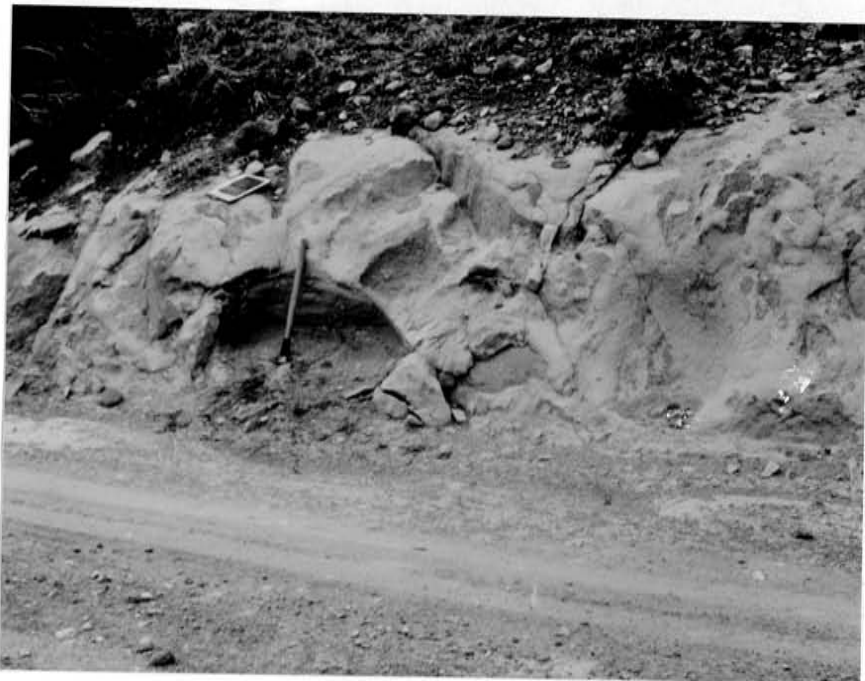


Figure 22. Massive, poorly sorted sandstone distinctive of the sandstone of Inman Ranch. The photograph was taken on the road into Scales Canyon. The hammer is about 75 cm long.



Figure 23. Exposures of the Gila Conglomerate at Wall Lake (foreground).



Figure 24. View of the west flank of the Black Range from near Paramount Canyon. The near hill on the skyline is Alexander Peak. This photograph exhibits the dimensions of the piedmont slope in the area. The far hills on the skyline are 20 to 30 km distant. Round Mountain, near Diamond Creek, is barely visible as a low rounded hill below the skyline to the right of Alexander Peak.

Figure 25. Geologic sketch map of the intrusive rhyolite porphyry of Kline Mountain and surrounding rocks with alteration zones overlain.

Geography

KM Summit of Kline Mountain.  
CP Clay pits.

Geology

Q Quaternary deposits undivided.  
Tlj La Jencia Tuff.  
Tkm Tuff of Kline Mountain.  
Tdp Rhyolite of Dolan Peak  
Tsp Rhyolite of Sawmill Peak  
Tsc Tuff of Stiver Canyon  
Tpc Basaltic andesite of Poverty Creek.  
Tkmp Rhyolite porphyry of Kline Mountain.

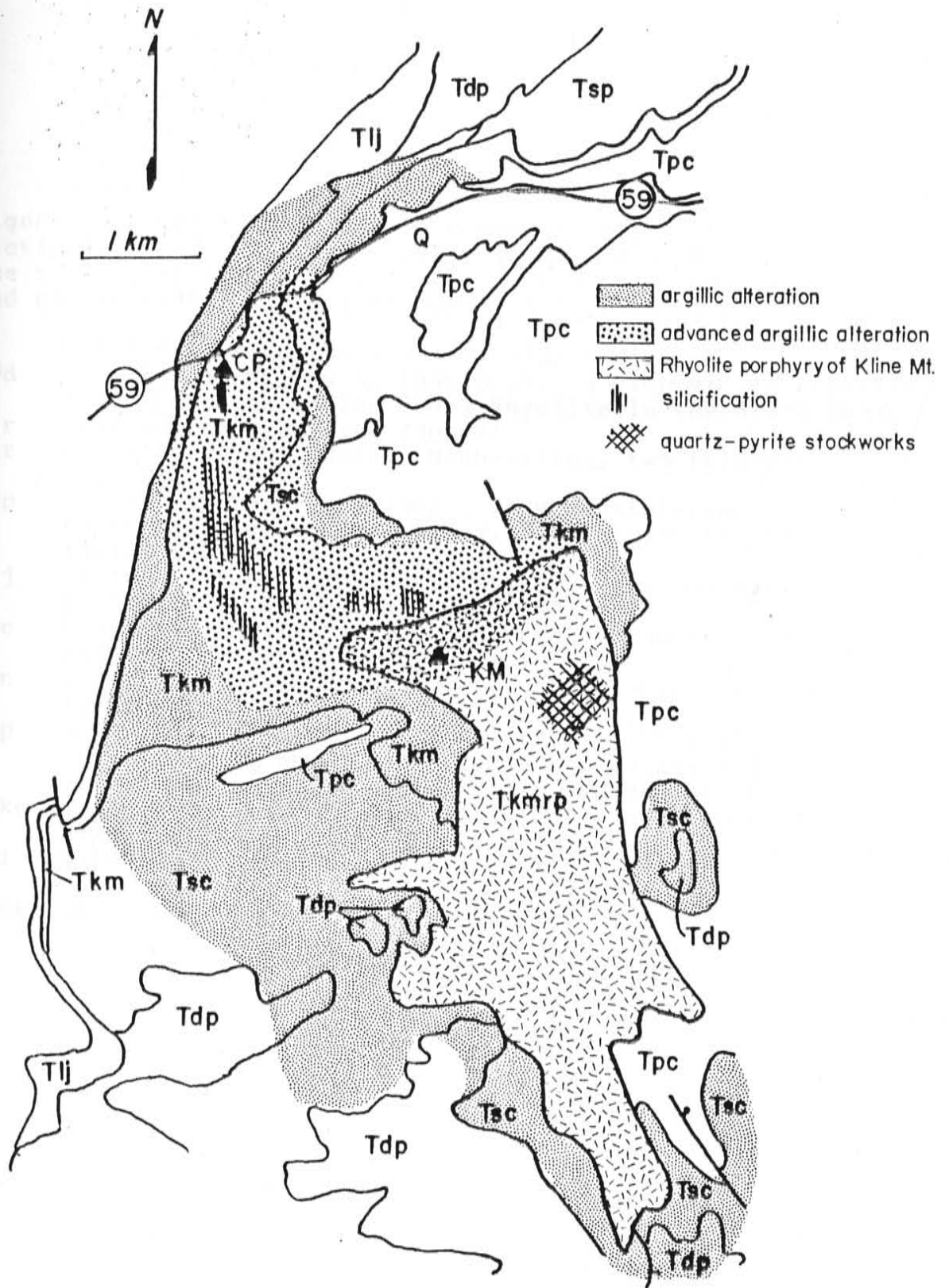
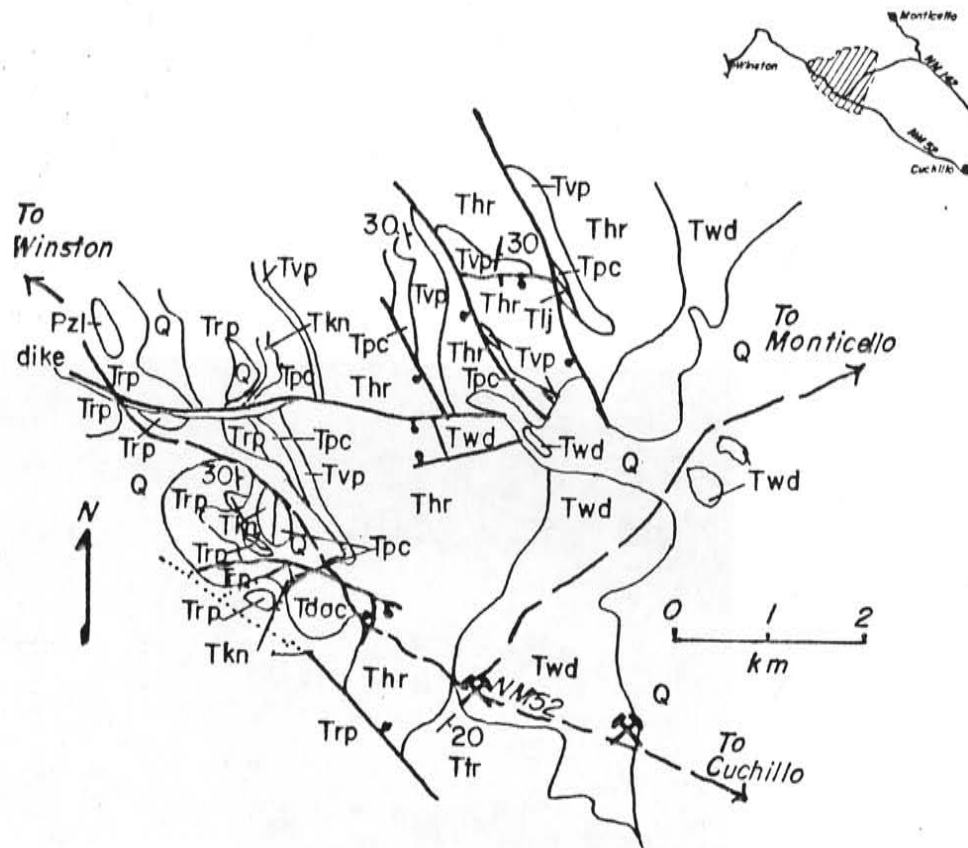


Figure 26. Generalized geologic map and stratigraphic section for volcanic rocks in the Sierra Cuchillo. Dates on the stratigraphic column are  $^{40}\text{Ar}/^{39}\text{Ar}$  dates from McIntosh and others (1986). Inset at top is a regional location map.

- Q Quaternary alluvium and colluvium undivided.
- Twd Rhyolite of Willow Springs Draw. A high silica rhyolite similar to the Taylor Creek Rhyolite in the Black Range.
- Ttr unnamed trachyte lava (dome?)
- Thr Rhyolite of HOK Ranch. High-silica, two feldspar rhyolite lava.
- Tvp Vicks Peak Tuff. Regional, very crystal-poor, moderately to densely welded, high-silica rhyolite ignimbrite.
- Tlj La Jencia Tuff. Regional, crystal-poor, densely welded, high silica rhyolite ignimbrite.
- Tpc Basaltic andesite of Poverty Creek. Numerous basaltic andesite lava flows.
- Tkn Kneeling Nun Tuff. Regional, crystal-rich, rhyolitic ignimbrite.
- Trp Rubio Peak Formation. This formation consists of mafic flows, felsic flows and pyroclastic rocks, and voluminous coarse volcanoclastic sedimentary rocks.
- dike White rhyolite dike. Lithologically similar to Thr and may be a feeder to the Thr flows.
- Pzl Paleozoic limestone undifferentiated.
- pick and shovel symbols are tin occurrences.





Q	
Twd / Ttr	
Thr	
Tvp	28.5
Tlj	28.8
Tpc	
Tkn	35.2
Trp	
Pzl	

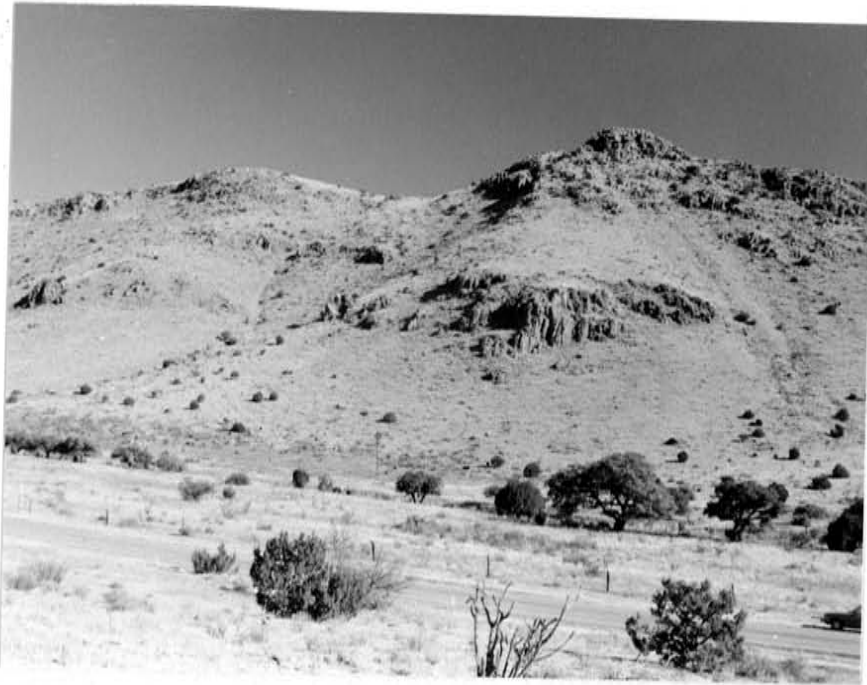


Figure 27. Photograph of the southwest side of Burro Ridge in the Sierra Cuchillo. The ridge is capped by the rhyolite of HOK Ranch. The ledges in the center part of the hill are the Vicks Peak Tuff separated from the HOK Ranch by a thin sedimentary rock interval. The base of the hill consists of the basaltic andesite of Poverty Creek. Extreme foreground is the Kneeling Nun Tuff.

CHAPTER 2

The data presented in this chapter and the interpretation of that data is the responsibility of Ted L. Eggleston. David I. Norman advised this thesis. Ted L. Eggleston collected the oxygen isotope data in the laboratory of Samuel Savin.

INTENSE VAPOR-PHASE CRYSTALLIZATION: MINERALOGICAL AND  
CHEMICAL EFFECTS IN HIGH-SILICA RHYOLITE LAVAS

Ted L. Eggleston and David I. Norman  
New Mexico Institute of Mining and Technology  
Socorro, New Mexico

and

Samuel M. Savin  
Case Western Reserve University  
Cleveland, Ohio

ABSTRACT

Vapor-phase crystallization (VPC) is widespread in the high-silica rhyolite domes of the tin-bearing Taylor Creek Rhyolite in the Black Range of southwestern New Mexico. Three intensities of VPC are recognized: mild, moderate and intense. Mild VPC is pervasive and is characterized by mild bleaching of the rhyolite and deposition of quartz and

sanidine in open space along flowbanding. Moderate VPC is restricted to thin zones around areas of intense VPC. The zones of moderate VPC are intensely bleached and quartz, sanidine, hematite, pseudobrookite, bixbyite, topaz, beryl, and cassiterite are deposited in lithophysae. Selvages on lithophysae have undergone intense VPC. Small zones of intense VPC typically several tens of meters across are distinct and consist of "punky", flowbanded rhyolite lava. Overgrowths on quartz and sanidine phenocrysts, dramatically increased groundmass crystallite size, and recrystallization of spherulites to granophyre are typical mineralogical changes. Intense VPC occurs within a few tens of meters of the paleosurface of the affected domes.

Most elements were mobilized by the fluids responsible for VPC. Ba, Cs, Y, and the rare earth elements (REE) are dramatically enriched in the zones of intense VPC relative to mildly vapor-phase crystallized rhyolite; Ti, Nb, Pb, Sb, U, and Sn are depleted; As, Cl, F, Sc, Sr, and Zn exhibit both enrichments and depletions. Enrichments and depletions in zones of moderate VPC are similar to those in zones of intense VPC, except that F, Mn, Mg, Se, and Sr are enriched in these zones. Sn,  $Fe_2O_3$ , As, Sb, Pb, W, U, Sc, Ta, Cs, Co, and Cr are enriched in the tin deposits that occur in and above the zone of moderate VPC (lithophysal zone). Ga, Hf, Zr, and Th are apparently immobile. Oxygen-isotope compositions of quartz from lithophysae suggest that the fluids responsible for VPC were magmatic. Fluid inclusion homogenization temperatures in quartz overgrowths and quartz

from lithophysae are  $>720^{\circ}$  C, also suggesting that the fluids were of magmatic origin.

High temperature, magmatic fluids that transported and deposited most major and trace elements were responsible for VPC.

#### INTRODUCTION

Vapor-phase crystallization (VPC) is characterized by growth of tridymite, alkali feldspar and other minerals in pore spaces in felsic ignimbrites and lavas from a vapor phase (Smith, 1960). Ross and Smith (1961) later defined vapor-phase crystallization as the formation of crystals in open spaces under the influence of a vapor phase. Other minerals that may form during VPC include magnetite, biotite, fayalite, aegirine, and sodic amphibole. The results of this process have been described by numerous authors (see Smith, 1960 for a partial list of descriptions), but little work has been done to characterize the process in terms of the chemical effects of VPC and the physiochemical conditions prevalent during VPC. Lipman and Christinansen (1964) reported no detectable major element variations between crystallized (devitrified) tuff and vapor-phase crystallized tuff, but did not discuss trace element variations.

This paper reports on a study of vapor-phase crystallized rhyolite lavas done as part of a larger study of tin mineralization associated with those lavas (Eggleston and Norman, 1987a, b,; Eggleston and others, 1987a, b). The

lavas all exhibit pervasive, mild VPC with local zones of intense VPC. The zones of intense VPC form pipe-like bodies a few hundred meters in diameter within the domes. Tin mineralization is found near these zones and is believed genetically related to them.

Eggleston and others (1987b) report analyses of volatile components in the fluid inclusions. Water is the dominant volatile in most samples, but  $\text{CO}_2$  dominates in some samples and typically comprises 5 to 10 mol% of the total. The  $\text{CO}_2$  content in the fluid inclusion volatiles is similar to the  $\text{CO}_2$  content of active volcanic fumaroles (Gerlach and Casadevall, 1986; Le Guern and others, 1982; Matsuo and others, 1982).

The  $f_{\text{O}_2}$  of felsic magmas and the fluids that evolve from them typically fall between the quartz-fayalite-magnetite (QFM) and nickel-nickel oxide (NNO) oxygen buffers (Haggerty, 1976; Christiansen and others, 1986). Analyses of volatiles from fluid inclusions in topaz (Eggleston and others, 1987b) indicate that the  $f_{\text{O}_2}$  of the fluids that deposited the topaz were about midway between the buffers. Analyses of volatiles in fluid inclusions in cassiterite and wood tin indicate that when the fluids deposited some of the wood tin, the  $f_{\text{O}_2}$  of the fluids was above the magnetite-hematite (MH) buffer. When cassiterite was deposited, the  $f_{\text{O}_2}$  of the fluids was between the NNO and MH buffers. Because cassiterite was deposited deeper in the veinlets than the wood tin, the  $f_{\text{O}_2}$  appears to increase as the fluids near the paleosurface. Eggleston and others (1987) suggest that



the increase in  $f_{O_2}$  is due to mixing of air with the fluid.

## GEOLOGY

The Taylor Creek Rhyolite is a group of Tertiary high-silica rhyolite lavas in the Black Range of southwestern New Mexico (Fig. 1). McIntosh and others (1986) report a high precision,  $^{40}\text{Ar}/^{39}\text{Ar}$  date of  $28.18 \pm 0.15$  Ma for the Taylor Creek Rhyolite. The following geologic descriptions are from Eggleston and Norman (1987a). These rhyolite lavas host numerous tin occurrences that consist of veinlets of hematite, cassiterite and wood tin (a microcrystalline form of cassiterite). The Taylor Creek Rhyolite is near the top of the volcanic section in the east-central part of the Mogollon-Datil volcanic field that consists of voluminous mafic to felsic lavas and felsic ignimbrites. The volcanic stratigraphy can be separated into two age groups, a pre-35 Ma group and a 30 to about 26 Ma group (McIntosh and others, 1986). The older group consists of intermediate to felsic lavas with minor felsic pyroclastic rocks. Volcaniclastic sedimentary rocks are common and locally dominate the section (Harrison, 1986). The younger group consists of a bimodal sequence of basaltic andesite and high-silica rhyolite. The basaltic andesite sandwiches the high-silica rhyolite that is as much as 700 m thick.

The high-silica rhyolite consists of numerous domes and lava flows as well as voluminous ignimbrites. Two high-silica rhyolite units have been identified on the basis of

phenocryst mineralogy; a lower group consisting of the rhyolite of Dolan Peak and an upper group consisting of the Taylor Creek Rhyolite. The rhyolite of Dolan Peak is characterized by a phenocryst assemblage of about 10% sanidine and about 2% quartz with a trace of biotite and plagioclase. The Taylor Creek Rhyolite typically contains 15 to 30% phenocrysts of quartz and sanidine in subequal proportions. Plagioclase and biotite are present in minor quantities. Accessory minerals include zircon, sphene, and opaque oxide minerals. Both of these rhyolite units consist of a number of discrete rhyolite domes with associated short flows. The domes are as much as 300 m high and in cross section, consist of an outer carapace breccia with a flow banded interior (Fig. 2). The carapace breccia is as much as 200 m thick around the margins of the domes. Vent areas have not been defined for any of the domes.

Pyroclastic rocks consisting of ignimbrites, fall-out deposits, surge deposits, and local agglutinates mantle the domes (Kyle and others, 1986; Eggleston and Norman, 1987a). These pyroclastic rocks are chemically and lithologically similar to the domes that they mantle. Vapor-phase crystallization affects both the rhyolite of Dolan Peak and the Taylor Creek Rhyolite, but the Taylor Creek is the best studied of the two units and will be the basis of the following discussion.

## ANALYTICAL PROCEDURES

Major elements and Ba, Ga, Nb, Pb, Rb, Sn, Sr, Th, U, Y, Zn, and Zr were analyzed by X-ray fluorescence spectrometry using techniques similar to those described by Norrish and Chappell (1977) and Norrish and Hutton (1969). As, Cs, Hf, Sc, Se, Ta, Th, and U were analyzed by instrumental neutron activation analysis (INAA) at the New Mexico Institute of Mining and Technology using the techniques of Jacobs and others (1977). INAA data was reduced by the software package TEABAGS (Lindstrom and Korotev, 1982). U and Th from the INAA analyses are reported when available. Cl and F were analyzed by wet chemical methods (American Public Health Association, 1976; Bodkin, 1977). Oxygen-isotopic analyses were performed at the laboratory of S. Savin, Case Western Reserve University, Cleveland, Ohio, using the  $\text{BrF}_5$  extraction technique of Clayton and Mayeda (1963). Fluid inclusion analyses were performed using a Linkham TH-600 heating-freezing stage and a Linkham TH-1500 heating stage. Both stages were calibrated with high purity organic and inorganic melting point reference materials. Precision is estimated to be better than  $\pm 3^\circ \text{C}$  for the TH-600 stage and  $\pm 15^\circ$  for the TH-1500 stage.

## VAPOR-PHASE CRYSTALLIZATION

Table 1 lists geochemical analyses from three of the Taylor Creek Rhyolite domes. No non-hydrated vitrophyres were discovered during this study so a pristine starting composition was not obtained. In the Boiler Peak dome, hydrated vitrophyre (sample #143) is assumed to most closely represent the original composition and is used for comparison with vapor-phase crystallized samples. In the Nugget Gulch and Indian Peaks domes, mildly vapor-phase crystallized samples (#149 and 205 respectively) are used for comparison with intensely vapor-phase crystallized samples.

## Physical and Mineralogical Changes

In the Taylor Creek Rhyolite, VPC can be conveniently divided into mild, moderate, and intense VPC, depending on the physical nature of the resultant rocks. Mild VPC is characterized by bleaching of the groundmass and by deposition of K-feldspar and various silica minerals in the pore spaces in the rhyolite lava. The crystallography of these secondary minerals was not investigated during this study; however, Smith (1960) suggests that the most common silica polymorph introduced during VPC is tridymite. The structural state of the feldspar is not known, but the high temperatures of formation suggest that it is sanidine (see later section). The groundmass is granophyric and the

crystallite size is typically  $\ll 0.1$  mm, thus optical determination of the mineralogy of the groundmass is difficult (Fig. 3). Biotite and amphibole are converted to opaque oxide minerals by mild VPC. Other phenocryst minerals are unaffected.

Boundaries of the intense VPC with mild VPC are gradational over a few meters and are not well exposed. Lithophysal zones that overlie zones of intense VPC typically exhibit characteristics typical of both mild and intense VPC and will be considered to be the product of moderate VPC. The zones of intense VPC consist of porous, "punky", extremely bleached rhyolite that resemble poorly welded ignimbrite (Fig. 4). Overgrowths of quartz on quartz phenocrysts increase the phenocryst size by as much as 200% (Fig. 3). The boundary of the overgrowths is marked by innumerable solid and fluid inclusions. Overgrowths on sanidine phenocrysts are likewise marked by inclusions, but these overgrowths rarely add more than a few percent to the size of the phenocryst. Groundmass crystallite size is increased from  $< 0.1$  mm to  $> 0.5$  mm in local areas. Few inclusions were observed in the groundmass crystallites. Spherulites have been recrystallized to granophyric textures with radiating opaque oxide minerals delineating the relict texture.

No biotite or amphibole survives intense VPC. Opaque oxide minerals form rare pseudomorphs after biotite, and more rarely pseudomorph amphibole. Amphibole sites and some biotite sites are marked by a core of dense opaque oxide

minerals surrounded by a halo of disseminated opaque oxides that grades out away from the core. Sphene is replaced by opaque oxide minerals in many of the zones of intense VPC. In the hematite-cassiterite veinlets associated with the intense VPC, hematite pseudomorphs after magnetite are common, indicating that magnetite was deposited from the fluids and was later replaced by hematite (Eggleston and others, 1987b). Plagioclase is rarely preserved. In local areas, it appears to have been replaced by alkali-feldspar; however, in most areas, little evidence for plagioclase remains. Magnetite is locally replaced by hematite. Ilmenite exsolution lamellae in opaque oxides are unaffected by VPC.

Overlying zones of intense VPC zone is a zone a few tens of meters thick that contains abundant lithophysae (Fig. 4). The lithophysae increase in size upward and near the top of the lithophysal zone, lithophysae are as much 3 cm in diameter (Fig. 5). The top of the zones of intense VPC is immediately below the carapace breccia and within a few tens of meters of the paleosurface.

The lithophysae contain drusy linings of quartz, sanidine, topaz, pseudobrookite, bixbyite, and rarely red beryl and cassiterite (Lufkin, 1976). Fries and others (1942) report that garnet may be present at some localities. The presence of garnet and/or cassiterite in lithophysae was not confirmed by subsequent studies. Many of the lithophysae have "punky" borders that appear to be small zones of intense VPC. Lithophysae are presumably produced by gas expansion while the lava is still hot enough to be plastic and the



drusy linings were deposited by fluids moving through the lithophysae.

Tin deposits are associated with the zones of intense VPC and typically occur in the upper parts of the lithophysal zones. These small deposits consist of cassiterite and/or wood tin (a botryoidal, microcrystalline form of cassiterite) with variable amounts of hematite, quartz, and rare fluoroarsenates in veinlets typically less than 10 X 10 m X 3 cm (Eggleston and others, 1987b; Foord and others, 1985; Maxwell and others, 1986; Lufkin, 1972). This mineralization contains high concentrations of  $Fe_2O_3$ , Sn, As, Sb, Pb, W, U, Sc, Ta, Cs, Co, and Cr (Eggleston and others, 1987b).

#### Chemical Changes

An enrichment-depletion diagram comparing the major and trace element chemistry of a mildly vapor-phase crystallized rhyolite sample with a moderately vapor-phase crystallized sample (from a lithophysal zone) and an intensely vapor-phase crystallized sample from the Nugget Gulch area indicates that Ca is the only major element depleted in the zone of intense VPC (Fig. 6a). Ca is enriched in the lithophysal zone. Other major elements exhibit no significant trends. Mn, Mg, and P are present in concentrations near the detection limit and thus the apparent enrichments are problematic. Trace element enrichments in zones of intense VPC include Ba, Cs, F, Cl, Rb, Sc, Y, Zn, and the rare-earth elements (REE); depleted trace elements include As, Sb, Se, Sn, Pb, Sr, and



U, Ga, Hf, Nb, Ta, Th, and Zr remain unchanged during intense VPC. Trace element enrichments and depletions are similar for the lithophysal rhyolite, with the exception of Cs and Nd, which are depleted in the lithophysal zone, and Pb and Sr which are enriched in the lithophysal rhyolite.

Figure 6b is an enrichment-depletion diagram for the Paramount Canyon area of the Boiler Peak dome. Ti is depleted and Ca is enriched in both the zone of moderate VPC and in the zone of intense VPC. Ba, Cl, Cs, Nb, Pb, Sb, Sn, Ta, U, and Zn are depleted and Rb, Y, and the rare earth elements except Eu are enriched in the zone of intense VPC. Ga, Hf, Se, and Sr exhibit no trends. As, F, Sc, Th, and Eu exhibit inconsistent enrichments and depletions. The zone of moderate VPC exhibits similar trends except that As, F, and Eu are enriched.

Figure 6c is a similar enrichment-depletion diagram for the rhyolite dome at Indian Peaks. Ti, Ca, Sb, and Sn are depleted and As, Cs, U, Y, Zn, and the REE are enriched in the zone of intense VPC. These trends are similar to the trends in the other domes.

The REE are enriched in zones of intense VPC (Fig. 6 and 7). The heavy REE exhibit a larger enrichment than the light REE indicating that the REE are fractionated during VPC. Eu and, to a lesser extent, Ce exhibit marked negative anomalies on Figure 6 indicating that those elements are less enriched than other REE. The relative depth of the negative Eu anomaly in the zones of intense VPC is thus increased relative to the zones of mild VPC (Fig. 7).

Mobility of the elements appears to be grossly similar in the three domes; however, the magnitude of the enrichments and depletions differs substantially (Fig. 8). The reasons for the differences in magnitude are problematic, but may relate to the composition of the fluid, the length of time the fluid was in contact with the rock, or to fluid/rock ratios.

The fact that quartz, sanidine, hematite, bixbyite, pseudobrookite, topaz, and rarely red beryl and cassiterite are deposited in lithophysae indicate that  $\text{SiO}_2$ ,  $\text{Fe}_2\text{O}_3$ ,  $\text{TiO}_2$ ,  $\text{Al}_2\text{O}_3$ ,  $\text{MnO}$ ,  $\text{K}_2\text{O}$ ,  $\text{Na}_2\text{O}$ ,  $\text{Sn}$ , and  $\text{Be}$  are mobile during VPC. With the exception of  $\text{Sn}$  and possibly  $\text{Fe}_2\text{O}_3$ , none of these elements exhibit any detectable changes in concentration in zones of intense VPC.

$\text{Ga}$ ,  $\text{Hf}$ ,  $\text{Zr}$ , and  $\text{Th}$  are apparently immobile in these fluids. No significant changes are observed in these elements in the vapor-phase crystallized rocks and they are not concentrated in the tin-bearing veinlets.

#### Oxygen Isotope Changes

The oxygen isotopic composition (in ‰ SMOW) of samples of rhyolite exhibiting different degrees of VPC from four domes was determined to evaluate the effect of VPC on the oxygen isotope systematics of the rhyolite (Table 2). Quartz separates from four of the samples were also analyzed. The  $\delta^{18}\text{O}$  of the least vapor-phase crystallized samples fall in the range 7.3 to 9.0 per mil and the quartz separates

range from 7.5 to 7.8 per mil. Vapor-phase crystallized rocks exhibit a wide range of  $\delta^{18}\text{O}$  values, ranging from 6.1 ‰ to 9.9 ‰. A single sample of quartz from a lithophysal cavity yields a  $\delta^{18}\text{O}$  of 7.5 ‰. No differences in  $\delta^{18}\text{O}$  compositions between intense VPC and mild VPC can be seen in the data.

The large range of whole-rock oxygen isotopic compositions and the small compositional range of quartz separates suggests that the whole-rock samples have undergone post-eruptive  $^{18}\text{O}$  exchange. Quartz exchanges oxygen with latter fluids slowly relative to other common minerals and can thus be used as an indicator of magmatic  $\delta^{18}\text{O}$  values (Criss and Taylor, 1979). If the  $\delta^{18}\text{O}$  of magmatic quartz has been determined, plagioclase equilibria can be used to estimate the magmatic whole-rock oxygen isotopic composition (Taylor, 1979). The fractionation between quartz and plagioclase (An 30) is about 1 ‰ at  $700^\circ$  using the fractionation factors of Bottinga and Javoy (1973). Plagioclase (An 30) in equilibrium with phenocryst quartz would thus be expected to have a  $\delta^{18}\text{O}$  of about 6.5 to 6.8 ‰, which should closely approximate the magmatic whole rock compositions.

The fractionation between plagioclase (An 30) and water at  $700^\circ\text{C}$  is approximately  $-0.4$  ‰ at  $700^\circ\text{C}$ . The primary magmatic water  $\delta^{18}\text{O}$  of the Taylor Creek Rhyolite could thus be expected to be between 6.9 and 7.1 per mil which is within the range of primary magmatic water of Taylor (1968; 1979).

The whole-rock  $\delta^{18}\text{O}$  of 6.1 to 9.9 imply oxygen isotopic

exchange between the rocks and water.  $\delta^{18}\text{O}$  enrichments and depletions are observed; however, only one sample is depleted relative to the estimated magmatic  $\delta^{18}\text{O}$  of the lavas. The  $\delta^{18}\text{O}$  enrichments may be due to interaction of the rhyolite lavas with cooling magmatic fluids responsible for VPC. The  $\delta^{18}\text{O}$  of quartz from lithophysae has a  $\delta^{18}\text{O}$  similar to the bulk of the rhyolite samples and is consistent with growth of the quartz from water with the calculated magmatic water composition at  $700^\circ\text{C}$ . Enrichment of  $^{18}\text{O}$  in the whole-rocks may have occurred as these fluids were cooling. At  $500^\circ\text{C}$ , the fractionation between plagioclase (An 30) and water is about  $1\text{ }^\circ/\text{oo}$  and at  $300^\circ\text{C}$ , the fractionation is about  $5\text{ }^\circ/\text{oo}$ . The observed  $\delta^{18}\text{O}$  compositions of the whole-rock samples are consistent with exchange of  $^{18}\text{O}$  between the rocks and the cooling magmatic fluid. Other factors, such as post-eruptive hydrothermal alteration and post-eruptive hydration (Cerling and others, 1985) may also enrich  $^{18}\text{O}$  in these rocks, but the importance of those processes is difficult to assess. Hydrothermal alteration may be responsible for the single  $^{18}\text{O}$ -depleted sample.

#### Fluid Inclusions

Two types of inclusions occur in overgrowths on quartz phenocrysts and in topaz, quartz, and cassiterite from lithophysae and the tin mineralization. Both types occur together in secondary and pseudosecondary planes indicating that they are cogenetic. Type 1 inclusions are vapor

inclusions locally as large as 50  $\mu\text{m}$  and occur as primary, secondary, and pseudosecondary inclusions (see Roedder (1984) for nomenclature). Type 1 inclusions enclose at least one and possibly two orders of magnitude more volume than Type 2 inclusions. Type 2 inclusions are primary, secondary and pseudosecondary solid inclusions that are typically  $< 10 \mu\text{m}$  in diameter (Fig. 3b; Fig. 9). At room temperature, these inclusions consist of a crystalline solid, vapor bubble, and as many as 4 daughter minerals. A small amount of aqueous liquid is visible in rare inclusions. One of the daughter minerals occurs as translucent, rhombohedral(?) crystals (Fig. 9a,b) and may be a carbonate. Two other translucent daughter minerals and an opaque daughter mineral occur in Type 2 inclusions. The opaque daughter mineral exhibits rare red fringes and may be hematite. One of the two small daughter minerals in Figure 9b is roughly cubic and may be a halide, possibly NaCl. In some Type 2 inclusions, a distinctly cubic daughter mineral is the only daughter mineral present. The other translucent daughter mineral may also be a halide, but it is typically rounded, thus the crystal system can not be determined. The daughter minerals are generally not visible in the inclusions unless the inclusion is liquid (that is  $>350^\circ \text{C}$ ), thus petrographic examination of them is difficult. Type 2 inclusions should not be confused with primary magmatic melt inclusions that occur within quartz and sanidine phenocrysts. Primary magmatic inclusions are solid-vapor inclusions, but did not homogenize when heated to  $1200^\circ \text{C}$  for one half hour.

A limited number of heating experiments were performed on fluid inclusions in the overgrowths on quartz phenocrysts and in drusy quartz and topaz from lithophysae. No phase changes were noted in Type 1 inclusions between 180° to 650° C. The crystalline solid that is the dominant phase in Type 2 inclusions melts between 350 and 530° C to form a liquid-vapor-daughter mineral inclusion that homogenizes to liquid at 650 to 730° C (Table 3). The daughter minerals dissolve between 400 and 630° C with the exception of the opaque daughter mineral, which did not dissolve when vapor-liquid homogenization occurred. The octahedral daughter mineral in Figure 9b dissolves at about 408° C. In order to preserve that inclusion, it was not heated above 450° C, thus the solution temperatures of the other two translucent daughter minerals in that inclusion are not known. In other inclusions, one daughter mineral dissolved between 500 and 550° C. Another daughter dissolved between 600 and 650° C.

In inclusions in overgrowths on quartz phenocrysts collected several tens of meters below the lithophysal rhyolite, the crystalline solid in Type 2 inclusions melts between 470 to 530° C and homogenize to liquid between 720 and 730° C. Daughter minerals dissolve above 530° C. The crystalline solid in Type 2 inclusions in quartz and topaz from lithophysae and in cassiterite from the tin-bearing veinlets melt between 350 and 360° C and homogenize to liquid between 650 and 670° C.

The similarity of the inclusions in the overgrowths in quartz phenocrysts, in quartz and topaz from lithophysae and



in the tin deposits suggests that the fluids were the same fluid. The higher homogenization temperatures for inclusions in overgrowths on quartz phenocrysts than in the lithophysae and in the tin deposits can be explained by a vertical temperature gradient of several  $^{\circ}$  C/meter.

#### DISCUSSION

The fluid inclusion data indicate that VPC occurs at temperatures in excess of  $670^{\circ}$  C. This temperature estimate is in agreement with the temperatures estimated by Lufkin (1976) based on pseudobrookite equilibria. Those temperatures preclude the possibility that the systems are the upper portions of a typical hydrothermal system because of the proximity of the high temperatures to the paleosurface. The vertical temperature gradient defined by fluid inclusion homogenization temperatures would presumably be extreme near the surface where the  $650^{\circ}$  C fluids would cool in a few tens of meters to ambient surface temperatures.

The fact that vapor and crystalline solid inclusions are spatially associated suggests that the two inclusion types are genetically related. The coexistence of vapor-dominated and liquid-dominated inclusions that homogenize at the same temperature is frequently cited as evidence that hydrothermal systems were boiling Roedder (1984). In mineral deposits formed under boiling conditions at about  $300^{\circ}$  C and 100 bars, a small amount of condensed water is visible in vapor



dominated inclusions. The density of fluids under those conditions will be 0.7 to 0.9 g\*cm<sup>-3</sup>. The calculated density of the fluids responsible for VPC at the prevailing conditions (650° C and 1 bar) is about 0.0004 g\*cm<sup>-3</sup>. This very low density is consistent with the lack of observable fluid in the inclusions.

The origin of Type 2 inclusions is problematic. Inclusions believed to be trapped magma occur in the quartz phenocrysts and are distinctly different than Type 2 inclusions. The spatial association of Type 1 and Type 2 inclusions indicates that they are cogenetic, suggesting that Type 2 inclusions are condensates from the low density fluids trapped in the vapor-dominated inclusions. Eggleston and Norman (1986) postulated that the composition of the crystalline solid in Type 2 inclusions is a lithium-boron compound similar to the diomignite (lithium tetraborate) reported by London (1986) in spodumene from the Tanco pegmatite. If this interpretation is correct, none of the crystalline-solid will be preserved outside the inclusions because of its high solubility in water.

The oxygen-isotope data from the lithophysal rhyolite indicate that the fluid responsible for deposition of the vapor-phase minerals was magmatic. The increase in d<sup>18</sup>O in the whole-rock samples can be explained by interaction of the rhyolite with a magmatic fluid at less than magmatic temperatures.

Chemical changes due to intense VPC are dramatic. Most elements are mobile in the fluids responsible for VPC as

evidenced by the enrichments and depletions observed from zones of intense VPC (Fig. 10). Enrichments of elements in such zones imply that F, Rb, Sc, Y, and rare earth elements for examples, were saturated in the fluid at some level below the zones of intense VPC. The elements enriched in the zones of intense VPC are typically incompatible with the mineralogy of the rhyolites and may be fractionated into the fluid phase from the melt prior to separation of the fluid from the melt. Elements such as As, Nb, Sb, Sn, and U that are depleted in zones of intense VPC were not saturated in the fluids and were thus able to be dissolved from the zones of intense VPC. The tin mineralization contains high concentrations of those elements, suggesting that they were deposited at higher levels in the system. Drusy linings of quartz, sanidine, hematite, topaz, pseudobrookite, bixbyite, red beryl, and cassiterite indicate that  $\text{SiO}_2$ ,  $\text{TiO}_2$ ,  $\text{Al}_2\text{O}_3$ ,  $\text{Fe}_2\text{O}_3$ , and  $\text{MnO}$  are also mobile in the fluids; but were near saturation in the fluids and thus those elements were neither enriched nor depleted.

The HREE are enriched in the zones of intense VPC more than the LREE. This fractionation of the REE may be due to the composition of the transporting fluid. The REE are transported in aqueous fluids as complexes with  $\text{CO}_3^{2-}$ , F, Cl, and  $\text{SO}_4^{2-}$  (Kosterin, 1959; Flynn and Burnham, 1978). REE tend to partition to the melt in aqueous fluid-melt systems, but high chlorine concentrations in the aqueous fluid and low  $\text{H}_2\text{O}$  pressures enhance the partitioning of the REE to Cl-rich fluid phases at pressures  $<4\text{kb}$  (Flynn and Burnham, 1978).

LREE have been shown to be more soluble in a CO<sub>2</sub>-rich fluid than the HREE (Kosterin, 1959). Conversely, the HREE are more soluble in Cl- and F-rich fluids than the LREE and the HREE tend to form more stable complexes with Cl and F than the LREE (Minayev, 1963; Humphries, 1984). Topaz was deposited from the fluids responsible for VPC indicating that F was present in high concentrations in the fluids and is thus available to complex and transport the REE. These data suggest that the REE were transported as F complexes and that the fractionation of the REE was due to stronger complexing of HREE relative to the LREE.

#### MODEL

The data suggest the following sequence of events; magmatic fluids saturated with SiO<sub>2</sub>, Al<sub>2</sub>O<sub>3</sub>, Fe<sub>2</sub>O<sub>3</sub>, F, Rb, Y, and rare earth elements separated from the magma and ascended along flow planes within the affected rhyolite lava. The fluids reached saturation with respect to Rb, F, Y, and REE and enriched the rhyolite with those elements. As, Sb, Sn, and U were undersaturated in the fluids and were dissolved from the rhyolite. Overgrowths on quartz and sanidine were deposited and the groundmass crystallite size increased at this time. Biotite and amphiboles were converted to opaque oxides and any remaining groundmass glass was destroyed. The fluids were rich in HF and possibly HCl.

Near the surface, upward migration of these fluids was interrupted by a plastic zone immediately below the carapace

breccia of the dome. Lithophysae were produced in the plastic zone and drusy minerals grew in the voids. This plastic zone was important in that it allows fluids at temperatures near  $700^{\circ}$  C to migrate to within a few tens of meters of the paleosurface of the dome and to be trapped there. When the plastic zone containing lithophysae cooled sufficiently to fracture, the lithophysal zone ruptured, releasing the fluids to the surface of the dome as fumaroles. As the fluids ascended, they mixed with air and the proportion of admixed air increased as the fluids near the surface, thus increasing the  $f_{O_2}$  of the fluids. The extreme thermal gradients and the oxidizing environment in the upper few meters of the dome served to deposit Sn, As, Sb, and U as well as rare earth elements, F, and Sc in the fumaroles.

#### CONCLUSIONS

The fluids responsible for VPC are high-temperature, magmatic fluids derived from the affected rhyolites. Most elements were mobile in the fluid, but, a two-stage evolution for the fluid is envisioned. First, F, Rb, Y, Sn, and rare earth elements were partitioned into the fluid from the magma. These elements were deposited in zones of intense VPC. Second, elements such as As, Sb, Sn, and U were leached from partially crystallized zones undergoing intense VPC and deposited in the fumaroles that resulted when the fluids reached the surface of the domes.

## ACKNOWLEDGEMENTS

Charles Chapin, Donald Richter, Philip Kyle, and Kent Condie are thanked for critical reviews of early versions of this manuscript. The Geological Society of America, New Mexico Geological Society, the National Science Foundation (Grants EAR 8319913 and EAR 8410481 to DIN), the New Mexico Bureau of Mines and Mineral Resources and the U.S. Department of Interior's Mineral Institutes program administered by the U.S. Bureau of Mines (allotment grant G1164135 to DIN) funded various aspects of the study. Lynn Brandvold, New Mexico Bureau of Mines and Mineral Resources, provided the F and Cl analyses. Irradiation costs were defrayed by the Department of Energy's reactor sharing program. Irradiations were performed at the research reactor at the University of Missouri, Columbia.

## BIBLIOGRAPHY

- American Public Health Association, 1976, Standard methods for the examination of water and waste water: American Public Health Association, Washington, D.C., 193 p.
- Bodkin, J.B., 1977, Determination of fluorine by the use of ion-specific electrode following fusion with lithium metaborate: *Analyst*, v. 102, p. 409-413.
- Bottinga, Y., and Javoy, M., 1973, Comments on oxygen isotope geothermometry: *Earth and Planetary Science Letters*, v. 20, p. 250-265.
- Cerling, T.E., Brown, F.H., and Bowman, J.R., 1985, Low-temperature alteration of volcanic glass: hydration, Na, K,  $^{18}\text{O}$ , and Ar mobility: *Chemical Geology (Isotope Geoscience Section)*, v. 52, p. 281-293.
- Christiansen, E.H., Sheridan, M.F., and Burt, D.M., 1986, The geology and geochemistry of Cenozoic topaz rhyolites from the western United States: *Geological Society of America Special Paper 205*, 82 p.
- Clayton, R.N., and Mayeda, T.K., 1963, The use of bromine penta-fluoride in the extraction of oxygen from oxides and silicates for isotopic analysis: *Geochimica et Cosmochimica Acta*, v. 27, p. 43-52.
- Criss, R.E. and Taylor, H.P., Jr., 1983, An  $^{18}\text{O}/^{16}\text{O}$  and D/H study of Tertiary hydrothermal systems in the southern half of the Idaho Batholith: *Geological Society of America Bulletin*, v. 94, p. 640-663.

- Eggleston, T.L., and Norman, D.I., 1986, The Taylor Creek tin deposits: products of magmatic processes (abs.): in Genesis of tin-tungsten deposits & their associated granitoids: Australian Bureau of Mineral Resources Record 1986/10, p. 18-19.
- Eggleston, T.L., and Norman, D.I., 1987, Geology of the Taylor Creek district, Black Range, New Mexico: New Mexico Bureau of Mines and Mineral Resources Bulletin, in prep.
- Eggleston, T.L., Norman, D.I., and Savin, S.M., 1987a, Petrology of the tin-bearing rhyolites, northern Black Range and Sierra Cuchillo, New Mexico: in prep.
- Eggleston, T.L., Norman, D.I., and Savin, S.M., 1987b, Origin of tin mineralization associated with topaz rhyolites, Black Range, New Mexico: in prep.
- Flynn, R.T. and Burnham, C.W., 1978, An experimental determination of rare earth partition coefficients between a chloride containing vapor phase and silicate melts: *Geochimica et Cosmochimica Acta*, v. 42, p. 685-701.
- Foord, E.E., Oakman, M.R., and Maxwell, C.H., 1985, Durangite from the Black Range, New Mexico and new data on durangite from Durango and Cornwall: *Canadian Mineralogist*, v. 23, p. 241-246.
- Fries, C. Jr., Schaller, W.T., and Glass, J.J., 1942, Bixbyite and pseudobrookite from the tin-bearing rhyolite of the Black Range, New Mexico: *The American Mineralogist*, v. 27, p. 305-322.



- Gerlach, T.M. and Casadevall, T.J., 1986, Fumarole emissions at Mount St. Helens volcano: June 1980 to October 1981: degassing of a magma-hydrothermal system: *Journal of Volcanology and Geothermal Research*, v. 28, p. 141-160.
- Haas, J.L., Jr., 1971, The effect of salinity on the maximum thermal gradient of a hydrothermal system at hydrostatic pressure: *Economic Geology*, v. 66, p. 940-946.
- Haggerty, S.E., 1976, Opaque mineral oxides in terrestrial igneous rocks: in Rumble, D., III., ed., Oxide minerals: Mineralogical Society of America Reviews in Mineralogy, v. 3, p. Hg101-Hg300.
- Harrison, R.W., 1986, General geology of Chloride Mining district, Sierra and Catron Counties, New Mexico: *New Mexico Geological Society Guidebook 37*, p. 265-272.
- Humphries, S.E., 1984, The mobility of rare earth elements in the crust: in Rare earth element geochemistry: Elsevier, Amsterdam, p. 317-342.
- Jacobs, J.W., Korotev, R.L., Blanchard, D.P., and Haskin, L.A., 1977, A well-tested procedure for instrumental neutron activation analysis of silicate rocks and minerals: *Journal of Radioanalytical Chemistry*, v. 40, p. 93-114.
- Jezek, P.A. and Noble, D.C., 1978, Natural hydration and ion exchange of obsidian: an electron microprobe study: *American Mineralogist*, v. 63, p. 266-273.
- Kosterin, A.V., 1959, The possible modes of transport of the rare earth elements by hydrothermal solutions: *Geochemistry*, 4, p. 381-387.

- Kyle, P.R., Eggleston, T.L., McIntosh, W.C., Dunbar, N.,  
Hammond, C.M., Johnson, W.D., Knoper, M., and Moore, J.,  
1986, Pyroclastic rocks associated with the Taylor Creek  
Rhyolite, Scales Canyon, New Mexico: New Mexico  
Geological Society Guidebook 37, p. 197-201.
- Le Guern, F., Gerlach, T.M., and Nohl, A., 1982, Field gas  
chromatography analyses of gases from a glowing dome at  
Merapi volcano, Java, Indonesia, 1977, 1978, 1979:  
Journal of Volcanology and Geothermal Research, v. 14,  
p. 223-245.
- Lindstrom, D.J. and Korotev, R.L., 1982, TEABAGS: computer  
programs for instrumental neutron activation analysis:  
Journal of Radioanalytical Chemistry, v. 70, p. 439-458.
- Lipman, P.W. and Christiansen, R.L., 1964, Zonal features of  
an ash-flow sheet in the Piapi Canyon Formation,  
southern Nevada: U.S. Geological Survey Professional  
Paper 501-B, p. B74-B78.
- London, D., 1986, Magmatic-hydrothermal transition in the  
Tanco rare-element pegmatite: evidence from fluid  
inclusions and phase-equilibrium experiments: The  
American Mineralogist, v. 71, p. 376-395.
- Lufkin, J.L., 1972, Tin mineralization within rhyolite flow-  
domes, Black Range, New Mexico: Ph.D. Dissertation,  
Stanford University, Stanford, 149 p. and New Mexico  
Bureau of Mines and Mineral Resources Open-File Report  
57.

- Lufkin, J.L., 1976, Oxide minerals inmiarolitic cavities, Black Range, New Mexico: *The American Mineralogist*, v. 61, p. 425-430.
- Matsuo, S., Ohsaka, J., Hirabayashi, J., Ozawa, T., and Kimishima, K., 1982, Chemical nature of volcanic gases at Usu volcano in Japan: *Bulletin Volcanologique*, v. 45, p. 261-264.
- Maxwell, C.H., Foord, E.E., Oakman, M.R., and Harvey, D.B., 1986, Tin deposits in the Black Range tin district: *New Mexico Geological Society Guidebook 37*, p. 273-281.
- McIntosh, W.C., Sutter, J.L., Chapin, C.E., Osburn, G.R., and Ratte', J.C., 1986, A stratigraphic framework for the eastern Mogollon-Datil volcanic field based on paleomagnetism and high-precision  $^{40}\text{Ar}/^{39}\text{Ar}$  dating of ignimbrites--a progress report: *New Mexico Geological Society Guidebook 37*, p. 183-195.
- Minayev, D.A., 1963, Geochemical differentiation of the rare earths: *Geochemistry*, 12, p. 1129-1149.
- Norrish, K., and Chappell, B.W., 1977, X-ray fluorescence spectrometry: in Zussman, J., ed. *Physical methods in determinative mineralogy*: Academic Press, p. 201-272.
- Norrish, K., and Hutton, J.T., 1969, An accurate x-ray spectrographic method for the analysis of a wide range of geologic samples: *Geochimica et Cosmochimica Acta*, v. 33, p. 431-453.

- Robie, R.A., Hemingway, B.S., and Fisher, J.R., 1979, Thermodynamic properties of minerals and related substances at 298.15 K and 1 bar ( $10^5$  pascals) pressure and at higher temperatures: U.S. Geological Survey Bulletin 1452, 465 p.
- Roedder, E., 1984, Fluid inclusions: Mineralogical Society of America, Reviews in Mineralogy, v. 12, 644 p.
- Ross, C.S., and Smith, R.L., 1961, Ash-flow tuffs: their origin, geologic relations, and identification: U.S. Geological Survey Professional Paper 388, 81 p.
- Smith, R.L., 1960, Ash flows: Geological Society of America Bulletin, v. 71, p. 795-842.
- Taylor, H.P., Jr., 1968, The oxygen isotope geochemistry of igneous rocks: Contributions to mineralogy and Petrology, v. 19, p. 1-71.
- Taylor, H.P., Jr., 1978, Oxygen and hydrogen isotope studies of plutonic granitic suites: Earth and Planetary science Letters, v. 38, p. 177-210.
- Taylor, H.P., Jr., 1979, Oxygen and Hydrogen isotope relationships in hydrothermal mineral deposits: in Barnes, H.L., ed., Geochemistry of hydrothermal ore deposits: John Wiley and Sons, New York, p. 236-277.

Table 1. Selected geochemical analyses of hydrated vitrophyre and mildly, moderately, and intensely vapor phase crystallized samples from three Taylor Creek Rhyolite domes.

Location * Intensity SAMPLE #	Nugget mild 143	Gulch mod 142	dome ¶ int 140	Boiler vit 149	Peak mod 131	dome ¶ int 152	Indian mild 207	Pk dome int 205
SiO <sub>2</sub>	77.15	77.05	76.91	74.54	76.26	76.59	76.39	76.67
TiO <sub>2</sub>	0.12	0.12	0.12	0.09	0.08	0.08	0.11	0.10
Al <sub>2</sub> O <sub>3</sub>	11.70	11.72	11.81	12.05	12.55	12.25	11.95	12.00
Fe <sub>2</sub> O <sub>3</sub>	1.23	1.19	1.18	1.13	1.24	1.20	1.17	1.21
MnO	0.03	0.05	0.05	0.06	0.05	0.07	0.05	0.05
MgO	0.16	0.28	0.17	0.13	0.15	0.16	0.02	0.01
CaO	0.26	0.46	0.22	0.40	0.53	0.44	0.23	0.17
Na <sub>2</sub> O	3.23	3.16	3.45	3.74	3.69	3.77	3.66	3.82
K <sub>2</sub> O	4.86	4.71	4.82	4.69	4.92	4.81	4.87	4.90
P <sub>2</sub> O <sub>5</sub>	0.01	0.02	0.02	0.01	0.01	0.01	0.01	0.01
LOI	0.50	0.84	0.43	2.36	0.50	0.46	0.26	0.04
TOTAL	99.25	99.60	99.18	99.20	99.98	99.84	98.72	98.98
As	16.4	4.3	4.3	2.4	4.1	<1.5	1.4	6.8
Ba	29	33	37	<16	<16	<16	19	31
Cl(%)	0.002	0.005	0.004	0.003	0.002	0.002	---	---
Cs	5.7	5.0	7.1	10.3	6.8	8.3	3.5	8.2
F(%)	0.06	0.17	0.16	0.2	0.26	0.15	---	---
Ga	20	19	19	22	22	22	21	21
Hf	7.2	7.1	7.8	7.9	8.0	7.8	7.8	7.9
Nb	35	33	34	47	44	41	50	48
Pb	24	26	16	36	32	30	28	28
Rb	293	288	290	360	416	420	392	393
Sb	0.6	0.4	0.1	0.4	0.1	0.2	0.2	0.1
Sc	2.4	2.6	2.9	2.4	2.4	2.2	1.8	1.9
Se	0.5	0.4	0.5	0.6	0.6	0.6	<2.1	<1.2
Sn	6	6	<5	11	<5	<5	5	<5
Sr	7	9	6	2	3	2	3	3
Ta	4.0	3.7	4.2	4.8	4.7	4.7	4.5	4.6
Th	31	30	32	41	43	39	35	37
U	10	7	8	14	11	8	6	9
Y	64	94	150	131	156	164	58	111
Zn	31	32	32	73	35	56	28	39
Zr	168	160	172	168	158	158	173	176
La	47	48	58	40	46	44	26	48
Ce	110	110	125	98	109	98	71	114
Nd	47	40	56	37	49	45	18	42
Sm	10.0	10.3	15.7	11.6	13.2	13.2	5.10	12.0
Eu	0.33	0.33	0.38	0.17	0.18	0.12	0.17	0.26
Tb	1.5	1.8	2.6	2.3	2.9	2.9	1.0	2.4
Yb	9.5	10.8	16.3	13.8	19.9	18.5	6.1	13.1
Lu	1.21	1.57	2.35	1.94	2.64	<2.50	0.99	2.17

\*

vit-vitrophyre; mild-mild vapor phase crystallization; mod-moderate vapor phase crystallization (lithophysal rhyolite); int-intense vapor phase crystallization.

Table 2. Oxygen isotope analyses for whole rock rhyolite samples and mineral separates. Values in per mil SMOW.

#	per mil	loc.*	remarks
116	7.6	MC	very mild VPC
	7.7	MC	quartz separate from 116
115	9.9	MC	mild VPC
122	9.3	MC	intense VPC
149	8.8	PC	vitrophyre (hydrated)
	7.5	PC	quartz separate from 149
131	6.1	PC	intermediate VPC (lithophysae)
	7.5	PC	quartz from lithophysae in 131
152	7.5	PC	intense VPC
136	7.3	NG	very mild VPC
	7.7	NG	quartz separate from 136
140	7.6	NG	intense VPC
141	7.2	NG	intense VPC
167	9.0	KM	very mild VPC
	7.8	KM	quartz separate from 167
168	8.4	KM	intense VPC

#--Sample Number

\*--location

MC--Monticello Cutoff

PC--Paramount Canyon

NG--Nugget Gulch

KM--Kemp Mesa

Table 3. Fluid inclusion microthermometric data for overgrowths on quartz phenocrysts and quartz and topaz from lithophysal cavities.

---

Sample (1)	Loc. (2)	Min. (3)	Type (4)	Tmc (5)	Th (6)
LQTZ1	SC	QUARTZ	PS-S	364	>600
	SC	QUARTZ	PS-S	360	>600
LQTZ2	PC	QUARTZ	P-PS	350	>600
TOPAZ1	RM	TOPAZ	P	350	>600
	RM	TOPAZ	P	352	>600
	RM	TOPAZ	P	---	>600
	RM	TOPAZ	P	353	>600
	RM	TOPAZ	P	350	680
	RM	TOPAZ	P	360	>600
TOPAZ2	BP	TOPAZ	PS-S	325	>600
RHYOLITE	PC	QUARTZ	P	470	>600
	PC	QUARTZ	P	500	>600
	PC	QUARTZ	P	500	>600
	PC	QUARTZ	P	530	>600
	PC	QUARTZ	P	---	730
	PC	QUARTZ	P	---	720

---

- 1) LQTZ1 and LQTZ2- quartz from lithophysae  
TOPAZ1 and TOPAZ2- topaz from lithophysae  
RHYOLITE- rhyolite from intense VPC zone
- 2) Location SC-Scales Canyon; PC-Paramount Canyon;  
RM-Round Mountain; BP- Boiler Peak
- 3) Host mineral
- 4) Type of inclusion  
P-primary  
PS-pseudosecondary  
S-secondary
- 5) Melting temperature of crystalline solid in ° C.
- 6) Homogenization temperature in ° C.



Figure 1. Location map for the zones of intense vapor-phase crystallization described in the text. Locations of domes discussed in text are underlined. Taylor Creek Rhyolite domes: MC-Monticello cutoff; IP-Indian Peaks; NNG-North Nugget Gulch; NG-Nugget Gulch; SC-Squaw Creek; NPC-North Paramount Canyon; BP-Boiler Peak; PC-Paramount Canyon area of Boiler Peak dome; AC-Alexander Cienega; RM-Round Mountain; IC-Indian Creek; TC-Taylor Creek; KM-Kemp Mesa. DP-rhyolite of Dolan Peak. IM-granite of Iron Mountain. MC-rhyolite of Willow Springs Draw.

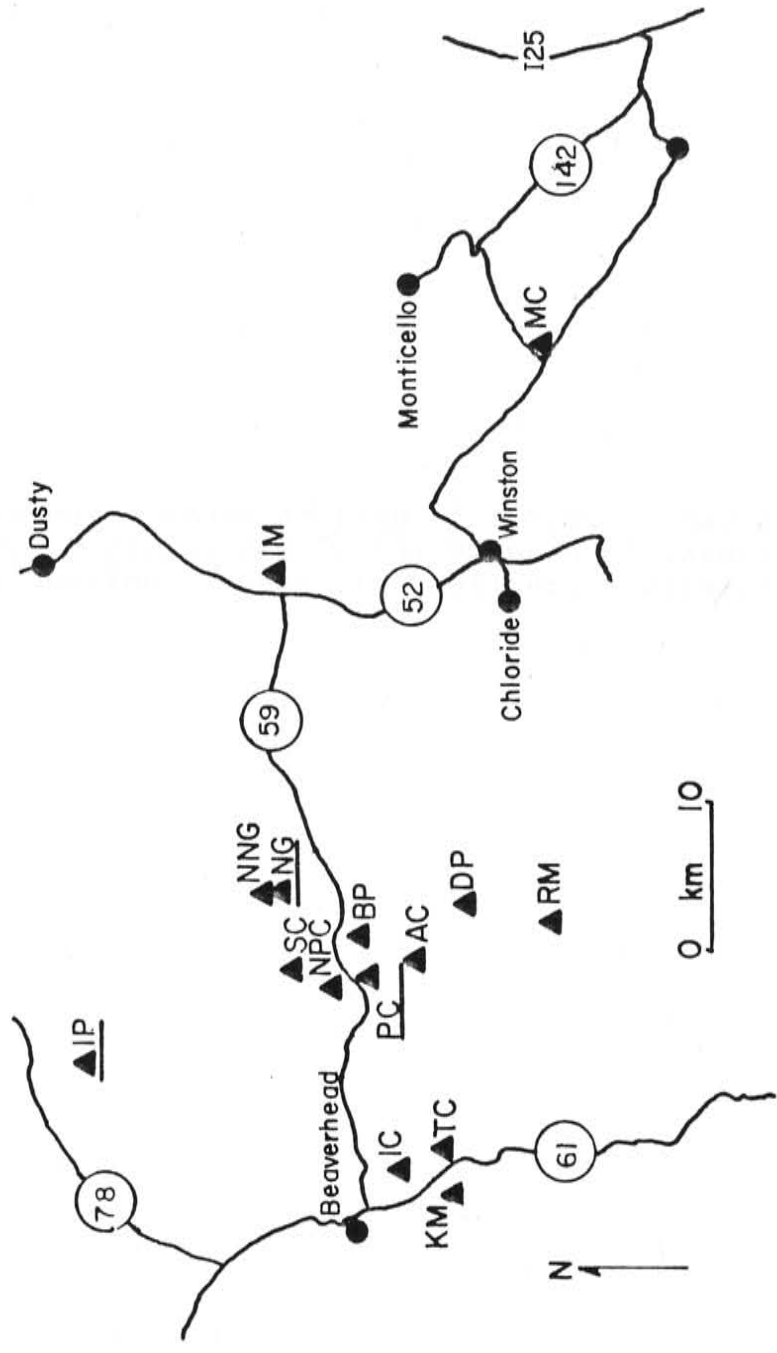
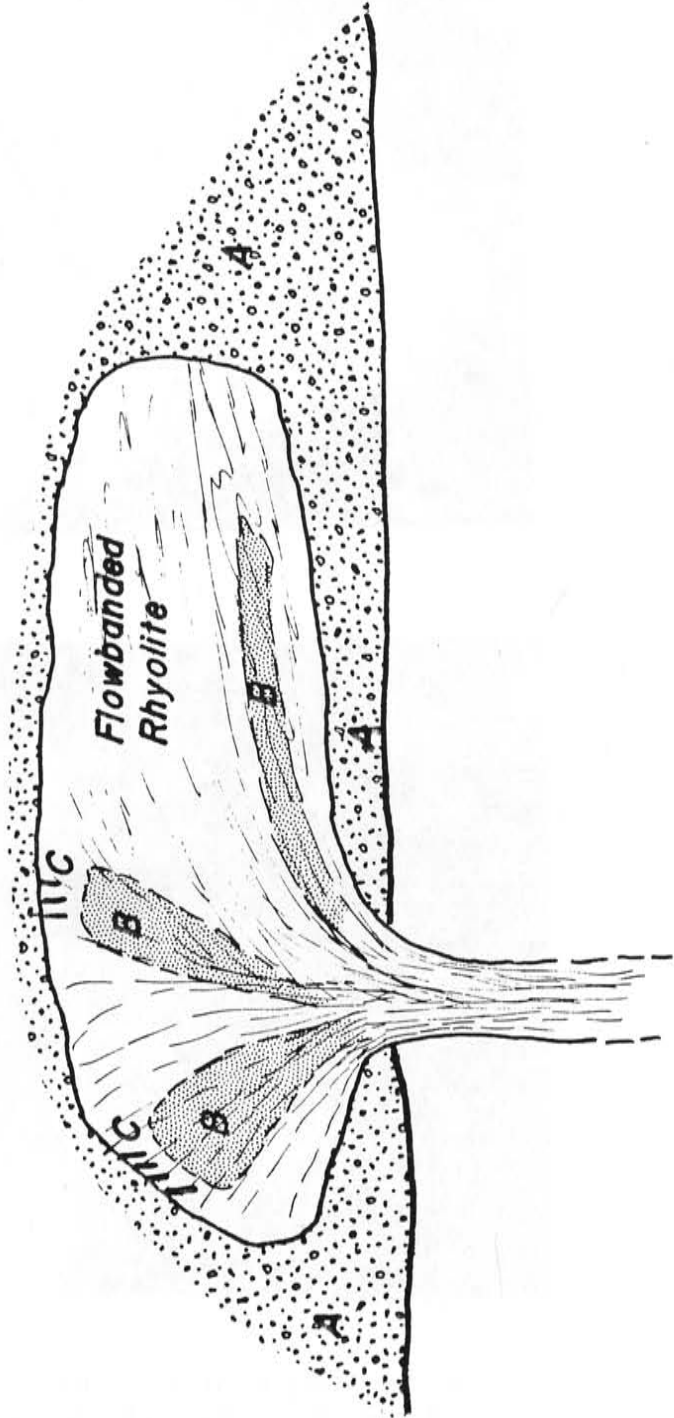
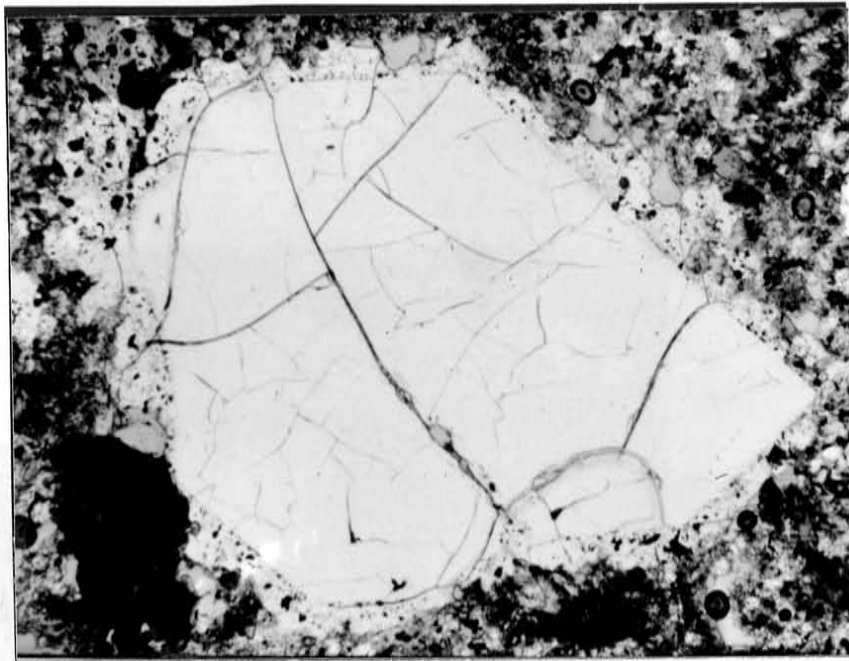
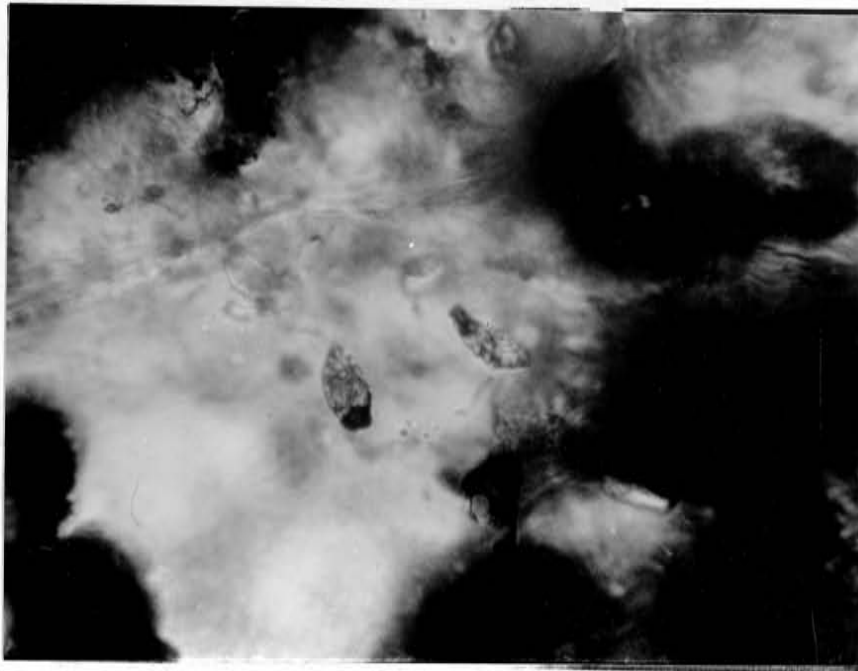


Figure 2. Schematic cross section of a typical Taylor Creek Rhyolite dome. A-carapace breccia; B-zones of intense vapor-phase crystallization; C-hematite-cassiterite veinlets.



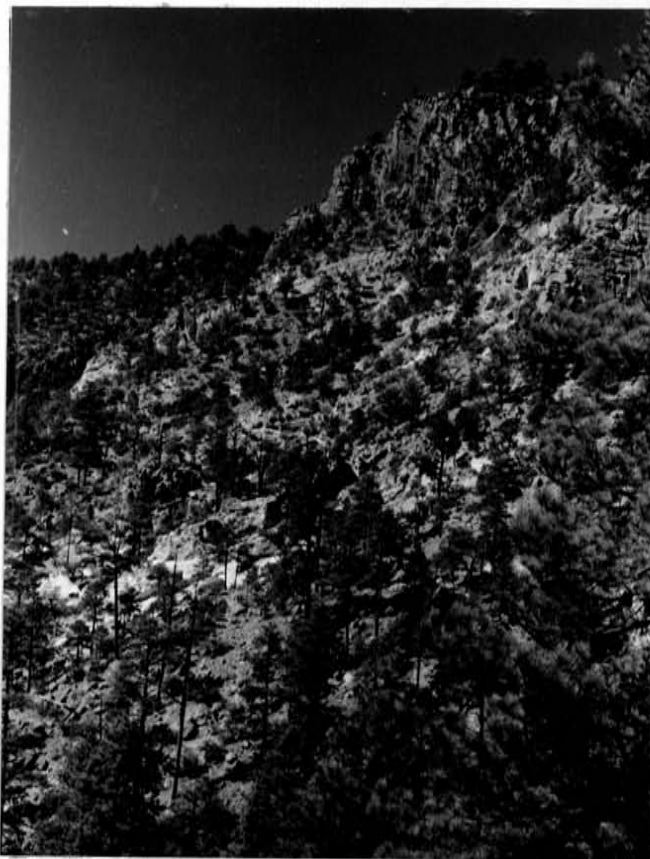


a



b

Figure 3. a) Photograph of a quartz phenocryst with an overgrowth (Field of view =2.5 mm). The overgrowth is marked by numerous multisolid-vapor and vapor inclusions. b) Multisolid-vapor inclusion in overgrowth above. Inclusion in the center of B is about 10  $\mu$ m long. Note the granophyric groundmass surrounding the phenocryst.



Lithophysal rhyolite

Zone of intense vapor-  
phase crystallization

Figure 4. Typical exposure of zones of intense vapor-phase crystallization. The white material in the foreground is "punky", intensely vapor-phase crystallized rhyolite. The cliffs at the top of the photograph are lithophysal rhyolite. Lithophysae increase in size upward from the base of the cliff.

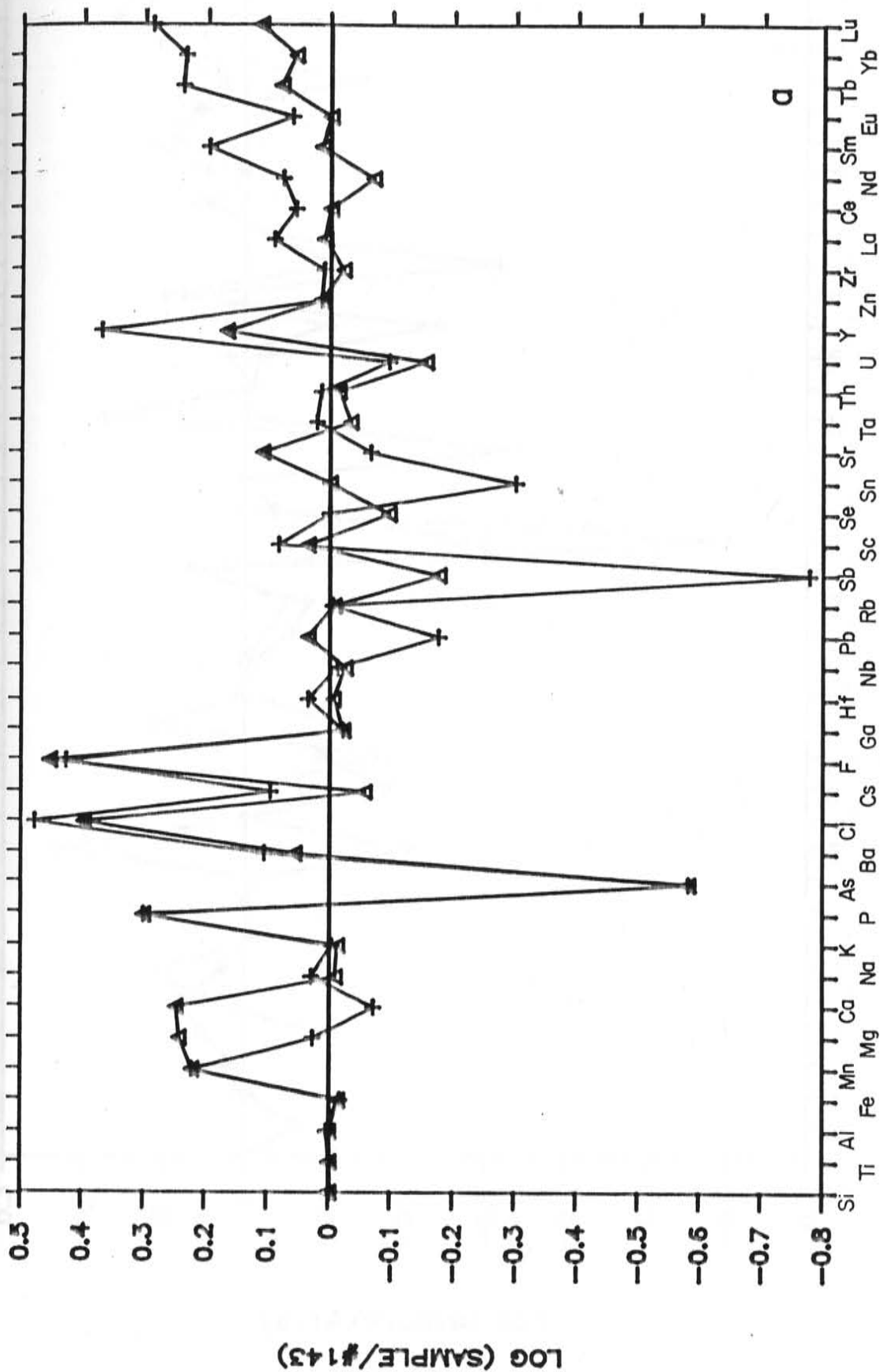


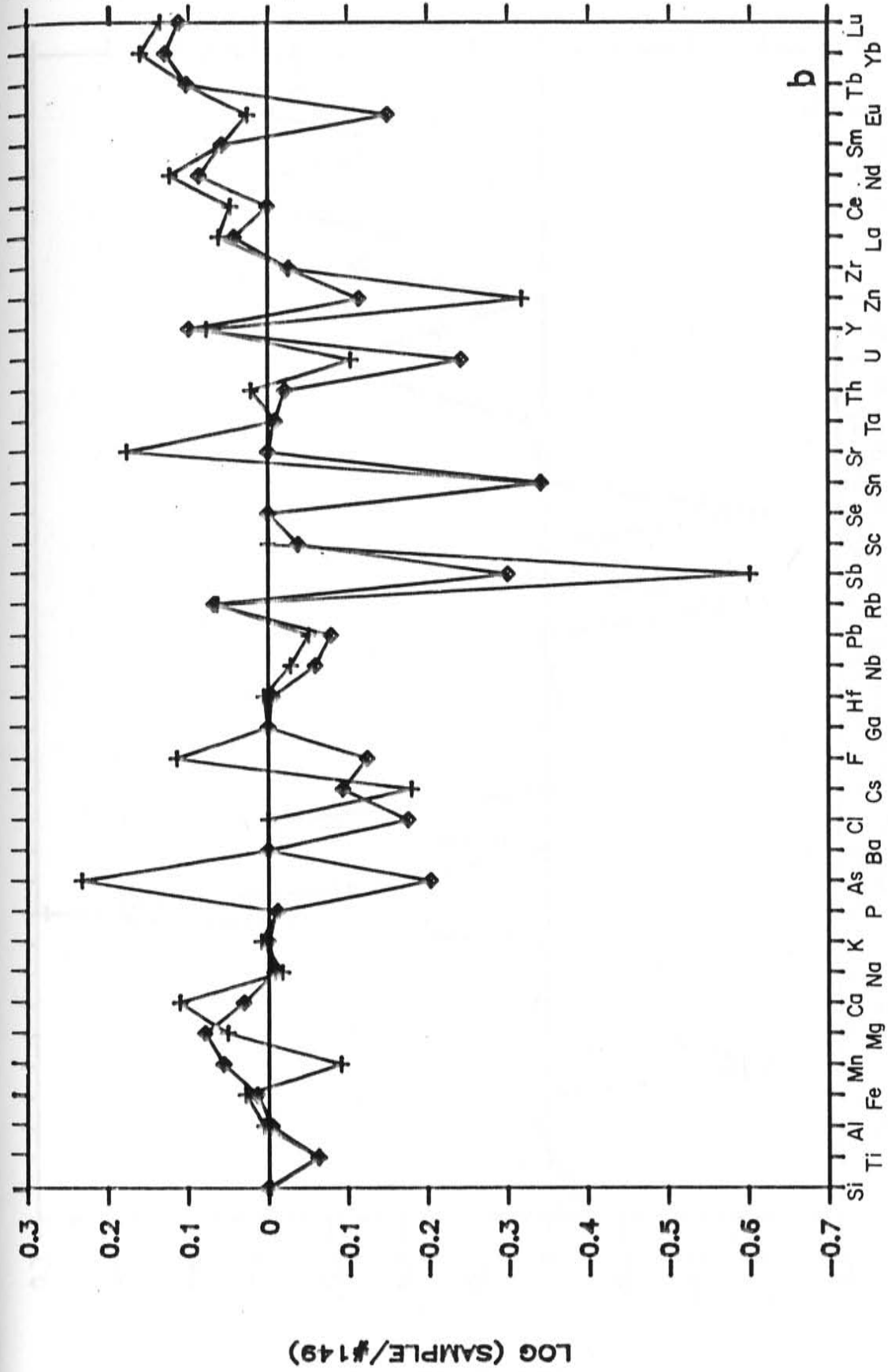
Figure 5. Photograph of lithophysal, flow banded rhyolite from the exposures at the top of Figure 4.



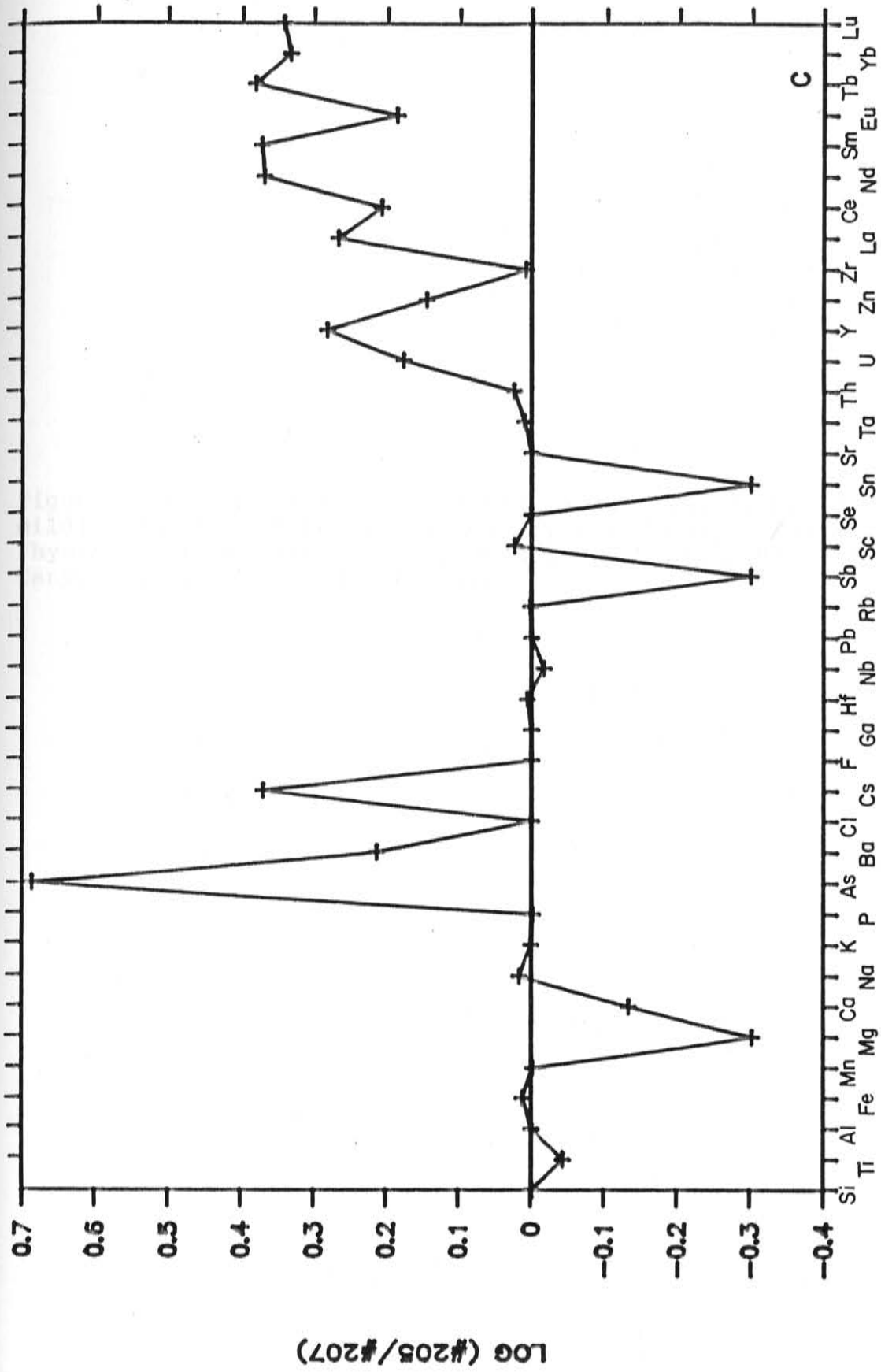
Figure 6. Enrichment-depletion diagrams for moderate and intense VPC compared to mild VPC.

- a) Nugget Gulch dome normalized to sample #143 (Table 1). Crosses-#140, intense VPC; Triangles-#142, moderate VPC, lithophysal rhyolite. Sn in #142 is <5 ppm.
- b) Paramount Canyon area of Boiler Peak dome normalized to sample #149. Crosses-#131, moderate VPC, lithophysal rhyolite. Ba <16 ppm, Sn <5 ppm. Diamonds-#152, intense VPC. As <1.5 ppm, Ba <16, Sn <5, Lu <2.5 ppm. Ba in normalizing sample (#149) <16 ppm.
- c) Indian Peaks dome normalized to sample 207. #205-Intense VPC only. F, Cl not determined, Se < detection, Sn in # #205 <5 ppm.





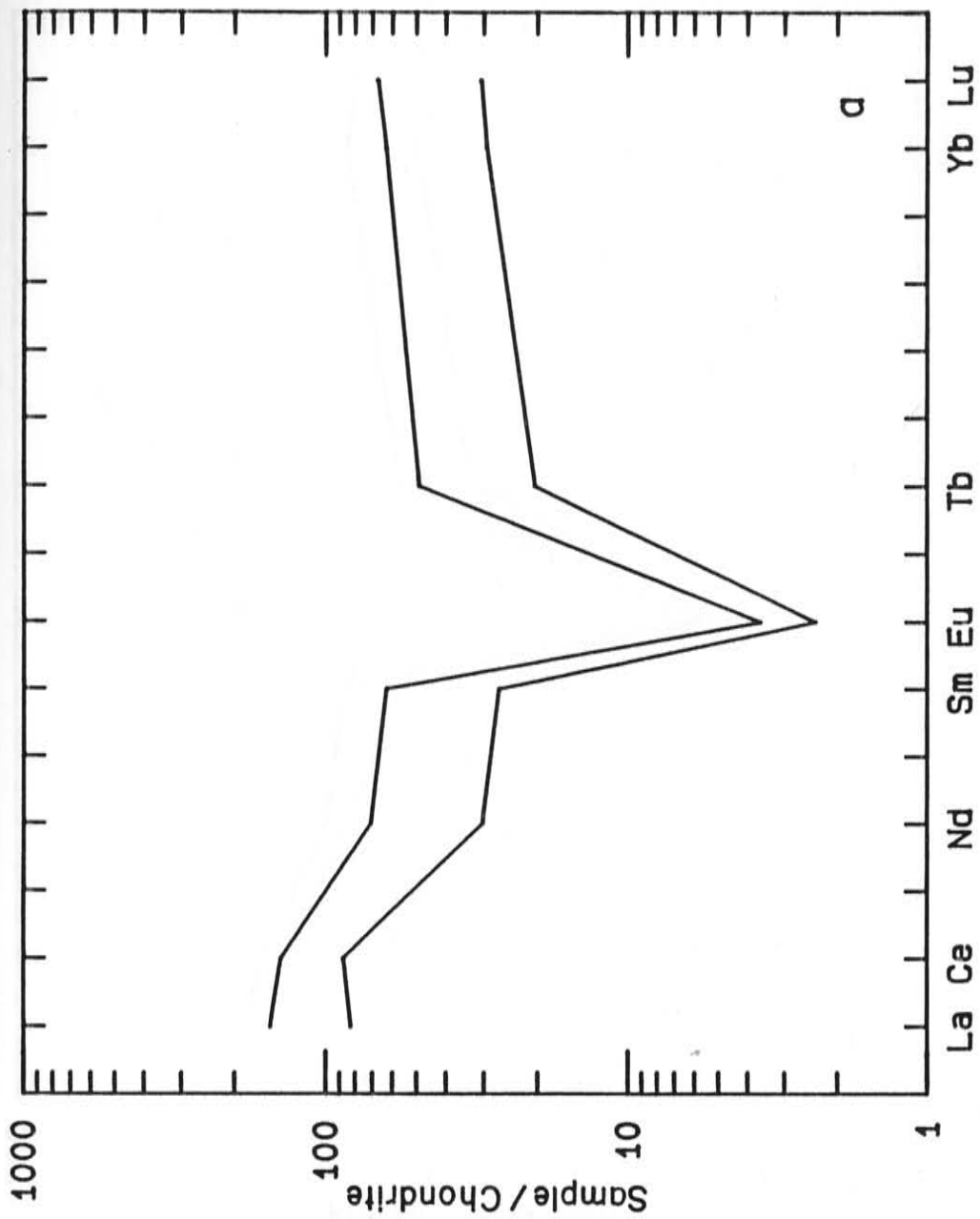
b

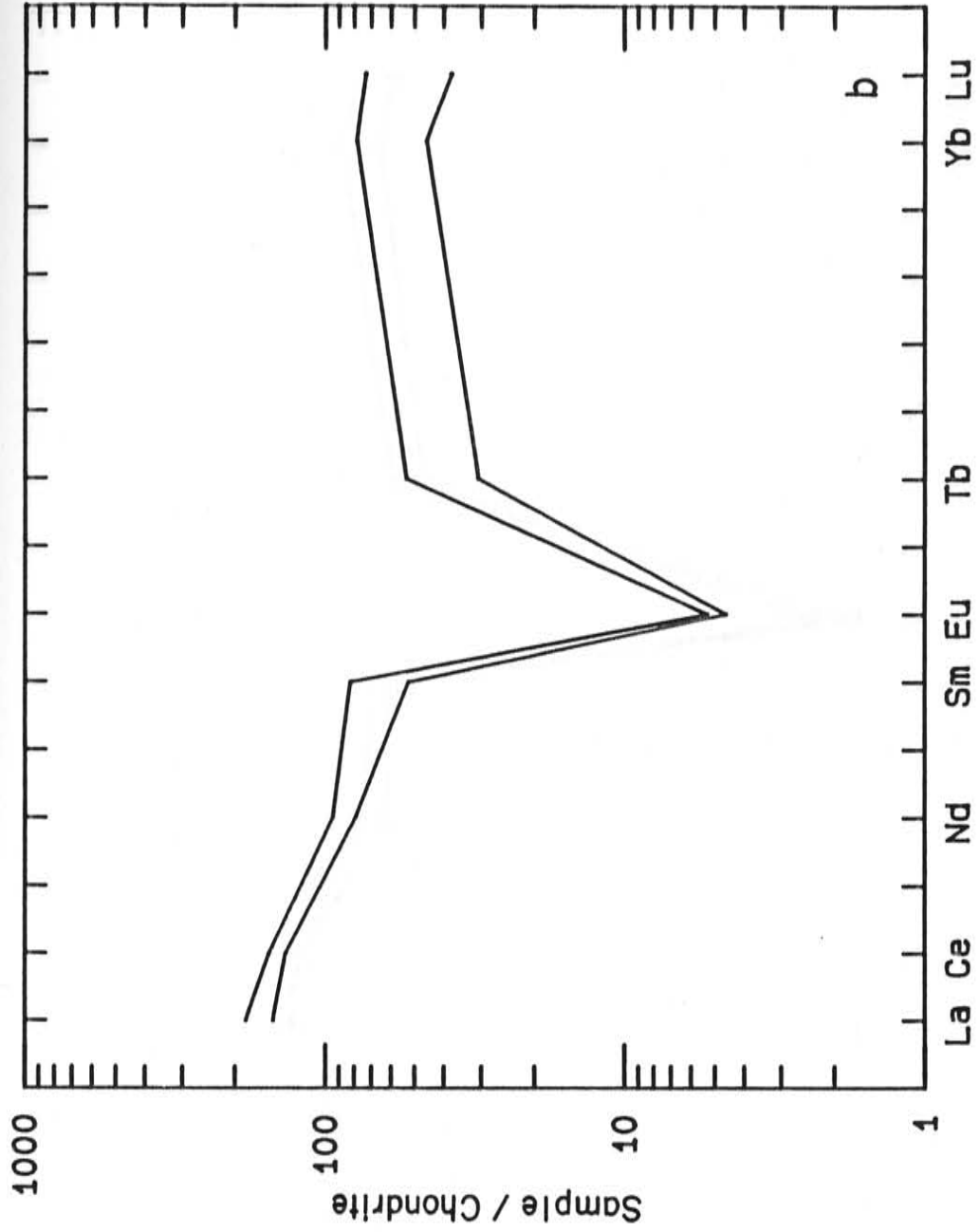


ELEMENTS

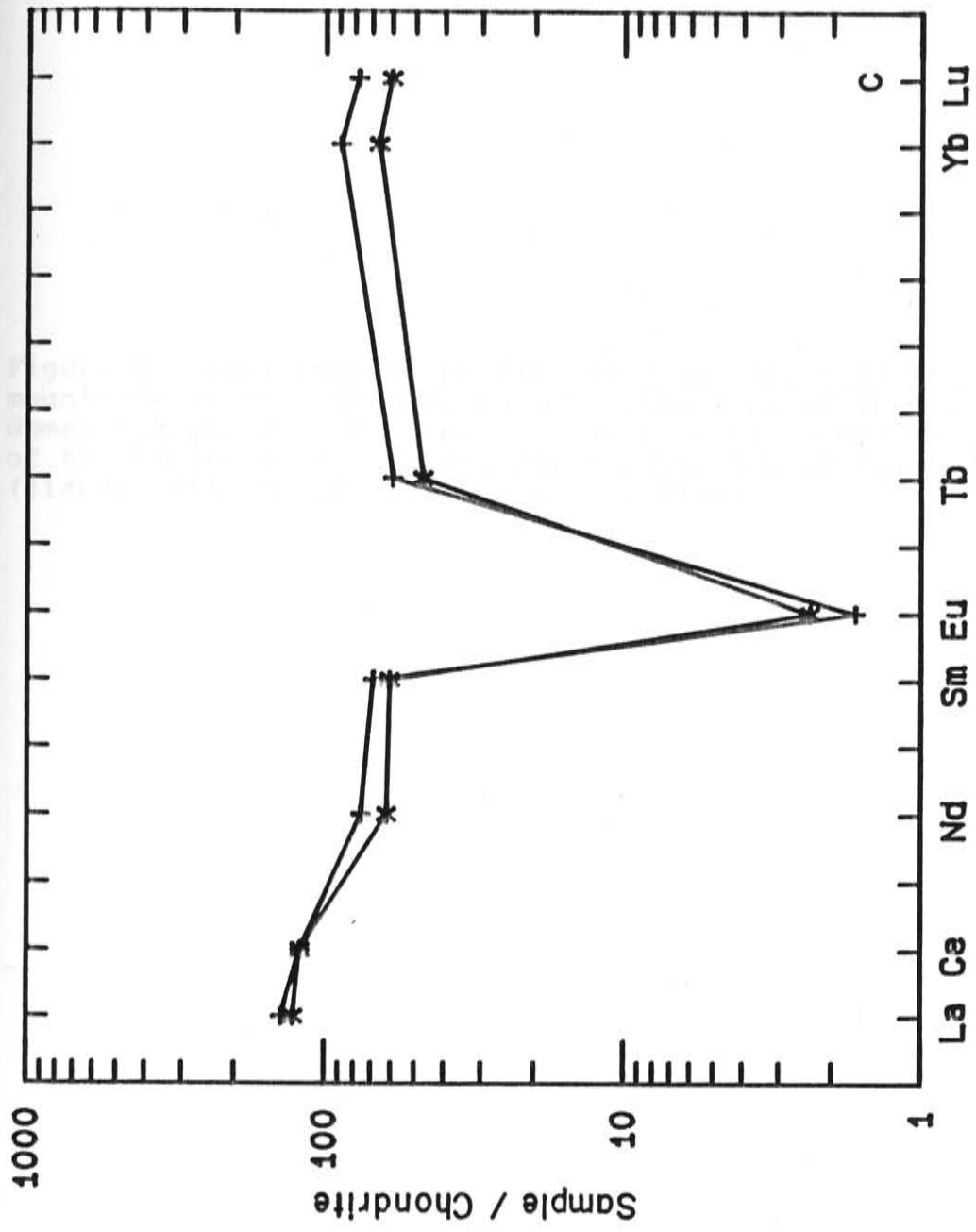
C

Figure 7. Chondrite normalized rare earth element plots for mildly (lower pattern) and intensely vapor-phase crystallized rhyolite (upper pattern). A) Nugget Gulch area, B) Paramount Canyon area, C) Indian Peaks area.









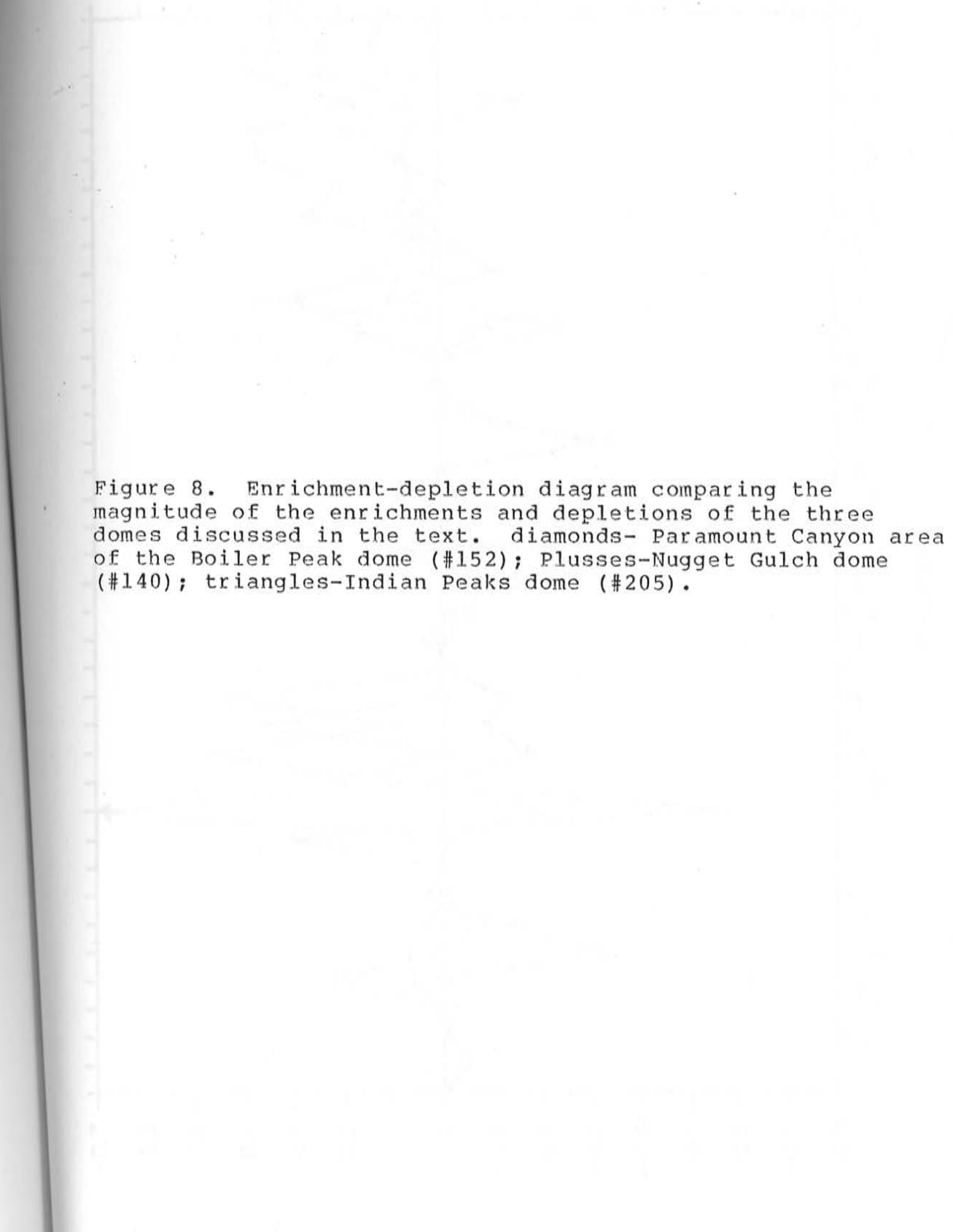
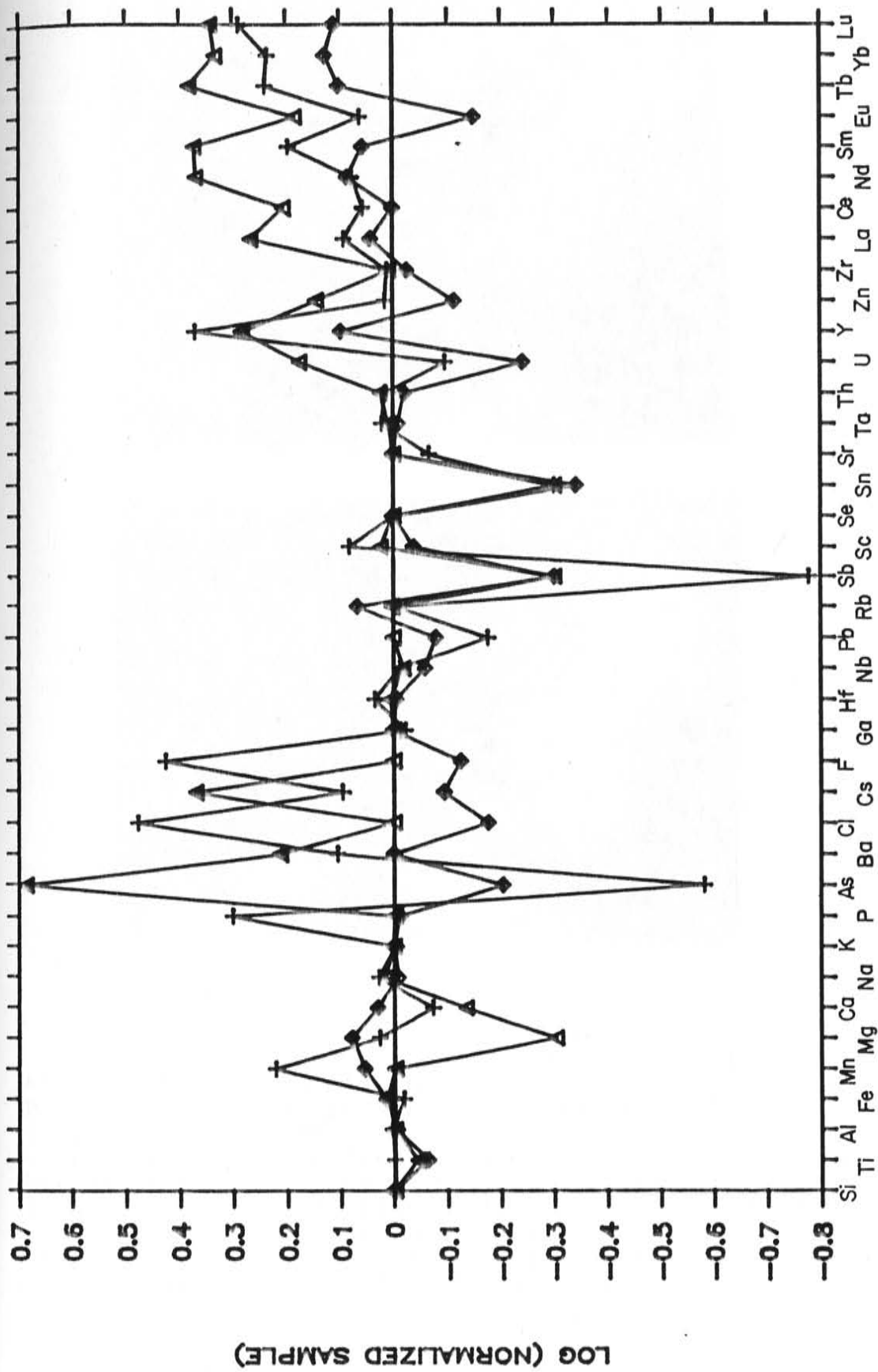
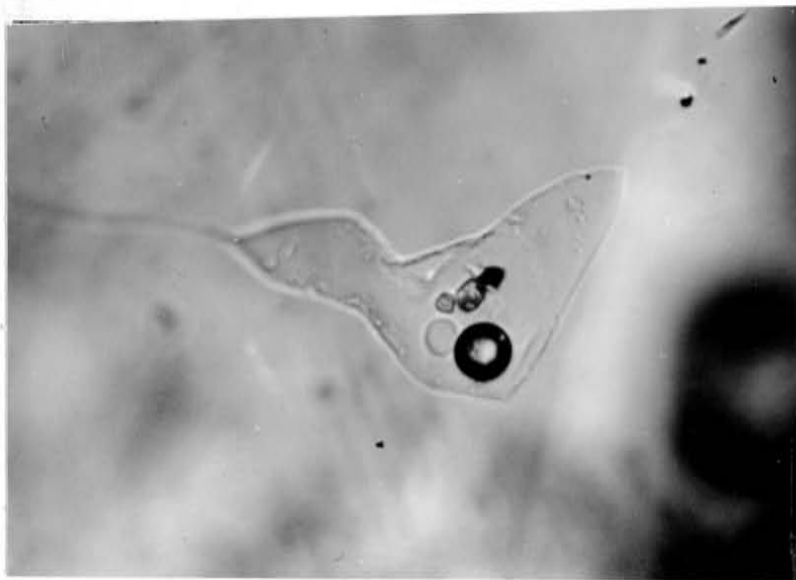


Figure 8. Enrichment-depletion diagram comparing the magnitude of the enrichments and depletions of the three domes discussed in the text. diamonds- Paramount Canyon area of the Boiler Peak dome (#152); Plusses-Nugget Gulch dome (#140); triangles-Indian Peaks dome (#205).





a

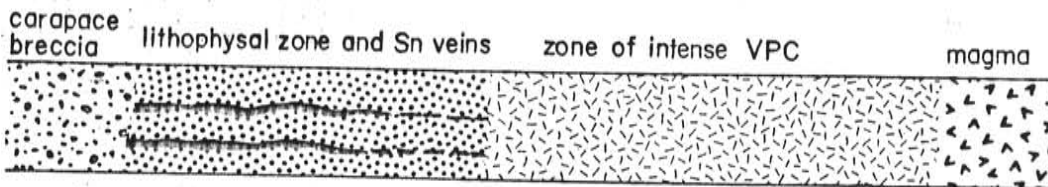


b

Figure 9. Large multisolid-vapor inclusion in topaz from Round Mountain (Figure 1). a) The inclusion is about 80  $\mu\text{m}$  long and at 25° C, consists of a microcrystalline solid with a large rhombohedral(?) daughter mineral and a vapor bubble that is deformed by the microcrystalline solid. b) At 400° C, the crystalline solid is molten and the large rhombohedral daughter mineral is nearly dissolved (round crystal touching vapor bubble). Three other daughter minerals are visible below the vapor bubble.

Figure 10. Schematic diagram of VPC system showing the temperatures, depth,  $f_{O_2}$ , and chemical trends exhibited by each zone. The  $f_{O_2}$  of air at the surface is that of air at 25° C. Other  $f_{O_2}$ 's are calculated at 650° C from the data of Robie and others (1979). The  $f_{O_2}$  of the magma is estimated from the diagrams of Haggerty (1976) at 800° C. Temperatures are fluid inclusion homogenization temperatures.

authigenic minerals	no change	chemical trends	inconsistent	log $f_{O_2}$	temp depth
	enrichments	depletions		o C	meters
wood tin				-0.7	25
quartz	Sn, As, Sb, Fe, Co, Cr, W, U, Pb				
hematite	Si, Al,		As, Cl, Pb,		20-
cassiterite	Fe, Na,	Ti, Cs,	Rb, Zn	-14	650
pseudo- brookite	P, Ga, Hf, Sc, Ta,	Nb, Sb, Sn, U			
bixbyite	Th, Zr				
topaz					
beryl					
quartz					
sanidine(?)					<100
quartz	Si, Al, Fe				
sanidine	Mn, Mg, Ca	Ba, Cs, Y, REE	As, Cl, F		
hematite(?)	Na, K, P, Ga, Hf, Rb Se, Ta, Th Zr	Ti, Nb, Pb Sb, Sn, U	Sc, Sr, Zn	-15	730
					>200
				-15	>800



In the magma chamber, the fluids are saturated with: Si, Al, Ca, Na, K, P, Rb, Y, Th, REE

CHAPTER 3

With the exception of the strontium isotope data, all data in this chapter was collected by Ted L. Eggleston. David I. Norman collected the strontium isotope data and advised this thesis. Ted L. Eggleston is responsible for interpreting all the data. Ted L. Eggleston collected the oxygen isotope data in the laboratory of Samuel M. Savin.



(196)

PETROLOGY OF TIN-BEARING RHYOLITES,  
NORTHERN BLACK RANGE AND SIERRA CUCHILLO,  
NEW MEXICO

Ted L. Eggleston and David I. Norman  
New Mexico Institute of Mining and Technology  
Socorro, New Mexico

and

Samuel M. Savin  
Case Western Reserve University  
Cleveland, Ohio

ABSTRACT

Three Oligocene tin-bearing, high-silica rhyolite formations occur in the northern Black Range and Sierra Cuchillo of southwestern New Mexico. Each of the tin-bearing rhyolite formations consists of widely separated lava domes and short flows containing variable proportions of quartz and sanidine phenocrysts in a granophyric groundmass.

Quartz/sanidine ratios are variable. Plagioclase, biotite, and amphibole are minor phases and zircon and sphene are present in trace quantities.

These rhyolite lavas are enriched in  $\text{SiO}_2$ ,  $\text{K}_2\text{O}$ , Rb, Nb, Th, and U and depleted in CaO, Sr, and Ba compared to average rhyolite and granite. The major element composition of the lavas is virtually identical with the exception of  $\text{TiO}_2$ .  $\text{TiO}_2$  decreases from with increasing Rb. Nb, Ta, and Th increase with increasing Rb and Ba, Sc, and Sr decrease with increasing Rb in the magmas. Rare-earth element patterns are flat with large negative Eu anomalies. The middle rare-earth elements exhibit a distinct sag relative to the light and heavy rare earth elements.

Initial  $^{87}\text{Sr}/^{86}\text{Sr}$  ratios for the tin-bearing rhyolites are between 0.708 and 0.713. The oxygen-isotopic composition of quartz phenocryst separates from the rhyolites are between 7.5 and 7.8 ‰.

Crystal-liquid fractionation models suggest that crystallization of plagioclase, K-feldspar, and quartz in a shallow magma chamber produced trace element covariations observed in the rhyolites and controlled the major element concentrations in the rhyolite magmas. The rare earth concentrations were controlled by plagioclase, allanite, and sphene crystallization. Variable contamination of the rhyolite magmas produced the variations of initial  $^{87}\text{Sr}/^{86}\text{Sr}$  ratios. Major and trace element modeling with the mode present in the rocks will not produce the elemental trends observed in the rocks; however, modelling with the same

minerals in different ratios will produce most of the trace element variations observed in the tin-bearing rhyolite lavas.

The lack of intermediate composition volcanic rocks associated with the tin-bearing rhyolites argues against an upper mantle source for the tin-bearing rhyolite magmas because of the large amounts of crystal-liquid fractionation required to produce the tin-bearing rhyolites from mantle derived, alkali basalts. Partial melting of lower to mid-crustal, felsic granulites can produce magmas very similar to A-type granites in composition. Crystallization of plagioclase and amphibole from the A-type granite composition melts produced the most mafic of the tin-bearing rhyolite magmas.

## INTRODUCTION

Tin-mineralized, high-silica rhyolite lavas occur in the upper parts of the Tertiary volcanic section of the northern Black Range of New Mexico and Sierra Cuchillo of southwestern New Mexico (Fig. 1; Eggleston and Norman, 1987). These chemically and petrographically similar rhyolites overlie a thick pile of basaltic andesite lava flows. Tin mineralization associated with these rhyolite lavas was deposited from high-temperature ( $>700^{\circ}$  C) magmatic fluids (Eggleston and others, 1987b) in a very near-surface environment. Understanding the origin of the magmatic fluids

and the magmas that produced them are thus important to understanding the genesis of the tin deposits.

In this paper we investigate the petrogenesis of the tin-bearing rhyolites using major, trace, and rare-earth element and strontium and oxygen-isotope geochemistry. Geochemical data for the underlying basaltic andesites and rhyolites in the upper part of the Tertiary volcanic section are also presented. Duffield (1986) and Ruiz and others (1986) discussed the petrology of the Taylor Creek Rhyolite and reported  $E_{Nd}$  values of -5.2 to -6.2 and initial  $^{87}Sr/^{86}Sr$  values of 0.707 to 0.714 for the Taylor Creek Rhyolite. They concluded that the Taylor Creek Rhyolite had a lower crustal origin with a possible upper mantle-derived component.

Huspeni and others (1984) published an account of the petrogenesis of the tin-bearing rhyolite lavas of Durango, Mexico. They concluded that the tin-bearing rhyolites in Mexico formed "as extreme differentiates in high-level magma chambers closely related to caldera development". They reported initial  $^{87}Sr/^{86}Sr$  ratios of 0.706 to 0.707 and concluded that those values were not distinctive of either an upper mantle or a lower crustal source for the parent magmas. Ruiz and others (1986) also investigated the strontium and neodymium isotope systematics of the tin-bearing rhyolites in Mexico and reported initial  $^{87}Sr/^{86}Sr$  ratios of 0.706 to 0.707 and  $E_{Nd}$  values of 0 to -2. The strontium and neodymium values for the rhyolites are similar to granulite xenoliths in the region leading Ruiz and others (1986) to conclude that the tin-bearing rhyolites were derived from the crust.

Studies of broadly similar, tin-barren high-silica, topaz rhyolites in the western U.S. have been published by Burt and others (1982), Christiansen (1981), and Christiansen and others (1983, 1984, 1986). These rhyolites contain as much as 40% phenocrysts of quartz and sanidine with little biotite and/or amphibole and are thus believed to be relatively dry melts. The tin-bearing rhyolites of Durango, Mexico (Huspeni and others, 1984), the ongonites of Mongolia and the Trans-Baikal region of the U.S.S.R. (Kovalenko and Kovalenko, 1984), the tin-bearing rhyolites of the Sheep Creek Range in Nevada (Fries, 1942), and the stocks that host Climax-type Mo porphyry systems (Burt and others, 1981) are similar rocks. The similarities have been discussed at length by Christiansen and others (1986).

#### REGIONAL GEOLOGIC AND TECTONIC SETTING

##### Regional Geologic Setting

The Black Range forms the eastern margin of the Mogollon Plateau, which has been little affected by faulting associated with the Rio Grande rift to the east (Fig. 1). This plateau is a highland area about 125 km in diameter that has acted as a stable block since the middle Tertiary. The Sierra Cuchillo, in contrast, is a horst block situated between the Winston Graben and the Palomas Basin of the Rio Grande rift (Kelley, 1979). Although the Winston Graben now separates the Black Range from the Sierra Cuchillo, the similar stratigraphic sections indicate that the volcanism

was continuous over the region.

The Taylor Creek Rhyolite is situated near the top of the Tertiary volcanic pile near the center of the Mogollon-Datil volcanic field. Details of the stratigraphy can be found in Eggleston and Norman (1987). The volcanic stratigraphy can be divided into two large age groups. The lower group consists of dominantly andesitic lavas and volcanoclastic sedimentary rocks known as the Rubio Peak Formation. Felsic ignimbrites, believed to be products of caldera eruption, are common in the uppermost part of the lower group (Elston, 1984). The age of this group is between about 44 and 35 Ma (Elston, 1976; McIntosh and others, 1986).

The upper group consists of basaltic andesite lavas and high-silica rhyolite lavas and ignimbrites (Table 1). The tin-bearing rhyolite lavas, are located near the top of this group. These rhyolite lavas and ignimbrites were erupted between about 30 and 27 Ma (McIntosh and others, 1986). Elsewhere in the Mogollon-Datil volcanic field, numerous major caldera eruptions produced several thousand km<sup>3</sup> of rhyolite ignimbrites (McIntosh and others, 1986). Most of those ignimbrites were high-silica rhyolite. Basaltic andesite lava flows are intercalated with the ignimbrites in many parts of the region.

#### Tectonic Setting

Cather (1986) and Elston (1984) suggest that extension began in this segment of the Rio Grande rift before 36 Ma. The beginning of extension was marked by a change from

calcalkaline volcanism to bimodal basaltic andesite-rhyolite volcanism and basin formation in much of what is now the Rio Grande rift. The hiatus in pyroclastic volcanism between 35 and 28 Ma appears to be an essentially anorogenic period or a period of very slow extension. At about 28-29 Ma, extension accelerated and is marked by the voluminous, regional ignimbrites erupted between 29 and 27 Ma (Chapin and Seager, 1975; Seager and Morgan, 1979; McIntosh and others, 1986). The tin-bearing rhyolites were erupted during this period of accelerated extension.

#### LOCAL GEOLOGY

Figure 2 is a geologic sketch map of a portion of the northern Black Range, New Mexico. Two tin-bearing rhyolite formations occur in the Black Range; the Taylor Creek Rhyolite and the rhyolite of Dolan Peak. Exposures of the Taylor Creek Rhyolite are found in a north-south trending belt 50 km long by 25 km wide. Reconnaissance mapping of the rhyolite of Dolan Peak indicates that the rhyolite of Dolan Peak is restricted to a north-south-trending belt 10 km long by 5 km wide, east of the Taylor Creek Rhyolite exposures. The stratigraphy of the Sierra Cuchillo is virtually identical to that of the Black Range.

These tin-bearing rhyolites are among the youngest volcanic units the northern Black Range and Sierra Cuchillo.  $^{40}\text{Ar}/^{39}\text{Ar}$  dating of regional ignimbrites above and below the



Taylor Creek Rhyolite bracket it between  $28.18 \pm 0.15$  Ma and  $28.76 \pm 0.15$  Ma (McIntosh and others, 1986). A single  $^{40}\text{Ar}/^{39}\text{Ar}$  date of  $28.18 \pm 0.15$  Ma has been determined by B. McIntosh (1986, oral communication). Heyl and others (1983) report a fission track date of  $27.8 \pm 1$  Ma for the tin-bearing rhyolite in the Sierra Cuchillo.

The rhyolite of Dolan Peak underlies a  $28.76 \pm 0.15$  Ma ignimbrite at the base of the Taylor Creek Rhyolite (Eggleston and Norman, 1987). Both tin-bearing rhyolite units comprise numerous discrete domes and flows that locally coalesce to form eruptive centers as much as 15 km across. An individual dome-flow complex is typically 3 to 5 km long, 2 to 4 km wide, and as much as 300 m thick. Volume of the individual domes is between 2 and  $6 \text{ km}^3$ . More than  $100 \text{ km}^3$  of tin-bearing, high-silica rhyolite lavas were erupted. Small volume pyroclastic flows, surge deposits, and fall deposits typically enclose the individual domes (Fig. 2) and are believed cogenetic with the domes. Within these eruptive centers, the relative age of the domes is determined by overlapping relations between the domes.

The tin-bearing rhyolites are divided into Groups, A, B, C, and D based on phenocryst mineralogy, relative age and similarities of trace element compositions (Table 2). Each of the groups form a cluster on trace element variation diagrams. Age, mineralogical and chemical differences between the four groups will be discussed in the appropriate sections.

Immediately below the tin-bearing rhyolite section is 40

to 50 m of brick-red, flow-banded rhyolite lava informally known as the rhyolite of Sawmill Peak that, in turn, overlies as much as 200 m of basaltic andesite of Poverty Creek. The age of the rhyolite of Sawmill Peak and the basaltic andesite of Poverty Creek is between 28.8 and 35.2 Ma (McIntosh and others, 1986).

In the extreme southwestern corner of the study area, three rhyolite domes underlie the Taylor Creek Rhyolite and overlie an unknown thickness of andesite (Fig. 2) (Richter and others, 1986). The age of these rocks is unknown, but they are older than the Taylor Creek.

A fine-grained, aplitic granite associated with fluorine-rich skarn mineralization occurs in the northern Sierra Cuchillo (Jahns, 1944). This intrusive, the granite of Iron Mountain, is chemically similar to the tin-bearing rhyolite lavas (Table 1) and has been dated by conventional K-Ar at  $29.9 \pm 1.1$  Ma (Chapin and others, 1978). This granite occurs as a north-south trending elongate mass about 5 km long by 2 km wide. The aplitic textures and stratigraphic position suggests that the intrusive crystallized at shallow levels. Burt and Sheridan (1982) suggested that the granite of Iron Mountain is a subvolcanic equivalent of the tin-bearing rhyolites in the region.

## ANALYTICAL PROCEDURES

Major elements were determined on fusion disks by X-ray fluorescence spectrometry (Norrish and Hutton, 1969). Trace elements were determined on pressed pellets using either the rhodium K-alpha compton peak or calculated mass absorption coefficients to correct for mass absorption (Norrish and Chappel, 1977). Instrumental neutron activation analyses for the rare earth elements and trace elements used the technique of Jacobs and others (1977). Data reduction used either Nuclear Data software of the software package TEABAGS (Lindstom and Korotev, 1982). Chlorine was determined by titration (American Public Health Association, 1976). Fluorine was determined by ion-specific electrode (Bodkin, 1977). Details of the instrumental procedures are found in Eggeston and Norman (1987a).

Oxygen-isotopic analyses were performed on a Nier Type mass spectrometer following extraction of oxygen by the bromine pentafluoride technique of Clayton and Mayeda (1963). Sr isotopic and Rb and Sr isotope dilution analyses were performed on a VG model 354 mass spectrometer at the Mineralogisk-Geologisk Museum, Oslo, Norway. Twenty-three replicate analyses of NBS 987 performed before and during the analyses reported here yield  $^{87}\text{Sr}/^{86}\text{Sr} = 0.71020 \pm 13$  (2 sigma).  $^{87}\text{Sr}/^{86}\text{Sr}$  values were normalized to  $^{86}\text{Sr}/^{88}\text{Sr} = 0.1194$ .

### Tin-Bearing Rhyolites

Group A rhyolites consist of phenocrysts of sanidine, quartz, and biotite in a granophyric to vitric groundmass. Biotite and the rare amphiboles are partially to completely altered to opaque oxide minerals. Zircon and sphene are present in trace quantities.

Group B rhyolites contain 30 to 40% phenocrysts of quartz, sanidine, plagioclase, and copper-colored biotite in a granophyric groundmass. Amphibole is apparently absent from this group. Sphene, zircon and opaque-oxide minerals are important accessory minerals.

Group C and Group D rhyolites contain 12 to 16% phenocrysts of quartz, sanidine, plagioclase, green amphibole, and copper-colored biotite in granophyric groundmass. Sphene was not observed in these groups. Biotite is rare and typically is altered to opaque oxides.

Sanidine in all groups is typically about  $Or_{50}$  and plagioclase is about  $An_{20}$  (Correa, 1981). Quartz and sanidine are locally rounded and embayed. Glomeroporphyritic sanidine is common and typically surrounds a single plagioclase crystal. Isolated plagioclase crystals are locally rimmed by a thin layer of sanidine. Zircon occurs as poikilitic inclusions in biotite and in late crystallizing opaque-oxide minerals.

Vapor-phase minerals typically form drusy linings in

lithophysae and along flow foliations and include quartz, hematite, sanidine, pseudobrookite, bixbyite, topaz, red beryl, and cassiterite (Lufkin, 1972; Fries and others, 1942). Small tin-bearing veinlets locally occur beneath the carapace breccias that mantle the domes. Minerals in the tin occurrences include cassiterite, hematite, topaz, quartz, clinopyroxene and various fluoroarsenates, the most common of which is durangite (Foord and others, 1985; Maxwell and others, 1986). The tin mineralization is postulated by Eggleston and others (1987b) to be fumarolic incrustations deposited by fluids responsible for vapor-phase crystallization.

#### Rhyolite of Sawmill Peak

The rhyolite of Sawmill Peak consists of as much as 10% of 0.5 to 1-cm-long sanidine phenocrysts in a brick-red, flow-banded, granophyric to vitric groundmass. Biotite and clinopyroxene are present in trace quantities. Both minerals are locally altered to opaque minerals. Zircon comprises as much as 0.1% of the rock and occurs as discrete microphenocrysts as well as inclusions in opaque minerals, biotite, pyroxene, and late sanidine indicating that it crystallized early relative to those phases. Small amounts of apatite are present as microphenocrysts and as inclusions in pyroxenes.

#### Older Rhyolites

The rhyolites that underlie the Taylor Creek Rhyolite in

the southwestern part of Figure 2 consist of crystal-poor rhyolite lavas. These rhyolites contain phenocrysts of quartz, sanidine, plagioclase, biotite, and amphibole in a microtrachytic to vitric groundmass. The groundmass is typically perlitic.

#### Trachytes

Two trachytes interfinger with the high-silica rhyolite section in the Sierra Cuchillo and consist of phenocrysts of plagioclase (5%), sanidine (5%), and biotite (tr to 1%) in a trachytic groundmass that is locally granophyric. Green clinopyroxenes are present in trace quantities. Euhedral apatite is a common accessory mineral and is generally included in opaque oxides. Zircon occurs as large (0.1 mm) isolated microphenocrysts and as inclusions in opaque oxide-minerals.

#### Mafic Rocks

The basaltic andesite of Poverty Creek consists of as much as 10% phenocrysts of plagioclase and clinopyroxene in a microtrachytic groundmass. Iddingsite and bowlingite alteration after olivine, comprise as much as 10% of the rock. The plagioclase content of the lavas increases upward, but does not exceed about 3%. Opaque minerals comprise as much as 2% of the rock.

## PETROCHEMISTRY

## Samples

Vitrophyres preserved in the carapace breccia of the domes are hydrated. All of the tin-bearing rhyolite domes has undergone incipient to intense vapor-phase crystallization. Samples exhibiting effects of intense vapor-phase crystallization were avoided because of the compositional changes due to intense vapor-phase crystallization reported by Eggleston and others (1987a). Samples exhibiting mild vapor-phase crystallization were collected, because no other material is available on most of the rhyolite domes examined. Hydrated vitrophyres were collected from two domes and exhibit little compositional differences compared to mildly vapor-phase crystallized samples; for example, see sample pairs 149/224 and 153/223 in Table 1. The small compositional differences in elements of petrologic interest between the samples were judged to be insignificant.

## Major Elements

The tin-bearing rhyolites have strikingly similar major element compositions (Table 1; Figure 3). Titanium is the only major element to exhibit systematic variations between the various rhyolite groups (Fig. 3). Group A and B rhyolites have the highest  $\text{TiO}_2$  content (0.2%); Group D rhyolites have the lowest  $\text{TiO}_2$  content (0.09%).



The rhyolites are enriched in  $\text{SiO}_2$  and  $\text{K}_2\text{O}$  and depleted in  $\text{TiO}_2$ ,  $\text{Fe}_2\text{O}_3$ , and  $\text{CaO}$  relative to average rhyolite (Fig. 4). Corundum is present in the CIPW norms of most of the tin-bearing rhyolite samples indicating that the rhyolites are mildly peraluminous to mildly metaluminous (Fig. 5); the differentiation index (Thornton and Tuttle, 1960) of the tin-bearing rhyolite is 94 to 97. The tin-bearing rhyolites fall very near the 0.5 kb granite minimum of Tuttle and Bowen (1958) (Fig. 6).

The rhyolite of Sawmill Peak contains lower  $\text{SiO}_2$  and higher  $\text{Al}_2\text{O}_3$ ,  $\text{Fe}_2\text{O}_3$ , and alkalis than the tin-bearing rhyolites (Table 1). The differentiation index of these lavas is about 94 and the agpaitic index is between 0.95 and 1.1, indicating that the unit has peralkaline tendencies (Fig. 5).

The older rhyolites in the northern Black Range contain 71 to 77%  $\text{SiO}_2$  and the  $\text{CaO}$ ,  $\text{Fe}_2\text{O}_3$ ,  $\text{MgO}$ , and  $\text{TiO}_2$  are higher than in the tin-bearing rhyolites. The basaltic andesite of Poverty Creek contains 52 to 57%  $\text{SiO}_2$ . With increasing  $\text{SiO}_2$ ;  $\text{TiO}_2$ ,  $\text{Fe}_2\text{O}_3$ , and  $\text{CaO}$  decrease;  $\text{Al}_2\text{O}_3$ ,  $\text{Na}_2\text{O}$ , and  $\text{K}_2\text{O}$  increase.

Trachytes in the Sierra Cuchillo contain about 66%  $\text{SiO}_2$  and have higher  $\text{TiO}_2$ ,  $\text{Fe}_2\text{O}_3$  and  $\text{CaO}$  than the tin-bearing rhyolite.  $\text{Na}_2\text{O}$  is markedly higher than that of the tin-bearing rhyolite and  $\text{K}_2\text{O}$  is moderately enriched relative to the tin-bearing rhyolite. On the alkali- $\text{SiO}_2$  diagram of Irvine and Baragar (1971) (Fig. 7), the trachytes plot in the alkaline field. All other rocks in this study plot in the

subalkaline field of Irvine and Baragar (1971) (Fig. 7).

A distinct gap in  $\text{SiO}_2$  between 60.5 and 71.5% occurs in major element variation diagrams (Fig 3). This gap suggests that the sequence in the northern Black Range is bimodal and indeed, if the northern Black Range is considered in isolation, it is distinctly bimodal. The samples in the middle of the gap are trachytes in the Sierra Cuchillo that are very small, isolated units relative to the basaltic andesites and high-silica rhyolites. The gap in  $\text{SiO}_2$  may be due to restricted sampling but each volcanic unit exposed in the area has been sampled and the trachytes in the Sierra Cuchillo are the only units that have compositions within the gap.

#### Trace Elements

The tin-bearing rhyolites are strongly enriched in Rb, Nb, F, Hf, Th, U, Y, Ta and strongly depleted in Ba, Sc, Sr, V, and Eu relative to an average low Ca granite (Fig. 4). Cs, Ga, Pb, Ta, Zn, and Zr exhibit mild enrichments and depletions that may not be significant when the precision of the analyses is considered. The high concentrations of Rb and Nb and low concentrations of Sr and Ba indicate that these tin-bearing rhyolites are extremely differentiated rocks.

Because Rb is incompatible with plagioclase, sanidine, and quartz in the high-silica rhyolites it will tend to be enriched with differentiation and can thus be used as an indicator of differentiation. Using Rb as the comparator,

Ga, Nb, Ta, and Th increase with increasing Rb content and Ba, Sc, and Sr are depleted (Fig. 8). Cs, Pb, Y, and Zr exhibit no consistent trends.

The rhyolite of Sawmill Peak contains less Cs, Nb, Rb, Ta, and Th and more Hf, Sc, Zn, and Zr than the tin-bearing rhyolites. Other trace elements are comparable between the two units. The rhyolite of Sawmill Peak contains more than 700 ppm Zr, supporting the contention based on major elements that the unit may be peralkaline.

The older rhyolites in the northern Black Range contain 700 to 1100 ppm Ba, 70 to 250 ppm Sr, 39 ppm Y, and 140 to 240 ppm Rb. Ba and Sr are enriched and Y and Rb are depleted relative to the tin-bearing rhyolites. These rhyolites are thus significantly different than the tin-bearing rhyolites.

#### Rare Earth Elements

Chondrite normalized rare-earth element (REE) plots for the tin-bearing rhyolites are flat with large negative Eu anomalies (Fig. 9). The light REE's (LREE) are typically 100 to 200 times chondrite, the heavy REE's (HREE), 50 to 100 times chondrite. The La/Lu ratios vary from about 40 in Group A to about 23 in Group C. The variation in La/Lu ratios reflects both depletion of the LREE's and enrichment of the HREE's relative to chondrites. LREE's vary from 400 X chondrite in Group A rhyolites to 100 X chondrite in Group C rhyolites. HREE's vary from 45 X chondrite in group A rhyolites to 60 X chondrite in group C rhyolites (Fig. 9d). The negative Eu anomalies typical of these rocks is greater

in Group C rhyolites than in Group A rhyolites and the Tb/Lu and La/Sm ratios are lower in Group C rhyolites than in Group A rhyolites (Table 2; Fig. 9). Group B domes have Eu anomalies and Tb/Lu and La/Sm ratios intermediate between Groups A and C. The rhyolite of Sawmill Peak has a very small negative Eu anomaly, but the pattern is otherwise similar to the tin-bearing rhyolites.

#### STRONTIUM ISOTOPES

Most of the samples analyzed for their strontium isotopic composition have undergone mild vapor-phase crystallization; however, some were from zones of intense vapor-phase crystallization. Eggleston and others (1987a) discussed the effects of vapor-phase crystallization and concluded that the vapors involved were in fact supercritical magmatic fluids derived from the cooling lavas. Sr and to a lesser extent, Rb, have been redistributed in the domes due to vapor-phase crystallization. Because the redistribution occurred while the dome was cooling, initial  $^{87}\text{Sr}/^{86}\text{Sr}$  ratios calculated from the measured isotopic ratios reflect the initial ratios of the domes.

Table 3 presents the Sr analyses for the tin-bearing rhyolites and other units in the area as well as the calculated initial  $^{87}\text{Sr}/^{86}\text{Sr}$  ratios for the units. The data for the tin-bearing rhyolite domes yield very straight lines and many appear to be isochrons (Fig. 10); however, the dates indicated by most of the regression lines are 1 to 2 Ma older

than the  $28.2 \pm 0.15$  Ma, high precision  $^{40}\text{Ar}/^{39}\text{Ar}$  date for the Taylor Creek Rhyolite (B. McIntosh, 1986, oral communication). The straight lines with older than permissible dates are probably mixing lines indicating mixing of two sources of strontium.

Strontium evolution diagrams for some of domes converge to a point at the age and initial  $^{87}\text{Sr}/^{86}\text{Sr}$  ratios indicated by the regression lines, but only the Boiler Peak data is within the window of time allowable for the tin-bearing rhyolites (Figure 11). The Indian Peaks dome converges to a point 1.2 to 1.7 Ma older than is stratigraphically permissible. This older date suggests uniform mixing of the tin-bearing rhyolites with a reservoir of Sr with an  $^{87}\text{Sr}/^{86}\text{Sr}$  ratio lower than that of the tin-bearing rhyolite (Fig. 12). Rocks in the region that may have  $^{87}\text{Sr}$  ratios lower than the tin-bearing rhyolite magmas include mafic volcanic rocks and Paleozoic, marine carbonates.

Assimilation of even small amounts of mafic rocks in the area the by tin-bearing magmas with would dramatically increase the Ba and Sr concentrations in the magma. Assimilation of marine carbonate rocks, which typically have  $^{87}\text{Sr}/^{86}\text{Sr}$  ratios of about 0.708 (Faure, 1977), would increase the CaO concentration in the magmas. A possible mixing mechanism that will allow the major element concentrations to remain relatively constant is to mix strontium contaminated cupolas with high  $^{87}\text{Sr}/^{86}\text{Sr}$  ratios with the main magma chamber with relatively lower  $^{87}\text{Sr}/^{86}\text{Sr}$  ratios. The effects on the major element concentrations would be minimal and the amount of

strontium needed to contaminate the magmas is very small.

The strontium isotope evolution diagrams for most of the domes exhibit widely scattered intersections and no definable initial  $^{87}\text{Sr}/^{86}\text{Sr}$  ratio (Fig 11). The scatter in these data suggests assimilation of an inhomogenous source of contaminant strontium.

The initial  $^{87}\text{Sr}/^{86}\text{Sr}$  ratios calculated from the regressions probably have little petrologic significance, thus ratios calculated using 28.2 Ma are used to estimate the initial  $^{87}\text{Sr}/^{86}\text{Sr}$  ratios for these rocks (Table 3). An additional complicating factor is the high Rb/Sr ratios. These high ratios cause the apparent initial  $^{87}\text{Sr}/^{86}\text{Sr}$  ratio to grow very rapidly (Table 3) and unless the ages between the individual lavas is known to within  $10^5$  years, the initial ratios of the lavas can not be precisely determined. The initial  $^{87}\text{Sr}/^{86}\text{Sr}$  ratios calculated at 28.2 Ma are used as the best estimates of the actual initial  $^{87}\text{Sr}/^{86}\text{Sr}$  ratios and range from 0.707 to 0.715. The scatter in the calculated initial  $^{87}\text{Sr}/^{86}\text{Sr}$  ratios (28.2 Ma) suggests that the rhyolite magmas were variably contaminated by strontium. The amount of strontium contamination can not be determined from the data.

#### OXYGEN ISOTOPES

Whole-rock  $\delta^{18}\text{O}$  values for the tin-bearing rhyolites range from 7.3 to 9.0 ‰. Quartz phenocryst separates



cluster between 7.5 and 7.8 ‰ and sanidine phenocryst separates have  $\delta^{18}\text{O}$  compositions between 6.7 and 7.7 permil. A single magnetite separate has a  $\delta^{18}\text{O}$  of 2.4 ‰.

Phenocryst quartz is believed to be a good indicator of initial magmatic  $\delta^{18}\text{O}$  because quartz does not readily exchange oxygen with later fluids (Criss and Taylor, 1983). The tight clustering of the  $\delta^{18}\text{O}$  of the phenocryst quartz separates and the larger range of whole-rock compositions suggest that the whole-rock oxygen-isotope compositions have been disturbed since the quartz phenocrysts crystallized from the melt. Plagioclase (An 30) oxygen isotope compositions calculated from quartz-plagioclase equilibria can be used to approximate the magmatic  $\delta^{18}\text{O}$  of whole-rock samples (Taylor, 1979). The fractionation between coexisting quartz and plagioclase (An 30) at 800° C is about 1 ‰, thus the estimated, magmatic  $\delta^{18}\text{O}$  (based on quartz-plagioclase equilibria) of samples 116, 136, 149, and 167 is 6.7, 6.7, 6.5, and 6.8 ‰ respectively. The data suggest that no  $\delta^{18}\text{O}$  differences exist in the calculated whole-rock  $\delta^{18}\text{O}$  between Groups B and C lavas.

All of the whole-rock samples thus appear to have experienced significant  $\delta^{18}\text{O}$  enrichment after the quartz phenocrysts crystallized from the melt. This enrichment can be explained by oxygen exchange between the rhyolites and the fluids responsible for vapor-phase crystallization. Cooling of magmatic fluids from 800° to 600° will produce a fractionation of about 0.5 permil and increase the whole-rock  $\delta^{18}\text{O}$  by that amount. As the fluids continue to cool, the



fluid-mineral fractionation will increase, thus increasing the mineral  $^{18}\text{O}$  enrichment.

Using the equations of Bottinga and Javoy (1973), the equilibrium temperatures of mineral pairs in Table 4a have been calculated (Table 4b). Temperatures range from 707 to  $1335^{\circ}\text{C}$ . The large range of calculated temperatures suggests that sanidine and magnetite have also exchanged oxygen with later fluids. Several of the temperatures; however, cluster near the temperatures indicated for intense vapor-phase crystallization by fluid-inclusion homogenization temperatures ( $720$  to  $730^{\circ}\text{C}$ ; Eggleston and others, 1987a), suggesting that the oxygen-isotope composition of the rocks and the magmatic fluid equilibrated near that temperature.

## DISCUSSION

## Petrologic Affinities of the Tin-Bearing Rhyolites.

The tin-bearing rhyolites in New Mexico are typical of what Burt and Sheridan (1981) called topaz rhyolites. They are high  $\text{SiO}_2$ , high  $\text{K}_2\text{O}$ , F-rich magmas that typically erupt as lava flows and domes with minor pyroclastic material. Burt and Sheridan (1981) suggested that topaz rhyolites are extrusive equivalents of A-type granites (Loiselle and Wones, 1979). Table 5 compares representative examples of S-, I-, and A-type granites with the tin-bearing rhyolites. The high  $\text{SiO}_2$ , low  $\text{Fe}_2\text{O}_3$  and  $\text{CaO}$ , high  $\text{Na}_2\text{O}$  and  $\text{K}_2\text{O}$ , and high  $\text{Ga}/\text{Al}_2\text{O}_3$  of the tin-bearing rhyolites are indeed similar to A-type granites.

Several trace elements in the tin-bearing rhyolites; however, are not similar to A-type granites. In particular, the Ba and Sr content of the average A-type granitoids is much higher than in the tin-bearing rhyolites. This suggests that although the tin-bearing rhyolites may have started as A-type granite magmas, differentiation is necessary to produce the rhyolite magmas.

## Constraints on Evolution of the Tin-Bearing Rhyolites

Trace element covariations in the tin-bearing rhyolites suggest that these rocks are the products of progressive crystal-liquid fractionation and periodic eruption of a

single, large magma chamber (Fig. 8). The major element composition of the tin-bearing rhyolites is very near the 0.5 kb granite minimum of Tuttle and Bowen (1958); thus sanidine, quartz, and plagioclase will be the dominant crystallizing phases and crystal-liquid fractionation will produce little change in the major element concentrations (Fig. 3).

The trace element data suggest that plagioclase, and sanidine were the major crystallizing phases during crystal-liquid fractionation of the tin-bearing rhyolites and that allanite and sphene were important accessory minerals (see Tables 7 and 8 for models). The large range of values for published crystal-liquid partition coefficients, none of which are for topaz rhyolites, complicates modeling of trace element trends; however, general relationships defined by the published coefficients can be used to constrain a petrogenetic model.

The low Sr and Ba content of these rhyolites indicates that plagioclase and sanidine crystallized and were removed from the melt. Sc exhibits compatible behaviour and may have been removed from the melt by crystallization of zircon or allanite. Ta enrichment suggests that zircon was not removed from the melt in significant quantities and that the concentration of Sc in the magma was thus controlled by allanite rather than zircon.

Rb, Nb and Cs exhibit similar incompatible behaviour (Fig. 8). All three elements are strongly enriched in the tin-bearing rhyolites relative to typical rhyolites and granites (Fig. 4) and exhibit a progressive enrichment from

Group A to Group D rhyolites (Fig. 8). Because Rb, Nb, and Cs partition into biotite, biotite must not have been a major crystallizing phase. Th exhibits similar enrichment trends to Rb and Nb and is compatible with clinopyroxene and amphibole as well as biotite, suggesting that those phases were not crystallizing during crystal-liquid fractionation of the rhyolite magmas.

The tin-bearing rhyolites exhibit a progressive depletion of LREE, enrichment of HREE, and an increase in the depth of Eu anomaly from Group A to Group C. These trends are consistent with crystallization of plagioclase and allanite (Table 7). The middle rare earth elements (MREE) typically sag suggesting sphene crystallization. Sphene has higher partition coefficients for MREE than HREE and LREE and sphene crystallization is required to balance the MREE in trace element modelling studies (Table 7). The depth of the sag increases from Group A to Group B rhyolites and correlates with the lower  $\text{TiO}_2$  content of Group B rhyolites relative to Group A rhyolites. The presence of sphene in Group B rhyolites confirms that sphene was a crystallizing phase.

Trace element modeling studies indicate that the trace element variations between the various rhyolite groups can not be produced by crystal-liquid fractionation using the phenocryst modes present in the lavas (Table 7; Table 8). For example, in order to balance Sr and Ba concentrations in the rhyolites, plagioclase must be crystallized in proportions similar to that of sanidine. Plagioclase phenocrysts;

however, occur in trace amounts whereas sanidine comprises as much as 20% of the rhyolite. This apparent problem can be resolved by allowing crystal-liquid fractionation to occur in a convecting, compositionally stratified magma chamber and by allowing the crystallizing phases to crystallize along the walls of the magma chamber. The phases crystallizing along the relatively cooler walls are not necessarily crystallizing in the hotter, convecting magma chamber. Such a model was proposed by McBirney and coworkers and described in detail by McBirney and others (1986), Nilson and others (1986), Barker and McBirney (1986), and Lowell (1985) and will not be detailed here.

The trace element covariations suggest that Groups B, C, and D are comagmatic; however, the initial  $^{87}\text{Sr}/^{86}\text{Sr}$  ratios are not consistent with that interpretation. The low concentration of strontium in these rhyolites make them very susceptible to upper crustal contamination. Contamination of the rhyolite magmas by as little as 1% of average crustal material containing 350 ppm Sr (Taylor and McLennan, 1985) and having an  $^{87}\text{Sr}/^{86}\text{Sr}$  ratio of 0.72 can produce the observed variations in the initial  $^{87}\text{Sr}/^{86}\text{Sr}$  ratios. If the strontium contamination is from granites similar to those exposed in the Franklin Mountains with present day  $^{87}\text{Sr}/^{86}\text{Sr}$  ratios greater than 1 (Norman and others, 1987), the amount would be substantially less than 1%. The variations between individual rhyolite domes can be explained by variable contamination of compositionally stratified cupolas at the top of the main magma chamber by upper crustal strontium.

The compositional stratification will tend to prevent contamination of the main magma chamber because the contaminating strontium will have to diffuse across the compositional boundary layer (Fridrich and Mahood, 1987).

#### The Role of Fluorine

The role of fluorine in the evolution of these magmas is problematic. The high fluorine concentrations (as much as 0.6%, Eggleston and Norman, 1987) in the tin-bearing rhyolites indicate that hydroxyl-bearing phases like biotite and amphibole did not crystallize in large quantities late in the differentiation history of these rhyolites. Collins and others (1982) suggest that fluorine is important in the production of A-type granites because it will stabilize amphibole early in the differentiation history, thus producing peraluminous melts. They argue that the absence of early amphibole will tend to produce peralkaline magmas. This may explain the origin of the mildly peralkaline rhyolite of Sawmill Peak.

The tendency of fluorine to lower the liquidus and solidus temperatures of felsic magmas is well documented. Manning (1981) reports that 4% fluorine in a Q-Ab-Or melt will lower the liquidus from 730° C to 630° C and that the solidus for the system may be as low as 550° C. Fluorine has much the same effect on the melt as H<sub>2</sub>O has in that it depolymerizes the melt and thus decreases the viscosity of the melt (Dingwell and others, 1985). Fluorine is more soluble in a silicate melt than H<sub>2</sub>O and is strongly

partitioned to the melt (Koster Van Groos and Wyllie, 1968; Fuge, 1977; Bailey, 1977). Fluorine also increases the solubility of  $H_2O$  in silicate melts, thus forestalling  $H_2O$  saturation (Koster Van Groos and Wyllie, 1968). Lowering of the viscosity and solidus temperatures and forestalling  $H_2O$  saturation may have allowed the crystal-rich magmas to reach the surface as lavas rather than crystallizing as buried plutons. The increased solubility of  $H_2O$  may also account for the pervasive vapor-phase crystallization because  $H_2O$  may have not been saturated in the magma until it was very near the surface.

Pearce and Gale (1977) and Manning (1981) suggest that fluorine enhances the solubility of Sn to the liquid and fluid phases of a magmatic system. Complexing of W, Zr, Th, Y, Nb, and the rare earth elements with fluorine may enhance partitioning of those elements into the melt and thus increase their concentration in more differentiated phases like the tin-bearing rhyolites (Plimer, 1984; Harris, 1981).

#### Source Region Constraints

The lowest calculated initial  $^{87}Sr/^{86}Sr$  ratios for the tin-bearing rhyolites are about 0.708 and may closely approximate the actual initial  $^{87}Sr/^{86}Sr$  ratios for these lavas. That ratio is not distinctive of any source area. The parent magmas may have been produced in the upper mantle and been contaminated by crustal strontium or the parent magmas may have been direct partial melts of lower or mid-crustal rocks and experienced contamination only during the



late differentiation history of the magmas.

In order to concentrate Rb, Nb, and Th to the levels observed in the tin-bearing rhyolites, a mantle derived, alkali basalt containing 50 ppm Rb, 5ppm Nb, and 4 ppm Th would have to undergo >80% fractional crystallization to produce the concentrations of those elements observed in the tin-bearing rhyolites, assuming a bulk distribution for those elements of 0.001. During fractional crystallization; however, large volumes of intermediate-composition magma will be produced and little intermediate-composition material is associated with the tin-bearing rhyolites. This argues against, but by no means precludes, a mantle source for the parental magmas.

Lower-crustal granulite xenoliths in the alkali basalts at Kilbourne Hole have present-day  $^{87}\text{Sr}/^{86}\text{Sr}$  ratios between 0.7034 and 0.7753 (James and others, 1980) indicating that the tin-bearing rhyolite magmas could be partial melts of lower-crustal granulites. Baldrige and Perry (1986) and Crowley and others (1986) report  $E_{\text{Nd}}$  determinations for the mantle beneath the Rio Grande Rift of between 0 and +8. Ruiz and others (1986) reported initial  $^{87}\text{Sr}/^{86}\text{Sr}$  ratios similar to those reported here as well as  $E_{\text{Nd}}$  values of -5.2 to -6.2 for the Taylor Creek Rhyolite. They suggest that the lower crust of New Mexico may have  $E_{\text{Nd}}$  of about -11, similar to the values reported by DePaolo (1981) for the lower crust of Colorado, and conclude that the Taylor Creek magmas may have had a mantle component. Ruiz and others (1986) also reported that the tin-bearing rhyolites in Mexico have  $^{87}\text{Sr}/^{86}\text{Sr}$

ratios of 0.706 to 0.707 and  $E_{Nd}$  values of 0 to -2.5. The initial  $^{87}Sr/^{86}Sr$  ratios and  $E_{Nd}$  values for the tin-bearing rhyolites are similar to granulite xenoliths found in the region leading Ruiz and others (1986) to postulate a crustal source for those tin-bearing rhyolites.

The oxygen isotope composition of the tin-bearing rhyolites are also not distinctive. The Taylor Creek Rhyolite has a  $d^{18}O$  of about +6.7 per mil (SMOW), which is a composition typical of most felsic igneous rocks (Taylor, 1968; 1978), but not of S-type granites (Beckinsale, 1979). The isotopic systematics can therefore only constrain the source region to be the lower to middle crust or upper mantle; however, the neodymium isotopic data strongly suggests that the lower crust was the dominant source region.

#### Composition of the Parent Magma

Major and trace element modeling studies using the mafic rocks in the Black Range and Sierra Cuchillo suggest that the tin-bearing rhyolites could not be the end products of fractional crystallization of magmas with those compositions (Table 9). In particular,  $Na_2O$  and  $K_2O$  concentrations in the tin-bearing rhyolites can not be successfully modeled with a basaltic andesite parent.  $Na_2O$  is invariably too high and  $K_2O$  too low in the calculated daughter liquid (Table 9b). Trace element modeling studies indicate that 40% fractionation of plagioclase and sanidine will balance Ba and Sr, but much larger amounts of total fractionation are required to balance Rb (Table 9).

The high Ba and Sr content of the rhyolite of Whitetail Canyon required >70% crystallization of sanidine, plagioclase, and biotite to attain the low levels of Ba and Sr and high concentrations of Rb observed in the tin-bearing rhyolites (Table 10); however, HREE concentrations in the tin-bearing rhyolites are not consistent with the rhyolite of Whitetail Canyon as parent. Models using the rhyolite of Sawmill Peak as the starting composition encounter problems balancing Zr and the alkalis (Table 11). These modeling studies strongly suggest that none of the volcanic rocks exposed in the Black Range or Sierra Cuchillo can be the parent materials for the tin-bearing rhyolites.

The petrologic similarities of the tin-bearing rhyolites to A-type granites suggest that the parent magma may have been similar to A-type granites in composition. Major element modeling using an average A-type granite from the Lachlan fold belt in Australia (White and Chappell, 1983) as a starting composition indicates that 10% crystallization of sanidine, plagioclase and calcic amphibole from that granite will produce the major element concentrations observed in Group A rhyolites (Table 12). Trace element models; however, suggest that plagioclase, sanidine, and biotite are the major crystallizing phases (Table 13) and that much more total fractionation is needed to balance the trace elements than is necessary to balance the major elements. This apparent discrepancy is explained by the fact that the tin-bearing rhyolites compositions are near the granite minima and when the melt composition reaches the granite minima by

crystallization of plagioclase, sanidine and amphibole, continued fractionation will not change the major element concentrations of the magma, but will dramatically affect the trace element concentrations.

#### Source Rocks For The Parent Magmas

Padovani and Carter (1977a; b) describe lower crustal granulite xenoliths from Kilbourne Hole, New Mexico, some of which have strontium and oxygen isotopic compositions similar to those of the tin-bearing rhyolites. They also report interstitial glass in garnet-bearing quartzofeldspathic granulite xenoliths from Kilbourne Hole, New Mexico, that have major element compositions similar to granites. That glass presumably resulted from partial melting of the host granulite.

Biotite or phlogopite in the source rocks would greatly facilitate enrichment of Rb, Nb, and Sn in daughter melts if the micas are completely destroyed during partial melting. Rb, Nb, and Sn are strongly partitioned to biotite (Munoz and Ludington, 1974; Pearce and Norry, 1979; Arth and Hanson, 1975) and will remain in the source region if the micas are not completely consumed during partial melting.

The high concentration of HREE's in the tin-bearing rhyolites suggests that the granulites contained zircon and/or garnet that were totally consumed during partial melting. Incompletely consumed zircon or garnet that remain in the source region will contain very high concentrations of HREE because both garnet and zircon have high (>10) partition

coefficients for the HREE;

Pelitic rocks are not a possible source material because melting of rocks containing muscovite and/or aluminosilicates typically produce strongly peraluminous magmas (Thompson and Tracey, 1977), rather than the mildly peraluminous to mildly metaluminous rocks typical of these high-silica rhyolites (Fig. 5).

The source rocks for the parent magmas of the tin-bearing rhyolites must therefore contain biotite and/or phlogopite and zircon and/or garnet. Both the upper mantle and the lower crust can contain this mineral assemblage; however, the neodymium isotopic data and the granitic compositions of some of the glass from Kilbourne Hole suggest that the source of the parent magmas were lower crustal, quartzofeldspathic granulites.

These observations suggest that the source rocks for the tin-bearing rhyolites were probably plagioclase, K-feldspar-, quartz-, biotite-bearing granulites. Garnet and/or zircon are probably present in the source rock, but must be consumed during partial melting.

#### Petrogenesis of Tin-Bearing Rhyolites

The data suggest the following petrogenesis for the tin-bearing rhyolites in southwestern New Mexico. The parent magmas of the tin-bearing rhyolites were A-type granitic melts derived by small amounts of partial melting of lower crustal quartzofeldspathic granulites. The source granulites initially contained fluorine-rich biotite and/or phlogopite

and zircon and/or garnet. Melting continued until the hydrous, fluorine-bearing phases were consumed. Melting was induced by intrusion of mantle-derived basaltic andesite magmas that eventually erupted as the basaltic andesite of Poverty Creek. A portion of these magmas may have mixed with the granitic melts.

Crystal-liquid fractionation in a shallow magma chamber modified the original melt and produced the progressive enrichments of Rb, Nb, Ta, and Th and the progressive depletions of Sr, Ba, and Sc observed in the tin-bearing rhyolites. The major crystallizing phases were plagioclase, sanidine, and quartz. Continued differentiation produced little change in the major element compositions and thus explains the lack of major element variation of the rhyolite magma. Rare earth element concentrations were controlled by crystallization of allanite and zircon. The initial  $^{87}\text{Sr}/^{86}\text{Sr}$  ratios of the rhyolites were modified by assimilation of small amounts of upper-crustal rocks. The assimilation and isotopic homogenization occurred in cupolas above the main magma chamber.

#### CONCLUSIONS

Conclusions reached from this study are: 1) The tin-bearing rhyolites in the northern Black Range of New Mexico are high-silica, very evolved rhyolites that were probably derived by crystal-liquid fractionation of a single, large



magma chamber. Major crystallizing phases included plagioclase, sanidine, and quartz. Allanite and sphene controlled the concentration of rare earth elements. The upper parts of the magma chamber were probably compositionally stratified and the rhyolites probably erupted from cupolas. 2) The source region for these rhyolites was probably the lower crust. The upper mantle may have contributed to the magmas, but the extent of that possible contribution is not known. 3) Felsic granulites containing biotite and/or phlogopite and zircon and/or garnet were probably the source rocks. Aluminosilicate minerals and white micas were not present in the source region. 4) Variable amounts of assimilation of upper crustal rocks by individual cupolas is responsible for producing the strontium isotope variations observed in the rhyolites. 5) Fluorine is important in the production of these magmas because it lowers the viscosity and solidus temperatures, increases the solubility of  $H_2O$ , stabilizes amphibole in these melts, and may increase the solubility of Sn in the melts.

#### ACKNOWLEDGEMENTS

FRM Minerals, the Geological Society of America, the Norwegian Marshall Fund, the New Mexico Geological Society, Rock Mountain Federation of Mineralogical Societies, the National Science Foundation (Grants EAR 8319913 and EAR 8410481 to DIN) and the U.S. Department of Interior's Mineral



Institutes program administered by the U.S. Bureau of Mines (allotment grant G1164135 to DIN) funded various aspects of this research. Philip Kyle, Kent Condie, Charles Chapin, and Donald Richter are thanked for critical reviews of early versions of this manuscript. The New Mexico Bureau of Mines and Mineral Resources provided a graduate research assistantship to the senior author. Irradiation costs were defrayed by the U.S. Department of Energy's reactor sharing program. Irradiations were performed at the research reactor at the University of Missouri, Columbia.

## BIBLIOGRAPHY

- Abitz, R.J., 1984, Volcanic geology and geochemistry of the northeastern Black Range Primitive Area and vicinity, Sierra County, New Mexico: M.S. Thesis, The University of New Mexico, Albuquerque, 121 p.
- American Public Health Association, 1976, Standard methods for the examination of water and waste water: American Public Health Association, Washington, D.C., 193 p.
- Arth, J.G. and Hanson, G.M., 1975, Geochemistry and origin of the early Precambrian crust of northeastern Minnesota: *Geochimica et Cosmochimica Acta*, v. 39, p. 325-362.
- Bailey, J.C., 1977, Fluorine in granitic rocks and melts: a review: *Chemical Geology*, v. 19, p. 1-42.
- Baldrige, W.S., and Perry, F.V., 1986, Late Cenozoic volcanism of the central Rio Grande Rift and southeastern Colorado Plateau: constraints on rift processes: *Geological Society of America Abstracts with Programs*, v. 18, p. 533.

- Barker, B.H. and McBirney, A.R., 1985, Liquid fractionation. part III: geochemistry of zoned magmas and the compositional effects of liquid fractionation: *Journal of Volcanology and Geothermal Research*, v. 24, p. 55-81.
- Beckinsale, R.D., 1979, Granite magmatism in the tin belt of Southeast Asia: in, Atherton, M.P. and Tarney, J., eds., *Origin of granite batholiths, geochemical evidence*: Shiva Publishing Limited, Cheshire, p. 34-44.
- Bodkin, J.B., 1977, Determination of fluorine in silicates by use of ion-selective electrode following fusion with lithium metaborate: *Analyst*, v. 102, p. 409-413.
- Bottinga, Y., and Javoy, M., 1973, Comments on oxygen isotope geothermometry: *Earth and Planetary Science Letters*, v. 20, p. 250-265.
- Burt, D.M. and Sheridan, M.F., 1981, Model for the formation of uranium/lithophile element deposits in fluorine-rich volcanic rocks: *American Association of Petroleum Geologists Studies in Geology*, No. 13, p. 99-109.
- Burt, D.M., Sheridan, M.F., Bikum, J.V., and Christiansen, E.H., 1982, Topaz rhyolites-distribution, origin, and significance for exploration: *Economic Geology*, v. 72, p. 1818-1836.
- Cather, S.M., 1986, Tectonic and petrogenetic implications of the Datil Group (latest Eocene-early Oligocene), west-central New Mexico: *Geological Society of America Abstracts With Programs*, v. 18, p. 560.

- Chapin, C.E. and Seager, W.R., 1975, Evolution of the Rio Grande rift in the Socorro and Las Cruces areas: New Mexico Geological Society Guidebook 26, p. 297-231.
- Chapin, C.E., Jahns, R.H., Chamberlin, R.M., and Osburn, G.R., 1978, First day roadlog from Socorro to Truth or Consequences via Magdalena and Winston: in, Chapin, C.E., and Elston, W.E., eds., Field guide to selected cauldrons and mining districts of the Datil-Mogollon volcanic field, New Mexico: New Mexico Geological Society Special Publication 7, p. 114-129.
- Chappell, B.W. and White, A.J.R., 1974, Two contrasting granite types: *Pacific Geology*, v. 8, p. 173-174.
- Christiansen, E.H., 1981, Geology and geochemistry of topaz rhyolites from the western United States: Ph.D. Dissertation, Arizona State University, Tempe, 351 p.
- Christiansen, E.H., Bikum, J.V., Sheridan, M.F., and Burt, D.M., 1984, Geochemical evolution of topaz rhyolites from the Thomas Range and Spor Mountain, Utah: *American Mineralogist*, v. 69, p. 223-236.
- Christiansen, E.H., Burt, D.M., Sheridan, M.F., and Wilson, R.T., 1983, The petrogenesis of topaz rhyolites from the western United States: *Contributions to Mineralogy and Petrology*, v. 83, p. 16-30.
- Christiansen, E.H., Sheridan, M.F., and Burt, D.M., 1986, The geology and geochemistry of Cenozoic topaz rhyolites from the western United States: *Geological Society of America Special Paper* 205, 82p.

- Clayton, R.N. and Mayeda, T.K., 1963, The use of bromine pentafluoride in the extraction of oxygen from oxides and silicates for isotopic analysis: *Geochimica et Cosmochimica Acta*, v. 27, p. 34-52.
- Collins, W.J., Beams, S.D., White, A.J.R., and Chappell, B.W., 1982, Nature and origin of A-type granites with particular reference to southeastern Australia: *Contributions to Mineralogy and Petrology*, v. 80, p. 189-200.
- Correa, B.P., 1981, The Taylor Creek Rhyolite and associated tin deposits, southwestern New Mexico: M.S. Thesis, Arizona State University, Tempe, 105 p.
- Crecraft, H.R., Nash, W.P., and Evans, S.H., Jr., 1981, Late Cenozoic volcanism at Twin Peaks, Utah: geology and petrology: *Journal of Geophysical Research*, v. 86, p. 10303-10320.
- Criss, R.E. and Taylor, H.P., Jr., 1983, An  $^{18}\text{O}/^{16}\text{O}$  and D/H study of Tertiary hydrothermal systems in the southern half of the Idaho Batholith: *Geological Society of America Bulletin*, v.94, p. 640-663.
- Crowley, J.C., Neimeyer, S., and Shaw, H.F., 1986, Source characteristics of Rio Grande rift basalts inferred from Nd, Sr, and Pb systematics: *Geological Society of America Abstracts with Programs*, v. 18, p. 577.
- Davis, L.L., 1986, The Reilly Peak Tertiary(?) intrusive- a high-silica rhyolite: *New Mexico Geological Society Guidebook 37*, p. 167-171.

- De Paolo, D.J., 1981, Neodymium isotopes in the Colorado Front Range and crust-mantle evolution in the Proterozoic: *Nature*, v. 291, p. 193-196.
- Di Girolamo, P., 1984, Magmatic character and geotectonic setting of some Tertiary-Quaternary Italian volcanic rocks: orogenic, anorogenic, and <<transitional>> associations: a review: *Bulletin Volcanologique*, v. 47, p. 421-432.
- Dingwell, D.B., Scarfe, C.M., and Cronin, D.J., 1985, The effects of fluorine on viscosities in the system  $\text{Na}_2\text{O}-\text{Al}_2\text{O}_3-\text{SiO}_2$ : implication for phonolites, trachytes, and rhyolite: *American Mineralogist*, v. 70, p. 80-87.
- Duffield, W.A., 1986, Preliminary field and chemical characteristics of the Taylor Creek Rhyolite, New Mexico: *Geological Society of America Abstracts with Programs*, v. 18, p. 352-353.
- Eggleston, T.L. and Norman, D.I., 1987, Geology of the Taylor Creek district, Black Range, New Mexico: *New Mexico Bureau of Mines and Mineral Resources Bulletin*, in prep.
- Eggleston, T.L., Norman, D.I., and Savin, S.M., 1987a, Intense vapor phase crystallization: mineralogical and chemical effects in high-silica rhyolites: in prep.
- Eggleston, T.L., Norman, D.I., and Savin, S.M., 1987b, Origin of tin mineralization associated with high-silica, topaz rhyolites, Black Range and Sierra Cuchillo, New Mexico: in prep.

- Elston, W.E., 1976, Glossary of stratigraphic terms of the Mogollon-Datil volcanic province, New Mexico: in, Elston, W.E., and Northrup, S.A., eds., Cenozoic volcanism in southwestern New Mexico: New Mexico Geological Society Special Publication 5, p. 131-144.
- Ewart, A., 1979, A review of the mineralogy and chemistry of Tertiary-Recent dacitic, latitic, and rhyolitic and related salic volcanic rocks: in Barker, F., ed., Trondhjemites, dacites, and related rocks: Elsevier Scientific Publishing, Amsterdam, 472 p.
- Elston, W.E., 1984, Subduction of young oceanic lithosphere and extensional orogeny in southwestern North America during mid-Tertiary time: *Tectonics*, v. 3, p. 229-250.
- Faure, G., 1977, Principles of isotope geology: John Wiley and Sons, New York, 464 p.
- Feigenson, M.D., 1986, Continental alkali basalts as mixtures of kimberlite and depleted mantle: evidence from Kilbourne Hole maar, New Mexico: *Geophysical Research Letters*, v. 13, p. 965-968.
- Foord, E.E. Oakman, M.R., and Maxwell, C.H., 1985, Durangite from the Black Range, New Mexico, and new data on durangite from Durango and Cornwall: *Canadian Mineralogist*, v. 23, p. 241-246.
- Fridrich, C.J. and Mahood, G.A., 1987, Compositional layers in the zoned magma chamber of the Grizzly Peak Tuff: *Geology*, v. 15, p. 299-303.



- Fries, C., Jr., 1942, Tin deposits of north Lander County, Nevada: U.S. Geological Survey Bulletin 931-1, p. 279-294.
- Fries, C., Jr., Schaller, W.T., and Glass, J.J., 1942, Bixbyite and pseudobrookite from the tin-bearing rhyolite of the Black Range, New Mexico: *The American Mineralogist*, v. 27, p. 305-322.
- Fuge, R., 1977, On the behavior of fluorine and chlorine during magmatic differentiation: *Contributions to Mineralogy and Petrology*, v. 61, p. 245-249.
- Harris, N.B.W., 1981, The role of fluorine and chlorine in the petrogenesis of a peralkaline complex from Saudi Arabia: *Chemical Geology*, v. 31, p. 303-310.
- Heyl, A.V., Maxwell, C.H., and Davis, L.L., 1983, Geology and mineral deposits of the Priest Tank quadrangle, Sierra County, New Mexico: U.S. Geological Survey Miscellaneous Field Studies Map MF-1665.
- Huspeni, J.R., Kesler, S.E., Ruiz, J., Tuta, Z., Sutter, J.F., and Jones, L.M., 1984, Petrology and geochemistry of rhyolites associated with tin mineralization in northern Mexico: *Economic Geology*, v. 79, p. 87-105.
- Irvine, T.N. and Baragar, W.R.A., 1971, A guide to the chemical classification of the common volcanic rocks: *Canadian Journal of Earth Sciences*, v. 8, p. 523-548.

- Jacobs, J.W., Korotev, R.L., Blanchard, D.P., and Haskin, L.A., 1977, A well-tested procedure for instrumental neutron activation analysis of silicate rocks and minerals: *Journal of Radioanalytical Chemistry*, v. 40, p. 93-114.
- Jahns, R.H., 1944, Beryllium and tungsten deposits of the Iron Mountain district, Sierra and Socorro Counties, New Mexico: *U.S. Geological Survey Bulletin*, 945-C, p. 45-79.
- James, D.E., Podavani, E.R., and Hart, S.R., 1980, Preliminary results on the oxygen isotopic compositions of the lower crust: Kilbourne Hole maar, New Mexico: *Geophysical Research Letters*, v. 7, p. 321-324.
- Kelley, J.L. and Kudo, A.M., 1986, Petrology and petrogenesis of alkalic and tholeiitic Pliocene lavas from the eastern margin of the southern Rio Grande rift: *EOS*, v. 67, p. 1267.
- Kelley, V.C., 1979, Tectonics, middle Rio Grande rift, New Mexico: in Reicker, R.E., ed. *Rio Grande Rift: tectonics and magmatism*: American Geophysical Union, Washington, p. 57-70.
- Koster van Groos, A.F.K. and Wyllie, P.J., 1968, Melting relationships in the system  $\text{NaAlSi}_3\text{O}_8\text{-NaF-H}_2\text{O}$  at 4 Kb pressure: *Journal of Geology*, v. 76, p. 50-70.

- Kovalenko, V.I. and Kovalenko, N.F., 1984, Problems of the origin, ore-bearing and evolution of rare-metal granitoids: *Physics of the Earth and Planetary Interiors*, v. 35, p. 51-62.
- Le Maitre, R.W., 1984, A proposal by the IUGS subcommission on the systematics of igneous rocks for a chemical classification of volcanic rocks based on the total alkali-silica (TAS) diagram: *Australian Journal of Earth Sciences*, v. 31, p. 243-255.
- Lindstrom, D.J. and Korotev, R.L., 1982, TEABAGS: computer programs for instrumental neutron activation analysis: *Journal of Radioanalytical Chemistry*, v. 70, p. 439-458.
- Loiselle, M.G. and Wones, D.R., 1979, Characteristics and origins of anorogenic granite: *Geological Society of America Abstracts with Programs*, v. 11, p. 468.
- Lowell, R.P., 1985, Double-diffusive convection in partially molten silicate systems: its role during magma production and in magma chambers: *Journal of Volcanology and Geothermal Research*, v. 26, p. 1-24.
- Lufkin, J.L., 1972, Tin mineralization within rhyolite flow-domes, Black Range, New Mexico: Ph.D. Dissertation, Stanford University, Stanford, 149 p.
- Mahood, G. and Hildreth, W., 1983, Large partition coefficients for trace elements in high-silica rhyolites: *Geochimica et Cosmochimica Acta*, v. 47, p. 11-30.

- Manning, D.A.C., 1981, The effects of fluorine on liquidus phases in the system Qz-Ab-Or with excess water at 1 Kb: Contributions to Mineralogy and Petrology, v. 76, p. 206-215.
- Maxwell, C.H., Foord, E.E., Oakman, M.R., and Harvey, D.B., 1986, Tin deposits in the Black Range tin district: New Mexico Geological Society Guidebook 37, p. 273-281.
- McBirney, A.R., Barker, B.H., and Nilson, R.H., 1985, Liquid fractionation. Part I: basic principles and experimental simulations: Journal of Volcanology and Geothermal Research, v. 24, p. 1-24.
- McIntosh, W.C., Sutter, J.L., Chapin, C.E., Osburn, G.R., and Ratte, J.C., 1986, A stratigraphic framework for the eastern Mogollon-Datil volcanic field based on paleomagnetism and high-precision  $^{40}\text{Ar}/^{39}\text{Ar}$  dating of ignimbrites--a progress report: New Mexico Geological Society Guidebook 37, p. 183-195.
- Michael, P.J., 1983, Chemical differentiation of the Bishop Tuff and other high-silica magmas through crystallization processes: Geology, v. 11, p. 31-34.
- Munoz, J.L. and Ludington, S.D., 1974, Fluorine-hydroxyl exchange in biotite: American Journal of Science, v. 274, p. 369-413.
- Nilson, R.H., McBirney, A.R., and Baker, B.H., 1985, Liquid fractionation. part II: fluid dynamics and quantitative implications for magmatic systems: Journal of Volcanology and Geothermal Research, v. 24, p. 25-54.

- Norman, D.I., Condie, K.C., Smith, R.W., and Thoman, W.F., 1987, geochemical and Sr and Nd isotopic constraints on the origin of late Proterozoic volcanics and associated tin-bearing granites from the Franklin Mountains, west Texas: Canadian Journal of Earth Science, in press.
- Norrish, K., and Chappell, B.W., 1977, X-ray fluorescence spectrometry: in Zussman, J., ed., Physical methods in determinative mineralogy: Academic Press, New York, p. 201-272.
- Norrish, K., and Hutton, J.T., 1969, An accurate method for the analysis of a wide range of geologic samples: Geochimica et Cosmochimica Acta, v. 33, p. 432-453.
- Padovani, E.R. and Carter, J.L., 1977 a, Aspects of the deep crustal evolution beneath south central New Mexico: in Heacock, J.G., ed., The Earth's Crust: American Geophysical Union Monograph 20, p. 19-55.
- Padovani, E.R. and Carter, J.L., 1977 b, Non-equilibrium partial fusion due to decompression and thermal effects in crustal xenoliths: in Magma genesis, proceedings of the American Geophysical Union Chapman conference on partial melting in the earth's upper mantle: State of Oregon Department of Geology and Mineral Industries Bulletin 96, p. 43-57.

- Pearce, J.A. and Gale, G.H., 1977, Identification of ore-deposition environments from trace-element geochemistry of associated igneous host rocks: in Volcanic Processes in Ore Genesis: Geological Society of London Special Publication 7, p. 14-24.
- Pearce, J.A. and Norry, M.J., 1979, Petrogenetic implications of Ti, Zr, Y, and Nb variations in volcanic rocks: Contributions to Mineralogy and Petrology, v. 69, p. 33-47.
- Peccerillo, A. and Taylor, S.R., 1976, Geochemistry of Eocene calc-alkaline volcanic rocks from Kastamonu area, northern Turkey: Contributions to Mineralogy and Petrology, v. 58, p. 63-81.
- Plimer, I.R., 1984, The role of fluorine in submarine exhalative systems with special reference to Broken Hill, Australia: Mineralium Deposita, v. 19, p. 19-25.
- Richter, D.L., Eggleston, T.L., and Duffield, W., 1986, Geologic map of the Wall Lake quadrangle, Catron County, New Mexico: U.S. Geological Survey Miscellaneous Field Studies Map, MF-1909.
- Rose, W.I., Jr., Grant, N.K., and Easter, J., 1979, Geochemistry of the Los Chocoyos ash, Quezaltenago, Guatemala: in, Chapin, C.E. and Elston, W.E., eds., Ash-flow tuffs: Geological Society of America Special Paper 180, p. 87-99.

- Ruiz, J., Duffield, W.A., and Burt, D.M., 1986, Sm-Nd and Rb-Sr isotopic compositions of mid-Tertiary, high silica rhyolites from the Black Range, New Mexico and Sierra Madre Occidental, Mexico: Geological Society of America Abstracts with Programs, v. 18, p. 736.
- Seager, W.R. and Morgan, P., 1979, Rio Grande rift in southern New Mexico, west Texas, and northern Chihuahua: in Riecher, R.E., ed. Rio Grande rift: tectonics and magmatism: American Geophysical Union, Washington, D.C., p. 87-106.
- Shand, S.J., 1927, Eruptive Rocks: John Wiley and Sons, New York.
- Taylor, H.P., 1968, The oxygen isotope geochemistry of igneous rocks: Contributions to Mineralogy and Petrology, v. 19, p. 1-71.
- Taylor, H.P., Jr., 1978, Oxygen and hydrogen isotope studies of plutonic granitic rocks: Earth and Planetary Science Letters, v. 38, p. 177-210.
- Taylor, H.P., Jr., 1979, Oxygen and hydrogen isotope relationships in hydrothermal mineral deposits: in Barnes, H.L., ed., Geochemistry of hydrothermal ore deposits: John Wiley and Sons, New York, p. 236-277.
- Taylor, S.R. and McLennan, S.M., 1985, The continental crust: its composition and evolution: Blackwell Scientific Publications, Oxford, 312 p.
- Thompson, A.B. and Tracy, R.J., 1977, Anatectic melting reactions in pelitic rocks: EOS, v. 58, p. 520.



- Thornton, C.P. and Tuttle. O.F., 1960, Chemistry of igneous rocks. I. differentiation index: American Journal of Science, v. 258, p. 664-684.
- Turekian, K.K., and Wedepohl, K.H., 1961, Distribution of the elements in some major units of the earth's crust: Geological Society of America Bulletin, v. 72, p. 175-192.
- Tuttle, D.F., and Bowen, N.L., 1958, Origin of granites in the light of experimental studies in the system  $\text{NaAlSi}_3\text{O}_8$ - $\text{KAlSi}_3\text{O}_8$ - $\text{SiO}_2$ - $\text{H}_2\text{O}$ : Geological Society of America Memoir 74, 153 p.
- White, A.J.R., 1979, Sources of Granite Magmas: Geological Society of America Abstracts with Programs, v. 11, p. 539.
- White, A.J.R. and Chappell, B.W., 1983, Granitoid types and their distribution in the Lachlan fold belt, southeastern Australia: Geological Society of America Memoir 159, p. 21-33.
- Wones, D.R., 1979, Intensive parameters during the crystallization of granitic plutons: Geological Society of America Abstracts with Programs, v. 11, p. 543.
- Woodard, T.W., 1982, Geology of the Lookout Mountain area, northern Black Range, Sierra County, New Mexico: M.S. Thesis, The University of New Mexico, Albuquerque, 95 p.
- York, D., 1966, Least-squares fitting of a straight line: Canadian Journal of Physics, v. 44, p. 1079-1086.

Table 1. Representative geochemical analyses of the various volcanic units in the Black Range and Sierra Cuchillo. Groups explained in text.

Tpc-basaltic andesite of Poverty Creek; Tkt-rhyolite of Keith Tank; Thc-rhyolite of Hoyt Creek; Twc-rhyolite of Whitetail Canyon; Ttr-trachytes in the Sierra Cuchillo; Tsp-rhyolite of Sawmill Peak; Tdp-rhyolite of Dolan Peak; Thok-rhyolite of HOK Ranch; Tws-rhyolite of Willow Springs Draw; NG-Taylor Creek Rhyolite, Nugget Gulch dome; Tc-Taylor Creek Rhyolite, Taylor Creek dome; KM-Taylor Creek Rhyolite, Kemp Mesa Dome; IC-Taylor Creek Rhyolite, Indian Creek dome; NNG-Taylor Creek Rhyolite, North Nugget Gulch Dome; BP-Taylor Creek Rhyolite, Boiler Peak Dome; AC-Taylor Creek Rhyolite, Alexander Cienega dome; NPC-Taylor Creek Rhyolite, North Paramount Canyon Dome; IP-Taylor Creek Rhyolite, Indian Peaks Dome; RM-Taylor Creek Rhyolite, Round Mountain Dome; Tg-granite of Iron Mountain.

Leaders indicate no analysis. Major elements, Ba, Cr, Ga, Mo, Nb, Ni, Pb, Rb, Sn, Sr, Th, U, V, Y, Zn, and Zr analyzed by XRF. \*-indicates INAA analyses. As, Br, Nf, Sb, Sc, Se, Ta, and REE's by INAA. F by ion-specific electrode. Cl by mercuric nitrate titration. Precision estimates:  $\text{SiO}_2$ ,  $\text{Al}_2\text{O}_3$ ,  $\text{K}_2\text{O} = \pm 0.5\%$ ,  $\text{CaO}$  and  $\text{Na}_2\text{O} = \pm 4\%$  at  $77\% \text{SiO}_2$ . Y, Nb, Zn, Ga, REE, Rb, Cs, Hf are better than  $\pm 2\%$ ; Zr, Th, Pb, Ni, Sc, Se, Ta, and U are better than  $\pm 5\%$ . Others are typically better than  $\pm 10\%$ . Sr at 2 ppm is  $\pm 30\%$  and at 450 ppm is  $\pm 0.1\%$ .

Total Fe as  $\text{Fe}_2\text{O}_3$

UNIT SAMPLE	Tpc 41	Tpc 52	Tpc 40	Tkt 218	Thc 259	Twc 260	Ttr 237	Ttr 239	Tsp 22
SiO <sub>2</sub>	52.23	54.77	56.93	73.71	73.83	69.20	65.18	66.11	71.45
TiO <sub>2</sub>	1.11	1.17	1.00	0.19	0.12	0.35	0.44	0.44	0.48
Al <sub>2</sub> O <sub>3</sub>	16.34	16.85	16.55	12.58	12.34	14.23	17.15	16.36	14.24
Fe <sub>2</sub> O <sub>3</sub>	9.04	8.00	7.21	1.26	0.94	2.00	3.07	2.93	2.03
MnO	0.14	0.08	0.14	0.06	0.04	0.07	0.12	0.17	0.02
MgO	6.29	3.99	1.57	0.55	0.29	0.71	0.52	0.49	0.27
CaO	8.44	7.40	4.91	0.84	0.86	1.62	1.14	1.00	0.33
Na <sub>2</sub> O	3.50	3.93	4.07	3.28	3.44	4.10	6.09	5.86	5.11
K <sub>2</sub> O	1.32	1.94	2.79	4.91	4.28	4.32	5.56	5.66	6.13
P <sub>2</sub> O <sub>5</sub>	0.25	0.58	0.51	0.03	0.02	0.10	0.17	0.16	0.07
LOI <sup>5</sup>	1.39	2.15	3.94	3.25	4.46	3.74	0.46	0.64	0.45
TOTAL	100.05	100.86	99.62	100.66	100.62	100.44	99.90	99.82	100.58
As	<1.0	<0.1	--	3.8	0.6	0.5	<0.3	1.4	<0.2
Ba	526	916	1278	1010	681	913	2210	1330	81
Br	<1.0	<1.0	--	0.5	2.8	2.9	--	0.8	<1.0
Cl(%)	--	--	--	--	--	--	--	--	--
Cr	272*	67*	52	<3*	<1*	<1*	<1*	<1*	<1*
Cs	1.3	0.3	--	6.4	5.1	2.8	0.5	0.7	2.8
F(%)	--	--	--	--	--	--	--	--	--
Ga	19	21	20	18	--	--	--	--	21
Hf	4.3	5.8	--	6.4	3.3	7.4	13.4	15.5	18.5
Mo	--	--	--	3	2	2	--	--	2
Nb	6	11	13	21	15	17	55	63	27
Ni	122	51	27	<5	<33*	<15*	--	<12	<5
Pb	7	5	11	30	27	23	20	23	23
Rb	23	29	51	236	222	141	109	119	171
Sb	0.2	<0.1	--	0.5	0.2	0.1	<0.1	<0.1	<0.1
Sc	20.9	18.8	--	3.0	2.3	2.8	6.6	6.6	10
Se	<1.0	<0.2	--	<0.3	<1.2	<0.4	<0.8	<0.2	<1.0
Sn	<5	<5	<5	<5	<5	<5	<5	<5	<5
Sr	581	1110	920	67	73	250	97	60	3
Ta	0.4	0.6	--	1.7	1.6	1.4	3	3.5	2.1
Th	<3	3	<3	27	24	16	16	18	18
U	<3	<1*	<3	6	6	4	3	3	5
V	183	157	120	7	<3	11	<3	<3	<3
Y	20	27	20	38	39	39	46	56	89
Zn	87	97	102	36	--	--	--	--	94
Zr	153	220	266	175	116	282	601	706	763
La	17	43	--	40	40	46	85	99	68
Ce	41	91	--	76	80	96	168	187	153
Nd	26	45	--	21	27	37	66	77	78
Sm	5	7.5	--	3.5	5.1	6.3	10.6	12	15.7
Eu	1.46	2	--	0.31	0.62	1.15	2.9	2.7	3.37
Tb	0.6	0.9	--	0.6	0.9	0.9	1.4	1.6	2.5
Yb	1.7	2.4	--	3.6	3.4	3.5	4.4	5.5	8.2
Lu	0.27	0.34	--	0.63	0.55	0.58	0.73	0.89	1.3

UNIT SAMPLE	Group A			Group B					
	Tsp 43	Tdp 55	Tdp 219	Thok 180	Tws 115	Tws 122	NG 142	NG 143	TC 9
SiO <sub>2</sub>	71.95	76.41	75.02	76.47	76.47	76.66	77.05	77.15	76.82
TiO <sub>2</sub>	0.48	0.18	0.16	0.16	0.15	0.16	0.12	0.12	0.16
Al <sub>2</sub> O <sub>3</sub>	13.72	12.09	11.82	11.98	12.28	12.12	12.72	11.70	11.37
Fe <sub>2</sub> O <sub>3</sub>	2.64	1.65	1.79	1.61	1.12	1.21	1.05	1.23	1.03
MnO	0.03	0.03	0.06	0.04	0.06	0.06	0.05	0.03	0.06
MgO	0.11	0.16	0.25	0.28	0.21	0.48	0.28	0.16	0.34
CaO	0.29	0.23	0.15	0.41	0.31	0.47	0.46	0.26	0.46
Na <sub>2</sub> O	4.01	3.64	3.34	3.11	3.45	2.79	3.16	3.23	3.64
K <sub>2</sub> O	5.77	5.27	4.89	4.96	5.16	5.00	4.71	4.86	4.80
P <sub>2</sub> O <sub>5</sub>	0.05	0.02	0.02	0.03	0.02	0.02	0.02	0.01	0.02
LOI	0.75	0.58	0.99	0.87	0.51	0.95	0.84	0.50	0.48
TOTAL	99.80	100.26	98.49	99.92	99.74	99.92	99.46	99.25	99.18
As	--	1.3	<1.4	1	36	3.2	10.3	16.4	--
Ba	82	<16	24	355	85	87	33	29	67
Br	--	<0.5	<0.6	1.1	--	--	--	--	--
Cl(%)	--	--	--	--	0.004	0.005	0.002	--	--
Cr	<10*	<1*	<1*	<1*	<9*	<10	<7*	<10	<6*
Cs	--	2.5	12.3	5.2	4.2	4	5.0	5.7	6.8
F(%)	--	--	--	--	0.19	0.06	0.17	0.06	0.15
Ga	20	19	20	21	19	19	19	20	19
Hf	--	12.2	3	8.4	7.6	7.5	7.1	7.6	6.7
Mo	2	2	1	--	1	--	3	--	--
Nb	25	32	33	39	36	33	33	35	36
Ni	<5	<5	<5	<5	8	<5	<5	<5	<5
Pb	25	30	20	28	21	37	26	24	22
Rb	162	223	228	313	259	232	288	293	247
Sb	--	0.1	<0.1	0.3	9	<0.1	0.4	0.6	<0.1
Sc	--	4.8	4.7	4.0	3.3	3.1	2.6	2.4	3.2
Se	--	<1.5	<0.2	<1.0	0.4	0.5	0.4	0.5	0.7
Sn	7	9	5	<5	25	<5	6	6	<5
Sr	13	4	7	92	16	18	9	7	55
Ta	--	2.5	2.8	3.7	3.5	3.7	3.7	4.0	5.4
Th	18	25	26	41	29	28	30	31	30
U		6	6	9	8	8	7	10	9
V	<3	<3	<3	3	<3	15	16	3	<3
Y	91	124	76	103	116	68	94	64	101
Zn	75	73	56	51	57	39	42	31	37
Zr	713	256	372	200	187	180	160	168	151
La	--	122	53	55	59	52	48	47	45
Ce	--	213	161	140	132	117	110	110	106
Nd	--	115	59	59	61	71	40	47	41
Sm	--	21.9	12.2	12.3	12.9	10.5	10.3	10.0	10.1
Eu	--	0.96	0.67	0.65	0.51	0.47	0.33	0.33	0.4
Tb	--	3.4	2.1	2.2	2.2	1.8	1.8	1.5	1.9
Yb	--	10.0	7.9	11.1	10.6	9.0	10.8	9.5	10.3
Lu	--	1.49	1.23	1.75	1.42	1.01	1.57	1.21	1.32

UNIT SAMPLE	Group B				π IC 8	Group C			
	TC 10	KM 1	KM 167	IC 6		NNG 136	NNG 236	BP 149	BP 224
SiO <sub>2</sub>	76.57	77.87	75.67	77.64	77.22	77.24	77.25	74.54	75.91
TiO <sub>2</sub>	0.17	0.14	0.13	0.15	0.16	0.08	0.11	0.09	0.11
Al <sub>2</sub> O <sub>3</sub>	12.25	11.71	12.56	12.59	11.84	12.53	11.98	12.05	12.17
Fe <sub>2</sub> O <sub>3</sub>	1.14	1.06	1.14	1.10	1.10	1.08	1.13	1.13	1.15
MnO	0.07	0.05	0.05	0.07	0.05	0.06	0.05	0.06	0.03
MgO	0.18	0.20	0.32	0.07	0.22	0.15	0.18	0.13	0.06
CaO	0.30	0.26	0.33	0.30	0.30	0.19	0.23	0.40	0.26
Na <sub>2</sub> O	3.50	3.42	3.29	3.58	3.64	3.76	3.72	3.74	3.57
K <sub>2</sub> O	5.19	5.14	5.33	5.06	4.94	4.89	4.87	4.69	4.80
P <sub>2</sub> O <sub>5</sub>	0.01	0.01	0.01	0.01	0.01	0.02	0.01	0.01	0.02
LOI	0.34	0.15	0.76	0.39	0.31	0.38	0.36	2.36	0.37
TOTAL	99.72	99.98	99.59	100.96	99.79	100.38	99.89	99.20	98.45
As	--	7.0	3.3	--	--	<1.3	--	2.4	3.5
Ba	81	69	66	100	55	19	19	19	<16
Br	--	--	--	--	--	0.2	--	--	<0.4
Cl(%)	--	--	0.005	--	--	0.002	--	0.003	--
Cr	<10	<10	<10	18	<10	<7*	23	14	<2*
Cs	--	4.5	4.0	--	--	4.7	--	10.3	4.0
F(%)	--	--	0.08	--	--	0.07	--	0.2	--
Ga	21	20	19	19	19	22	--	22	21
Hf	--	7.2	7.4	--	--	7.4	--	7.9	8.0
Mo	--	--	--	--	--	4	--	5	--
Nb	40	44	44	39	37	46	45	47	47
Ni	<5	<5	<5	<5	<5	<5	--	<5	<5
Pb	21	27	43	25	26	26	29	36	40
Rb	266	294	300	268	257	376	357	360	379
Sb	--	0.3	0.2	--	--	<0.1	--	0.4	0.1
Sc	--	3.2	3	--	--	2.6	--	2.4	2.0
Se	--	0.6	0.6	--	--	0.6	--	0.6	<0.8
Sn	<5	6	7	<5	<5	<5	7	11	5
Sr	12	10	21	12	11	2	2	2	6
Ta	--	--	4.6	--	--	5.4	--	4.8	4.6
Th	33	33	36	33	30	30	37	41	36
U	<3	10*	17	3	<3	7	6	14	7
V	<3	44	6	<3	6	<3	4	<3	14
Y	95	114	105	86	77	73	57	131	100
Zn	48	42	40	44	42	52	--	73	69
Zr	176	162	158	161	156	158	160	168	173
La	--	41	41	--	--	31	--	40	35
Ce	--	103	107	--	--	97	--	98	123
Nd	--	47	41	--	--	27	--	37	37
Sm	--	10.3	10.1	--	--	7.8	--	11.6	9.3
Eu	--	0.33	0.32	--	--	0.20	--	0.17	0.16
Tb	--	2.2	2.2	--	--	1.4	--	2.3	2.1
Yb	--	11.9	13.0	--	--	9.9	--	13.8	10.5
Lu	--	1.52	1.74	--	--	1.27	--	1.94	1.65

UNIT SAMPLE	Group C					Group D			Tg 198
	AC 215	AC 251	NPC 153	NPC 223	IP 205	IP 207	RM 134	RM 135	
SiO <sub>2</sub>	76.71	77.14	76.00	76.53	76.67	76.39	76.49	75.93	77.87
TiO <sub>2</sub>	0.11	0.11	0.08	0.11	0.10	0.11	0.07	0.07	0.07
Al <sub>2</sub> O <sub>3</sub>	11.94	12.18	12.26	12.33	12.00	11.95	12.95	12.87	11.98
Fe <sub>2</sub> O <sub>3</sub>	1.08	1.11	1.14	1.07	1.21	1.17	1.15	1.08	0.68
MnO	0.05	0.10	0.06	0.05	0.05	0.05	0.03	0.06	0.03
MgO	0.24	0.07	0.15	0.01	0.01	0.02	0.10	0.12	0.03
CaO	0.23	0.37	0.37	0.18	0.17	0.23	0.12	0.35	0.38
Na <sub>2</sub> O	3.53	3.96	3.46	3.55	3.82	3.66	3.47	3.92	4.15
K <sub>2</sub> O	5.04	4.83	5.02	4.82	4.90	4.87	5.11	4.95	4.53
P <sub>2</sub> O <sub>5</sub>	0.02	0.01	0.01	0.02	0.01	0.01	0.01	0.01	0.02
LOI	0.56	0.50	0.98	0.69	0.04	0.26	0.57	0.47	0.28
TOTAL	99.51	100.38	99.53	99.44	98.98	98.72	100.07	99.83	100.02
As	8.1	1.2	--	1.9	6.8	1.4	--	--	--
Ba	38	36	34	44	31	19	20	17	44
Br	0.3	--	--	<0.3	0.2	<0.1	--	--	--
Cl(%)	--	--	--	--	--	--	0.01	--	0.003
Cr	<0.7	<2.0	20	<1	<3*	<5*	27	<10	14
Cs	5.0	5.3	--	8.2	8.2	3.5	--	--	--
F(%)	--	--	--	--	--	--	0.06	0.11	0.24
Ga	21	--	23	22	21	21	24	24	28
Hf	8.0	8.6	--	8.2	7.9	7.8	--	--	--
Mo	--	--	--	--	--	--	--	--	--
Nb	47	49	49	49	48	50	59	55	82
Ni	<5	<35*	<5	<5	8	<5	<5	6	<5
Pb	29	35	39	26	28	28	28	33	30
Rb	349	377	397	375	393	392	463	476	404
Sb	0.4	0.1	--	0.1	0.1	0.2	--	--	--
Sc	2.0	2.1	--	2.1	1.9	1.8	--	--	--
Se	<0.1	<0.2	--	<0.4	<1.2	<2.1	--	--	--
Sn	6	<5	11	6	<5	5	10	<5	<5
Sr	4	5	10	5	3	3	1	1	8
Ta	4.3	4.2	--	4.4	4.6	4.5	--	--	--
Th	32*	42	38	34	37*	35*	12	42	--
U	8*	6*	6	5	9*	6*	5	3	--
V	40	4	<3	<3	18	<3	<3	<3	<3
Y	112	160	67	69	111	58	12	143	89
Zn	45	--	173	37	39	28	45	68	23
Zr	175	160	159	177	176	173	142	151	134
La	37	55	--	26	48	26	--	--	--
Ce	91	108	--	122	114	71	--	--	--
Nd	41	59	--	25	42	18	--	--	--
Sm	10.4	16.7	--	7.1	12.0	5.1	--	--	--
Eu	0.22	0.18	--	0.21	0.26	0.17	--	--	--
Tb	2.4	3.7	--	1.7	2.4	1.0	--	--	--
Yb	11.2	18.0	--	8.6	13.1	6.1	--	--	--
Lu	1.77	2.96	--	1.34	2.17	0.99	--	--	--

Table 2. Characteristics of the four tin-bearing rhyolite groups in the Black Range and Sierra Cuchillo of New Mexico.

Characteristic	Group A	Group B	Group C	Group D
Relative age (oldest=1)	1	2	3	4(?)
Phenocrysts (volume %)				
quartz	1-2	15-20	6-8	6-8
sanidine	5-13	15-20	6-8	6-8
plagioclase	--	0.5-2	<1	<1
biotite	tr	tr	tr	tr
amphibole	tr	--	tr	tr
zircon	tr	tr	tr	tr
sphene	tr	tr	--	--
opaque oxides	tr	tr	tr	tr
Total phenocrysts (%)	15	40	15	15
Quartz/sanidine ratio	0.1	1	1	1
Rb (ppm)	225	288	360	470
Sr (ppm)	6	16	5	1
Nb (ppm)	33	40	45	57
Ba (ppm)	20	65	29	19
La/Lu	40	33	23	--
La/Sm	4.3	4.3	3.9	--
Tb/Lu	1.7	1.5	1.2	--
LREE (/chondrite)	400	120	115	--
HREE (/chondrite)	45	50	60	--

Formations and individual domes included in the various tin-bearing rhyolite groups

Group A-rhyolite of Dolan Peak, Black Range

Group B-Taylor Creek Rhyolite (North Nugget Gulch Dome, Taylor Creek Dome, Kemp Mesa Dome, Indian Creek Dome, Squaw Creek Dome), Black Range; rhyolite of Willow Springs Draw, Sierra Cuchillo; rhyolite of HOK Ranch, Sierra Cuchillo.

Group C-Taylor Creek Rhyolite (Nugget Gulch Dome, Poiler Peak Dome, Alexander Cienega Dome, North Paramount Canyon Dome, Indian Peaks Dome), Black Range.

Group D-Taylor Creek Rhyolite (Round Mountain Dome); Black Range.



Table 3.  $^{87}\text{Sr}/^{86}\text{Sr}$  initial ratios for tin-bearing rhyolites in the northern Black Range and Sierra Cuchillo, New Mexico.

SAMPLE	Rb	Sr	$^{87}\text{Rb}/^{86}\text{Sr}$	$^{87}\text{Sr}/^{86}\text{Sr}$	Error	$^{87}\text{Sr}/^{86}\text{Sr}$	
						28.2 Ma	28.5 Ma
Taylor Creek Rhyolite; Boiler Peak dome							
131	416*	3.83	318.1	0.83411	21	0.7067	0.7053
149	347.7	2.716	376.0	0.86338	1	0.7128	0.7112
150	393.8	2.474	469.3	0.90139	6	0.7134	0.7114
190	366.7	16.1	66.07	0.73452	29	0.7081	0.7078
221	357.9	5.275	197.9	0.78940	1	0.7101	0.7093
226	376.3	5.635	194.7	0.78811	2	0.7101	0.7093
227	360.0	3.641	289.4	0.82724	9	0.7113	0.7101
Nugget Gulch dome							
140	290*	7.143	118.1	0.75959	11	0.7123	0.7118
141	288.5	6.885	121.9	0.76040	18	0.7116	0.7111
142	288*	10.18	82.13	0.74259	15	0.7097	0.7093
196	8.03	199.6	0.116	0.70880	10	0.7088	0.7088
Squaw Creek dome							
30	470*	75*	18.15	0.71770	20	0.7104	0.7104
31	676*	47*	41.7	0.72737	26	0.7107	0.7105
33	617*	174*	10.27	0.71470	18	0.7106	0.7105
Kemp Mesa dome							
2	274.0	9.638	82.56	0.74601	15	0.7129	0.7126
3	326.0	15.82	59.79	0.73566	11	0.7117	0.7115
4	285.9	11.24	73.86	0.74165	14	0.7121	0.7118
167	292.2	19.24	44.03	0.72918	13	0.7115	0.7114
168	306.5	10.20	87.28	0.74710	10	0.7121	0.7118
268	264.3	11.01	69.68	0.74015	5	0.7122	0.7119
Indian Peaks dome							
207	368.39	4.087	263.7	0.82106	18	0.7154	0.7143
208	300.2	10.086	86.43	0.74505	23	0.7104	0.7101
211	300.7	7.973	110.3	0.75529	10	0.7111	0.7106
Taylor Creek dome							
155	281.3	22.01	37.05	0.72653	9	0.7117	0.7115
165	261.5	9.222	82.38	0.74973	17	0.7149	0.7146
Alexander Cienega dome							
213	364.3	4.790	213.8	0.79187	2	0.7062	0.7053
214	352.8	3.235	319.6	0.83799	2	0.7100	0.7086
North Paramount Canyon dome							
223	287.0	6.231	134.19	0.77874	1	0.7250	0.7244
North Nugget Gulch dome							
136	365.6	3.104	345.65	0.85374	1	0.7153	0.7138
Rhyolite of Dolan Peak							
219	223.1	8.48	76.43	0.74952	1	0.7189	0.7186
220	288.9	8.647	99.07	0.75049	1	0.7108	0.7104
Rhyolite of Willow Springs Draw (Sierra Cuchillo)							
115	259*	15.28	49.17	0.73103	25	0.7143	0.7141
116	235*	13.49	50.53	0.73423	15	0.7140	0.7138
117	250*	16.33	44.40	0.73198	19	0.7142	0.7140
Granite of Iron Mountain (Sierra Cuchillo)							
198	395.6	9.576	120.1	0.75567	1	0.7076	0.7071
199	359.6	11.696	89.25	0.74182	1	0.7061	0.7057
200	601.1	4.416	400.0	0.86676	2	0.7066	0.7048
201	469.5	4.49	306.1	0.83009	12	0.7075	0.7062

\* determined by XRF, other Rb and Sr by isotope dilution.

Table 4A. Oxygen isotope compositions and temperatures for mineral pairs from the Taylor Creek Rhyolite and rhyolite of Willow Springs Draw.

<u>Sample</u>	<u><math>\delta^{18}\text{O}</math></u>	<u>REMARKS</u>
1	8.0	Mild VPC* whole rock rhyolite
9	8.8	Mild VPC whole rock rhyolite
116	7.6	Mild VPC whole rock rhyolite
	7.7	Quartz separate from 116
	6.8	sanidine separate from 116
136	7.3	Mild VPC whole rock rhyolite
	7.6	Quartz separate from 136
	7.0	Sanidine separate from 136
	2.4	Magnetite separate from 136
149	8.8	Hydrated vitrophyre
	7.5	Quartz separate from 149
	6.7	Sanidine separate from 149
167	9.0	Mild VPC whole rock rhyolite
	7.8	Quartz separate from 167
	7.7	Sanidine separate from 167

4B. Oxygen isotope temperatures from mineral pairs. Errors are about  $\pm 100^\circ\text{C}$ .

<u>Sample</u>	<u>Pair</u>	<u>Temperature (<math>^\circ\text{C}</math>)</u>
116	quartz-sanidine	707
136	quartz-sanidine	876
	quartz-magnetite	757
	sanidine-magnetite	730
149	quartz-sanidine	753
167	quartz-sanidine	1335

sample locations (Fig. 2); 1-Kemp Mesa dome; 9-Taylor Creek Dome; 116-Monticello Cutoff (rhyolite of Willow Springs Draw); 136-North Nugget Gulch dome; 149-Boiler Peak Dome, Paramount Canyon; 167-Taylor Creek Dome.

Table 5. Comparison of average tin-bearing rhyolites of New Mexico with the I-, S-, and A-Type granites. Granite data compiled from White and Chappell (1983), Chappell and White (1974), Loiselle and Wones (1979), Wones (1979), and White (1979).

	I-Type	S-type	A-type	Average Rhyolite
Chemistry				
SiO <sub>2</sub>	68	69	74	77
Al <sub>2</sub> O <sub>3</sub>	14.5	14.3	12.7	12.4
Fe <sub>2</sub> O <sub>3</sub>	4.1	4.3	2.9	1.1
CaO	3.8	2.5	1.1	0.4
Na <sub>2</sub> O	2.9	2.2	3.3	3.9
K <sub>2</sub> O	3.1	3.6	4.5	4.8
Ba	520	480	605	19
Rb	132	180	199	360
Sr	253	139	105	10
Nb	9	11	22	47
Y	29	32	76	131
Zr	143	170	342	168
Th	16	19	23	41
U	3	3	5	14
Ga	16	17	21	22
Sc	15	14	14	2.4
La	29	31	55	40
Ce	63	69	134	98
$\delta^{18}\text{O}$	6-10	>10		6.5-6.8
$f_{\text{O}_2}$	high	low	low to moderate	moderate
( <sup>87</sup> Sr/ <sup>86</sup> Sr) <sub>i</sub>	<0.708	>0.708	0.703-0.712	0.708-0.712
% C in norm	<1%	>>1%	+1	+1
Ga/Al	low	moderate	high	high
K <sub>2</sub> O/Na <sub>2</sub> O	low	high	high	high
Hf/H <sub>2</sub> O <sub>2</sub>	low	low	high	high

Table 6. Crystal-liquid partition coefficients used in this study. Data from Mahood and Hildreth (1983), Michael (1983) Crecraft and others (1981), and Rose and others (1979).

el.	Plag.	San.	Bio.	Cpx.	Amph.	Zir.	Sphene	Allanite
Ba	0.6-1	3-22	2-18	0.2	0.2	--	--	--
Sr	4-15	3.1	0.2	0.5	0.7	--	0.9	40
Rb	0.06	0.4-1	2-12	0.03	0.07	--	--	--
Nb	0.06	--	3-9	0.8	--	--	--	--
Sc	0.15	0.3	4-19	25-100	26	60-77	3.9	49-62
Zr	0.25	0.3	1.2	0.6	1	>>500	--	--
Ta	--	--	1	--	--	30-50	--	--
Th	0.05	0.02	0.2-4	.01-7	0.1-9	62-91	--	420-548
La	0.4	0.3	0.8-10	0.5-13	0.4	2-27	19-45	1400- 3500
Ce	0.4	0.4	0.8-10	0.4-11	0.5-6.4	2-24	34-70	1300- 2500
Sm	0.2	0.3	0.9-4	1.5-11	3-7	3-18	102-352	730-977
Eu	3	2-9	0.3-3	1.1-5	2.5-5.8	1-20	99-189	100- 300
Tb	0.1	0.3	0.1-4	10	4-10	37	--	20-311
Lu	0.25	0.2	0.5-3	1.3-5	3-9	280- 650	27-105	15-44

Table 7. Trace element crystal-liquid fractionation models for fractionation from Group B rhyolites to Group C rhyolites. Partition coefficients from Michael (1983).

El.	Parent	model 1	model 2	model 3	model 4	Daughter
Ba	66	21.3	21.3	21.3	21.3	19
Sr	21	2.3	2.3	2.3	2.3	2.0
Rb	300	357	357	357	358	360
Nb	44	55	55	55	55	40
La	41	48	40	40	41	40
Ce	107	128	112	112	107	98
Sm	10	12.5	12.1	12.0	10.3	11.6
Eu	0.3	0.1	0.1	0.1	0.1	0.2
Yb	13.0	16.3	16.3	14.8	13.9	13.8
Lu	1.7	2.1	2.1	1.9	1.7	1.9

Parent fractionated by (%)

plagioclase	17.0	17.0	17.0	17.0
sanidine	6.0	6.0	6.0	6.0
biotite	0.5	0.5	0.5	0.5
allanite	0.0	0.046	0.046	0.03
zircon	0.0	0.0	0.015	0.015
spene	0.0	0.0	0.0	0.15

Chi <sup>2</sup>	13.1	4.3	3.8	2.9
------------------	------	-----	-----	-----

Bulk distribution coefficients

Ba	5.2298	5.2288	5.2254	5.1927
Sr	9.1947	9.2007	9.1948	9.1402
Rb	0.3481	0.3480	0.3478	0.3456
Nb	0.1498	0.1498	0.1497	0.1487
La	0.4328	1.0883	1.0922	1.0173
Ce	0.3281	0.8369	0.8427	0.9976
Sm	0.19532	0.3391	0.3460	0.9406
Eu	5.5936	5.6512	5.6605	6.2449
Yb	0.1553	0.1563	0.51587	6.2449
Lu	0.2098	0.2127	0.6258	0.7920

Partition coefficients

	Plagioclase	Sanidine	Biotite	Zircon	Sphene	Allanite
Ba	1.7	15.0	8.0	0.00	0.00	0.00
Sr	12.0	2.0	0.15	0.00	0.90	40.0
Rb	0.14	0.55	5.0	0.00	0.00	0.00
Nb	0.06	0.00	5.0	0.00	0.00	0.00
La	0.45	0.12	3.6	7.2	25	3350
Ce	0.35	0.06	2.8	10.0	53	2600
Sm	0.2	0.04	1.9	11.	102	735
Eu	6.0	4.8	1.3	20	101	300
Yb	0.18	0.04	0.7	564	37	5
Lu	0.25	0.03	1.0	648	27	15

Table 8. Crystal-liquid fractionation models of fractionation of Group C rhyolites to Group D rhyolites. Partition coefficients from Michael (1983).

El.	Parent	model 1	model 2	model 3	daughter
Nb	47	69	55	63	59
Ba	25	1	18	16	18
Rb	360	465	413	466	463
Sr	5	0.5	0.9	0.2	1
Th	35	52	41	47	42

Parent fractionated by (%)

plagioclase	15	14	25
sanidine	18	1.5	1.5
Chi <sup>2</sup>	20.2	5.6	1.7

Bulk distribution coefficients

Nb	0.0273	0.0542	0.0566
Ba	8.9546	2.9871	2.4528
Rb	0.3636	0.1797	0.1632
Sr	6.5454	11.0323	11.4340
Th	0.0336	0.0471	0.0483

partition coefficients

	Plagioclase	Sanidine
Nb	0.06	0.00
Ba	1.7	15
Rb	0.14	0.55
Sr	12	2
Th	0.05	0.02

Table 9a. Trace element crystal-liquid fractionation model for fractionating the basaltic andesite of Poverty Creek to Group B tin-bearing rhyolites. Partition coefficients as in Table 7 except for Hf, which is 3350 for Hf in zircon.

	Parent	Model	Daughter	Bulk D	Fractionated by
Ba	1278	70	66	6.6875	25% plagioclase
Sr	920	23	25	8.2500	15% sanidine
Rb	51	73	300	0.2938	
Hf	6.2	9.7	7.1	0.1288	
La	43	61	41	0.3263	
Ce	91	134	107	0.2413	
Sm	7.5	11.6	10.1	0.1400	
Eu	2.0	0.2	0.3	5.5500	
Yb	2.4	3.7	13	0.1275	
Lu	0.3	0.5	1.7	0.1675	

Table 9b. Major element mixing model for the basaltic andesite of Poverty Creek and Group B tin-bearing rhyolites.

	Parent *	An 40 *	Amph *	Biot *	Apat *	Daughter *	Calc *
SiO <sub>2</sub>	59.94	58.16	38.94	36.68	1.03	76.66	75.94
TiO <sub>2</sub>	1.05	0.00	2.79	4.53	0.00	0.13	0.58
Al <sub>2</sub> O <sub>3</sub>	17.43	26.57	9.02	12.88	0.02	12.73	12.37
Fe <sub>2</sub> O <sub>3</sub>	6.83	0.00	33.31	25.86	0.71	1.04	0.98
MnO	0.15	0.00	0.66	0.41	0.19	0.05	0.08
MgO	1.66	0.00	0.05	8.65	0.06	0.32	1.53
CaO	5.17	8.35	10.29	0.01	55.23	0.33	0.44
Na <sub>2</sub> O	4.29	6.92	2.29	0.45	0.08	3.33	3.50
K <sub>2</sub> O	2.94	0.00	1.65	9.48	0.00	5.39	4.19
P <sub>2</sub> O <sub>5</sub>	0.54	0.00	0.00	0.00	41.58	0.01	-0.14

Cumulates = 61.6% of the system

Liquid = 38.4% of the system

Cumulate composition (%):

Plagioclase (An 40)	62.00
Amphibole	15.93
Biotite	19.77
Apatite	2.30

\* Parent - Parent analysis      An 40 - Plagioclase (An 40)  
 Amph - Amphibole                  Biot - Biotite  
 Apat - Apatite                      Daughter - Daughter analysis  
 Calc - Calculated daughter composition



Table 10. Trace element crystal-liquid fractionation model to produce the tin-bearing rhyolite magmas from the older rhyolites in the Black Range. Partition coefficients from numerous sources (K. Condie, 1987, written communication).

Rhyolite of Whitetail Canyon

	Parent	Model	Daughter	Bulk D	Fractionated by	
Ba	913	44	66	3.3091	44%	plagioclase
Sr	250	27	25	2.6927	21%	sanidine
Rb	141	296	300	0.4339	8%	biotite
Nb	17	48	44	0.2005	0.012%	allanite
La	46	44	41	1.0389		
Ce	96	91	107	1.0389		
Sm	6.3	8.1	10.1	0.8085		
Eu	1.1	1.0	0.3	1.1156		
Yb	3.5	11.3	13.0	0.1053		
Lu	0.6	1.9	1.7	0.1053		

Rhyolite of Hoyt Creek

	Parent	Model	Daughter	Bulk D	Fractionated by	
Ba	681	66	66	5.2848	15%	plagioclase
Sr	73	25	25	2.9995	27%	sanidine
Rb	222	300	306	0.4107	0.007%	allanite
Nb	15	26	44	0.0214		
La	40	41	41	0.9725		
Ce	80	81	107	0.9725		
Sm	5.1	5.8	10.1	0.7573		
Eu	0.6	0.5	0.3	1.2938		
Yb	3.4	5.7	13	0.0481		
Lu	0.6	0.9	1.7	0.0481		

Partition coefficients

	Plag	San	Bio	Amph	Zir	Sph	All
Ba	0.4	8.0	7.0	0.05	0.0	0.0	0.0
Sr	3.0	3.0	0.2	0.3	0.0	0.0	0.0
Rb	0.07	0.6	2.0	0.02	0.0	0.0	0.0
Nb	0.06	0.0	1.5	0.0	0.0	0.0	0.0
La	0.3	0.05	0.2	1.0	3.0	50	5000
Ce	0.3	0.05	0.2	2.0	3.0	80	5000
Sm	0.2	0.03	0.2	5.0	4.0	125	5000
Eu	5.0	1.25	0.2	4.0	3.0	60	800
Yb	0.07	0.10	0.4	5.0	250	60	100
Lu	0.07	0.01	0.4	5.0	300	50	100

Table 11a. Trace element crystal-liquid fractionation model for fractionating the rhyolite of Sawmill Peak to produce the Group B tin-bearing rhyolite lavas. The distribution coefficients are the same as in Table 7 except for Hf in zircon. The distribution coefficient for Hf in zircon = 3350.

	Parent	Model	Daughter	Bulk D	Fractionated by
Ba	81	66	66	14.7248	1.5% sanidine
Sr	3	3	25	1.9646	0.027% zircon
Rb	171	172	300	0.5403	
Hf	18.5	7.5	7.1	59.2436	
La	68	69	41	0.2452	
Ce	153	155	107	0.2358	
Sm	15.7	15.9	10.1	0.2338	
Eu	3.4	3.2	0.3	5.0688	
Yb	8.2	7.1	13.0	10.0118	
Lu	1.3	1.1	1.7	11.4872	

Table 11b. Major element mixing model for the rhyolite of Sawmill Peak and Group B tin-bearing rhyolites.

Input compositions

	Parent analysis	San. (Or 70)	Plag. (An 14)	Amph.	Daughter analysis	Calc. daughter
SiO <sub>2</sub>	71.49	65.91	64.10	50.23	76.66	75.83
TiO <sub>2</sub>	0.49	0.00	0.00	2.31	0.13	0.60
Al <sub>2</sub> O <sub>3</sub>	14.26	18.64	21.68	0.64	12.73	12.35
Fe <sub>2</sub> O <sub>3</sub>	1.83	0.00	0.00	29.14	1.04	0.96
MnO	0.02	0.00	0.00	0.56	0.05	0.00
MgO	0.27	0.00	0.00	3.72	0.32	0.18
CaO	0.33	0.00	2.93	4.77	0.33	0.18
Na <sub>2</sub> O	5.12	3.40	9.25	6.33	3.39	4.66
K <sub>2</sub> O	6.14	12.05	1.05	1.29	5.39	5.82
P <sub>2</sub> O <sub>5</sub>	0.07	0.00	0.00	0.00	0.01	0.11

Cumulates = 35.4% of the system  
 Liquid = 64.6% of the system

Cumulate composition (%):

Sanidine (Or 70) = 50.987  
 Plagioclase (An 14) = 37.321  
 Amphibole = 11.692

Table 12. Major element mixing model for fractionation of A-type granite to Group B tin-bearing rhyolite lava.

	Input Compositions				
	Parent	An 14	Or 50	Amph	Daughter
SiO <sub>2</sub>	74.61	64.74	66.03	40.47	77.09
TiO <sub>2</sub>	0.33	0.00	0.00	2.90	0.09
Al <sub>2</sub> O <sub>3</sub>	12.86	21.89	18.67	9.37	12.46
Fe <sub>2</sub> O <sub>3</sub>	2.65	0.00	0.00	34.62	1.05
MnO	0.06	0.00	0.00	0.69	0.06
MgO	0.33	0.00	0.00	0.05	0.13
CaO	1.09	2.96	0.00	10.71	0.41
Na <sub>2</sub> O	3.39	1.06	8.63	2.38	3.84
K <sub>2</sub> O	4.58	1.06	8.63	1.71	4.85
P <sub>2</sub> O <sub>5</sub>	0.09	0.00	0.00	0.00	0.01

	Model Calculations		
	Parent analysis	Daughter analysis	Daughter calculated
SiO <sub>2</sub>	74.61	77.09	76.31
TiO <sub>2</sub>	0.33	0.09	0.21
Al <sub>2</sub> O <sub>3</sub>	12.86	12.46	12.62
Fe <sub>2</sub> O <sub>3</sub>	2.65	1.04	0.98
MnO	0.06	0.06	0.03
MgO	0.33	0.13	0.36
CaO	1.09	0.41	0.54
Na <sub>2</sub> O	3.39	3.84	3.23
K <sub>2</sub> O	4.58	4.85	4.70
P <sub>2</sub> O <sub>5</sub>	0.09	0.01	0.10

Cumulate = 9.2% of the starting liquid

Cumulate minerals:

Plagioclase (An 14)	24.20%
Sanidine (Or 50)	19.13%
Amphibole	56.67%

Table 13. Crystal-liquid fractionation model for fractionation of A-type granites to Group B tin-bearing rhyolites. Partition coefficients from numerous sources (K. Condie, 1986, written communication).

El.	Parent	Model	Daughter	Bulk D	Fractionated by	
----	-----	-----	-----	-----	-----	-----
Ba	605	66	66	3.7741	30.0%	Plagioclase
Sr	105	25	25	2.7907	21.0%	Sanidine
Rb	199	319	300	0.4119	4.0%	Biotite
Nb	22	44	44	0.1415	0.1%	Zircon
La	55	44	41	1.2910	0.012%	Allanite
Ce	134	106	107	1.2910		
Sm	15.0	12.5	10.1	1.2308	Chi <sup>2</sup> =1.9	
Eu	2.4	0.4	0.3	3.3922		
Yb	8.7	12.5	13	0.5463		
Lu	1.4	1.8	1.7	0.6371		

Partition coefficients

	Plag	San	Bio	Amph	Zir	Sph	All
	----	-----	-----	-----	-----	-----	-----
Ba	0.4	8.0	7.0	0.05	0.0	0.0	0.0
Sr	3.0	3.0	0.2	0.3	0.0	0.0	0.0
Rb	0.07	0.6	2.0	0.02	0.0	0.0	0.0
Nb	0.06	0.0	1.5	0.0	0.0	0.0	0.0
La	0.3	0.05	0.2	1.0	3.0	50	5000
Ce	0.3	0.05	0.2	2.0	3.0	80	5000
Sm	0.2	0.03	0.2	5.0	4.0	125	5000
Eu	5.0	1.25	0.2	4.0	3.0	60	800
Yb	0.07	0.10	0.4	5.0	250	60	100
Lu	0.07	0.01	0.4	5.0	300	50	100

Plag-plagioclase

San- sanidine

Bio- biotite

Amph-amphibole

Zir- zircon

Sph- sphene

All- allanite

Figure 1. Location map for the Taylor Creek district in southern New Mexico and its relationship to the Rio Grande rift. Inset shows detail of the region near Figure 2 and includes the tin-bearing rhyolites investigated during this study. MC-Monticello Cutoff; IM-Iron Mountain; NNG-North Nugget Gulch; NG-Nugget Gulch; SC-Squaw Creek; NPC-North Paramount Canyon; BP-Boiler Peak; AC-Alexander Cienega; DP-Dolan Peak; RM-Round Mountain; IC-Indian Creek; TC-Taylor Creek; KM-Kemp Mesa; IP-Indian Peaks; PC-The Paramount Canyon area of the Boiler Peak dome.

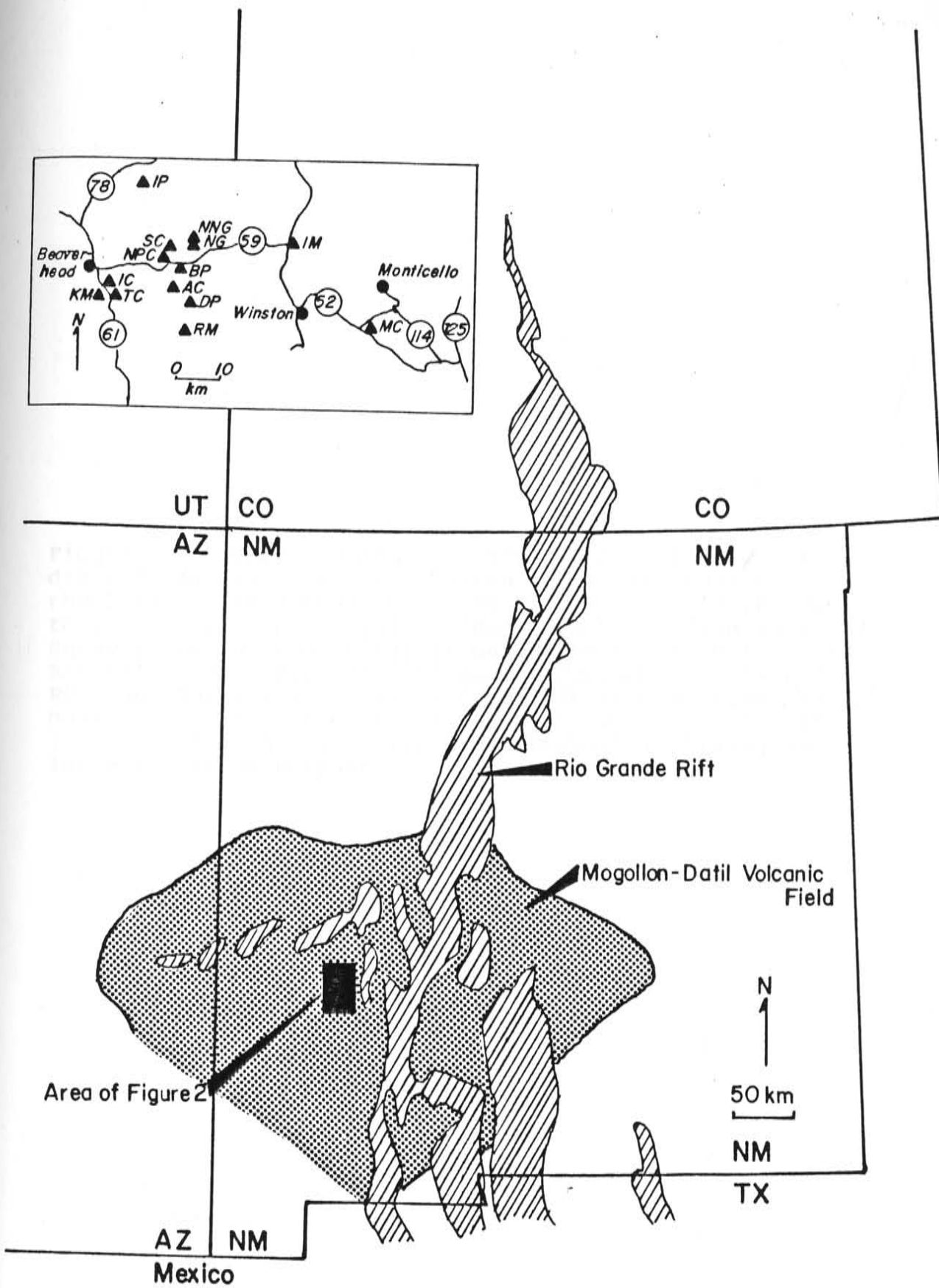


Figure 2. Generalized geologic map of the Taylor Creek district showing the distribution of the tin-bearing rhyolites. Tin-bearing rhyolite groups are described in the text. Taylor Creek Rhyolite domes are; IP-Indian Peaks; SC-Squaw Creek; NNG-North Nugget Gulch; NG-Nugget Gulch; SP-Sawmill Canyon; NPC-North Paramount Canyon; BP-Boiler Peak; RM-Round Mountain; TC-Taylor Creek; IC-Indian Creek; KM-Kemp Mesa. DP is the rhyolite of Dolan Peak. OR is rhyolite lavas older than the Taylor Creek Rhyolite. Triangles indicate tin occurrences.



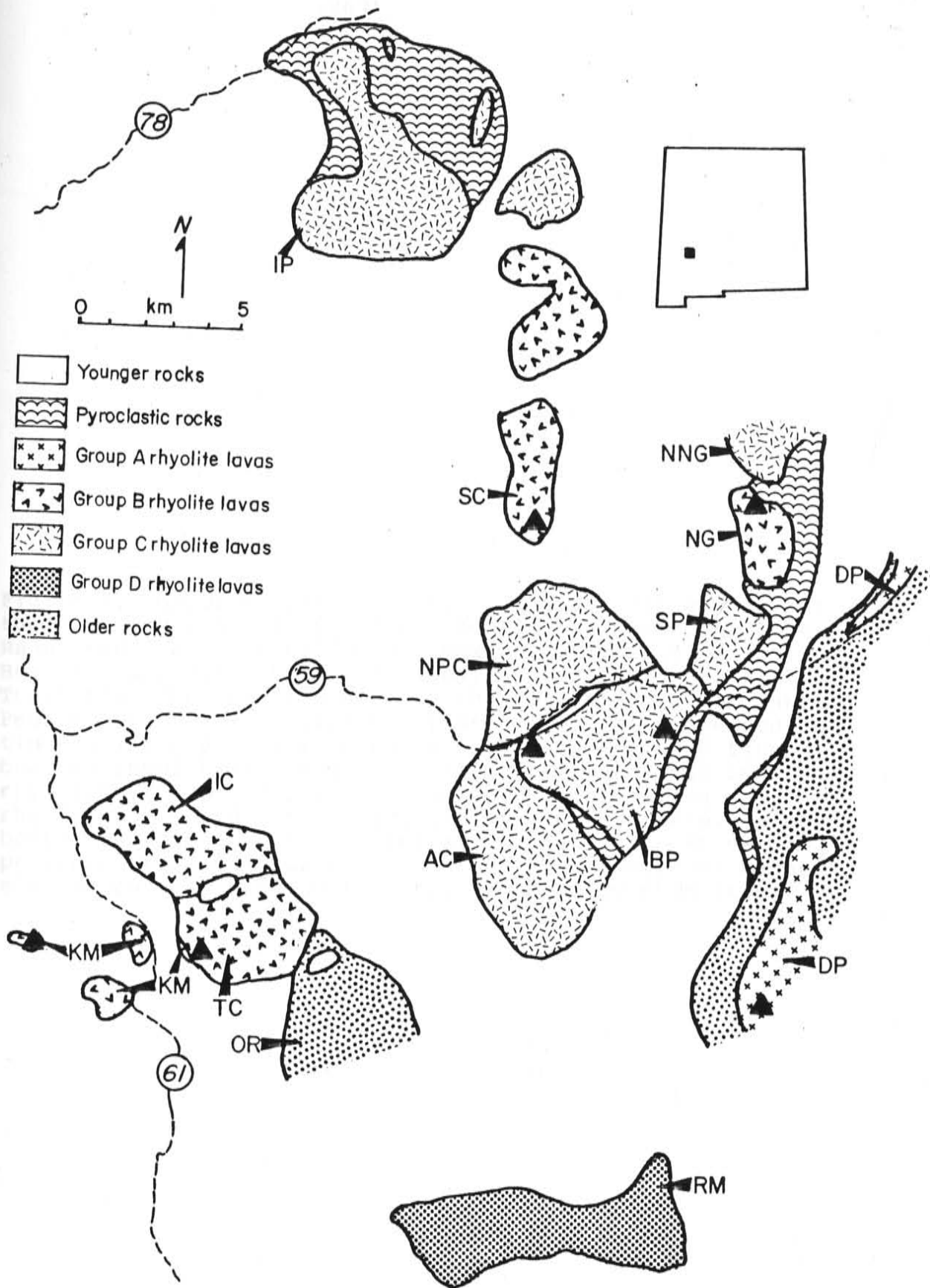
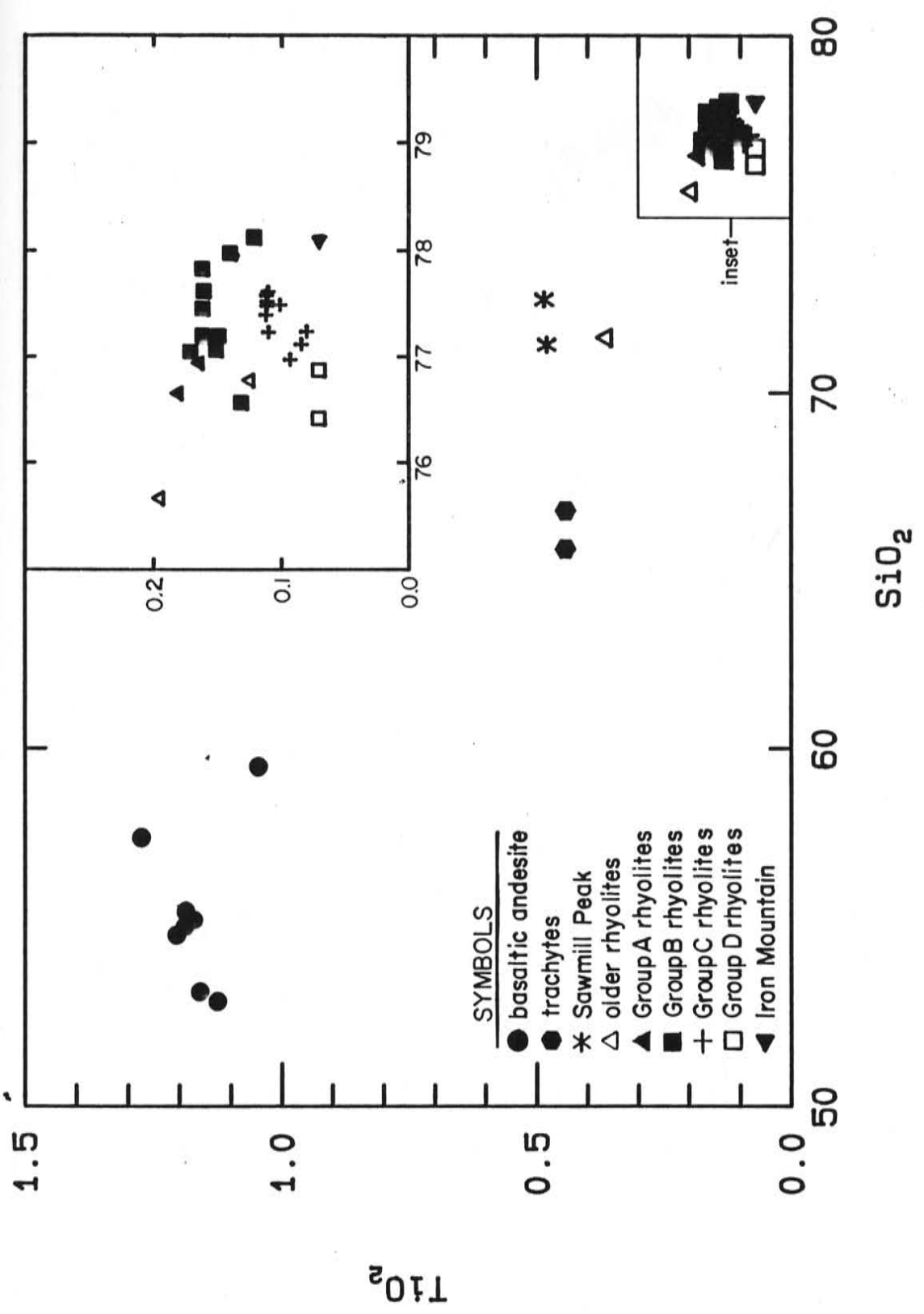
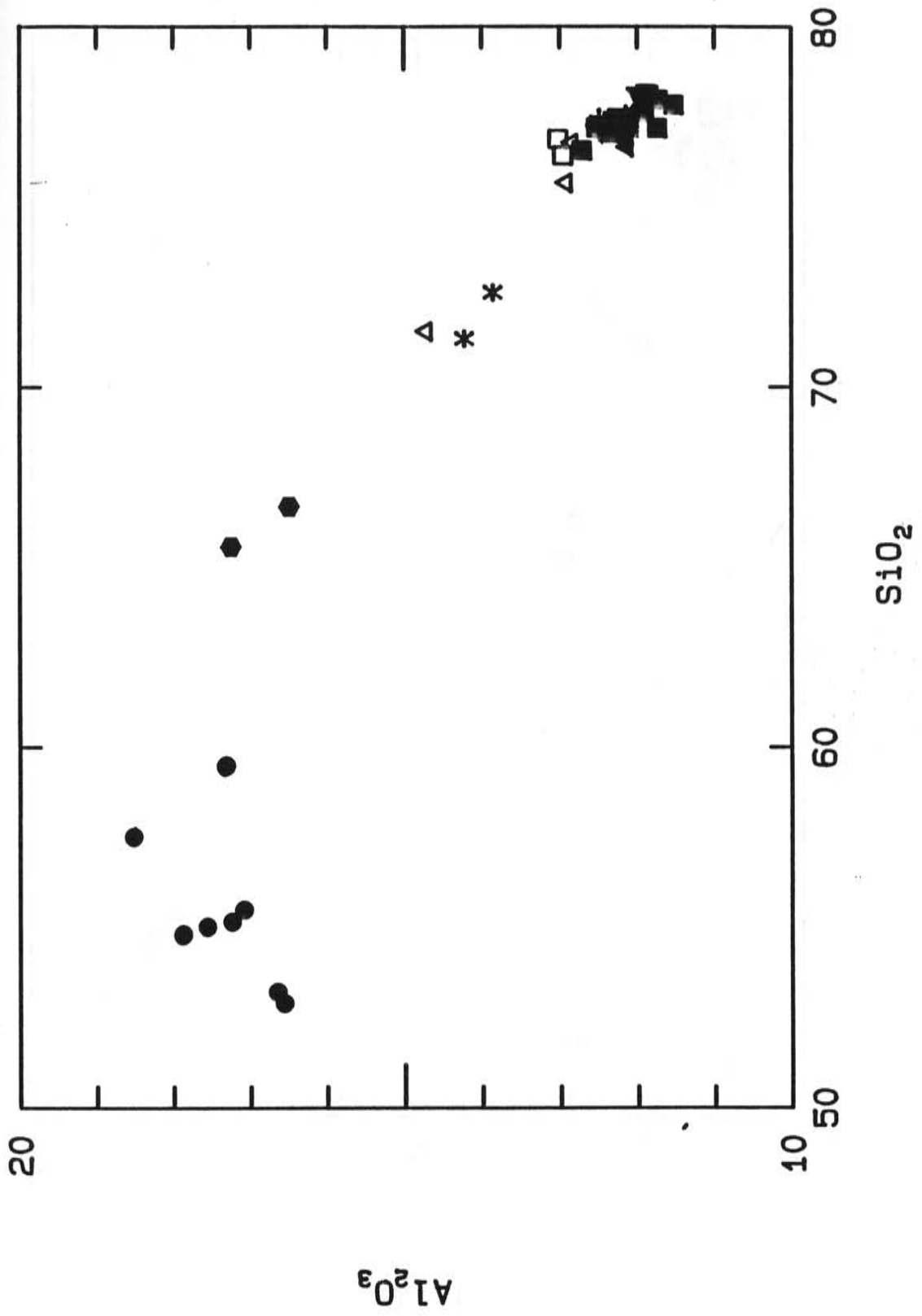
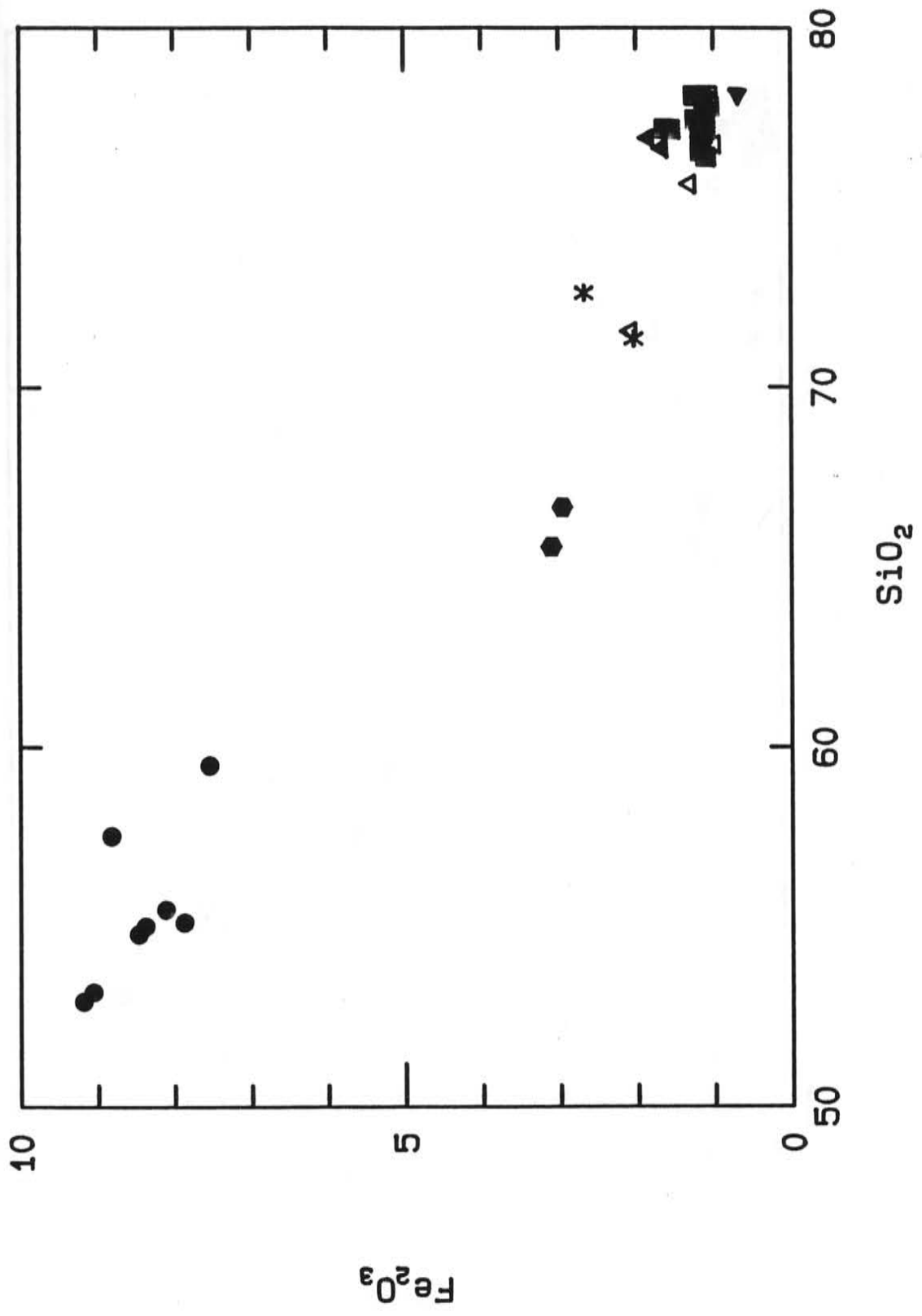
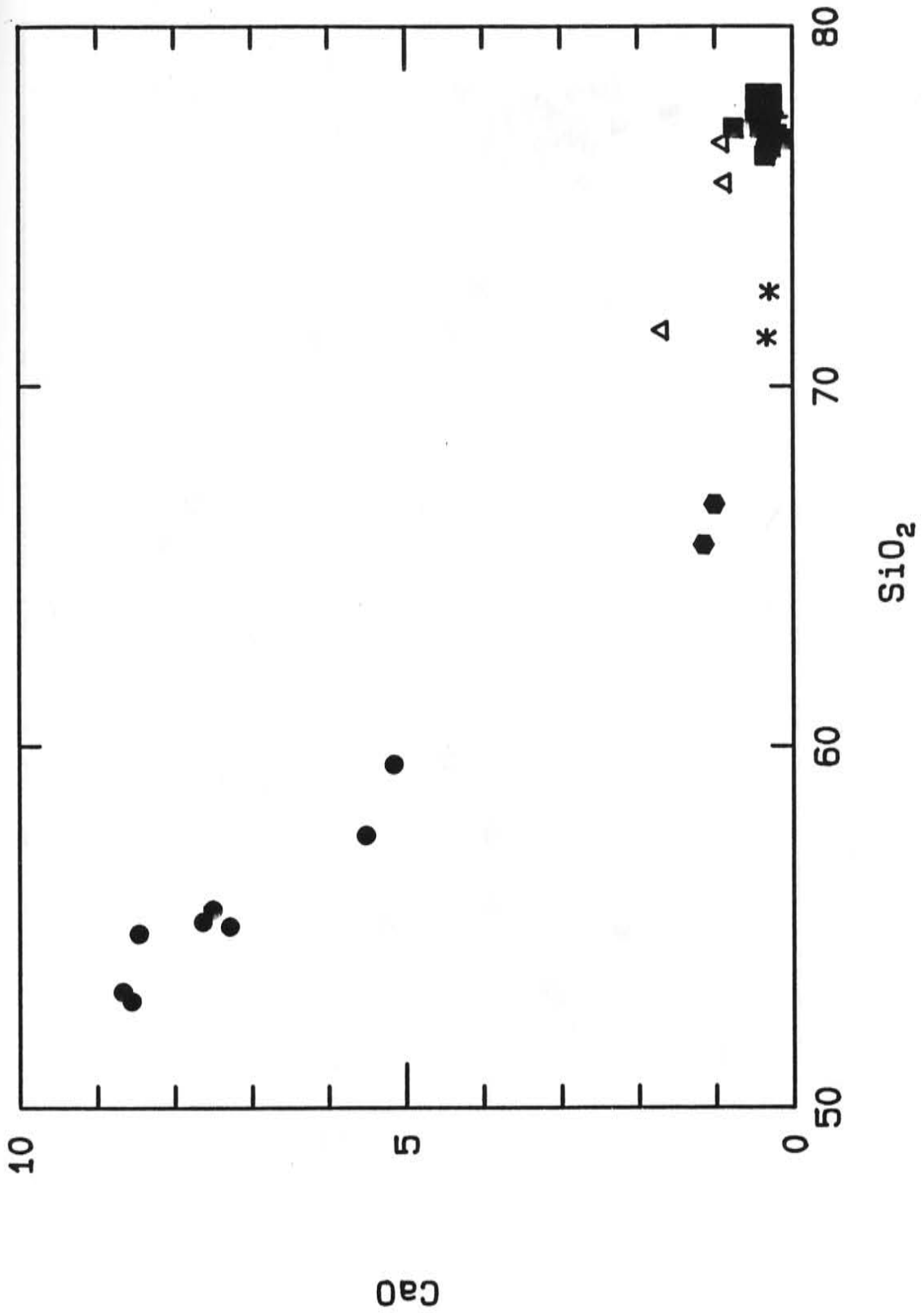


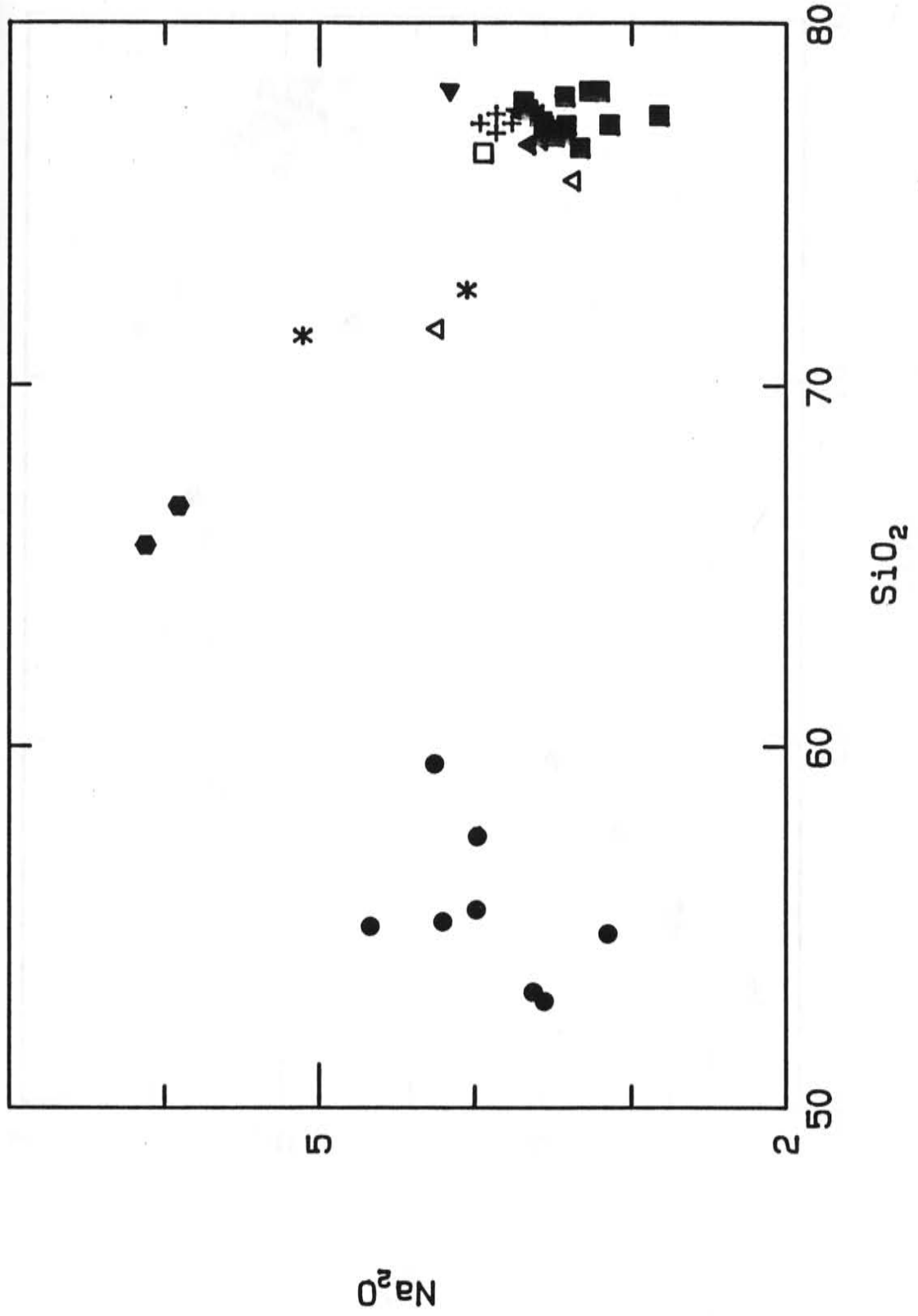
Figure 3. Major element variation diagrams (in wt. %) for the Tertiary volcanic units exposed in the northern Black Range and Sierra Cuchillo, New Mexico. Explanation: Basaltic andesite--basaltic andesite of Poverty Creek; Trachytes--unnamed trachytes in the Sierra Cuchillo; Sawmill Peak--rhyolite of Sawmill Peak; Group A rhyolites--Group A tin-bearing rhyolites; Group B rhyolites--Group B tin-bearing rhyolites; Group C rhyolites--Group C tin-bearing rhyolites; Group D rhyolites--Group C tin-bearing rhyolites; Iron Mountain--granite of Iron Mountain. Tin-bearing rhyolite groups described in the text. Rb vs SiO<sub>2</sub> presented to emphasize the fact that no significant major element changes occur within the tin-bearing rhyolites.



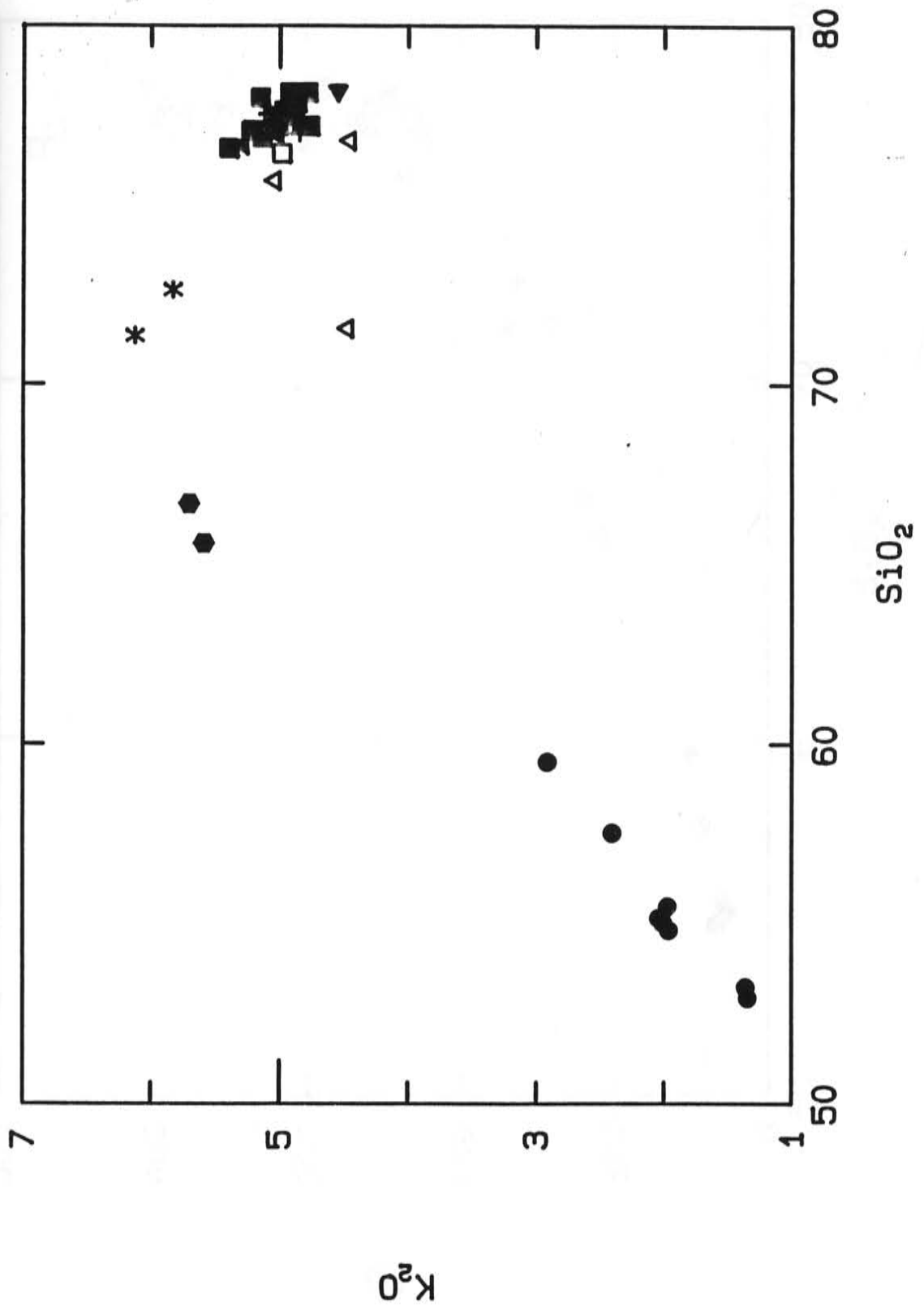












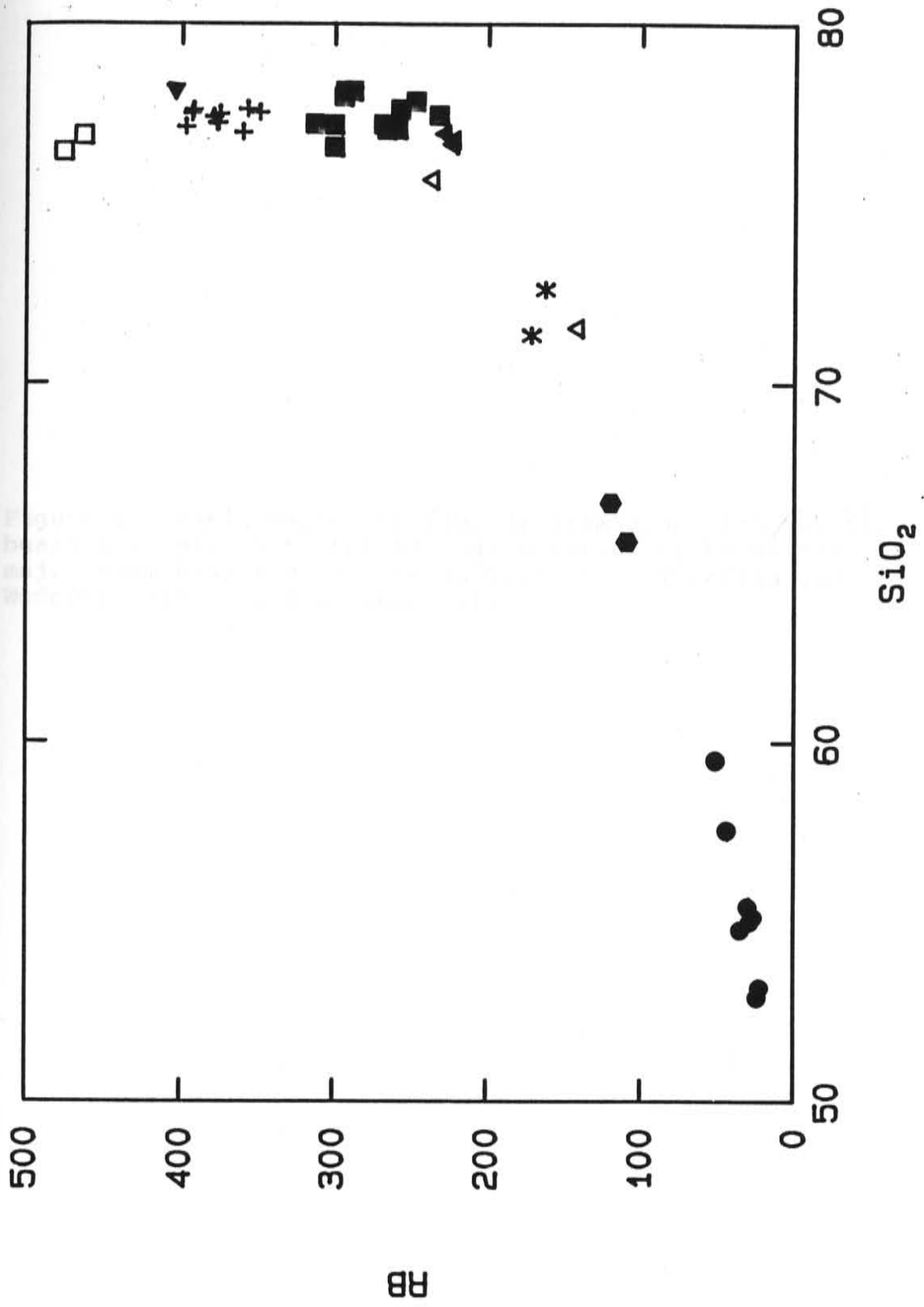


Figure 4. Enrichment-depletion diagram comparing the tin-bearing rhyolites to the average rhyolite of Le Maitre (1976; major elements) and the low Ca granite of Turekian and Wedepohl (1961; trace elements).

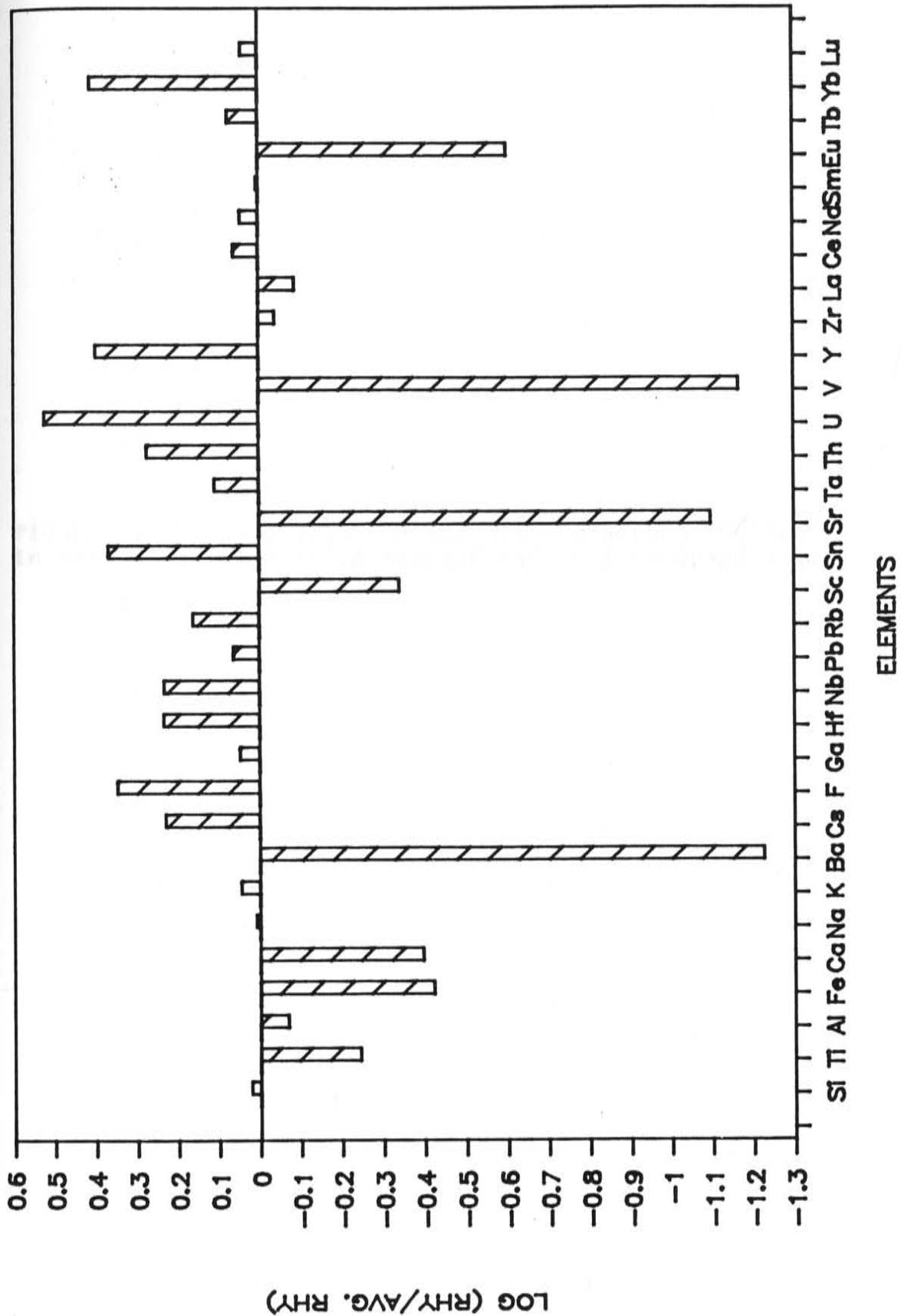


Figure 5. Ternary  $\text{Al}_2\text{O}_3$ - $\text{CaO}$ - $\text{Na}_2\text{O}+\text{K}_2\text{O}$  diagram. Oxides in mol units. The field boundaries are from Shand (1927).

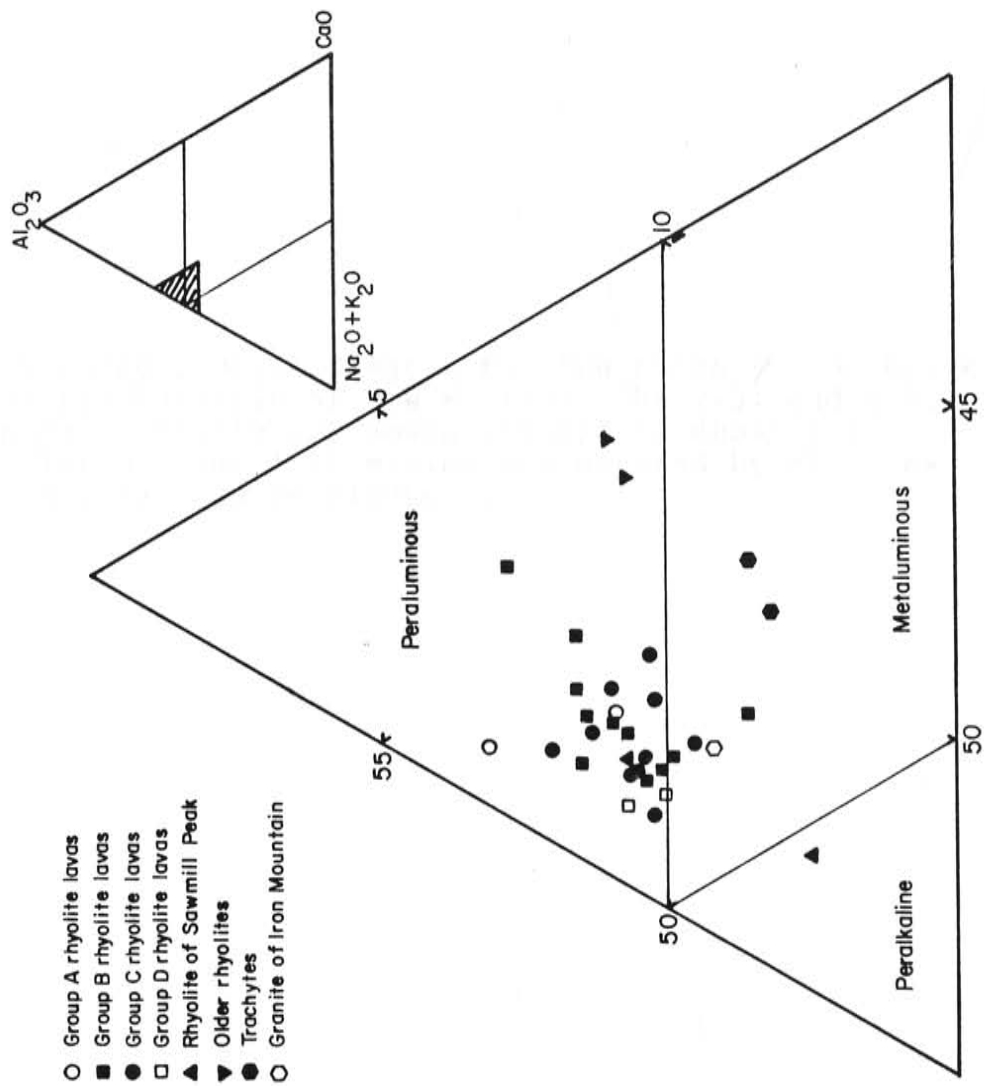


Figure 6. Ternary Q-Or-Ab diagram for the rocks in the Black Range and Sierra Cuchillo of New Mexico. The 2,3, and 4 kb ternary minima of Tuttle and Bowen (1958) are shown for reference. The 0.5 and 1 kb minima are covered by the mass of data points. Symbols as Figure 3.



Fig. 1  
Map  
and  
Fig.

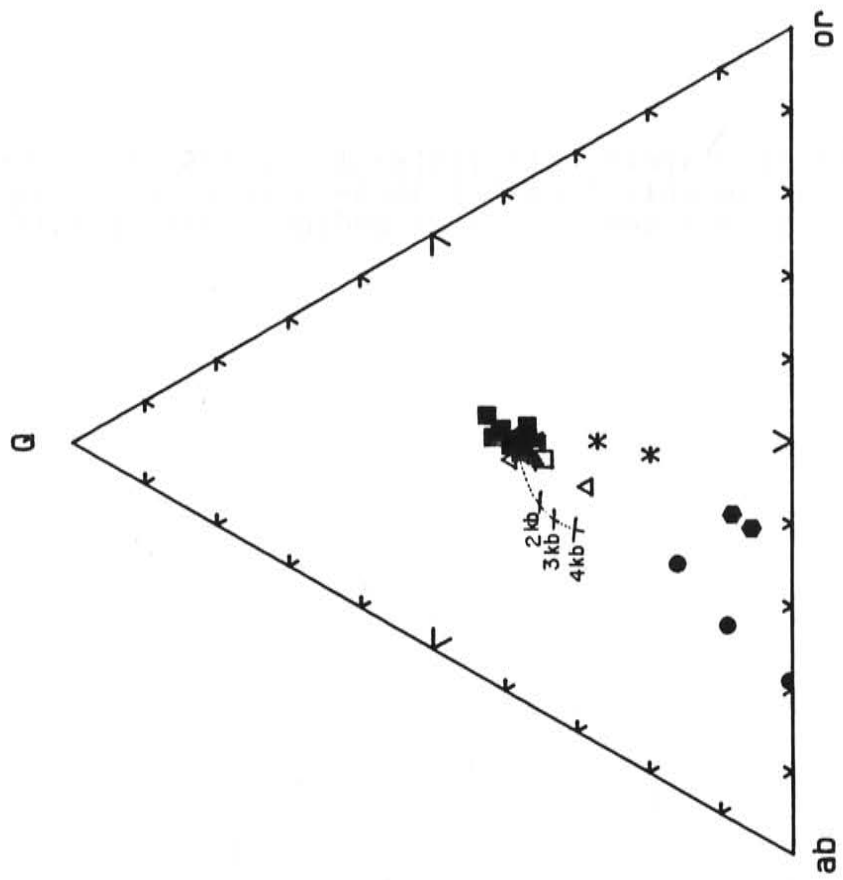


Figure 7.  $\text{SiO}_2$ -total alkalis classification diagram of Le Maitre (1984) with the alkaline-subalkaline fields of Irvine and Baragar (1971; diagonal dashed line). Symbols as in Figure 3.

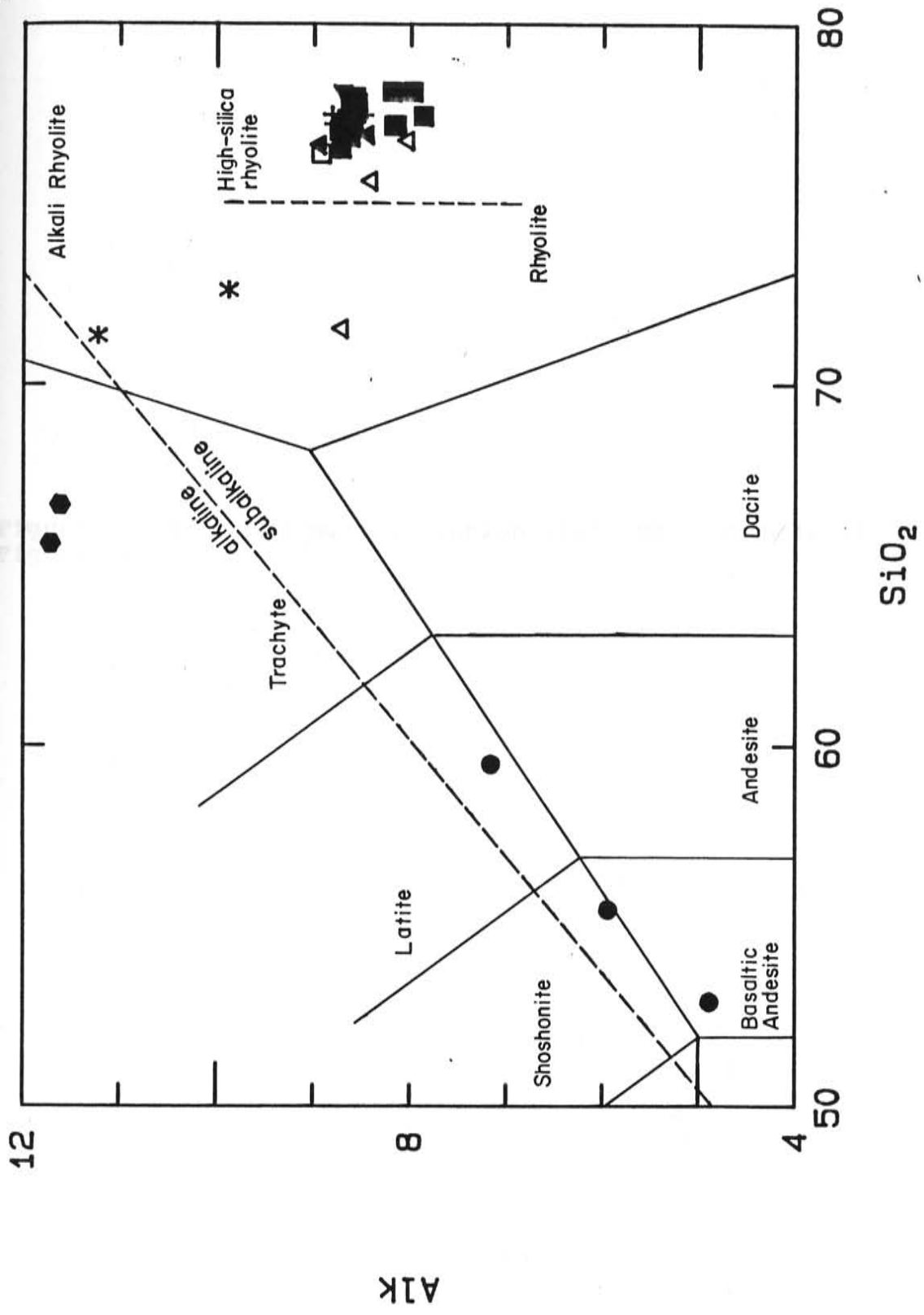
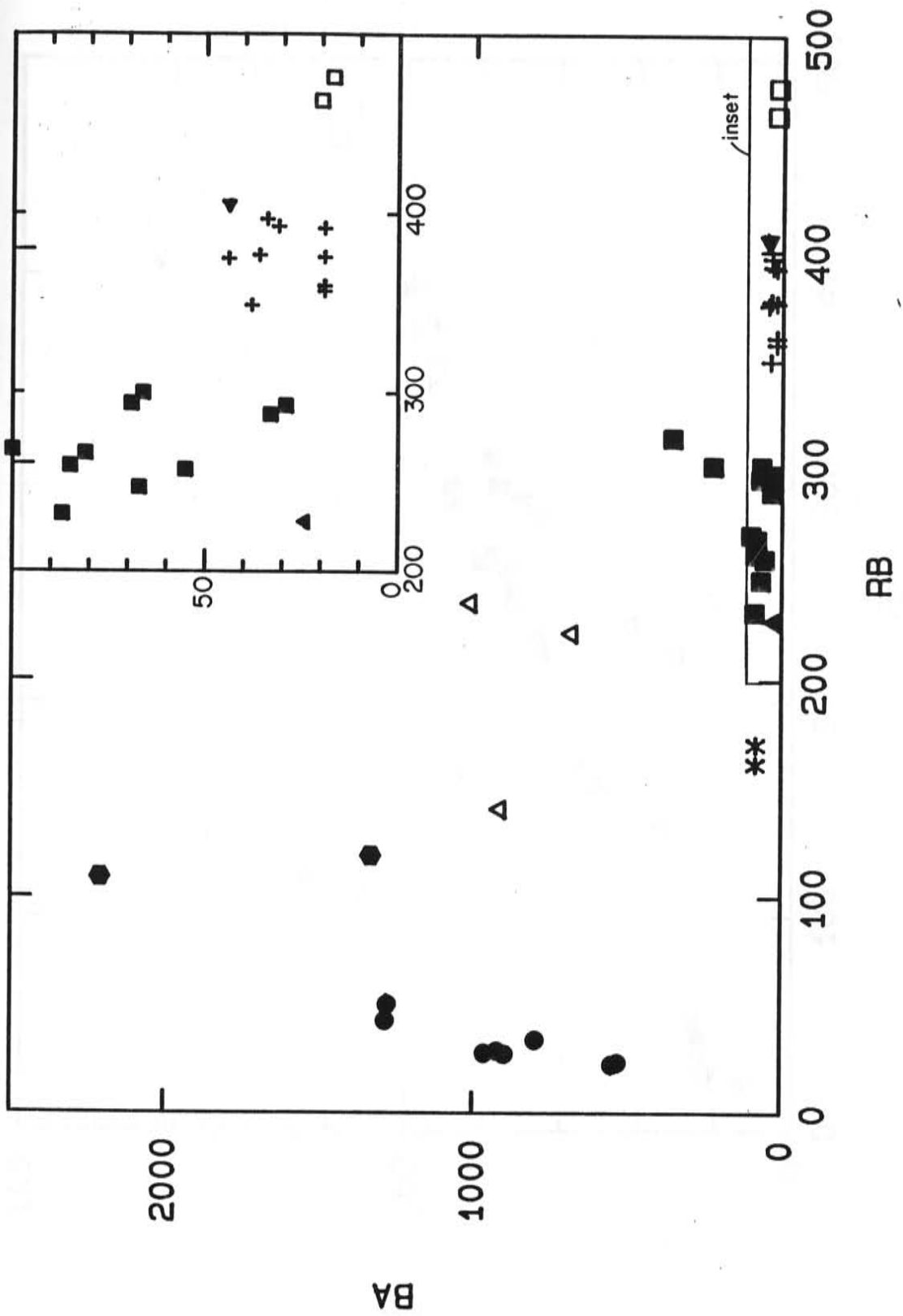
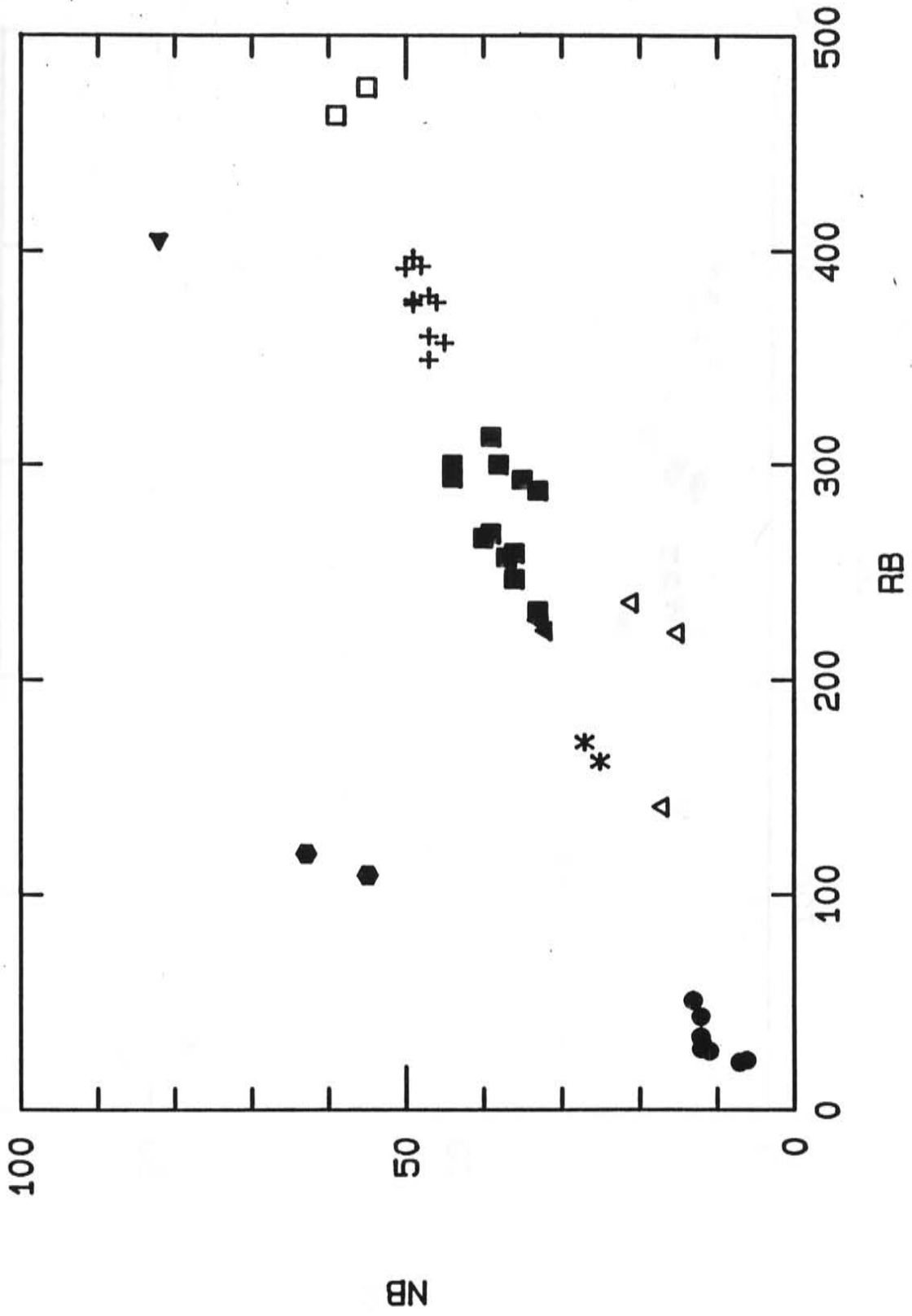
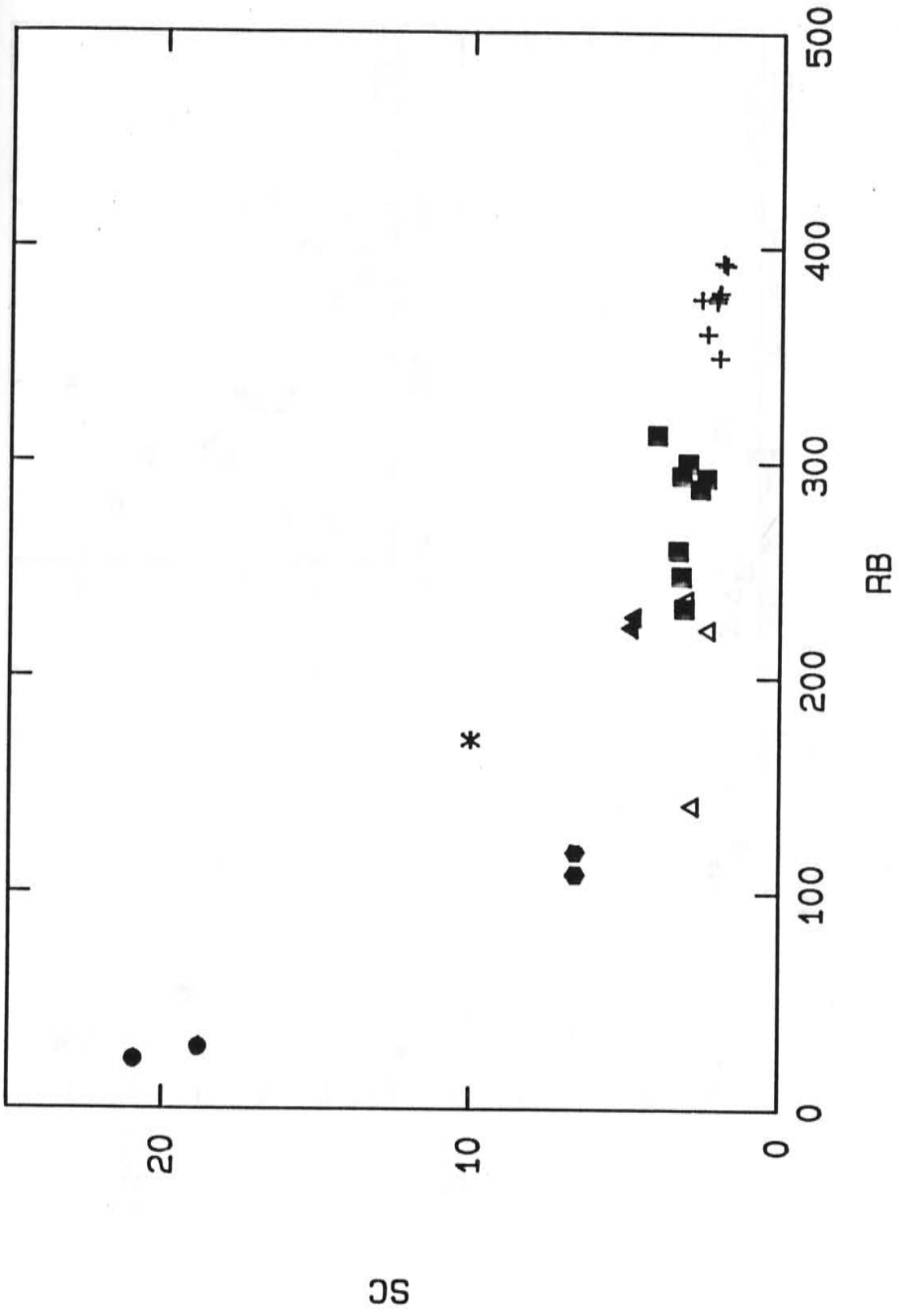
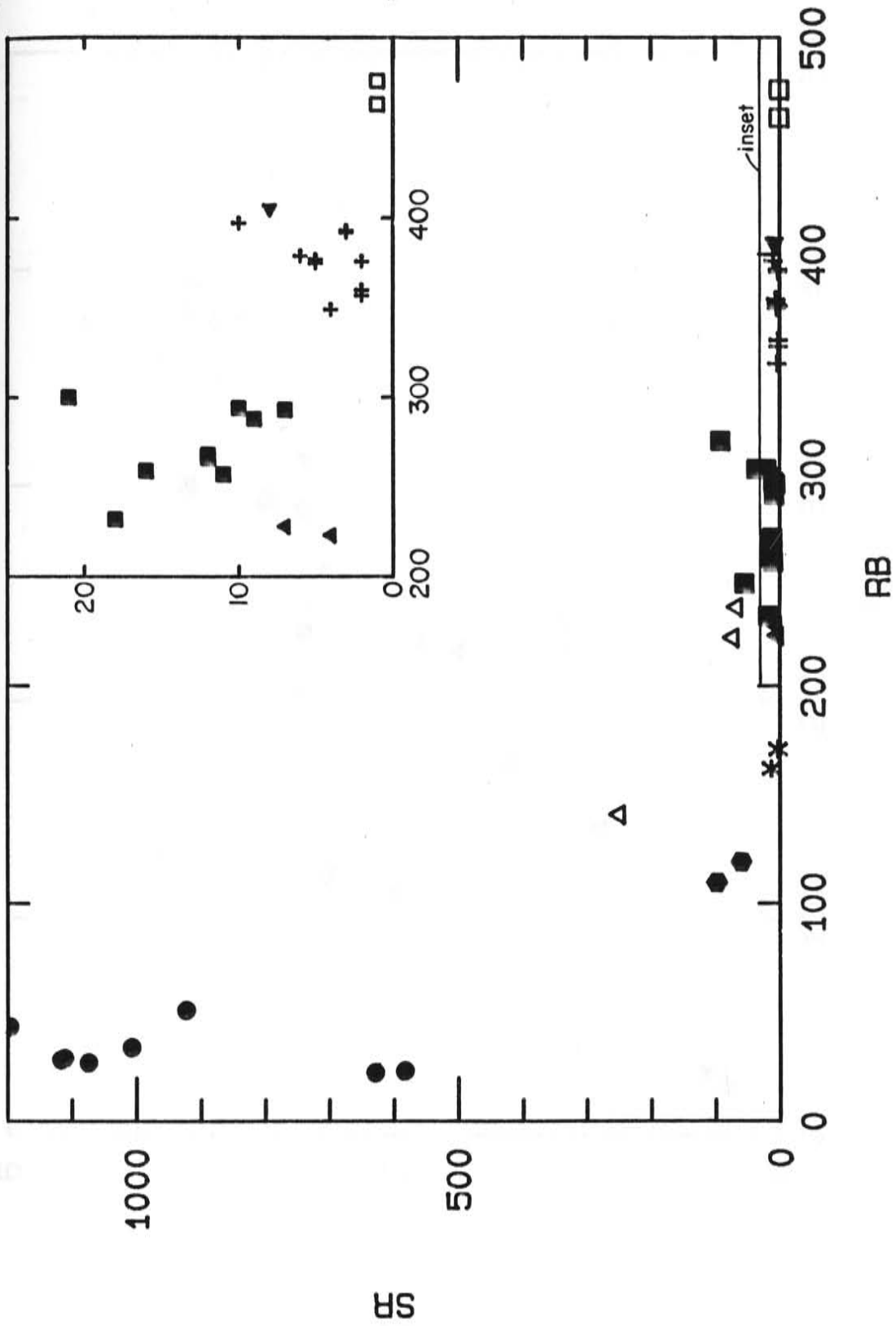


Figure 8. Trace element variation diagrams. Symbols as in Figure 3.

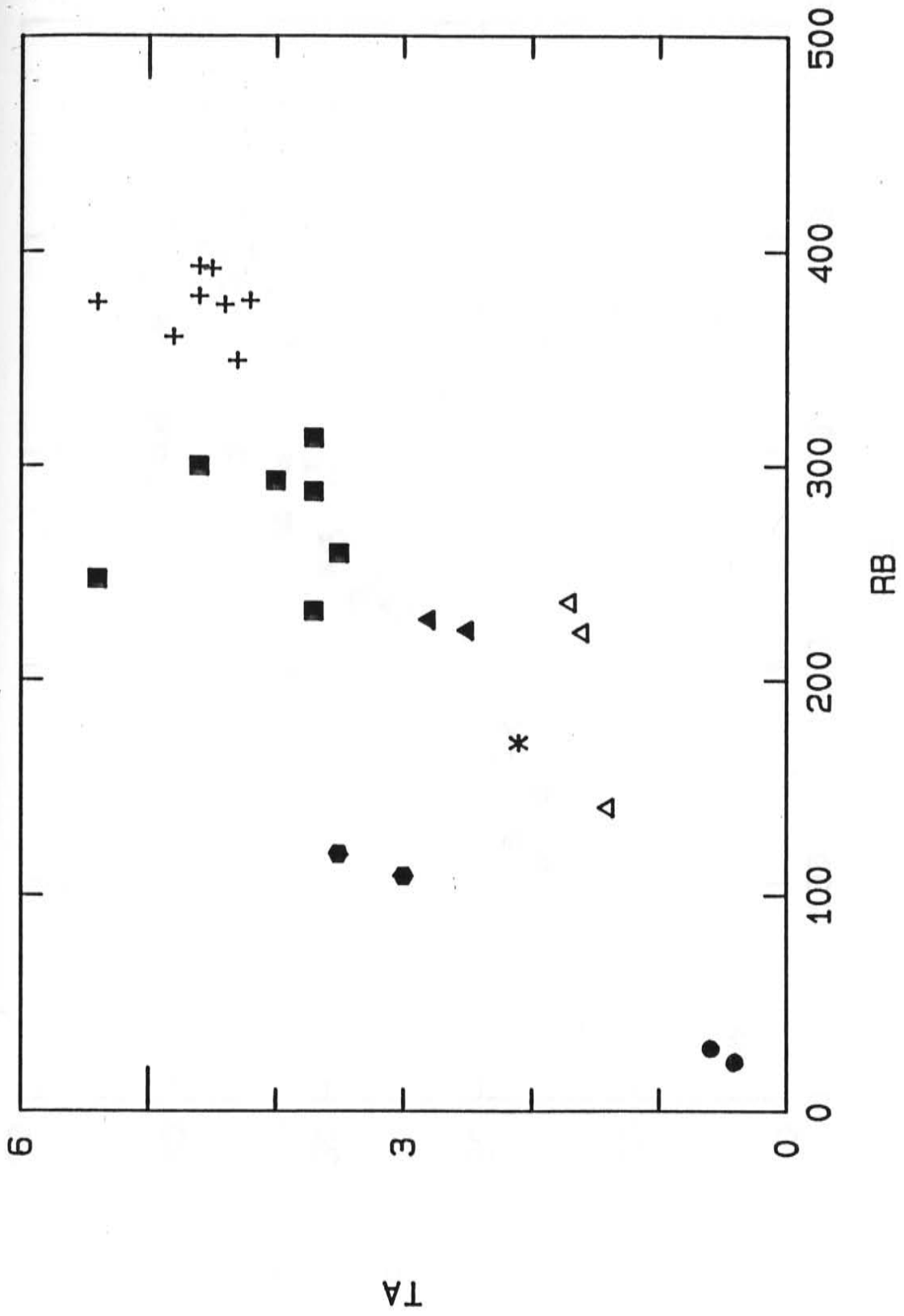


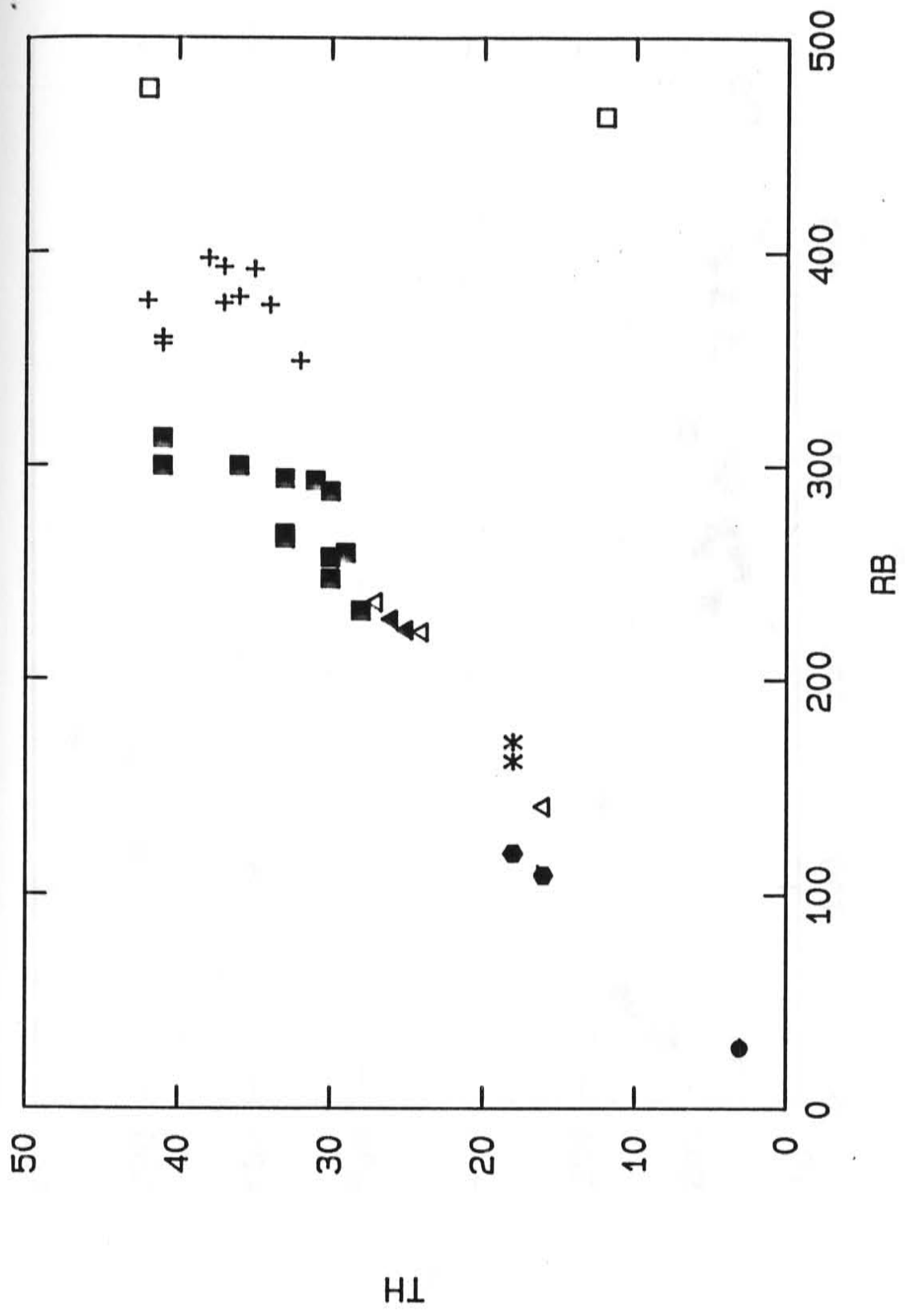


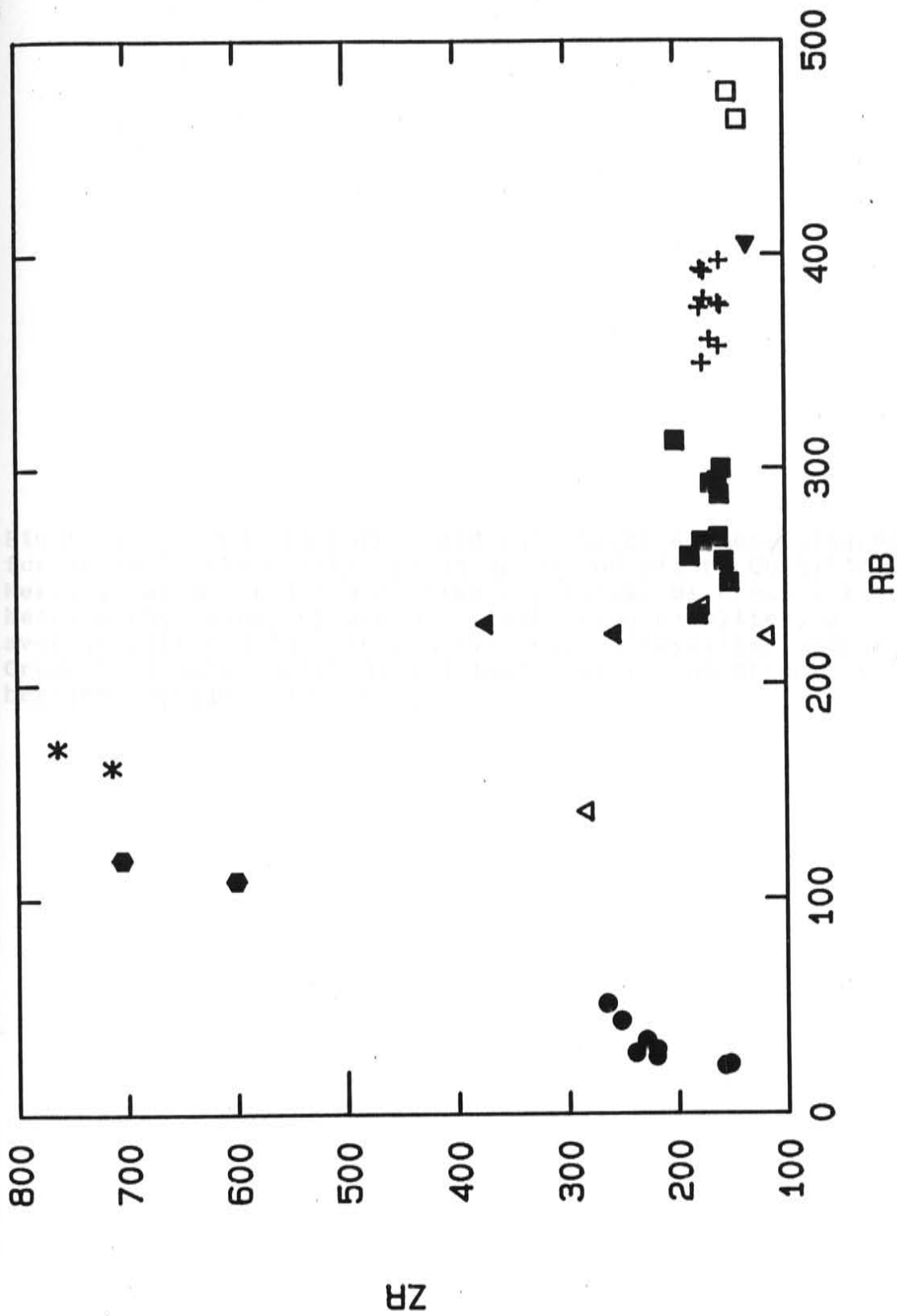












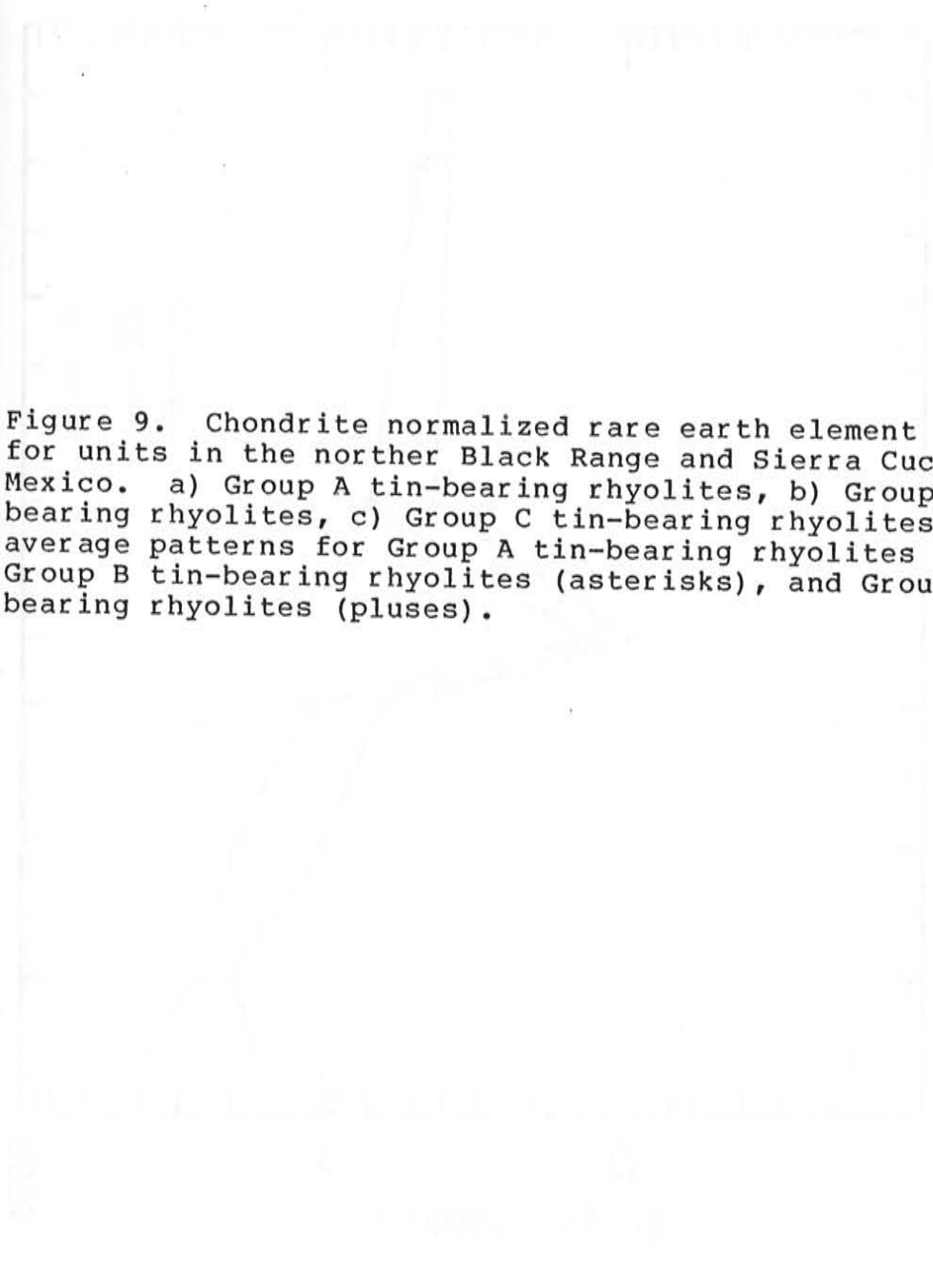
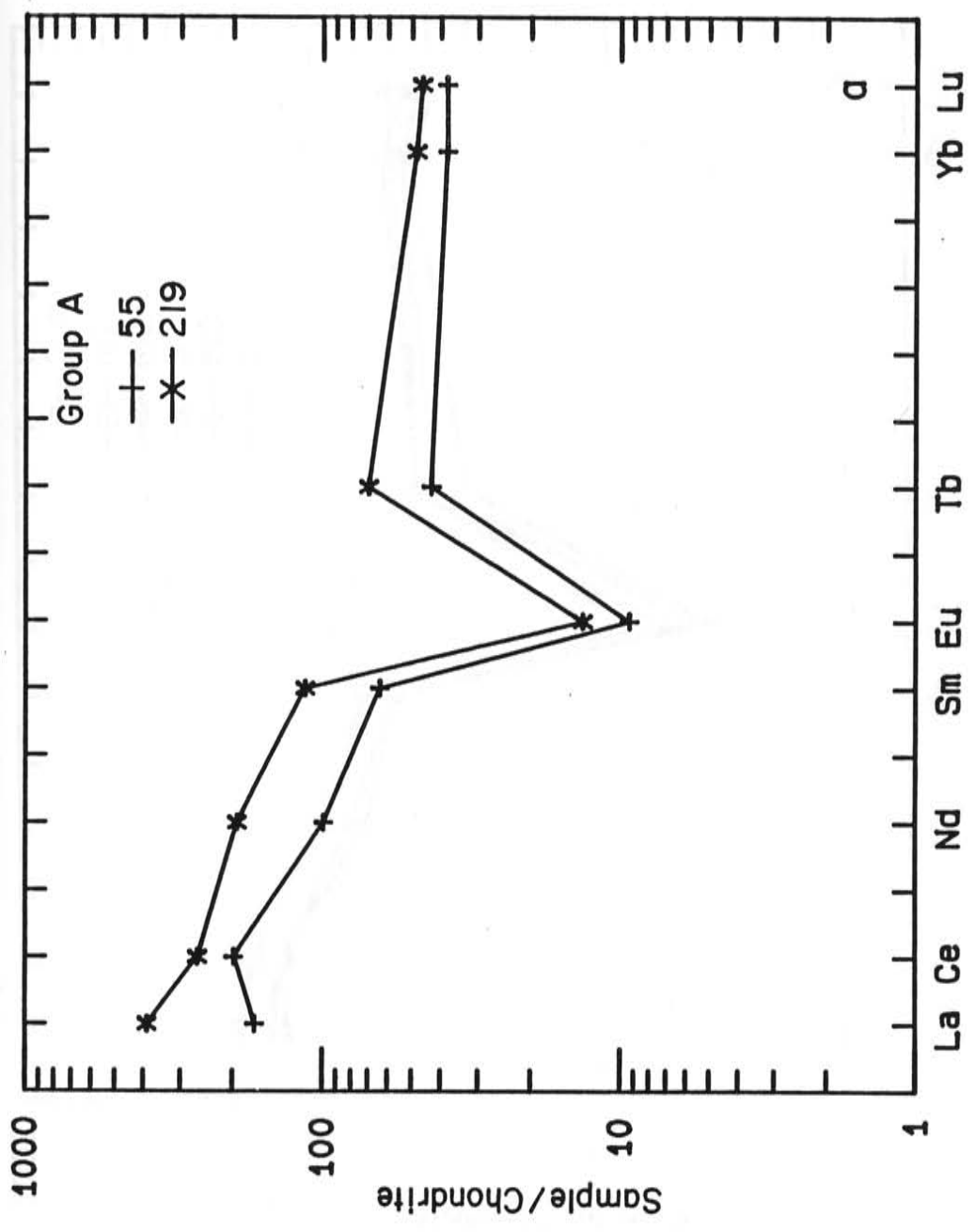
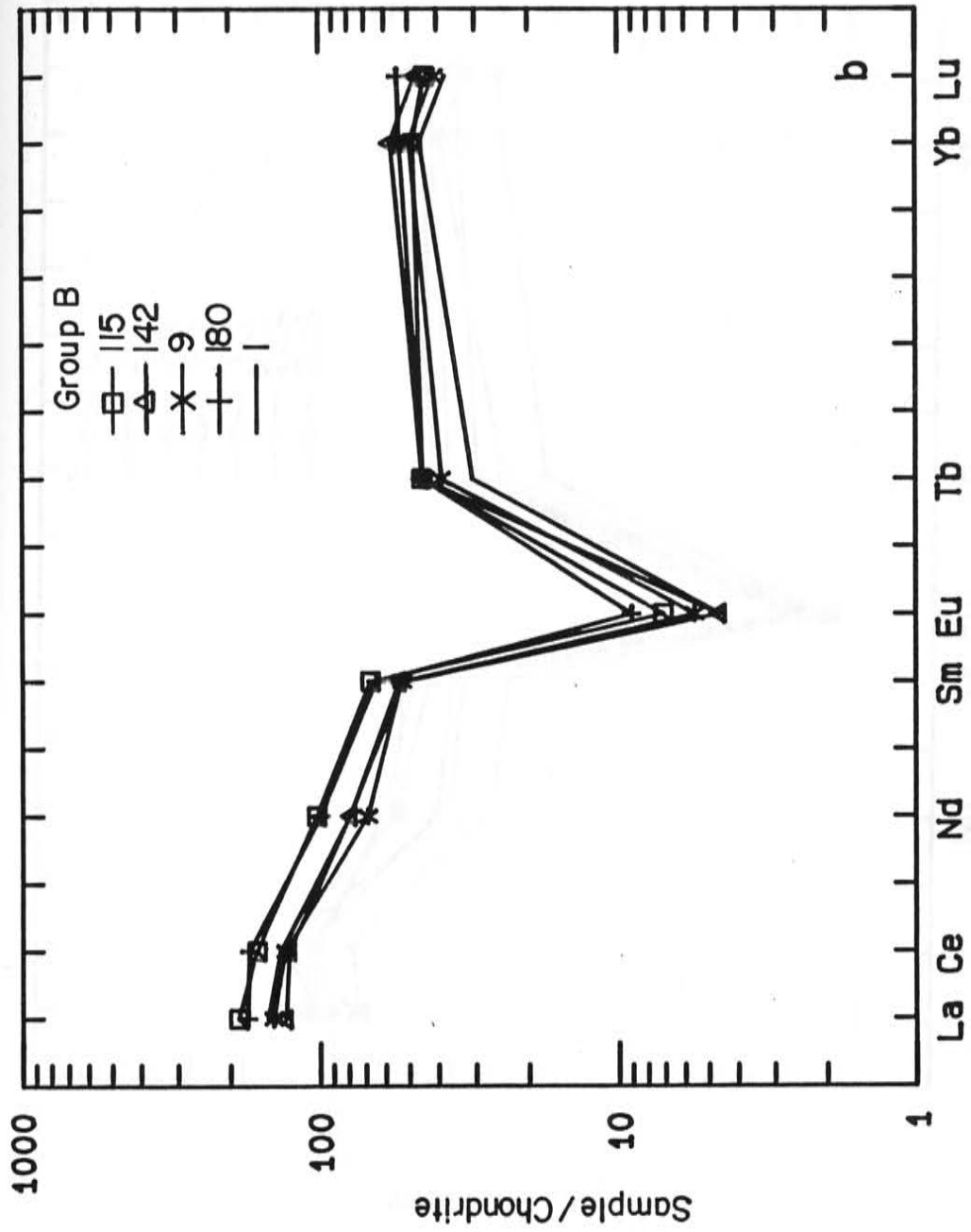
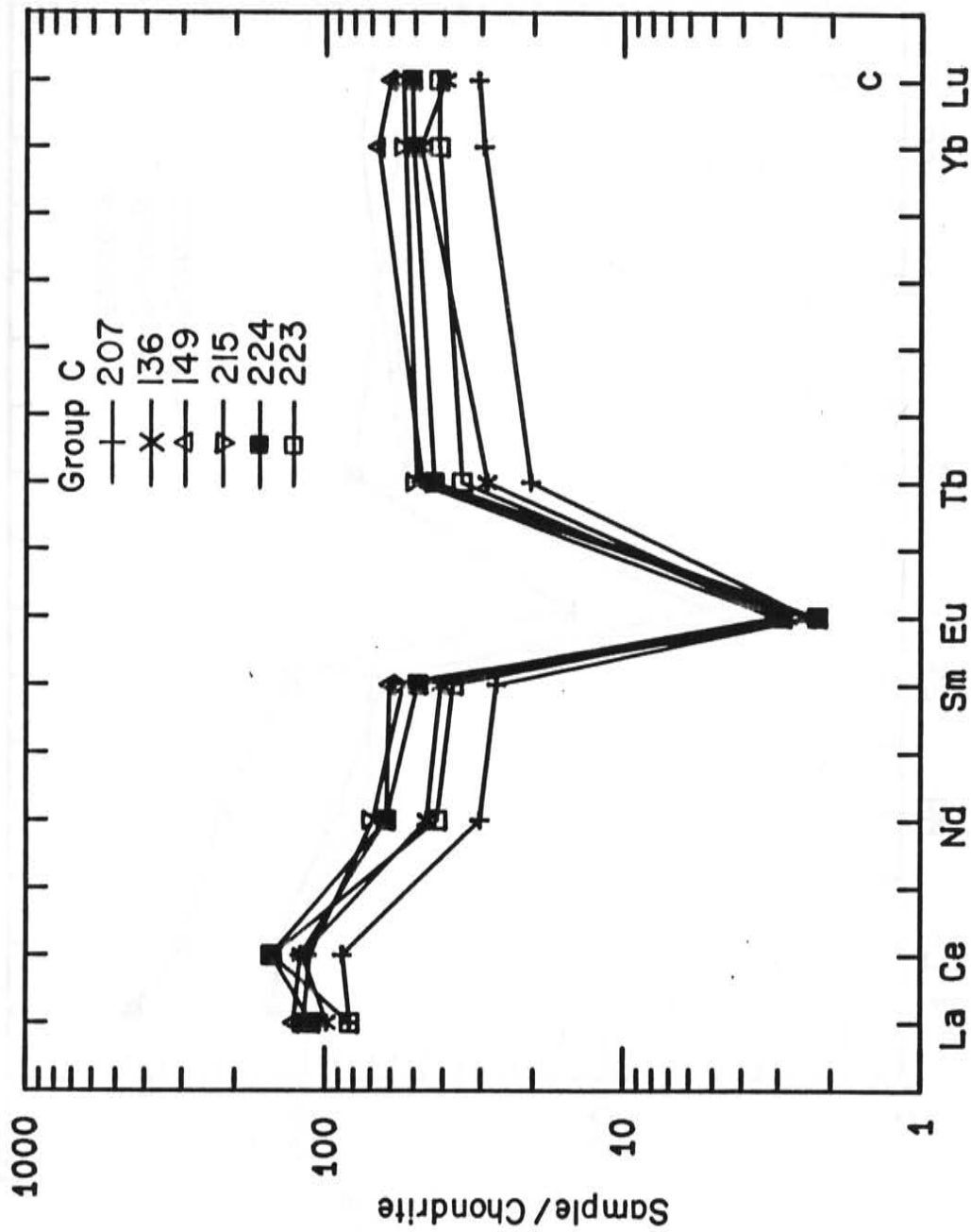


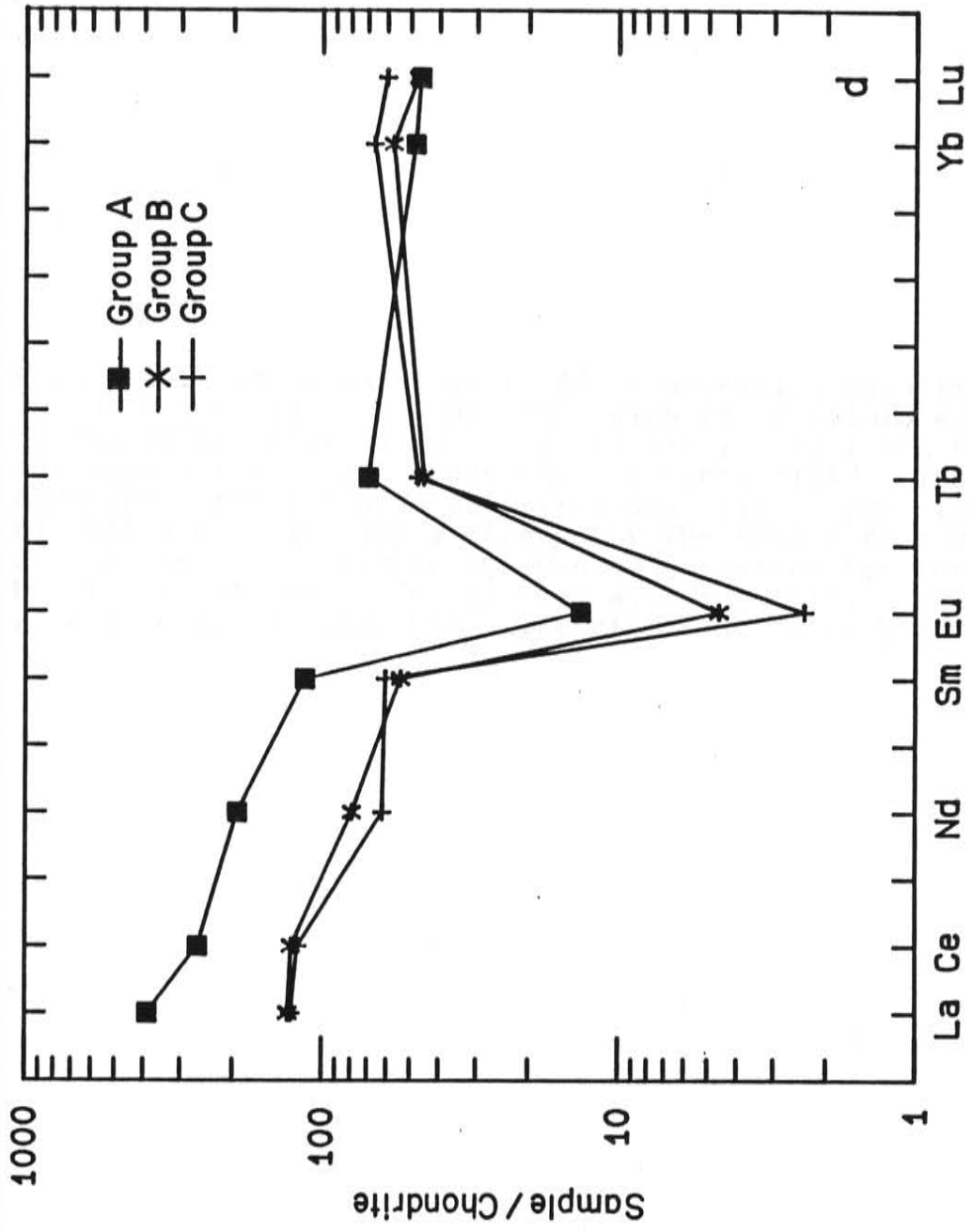
Figure 9. Chondrite normalized rare earth element diagrams for units in the northern Black Range and Sierra Cuchillo, New Mexico. a) Group A tin-bearing rhyolites, b) Group B tin-bearing rhyolites, c) Group C tin-bearing rhyolites, d) average patterns for Group A tin-bearing rhyolites (squares), Group B tin-bearing rhyolites (asterisks), and Group C tin-bearing rhyolites (pluses).



a







(123)



Figure 10. Isochron diagrams for tin-bearing rhyolite domes in the Black Range, New Mexico. With the possible exception of the Boiler Peak data, the lines are mixing lines because the apparent ages are older than is permissible. The apparent initial  $^{87}\text{Sr}/^{86}\text{Sr}$  ratios have little petrologic significance. The age indicated by the Boiler Peak data is within the stratigraphic age window permitted for the tin-bearing rhyolites. The apparent ages and initial ratios were calculated using the regression routine of York (1966).

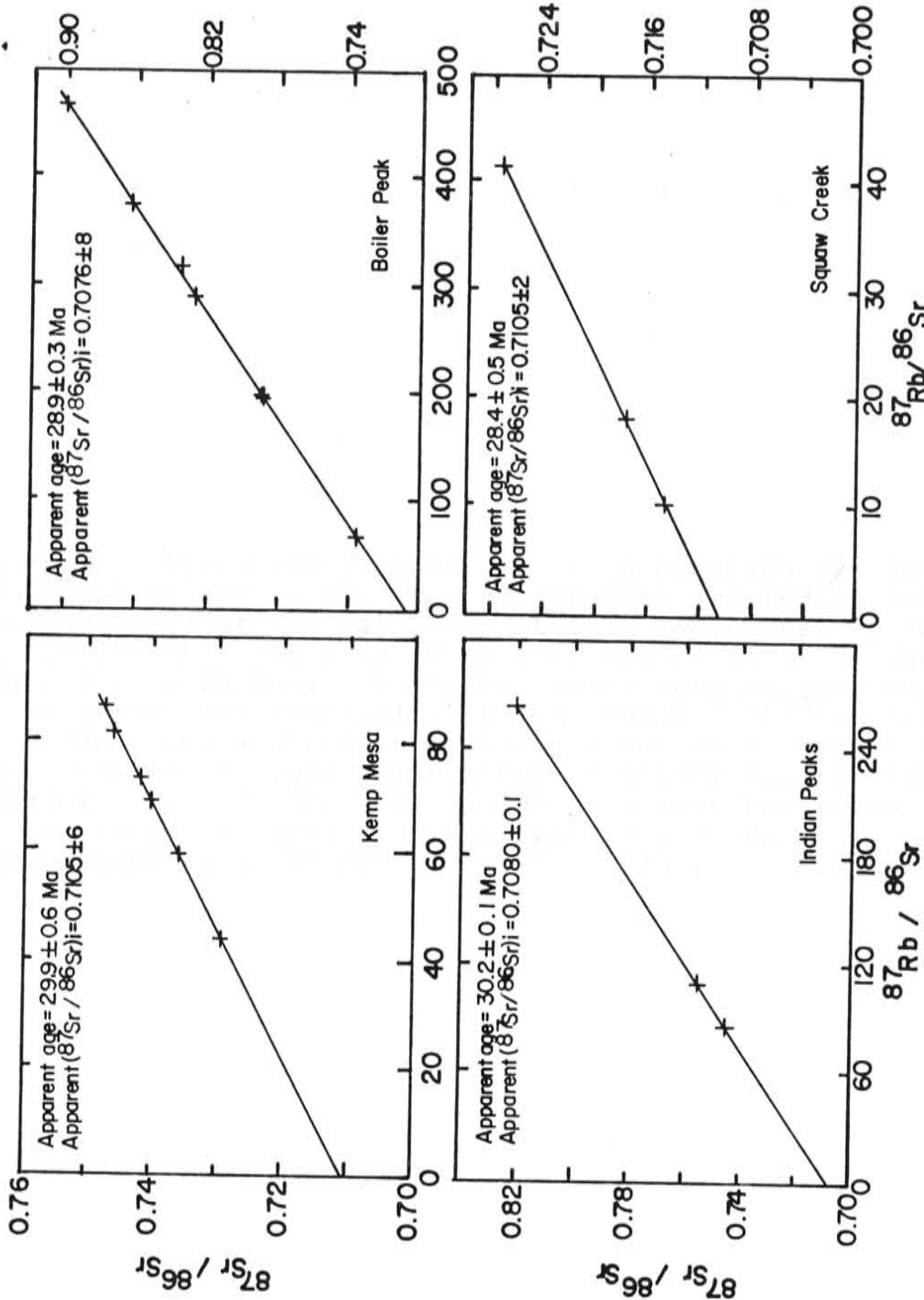


Figure 11. Strontium isotope evolution diagrams for the four domes in Figure 10. The Boiler Peak and Indian Peaks data intersect at the age calculated by linear regression, but the Indian Peaks data is outside the permissible age window (28 to 29 Ma). The Indian Peaks data suggest mixing of the magma with material with homogenous  $^{87}\text{Sr}/^{86}\text{Sr}$  ratios. The Squaw Creek and Kemp Mesa data do not intersect at a point, rather, the evolution lines intersect over a wide range of time and  $^{87}\text{Sr}/^{86}\text{Sr}$ , suggesting that the magmas were variably contaminated by strontium that was inhomogenous with respect to  $^{87}\text{Sr}/^{86}\text{Sr}$  ratios.

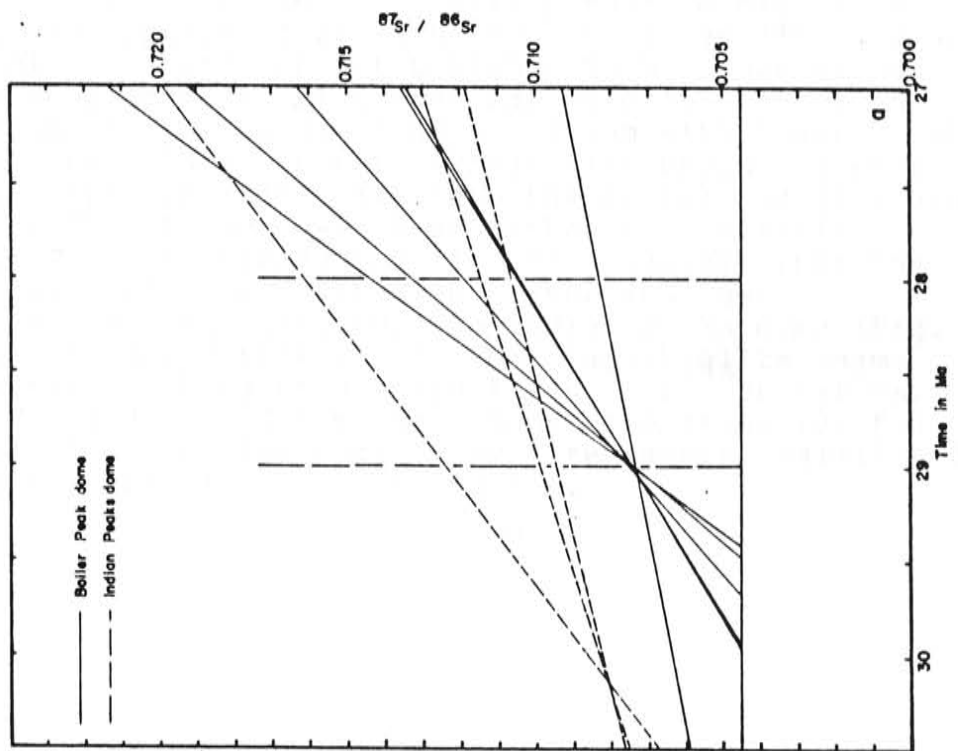
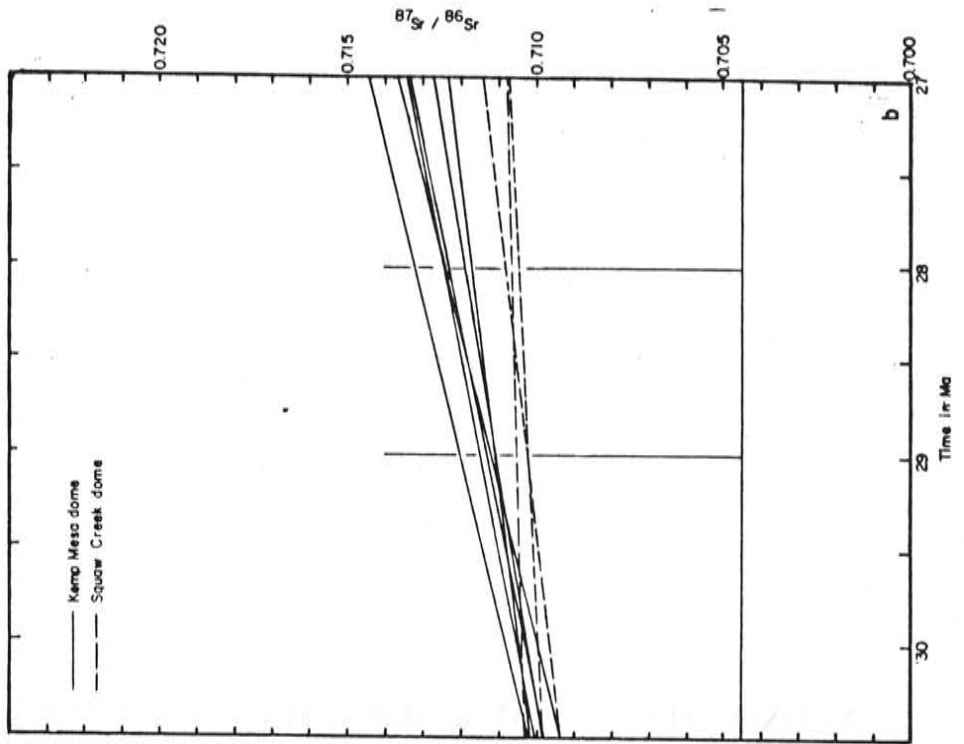
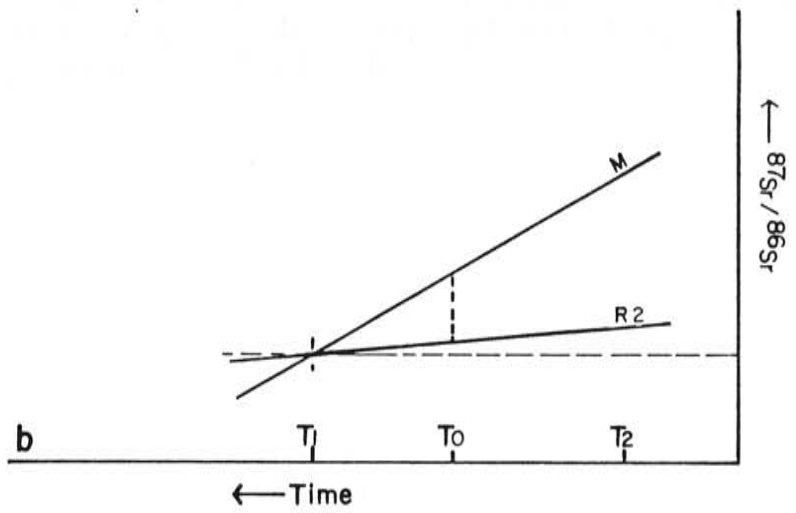
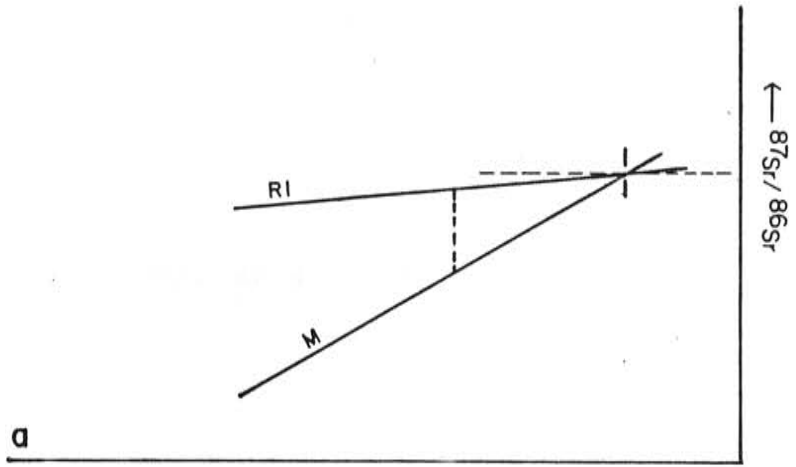


Figure 12. Strontium mixing models for the tin-bearing rhyolite magmas. a) Contamination of a tin-bearing rhyolite magma (M) by a source of strontium with lower Rb/Sr ratios and higher  $^{87}\text{Sr}/^{86}\text{Sr}$  ratios (R1) will produce a mixture with an apparent age younger (T2) than the actual age (T0) and an apparent initial  $^{87}\text{Sr}/^{86}\text{Sr}$  ratio higher than either of the two mixing components. b) Contamination of a tin-bearing rhyolite magma (M) by a source of strontium with lower Rb/Sr ratios and lower  $^{87}\text{Sr}/^{86}\text{Sr}$  ratios (R2) will produce a rock with an apparent age older (T1) than the actual age (T0) and with an  $^{87}\text{Sr}/^{86}\text{Sr}$  ratio lower than either of the mixing materials. The tin-bearing rhyolite data suggest that the magmas assimilated rocks with both higher and lower  $^{87}\text{Sr}/^{86}\text{Sr}$  ratios. The data for the Indian Peaks dome (Fig. 10; Fig. 11) suggests that the tin-bearing rhyolite magma mixed primarily with material with lower  $^{87}\text{Sr}/^{86}\text{Sr}$  ratios. The Squaw Creek dome and Kemp Mesa dome data (Fig. 10; Fig. 11) suggest that the tin-bearing rhyolite magmas assimilated material with variable  $^{87}\text{Sr}/^{86}\text{Sr}$  ratios.



CHAPTER 4

The data presented in this chapter was collected and interpreted by Ted L. Eggleston. David I. Norman was advisor for this thesis. Oxygen isotope data was collected by Ted L. Eggleston in the laboratory of Samuel M. Savin.

ORIGIN OF TIN MINERALIZATION ASSOCIATED  
WITH HIGH-SILICA, TOPAZ RHYOLITES,  
BLACK RANGE, NEW MEXICO

Ted L. Eggleston and David I. Norman  
New Mexico Institute of Mining and Technology  
Socorro, New Mexico

and

Samuel M. Savin  
Case Western Reserve University  
Cleveland, Ohio

ABSTRACT

Tin mineralization is associated with mid-Tertiary, high-silica rhyolite lavas in the Black Range and Sierra Cuchillo of southwestern New Mexico. Lode tin mineralization consists of hematite-cassiterite-wood tin veinlets located near the paleosurface of the rhyolite domes. Very small



amounts of quartz-calcite-fluorite mineralization fills open space that remained after tin deposition was complete. The tin mineralization is intimately associated with small zones of intense vapor phase crystallization of the host rhyolite.

Fluid inclusion homogenization temperatures ( $T_h$ ) in cassiterite, quartz and topaz in the tin mineralization are  $>650^\circ$  C. Overgrowths on quartz phenocrysts in zones of intense vapor phase crystallization contain inclusions with  $T_h$  of  $730^\circ$  C. Fluid inclusion  $T_h$  in quartz-calcite-fluorite mineralization are between  $380$  to  $130^\circ$  C. The oxygen isotope composition of quartz associated with the tin mineralization is about  $7.5^\circ$ /oo. Quartz in the quartz-calcite-fluorite has  $d^{18}O$  compositions of  $5$  to  $11^\circ$ /oo. Whole rock rhyolite samples near the tin mineralization has  $d^{18}O$  values of  $6.1$  to  $9.9$ . Estimated magmatic values for the whole rock samples are  $6.5$  to  $6.8^\circ$ /oo suggesting that the whole rock samples were enriched with  $^{18}O$ . Fluid inclusion gases in the tin minerals are similar to recently active volcanic fumaroles.

Calculated  $f_{O_2}$  of fluid inclusion gases in wood tin and cassiterite indicate that the  $f_{O_2}$  of the fluids ranged from  $10^{-20}$  to  $10^{-10}$  at  $627^\circ$  C. The higher  $f_{O_2}$  values were for tin mineralization very near the paleosurface. The  $f_{O_2}$  of the fluid inclusion gases in tin minerals decreased with depth of the host mineral. Fluid inclusion gases in the quartz-calcite-fluorite mineralization are organic-rich fluids similar to fluid inclusion gases in many epithermal deposits.

The data strongly suggest that the fluids responsible for the tin mineralization were magmatic fluids derived from

the host rhyolite and that the tin was deposited as fumarolic incrustations. Fluids responsible for quartz-calcite-fluorite mineralization were meteoric water, but had an undetermined magmatic water component. The small volume of the quartz-calcite-fluorite mineralization and the lack of  $d^{18}O$  depletion in the host rhyolite indicate that the meteoric water dominated hydrothermal system that deposited the quartz-calcite-fluorite mineralization was short lived.

The host rhyolites probably originated as partial melts of lower crustal, biotite-bearing granulites with a small, but undetermined upper mantle component. The parent liquids were probably similar to A-type granites. Crystallization of plagioclase, K-feldspar, and quartz from the parent liquid in a high level magma chamber enriched Rb, Nb, Ta, Th, and Sn and depleted Sr and Ba in the tin-bearing rhyolites. Tin was probably transported as  $SnCl^+$  in magmatic, supercritical fluids and was deposited as near surface, fumarole incrustations by decreasing temperatures and increasing  $f_{O_2}$ . Fluid flow rates determined the texture of the resulting tin mineralization. Tin was probably enriched in the magma by crystal-liquid fractionation processes.

Economic potential for the rhyolite-hosted tin mineralization is low. Potential for tin- and tungsten-bearing skarn mineralization and lode deposits at depth is very good, but the depth to the deposits may be prohibitive.

## INTRODUCTION

Cassiterite and wood-tin bearing veinlets associated with Tertiary high-silica rhyolite lavas have been known from Durango, Mexico since the time of the Aztecs (Ingalls, 1896). Wood tin, the microcrystalline, botryoidal form of cassiterite, is probably the most important tin mineral in these deposits. Baron von Richthofen (1869, as reported in Ingalls, 1896) suggested that these deposits formed as the result of solfataric action. Since that time, the origin of these "Mexican" type tin deposits has been controversial. Genetic models that have been proposed are; 1) tin was deposited from magmatic fluids generated during cooling of the host rhyolite (von Richthofen, 1869 and Vogt, 1894 as reported by Ingalls, 1896; Fries, 1940; Lufkin, 1976; Correa, 1981, Duffield and others, 1984); 2) tin deposition from low temperature hydrothermal fluids that are not derived from the host rhyolites (Pan, 1974; Ypma and Simons, 1970); and 3) deposition occurred from high temperature fluids derived from intrusive bodies beneath the host rhyolite lavas (Rye and others, 1984; Harvey, 1985; Maxwell and others, 1986).

Tin mineralization similar to the Mexican deposits occurs sporadically in the northern Black Range and Sierra Cuchillo of southwestern New Mexico (Fig. 1). Estimated production has been about 70 tons of concentrate averaging 40 to 50% Sn from placer deposits near the sources of primary

tin mineralization (Maxwell and others, 1986). This paper reports field, fluid inclusion, oxygen isotopic, mineralogic, and geochemical studies of the tin deposits and rhyolite host rocks in southwestern New Mexico. The objective of these studies was to determine the genesis of the tin mineralization.

#### REGIONAL GEOLOGIC SETTING

Tin deposits in the Taylor Creek district and Sierra Cuchillo are hosted by Tertiary rhyolite lavas that are part of the Mogollon-Datil volcanic field in southwestern New Mexico (Fig. 1). In the region surrounding the Taylor Creek district, the Mogollon-Datil volcanic field consists of more than 2 km of Oligocene to lower Miocene lava flows, pyroclastic rocks, and volcanoclastic sedimentary rocks (Harrison, 1986). Details of the geology of the region are reported in Eggleston and Norman (1987), Lawrence and Richter (1986), Ratte' and others (1984), and Richter and others (1986 a and b), Richter (1978), Correa (1981), and Goerold (1981).

The Mogolon-Datil volcanic field rests unconformably on Mesozoic, Paleozoic, and Precambrian rocks. The exposed Precambrian section consists of schists, gneisses, and felsic to mafic igneous rocks that range in age from about 0.9 to about 1.4 Ga (Condie and Budding, 1979). In the Franklin Mountains of west Texas and eastern New Mexico, the Precambrian is dominated by felsic volcanic and intrusive

rocks. One granite, the 1065 Ma Red Bluff granite, is known to host tin deposits (Harbour, 1972; Norman and others, 1987). Norman and others (1987) report present day  $^{87}\text{Sr}/^{86}\text{Sr}$  ratios for the granite of 0.9243 to 1.3464 with  $^{87}\text{Rb}/^{86}\text{Sr}$  ratios of 14.67 to 42.83.

The Mogollon-Datil volcanic field can be divided into two age groups. The lower group is as much as 1 km thick and consists of mafic to intermediate lava flows and felsic pyroclastic rocks erupted between 44 and 35 Ma (Seager and others, 1984; McIntosh and others, 1986).

After an hiatus in volcanism of 5 to 6 Ma, a bimodal sequence of basaltic andesite lava flows and high-silica rhyolite lavas and pyroclastic rocks was erupted. The high-silica rhyolites, including the tin-bearing Taylor Creek Rhyolite, rhyolite of Dolan Peak, and rhyolite of Willow Springs Draw, overlie the basaltic andesites. McIntosh and others (1986) report  $^{40}\text{Ar}/^{39}\text{Ar}$  dates in this group from about 29 Ma for the oldest rocks to about 27 Ma for the youngest rocks. Dating of volcanic rocks that bracket the Taylor Creek Rhyolite indicates that it erupted between 28.8 and 28.2 Ma (McIntosh and others, 1986). Eggleston and Norman (1987) summarize the geochronological data on the Taylor Creek Rhyolite. A zircon and apatite fission track date of  $27.8 \pm 1$  Ma for the rhyolite of Willow Springs Draw in the Sierra Cuchillo was reported by Heyl and others (1983).

The granite of Iron Mountain, exposed in the northern Sierra Cuchillo (Fig. 1), consists of high-silica, aplitic and porphyritic granite (Table 1). Both phases of the

granite of Iron Mountain consist of quartz, K-feldspar, and oligoclase with accessory biotite, fluorite, zircon, and apatite. The aplitic phase contains accessory topaz. Biotite in the aplitic phase is associated with crosscutting quartz-fluorite veinlets and is in part secondary. Fluorite, although for the most part, secondary, locally occurs as anhedral blebs in the matrix of the granite and may be a late crystallizing phenocryst. The granite is surrounded by tungsten-, beryllium- and tin-bearing fluorite-magnetite (wrigglite) skarns in the Paleozoic rocks that it intrudes (Jahns, 1944). Chapin and others (1978) report a conventional K-Ar date of  $29.9 \pm 1.2$  Ma (recalculated with new constants) for this granite. The chemistry of the granite and the associated mineralization led Burt and Sheridan (1986) to suggest that the granite of Iron Mountain is the intrusive equivalent of topaz rhyolites.

#### ANALYTICAL PROCEDURES

Fluid inclusion heating and freezing experiments were performed on doubly polished, thick sections in a Linkham TH 600 heating-freezing stage equipped with a Linkham electronic controller. Calibration of the stage was done using organic melting point standards, double distilled, deionized water, and high purity, inorganic compounds. Precision of homogenization temperature measurements is  $\pm 2^{\circ}$  C. Precision of freezing point depression measurements is better than  $\pm 0.2^{\circ}$  C. A limited number of heating experiments were



performed with a Linkham TH 1500 heating stage. Precision of measurements of this stage is better than  $\pm 15^{\circ}$  C. The stage was calibrated using high purity, inorganic materials for reference points. Fluid inclusion volatiles were analyzed in a quadrupole mass spectrometer following release of the volatiles from the host inclusions by thermal decrepitation of the fluid inclusions using the techniques described in Norman and Sawkins (1987).

Oxygen isotopic analyses were performed at the laboratory of S. Savin, Case Western Reserve University using a Nier type, 6 inch, 60 degree sector ratio mass spectrometer. Oxygen was liberated from the samples by the bromine pentafluoride technique described by Clayton and Mayeda (1963). Estimated precision is better than  $\pm 0.2$  ‰.

Major and trace elements were determined by X-ray fluorescence spectrometry (XRF) (Norrish and Hutton, 1969; Norrish and Chappell, 1977) and instrumental neutron activation analysis (INAA) (Jacobs and others, 1977). F was determined by ion-specific electrode following digestion of the sample in lithium metaborate (Bodkin, 1977). Precision of all geochemical analyses is discussed in Eggleston and Norman (1987).

## LOCAL GEOLOGY

## Tin-Bearing Rhyolites

There are three discrete, although very similar, groups of rhyolite lavas that host tin mineralization in southwestern New Mexico; the Taylor Creek Rhyolite and the rhyolite of Dolan Peak in the Black Range and the rhyolite of Willow Springs Draw in the Sierra Cuchillo (Fig. 1). Each of the rhyolite units consists of roughly time equivalent, widely separated eruptive centers that comprise one or more discrete rhyolite domes.

## Lithology and geometry

The tin-bearing rhyolite lavas contain 15 to 30 % phenocrysts of quartz and sanidine, minor plagioclase, and traces of biotite, amphibole, zircon, sphene, and opaque oxides. Lithophysae contain euhedral to anhedral crystals of quartz, sanidine, hematite, pseudobrookite, bixbyite, topaz, and rare cassiterite. The groundmass texture is typically granophyric with rare relict spherulites. Hydrated vitric blocks are locally preserved in carapace breccia. Incipient to intense vapor phase crystallization has bleached the rhyolites and locally, extensively recrystallized the groundmass. Flowbanding is found throughout the rhyolites (Fig. 2a). Carapace breccia consisting of monolithic breccias produced by brecciation of the outer skin of the growing domes mantles much of the rhyolite (Fig. 2b). The



geometry of the rhyolite lava bodies indicates that they are rhyolite domes with associated short lava flows (Fig. 3.). Carapace breccia and pyroclastic deposits that mantle domes mark the boundary between domes that have coalesced.

#### Geochemistry

The three tin-bearing rhyolite lavas are high-silica (75-77 %  $\text{SiO}_2$ ), high K rhyolites typical of what Burt and others (1982) termed "topaz" rhyolites (Table 1). They have significant enrichments of Rb, Cl, F, Th, U, and heavy rare earth elements and depletions of CaO, Ba, Sr, V, and light rare earth elements when compared to average granite and low Ca granite (Eggleston and others, 1987b). The Sr, Ba, and Eu depletions and Rb, U, and Th enrichments indicate that the rhyolites are extremely differentiated rocks. The 5 to 15 ppm Sn content of these rhyolites is not particularly high when compared to the 20 to 50 ppm reported in tin granites (Chatterjee and others, 1983; Du Bray, 1985; Ishihara and others, 1980). Chondrite normalized rare earth element patterns are flat with large negative Eu anomalies (Fig. 4).

The major and trace element composition of the granite of Iron Mountain is very similar to that of Taylor Creek Rhyolite (Table 1). Robertson (1985) reports rare earth element analyses that are likewise virtually identical to the topaz rhyolites (Fig. 4). Tin-bearing rhyolites in Durango, Mexico (Huspeni and others, 1984) are similar to the tin-bearing rhyolites in New Mexico (Table 1).

## vapor-Phase Crystallization

Pervasive, mild vapor phase crystallization (VPC) is characteristic of the tin-bearing rhyolites. The effects of VPC include bleaching, increased porosity, and recrystallization of groundmass minerals. Biotite and amphibole, the dominant ferromagnesian minerals in these rhyolites are converted to opaque oxides. Magnetite has been converted to hematite, but ilmenite(?) exsolution lamellae have been unaffected by VPC. Overgrowths on quartz phenocrysts locally increase the size of the phenocrysts by as much as 300% (Fig. 12a). Sanidine phenocrysts exhibit rare overgrowths. The overgrowths on both quartz and sanidine are marked by innumerable fluid inclusions (Fig. 12b).

Zones of intense vapor phase crystallization form punky areas within normally dense rhyolite (Fig. 6). Flow bands pass into and out of these zones, precluding the possibility that these zones are poorly welded pyroclastic deposits that they superficially resemble. The borders of these zones of intense VPC are gradational over a few meters to dense rhyolite lava that has undergone only mild to incipient VPC.

The zones of intense VPC are randomly scattered near the paleosurface of the domes and are typically capped by as much as 30 m of dense rhyolite lava that contains numerous lithophysal cavities. Those lithophysae increase in size upward and are as much as 5 cm in diameter at the top of the lithophysal zone. The borders of many of these lithophysae exhibit locally intense VPC. Tin mineralization

occurs within the lithophysal zone above zones of intense VPC (Fig. 3). A number of zones of intense VPC are known that have no associated tin mineralization.

Timing of VPC can be constrained by overlapping relationships between tin-bearing domes. Domes overlying zones of intense VPC typically have thin, vitric bases indicating that VPC was complete in the older dome prior to emplacement of the younger dome.

#### Comparison With Tin-Bearing Granites

Two different types of granites host tin deposits: the S-type granites of Chappell and White (1974) and the A-type granites (Loiselle and Wones, 1979). The tin-bearing, S-type granites of Cornwall, Southeast Asia and parts of the Lachlan Fold Belt of Australia are strongly peraluminous granites and have  $\text{SiO}_2$  contents between 71 and 74% (Table 1; Alderton and others, 1980). Chondrite normalized rare earth element diagrams have steep slopes ( $\text{La/Lu}=20$ ) with small negative Eu anomalies (Fig. 4). Tin-bearing granitoids in Saudi Arabia, western Africa, and parts of the Lachlan Fold Belt in Australia are peralkaline to mildly peraluminous A-type granites that contain 75 to 77%  $\text{SiO}_2$ . These granites have major and trace element compositions similar to the tin-bearing rhyolites in New Mexico (Fig. 5). The chondrite normalized rare earth element patterns for these granitoids are flat with deep negative Eu anomalies, similar to the tin-bearing rhyolites (Fig. 4).

## TIN DEPOSITS

## Types of Deposits

Both lode and placer tin deposits occur in the region. The most important in terms of economic value are the placer deposits, which are both alluvial and colluvial types. The alluvial placer deposits consist of unconsolidated sand and gravel deposits in the bottoms of presently active valleys. These placers are long (>2 km), narrow (<100 m), and rarely exceed 2 or 3 m in depth. Colluvial placer deposits mantle the tin-bearing rhyolite domes and have produced most of the tin in the district. Thickness of the colluvial deposits is variable over short distances and does not exceed 2 to 3 m in the Nugget Gulch prospect, where the tin-bearing colluvium has been exploited. Cassiterite and wood tin are concentrated near the base of the colluvium. Wood tin nuggets larger than 10 cm have been found and wood tin is the predominant tin-bearing mineral in the placer deposits (Fig. 7). The richest colluvial placer deposits were found on the flanks of rhyolite domes, within a few tens of meters of the carapace of the domes.

Lode tin occurs as cassiterite and wood tin in veinlets with variable proportions of hematite (Fig. 8). We use the term cassiterite in reference to coarsely crystallized, red to pale yellow  $\text{SnO}_2$ . The crystals rarely exceed 3 mm in diameter and locally form coarse, anhedral aggregates. Wood tin is micro- and cryptocrystalline cassiterite that is finely banded, botryoidal, and generally opaque.  $\text{SnO}_2$

exhibits a continuous spectrum of grain size, however, the fine and coarse end members are the most common. Gangue consisting of quartz, calcite, fluorite, topaz, various fluoroarsenates, antimonides, pyroxenes, and zeolites in extremely variable proportions locally coat the veinlets (Foord and others, 1985; Maxwell and others, 1986). Calcite, and quartz veinlets with no associated tin mineralization are common in some deposits.

Exposed tin-bearing veinlets are a few meters in length and height and as much as 5 cm wide. The large wood tin nuggets found in many of the placer deposits suggest that some veins were wider. At some localities, the veinlets form anastomosing networks several meters long and wide. Vertical dimensions in excess of 20 m are not known. Disseminated cassiterite and hematite selvages in the wallrock extend a few cm away from many of the veinlets. With rare exception, the mineralization is restricted to lithophysal zones above zones of intense VPC and a below the carapace breccia of the domes (Fig. 3). The Nugget Gulch prospect is a notable exception because tin-bearing veinlets are exposed within the carapace breccia within a few tens of meters of the paleosurface of the dome.

Only the Juniper deposit (Fig. 1) is not hosted by rhyolite lava. Rather, it is hosted by high-silica rhyolite ignimbrite that preceded the eruption of the immediately overlying rhyolite dome-flow complex (Lawrence and Richter, 1986). Although the tin deposit is located several hundred meters from the nearest rhyolite lava, it apparently was once

covered by rhyolite lava (Lawrence and Richter, 1986). The mineralogy, paragenesis, and fluid inclusion homogenization temperatures of the Juniper deposit are identical to those of the tin deposits hosted by rhyolite lava.

The open fractures that host the tin mineralization are not fault related. Lufkin (1972) concluded that the fractures were due to cooling of the rhyolite domes after modelling the stresses induced by heat loss.

### Paragenesis

The paragenesis of these deposits can be divided into an early hematite-cassiterite-wood tin stage and a later quartz-calcite-fluorite stage (Fig. 9). This paragenesis represents a composite for the region and the entire paragenesis has not been observed at any single locality.

During the hematite-cassiterite-wood tin stage, small amounts of topaz, quartz, and possibly sanidine were locally deposited on and in the wallrock prior to deposition of magnetite. Quartz, topaz, sanidine, hematite, pseudobrookite, bixbyite, red beryl and cassiterite were deposited in lithophysae. Massive and octahedral magnetite was then deposited in veinlets. Hematite containing sparse inclusions of cassiterite replaced the early magnetite and formed pseudomorphs after the octahedral magnetite. Bladed hematite then grew on the massive hematite. Cassiterite was deposited as both dark red crystals and as wood tin coevally with the bladed hematite. The proportion of hematite to cassiterite varies dramatically from deposit to deposit. At



one locality, cassiterite was deposited as dark red, euhedral crystals with little associated hematite (Fig 8a). At other deposits, coarse cassiterite, wood tin, and both massive and bladed hematite form alternating bands (Fig. 11). Wood tin veinlets with little associated hematite were deposited in and very near the carapace breccia (Fig. 8b).

The hematite-cassiterite-wood tin stage is followed by a stage consisting of various polymorphs of quartz, calcite, fluorite, various rare fluoroarsenates, and zeolites and possibly hematite. These minerals were deposited in no specific order.

In detailed studies of the mineralogy of the tin deposits of the region, Foord and others (1985) and Maxwell and others (1986) report durangite, two unnamed fluoroarsenates, an unnamed Sb-Sn-Fe-Ti oxide related to cassiterite, and an unidentified clinopyroxene that may be included with the hematite-cassiterite stage; but the rarity of these minerals makes assignment of a position in the paragenetic sequence tenuous. Hidalgoite, beudantite, jarosite, cryptomelane, todorokite, and possibly varlamoffite are also reported (Foord and others, 1985) and are postulated to be late in the paragenesis, possibly coeval with the quartz-calcite-fluorite mineralization, but again, the rarity of these minerals makes assignment in the paragenesis tenuous. Locally, clay minerals fill open spaces in the veinlets and are the last minerals to form.

Although the general paragenesis is simple, the detailed paragenesis of the first stage is quite complex.

Hematite locally replaces cassiterite and cassiterite replaces hematite. Exsolution of cassiterite from hematite is common and Lawrence (1985) reports exsolution of ilmenite from hematite. Skeletal hematite occurs at several localities as does euhedral hematite that has been etched. In all the deposits studied, coarse cassiterite and wood tin are concentrically banded (Fig. 10). Hematite bands commonly separate coarse cassiterite from wood tin. Individual bands can be traced throughout a single hand sample, but no stratigraphy was defined that was consistent from sample to sample in an individual deposit.

#### Hydrothermal alteration

Argillic alteration and silicification associated with tin mineralization at Nugget Gulch is restricted to zones a few meters in diameter near the top of the carapace breccia of the dome. At the Nugget Gulch deposit, the argillic alteration does not affect the overlying rhyolite lava or pyroclastic rocks that mantle the tin-bearing dome indicating that alteration was complete prior to emplacement of the overlying dome. The small zones of argillic alteration are closely related to small bodies of silica-replaced carapace breccia. These silica replacement bodies are typically less than 20 m in diameter and occur at the top of the dome. Selvages of intense silicification border many of the tin-bearing veinlets at the base of the carapace breccia.



## Chemistry of the Cassiterite and Hematite

Five hand-picked samples of minerals from the vein mineralization were analyzed by INAA to investigate the trace element composition of the hematite and cassiterite (Table 2). Cassiterite contains as much as 2.5%  $\text{Fe}_2\text{O}_3$  and the wood tin sample contains about 5%  $\text{Fe}_2\text{O}_3$ . Lufkin (1977) reported that wood tin contains as much as 8%  $\text{Fe}_2\text{O}_3$ . Cassiterite has higher concentrations of Sb, U, W, and U than the wood tin and wood tin has higher concentrations of As than the cassiterite. Cr, although not in high concentrations is significantly enriched in the tin samples relative to the host rhyolites. These differences in trace element composition between the wood tin and cassiterite suggest that the minerals were formed by somewhat different depositional processes. Sc, Sb, Ta, and Co typically substitute for iron in minerals and are enriched in the hematite relative to the host rhyolite. The rare earth element content of both the hematite and cassiterite is very low. Samples of tin-bearing vein material analyzed by XRF contain high concentrations of Pb, Rb, Sr, and Zn relative to the host rhyolites.

## FLUID INCLUSIONS

## petrography

Fluid inclusions in cassiterite, topaz, quartz, and calcite from these deposits were studied. Following the guidelines of Roedder (1984), primary inclusions are large, isolated inclusions and inclusion that follow primary growth bands. Pseudosecondary inclusions consist of veils of inclusions that are truncated by primary growth bands. Secondary inclusions form veils that fill fractures in the host mineral.

Three types of inclusions were observed in cassiterite, topaz and the quartz associated with the tin mineralization (Table 3). Type 1 inclusions are large (<50  $\mu\text{m}$ ), vapor-filled inclusions with no observable liquid phase and occur as primary, pseudosecondary and secondary inclusions (Fig. 12c). Heating to 600 $^{\circ}$  C and cooling to -180 $^{\circ}$  C produced no recognizable phase changes in type 1 inclusions.

Type 2 inclusions are small (<10  $\mu\text{m}$ ), multiphase solid-vapor inclusions that occur as primary, pseudosecondary and secondary inclusions (Fig. 12d). At room temperature, type 2 inclusions consist of a vapor bubble, and as many as four subhedral to euhedral daughter minerals in a pale-yellow, crystalline solid that fills most of the inclusion. Daughter minerals in type 2 inclusions are enclosed in the crystalline solid, thus they are visible only when the crystalline solid is molten, thus petrographic study of the daughter minerals

in type 2 inclusions was done at temperatures above 350° C. Three of the daughter minerals are translucent (Fig. 12j). The large, rhombohedral(?), birefringent daughter mineral in Figure 12i may be a carbonate. The smallest of the transparent daughter minerals is roughly cubic and may be a halide (Fig. 12j). The larger of the two is rounded and apparently isotropic; it may be KCl. The opaque daughter mineral has red rims on some grains, suggesting that it is hematite. Very small amounts of aqueous fluid was observed in a few of these inclusions at room temperature.

Type 2 inclusions also occur in overgrowths on quartz phenocrysts in zones of intense vapor phase crystallization. Type 1 and 2 inclusions typically occur together in pseudosecondary planes (Fig. 12f). This spatial association suggests that both types of inclusions were trapped simultaneously. Type 3 inclusions are rare liquid-vapor secondary inclusions in cassiterite and topaz.

Type 4 and 5 inclusions were observed in the quartz-calcite-fluorite mineralization. Type 4 inclusions occur as primary, pseudosecondary and secondary types and are vapor-dominated liquid-vapor inclusions. Type 5 inclusions occur as primary and pseudosecondary types and are liquid-dominated, liquid-vapor inclusions (Fig. 12e).

Type 6 inclusions (Fig. 12j) occur in quartz and sanidine phenocrysts and consist of glass and vapor. Type 6 inclusions in quartz phenocrysts (Fig. 12k) did not homogenize when heated to 1200° C for 20 minutes and are probably magmatic glass-vapor inclusions. These inclusions

are distinctly different than type 2 inclusions.

Most dark-red cassiterite became opaque when heated to  $400^{\circ}$  C and this effect was reversible. This limited the number of microthermometric determinations on cassiterite.

#### Microthermometric Studies

The crystalline solid in type 2 inclusions melts between  $350$  to  $370^{\circ}$  C to form typical three phase inclusions (Fig. 12h). Melting of the crystalline solid occurs over a  $10$  to  $20^{\circ}$  C interval, suggesting eutectic behaviour. Melting begins at the margins of the inclusions and as it proceeds, "rafts" of solid form, floating in the liquid. These rafts continue to melt as the temperature is increased until melting is complete. Supercooling by  $50^{\circ}$  to  $80^{\circ}$  C causes the liquid to instantly crystallize to a microcrystalline aggregate that deforms the vapor bubble. The microcrystalline aggregate exhibits a mottled appearance in transmitted light rather than the uniform, isotropic appearance of typical glass inclusions (Fig. 12j).

Homogenization of these inclusions to liquid occurs at temperatures between  $650^{\circ}$  and  $680^{\circ}$  C (Table 4). Daughter minerals dissolve between  $400^{\circ}$  and  $650^{\circ}$  C (Fig. 12j). A particularly large Type 2 inclusion in topaz contained four daughter minerals (Fig. 12i). The large, rhombohedral(?) daughter mineral in that inclusion dissolved at about  $408^{\circ}$  C. In order to preserve the inclusion, it was not heated above  $450^{\circ}$  C. In smaller inclusions that contain similar appearing

daughter minerals, the daughter minerals dissolve between 500° and 630° C. The opaque daughter mineral present in most Type 2 inclusions was not observed to dissolve on heating.

Type 2 inclusions in a single quartz overgrowth melted between 470 and 530° C and homogenized to liquid at 720° to 730° C. No daughter minerals were observed in these inclusions. Type 2 inclusions in the overgrowths are thus significantly different melting and homogenization temperatures than those in the vein minerals.

London (1986) describes similar melting phenomena in inclusions in spodumene from the Tanco Pegmatite in Canada. The melting phases were determined to be diomignite (lithium tetraborate), cookeite, albite, quartz, and a pollucite-analcime solid solution. Naumov and others (1977) report similar to type 2 inclusions in topaz from ongonites, but hazard no opinion on the composition of the solid. The composition of type 2 inclusions may be similar to the composition of the inclusions described by London (1986).

Type 3 secondary inclusions homogenize between 450 to 512° C. Decrepitation of fluid inclusions occurred in a number of cassiterite and topaz samples at about 400 to 460° C. The decrepitating inclusions were not observed. Decrepitation temperatures of fluid inclusions gives little other than maximum filling temperatures, but suggest upper limits of filling temperatures (Roedder, 1984).

Type 4 and Type 5 inclusions large enough to measure are sparse, in part because of the fine grain size of the minerals involved. Homogenization temperatures ( $T_h$ ) of Type

4 and Type 5 inclusions range from 130° to 390° C (Table 5; Fig. 13). Type 4 inclusions homogenize to vapor and Type 5 inclusions homogenize to liquid. The coexistence of Type 4 and Type 5 inclusions and the fact that both homogenize at similar temperatures indicates that the fluids were boiling (Roedder, 1984). Only one sample, #252, had measurable inclusions in both quartz and calcite. The values from both minerals are about the same. In all samples, inclusions representative of the entire range of Th were found in close proximity. Typically, inclusions with low Th decrepitated prior to homogenization of inclusions with high Th (>340° C), suggesting that inclusions with low Th were trapped later than inclusions with high Th.

A number of inclusions with Th below 150° C were observed. With one exception, these inclusions were in calcite. In samples MC-1 and MC-2, stretching of inclusions was found to increase Th by as much as 40° C if the inclusion was >10 um and was heated as little as 10° C above Th. Stretching was not found to be a problem in inclusions smaller than 10 um. This problem is mentioned because a number of chips of MC-1 and MC-2 were heated to over 200° C before the problem was identified and thus many of the temperatures in the 150 to 190° C range would probably homogenize at Th of about 130° C had they not been stretched. These problems were avoided in the high temperature inclusions by heating only to Th and then cooling prior to measuring another inclusion. No data was recorded for subsequent inclusions that had Th lower than the maximum



temperature the chip had attained. Salinities of Type 5 inclusions calculated from freezing point depressions in liquid-vapor inclusions are 0 to 2.4 equivalent wt.% NaCl (Table 5).

A sample of quartz from a quartz vein about 200 m from a tin occurrence contains type 1, 2, 4, and 5 inclusions. A number of apparently naturally decrepitated fluid inclusions (Fig. 12m) were observed, suggesting that the temperature of the mineralizing systems did not simply decrease, but rather, fluctuated with time, causing earlier formed inclusions with lower Th to decrepitate.

Eggleston and others (1987a) report homogenization temperatures of 720 to 730<sup>o</sup> C for inclusions in overgrowths on quartz phenocrysts that are similar to Type 2 inclusions. These overgrowths occur in zones of intense vapor phase crystallization several tens of meters below the tin mineralization. These differences in homogenization temperatures indicates a vertical temperature gradient of several <sup>o</sup> C/meter. Thermal gradients near the paleosurface of the domes may have been several tens of <sup>o</sup> C/meter.

#### Pressure Estimates

Geologic reconstructions of the surface of the domes indicates that many type 2 inclusions were trapped within 50 m of the paleosurface. The proximity of temperatures >650<sup>o</sup> C indicates that the fluids were in contact with rocks at magmatic temperatures very near the paleosurface of the host rhyolite domes. The high temperatures and low pressures of

mineralization indicate that the fluids responsible for VPC and tin mineralization were supercritical. The density of a 650° C, aqueous fluid at 1 bar is about  $10^{-4}$  g/cm<sup>3</sup> (Holloway, 1981). It is not surprising that no liquid is visible in type 1 inclusions. Type 2 inclusions are probably condensates from the low density, supercritical fluid responsible for tin mineralization.

Pressure estimates based on boiling at temperatures >330° of type 5 and 6 inclusions indicate pressures of 180 bars; suggest confining pressures equivalent to >700 m for a lithostatically pressured system and >1800 m for a hydrostatically pressured system (Haas, 1971). The distance to the tops of the host rhyolite domes from the mineralization could not have been more than 300 m and in many cases, could not have been more than 200 m, thus the fluids were overpressured. These pressures are conceivable if the fractures that the tin-bearing veinlets occupy were periodically blocked and trapped the fluids. When the fluid pressure overcame the confining pressure, brecciation of the pre-existing tin-bearing veinlets would occur as the fluids were released (Fig. 121).

The pressure required to prevent boiling of fluids at 200° C is 20 to 25 bars; equivalent to <200 m of hydrostatic load or <75m of lithostatic load (Haas, 1971) and are consistent with estimated cover on the deposits. The lack of coexisting vapor- and liquid-rich inclusions that homogenize at <200° C suggests that the fluids were not boiling and were trapped at pressures higher than 25 bars.



## Fluid Inclusion Gas Analyses

Volatiles in fluid inclusions from 13 samples were analyzed (Table 6). The condensible fraction (separated by liquid  $N_2$ ) consists of  $H_2O$ ,  $CO_2$ ,  $H_2S$ ,  $SO_2$ ,  $NO$ , and most organic compounds. The organic fraction is reported as total organic materials ( $C_NH_N$ ), however, identified organic compounds include propene, propane, benzene, and ethane. Other organic compounds are probably present, but overlapping mass peaks preclude their identification by mass quadrupole spectrometry.

Non-condensable phases include  $H_2$ ,  $He$ ,  $Ar$ ,  $N_2$ ,  $CH_4$ ,  $NO$ ,  $O_2$ , and  $CO$ . Overlapping peaks on the mass spectra are not the problem that they are for the condensible phases, thus these phases are easily identified and their ratios calculated. Metallic precipitates formed in the sample tubes when samples 5, 15, and 16 were heated to  $800^\circ C$  and most likely were  $Sn$ ,  $As$ , or  $Sb$ , which occur in high concentrations in the ores.

$H_2O$  and  $CO_2$  are the dominant volatiles in all samples with  $CO_2/H_2O$  ratios from about 0.1 to 0.6. Two samples of wood tin were decrepitated at 500 and then at  $800^\circ C$ . For those samples (#2/#3 and #4/#5),  $CO_2$  was higher in the low temperature decrepitation and  $H_2S$ ,  $SO_2$ , and  $H_2$  were higher in the high temperature decrepitation. Although somewhat different gas ratios were obtained by changes in decrepitation temperature, these differences are probably insignificant because the data for different decrepitation

temperatures cluster tightly on plots discussed below.

A plot of  $\text{CO}_2$  vs  $\text{N}_2$  (Fig. 14) shows that the wood tin and cassiterite have similar  $\text{CO}_2$  and  $\text{N}_2$  contents. The calcite samples likewise plot as a group, but are distinctly different from the tin minerals. Values of  $\text{SO}_2$  and  $\text{H}_2\text{S}$  exhibit distinct differences between the tin mineralization and the later mineralization.  $\text{SO}_2$  is the dominant S-bearing gaseous species in inclusions in the tin mineralization and  $\text{H}_2\text{S}$  is the dominant S-bearing gaseous species in inclusions in the later mineralization.

The gas ratios in the wood tin and cassiterite are similar to the gas ratios in porphyry Cu and Mo deposits and to many fumarole gases (Fig. 14) whereas the high organic and  $\text{N}_2$  content of the quartz-calcite samples plots in a field similar to those reported in many epithermal and sediment-hosted deposits (Norman and Sawkins, 1987).

Organic materials were identified in all but one sample. In two samples (#8 and 10), an unidentified, yellow, oily substance precipitated on the inside of the sample tube during heating of the sample. The yellow precipitate was partially soluble in soapy water and is believed to be a hydrocarbon compound. The origin of these organic compounds is problematic. Bacteria and algae are commonly observed at the top of hot springs and fumaroles. In the tin mineralization, the organic compounds in the fluid inclusions could represent organic material that entered the system from the surface. Alternatively, the organic components may have been leached from crustal rocks (Norman and Sawkins, 1987).

## OXYGEN ISOTOPE DATA

Quartz samples from the quartz-calcite-fluorite mineralization have  $\delta^{18}\text{O}$  compositions from 5.8 to 11.0 ‰ (Table 7). Clay minerals taken from open space in the center of a calcite vein has a  $\delta^{18}\text{O}$  of 10.6 ‰. Chalcedonic quartz from the silica replacement body associated with the tin mineralization in Nugget Gulch has a  $\delta^{18}\text{O}$  of 19.4 ‰ and a silicified selvage bordering a hematite veinlet has a  $\delta^{18}\text{O}$  of 17.2 ‰.

Temperatures of formation for the quartz-calcite-fluorite are in the range of 130 to 350°C, thus the fluids that precipitated those minerals had a  $\delta^{18}\text{O}$  of between -8 and +3 ‰ depending on the temperature of the fluid.

Eggleston and others (1987a) report a  $\delta^{18}\text{O}$  of 7.5 ‰ for quartz from lithophysae and concluded that the fluids responsible for vapor phase crystallization was magmatic fluid derived from the affected rhyolite. Measured whole rock  $\delta^{18}\text{O}$  range from 6.1 to 9.9 ‰ and the measured  $\delta^{18}\text{O}$  of quartz separates range from 7.5 to 7.8. They concluded that the  $\delta^{18}\text{O}$  composition of the whole-rock samples was modified by post-eruptive fluids and estimated that the magmatic  $\delta^{18}\text{O}$  of the tin-bearing rhyolites was between 6.5 to 6.8 ‰. We proposed that cooling magmatic water produced the  $^{18}\text{O}$  enrichment of the whole rock samples and that the fluid was probably the same fluid that was responsible for VPC.

Rye and others (1984) reported that cassiterite and

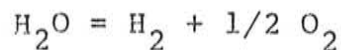
hematite  $\delta^{18}\text{O}$  compositions range from 4.2 to 1.2 ‰ and that the  $\delta^{18}\text{O}$  for quartz from lithophysae and cristobalite from veinlets range from 7.4 to 11.8 ‰; late silica had  $\delta^{18}\text{O}$  compositions of 22.5 to 28.9 ‰; and the difference in oxygen isotopic values for quartz-magnetite pairs was 0.7 to 0.1 ‰ and indicates temperatures in excess of 500° C. Their values are essentially the same as those reported here.

## DISCUSSION

 $f_{O_2}$  Of The Mineralizing Fluids

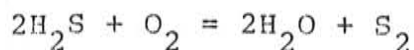
The  $f_{O_2}$  of the fluids can be expected to be similar to the  $f_{O_2}$  of the host rhyolite immediately after the fluids separate from the melt. The  $f_{O_2}$  of felsic magmas to be above the quartz-magnetite-fayalite (QFM) buffer and may be as much as 2 log  $f_{O_2}$  units above the Ni-NiO (NNO) buffer (Haggerty, 1976; Christiansen and others, 1986). The few data available for high-silica rhyolites indicate that  $f_{O_2}$  for these rocks can lie anywhere between the QFM buffer and 1 or 2 log  $f_{O_2}$  units above the NNO buffers (Christiansen and others, 1986). The presence of sphene in some of the Taylor Creek Rhyolite domes suggests that the  $f_{O_2}$  of the sphene-bearing domes was approximately on the Ni-NiO buffer (Haggerty, 1976). Pseudobrookite in lithophysae suggests that the  $f_{O_2}$  of the fluids was as much as 2 log units above the Ni-NiO buffer (Fig. 16) (Carmichael and Nicholls, 1967). Early magnetite deposited in the tin-bearing veins was replaced by hematite indicating that the  $f_{O_2}$  of the early fluids was below the magnetite-hematite (MH) buffer and that with time the fluids became more oxidizing. When the bulk of the tin-bearing material was deposited, the fluid had an  $f_{O_2}$  higher than that of the magnetite-hematite buffer.

The  $f_{O_2}$  of the fluid inclusion gases was calculated from the gas analyses with the equation;



from free energy data compiled by Robie and others (1979).

The  $f_{S_2}$  of the samples was calculated from the equation;



using the calculated  $f_{O_2}$  values. The calculated  $f_{O_2}$  and  $f_{S_2}$  are plotted on Figure 16.

The calculated  $f_{O_2}$  value of fluid inclusion gases in topaz agree with other estimates of the  $f_{O_2}$  of the rhyolites. Calculated  $f_{O_2}$  of fluids that deposited cassiterite agrees with the  $f_{O_2}$  required for the stability of pseudobrookite. Wood tin is deposited nearest the surface and has the highest calculated  $f_{O_2}$  values. The gas data from fluid inclusions suggest that the fluids were in equilibrium with the magma at near magmatic temperatures and became more oxidizing near the surface where atmospheric oxygen could be added to the fluids.

#### Origin of the Mineralizing Fluids

Th of fluid inclusions in cassiterite and associated quartz and topaz indicate fluid temperatures between 670 and 730° C. These temperatures agree with depositional

temperatures suggested by Lufkin (1976), Lawrence (1985), and Rye and others (1984) from mineral equilibria, ilmenite exsolution in hematite, and oxygen isotopes respectively. Together the data are strong evidence that the hematite-cassiterite mineralization occurred at near magmatic temperatures.

The spatial association of tin mineralization with zones of intense vapor phase crystallization, the occurrence of type 2 inclusions in zones of intense VPC and in the tin mineralization, and the magmatic temperatures recorded in type 2 inclusions indicate that the fluids responsible for VPC were also responsible for depositing the tin mineralization. The oxygen isotope data indicates that the fluids responsible for VPC was magmatic water, thus the tin mineralization was deposited from magmatic fluids.

Fluid inclusion gas analyses are similar to fumarolic gases in recently active volcanos (Fig. 14). This also indicates the magmatic nature of the fluid and suggests that the tin mineralization was deposited in fumaroles at the paleosurface of the rhyolite domes immediately after extrusion of the domes and while the domes were cooling.

The temperature of formation of the replacement silica body and the silicified selvages at Nugget Gulch was not possible to determine; however, because those deposits were formed within a few meters of the surface, temperatures could be expected to be somewhat above 100° C. At 100° C, the fluids that deposited the quartz would, by extrapolating the equations of Clayton and others (1972), have a  $\delta^{18}\text{O}$  of -2 to



-4 ‰. At 200° C, the water would have a  $\delta^{18}\text{O}$  of between 5 and 7 ‰, thus it is probable that the fluids were magmatic with an undetermined meteoric water component.

Fluids that deposited the quartz-calcite-fluorite mineralization have oxygen isotope compositions that suggest that they were mixed meteoric and magmatic fluids or exchanged meteoric water. The quartz that was analyzed for its oxygen isotopic composition was deposited over a wide range of temperatures, thus, it is not possible to ascertain the relative proportions of magmatic water or the degree of exchange. As much as 70% of the water could be magmatic if the bulk of the quartz were deposited from  $>300^\circ$  water. The low salinity of the water in these inclusions (<2 eq. wt% NaCl); however, suggests that the water was dominantly meteoric. The similarities of fluid inclusion gases in the quartz-calcite-fluorite mineralization to those that occur in epithermal ore deposits (Norman and Sawkins, 1987) also suggests a meteoric origin for the water. The small volume of the quartz-calcite-fluorite mineralization and the lack of  $^{18}\text{O}$  depletions near the deposits indicate that the systems were short lived meteoric water dominated hydrothermal systems.

The small size of the tin deposits and the lack of significant hydrothermal alteration argue that no external source of water is necessary. Large volumes of meteoric water flowing through these systems would be expected to produce a significant  $^{18}\text{O}$  depleted zone in the host rhyolites (Criss and Taylor, 1983). Whole-rock  $\delta^{18}\text{O}$  values indicate



enrichment of  $^{18}\text{O}$  in most samples. The small size of the zones of intense VPC also argue for a small water/rock ratio. Small volumes of water are consistent with the interpretation that the fluids responsible for the VPC and tin mineralization were from the host rhyolite dome.

#### Origin of Tin in the Rhyolites

The 5 to 15 ppm Sn in the tin-bearing rhyolites is higher than the 2.5 ppm in average crust (Taylor and McLennan, 1985) and average granite (Turekian and Wedepohl, 1961), but is less than the 20 to 50 ppm reported in many tin-bearing granites and in some other topaz rhyolites (Christiansen and others, 1986). The mild enrichment of tin relative to average granite and rhyolite can be explained by differentiation processes (Eggleston and others, 1987b; Lehman, 1982; Mitchell, 1979). Desborough and others (1980) and Desborough and Mihalik (1980) noted high concentrations of tin in the late crystallizing Fe and Ti oxide minerals in the Redskin Granite and Henderson molybdenum deposit. This indicates that tin is incompatible with earlier forming minerals in granitic systems, thus differentiation of the parental magma will concentrate incompatible elements such as Sn, Nb, and Rb in the most felsic parts of the magma. It is not necessary to invoke reworking of tin-rich source regions (Hutchison and Chakraborty, 1979; Routhier, 1976; and Turneure, 1977), leaching of tin from upper crustal, tin-rich granites (Jackson, 1979), or volatile transfer of tin (Sainsbury and Hamilton, 1967) to produce the mild tin

enrichment in the tin-bearing rhyolites.

#### Origin of the Tin-Bearing Rhyolites

Eggleston and others (1987b) suggest that the parent magmas for the tin-bearing magmas were derived by partial melting of a biotite/phlogopite-bearing lower crustal granulite with a possible upper mantle contribution. Lower crustal granulites are believed to have formed by extraction of a hydrous, granitic melt (Collins and others, 1982). Because most of the water will be removed by the early melting episode, subsequent melting episodes will be relatively dry and thus melt at a higher temperature. Plagioclase, K-feldspar, quartz, pyroxene, garnet, aluminosilicate minerals, biotite, phlogopite, zircon, and rutile are typical minerals in granulites (Padovani and Carter, 1977). Fe-Mg mica in the source contribute F, Rb, Nb, and Sn to the melt. Sr and Ba would have been depleted in the source region by the early melting event and will thus be relatively depleted in subsequent magmas produced in the source region. Eggleston and others (1987b) suggest that the parental magma for the tin-bearing rhyolites is similar in composition to A-type granites described by Loiselle and Wones (1979).

Crystal-liquid fractionation is a suggested mechanism to produce the high Rb, Nb, Th, and U concentrations and the low Ba and Sr concentrations in the tin-bearing rhyolites. Plagioclase, sanidine, quartz, and amphibole were probably major crystallizing phases; however, crystallization of

allanite and sphene are necessary to control the earth element concentrations. Biotite can not have been an important crystallizing phase because it would have removed Rb, Nb and Sn from the melt, precluding concentration of those elements in the melt. Contamination of the magmas by upper crustal rocks and isotopic homogenization late in the differentiation history of the magma probably occurred, but that contamination was minimal (Eggleston and others, 1987b) and produced only minor changes in the trace element concentrations and initial  $^{87}\text{Sr}/^{86}\text{Sr}$  ratios.

#### Transport of Tin

Tin can be volatilized and transported as a metallic vapor at magmatic temperatures and occurs in fumarolic incrustations (Daubree', 1879; Zies, 1929; Krauskopf, 1957; Stoiber and Rose, 1974; Oskarsson, 1981; Symonds and others, 1984; Bernard and Le Guern, 1986); however, the vapor pressure of tin is  $<10^{-13}$  bars at  $600^{\circ}\text{C}$ , thus vapor transport is not a particularly attractive mechanism for the formation of the deposits in New Mexico (Krauskopf, 1957; 1964). Cassiterite has been reported in fumarole incrustations by Stoiber and Rose (1974), but, Sn typically occurs as contaminants in crystalline sublimates around high temperature ( $>300^{\circ}\text{C}$ ) fumaroles. In reported occurrences of tin in sublimates, the tin occurs in phases that condense at temperatures between  $300$  and  $500^{\circ}\text{C}$ , much lower temperatures than those indicated for the Taylor Creek deposits (Bernard and Le Guern, 1986; Stoiber and Rose, 1974; Oskarsson, 1981).

These observations argue that another transport mechanism is probably responsible for tin transport in these systems.

Transporting tin as Cl complex in supercritical fluids appears to be more probable than vapor transport of tin metal. Data from Eugster and co-workers (Eugster, 1986; Eugster and Wilson, 1985; Wilson and Eugster, 1984) that the solubility of tin in supercritical, chloride solutions is favored by high temperatures and low  $f_{O_2}$  (Fig. 17) and that tin is carried in solution as  $SnCl^+$ . Chou and Eugster (1977) found that Fe is about 100 times as soluble in chloride-bearing supercritical fluids as Sn, thus offering an explanation for the predominance of hematite in the tin-bearing veinlets.

The proximity of the tin mineralization to the paleosurface and the high depositional temperatures indicate a low pressure, high temperature environment for deposition. A thermal gradient of several degrees per meter are indicated between the zone of intense vapor phase crystallization and the paleosurface. Cooling and the increasing  $f_{O_2}$  of the fluids as the fluids neared the paleosurface decreased the solubility of  $SnCl^+$  in the fluids and precipitate tin.

#### The Wood Tin Problem

The origin of wood tin has been debated since Hanks (1876) reported wood tin in the rhyolite-hosted tin deposits in Mexico. He suggested that wood tin was forming in the veins as a result of supergene processes based on a verbal report by a Mr. J.F. Boyd who stated that he found films of

cassiterite and wood tin that formed in a mine between 1864 and 1870. Collins (1880) described deer horns recovered from placer deposits in Cornwall that contained several per cent cassiterite. The cassiterite (wood tin) pseudomorphed the internal structure of the horn indicating low temperature formation for wood tin. Scrivenor (1909, as reported in Ferguson and Bateman, 1912) examined the horns and concluded that the cassiterite was mechanically impregnated in the horn, but did not discuss the pseudomorphous character of some of the cassiterite. Since those early reports, Jones (1925), Singh and Bean (1967), Smith and Hosking (1974), and Pan (1974) speculated on various low temperature processes to form wood tin. Pan's (1974) experimental studies suggested that wood tin was not stable above  $140^{\circ}$  C.

In the Taylor Creek district, interbanding of cassiterite and wood tin and the continuous cassiterite crystal size spectrum argue that the coarse cassiterite was formed at temperatures similar to that of wood tin, but under somewhat different chemical, pressure, or temperature conditions. The delicate interbanding of the two end member grain sizes suggests that the physiochemical conditions of deposition were rapidly fluctuating. The differences in grain size can be explained by variations in the rate that the supercritical fluids reach the paleosurface. Quiescent flow in an open fracture will allow for coarse, nearly pure cassiterite and hematite to grow from Sn and Fe saturated solutions. Rapid fluid flow on the other hand will cause telescoping of the relatively high temperature and low  $f_{O_2}$

fluid to within a few meters of the paleosurface where extreme temperature and  $f_{O_2}$  gradients will lead to supersaturation of Sn and Fe that in turn will favor rapid precipitation of cassiterite and thus finer grains, that is, wood tin.

Multiple pulses of rapidly flowing, supersaturated fluids will produce the banding observed in the wood tin nuggets. Periodic blockage of the fluid channels by mineral growth will cause overpressure that will result in almost explosive flow rates when the overpressure exceeds the confining pressure.

The high concentration of Fe and As in wood tin can be explained by rapid precipitation of wood tin. Fe will be trapped in the wood tin as fine grained hematite that will not diffuse out of the wood tin. Arsenic, which has a vapor pressure of about 0.8 bars at 600° C (Krauskopf, 1957), will also be incorporated in the wood-tin rather than the more slowly crystallizing cassiterite because As will be transported as a vapor until it is cooled and deposited near the surface.

#### Model

The following sequence of events is suggested by the data (Fig. 18). A relatively anhydrous, A-type granitic magma was generated by partial melting of a lower crustal granulite. The upper mantle may have contributed to the magma, but the extent of that contribution is not known. Melting of residual biotite in the granulite provided the Sn



and relatively high initial concentrations of F, Rb, Nb. Residual plagioclase prevented Sr and Eu from entering the melt. Differentiation in shallow magma chambers enriched Rb, Nb, Ta, Th, U, and depleted Ba, Sr, and Sc in the tin-bearing rhyolites. Differentiation concentrated Sn in the most felsic phases. Rapid ascent of the magma from the shallow magma chamber to the surface was facilitated by the viscosity decrease induced by the high F content (Mysen and Virgo, 1985). As the lava was erupted and the dome growth proceeded endogenously, exsolving fluids were channeled along flow banding and progressed toward the surface. The abundance of quartz, hematite, and other minerals suggests that fluids migrated through the lithophysae. The lithophysal zones formed caps on zones of intense vapor phase crystallization, temporarily trapping magmatic fluids that migrated along flowbanding. Localized zones of intense VPC formed in an otherwise mildly vapor phase crystallized rhyolite dome. While the fluids were temporarily trapped, phenocrystic magnetite, hematite, biotite and other ferromagnesian minerals were converted to hematite, releasing any contained tin to the already tin-rich fluid. As the lithophysal zones cooled enough to become brittle, they fractured, releasing the trapped fluids that contained high concentrations of Sn and Fe. The hematite-cassiterite mineralization was deposited as incrustations in fumaroles by a combination of  $f_{O_2}$  increase and temperature decrease. Periodic blockage of the fractures and quiescent fluid flow allowed coarse cassiterite and hematite to precipitate. Rapid venting of

the fluids favored wood tin precipitation.

The process continued throughout the degassing history of the lavas, lasting no more than a few hundred years. Condensation of the vapor phase created acidic waters that argillically altered very small areas of the carapace breccias of the domes. This condensate is probably also responsible for the silicification of the carapace breccia.

As the lavas cooled to the 300 to 400° C range, very short lived epithermal systems commenced. These systems were meteoric water dominated and produced quartz-calcite-fluorite mineralization. Magmatic fluids that had not escaped in the initial degassing period mixed with the epithermal waters. Cooling to less than 100° C occurred in 30 to 300 years.

#### Implications for Other Deposit Types

Burt and Sheridan (1986) suggested that topaz rhyolites may be surface expressions of Climax-type molybdenum porphyry systems, and they note that fault reconstructions at Climax, Colorado suggest that the Chalk Mountain topaz rhyolite is related to the Climax intrusives. Low molybdenum contents of the tin-bearing rhyolites, lack of sulfur in the systems and the postulated low water content of the tin-bearing rhyolite magmas however, argues against the possibility of a Climax type porphyry molybdenum system underlying the tin-bearing rhyolites. Molybdenum mineralization, although sparse, is present in the Iron Mountain, New Mexico, skarns as is W and tin mineralization. Skarns similar to those at Iron Mountain,



New Mexico and Lost River, Alaska (Robertson, 1985; Dobson, 1982), are probably present in carbonate rocks that underlie the region; however, depth to that type mineralization may be prohibitive.

Granitic rocks that are chemically similar to the tin-bearing rhyolites in New Mexico host greisen mineralization in Tasmania and west Africa (Higgins and others, 1985; Bowden, 1982) and porphyry tin deposits in Bolivia (Grant and others, 1980). Depth to this type of mineralization could be expected to be as much as 2 to 5 km, and thus may not be attractive exploration targets.

#### Tin-Bearing and Tin-Barren High-Silica Rhyolites

Christiansen and others (1986) report 26 topaz rhyolite localities in the western United States. Of those localities, only 3 contain reported tin mineralization; the Black Range of New Mexico, the Sheep Creek Range of Nevada, and the Wah Wah Mountains area in Utah. All of the rhyolites appear to have had similar evolutionary histories. The most plausible explanation is that the tin-bearing rhyolites contain less water than do the tin-barren rhyolites. Biotite is a sparse mineral in the tin-bearing rhyolites in New Mexico and Utah and relatively common in other topaz rhyolites (Christiansen and others, 1986). If the water content of the tin-barren rhyolites were high enough to stabilize biotite as a liquidus phase, tin would be incorporated into the biotites thus removing it from the melt and precluding its concentration in the aqueous phase released at  $H_2O$

saturation. Other possibilities include differences in halogen content of the tin-bearing and tin-barren rhyolites, but the sparse data that are available suggest that no such differences exist.

### Conclusions

The tin-bearing rhyolites in the Black Range and Sierra Cuchillo in New Mexico are the products of extreme differentiation of A-type granitoid parent magmas that were probably derived by partial melting of a felsic granulite parent; however, isotopic evidence suggests that the upper mantle contributed to the parent magmas. Sn and F was introduced into the magma by melting of biotite in the granulite and concentrated in the residual magma and ultimately in the aqueous phase by differentiation processes. Sr isotopic systematics indicate that the tin-bearing rhyolites can not have been contaminated to any extent by the older tin-bearing granites in the region, thus little tin could have been contributed by tin-rich, older granites. Tin was transported at temperatures greater than 650° C in the magmatic aqueous phase as Sn-Cl complexes and deposited as cassiterite and wood tin in a near surface, fumarolic environment by a combination of temperature decrease and  $f_{O_2}$  increase. Timing of the mineralizing event indicates that the magmatic fluids were derived from the host rhyolite. The tin-mineralizing event was followed by a short lived epithermal event that deposited quartz, calcite, and fluorite from meteoric water dominated fluids with a variable magmatic

water component.

Although the tin-bearing rhyolites are chemically similar to many tin-bearing granitoids as well as intrusives that host Climax-type porphyry molybdenum deposits, the possibility of greisen or porphyry tin or molybdenum ore at depth is questionable and the depth to potential targets may be 2 to 5 km. Skarn mineralization similar to the mineralization at Iron Mountain may occur at depth.

The very small size of the exposed lode tin deposits and the proposed origin for those deposits render them very unattractive exploration targets. The placer deposits have limited potential for small operations.

#### ACKNOWLEDGEMENTS

We thank Charles Chapin, Philip Kyle, Donald Richter and Kent Condie for critically reviewing this manuscript. Charles Maxwell and Wendell Duffield are thanked for many hours of stimulating discussions about these deposits. Funding for this study was provided by the New Mexico Geological Society, the Geological Society of America, FRM Minerals, the National Science Foundation (Grants EAR 8319913 and EAR 8410481 to DIN), the Rocky Mountain Federation of Mineralogical Societies, and the U.S. Department of Interior's Mineral Institutes program administered by the U.S. Bureau of Mines (Allotment grant G1164135 to DIN). The New Mexico Bureau of Mines and Mineral Resources provided a graduate assistantship to the senior author and are thanked

for the assistance. The irradiation costs were defrayed by the U.S. Department of Energy's Reactor Sharing Program. Irradiations were performed at the research reactor of the University of Missouri, Columbia.

## BIBLIOGRAPHY

- Alderton, D.H.M., Pearce, J.A., and Potts, P.J., 1980, Rare earth element mobility during granite alteration: evidence from southwest England: *Earth and Planetary Science Letters*, v. 49, p. 149-165.
- Bernard, A. and Le Guern, F., 1986, Condensation of volatile elements in high-temperature gases of Mount St. Helens: *Journal of Volcanology and Geothermal Research*, v. 25, p. 91-105.
- Bodkin, J.B., 1977, Determination of fluorine in silicates by ion-selective electrode following fusion with lithium metaborate: *Analyst*, v. 102, p. 409-413.
- Bowden, P., 1982, Magmatic evolution and mineralization in the Nigerian younger granite province: in, Evans, A.M., ed., *Metallization Associated with Acid Magmatism*, Chichester, John Wiley and Sons, Ltd., p. 51-61.
- Bowden, P., 1985, The geochemistry and mineralization of alkaline ring complexes in Africa (a review): *Journal of African Earth Sciences*, v. 3, p. 17-39.
- Burt, D.M. and Sheridan, M.F., 1986, Mineral deposits related to topaz rhyolites in the Southwest: *Arizona Geological Society Digest*, v. 16, p. 170-178.
- Burt, D.M., Sheridan, M.F., Bikum, J.V., and Christiansen, E.H., 1982, Topaz rhyolites- distribution, origin, and significance for exploration: *Economic Geology*, v. 77, p. 1818-1836.

- Carmichael, I.S.E. and Nicholls, J., 1967, Iron-titanium oxides and oxygen fugacity in volcanic rocks: *Journal of Geophysical Research*, v. 72, p. 4665-4687.
- Chapin, C.E., Jahns, R.H., Chamberlin, R.M., and Osburn, G.R., 1978, First day roadlog from Socorro to Truth or Consequences via Magdalena and Winston: in Chapin, C.E. and Elston, W.E., eds., Field guide to selected cauldrons and mining districts of the Datil-Mogollon volcanic field, New Mexico: New Mexico Geological Society Special Publication 7, p. 1-32.
- Chappell, B.W. and White, A.J.R., 1974, Two contrasting granite types: *Pacific Geology*, v. 8, p. 173-174.
- Chatterjee, A.K., Strong, D.F., and Muecke, G.K., 1983, A multivariate approach to geochemical distinction between tin-specialized and uranium-specialized granites of southern Nova Scotia: *Canadian Journal of Earth Sciences*, v. 20, p. 420-430.
- Chou, I. and Eugster, H.P., 1977, Solubility in supercritical chloride solutions: *American Journal of Science*, v. 277, p. 1296-1314.
- Christiansen, E.H., Sheridan, M.F., and Burt, D.M., 1986, The geology and geochemistry of Cenozoic topaz rhyolites from the western United States: *Geological Society of America Special Paper 205*, 82 p.

- Clayton, R.N., and Mayeda, T.K., 1963, The use of bromine penta-fluoride in the extraction of oxygen from oxides and silicates for isotopic analysis: *Geochimica et Cosmochimica Acta*, v. 27, p. 43-52.
- Clayton, R.N., O'Neil, J.R., and Mayeda, T.K., 1972, Oxygen isotope exchange between quartz and water: *Journal of Geophysical Research*, v. 77, p. 3057-3067.
- Collins, J.H., 1880, On some Cornish tin-stones and tin-capels: second paper: *The Mineralogical Magazine*, v. 4, p. 103-116.
- Collins, W.J., Beams, S.D., White, A.J.R., and Chappell, B.W., 1982, Nature and origin of A-type granite with particular reference to southeastern Australia: *Contributions to Mineralogy and Petrology*, v. 80, p. 189-200.
- Condie, K.C. and Budding, A.J., 1979, *Geology and geochemistry of Precambrian rocks, central and south-central New Mexico: New Mexico Bureau of Mines and Mineral Resources Memoir 35*, 58p.
- Correa, B.P., 1981, *The Taylor Creek Rhyolite and associated tin deposits, southwestern New Mexico: M.S. Thesis, Arizona State University, Tempe*, 105 p.
- Criss, R.E. and Taylor, H.P., Jr., 1983, An  $^{18}\text{O}/^{16}\text{O}$  and D/H study of the Tertiary hydrothermal systems in the southern half of the Idaho Batholith: *Geological Society of America Bulletin*, v. 94, p. 640-663.



- Daubree, A., 1879, Etudes synthetique de geologie experimentale: Dunod, Editeur, Paris, 828 p.
- Desborough G.A. and Mihalik, P., 1980, Accessory minerals in the igneous host of molybdenum ore, Henderson Mine, Colorado: U.S. Geological Survey Open File Report 80-661, 16 p.
- Desborough, G.A., Ludington, S.D., and Sharp, W.N., 1980, Redskin Granite: a rare-metal-rich Precambrian pluton, Colorado, USA: Mineralogical Magazine, v. 43, p. 959-966.
- Dobson, D.C., 1982, Geology and alteration of the Lost River tin-tungsten-fluorine deposit, Alaska: Economic Geology, v. 77, p. 1033-1052.
- Du Bray, E.A., 1985, Geology of the Silsilah ring complex and associated tin mineralization, Kingdom of Saudi Arabia—a synopsis: American Mineralogist, v. 70, p. 1075-1086.
- Duffield, W.A., Ludington, S.D., Maxwell, C.H., Reed, B.L., and Richter, D.H., 1984, Tin mineralization in rhyolite lavas, Sierra Madre Occidental, Mexico: Geological Society of America Abstracts with programs, v. 16, p. 495.
- Eggleston, T.L. and Norman, D.I., 1987, Geology of the Taylor Creek District, Black Range, New Mexico: New Mexico Bureau of Mines and Mineral Resources Bulletin, in prep.



- Eggleston, T.L., Norman, D.I., and Savin, S.M., 1987a,  
Intense vapor phase crystallization: mineralogical and  
chemical effects in high-silica rhyolite lavas: in prep.
- Eggleston, T.L., Norman, D.I., and Savin, S. M., 1987b,  
Petrology of the high-silica Taylor Creek Rhyolite and  
associated rocks, Black Range, New Mexico: in prep.
- Eugster, H.P., 1986, Minerals in hot water: American  
Mineralogist, v. 71, p. 655-673.
- Eugster, H.P. and Wilson, G.A., 1985, Transport and  
deposition of ore-forming elements in hydrothermal  
systems associated with granites: in Halls, C., ed.,  
High heat production granites, hydrothermal circulation  
and ore genesis: Institute of Mining and Metallurgy,  
London, p. 87-98.
- Ferguson, H.G. and Bateman, A.M., 1912, Geological features  
of tin deposits: Economic Geology, v. 7, p. 209-262.
- Foord, E.E., Oakman, M.R., and Maxwell, C.H., 1985, Durangite  
from the Black Range, New Mexico and new data on  
durangite from Durango and Cornwall: Canadian  
Mineralogist, v. 23, p. 241-246.
- Fries, C., 1940, Tin deposits of the Black Range, Catron and  
Sierra Counties, New Mexico: U.S. Geological Survey  
Bulletin 922-M, p. 355-370.
- Gerlach, T.M. and Casadevall, T.J., 1986, Fumarole emissions  
at Mount St. Helens Volcano: June 1980 to October 1981:  
degassing of a magma-hydrothermal system: Journal of  
Volcanology and Geothermal Research, v, 28, p. 141-160.

- Goerold, W.T., 1981, Geology and geochemistry of tin occurrences in southwestern New Mexico: M.S. Thesis, The Pennsylvania State University, 120 p.
- Grant, J.N., Halls, C., Sheppard, M.R., and Avila, W., 1980, Evolution of the porphyry tin deposits of Bolivia: Mining Geology Special Issue No. 8, p. 151-173.
- Haas, J.L., Jr., 1971, The effect of salinity on the maximum thermal gradient of a hydrothermal system at hydrostatic pressure: *Economic Geology*, v. 66, p. 940-946.
- Haggerty, S.E., 1976, Opaque mineral oxides in terrestrial igneous rocks: in, Rumble, D., III, ed. *Oxide Minerals: Mineralogical Society of America Reviews in Mineralogy*, v. 3, p. Hg101-Hg300.
- Hanks, H.G., 1876, On the occurrence of durangite in the tin-bearing region of Durango, Mexico: *American Journal of Science*, 3rd series, v. 12, p. 274-276.
- Harbour, R.L., 1972, Geology of the northern Franklin Mountain, Texas and New Mexico: U.S. Geological Survey Bulletin 1298, 129 p.
- Harris, N.B.W., 1985, Alkaline complexes from the Arabian Shield: *Journal of African Earth Sciences*, v. 3, p. 83-88.
- Harrison, R.W., 1986, General geology of Chloride Mining District, Sierra and Catron Counties, New Mexico: New Mexico Geological Society Guidebook 37, p. 265-272.

- Harvey, D.B., 1985, Cassiterite mineralization in the Black Range tin district, Sierra and Catron Counties, New Mexico: M.S. Thesis, The University of Texas at El Paso, El Paso, 147 p.
- Heyl, A.V., Maxwell, C.H., and Davis, L.L., 1983, Geology and mineral deposits of the Priest Tank quadrangle, Sierra County, New Mexico: U.S. Geological Survey Miscellaneous Field Studies Map MF-1665.
- Higgins, H.C., Solomon, M., and Varne, R., 1985, The genesis of the Blue Tier Batholith, northeastern Tasmania, Australia: *Lithos*, v. 18, p. 129-149.
- Holloway, J.R., 1981, Compositions and volumes of supercritical fluids in the earth's crust: Mineralogical Association of Canada Short Course Handbook, v. 6., p. 13-38.
- Hudson, T. and Arth, J.G., 1983, Tin granites of the Seward Peninsula, Alaska: Geological Society of America Bulletin, v. 94, p. 768-790.
- Huspeni, J.R., Kesler, S.E., Ruiz, J., Tuta, Z.H., Sutter, J.F., and Jones, L.M., 1982, Petrology and geochemistry of rhyolites associated with tin mineralization in northern Mexico: *Economic Geology*, v. 79, p. 87-105.
- Hutchison, C.S. and Chakraborty, K.R., 1979, Tin: a mantle or crustal source?: Bulletin of the Geological Society of Malaysia, No. 11, p. 71-80.

- Ingalls, W.R., 1896, The tin deposits of Durango Mexico: American Institute of Mining Engineers Transactions, v. 25, p. 146-163.
- Ishihara, S., Sawata, H., Shibata, K., Terashima, S., Arrykul, S., and Sato, K, 1980, Granites and Sn-W deposits of peninsular Thailand: Mining Geology Special Issue 8, p. 223-241.
- Jackson, N.J., 1979, Geology of the Cornubian tin field "a review": Geological Society of Malaysia, Bulletin 11, p. 209-237.
- Jacobs, J.W., Korotev, R.L., Blanchard, D.P., and Haskin, L.A., 1977, A well-tested procedure for instrumental neutron activation analysis of silicate rocks and minerals: Journal of Radioanalytical Chemistry, v. 40, p. 93-114.
- Jahns, R.H., 1944, Beryllium and Tungsten deposits of the Iron Mountain district, Sierra and Socorro Counties, New Mexico: U.S. Geological Survey Bulletin 945C, p. 45-79.
- Jones, W.R., 1925, Tin fields of the World: London, Mining Publications Ltd., 423 p.
- Kinnaird, J.A., Bowden, P., Ixer, R.A., and Olding, N.W.A., 1985, Mineralogy, geochemistry, and mineralization of the Riwiwai complex, northern Nigeria: Journal of African Earth Sciences, v. 3., p. 185-222.
- Krauskopf, K.B., 1957, The heavy metal content of magmatic vapor at 600<sup>o</sup> C: Economic Geology, v. 52, p. 786-807.

- Krauskopf, K.B., 1964, The possible role of volatile metal compounds in ore genesis: *Economic Geology*, v. 59, p.22-45.
- Lawrence, V.A., 1985, A study of the Indian Peaks tin-bearing rhyolite flow-dome complex, northern Black Range, New Mexico (M. S. Thesis): Boulder, The University of Colorado, 112 p.
- Lawrence, V.A. and Richter, D.H., 1986, Geologic map of the Indian Peaks West quadrangle, Catron County, New Mexico: U. S. Geological Survey Miscellaneous Field Studies Map MF-1849.
- Le Guern, F., Gerlach, T.M., and Nohl, A., 1982, Field gas chromatography analyses of gases from a glowing dome at Merapi volcano, Java, Indonesia, 1977, 1978, 1979: *Journal of Volcanology and Geothermal Research*, v. 14, P. 223-245.
- Lehmann, B., 1982, Metallogeny of tin, magmatic differentiation versus geochemical heritage: *Economic Geology*, v. 77, p. 50-59.
- Loiselle, M.G. and Wones, D.R., 1979, Characteristics and origins of anorogenic granite: *Geological Society of America Abstracts with Programs*, v. 11, p. 468.
- London, D., 1986, Magmatic-hydrothermal transition in the Tanco rare-element pegmatite: evidence from fluid inclusions and phase-equilibrium experiments: *American Mineralogist*, v. 71, p. 376-395.

- Lufkin, J.L., 1972, Tin mineralization within rhyolite flow-domes, Black Range, New Mexico: Ph.D. Dissertation, Stanford University, Stanford, 149 p. and New Mexico Bureau of Mines and Mineral Resources Open-File Report 57.
- Lufkin, J.L., 1976, Oxide minerals in miarolitic rhyolite, Black Range, New Mexico: *American Mineralogist*, v. 61, p. 425-430.
- Lufkin, J.L., 1977, Chemistry and mineralogy of wood-tin, Black Range, New Mexico: *American Mineralogist*, v. 62, p. 100-106.
- Matsuo, S., Oosaka, J., Hirabayashi, J., Ozawa, T., and Kimishima, K., 1982, Chemical nature of volcanic gases of Usu Volcano in Japan: *Bulletin Volcanologique*, v. 45, p. 261-264.
- Maxwell, C.H., Foord, E.E., Oakman, M.R., and Harvey, D.B., 1986, Tin deposits in the Black Range Tin District: *New Mexico Geological Society Guidebook 37*, p. 273-281.
- McIntosh, W.C., Sutter, J.L., Chapin, C.E., and Osburn, G.R., 1986, A stratigraphic framework for the eastern Mogollon-Datil volcanic field based on paleomagnetism and high-precision  $^{40}\text{Ar}/^{39}\text{Ar}$  dating of ignimbrites--a progress report: *New Mexico Geological Society Guidebook 37*, 183-195.

- Mitchell, A.G.H., 1979, Geosynclinal and plate-tectonic hypotheses: significance of late-orogenic Himalayan tin granites and continental collision: in, M.J., ed., Proceedings of the Eleventh Commonwealth Mining and Metallurgical Congress, Hong Kong, 1978: Institute of Mining and Metallurgy, London, p. 79-91.
- Mutschler, F.E., Wright, E.G., Luddington, S., and Abbott, J.T., 1981, Granite molybdenite systems: Economic Geology, v. 76, p. 874-897.
- Mysen, B.O. and Virgo, D., 1985, Structure and properties of fluorine-bearing aluminosilicate melts: the system  $\text{Na}_2\text{O}-\text{Al}_2\text{O}_3-\text{SiO}_2-\text{F}$  at 1 atm: Contributions to Mineralogy and Petrology, v. 91, p. 205-220.
- Naumov, V.B., Kovalenko, V.I., Ivanova, G.F., and Vladykin, N.V., 1977, Genesis of topaz according to the data on microinclusions: Geochemistry International, v. 14, No. 2, p. 1-8.
- Nguene, F.R., 1982, Geology and geochemistry of the Mayo-Darle tin deposit, west-central Cameroon, Central Africa: Ph.D. Dissertation, New Mexico Institute of Mining and Technology, Socorro, 189 p.
- Norman, D.I. and Sawkins, F.J., 1987, Analysis of volatile fluid inclusions by mass spectrometry: Chemical Geology, v. 61 (in press).



- Norman, D.I., Condie, K.C., Smith, R.W., and Thoman, W.F., 1987, Geochemical and Sr and Nd isotopic constraints on the origin of late Proterozoic volcanics and associated tin-bearing granites from the Franklin Mountain, West Texas: *Canadian Journal of Earth Science*.
- Norrish, K. and Chappell, B.W., 1977, X-ray fluorescence spectrometry: in, Zussman, J., ed., *Physical methods in determinative mineralogy*: Academic Press, p. 210-272.
- Norrish, K. and Hutton, J.T., 1969, An accurate x-ray spectrographic method for the analysis of a wide range of geologic samples: *Geochimica et Cosmochimica Acta*, v. 33, p. 431-453.
- Oscarsson, N., 1981, The geochemistry of Icelandic lava incrustations and the latest stages of degassing: *Journal of Volcanology and Geothermal Research*, v. 10, p. 93-111.
- Padovani, E.R. and Carter, J.L., 1977, Aspects of the deep crustal evolution beneath south central New Mexico: in Heacock, J.G., ed. *The Earth's Crust*: American Geophysical Union Monograph 20, p. 19-55.
- Pan, Y.-S., 1974, The genesis of the Mexican type tin deposits in acidic volcanics: Ph.D. dissertation, Columbia University, New York, 286 p.
- Potter, R.W., II, Clynne, M.A., and Brown, D.L., 1978, Freezing point depression of aqueous sodium chloride solutions: *Economic Geology*, v. 73, p. 284-285.



- Price, R.C., 1983, Geochemistry of peraluminous granitoid suite from northeastern Victoria, southeastern Australia: *Geochimica et Cosmochimica Acta*, v. 47, p. 31-42.
- Ratte', J.C., Marvin, R.F., and Naeser, C.W., 1984, Calderas and ash-flow tuffs of the Mogollon Mountains, southwestern New Mexico: *Journal of Geophysical Research*, v. 89, p. 8713-8732.
- Richter, D.H., 1978, Geologic map of the Spring Canyon quadrangle, Catron County, New Mexico: U.S. Geological Survey Miscellaneous Field Studies Map, MF-966.
- Richter, D.H., Eggleston, T.L., and Duffield, W.A., 1986, Geologic map of the Wall Lake Quadrangle, Catron County, New Mexico: U. S. Geological Survey Miscellaneous Field Studies Map, MF-1909.
- Richter, D. H., Lawrence, V. A., and Duffield, W. A., 1986, Geologic map of the Indian Peaks East quadrangle, Catron County, New Mexico: U.S. Geological Survey Miscellaneous Field Studies Map, MF-1850.
- Robertson, D.E., 1985, Skarn mineralization at Iron Mountain, New Mexico: M.S. Thesis, The Arizona State University, Tempe.
- Robie, R.A., Hemingway, B.S., and Fisher J.R., 1979, Thermodynamic properties of minerals and related substances at 298.15 K and 1 bar ( $10^5$  pascals) pressure and at higher temperatures: U.S. Geological Survey Bulletin 1452, 465 p.

- Roedder, E., 1984, Fluid inclusions: Mineralogical Society of America, *Reviews in Mineralogy*, v. 12, 644 p.
- Routhier, P., 1976, A new approach to metallogenic provinces: the example of Europe: *Economic Geology*, v. 71, p. 803-811.
- Rye, R.O., Lufkin, J.L., and Wasserman, M.D., 1984, Genesis of tin occurrences in the Black Range, New Mexico, as indicated by oxygen isotope studies: *Geological Society of America Abstracts with Programs*, v. 16, p. 642.
- Sainsbury, C.L. and Hamilton, J.C., 1967, The geology of lode tin deposits: in Fox, W., ed. A second technical conference on tin: International Tin Council, London, p. 179-192.
- Scrivenor, J.B., 1909, The origin of tin deposits: Perak Chamber of Mines, Kuala Lumpur.
- Seager, W.R., Shafiqullah, M., Hawley, J.W., and Marvin, R.F., 1984, New K-Ar dates from basalts and the evolution of the southern Rio Grande Rift: *Geological Society of America Bulletin*, v. 95, p. 87-99.
- Singh, D.S. and Bean, J., H., 1967, Some general aspects of tin minerals in Malaysia: A second technical conference on tin: International Tin Council, London, p. 457-478.
- Smith, C.W.E.H. and Hosking, K.F.G., 1974, Wood tin from peninsular Malaysia: *Geological Society of Malaysia Newsletter*, No. 46, p. 1-7.
- Stoiber, R.E. and Rose, W.I., Jr., 1974, Fumarole incrustations at active Central American volcanoes: *Geochimica et Cosmochimica Acta*, v. 38, p. 495-516.

- Symonds, R.B., Rose, W.I., and Lichte, F.E., 1984, Transport and enrichment of elements in high temperature gases at Merapi Volcano, Indonesia: EOS, v. 65, p. 1133.
- Taylor, S.R. and McLennan, S.C., 1985, The continental crust: its composition and evolution: Blackwell Scientific Publications, Oxford, 312p.
- Turekian, K.K. and Wedepohl, K.H., 1961, Distribution of the elements in some major units of the earth's Crust: Geological Society of America Bulletin, v. 72, p. 175-192.
- Turneure, F.S., 1977, The Bolivian tin-silver province: Economic Geology, v. 66, p. 215-225.
- Vakin, E.A. and Kuttyev, F. Sh., 1982, Results of analyses of gas microinclusions in the minerals of abyssal xenoliths and composition of magmatic gases: Bulletin Volcanologique, v. 45, p. 273-276.
- Vogt, J.H.L., 1894, Uber die durch pneumatolytisch processe an granite gebundenen mineral- Neubildungen: Seitschrift fur Praktische Geology, December, 1894.
- von Richtohofen, Baron, 1869, Uber das alter der goldfuhrender gange und der von ihnen durchsetzten gesteine: Zeitschr. der d. Geol. Gesellschaft, v. 21, p. 723.
- Wilson, G.A. and Eugster, H.P., 1984, Cassiterite solubility and metal-chloride speciation in supercritical solutions: Geological Society of America Abstracts With Programs, v. 16, p. 696.

Ympma, P.S.M. and Simons, J.H., 1970, Genetical aspects of the tin mineralization in Durango, Mexico: in, Fox, W., ed., A second technical conference on tin: International Tin Council, London, p. 179-192.

Zies, E.G., 1929, The Valley of 10,000 Smokes, the fumarolic incrustations and their bearing on ore deposition: National Geographic Society Technical Paper, v. 1, No. 4, p. 61-79.

Table 1. Selected analyses of Sn-bearing rhyolites and granitoids.

UNIT*	Tdp	Ttc	Twd	IRON	CORN	AUSSIE	SAUDI	MEXICO
SiO <sub>2</sub>	76.41	74.54	76.66	77.87	70.92	77.00	75.00	77.00
TiO <sub>2</sub>	0.18	0.09	0.16	0.07	0.18	0.15	0.03	0.07
Al <sub>2</sub> O <sub>3</sub>	12.09	12.05	12.12	11.98	15.36	11.83	13.20	13.00
Fe <sub>2</sub> O <sub>3</sub>	1.65	1.13	1.21	0.68	1.82	1.57	0.73	1.10
MnO	0.03	0.06	0.06	0.03	0.04	0.04	0.02	0.02
MgO	0.16	0.13	0.48	0.03	0.44	0.04	0.05	0.24
CaO	0.23	0.40	0.47	0.38	0.88	0.61	0.38	0.37
Na <sub>2</sub> O	3.64	3.74	2.79	4.15	2.83	3.06	4.50	2.87
K <sub>2</sub> O	5.27	4.69	5.00	4.53	5.72	4.98	4.51	5.33
P <sub>2</sub> O <sub>5</sub>	0.02	0.01	0.02	0.02	0.23	0.02	0.02	0.00
LOI	0.58	2.36	0.95	--	0.77	0.54	0.48	--
Total	100.26	99.20	99.92	99.74	99.19	99.84	98.92	100.00
F(%)	--	0.2	0.06	0.04	--	--	0.31	0.31
Rb	223	360	232	404	212	230	669	548
Sr	4	2	18	8	96	50	20	5
Ba	16	19	87	44	--	655	15	--
Ga	19	22	19	28	--	20	--	--
Zr	256	168	180	134	63	187	116	90
Nb	32	47	33	82	--	18	50	--
Th	25	41	28	--	21	22	33	46
U	6	14	8	--	--	5	12	10.8
Sc	4.8	2.4	3.1	--	4	12.2	--	9.5
La	122	40	52	43	39	59	18	13
Ce	213	98	117	--	72	132	58	109
Nd	115	37	71	--	32.9	66	30	--
Sm	21.9	11.6	10.5	11	6.9	16.4	11.0	4.51
Eu	0.96	0.17	0.47	0.7	0.75	1.61	0.13	0.09
Tb	3.4	2.3	1.8	--	0.6	--	2.4	2.76
Yb	10.0	13.8	9.0	9	1.22	10.6	16.0	7.73
Lu	1.49	1.94	1.01	--	--	1.57	2.33	1.07

\* Tdp-rhyolite of Dolan Peak (this study); Ttc-Taylor Creek Rhyolite (this study); Twd (rhyolite of Willow Springs Draw (this study); Iron-granite of Iron Mountain (this study, rare earth elements from Robertson, 1986); Corn-Cornish tin granite (Alderton and others, 1980); Aussie-Australian A-type granite (Collins and others, 1982); Saudi-Saudi Arabian tin granite (Du Bray, 1985); Mexico-Mexican tin-bearing rhyolite (Huspeni and others, 1984). Analytical methods (this study): Major elements and Y, Rb, Sr, Y, Ga, Zn, Zr, Nb, Th, and U by XRF. REE and Sc by INAA. F by ion-specific electrode.

Table 2. Representative analyses of the tin mineralization.

Type	hem	cass1	cass2	w-tin	ore1	ore2	ore3
SAMPLE #	270	271	272	273	274	33	161
Fe <sub>2</sub> O <sub>3</sub>	85.50	0.70	2.50	4.78	21.46	4.42	6.49
Na <sub>2</sub> O	0.02	0.04	0.19	0.23	0.22	2.11	3.23
As	5.7	<0.1	37	2581	111	---	---
Ba	<50	480	<200	<100	<90	45	79
Br	<0.5	<0.5	<5	6.8	1.8	---	---
Co	17	<0.1	0.7	0.8	3.2	---	---
Cr	5	22	26	21	12	<10	10
Cs	0.5	2.3	7.2	69	41	---	---
Hf	4.7	0.5	0.8	0.2	0.9	---	---
Mo	---	---	---	---	---	3	---
Nb	---	---	---	---	---	73	103
Ni	<120	<0.5	<140	<100	<160	<5	5
Pb	---	---	---	---	---	860	1212
Rb	<30	<15	24	29	35	617	293
Sb	15.5	1830	2880	1262	836	---	---
Sc	74.2	0.9	1.1	0.9	2.3	---	---
Se	<3	<10	<9	<10	<7	---	---
Sn	---	---	---	---	---	9859	4531
Sr	---	---	---	---	---	174	65
Ta	22.3	0.9	<0.5	<0.3	0.8	---	---
Th	2	3	4	8	17	23	20
U	2	90	20	5	9	<3	<3
W	8	400	410	6	51	---	---
La	2	5	7	8	17	---	---
Ce	5	25	8	20	48	---	---
Nd	<20	27	<1	<20	30	---	---
Sm	0.7	<1.0	<0.3	1.5	6.2	---	---
Eu	0.06	<0.1	<0.5	0.16	0.26	---	---
Tb	0.1	<0.2	<0.3	0.3	1.4	---	---
Yb	2.9	4.0	3.4	2.1	5.9	---	---
Lu	0.37	0.35	0.16	0.18	0.8	---	---

Sample descriptions and locations: hem--hand picked hematite in panned concentrates from Boiler Peak; cass1--hand picked, translucent red cassiterite from Boiler Peak panned concentrates; cass2--hand picked, translucent red cassiterite in panned concentrate from Grogan Canyon; w-tin--wood tin from Nugget Gulch; ore1--hematite-cassiterite veinlet from Squaw Creek; ore2--hand sample with crosscutting hematite-cassiterite veinlet from Squaw Creek; ore3--vein wallrock with disseminated cassiterite and hematite from Taylor Creek. Samples analyzed by instrumental neutron activation analysis and XRF. Mo, Nb, Pb, Sn, and Sr by XRF, all others by INAA.

Table 3. Summary of fluid inclusion types defined in this study.

	Host <sup>1</sup>	Type <sup>2</sup>	Remarks
Type 1	C,T,Q	P,Ps,S	Vapor inclusions with little aqueous fluid. Coexist with Type 2 inclusions. No observable phase changes between -180 and +600° C.
Type 2	C,T,Q	P,Ps,S	Multisolid-vapor inclusions with rare aqueous fluid. Consists of a crystalline solid with as many as 4 daughter minerals. Crystalline solid melts at about 350° C to form liquid-vapor-multisolid inclusion. Th= 650 to 730° C.
Type 3	C,T,Q	S(?)	Liquid-vapor inclusions with variable liquid/vapor ratios. These inclusions are rare. Th= 400 to 600° C.
Type 4	Q,Cc	P,Ps	Vapor dominated liquid-vapor inclusions. Coexist with Type 5 inclusions. Th= 292-390° C.
Type 5	Q,Cc	P,Ps	Low salinity, liquid dominated liquid-vapor inclusions. Th= 135-384° C.
Type 6	Q,S	P	Magmatic inclusions in quartz and sanidine phenocrysts.

<sup>1</sup> Host minerals: C-cassiterite; T-topaz; Q-quartz; Cc-calcite  
S-sanidine

<sup>2</sup> P-primary; Ps-pseudosecondary; S-secondary



Table 4. Summary of microthermometric studies of Type 2 inclusions. Temperatures in degrees C.

Sample (1)	Host (2)	Type (3)	Tmc (4)	Th (5)	Ts1 (6)	Ts2 (7)	Decl (8)	Dec2 (9)
Lqtz1	lqtz	PS-S	364	>600	--	--	--	--
		PS-S	360	>600	--	--	--	--
Topaz1	topaz	P	350	>600	500	>600	425	--
		P	352	>600	--	--	--	--
		P	--	>600	--	--	453	--
		P	353	>600	--	--	--	--
		P	350	680	--	--	--	--
		P	360	>600	555	--	--	--
		-	--	--	--	--	460	650
Topaz2	topaz	PS-S	325	>600	--	--	--	--
Consl	cass	P	350	>603	--	--	--	--
		P	350	>603	--	--	--	--
		PS-S	370	>607	--	--	--	--
		P	355	>607	--	--	--	--
Cons3	cass	--	--	--	--	--	400	--
		P	385	660	--	--	--	--
		PS	353	>600	--	--	--	--
		S-PS	353	660	--	--	--	--
		P	370	650	--	--	--	--
		P	380	>602	--	--	--	--
		P	360	650	--	--	--	--
Lqtz2	qtz	P-PS	350	>600	--	--	--	--
Qtz1	qtz	PS-S	377	>600	--	--	--	--
		PS-S	383	>600	--	--	--	--
		S-PS	365	>600	--	--	--	--
		S-PS	385	>670	670	--	--	--
		S-PS	394	>600	--	--	--	--
119	qtz	PS-S	377	>600	--	--	--	--
		PS-S	357	>600	--	--	--	--
		PS-S	367	>600	--	--	--	--
		PS-S	376	>600	--	--	--	--
		PS-S	360	>600	--	--	--	--
Juniper	cass	P	365	655	600	--	--	--
		P	350	>525	--	--	--	--

1) sample locations: Lqtz1-Scales Canyon; Lqtz2-Paramount Canyon; Topaz1-Round Mountain; Topaz2-panned concentrate, Boiler Peak; Consl-panned concentrate, Dawson Mine; Cons3-panned concentrate, Miners Tank; Qtz1-Scales Canyon; Juniper-Juniper Claims, Indian Peaks

2) lqtz-lithophysal quartz; cass-cassiterite; qtz-quartz;

3) Type of inclusion: P-primary; PS-pseudosecondary; S-secondary

4) Melting temperature of solid inclusions

5) Homogenization temperature (to liquid in all cases)

6) Temperature first salt dissolved

7) Temperature second salt dissolved

8) First decrepitation

9) Second decrepitation



Table 5. Summary of microthermometric studies of Type 3, 4, and 5 fluid inclusions.

Sample (1)	Host (2)	Type (3)	Tm (4)	eq wt. % NaCl(5)	Th (6)	Hom. (7)	Decl (8)	Dec2 (9)
Cons2	cass.	3S	--	--	450	L	--	--
		4	--	--	--	--	400	--
Qtz1	qtz	4P	-1.2	2.06	344	L	--	--
		4S	-0.2	0.35	327	L	--	--
		4S	--	--	319	L	--	--
		4S	--	--	212	L	--	--
		4P	-0.4	0.70	378	L	--	--
		4S	--	--	216	L	--	--
		5S	--	--	303	V	--	--
		4S	--	--	180	L	--	--
		4S	--	--	217	L	--	--
		4S	--	--	164	L	--	--
157	qtz	4	--	--	--	--	420	--
		4P	--	--	258	L	--	--
		4P	--	--	234	L	378	--
		4P	--	--	379	L	--	--
		4P	--	--	350	L	380	--
		4P	--	--	364	L	--	--
158	fluor	4	--	--	--	--	390	480
114	cc	4S-PS	--	--	269	L	--	--
MC-1	cc	4S-PS	--	--	335	L	--	--
		5P	--	--	386	V	--	--
		5P	--	--	390	V	--	--
		4P	--	--	225	L	--	--
		4P	-0.3	0.53	208	L	--	--
		4P	-0.2	0.35	215	L	--	--
		4P	--	--	205	L	--	--
		4P	-0.1	0.18	196	L	--	--
		4P	--	--	303	L	--	--
MC-2	cc	5P	--	--	292	V	--	--
		4P	-1.4	2.40	254	L	--	--
		4P	-0.4	0.70	152	L	--	--
		4P	--	--	221	L	--	--
		4P	>-5	<8	267	L	--	--
		4S	--	--	130	L	--	--
		4P	--	--	208	L	--	--
		4S	0.0	0.0	135	L	--	--
		4S	--	--	174	L	--	--
		4P	--	--	168	L	--	--
		4S	--	--	165	L	--	--
		4P	--	--	247	L	--	--
252	cc	4P	--	--	215	L	--	--
		4P	--	--	384	L	300	--
		4P	--	--	330	L	345	--
Lqtz1	qtz	4P	--	--	332	L	--	--
5	z-c	3S	--	--	512	L	--	--
		4	--	--	--	--	250	350

Table 5 cont.

- 1) Sample locations: Cons3-panned concentrate, Miners Tank; Qtzl-Scales Canyon; MC-1-Monticello Cutoff; MC-2-Monticello Cutoff; Lqtzl-Scales Canyon; 5-Dawson Mine; 114-Monticello Cutoff; 157-Dawson Mine; 158-Dawson Mine; 252-Dawson Mine
- 2) cass-cassiterite; qtz-quartz; cc-calcite; fluor-fluorite; z-c-zeolite and cristobalite mix
- 3) Inclusion type: Type 3, 4, or 5 inclusions; P-primary; PS-pseudosecondary; S-secondary
- 4) Tm-temperature of final melt of ice in frozen inclusion
- 5) Calculated with the equations of Potter and others (1978)
- 6) Th-homogenization temperature
- 7) Type of homogenization: L-to liquid; V-to vapor
- 8) First decrepitation
- 9) Second decrepitation

Table 6. Fluid inclusion gas analyses including water (in mol %).

SAMPLE	1	2	3	4	5	6	7
He	0.0027	0.0005	0.0027	0.0002	0.0008	0.0205	0.0005
H <sub>2</sub>	0.6642	0.0010	0.0614	0.0002	0.0011	3.8765	0.0469
N <sub>2</sub>	0.3516	0.2872	3.0161	0.0436	---	2.4037	0.9109
Ar	0.0022	0.0011	0.0006	0.0002	0.0004	---	0.0005
O <sub>2</sub>	0.0993	---	---	---	---	---	---
NO	---	---	---	0.0059	0.5314	---	---
SO <sub>2</sub>	0.0036	0.0384	0.1980	---	0.1149	0.1400	0.0041
H <sub>2</sub> S	0.0051	---	0.0026	---	0.0002	0.0206	0.0085
CH <sub>4</sub>	0.0819	0.1031	---	0.0542	0.1252	2.9751	0.2566
C <sub>2</sub> H <sub>6</sub>	0.3580	0.1555	0.0731	0.0436	---	4.1151	0.8429
CO	---	0.0372	0.4643	---	---	0.8427	0.1896
CO <sub>2</sub>	0.6576	10.6298	17.9907	9.0562	7.4404	8.7477	5.2911
H <sub>2</sub> O *	97.5747	88.7463	78.1905	90.8159	91.7856	76.8580	92.4452
Temp	500	500	800	500	800	800	500

SAMPLE	8	9	10	11	12	13
He	0.0039	0.0005	0.0023	0.0008	0.0077	0.0083
H <sub>2</sub>	0.3622	0.0823	0.2027	0.1323	0.2224	0.0019
N <sub>2</sub>	0.0154	0.7006	2.3312	0.3324	17.4842	0.3822
Ar	0.0004	0.0020	0.0010	0.0017	---	0.0004
O <sub>2</sub>	---	---	---	---	---	---
NO	---	---	---	---	---	0.2422
SO <sub>2</sub>	---	0.0327	0.0716	0.0013	---	0.3864
H <sub>2</sub> S	0.0200	0.0044	0.0241	0.0006	0.0311	---
CH <sub>4</sub>	---	---	---	0.7542	---	0.1403
C <sub>2</sub> H <sub>6</sub>	3.6580	0.6177	3.8997	0.0637	3.6071	0.2488
CO	0.7335	0.1747	0.4925	0.0335	0.6425	0.0110
CO <sub>2</sub>	13.3044	2.6174	9.7909	0.1852	31.7568	65.2458
H <sub>2</sub> O *	76.9022	95.7676	83.1841	98.4844	46.2480	32.7685
Temp	500	500	500	500	800	800

SAMPLE DESCRIPTIONS (with sample numbers in parens) 1--Massive fluorite, Nugget Gulch; 2--Wood tin, Nugget Gulch 3--Wood tin, Nugget Gulch; 4--Wood tin, Texas Prospect 5--Wood tin, Texas Prospect; 6--Topaz, Round Mountain 7--Calcite, Monticello Cutoff (#114); 8--Calcite, Dawson Mine (#157); 9--Calcite, Monticello Cutoff; 10--Quartz/calcite, Monticello Cutoff; 11--Massive silica (#138), Nugget Gulch; 12--Cassiterite, Boiler Peak, hand picked separate; 13--Wood tin, Boiler Peak, Hand picked separate \* decrepitation temperature in °C.

Leaders indicate values below detection.

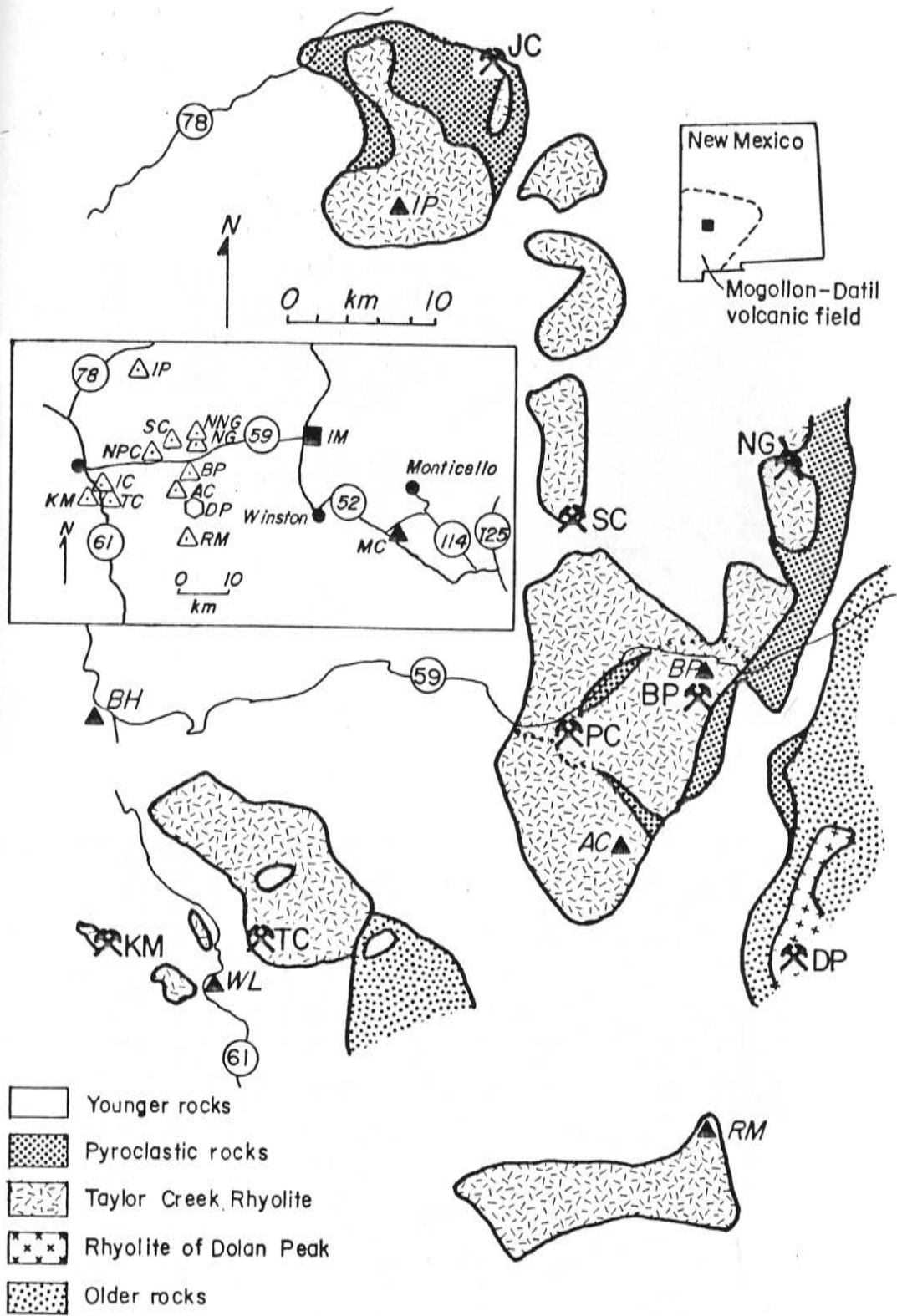
Table 7. Oxygen isotope analyses of whole rock and mineral separate samples from the Taylor Creek Tin District.

LOCATION	SAMPLE#	$\delta^{18}\text{O}\#$	REMARKS
Monticello Cutoff	115	9.9	mild VPC *
	116	7.6	very mild VPC
	122	9.3	intense VPC
Nugget Gulch	136	7.3	mild VPC
	138	19.4	silica replaced rhyolite
	140	7.6	intense VPC
	141	7.3	intense VPC
	146	17.2	silicified selvage on Sn vein
Paramount Canyon	131	6.1	lithophysal rhyolite
		7.5	drusey quartz from 131
	149	8.8	hydrated rhyolite vitrophyre
	152	7.5	quartz phenocrysts from 149 intense VPC
Taylor Creek	1	8.0	mild VPC
	157	5.8	vein quartz
	158	7.6	intense VPC
		11.0	vein quartz from 158
		10.6	clays from vein in 158
	163	8.7	vein quartz
Kemp Mesa	165	8.0	intense VPC
	167	9.0	mild VPC
		7.8	quartz phenocrysts in 167
	168	8.4	intense VPC

#- in permil SMOW

\*- VPC= vapor phase crystallization; these samples are all whole rock rhyolite.

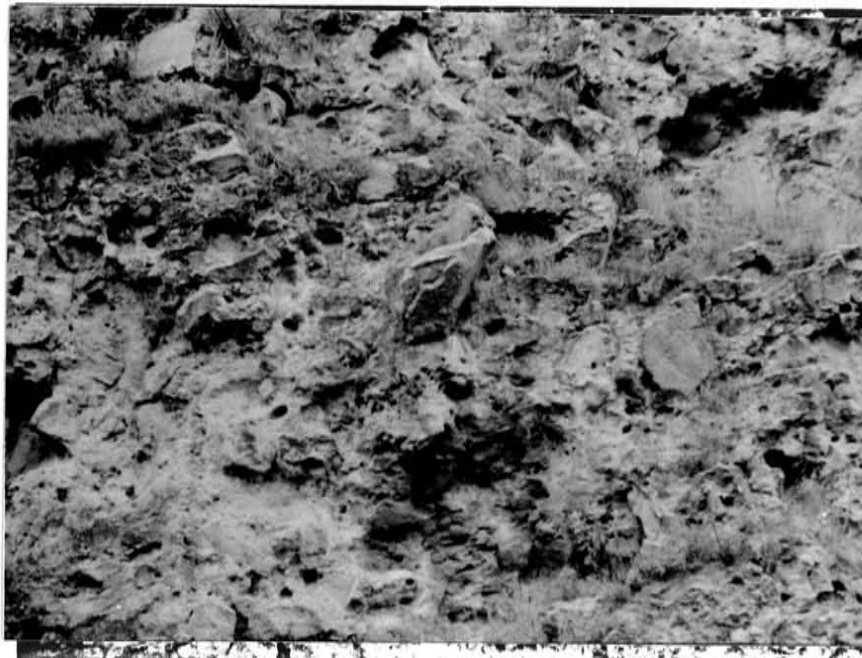
Figure 1. Generalized geologic map of the Taylor Creek District, New Mexico. Tin occurrences (pick and shovel): JC-Juniper Claims; SC-Squaw Creek; NG-Nugget Gulch; BP-Boiler Peak; PC-Paramount Canyon; KM-Kemp Mesa; TC-Taylor Creek. Geography (closed triangles): IP-Indian Peaks; BP-Boiler Peak; AC-Alexander Cienega; WL-Wall Lake; RM-Round Mountain. Inset: Taylor Creek Rhyolite domes: IP-Indian Peaks, NNG-North Nugget Gulch, NG-Nugget Gulch, SC-Squaw Creek, NPC-North Paramount Canyon, BP-Boiler Peak; IC-Indian Creek; TC-Taylor Creek; KM-Kemp Mesa, AC-Alexander Cienega; RM-Round Mountain. DP-rhyolite of Dolan Peak. IM-granite of Iron Mountain. MC-rhyolite of Willow Springs Draw at Monticello Cutoff.



- Younger rocks
- Pyroclastic rocks
- Taylor Creek Rhyolite
- Rhyolite of Dolan Peak
- Older rocks



a



b

Figure 2. Typical exposures of the Taylor Creek Rhyolite.  
a) Flow Banded rhyolite near the Paramount Canyon tin occurrence. 72 mm diameter lens cap on outcrop for scale b) Carapace breccia near the Taylor Creek tin occurrence. Large boulder in center of photo is 1.5 m top to bottom.

Figure 3. Schematic cross section of a typical Taylor Creek Rhyolite dome. A) Flow banded rhyolite lava; B) Carapace breccia; C) Zones of intense vapor-phase crystallization; D) Tin occurrences; E) Older rocks.



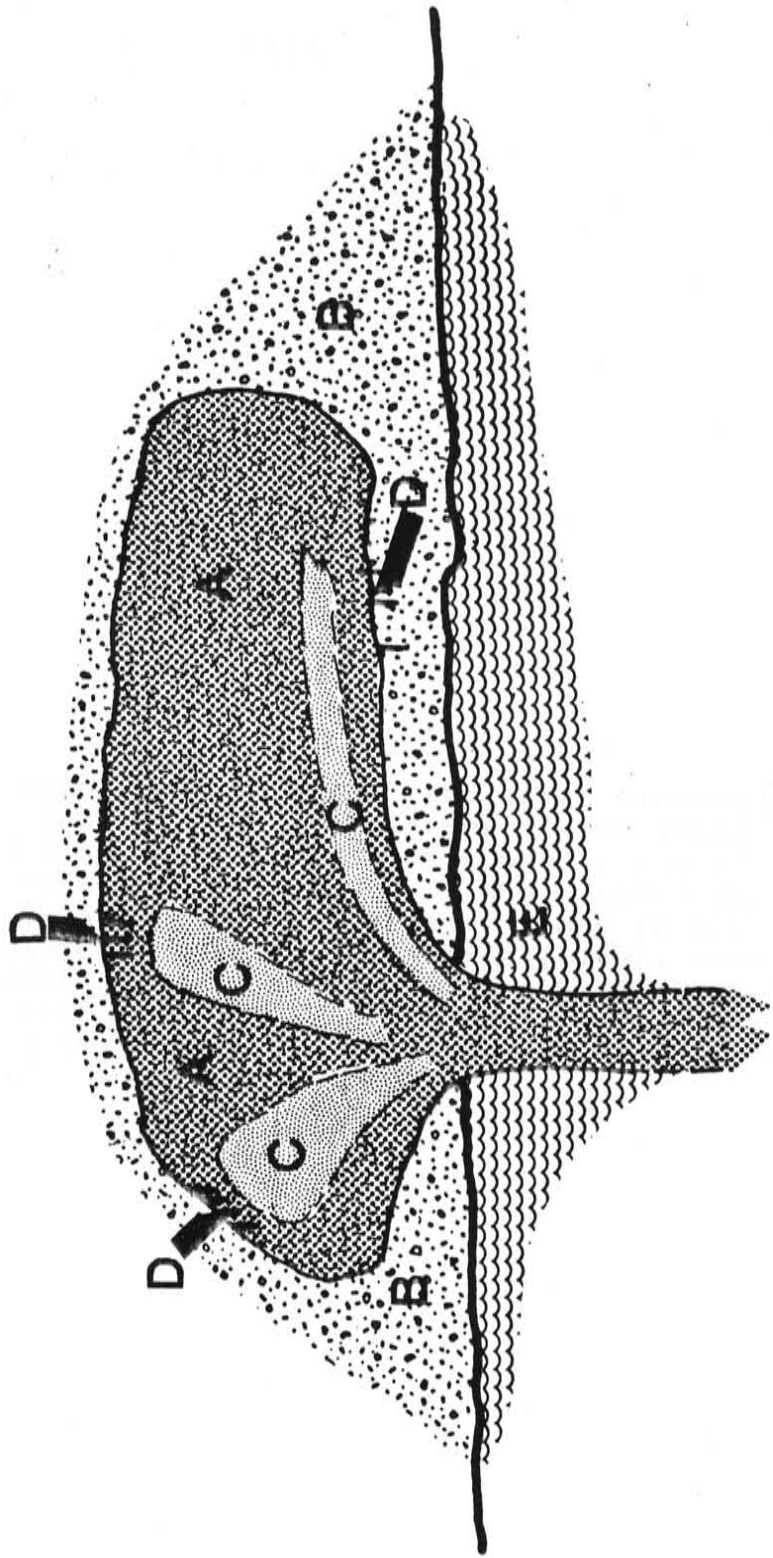


Figure 4. Chondrite normalized rare earth element patterns for the tin-bearing rhyolites in New Mexico (ruled pattern), tin-bearing S-type granitoids (dark band), and tin-bearing A-type granitoids (stipule pattern). The pattern for the granite of Iron Mountain is in heavy lines (Robertson, 1985). Data from Alderton and others (1980), Bowden (1985), Du Bray (1985), Eggleston and Norman (1987d), Harris (1985), Higgins and others (1985), Hudson and Arth (1983), Ishihara and others (1980), Kinnaird and others (1985), Nguene (1982), and Price (1983).

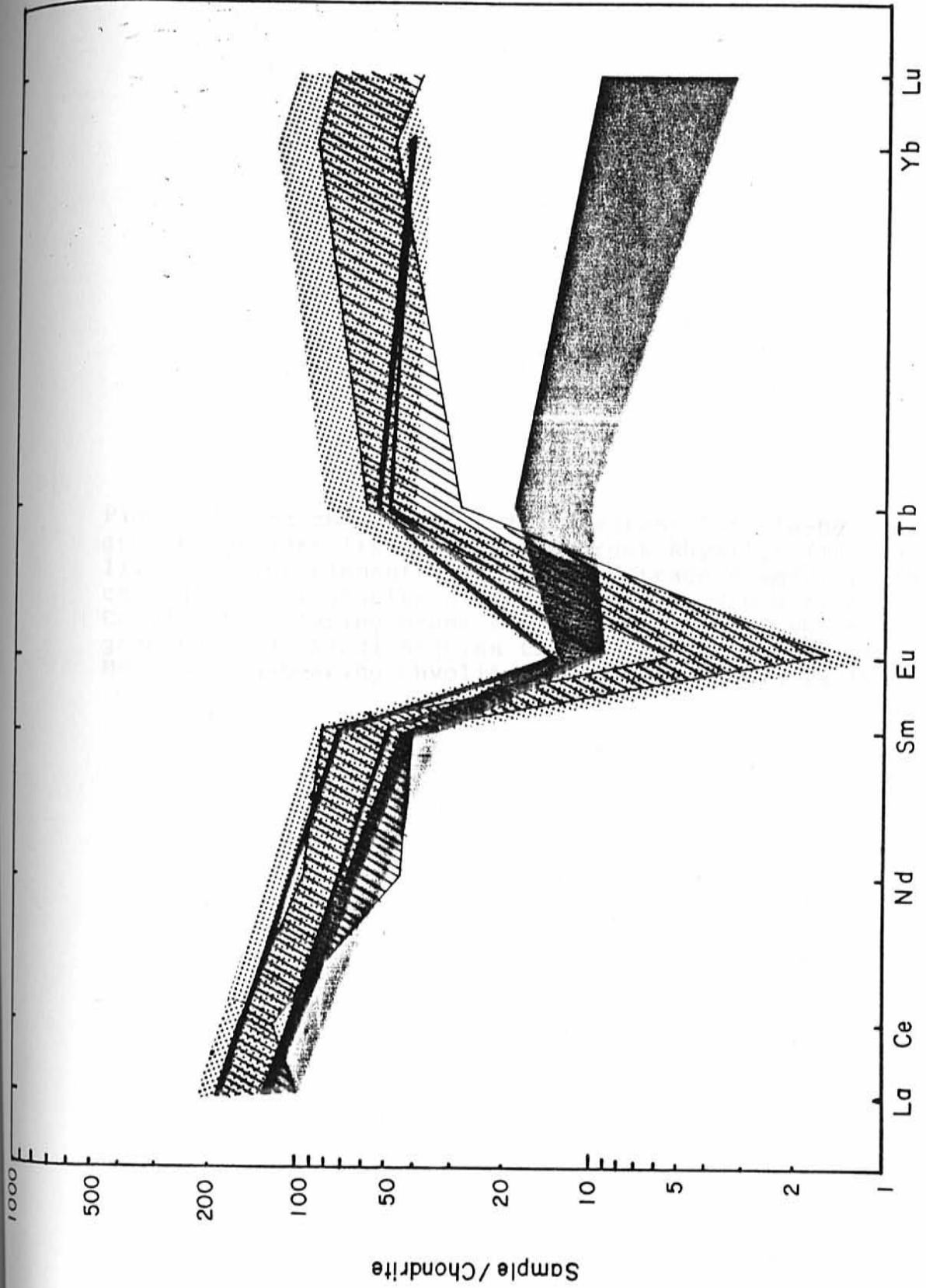
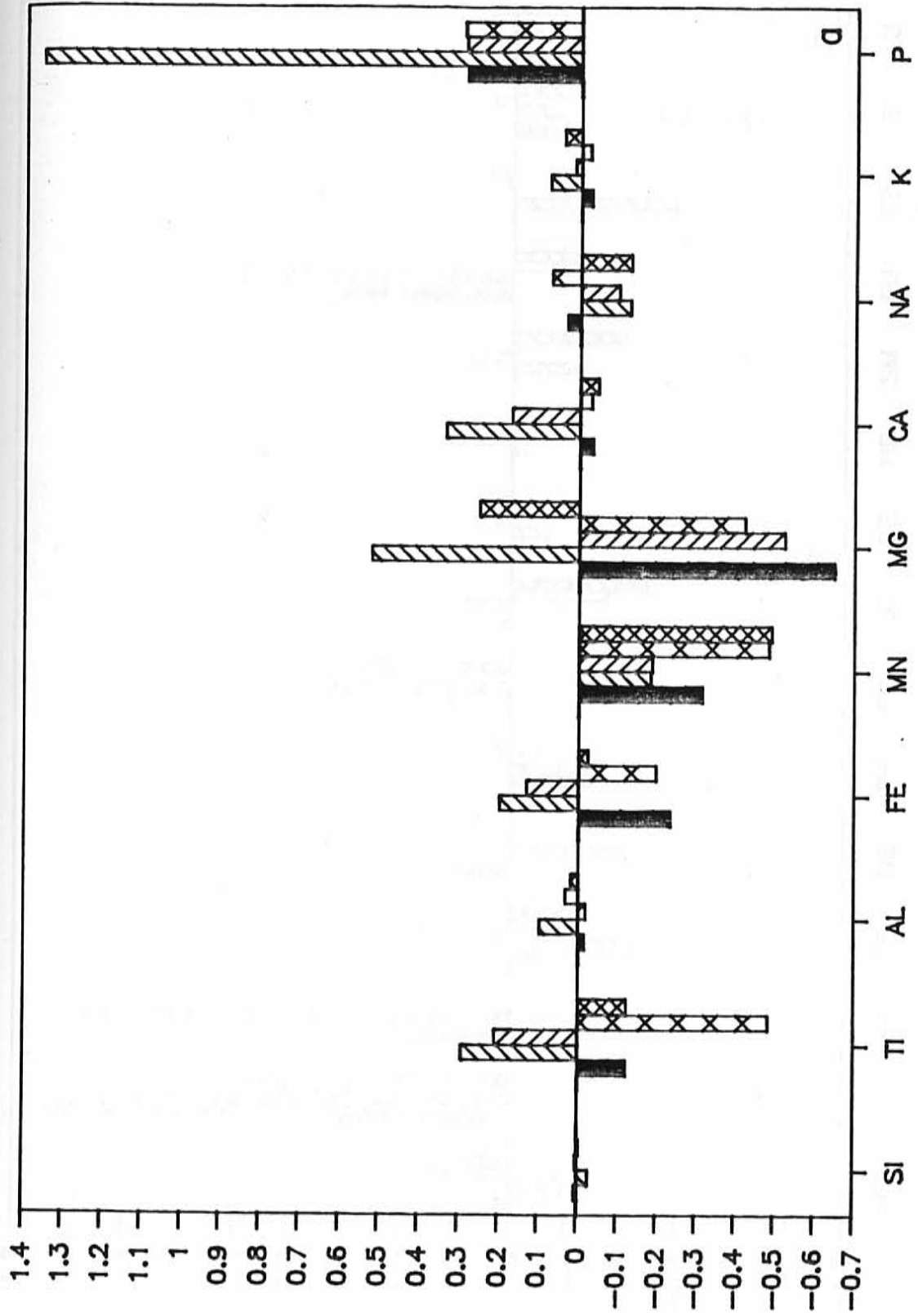


Figure 5. Enrichment-depletion diagrams for tin-bearing granitoids normalized to Taylor Creek Rhyolite (Ttc in Table 1). a) Major elements, b) selected trace elements. The columns are 1) granite of Iron Mountain, New Mexico, 2) Cornish tin-bearing granite, 3) Australian tin-bearing A-type granitoid, 4) Saudi Arabian tin-bearing granitoid, and 5) Mexican tin-bearing rhyolite. Data sources in Table 1.



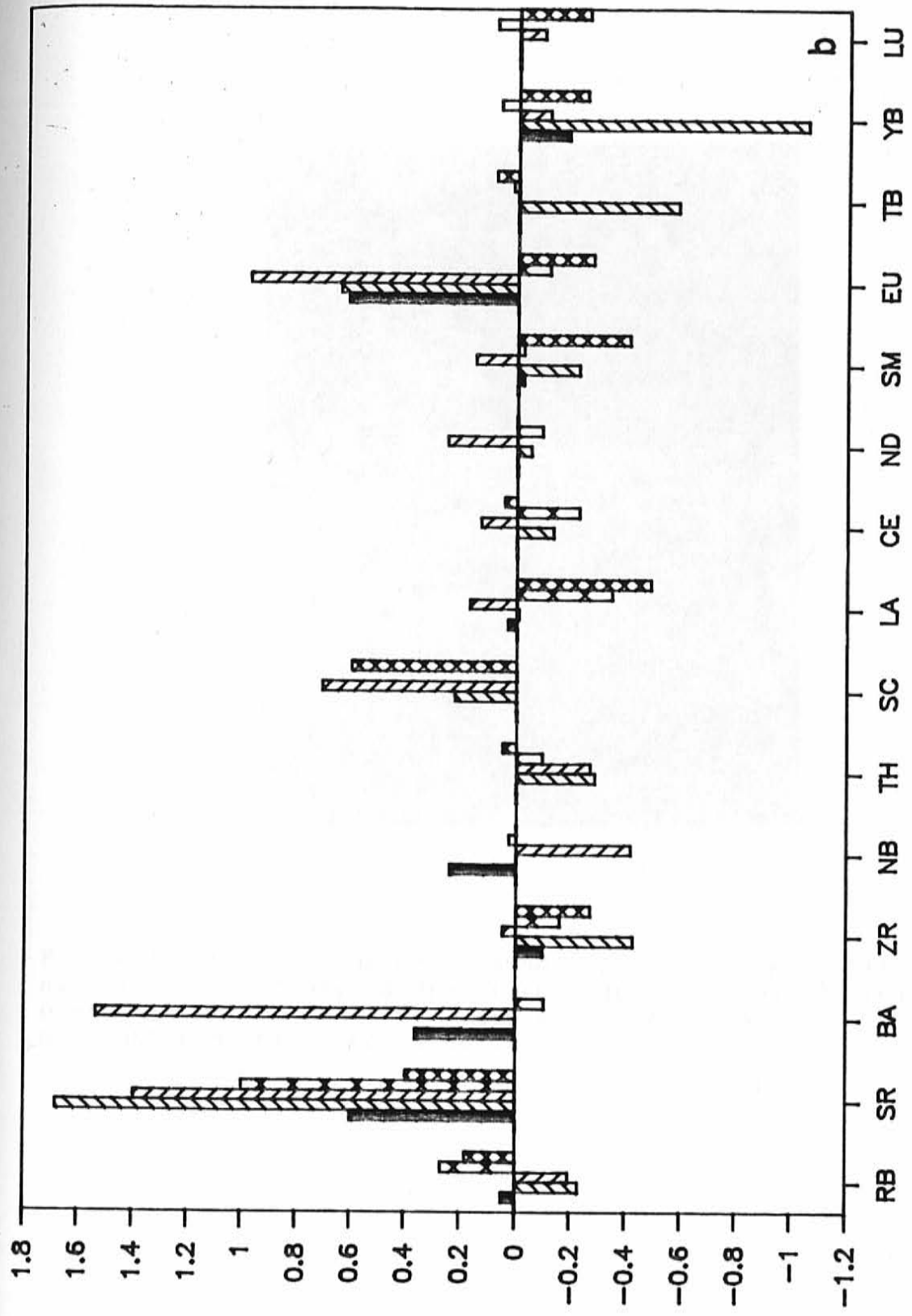




Figure 6. Typical zone of intense vapor-phase crystallization exhibiting the punky nature of the outcrop, flow banding, and overlying lithophysal zone (top right of photograph). Tree at right edge of photo is about 2.5 m high.



Figure 7. Wood tin nuggets recovered from the Nugget Gulch tin occurrence exhibit typical botryoidal character of wood tin associated with high-silica rhyolite lavas.





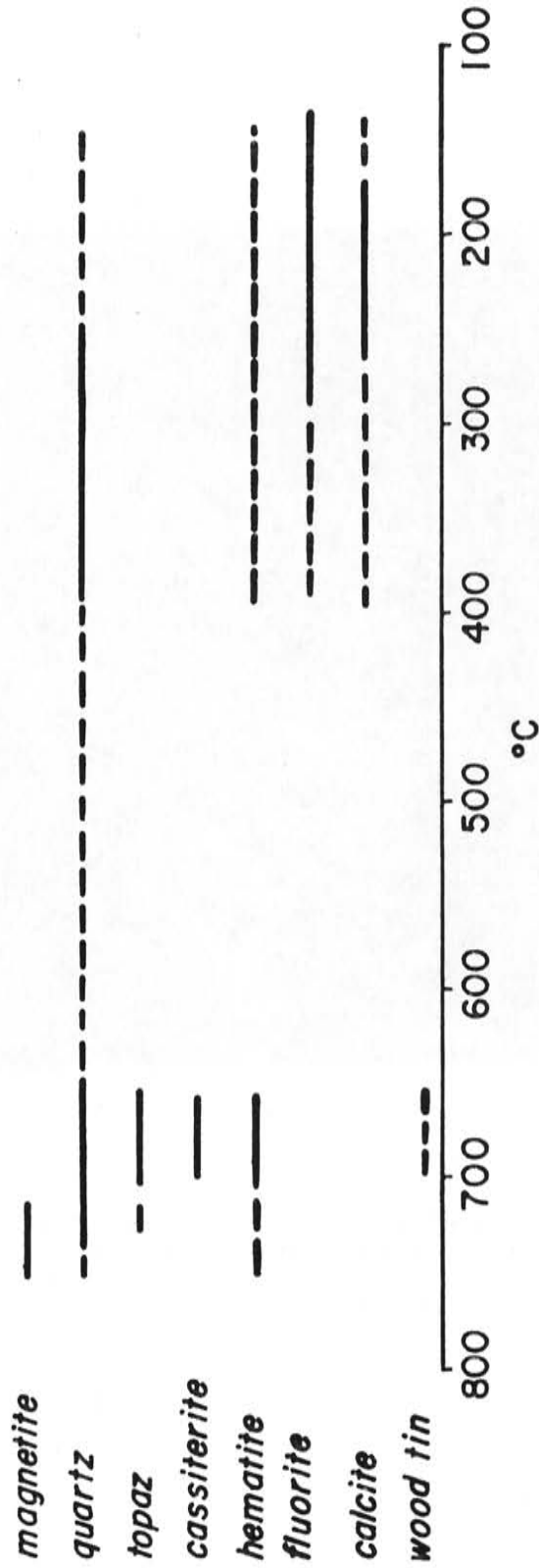
a



b

Figure 8. Typical lode tin occurrences in the Taylor Creek District. a) Nearly pure cassiterite (dark crystals) at the Squaw creek tin occurrence. b) Wood tin in chalcedony veinlet at the base of the carapace breccia in the Nugget Gulch tin occurrence. Large botryoids in center of photograph are about 2 mm diameter.

Figure 9. Paragenesis of the tin mineralization associated with high-silica rhyolites in New Mexico. The paragenesis is a composite of the region and does not occur in its entirety at any single locality.



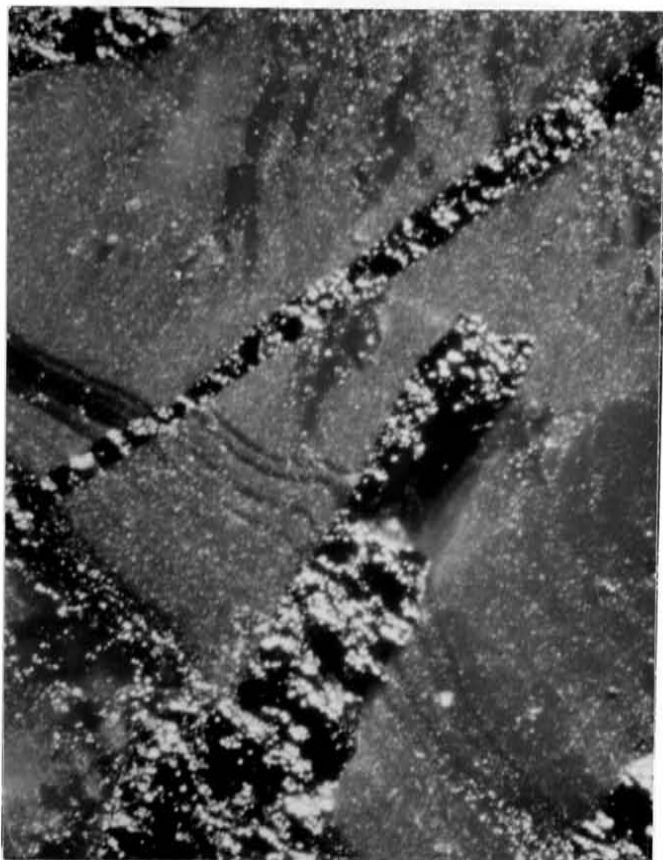


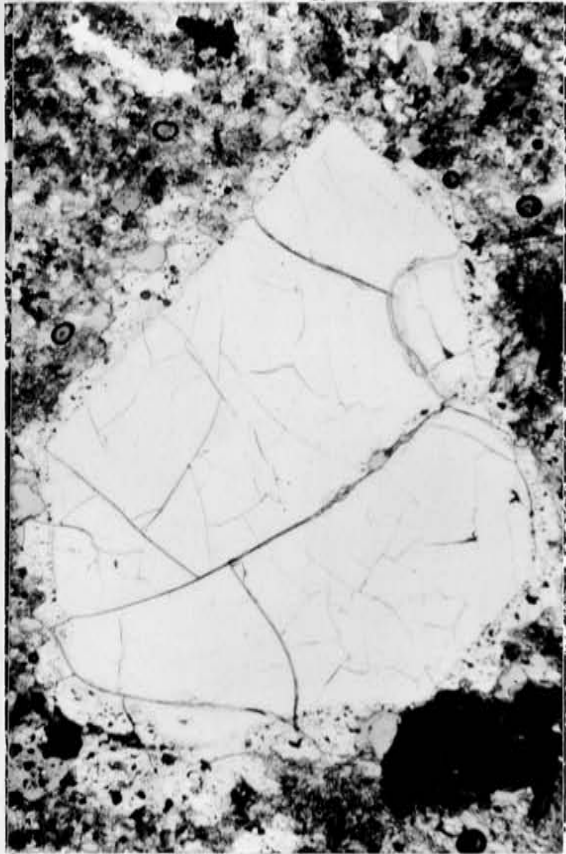
Figure 10. Bladed hematite with interbanded cassiterite and wood tin filling space between hematite blades. Field of view is about 2 mm.



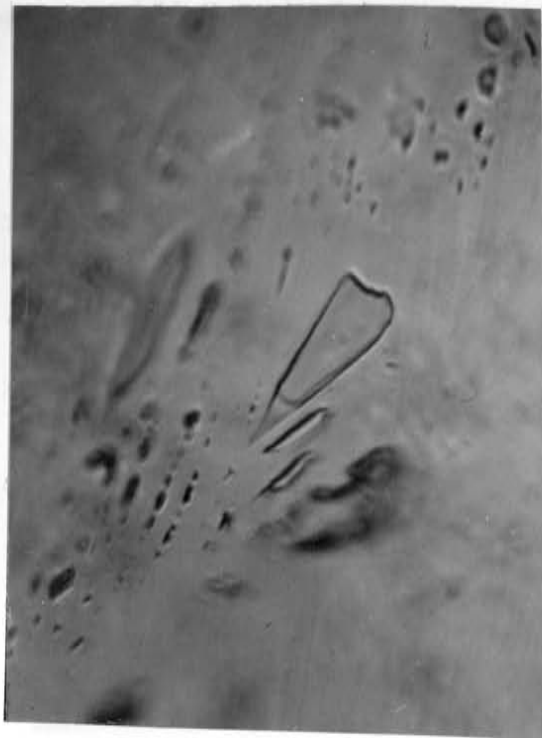
Figure 11. Interbanded hematite (black) and cassiterite (bright and medium dark bands). The field of view is about 2 mm.

Figure 12. Fluid inclusions in the tin mineralization and associated minerals in the tin-bearing rhyolites in New Mexico. a) Quartz phenocryst in host rhyolite with an inclusion-rich overgrowth. b) Type 2 inclusions in overgrowths on quartz phenocrysts in Figure 12a (25° C). c) Type 1 inclusions in quartz from lithophysae. d) Type 2 inclusions in topaz (25° C). e) Type 5 inclusion in calcite (25° C). f) Type 1 (large, dark inclusions) and Type 2 (small, clear inclusions) inclusions along a pseudosecondary plane in cassiterite. g) Large type 2 inclusion in topaz. The inclusion consists of a crystalline solid with 4 daughter minerals and contains numerous vapor bubbles. No aqueous fluid was observed. h) the same inclusion as in 12g, but at 320° C. note the liquid in the end of the inclusion and the euhedral termination on the solid. Four daughter minerals are visible near the vapor bubble. i) Type 2 inclusion after quenching from 400° C. Note the mottled, microcrystalline nature of the crystalline solid and the octahedral(?) daughter mineral near the vapor bubble. j) Type 2 inclusion at 400° C. Note that the crystalline solid is completely liquid. The round daughter mineral touching the vapor bubble is what remains of the octahedral daughter in Figure 12j. That daughter mineral totally dissolved at 408° C. The inclusion was not heated above 450° C, thus the other two transparent daughter minerals did not dissolve. Similar daughter minerals in other inclusions dissolve between 500 and 630° C. The opaque daughter mineral did not dissolve. k) Type 6 magmatic glass inclusions in the phenocryst in Figure 12a. l) Brecciated cassiterite (dark mineral) and hematite (black mineral) in a matrix of quartz and sanidine with minor topaz (not visible in this view). Field of view is about 2.5 mm. m) naturally decrepitated fluid inclusions in quartz. Note the dark crack leading away from the inclusion.

a



b



c

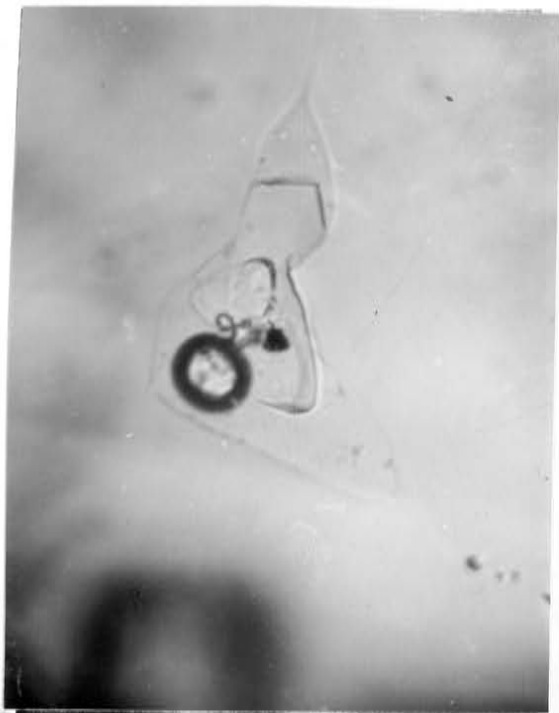
d



f



g



h

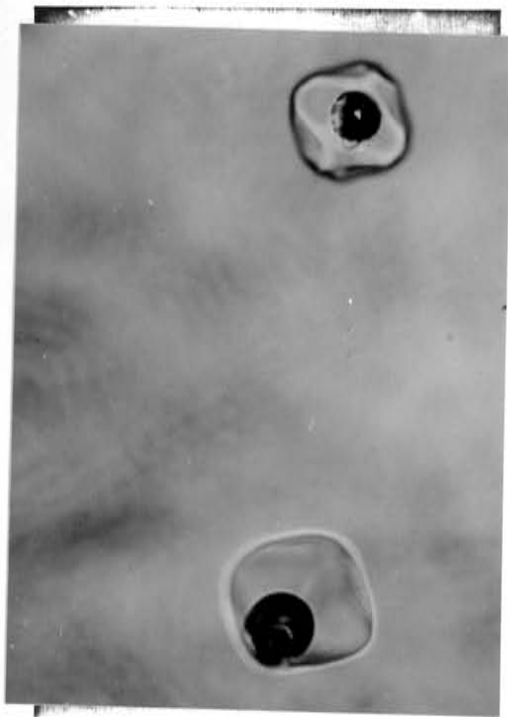
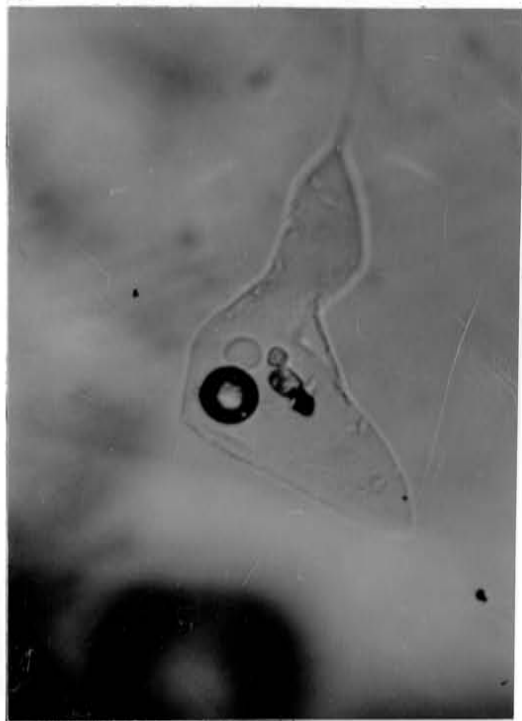


(392)

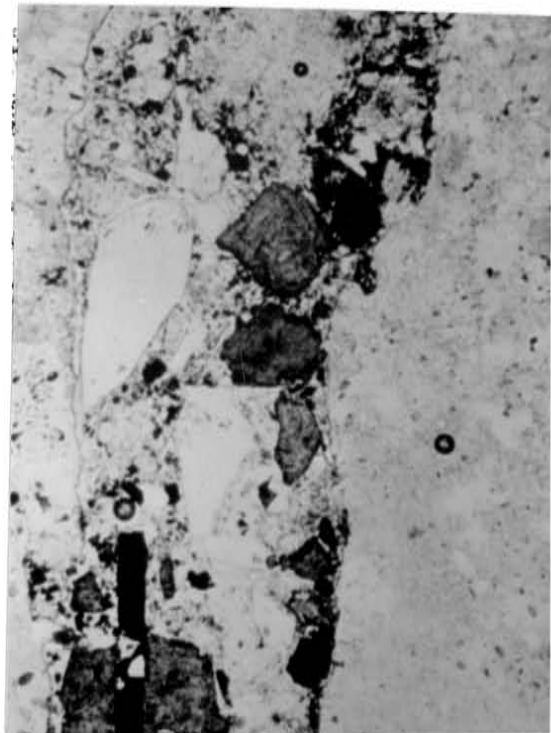
i



j



k



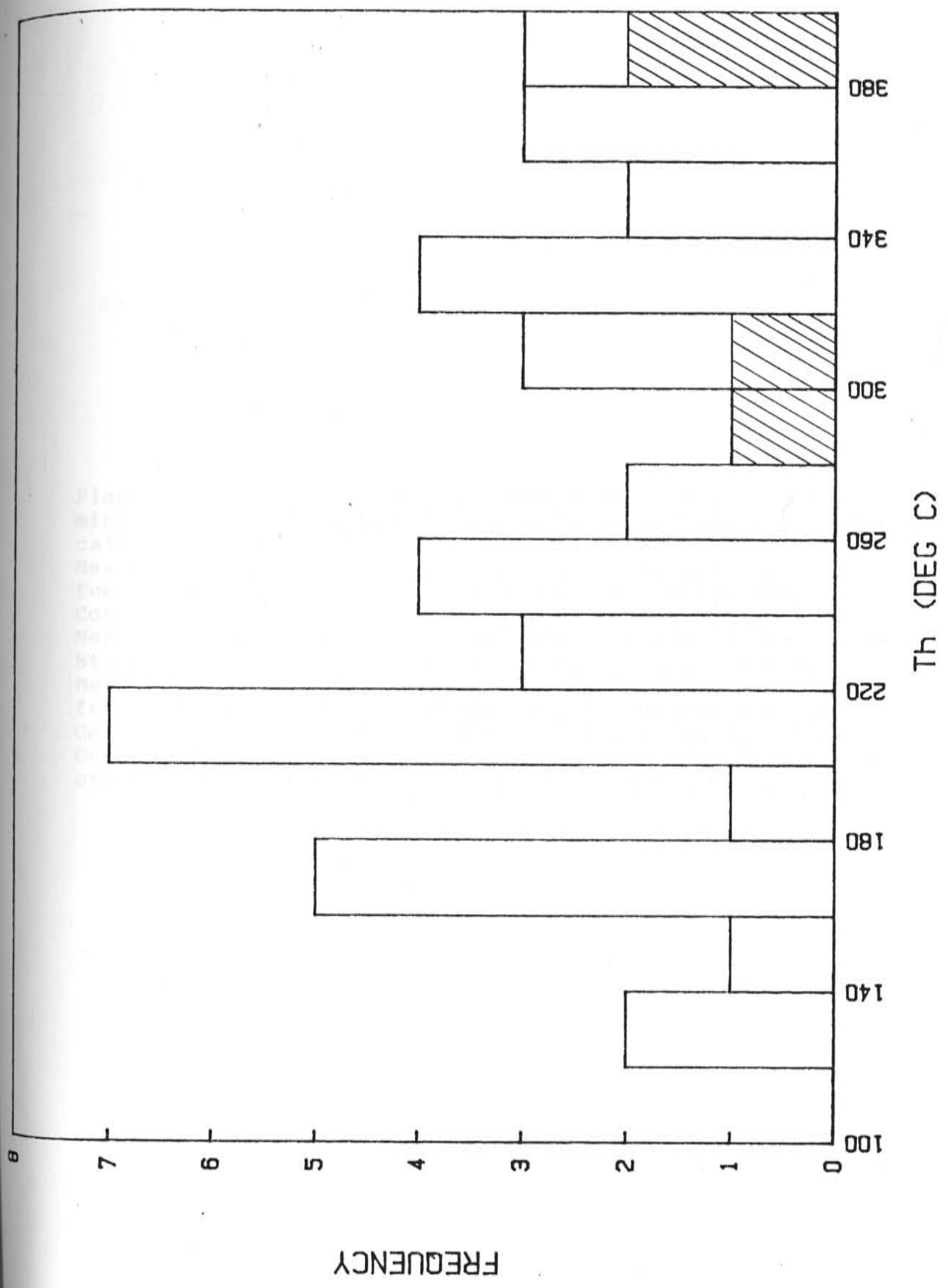
l

(393)

m



Figure 13. Histogram of homogenization temperatures for type 4 (ruled areas) and type 5 inclusions.



Flo  
al  
ca  
No  
Eu  
Co  
No  
St  
No  
ti  
Co  
Q  
or

Figure 14.  $\text{CO}_2$  vs  $\text{N}_2$  plot (in mol % without water) for tin minerals, fluorite and silica replacement bodies and quartz-calcite mineralization in the Taylor Creek District, New Mexico with analyses of porphyry Cu and Mo systems, and fumarolic gases from active volcanos for comparison. CF-Copper Flat, New Mexico, porphyry Cu system; Q-Questa, New Mexico, Climax-type Mo system; U-Usu Volcano, Japan; SH-Mt. St. Helens Volcano, Washington; K-Kamchatka, U.S.S.R.; M-Merapi Volcano, Indonesia. Data sources: Porphyry systems from Norman and Sawkins (1987); Mt. St. Helens data from Gerlach and Casadevall (1986); Merapi Volcano data from Le Guern and others (1982); Usu volcano data from Matsuo and others (1982); Kamchatka data from Vakin and Kutjev (1982).

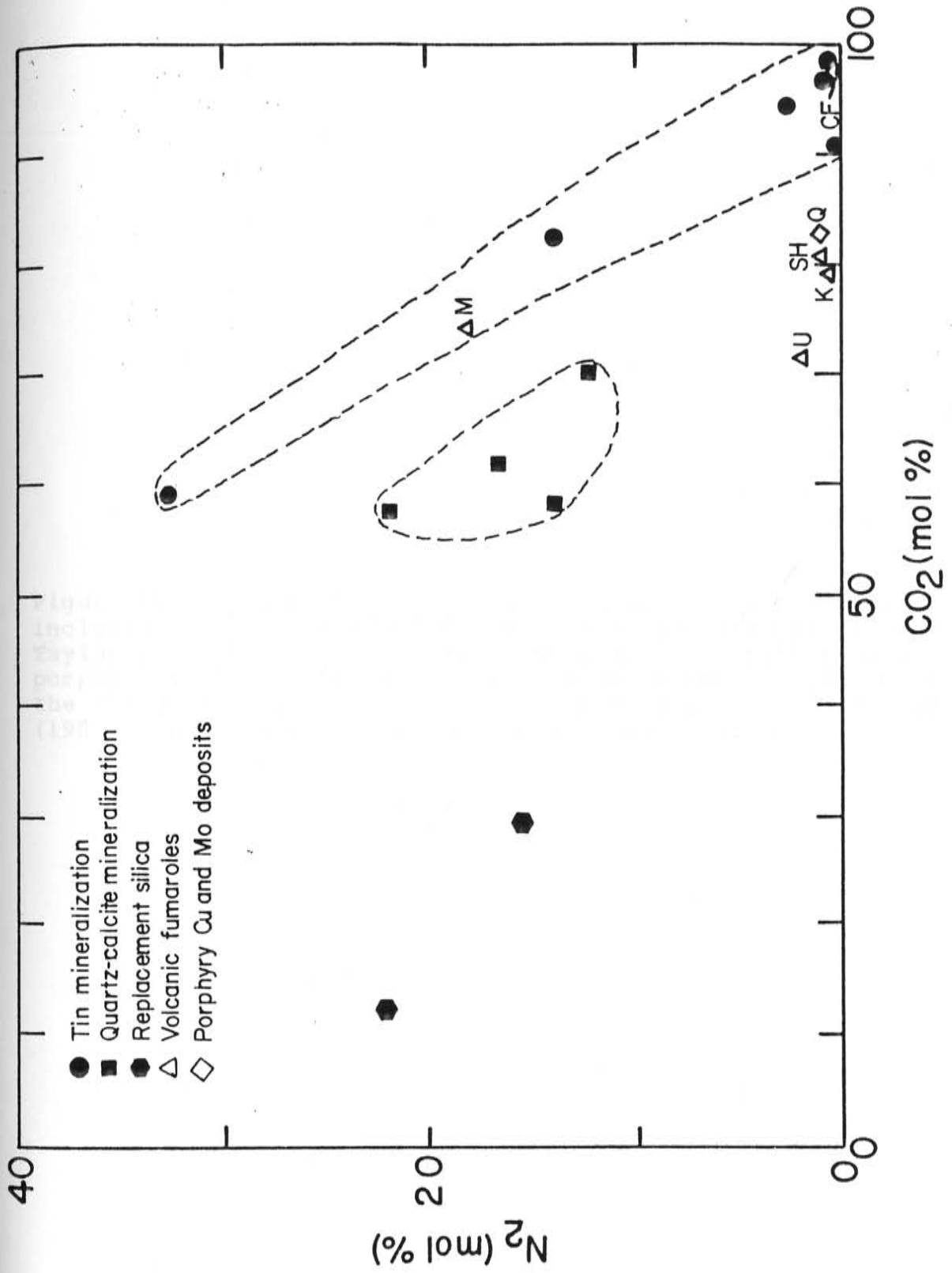


Figure 15. Ternary  $\text{CO}_2$ - $\text{C}_2\text{H}_6$  (total organics)- $\text{N}_2$  for fluid inclusion gases from tin minerals and gangue minerals in the Taylor Creek District. Also plotted are the epithermal and porphyry systems from Figure 14. An additional field, PC, is the field of porphyry copper deposits from Norman and Sawkins (1987). Data sources and symbols as Figure 14.

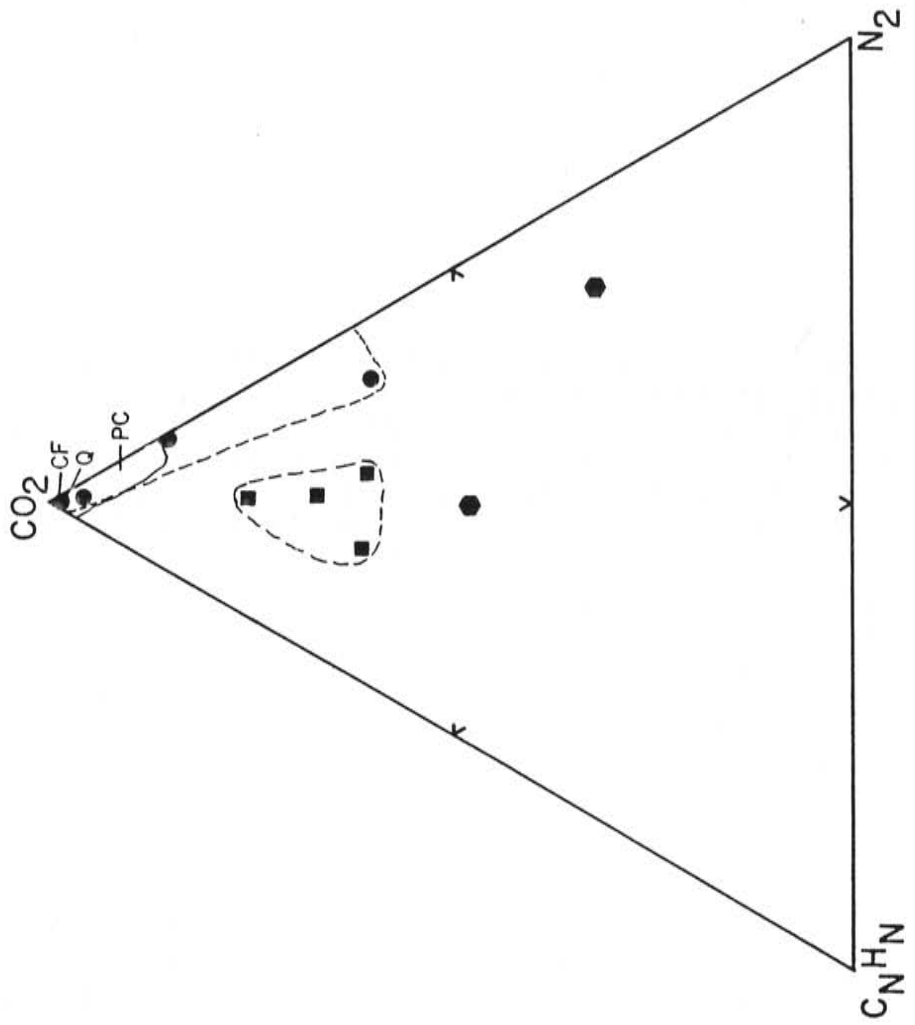


Figure  
space  
plot  
line  
buff  
pair  
of t



Figure 16. Stability of Fe- and Sn-bearing species in  $f_{O_2}$ - $f_{S_2}$  space.  $T=627^\circ\text{C}$  ( $900^\circ\text{K}$ ). Fluid inclusion gas analyses plotted as solid circles (T-topaz, C-cassiterite, W-wood tin). See text for calculations and discussion. FMQ and NNO buffers from Haggerty (1976). PS-Minimum stability of pseudobrookite from Carmichael and Nicholls (1967). Position of  $f_{O_2}$  air calculated at  $25^\circ\text{C}$ .

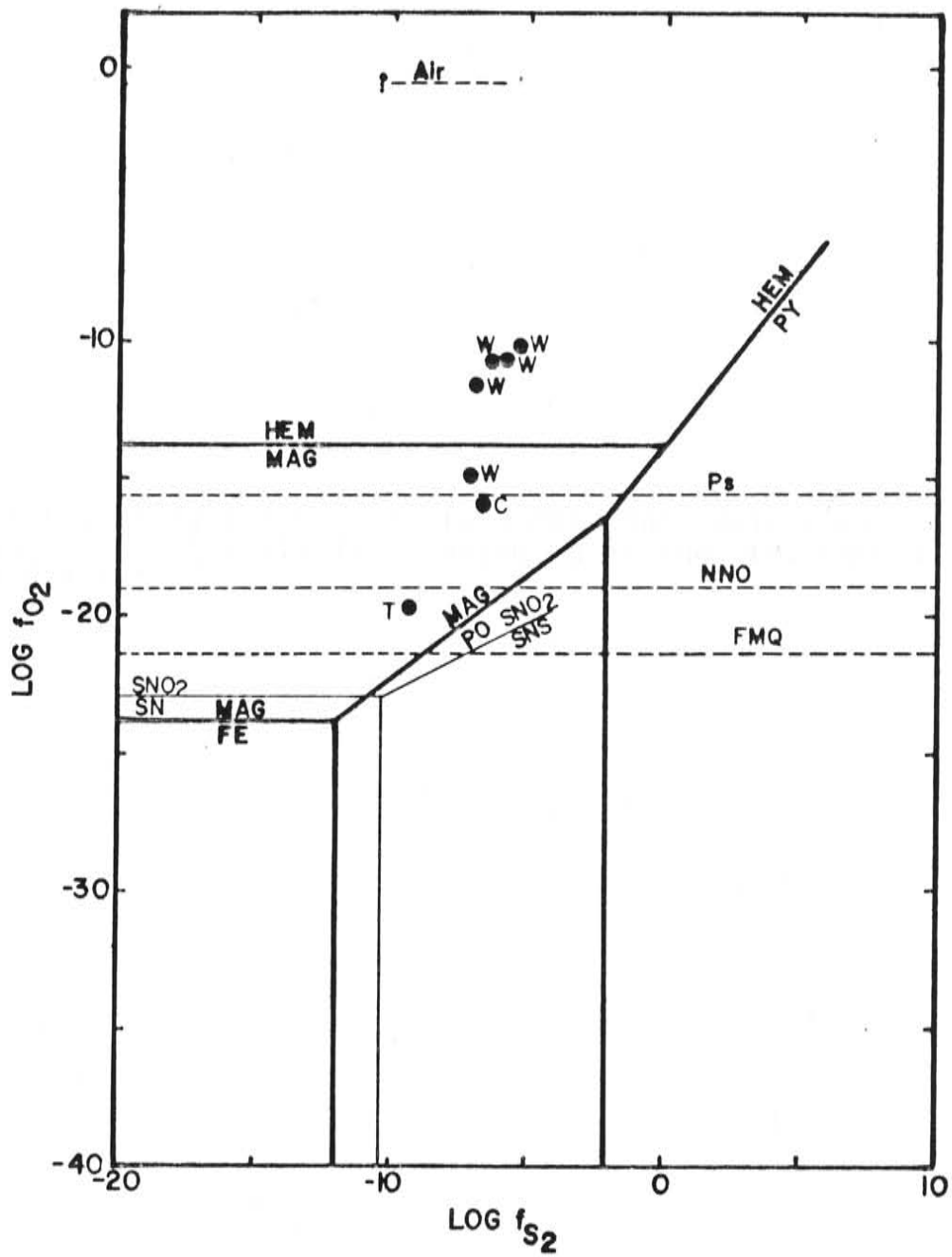


Figure 17. Solubility of Sn in 2 mol. NaCl solutions from Wilson and Eugster (1984). Contoured at the QFM, NNO, and MH  $f_{O_2}$  buffers.

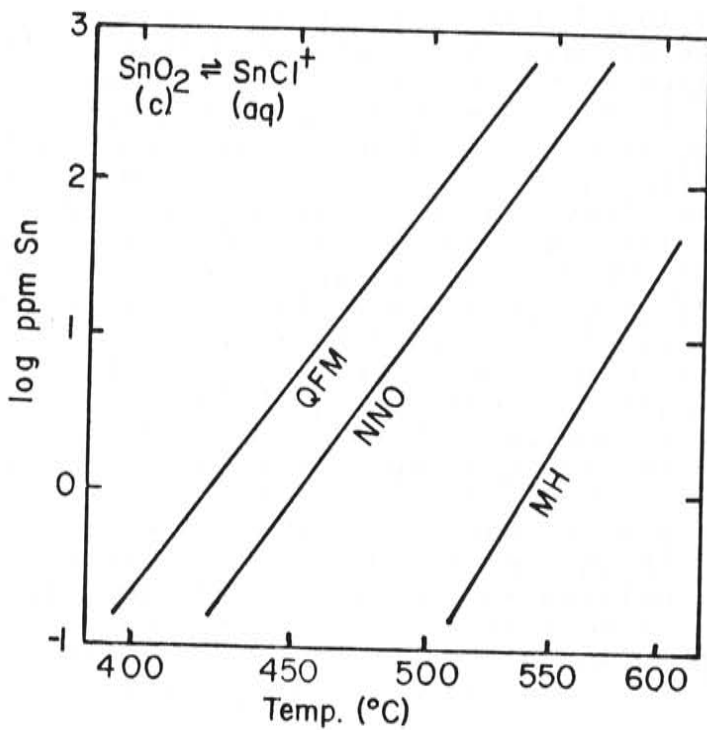
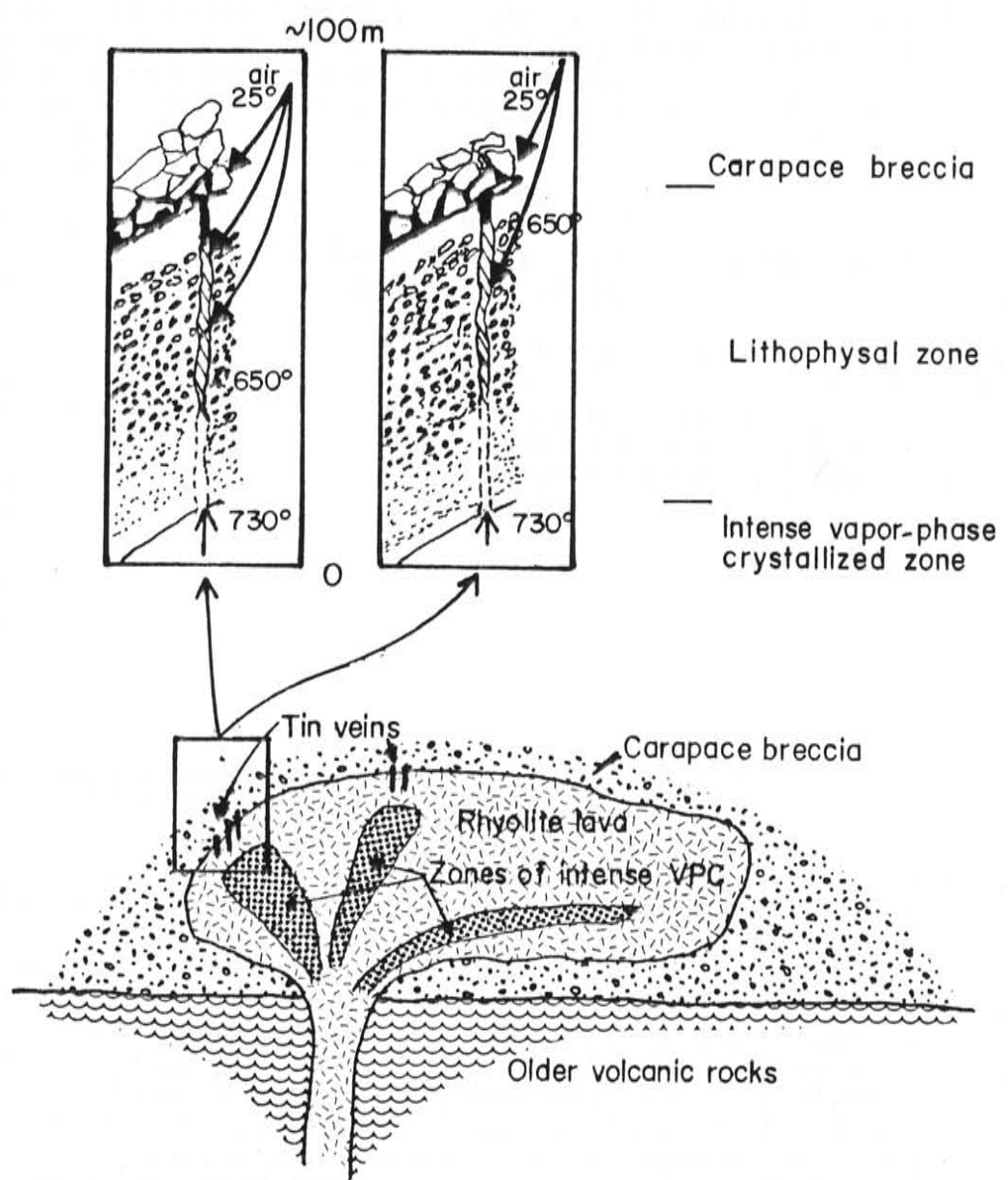


Figure 18. Model for the formation of rhyolite-hosted tin deposits. The process begins with extrusion of the rhyolite lava. Tin-rich magmatic fluids are focused to and travel along flow banding until they are trapped beneath a plastic zone where the lithophysae are forming. Intense vapor phase crystallization occurs while the fluids are trapped. Additional tin is scavenged from the host rhyolite by destruction of biotite. When the lithophysal zone becomes brittle enough to fracture, the trapped magmatic fluids are rapidly released as fumaroles. Mixing of air with the fluids and the extreme thermal gradients rapidly precipitate hematite, cassiterite and wood tin. Cassiterite will be favored under relatively more quiescent fluid flow (left inset) because it can be deposited from a saturated fluid. During periods of very rapid fluid flow, wood tin will be favored (right inset) because high temperatures will be closer to the surface. Mixing with air and cooling will cause supersaturation that will in turn rapidly precipitate the botryoidal wood tin. This model thus predicts that cassiterite will be the predominant Sn-bearing phase in the deeper veinlets (cross ruling) and that wood tin will be predominant closer to the surface and in the carapace breccia (black matte in the carapace breccia).



Appendix 1a.DETECTION LIMITS

The following calculated\* detection limits for various trace elements determined by XRF were used throughout this study. The detection limits for major elements was about 0.01% in all cases. Detection limits for trace elements determined by INAA are determined during reduction of the data for each sample and is based on the peak height relative to the background at the peak.

=====

(values in ppm)

Ba 16  
Cr 10  
Ga 3  
Nb 1  
Ni 5  
Pb 3  
Rb 1  
Sn 5  
Sr 1  
Th 3  
U 3  
V 3  
Y 1  
Zn 4  
Zr 2

\*the formula used to determine the detection limits is:

$$LLD = 3/M * \text{SQUARE ROOT} (R_b/T_b)$$

where M= counts/second/ppm  
 $R_b$  =background count rate  
 $T_b$  =count time on background

SAMPLE PREPARATION

With the exception of samples 270 to 274, all samples were prepared by first sawing slabs from large hand samples. The slab was cut approximately 1 cm thick and typically produced 150 to 200 g of sample. A thin section chip was also cut when the sample slab was cut. The slab was broken and ground in a tungsten carbide TEMA mill for approximately 1 minute. This procedure produced uniformly fine powder. Contamination of the sample by W and Co was extreme. Contamination by Ta was noted, but was too low (<0.05 ppm/100 ppm W) to affect these analyses. Samples 270-274 are hand-picked samples consisting of fine crystals and fragments of cassiterite, wood tin, and hematite. No further sample preparation was needed.

Appendix 1b. Geochemistry of samples collected in the northern Black Range and Sierra Cuchillo of New Mexico. Samples are described in Appendix 2.

- 1) leaders indicate no analysis
- 2) Less than symbol (<) in front of a number indicates below detection limit (see Appendix 1a).
- 3) \* indicates INAA data for an element normally analyzed by XRF.

The samples are arranged by stratigraphic unit starting at the bottom and by increasing  $\text{SiO}_2$  content. The analyses for units in the Sierra Cuchillo follow the Black range samples and are arranged similarly. Finally, 5 samples of ore material analyzed by INAA are at the end of the table.

The symbols in row 1 are as follows:

Black Range:

Tkn- Kneeling Nun Tuff  
 Tkw- tuff of Koko Well  
 Tpc- basaltic andesite of Poverty Creek  
 Tsc- Tuff of Stiver Canyon  
 Tsp- rhyolite of Sawmill Peak  
 Tkm- tuff of Kline Mountain  
 Tdp- rhyolite of Dolan Peak  
 Thc- rhyolite of Hoyt Creek  
 Twc- rhyolite of Whitetail Canyon  
 Tkt- rhyolite of Keith Tank  
 Tlj- La Jencia Tuff

Sierra Cuchillo:

Trp- Rubio Peak Formation  
 Tkn- Kneeling Nun Tuff  
 Tvp- Vicks Peak Tuff  
 Ttr- unnamed trachytes  
 Thok- rhyolite of HOK Ranch  
 Tdike- rhyolite porphyry dike  
 Twsd- rhyolite of Willow Springs Draw  
 Iron- granite of Iron Mountain

ore samples:

ore1- ore5

Taylor Creek Rhyolite domes

Ttsc- Squaw Creek dome  
 Ttng- Nugget Gulch dome  
 Ttnng- North Nugget Gulch dome  
 Ttbp- Boiler Peak dome  
 Ttnpc- North Paramount Canyon dome  
 Ttac- Alexander Cienega dome  
 Ttrm- Round Mountain dome  
 Tttc- Taylor Creek dome  
 Ttkm- Kemp Mesa dome  
 Ttip- Indian Peaks dome

Ttuff- Tuffs associated with the Taylor Creek Rhyolite

Tgc- tuff of Garcia Camp

Tbc- Bloodgood Canyon Tuff

Tbm- Bearwallow Mountain Fm.

Tkmp- rhyolite porphyry of Kline Mountain



SAMPLE	Tkn 19	Tkw 123	Tpc 41	Tpc 42	Tpc 175	Tpc 25	Tpc 46	Tpc 52	Tpc 64	Tpc 40
SiO <sub>2</sub>	72.60	69.80	52.23	52.31	53.22	53.96	54.63	54.77	56.54	56.93
TiO <sub>2</sub>	0.27	0.45	1.11	1.14	1.17	1.15	1.18	1.17	1.25	1.00
Al <sub>2</sub> O <sub>3</sub>	13.94	15.09	16.34	16.36	17.34	16.86	17.43	16.85	18.18	16.55
Fe <sub>2</sub> O <sub>3</sub>	1.77	2.15	9.04	8.91	8.20	7.70	8.31	8.00	8.65	7.21
FeO	--	--	--	--	--	--	--	--	--	--
MnO	0.02	0.01	0.14	0.13	0.11	0.07	0.06	0.08	0.49	0.14
MgO	0.57	0.42	6.29	5.83	3.47	4.00	3.24	3.99	0.90	1.57
CaO	0.99	0.28	8.44	8.51	8.20	7.45	7.23	7.40	5.42	4.91
Na <sub>2</sub> O	2.90	3.12	3.50	3.56	3.05	4.11	4.63	3.93	3.90	4.07
K <sub>2</sub> O	4.93	6.44	1.32	1.33	1.90	1.99	2.00	1.94	2.36	2.79
P <sub>2</sub> O <sub>5</sub>	0.06	0.08	0.25	0.26	0.44	0.55	0.58	0.58	0.58	0.51
LOI	1.04	1.27	1.39	1.87	2.59	2.15	1.49	2.15	1.90	3.94
TOTAL	99.09	99.11	100.05	100.21	99.69	99.99	100.78	100.86	100.17	99.62
As	--	--	<1.0	--	--	--	--	<1.0	--	--
Ba	599	1757	526	548	796	893	960	916	1280	1278
Br	--	--	<1.0	--	--	--	--	<1.0	--	--
Cl(%)	--	--	--	--	--	--	--	--	--	--
Cr	13	<10	272*	229	27	58	56	67*	63	52
Cs	--	--	1.3	--	--	--	--	0.3	--	--
F(%)	--	--	--	--	--	--	--	--	--	--
Ga	16	13	19	19	22	20	20	21	21	20
Hf	--	--	4.3	--	--	--	--	5.8	--	--
Mo	<1	--	2	--	--	1	--	--	--	--
Nb	18	18	6	7	12	11	12	11	12	13
Ni	<5	<5	122	114	29	41	53	51	50	27
Pb	21	21	7	7	6	<3	5	5	6	11
Rb	182	232	23	22	34	27	28	29	43	51
Sb	--	--	0.2	--	--	--	--	<0.1	--	--
Sc	--	--	20.9	--	--	--	--	18.8	--	--
Se	--	--	<1.0	--	--	--	--	<0.2	--	--
Sn	<5	<5	<5	<5	<5	<5	<5	<5	<5	<5
Sr	151	127	581	627	1008	072	1117	1110	1197	920
Ta	--	--	0.4	--	--	--	--	0.6	--	--
Th	28	27	<3	<3	<3	<3	<3	3*	<3	<3
U	<3	<3	<3	<3	<3	<3	<3	<1*	<3	<3
V	17	30	183	168	171	152	178	157	170	120
Y	29	60	20	21	28	30	26	27	25	20
Zn	30	38	87	87	92	84	97	97	94	102
Zr	134	478	153	157	229	220	239	220	251	266
La	--	--	17	--	--	--	--	43	--	--
Ce	--	--	41	--	--	--	--	91	--	--
Nd	--	--	26	--	--	--	--	45	--	--
Sm	--	--	5.0	--	--	--	--	7.5	--	--
Eu	--	--	1.46	--	--	--	--	2.00	--	--
Tb	--	--	0.6	--	--	--	--	0.9	--	--
Yb	--	--	1.7	--	--	--	--	2.4	--	--
Lu	--	--	0.27	--	--	--	--	.34	--	--

SAMPLE	Tpc 39	Tsc 96	Tsc 48	Tsc 112	Tsc 44	Tsc 23	Tsc 60	Tsc 49	Tsc 86	Tsc 61
SiO <sub>2</sub>	61.77	73.64	75.17	75.26	75.33	75.40	76.47	77.06	77.12	77.28
TiO <sub>2</sub>	1.05	0.25	0.15	0.16	0.17	0.16	0.18	0.16	0.17	0.15
Al <sub>2</sub> O <sub>3</sub>	17.50	13.29	11.62	12.07	12.31	11.96	11.93	12.07	11.32	11.37
Fe <sub>2</sub> O <sub>3</sub>	5.63	1.25	1.08	2.22	1.24	1.10	1.24	1.08	1.29	0.99
FeO	---	---	---	---	---	---	---	---	---	---
MnO	0.01	0.05	0.06	0.02	0.03	0.04	0.04	0.04	0.03	0.02
MgO	0.75	0.60	0.77	0.29	0.22	0.28	0.31	0.43	0.14	0.32
CaO	3.85	1.38	0.53	0.20	0.27	0.38	0.34	0.30	0.19	0.36
Na <sub>2</sub> O	4.30	0.92	3.57	1.92	2.65	2.85	2.35	3.15	0.18	2.22
K <sub>2</sub> O	3.09	2.47	5.63	5.83	6.02	5.58	5.25	5.28	8.09	4.98
P <sub>2</sub> O <sub>5</sub>	0.53	0.03	0.03	0.02	0.02	0.03	0.03	0.01	0.01	0.05
LOI	1.82	5.70	2.18	1.38	1.32	1.26	2.02	1.10	1.72	1.86
TOTAL	100.30	99.58	100.79	99.37	99.58	99.04	100.19	100.68	100.26	99.60
As	---	---	---	---	---	2.5	---	---	---	---
Ba	1328	542	64	34	96	82	100	76	42	72
Br	---	---	---	---	---	<1.00	---	---	---	---
Cl(%)	---	---	---	---	---	---	---	---	---	---
Cr	52	<10	<10	<10	<10	3*	<10	<10	<10	<10
Cs	---	---	---	---	---	2.6	---	---	---	---
F(%)	---	---	---	---	---	---	---	---	---	---
Ga	21	17	15	19	16	16	14	17	12	16
Hf	---	---	---	---	---	6.6	---	---	---	---
Mo	1	---	---	1	---	1	---	---	---	---
Nb	13	22	22	31	24	23	23	24	22	22
Ni	41	9	<5	<5	<5	<5	<5	<5	<5	<5
Pb	12	42	27	20	21	20	23	19	37	19
Rb	59	125	187	258	217	202	197	200	262	195
Sb	---	---	---	---	---	0.16	---	---	---	---
Sc	---	---	---	---	---	3.7	---	---	---	---
Se	---	---	---	---	---	<1.0	---	---	---	---
Sn	25	5	12	<5	<5	<5	<5	<5	<5	<5
Sr	906	771	26	13	20	18	26	20	16	26
Ta	---	---	---	---	---	1.8	---	---	---	---
Th	<3	21	25	26	23	23	25	24	25	22
U	<3	<3	<3	<3	<3	4*	<3	<3	<3	<3
V	124	15	<3	<3	<3	<3	20	<3	6	<3
Y	18	244	55	96	75	45	323	52	39	198
Zn	82	91	51	117	57	40	64	38	35	61
Zr	275	218	168	339	180	172	184	176	173	162
La	---	---	---	---	---	31	---	---	---	---
Ce	---	---	---	---	---	59	---	---	---	---
Nd	---	---	---	---	---	22	---	---	---	---
Sm	---	---	---	---	---	5.7	---	---	---	---
Eu	---	---	---	---	---	0.32	---	---	---	---
Tb	---	---	---	---	---	1.0	---	---	---	---
Yb	---	---	---	---	---	4.1	---	---	---	---
Lu	---	---	---	---	---	0.65	---	---	---	---

SAMPLE	Tsc	Tsc	Tsc	Tsc	Tsc	Tsc	Tsc	Tsp	Tsp	Tsp
	45	70	50	63	62	24	51	22	53	43
SiO <sub>2</sub>	77.50	77.55	77.68	77.70	77.94	78.14	79.73	71.45	71.81	71.95
TiO <sub>2</sub>	0.12	0.13	0.13	0.15	0.13	0.12	0.11	0.48	0.43	0.48
Al <sub>2</sub> O <sub>3</sub>	10.80	10.97	11.39	9.87	10.72	10.97	9.92	14.24	13.23	13.72
Fe <sub>2</sub> O <sub>3</sub>	0.98	1.03	0.97	0.92	0.98	0.87	0.79	2.03	3.17	2.64
FeO	--	--	--	--	--	--	--	--	--	--
MnO	0.02	0.13	0.03	0.01	0.03	0.03	0.05	0.02	0.40	0.03
MgO	0.62	0.45	0.38	0.32	0.21	0.29	0.61	0.27	0.21	0.11
CaO	0.37	0.32	0.29	0.40	0.32	0.23	0.42	0.33	0.26	0.29
Na <sub>2</sub> O	2.06	1.55	2.65	1.69	1.97	2.24	1.22	5.11	4.15	4.01
K <sub>2</sub> O	5.90	5.54	5.00	4.03	4.60	5.42	5.08	6.13	5.69	5.77
P <sub>2</sub> O <sub>5</sub>	0.02	0.01	0.01	0.02	0.09	0.01	0.01	0.07	0.05	0.05
LOI	1.52	1.86	1.40	2.53	2.34	1.27	2.22	0.45	0.80	0.75
TOTAL	99.91	99.54	99.93	97.64	99.33	99.59	100.16	100.58	100.20	99.80
As	--	--	--	--	--	3.2	--	<0.2	--	--
Ba	48	94	49	70	100	41	74	81	139	82
Br	--	--	--	--	--	0.13	--	<1.0	--	--
Cl(%)	--	--	--	--	--	--	--	--	--	--
Cr	<10	<10	<10	<10	<10	<1*	<10	<1*	<10	<10
Cs	--	--	--	--	--	2.8	--	2.8	--	--
F(%)	--	--	--	--	--	--	--	--	--	--
Ga	15	16	14	13	15	16	13	21	19	20
Hf	--	--	--	--	--	5.7	--	18.5	--	--
Mo	--	--	--	--	--	--	--	2	--	2
Nb	22	21	21	19	21	21	19	27	25	25
Ni	<5	<5	<5	<5	<5	<5	<5	<5	<5	<5
Pb	20	41	18	14	17	18	26	23	23	25
Rb	218	207	192	152	189	201	123	171	159	162
Sb	--	--	--	--	--	0.21	--	0.1	--	--
Sc	--	--	--	--	--	2.3	--	10.0	--	--
Se	--	--	--	--	--	<1.0	--	<1.0	--	--
Sn	<5	<5	<5	<5	<5	<5	8	<5	7	7
Sr	20	20	18	32	30	14	29	3	15	13
Ta	--	--	--	--	--	1.5	--	2.1	--	--
Th	24	22	24	18	21	22	20	18	18	18
U	<3	<3	<3	<3	<3	4*	<3	5*	<3	<3
V	<3	9	<3	3	3	<3	<3	<3	<3	<3
Y	71	46	41	113	154	39	40	89	103	91
Zn	75	47	37	55	48	37	48	94	85	75
Zr	140	138	145	158	150	131	118	763	687	713
La	--	--	--	--	--	28	--	68	--	--
Ce	--	--	--	--	--	57	--	153	--	--
Nd	--	--	--	--	--	16	--	78	--	--
Sm	--	--	--	--	--	4.4	--	15.7	--	--
Eu	--	--	--	--	--	0.25	--	3.37	--	--
Tb	--	--	--	--	--	0.8	--	2.5	--	--
Yb	--	--	--	--	--	3.3	--	8.2	--	--
Lu	--	--	--	--	--	0.53	--	1.30	--	--



SAMPLE	Tkm	Tkm	Tkm	Tkm	Tkm	Tkm	Tkm	Tkm	Tkm	Tkm
	58	78	67	57	90	95	85	80	94	84
SiO <sub>2</sub>	72.02	72.38	72.60	73.33	73.78	77.40	77.78	79.13	79.28	80.29
TiO <sub>2</sub>	0.23	0.22	0.14	0.14	0.21	0.18	0.19	0.16	0.24	0.12
Al <sub>2</sub> O <sub>3</sub>	12.53	12.33	11.80	11.96	15.24	15.24	10.33	8.51	12.25	10.53
Fe <sub>2</sub> O <sub>3</sub>	1.87	2.00	1.44	1.62	0.10	0.12	1.13	0.64	1.47	0.92
FeO	--	--	--	--	--	--	--	--	--	--
MnO	0.18	0.04	0.05	0.03	<0.01	0.01	0.02	0.05	<0.01	0.02
MgO	0.40	0.66	0.35	0.71	0.16	0.08	0.17	0.62	0.24	0.09
CaO	0.79	0.79	0.51	0.62	0.12	0.11	0.16	1.76	0.23	0.17
Na <sub>2</sub> O	1.66	1.59	2.07	1.86	0.06	0.01	0.33	0.75	0.22	1.12
K <sub>2</sub> O	5.00	4.02	4.87	4.96	1.04	0.10	8.33	2.24	0.58	4.43
P <sub>2</sub> O <sub>5</sub>	0.01	0.02	0.01	0.01	0.03	0.04	0.01	0.02	0.03	0.01
LOI	5.45	5.72	6.00	4.96	10.26	7.60	1.31	6.41	5.34	2.01
TOTAL	100.09	99.77	99.84	100.20	100.99	100.89	99.76	100.29	99.87	99.71
As	1.4	--	--	1.1	--	--	--	--	--	--
Ba	270	125	43	28	70	106	68	344	67	178
Br	2.7	--	--	2.2	--	--	--	--	--	--
Cl(%)	--	--	--	--	--	--	--	--	--	--
Cr	3*	<10	<10	<10	<10	<10	11	<10	<10	<10
Cs	19.1	--	--	14.6	--	--	--	--	--	--
F(%)	--	--	--	--	--	--	--	--	--	--
Ga	19	19	19	19	47	16	16	16	19	17
Hf	9.0	--	--	11.0	--	--	--	--	--	--
Mo	--	--	--	3	--	--	--	--	--	--
Nb	36	34	40	36	35	27	30	28	35	31
Ni	<5*	15	<5	<5	<5	<5	<5	7	7	<5
Pb	34	26	31	29	54	24	29	57	15	24
Rb	309	250	290	329	<1	<1	228	96	11	145
Sb	0.3	--	--	0.2	--	--	--	--	--	--
Sc	3.7	--	--	3.5	--	--	--	--	--	--
Se	<3.0	--	--	<1.5	--	--	--	--	--	--
Sn	9	7	9	9	6	6	<5	5	7	9
Sr	86	102	31	28	140	63	19	1089	34	18
Ta	2.8	--	--	2.8	--	--	--	--	--	--
Th	26	24	27	27	12	23	14	12	29	23
U	10*	<3	<3	7*	<3	<3	<3	<3	<3	<3
V	6	11	<3	<3	9	<3	12	8	12	<3
Y	102	226	104	126	9	16	58	100	190	41
Zn	85	145	85	100	11	14	31	23	32	31
Zr	226	214	231	290	206	169	176	132	213	226
La	54	--	--	58	--	--	--	--	--	--
Ce	128	--	--	123	--	--	--	--	--	--
Nd	44	--	--	55	--	--	--	--	--	--
Sm	11.4	--	--	12.9	--	--	--	--	--	--
Eu	0.53	--	--	0.49	--	--	--	--	--	--
Tb	2.3	--	--	2.6	--	--	--	--	--	--
Yb	9.2	--	--	11.0	--	--	--	--	--	--
Lu	1.52	--	--	1.82	--	--	--	--	--	--

SAMPLE	Tkm	Tkm	Tdp	Tdp	Tdp	Tdp	Tdp	Tdp	Tdp	Thc
	89	91	56	219	220	230	55	195	54	231
SiO <sub>2</sub>	82.80	95.99	73.93	75.02	75.42	75.44	76.41	76.50	79.27	70.91
TiO <sub>2</sub>	0.13	0.07	0.18	0.16	0.16	0.16	0.18	0.10	0.16	0.27
Al <sub>2</sub> O <sub>3</sub>	11.14	0.29	11.74	11.82	11.89	11.43	12.09	11.94	10.33	13.84
Fe <sub>2</sub> O <sub>3</sub>	0.35	0.27	1.66	1.79	1.85	1.88	1.65	1.17	1.59	1.65
FeO	--	--	--	--	--	--	--	--	--	--
MnO	<0.01	<0.01	0.05	0.06	0.04	0.04	0.03	0.06	0.03	0.06
MgO	0.12	0.15	0.31	0.25	0.20	0.60	0.16	<0.01	0.36	0.53
CaO	0.17	0.03	0.24	0.15	0.15	0.45	0.23	0.17	0.15	1.36
Na <sub>2</sub> O	0.05	0.02	2.62	3.34	3.57	3.29	3.64	2.98	2.93	3.67
K <sub>2</sub> O	0.07	0.03	6.03	4.89	5.17	5.63	5.27	6.09	4.68	4.70
P <sub>2</sub> O <sub>5</sub>	0.01	<0.01	0.01	0.02	0.02	0.21	0.02	0.02	0.03	0.07
LOI	5.22	3.16	3.62	0.99	0.88	1.04	0.58	0.57	0.76	2.51
TOTAL	100.05	100.00	100.39	98.49	99.35	100.17	100.26	99.59	100.29	99.57
As	--	--	--	<1.4	--	--	1.3	--	--	--
Ba	29	16	<16	24	32	27	<16	19	<16	840
Br	--	--	--	<0.6	--	--	<0.5	--	--	--
Cl(%)	--	--	--	--	--	--	--	--	--	--
Cr	16	11	<10	<6*	25	19	<16*	<10	<10	28
Cs	--	--	--	12.3	--	--	2.5	--	--	--
F(%)	--	--	--	--	--	--	--	--	--	--
Ga	16	<3	18	20	21	--	19	22	17	--
Hf	--	--	--	3.0	--	--	12.2	--	--	--
Mo	--	2	--	--	--	--	2	--	--	--
Nb	30	17	33	33	34	31	32	43	29	17
Ni	<5	<5	<5	<5	6	--	<5	<5	<5	--
Pb	25	7	35	20	29	17	30	32	41	24
Rb	<1	<1	255	228	239	257	223	407	178	226
Sb	--	--	--	<0.1	--	--	0.14	--	--	--
Sc	--	--	--	4.7	--	--	4.8	--	--	--
Se	--	--	--	<0.2	--	--	<1.5	--	--	--
Sn	8	7	7	5	6	<5	9	<5	9	<5
Sr	20	4	4	7	7	26	4	5	8	195
Ta	--	--	--	2.8	--	--	2.5	--	--	--
Th	16	3	28	26*	--	29	25	--	24	20
U	<3	<3	<3	6*	--	5	6*	--	<3	3
V	<3	<3	<3	<3	<3	<3	<3	<3	<3	7
Y	26	8	133	76	103	101	124	134	95	40
Zn	13	13	82	56	74	--	73	58	65	--
Zr	248	127	354	372	383	315	256	178	312	245
La	--	--	--	53	--	--	122	--	--	--
Ce	--	--	--	161	--	--	213	--	--	--
Nd	--	--	--	59	--	--	115	--	--	--
Sm	--	--	--	12.2	--	--	21.9	--	--	--
Eu	--	--	--	0.67	--	--	0.96	--	--	--
Tb	--	--	--	2.1	--	--	3.4	--	--	--
Yb	--	--	--	7.9	--	--	10.0	--	--	--
Lu	--	--	--	1.23	--	--	1.49	--	--	--



SAMPLE	Thc	Twc	Twc	Tkt	Tlj	Tlj	Tlj	Tlj	Tlj	Tlj
	259	260	232	218	176	72	71	76	75	177
SiO <sub>2</sub>	73.83	69.20	70.31	73.71	70.16	70.27	70.64	71.50	72.20	72.42
TiO <sub>2</sub>	0.12	0.35	0.41	0.19	0.38	0.44	0.44	0.30	0.33	0.35
Al <sub>2</sub> O <sub>3</sub>	12.34	14.23	15.13	12.58	14.34	14.65	14.84	13.77	14.01	13.51
Fe <sub>2</sub> O <sub>3</sub>	0.94	2.00	2.30	1.26	2.07	2.14	2.09	1.12	2.01	1.87
FeO	--	--	--	--	--	--	--	--	--	--
MnO	0.04	0.07	0.06	0.06	0.07	0.07	0.06	0.02	0.06	0.07
MgO	0.29	0.71	0.55	0.55	0.17	0.34	0.26	0.31	0.25	0.11
CaO	0.86	1.62	1.66	0.84	0.67	0.50	0.37	0.23	0.37	0.61
Na <sub>2</sub> O	3.44	4.10	4.33	3.28	4.27	4.50	4.51	3.63	3.92	4.34
K <sub>2</sub> O	4.28	4.32	4.46	4.91	5.95	5.88	5.83	5.35	5.07	5.41
P <sub>2</sub> O <sub>5</sub>	0.02	0.10	0.10	0.03	0.05	0.05	0.05	0.03	0.01	0.06
LOI	4.46	3.74	0.91	3.25	1.80	0.82	0.76	1.51	1.25	0.66
TOTAL	100.62	100.44	100.22	100.66	99.93	99.66	99.85	97.79	99.48	99.41
As	0.6	0.5	--	3.8	--	--	--	--	--	--
BA	681	913	981	101	75	67	107	54	115	109
Br	2.8	2.9	--	0.5	--	--	--	--	--	--
Cl(%)	--	--	--	--	--	--	--	--	--	--
Cr	<1*	<1*	<10	<3*	<10	<10	<10	<10	<10	<10
Cs	5.1	2.8	--	6.4	--	--	--	--	--	--
F(%)	--	--	--	--	--	--	--	--	--	--
Ga	--	--	--	18	20	20	20	20	20	20
Hf	3.3	7.4	--	6.4	--	--	--	--	--	--
Mo	2	2	--	3	--	--	--	--	--	--
Nb	15	17	17	21	30	28	28	33	30	26
Ni	<33*	<15*	--	<5	8	<5	<5	<5	12	6
Pb	27	23	21	30	32	23	25	32	15	25
Rb	222	141	146	236	159	147	141	160	159	138
Sb	0.2	0.1	--	0.5	--	--	--	--	--	--
Sc	2.3	2.8	--	3.0	--	--	--	--	--	--
Se	<1.2	<0.4	--	<0.3	--	--	--	--	--	--
Sn	<5	<5	<5	<5	7	<5	<5	<5	5	6
Sr	73	250	270	67	30	25	84	26	46	33
Ta	1.6	1.4	--	1.7	--	--	--	--	--	--
Th	24	16	16	27*	25	24	24	28	26	26
U	6*	4*	<3	6*	<3	<3	<3	<3	<3	3
V	<3	11	14	7	<3	9	8	5	10	8
Y	39	39	39	38	68	71	56	61	48	59
Zn	--	--	--	36	76	72	66	51	42	64
Zr	116	282	315	175	540	587	578	428	407	504
La	40	46	--	40	--	--	--	--	--	--
Ce	80	96	--	76	--	--	--	--	--	--
Nd	27	37	--	21	--	--	--	--	--	--
Sm	5.1	6.3	--	3.5	--	--	--	--	--	--
Eu	0.62	1.15	--	0.31	--	--	--	--	--	--
Tb	0.9	0.9	--	0.6	--	--	--	--	--	--
Yb	3.4	3.5	--	3.6	--	--	--	--	--	--
Lu	0.55	0.58	--	0.63	--	--	--	--	--	--







SAMPLE	Ttng 144	Ttng 140	Ttng 142	Ttng 143	Ttng 141	Ttng 137	Ttng 147	Ttng 146	Ttng 138	Ttng 196
SiO <sub>2</sub>	76.45	76.91	77.05	77.15	77.49	78.37	81.57	93.58	98.63	15.07
TiO <sub>2</sub>	0.11	0.12	0.12	0.12	0.12	0.13	0.12	0.11	<0.01	<0.01
Al <sub>2</sub> O <sub>3</sub>	9.60	11.81	11.72	11.70	11.75	9.90	9.29	2.98	0.23	0.26
Fe <sub>2</sub> O <sub>3</sub>	1.19	0.67	0.52	1.23	0.83	0.88	1.48	0.60	0.07	0.19
FeO	--	0.46	0.60	--	0.24	--	--	--	--	--
MnO	0.02	0.05	0.05	0.03	0.06	0.04	0.02	0.01	<0.01	<0.01
MgO	0.18	0.17	0.28	0.16	0.14	0.17	0.19	0.11	0.07	0.88
CaO	4.42	0.22	0.46	0.26	0.22	0.33	0.16	0.21	0.01	41.13
Na <sub>2</sub> O	0.39	3.45	3.16	3.23	3.38	2.64	0.59	0.06	<0.01	0.23
K <sub>2</sub> O	3.18	4.82	4.71	4.86	4.80	3.72	3.90	0.22	0.03	0.11
P <sub>2</sub> O <sub>5</sub>	0.02	0.02	0.02	0.01	0.02	0.01	0.01	0.01	0.01	0.08
LOI	3.26	0.43	0.84	0.50	0.30	2.90	1.27	1.38	0.27	4.49
TOTAL	99.82	99.13	99.53	99.25	99.35	99.09	98.60	99.27	99.33	63.31
As	--	4.3	10.0	16.4	<1.6	--	--	125.0	1.6	--
Ba	72	37	33	29	28	<16	44	67	<16	40
Br	--	--	--	--	--	--	--	--	--	--
Cl(%)	--	0.006	0.005	0.002	0.004	--	--	0.003	0.001	--
Cr	17	<10	<7	<10	11	11	<10	<10	<8*	10
Cs	--	7.1	5.0	5.7	6.9	--	--	10.5	0.8	--
F(%)	--	0.16	0.17	0.06	0.08	--	--	0.48	0.20	39.04
Ga	18	19	19	20	20	17	19	7	<3	4
Hf	--	7.8	7.1	7.2	7.3	--	--	6.7	3.0	--
Mo	--	3	3	--	--	--	--	--	--	--
Nb	33	34	33	35	34	41	32	25	1	5
Ni	10	12	<5	<5	12	<5	<5	5	17	6
Pb	57	16	26	24	16	28	60	52	4	7
Rb	164	290	288	293	288	285	351	9	<1	15
Sb	--	0.1	0.4	0.6	0.1	--	--	26.4	0.7	--
Sc	--	2.9	2.6	2.4	2.6	--	--	0.8	0.5	--
Se	--	0.5	0.4	0.5	0.5	--	--	0.5	0.5	--
Sn	45	<5	6	6	<5	11	13	17	8	<5
Sr	50	6	9	7	6	3	10	15	<1	193
Ta	--	4.2	3.7	4.0	4.1	--	--	3.8	4.2	--
Th	33	32	30	31	32	32	28	39	<3	--
U	7	8*	7*	10*	8*	6	8	22*	4*	--
V	13	9	16	3	<3	<3	7	7	<3	<3
Y	96	150	94	64	99	105	43	48	6	177
Zn	186	32	42	31	48	58	53	96	11	23
Zr	162	172	160	168	170	181	164	156	85	<2
La	--	58	48	47	51	--	--	51	1	--
Ce	--	125	110	110	116	--	--	79	4	--
Nd	--	56	40	47	44	--	--	54	<8	--
Sm	--	15.7	10.3	10.0	11.8	--	--	10.8	0.4	--
Eu	--	0.38	0.33	0.33	0.33	--	--	0.19	<0.01	--
Tb	--	2.6	1.8	1.5	2.0	--	--	1.4	<0.1	--
Yb	--	16.3	10.8	9.5	11.5	--	--	5.7	1.1	--
Lu	--	2.35	1.57	1.21	1.56	--	--	0.81	0.18	--

SAMPLE	Ttnng	Ttnng	Ttbp	Ttbp	Ttbp	Ttbp	Ttbp	Ttbp	Ttpb	Ttbp
	136	236	149	224	131	227	150	151	132	152
SiO <sub>2</sub>	77.24	77.25	74.54	75.91	76.26	76.22	76.35	76.46	76.57	76.59
TiO <sub>2</sub>	0.08	0.11	0.09	0.11	0.08	0.10	0.09	0.08	0.08	0.08
Al <sub>2</sub> O <sub>3</sub>	12.53	11.98	12.05	12.17	12.55	12.41	12.44	12.36	12.41	12.25
Fe <sub>2</sub> O <sub>3</sub>	0.84	1.13	1.13	1.15	1.24	1.13	1.21	0.99	1.11	0.78
FeO	0.29	--	--	--	--	--	--	0.15	--	0.38
MnO	0.06	0.05	0.06	0.03	0.05	0.04	0.07	0.06	0.05	0.07
MgO	0.15	0.18	0.13	0.06	0.15	<0.01	0.16	0.21	0.13	0.16
CaO	0.19	0.23	0.40	0.26	0.53	0.18	0.16	0.18	0.36	0.44
Na <sub>2</sub> O	3.76	3.72	3.74	3.57	3.69	4.27	3.66	3.51	3.85	3.77
K <sub>2</sub> O	4.89	4.87	4.69	4.80	4.92	4.75	4.85	4.79	4.89	4.81
P <sub>2</sub> O <sub>5</sub>	0.02	0.01	0.01	0.02	0.01	0.02	0.01	0.01	0.01	0.01
LOI	0.38	0.36	2.36	0.37	0.50	0.94	0.41	0.65	0.60	0.46
TOTAL	100.43	99.89	99.20	98.45	99.98	100.05	99.41	99.45	100.06	99.80
As	<1.3	--	2.4	3.5	4.1	--	--	2.0	20.1	<1.5
Ba	19	19	19	<16	<16	16	<16	<16	<16	<16
Br	0.15	--	--	<0.4	--	--	--	--	--	--
Cl(%)	0.002	--	0.003	--	0.002	--	0.003	--	0.003	0.002
Cr	<7*	23	14	<2*	<10	11	19	13	<10	12
Cs	4.7	--	10.3	4.0	6.8	--	--	6.4	16.0	8.3
F(%)	0.07	--	0.20	--	0.26	--	0.14	--	0.12	0.15
Ga	22	--	22	21	22	23	23	23	22	22
Hf	7.4	--	7.9	8.0	8.0	--	--	8.7	3.8	7.8
Mo	4	--	5	--	--	--	--	5	--	3
Nb	46	45	47	47	44	49	43	47	44	41
Ni	<5	--	<5	<5	7	<5	<5	<5	<5	<5
Pb	26	29	36	40	32	33	19	33	24	30
Rb	376	357	360	379	416	372	414	415	464	420
Sb	<0.1	--	0.4	0.1	0.1	--	--	0.1	0.1	0.2
Sc	2.6	--	2.4	2.0	2.4	--	--	2.3	2.3	2.2
Se	0.6	--	0.6	<0.8	0.6	--	--	0.6	0.4	0.6
Sn	<5	7	11	5	<5	<5	<5	<5	27	<5
Sr	2	2	2	6	3	2	2	4	2	2
Ta	5.4	--	4.8	4.6	4.7	--	--	4.6	3	4.7
Th	37	41	41	36*	43	--	37	41	44	39
U	7*	6	14*	7*	11*	--	7	9*	9*	8*
V	<3	4	<3	14	8	10	<3	<3	<3	<3
Y	73	57	131	100	156	94	35	28	117	164
Zn	52	--	73	69	35	33	33	48	42	56
Zr	158	160	168	173	158	182	157	159	155	158
La	31	--	40	35	46	--	--	15	40	44
Ce	97	--	98	123	109	--	--	103	61	98
Nd	27	--	37	37	49	--	--	10	38	45
Sm	7.8	--	11.6	9.3	13.2	--	--	3.1	10.7	13.2
Eu	0.20	--	0.17	0.16	0.18	--	--	0.14	1.50	0.12
Tb	1.4	--	2.3	2.1	2.9	--	--	0.6	1.2	2.9
Yb	9.9	--	13.8	10.5	19.9	--	--	4.9	15.2	18.5
Lu	1.27	--	1.94	1.65	2.64	--	--	0.70	1.91	<2.50

SAMPLE	Ttbp	Ttbp	Ttbp	Ttbp	Ttnpc	Ttnpc	Ttnpc	Ttac	Ttac	Ttac
	226	225	221	179	222	153	223	216	213	214
SiO <sub>2</sub>	76.72	76.80	77.33	78.15	75.88	76.00	76.53	74.09	76.02	76.93
TiO <sub>2</sub>	0.11	0.11	0.11	0.09	0.11	0.08	0.11	0.11	0.10	0.10
Al <sub>2</sub> O <sub>3</sub>	12.23	12.13	11.55	11.17	11.97	12.26	12.33	11.93	12.33	12.03
Fe <sub>2</sub> O <sub>3</sub>	1.16	1.21	1.13	1.11	1.03	1.14	1.17	1.12	1.13	1.15
FeO	--	--	--	--	--	--	--	--	--	--
MnO	0.07	0.05	0.05	0.06	0.04	0.06	0.05	0.07	0.05	0.07
MgO	0.01	0.05	0.02	<0.01	0.06	0.15	<0.01	0.21	0.07	<0.01
CaO	0.21	0.24	0.22	0.23	0.42	0.37	0.18	0.44	0.19	0.17
Na <sub>2</sub> O	3.32	3.55	3.40	3.39	3.62	3.46	3.55	3.95	4.71	3.58
K <sub>2</sub> O	4.95	4.87	4.79	4.69	4.73	5.02	4.82	4.46	4.87	4.79
P <sub>2</sub> O <sub>5</sub>	0.02	0.02	0.02	0.02	0.01	0.01	0.02	0.01	0.01	0.02
LOI	0.67	0.57	0.32	0.70	0.31	0.98	0.69	2.50	0.54	0.49
TOTAL	99.47	99.60	98.94	99.60	98.18	99.53	99.44	98.89	100.02	99.32
As	--	--	--	--	--	--	1.9	--	--	--
Ba	30	<16	<16	35	17	34	29	19	36	35
Br	--	--	--	--	--	--	<0.3	--	--	--
Cl(%)	--	--	--	--	--	--	--	--	--	--
Cr	16	12	<10	<10	23	20	<1*	28	24	25
Cs	--	--	--	--	--	--	8.2	--	--	--
F(%)	--	--	--	--	--	--	--	--	--	--
Ga	23	21	23	22	22	23	22	23	19	22
Hf	--	--	--	--	--	--	8.2	--	--	--
Mo	--	--	--	--	--	--	--	--	--	--
Nb	50	49	45	45	45	49	49	49	50	49
Ni	5	<5	<5	<5	<5	<5	<5	5	<5	<5
Pb	39	35	24	135	27	39	26	34	39	23
Rb	380	391	362	332	373	397	375	326	370	362
Sb	--	--	--	--	--	--	0.1	--	--	--
Sc	--	--	--	--	--	--	2.1	--	--	--
Se	--	--	--	--	--	--	<0.4	--	--	--
Sn	8	<5	<5	<5	6	11	<5	8	5	<5
Sr	4	5	4	13	1	10	5	5	4	2
Ta	--	--	--	--	--	--	4.4	--	--	--
Th	--	--	--	41	--	38	34*	--	--	--
U	--	--	--	6	--	6	5*	--	--	--
V	6	<3	<3	24	<3	<3	12	6	21	<3
Y	113	52	114	147	138	67	69	138	54	97
Zn	56	48	106	269	33	173	37	68	27	37
Zr	185	178	174	152	176	159	177	180	185	169
La	--	--	--	--	--	--	26	--	--	--
Ce	--	--	--	--	--	--	122	--	--	--
Nd	--	--	--	--	--	--	25	--	--	--
Sm	--	--	--	--	--	--	7.1	--	--	--
Eu	--	--	--	--	--	--	0.21	--	--	--
Tb	--	--	--	--	--	--	1.7	--	--	--
Yb	--	--	--	--	--	--	8.6	--	--	--
Lu	--	--	--	--	--	--	1.34	--	--	--



SAMPLE	Tttc	Tttc	Tttc	Tttc	Tttc	Tttc	Tttc	Tttc	Tttc	Ttkm
	10	165	9	163	11	164	233	253	158	7
SiO <sub>2</sub>	76.57	76.58	76.82	77.83	77.84	77.89	78.02	78.21	88.38	48.45
TiO <sub>2</sub>	0.17	0.15	0.16	0.12	0.15	0.03	0.16	0.14	<0.01	0.10
Al <sub>2</sub> O <sub>3</sub>	12.25	12.23	11.37	10.11	11.04	11.66	11.66	11.48	0.13	7.20
Fe <sub>2</sub> O <sub>3</sub>	1.14	1.18	1.03	1.20	1.02	1.11	1.06	0.85	0.05	0.67
FeO	--	--	--	--	--	--	--	--	--	--
MnO	0.07	0.06	0.06	0.06	0.07	0.06	0.07	0.06	<0.01	0.03
MgO	0.18	0.22	0.34	0.17	0.24	0.16	0.45	0.78	0.15	0.39
CaO	0.30	0.27	0.46	1.62	0.45	0.46	0.32	0.55	7.19	21.74
Na <sub>2</sub> O	3.50	3.41	3.64	2.81	2.85	3.46	3.58	2.49	0.16	2.22
K <sub>2</sub> O	5.19	5.07	4.80	4.20	4.93	4.74	4.79	4.63	0.04	3.14
P <sub>2</sub> O <sub>5</sub>	0.01	0.02	0.02	0.02	0.01	0.02	0.02	0.02	0.01	0.03
LOI	0.34	0.40	0.48	1.14	1.00	0.65	0.37	1.89	2.90	16.50
TOTAL	99.72	99.59	99.18	99.28	99.60	100.34	100.50	101.10	99.02	100.47
As	--	7.7	--	1.8	--	--	--	--	--	--
Ba	81	58	67	101	80	64	119	68	<16	37
Br	--	--	--	--	--	--	--	--	--	--
Cl(%)	--	0.004	--	0.004	--	0.001	--	--	--	--
Cr	<10	17	<6	17	<10	17	14	13	13	<10
Cs	--	10.6	6.8	6.9	--	--	--	--	--	--
F(%)	--	0.08	0.15	0.63	--	0.15	--	--	--	--
Ga	21	17	19	18	19	17	--	--	4	12
Hf	--	7.3	6.7	5.9	--	--	--	--	--	--
Mo	--	--	--	--	--	--	--	--	--	--
Nb	40	39	36	28	39	33	38	34	2	27
Ni	<5	9	<5	32	<5	15	--	--	16	<5
Pb	21	21	22	18	37	17	27	28	8	19
Rb	266	268	247	227	285	245	246	234	<1	168
Sb	--	1.1	<0.1	0.6	--	--	--	--	--	--
Sc	--	3.4	3.2	2.8	--	--	--	--	--	--
Se	--	0.5	0.7	0.4	--	--	--	--	--	--
Sn	<5	112	<5	109	5	9	<5	<5	<5	<5
Sr	12	13	55	103	21	11	13	41	17	18
Ta	--	3.9	5.4	3.3	--	--	--	--	--	--
Th	33	31	30	26	31	29	33	28	<3	18
U	<3	7*	9*	14*	<3	3	3	5	47	<3
V	<3	<3	<3	<3	<3	<3	20	24	<3	7
Y	95	108	101	97	109	91	93	173	76	82
Zn	48	29	37	30	75	34	--	--	10	41
Zr	176	161	151	139	158	146	161	147	11	98
La	--	55	45	42	--	--	--	--	--	--
Ce	--	125	106	98	--	--	--	--	--	--
Nd	--	56	41	44	--	--	--	--	--	--
Sm	--	13.1	10.1	9.4	--	--	--	--	--	--
Eu	--	0.47	0.40	0.37	--	--	--	--	--	--
Tb	--	2.3	1.9	1.9	--	--	--	--	--	--
Yb	--	11.1	10.3	9.8	--	--	--	--	--	--
Lu	--	1.59	1.32	1.16	--	--	--	--	--	--



SAMPLE	Ttkm 167	Ttkm 4	Ttkm 264	Ttkm 168	Ttkm 268	Ttkm 263	Ttkm 265	Ttkm 262	Ttkm 3	Ttkm 267
SiO <sub>2</sub>	75.67	75.98	76.04	76.27	76.33	76.33	76.40	76.50	76.72	76.73
TiO <sub>2</sub>	0.13	0.15	0.13	0.12	0.12	0.12	0.13	0.13	0.15	0.13
Al <sub>2</sub> O <sub>3</sub>	12.56	12.00	12.07	12.12	11.64	12.71	12.04	12.14	12.23	12.01
Fe <sub>2</sub> O <sub>3</sub>	1.14	1.04	1.03	1.19	1.10	1.16	1.06	1.04	1.38	1.11
FeO	--	--	--	--	--	--	--	--	--	--
MnO	0.05	0.06	0.06	0.06	0.06	0.07	0.06	0.06	0.09	0.06
MgO	0.32	0.23	0.21	0.17	0.17	0.32	0.23	0.18	0.26	0.22
CaO	0.33	0.36	0.27	0.34	0.38	0.31	0.31	0.26	0.17	0.39
Na <sub>2</sub> O	3.29	3.67	3.41	3.43	3.53	3.56	3.40	3.44	3.69	3.43
K <sub>2</sub> O	5.33	5.22	4.84	4.96	4.74	4.97	4.84	4.99	5.24	4.96
P <sub>2</sub> O <sub>5</sub>	0.01	0.01	0.02	0.02	0.01	0.02	0.01	0.02	0.02	0.01
LOI <sup>5</sup>	0.76	0.49	0.42	0.48	0.35	0.42	0.31	0.42	0.67	0.48
TOTAL	99.59	99.21	98.50	99.16	99.43	99.99	98.79	99.18	100.62	99.53
As	3.3	--	--	10.8	--	--	--	--	--	--
Ba	66	64	61	45	36	50	53	47	55	52
Br	--	--	--	--	--	--	--	--	--	--
Cl(%)	0.005	--	--	0.003	0.003	--	0.003	0.003	--	--
Cr	<10	<10	<10	<8*	<10	<10	<10	<10	11	21
Cs	4.0	--	--	9.4	--	--	--	--	--	--
F(%)	0.08	--	--	0.07	0.31	--	0.09	0.06	--	--
Ga	19	22	19	21	18	22	20	21	20	20
Hf	7.4	--	--	6.8	--	--	--	--	--	--
Mo	--	--	--	--	--	--	--	--	2	--
Nb	44	41	42	39	40	43	43	42	41	39
Ni	<5	<5	22	15	5	13	14	6	11	10
Pb	43	25	25	35	20	23	23	25	96	17
Rb	300	290	301	311	268	308	294	304	337	274
Sb	0.2	--	--	0.4	--	--	--	--	--	--
Sc	3.0	--	--	3.3	--	--	--	--	--	--
Se	0.6	--	--	0.9	--	--	--	--	--	--
Sn	7	5	5	37	<5	8	<5	38	1597	6
Sr	21	11	9	9	10	12	12	8	18	14
Ta	4.6	--	--	6.8	--	--	--	--	--	--
Th	36	34	34	31	32	33	35	34	29	30
U	17*	<3	5	9*	4	5	5	6	<3	4
V	6	4	<3	<3	<3	3	<3	<3	7	<3
Y	105	60	73	113	101	79	61	63	146	95
Zn	40	35	46	40	50	46	58	45	43	47
Zr	158	155	153	154	157	152	159	159	151	154
La	41	--	--	43	--	--	--	--	--	--
Ce	107	--	--	102	--	--	--	--	--	--
Nd	41	--	--	38	--	--	--	--	--	--
Sm	10.1	--	--	11.3	--	--	--	--	--	--
Eu	0.32	--	--	0.35	--	--	--	--	--	--
Tb	2.2	--	--	2.0	--	--	--	--	--	--
YB	13.0	--	--	12.5	--	--	--	--	--	--
Lu	1.74	--	--	1.63	--	--	--	--	--	--

SAMPLE	Ttkm	Ttkm	Ttkm	Ttkm	Ttkm	Ttkm	Ttkm	Ttip	Ttip	Ttip
	266	2	8	254	255	6	1	211	207	206
SiO <sub>2</sub>	76.85	76.97	77.22	77.43	77.60	77.64	77.84	76.26	76.39	76.40
TiO <sub>2</sub>	0.12	0.15	0.16	0.16	0.16	0.15	0.14	0.14	0.11	0.11
Al <sub>2</sub> O <sub>3</sub>	12.04	12.03	11.84	12.22	11.88	12.59	11.71	11.57	11.95	11.87
Fe <sub>2</sub> O <sub>3</sub>	1.06	1.01	1.10	1.15	1.30	1.10	1.06	1.23	1.17	1.07
FeO	--	--	--	--	--	--	--	--	--	--
MnO	0.08	0.05	0.05	0.11	0.06	0.07	0.05	0.06	0.05	0.04
MgO	0.20	0.34	0.22	0.28	0.32	0.07	0.20	<0.01	0.02	0.01
CaO	0.35	0.25	0.30	0.34	0.33	0.30	0.26	0.55	0.23	0.25
Na <sub>2</sub> O	3.36	3.69	3.64	3.13	3.22	3.58	3.42	3.39	3.66	3.63
K <sub>2</sub> O	4.84	5.24	4.94	5.45	4.71	5.06	5.14	4.90	4.87	4.84
P <sub>2</sub> O <sub>5</sub>	0.02	0.03	0.01	0.02	0.03	0.01	0.01	0.02	0.01	0.01
LOI	0.60	0.12	0.31	0.77	0.85	0.39	0.15	0.33	0.26	0.21
TOTAL	99.52	99.88	99.79	101.06	100.46	100.96	99.98	98.44	98.72	98.44
As	--	--	--	--	--	--	7.0	--	1.4	--
Ba	60	61	55	107	63	100	69	39	19	<16
Br	--	--	--	--	--	--	--	--	<0.1	--
Cl(%)	--	--	--	--	--	--	--	--	--	--
Cr	68	<10	<10	23	21	18	<10	13	<0.5*	<10
Cs	--	--	--	--	--	--	4.5	--	3.5	--
F(%)	--	--	--	--	--	--	--	--	--	--
Ga	21	20	19	--	--	19	20	19	21	20
Hf	--	--	--	--	--	--	7.2	--	7.8	--
Mo	--	--	--	--	--	--	3	--	--	--
Nb	45	39	37	39	42	39	44	35	50	42
Ni	6	<5	<5	--	--	<5	<5	8	<5	<5
Pb	16	23	26	32	29	25	27	27	28	32
Rb	301	280	257	263	278	268	294	311	392	380
Sb	--	--	--	--	--	--	0.31	--	0.2	--
Sc	--	--	--	--	--	--	3.2	--	1.8	--
Se	--	--	--	--	--	--	0.60	--	<2.1	--
Sn	10	<5	<5	6	<5	<5	9	<5	5	<5
Sr	12	9	11	18	13	12	10	7	3	3
Ta	--	--	--	--	--	--	--	--	4.5	--
Th	35	30	30	36	35	33	33	--	35*	--
U	5	<3	<3	4	5	3	10*	--	6*	--
V	<3	67	6	9	3	<3	44	7	<3	8
Y	91	116	77	95	73	86	114	131	58	78
Zn	78	27	42	--	--	44	42	33	28	34
Zr	159	158	156	167	155	161	162	189	173	178
La	--	--	--	--	--	--	41	--	26	--
Ce	--	--	--	--	--	--	103	--	71	--
Nd	--	--	--	--	--	--	47	--	18	--
Sm	--	--	--	--	--	--	10.3	--	5.1	--
Eu	--	--	--	--	--	--	0.33	--	0.17	--
Tb	--	--	--	--	--	--	2.2	--	1.0	--
Yb	--	--	--	--	--	--	11.9	--	6.1	--
Lu	--	--	--	--	--	--	1.52	--	0.99	--



SAMPLE	Ttip	Ttip	Ttuff	Ttuff	Ttuff	Ttuff	Ttuff	Ttuff	Ttuff	Ttuff
	205	208	228	192	191	190	188	178	12	235
SiO <sub>2</sub>	76.67	77.10	69.51	71.64	71.65	73.72	74.13	74.32	75.18	75.19
TiO <sub>2</sub>	0.10	0.14	0.26	0.10	0.09	0.09	0.08	0.09	0.18	0.14
Al <sub>2</sub> O <sub>3</sub>	12.00	11.39	13.54	12.56	12.83	12.23	11.84	11.98	10.76	12.02
Fe <sub>2</sub> O <sub>3</sub>	1.21	1.22	1.75	1.20	0.81	0.56	1.10	1.18	1.17	1.31
FeO	--	--	--	--	0.41	0.55	--	--	--	--
MnO	0.05	0.04	0.06	0.06	0.06	0.07	0.07	0.06	0.06	0.04
MgO	<0.01	0.07	0.42	0.75	1.07	0.27	<0.01	<0.01	0.54	0.47
CaO	0.17	0.17	0.45	0.86	0.73	0.51	0.53	0.45	1.48	0.49
Na <sub>2</sub> O	3.82	3.12	1.73	2.49	2.74	3.34	3.23	3.14	1.43	2.82
K <sub>2</sub> O	4.90	4.92	5.20	4.28	4.45	4.95	4.85	5.31	4.58	4.45
P <sub>2</sub> O <sub>5</sub>	0.01	0.03	0.02	0.01	0.01	0.01	0.01	0.01	0.02	0.02
LOI	0.04	0.58	6.35	5.27	4.92	3.63	3.67	3.20	2.88	2.74
TOTAL	98.97	98.78	99.29	99.22	99.77	99.93	99.50	99.73	98.28	99.69
As	6.8	--	--	--	5.7	3.5	--	--	--	--
Ba	31	42	64	68	<16	<16	<16	21	135	74
Br	0.2	--	--	--	3.1	3.6	--	--	--	--
Cl(%)	--	--	--	--	--	0.005	--	--	--	--
Cr	<3*	10	30	<10	<1*	<1*	<10	27	28	16
Cs	8.2	--	--	--	9.8	10.6	--	--	--	--
F(%)	--	--	--	--	--	0.20	--	--	--	--
Ga	21	20	22	23	25	24	24	22	15	--
Hf	7.9	--	--	--	8.6	8.4	--	--	--	--
Mo	--	--	--	--	--	--	--	--	--	--
Nb	48	35	36	49	54	52	49	48	35	41
Ni	8	5	10	<5	6	<5	<5	<5	21	--
PB	28	61	38	29	35	34	35	38	15	28
Rb	393	304	258	347	320	373	388	383	246	333
Sb	0.1	--	--	--	0.4	0.4	--	--	--	--
Sc	1.9	--	--	--	2.0	1.9	--	--	--	--
Se	<1.2	--	--	--	<1.5	<1.5	--	--	--	--
Sn	<5	51	6	9	12	11	14	10	15	63
Sr	3	9	23	59	43	15	5	5	1155	18
Ta	4.6	--	--	--	4.6	4.6	--	--	--	--
Th	37*	--	39	35	37*	36*	39	47	24	37
U	9*	--	5	6	12*	13*	10	10	<3	7
V	18	10	12	<3	12	<3	<3	<3	5	6
Y	111	116	128	114	152	149	142	144	111	115
Zn	39	139	88	87	83	79	78	74	46	--
Zr	176	200	249	165	186	183	155	162	147	161
La	48	--	--	--	41	43	--	--	--	--
Ce	114	--	--	--	101	100	--	--	--	--
Nd	42	--	--	--	40	42	--	--	--	--
Sm	12.0	--	--	--	11.6	11.2	--	--	--	--
Eu	0.26	--	--	--	0.14	0.14	--	--	--	--
Tb	2.4	--	--	--	3.0	2.8	--	--	--	--
Yb	13.1	--	--	--	14.6	14.0	--	--	--	--
Lu	2.17	--	--	--	2.41	2.32	--	--	--	--

SAMPLE	Ttuff	Ttuff	Ttuff	Ttuff	Tgc	Tbc	Tbc	Tbc	Tbc	Tbc
	154	189	13	14	209	15	18	17	16	202
SiO <sub>2</sub>	75.26	76.04	76.29	76.57	77.20	66.55	75.02	75.18	76.05	76.33
TiO <sub>2</sub>	0.11	0.09	0.15	0.17	0.16	0.11	0.21	0.20	0.18	0.20
Al <sub>2</sub> O <sub>3</sub>	12.78	11.91	10.75	12.28	11.37	7.36	13.20	12.09	11.94	12.13
Fe <sub>2</sub> O <sub>3</sub>	1.17	0.78	1.05	1.17	1.27	0.71	1.21	1.15	1.08	1.25
FeO	--	0.38	--	--	--	--	--	--	--	--
MnO	0.06	0.07	0.06	0.07	0.06	0.05	0.08	0.07	0.06	0.08
MgO	0.22	<0.01	0.41	1.03	0.12	0.73	0.29	0.21	0.49	0.15
CaO	0.29	0.43	1.85	0.43	0.23	10.90	0.31	0.71	0.34	0.41
Na <sub>2</sub> O	3.09	4.18	1.47	4.46	3.48	1.56	4.25	3.78	3.31	4.04
K <sub>2</sub> O	5.07	4.92	4.01	5.31	5.01	3.76	6.05	5.30	5.13	5.16
P <sub>2</sub> O <sub>5</sub>	0.01	0.03	0.01	0.03	0.02	0.01	0.02	0.04	0.01	0.10
LOI <sup>5</sup>	1.12	1.06	3.71	0.45	0.31	6.69	0.55	0.90	0.96	0.28
TOTAL	99.18	99.88	99.76	101.97	99.23	98.42	101.19	99.63	99.55	100.13
As	--	--	--	--	2.2	--	--	--	--	--
Ba	21	19	93	75	38	41	56	56	39	60
Br	--	--	--	--	<0.5	--	--	--	--	--
Cl(%)	--	0.003	--	--	--	--	--	--	--	--
Cr	<10	14	<10	<10	<0.6*	<10	<10	<10	<10	<10
Cs	--	--	--	--	4.2	--	--	--	--	--
F(%)	--	0.07	--	--	--	--	--	--	--	--
Ga	22	23	15	20	19	12	21	19	19	21
Hf	--	--	--	--	8.5	--	--	--	--	--
Mo	--	--	--	--	--	--	--	--	--	--
Nb	51	46	33	42	33	21	36	32	32	35
Ni	6	7	20	<5	6	<5	<5	<5	<5	7
Pb	37	24	17	24	24	37	26	30	26	--
Rb	415	283	222	293	289	146	293	256	260	263
Sb	--	--	--	--	0.1	--	--	--	--	--
Sc	--	--	--	--	2.5	--	--	--	--	--
Se	--	--	--	--	<0.5	--	--	--	--	--
Sn	5	<5	15	<5	<5	11	6	6	9	<5
Sr	11	30	1187	19	6	435	20	28	26	23
Ta	--	--	--	--	3.4	--	--	--	--	--
Th	41	--	24	33	29*	16	36	31	32	--
U	7	--	<3	<3	9*	<3	<3	<3	<3	--
V	<3	13	<3	3	5	5	32	18	11	<3
Y	88	144	90	72	94	54	94	85	89	89
Zn	53	50	41	37	33	47	64	58	57	62
Zr	171	171	132	164	209	119	218	208	195	206
La	--	--	--	--	50	--	--	--	--	--
Ce	--	--	--	--	120	--	--	--	--	--
Nd	--	--	--	--	50	--	--	--	--	--
Sm	--	--	--	--	11.2	--	--	--	--	--
Eu	--	--	--	--	0.37	--	--	--	--	--
Tb	--	--	--	--	2.3	--	--	--	--	--
Yb	--	--	--	--	9.9	--	--	--	--	--
Lu	--	--	--	--	1.61	--	--	--	--	--

SAMPLE	Tbc	Tbc	Tbc	Tbm	Tbm	Tbm	Tbm	Tkmp	Tkmp	Tkmp
	234	203	204	217	256	258	257	174	102	107
SiO <sub>2</sub>	76.92	77.09	77.64	58.49	59.55	59.87	60.17	39.67	71.31	75.42
TiO <sub>2</sub>	0.18	0.19	0.18	1.46	1.04	1.09	1.09	0.08	0.15	0.16
Al <sub>2</sub> O <sub>3</sub>	11.87	12.11	12.42	14.78	16.10	16.12	16.32	22.32	11.48	11.85
Fe <sub>2</sub> O <sub>3</sub>	1.10	1.14	1.15	7.24	6.61	6.60	6.89	0.28	5.75	1.78
FeO	--	--	--	--	--	--	--	--	--	--
MnO	0.08	0.08	0.08	0.10	0.10	0.12	0.09	<0.01	1.14	0.02
MgO	0.23	0.19	0.39	2.15	3.44	2.69	2.90	<0.01	0.16	0.18
CaO	0.19	0.43	0.26	4.28	5.57	5.63	5.37	<0.01	0.14	0.09
Na <sub>2</sub> O	3.48	4.07	3.84	5.77	3.45	3.70	3.73	0.10	0.61	0.60
K <sub>2</sub> O	5.08	4.99	5.06	3.86	2.58	3.32	3.13	6.25	6.15	7.38
P <sub>2</sub> O <sub>5</sub>	0.04	0.14	0.02	0.74	0.34	0.37	0.38	0.05	0.02	0.02
LOI	0.59	0.47	0.55	1.62	2.25	1.20	1.40	25.15	2.46	1.50
TOTAL	99.76	100.90	101.59	100.49	101.03	100.71	101.47	93.87	99.37	99.00
As	--	--	--	<1.4	<0.7	--	--	--	--	--
Ba	121	51	45	1584	1151	1032	1068	175	365	23
Br	--	--	--	<0.7	0.9	--	--	--	--	--
Cl(%)	--	--	--	--	--	--	--	--	--	--
Cr	10	<10	10	<1*	47*	40	53	<10	<10	18
Cs	--	--	--	2.1	0.9	--	--	--	--	--
F(%)	--	--	--	--	--	--	--	--	--	--
Ga	--	21	20	21	--	--	--	18	18	19
Hf	--	--	--	11.7	7.6	--	--	--	--	--
Mo	--	--	--	--	--	--	2	--	4	2
Nb	33	37	38	22	16	15	16	24	33	34
Ni	--	6	10	6	<38*	--	--	5	<5	<5
Pb	48	--	--	12	15	19	18	23	27	38
Rb	265	278	292	113	90	115	110	<1	279	365
Sb	--	--	--	>0.1	<0.1	--	--	--	--	--
Sc	--	--	--	12.5	13.9	--	--	--	--	--
Se	--	--	--	<0.9	<0.8	--	--	--	--	--
Sn	<5	7	<5	<5	<5	<5	<5	<5	<5	7
Sr	20	26	15	744	570	510	521	95	87	5
Ta	--	--	--	1.3	0.9	--	--	--	--	--
Th	36	--	--	10*	8	13	12	15	26	25
U	4	--	--	2*	1*	<3	3	<3	5	3
V	13	5	3	119	126	134	122	7	<3	<3
Y	76	75	80	63	40	40	40	26	102	61
Zn	--	61	73	103	--	--	--	5	116	20
Zr	217	194	199	475	304	335	335	226	332	356
La	--	--	--	73	49	--	--	--	--	--
Ce	--	--	--	168	101	--	--	--	--	--
Nd	--	--	--	89	48	--	--	--	--	--
Sm	--	--	--	15.6	9.0	--	--	--	--	--
Eu	--	--	--	3.51	1.81	--	--	--	--	--
Tb	--	--	--	1.9	1.1	--	--	--	--	--
Yb	--	--	--	5.4	3.3	--	--	--	--	--
Lu	--	--	--	0.82	0.51	--	--	--	--	--

SAMPLE	Tkmp	Tkmp	Tkmp	Tkmp	Tkmp	Tkmp	Tkmp	Tkmp	Tkmp	Tkmp
	127	124	103	105	125	104	126	108	173	106
SiO <sub>2</sub>	75.80	75.86	75.87	75.95	76.25	76.50	76.64	76.75	79.78	80.97
TiO <sub>2</sub>	0.16	0.15	0.15	0.16	0.15	0.16	0.15	0.14	0.18	0.12
Al <sub>2</sub> O <sub>3</sub>	12.48	11.66	12.17	11.92	12.07	12.44	11.66	11.59	12.17	10.03
Fe <sub>2</sub> O <sub>3</sub>	1.31	1.63	1.50	2.13	1.59	1.05	1.79	1.19	2.52	0.66
FeO	--	--	--	--	--	--	--	--	--	--
MnO	0.01	<0.01	0.01	0.02	<0.01	0.01	<0.01	<0.01	<0.01	0.01
MgO	0.17	0.15	0.22	0.23	0.18	0.11	0.21	0.13	<0.01	0.13
CaO	0.16	0.13	0.23	0.12	0.24	0.05	0.26	0.05	0.02	0.04
Na <sub>2</sub> O	0.67	0.58	0.68	0.82	2.52	0.76	2.00	0.96	0.07	0.48
K <sub>2</sub> O	7.25	7.34	6.43	7.35	5.56	6.71	5.38	7.08	0.12	6.29
P <sub>2</sub> O <sub>5</sub>	0.02	0.01	0.01	0.01	0.01	0.01	0.02	0.01	0.01	0.01
LOI	2.08	2.02	1.98	1.22	1.24	1.71	1.18	1.34	4.88	1.29
TOTAL	100.11	99.52	99.25	99.93	99.80	99.51	99.28	99.23	99.73	100.03
As	<1.2	--	--	--	<1.6	--	<1.8	--	--	<1.0
Ba	22	26	22	<16	<16	26	41	44	20	17
Br	--	--	--	--	--	--	--	--	--	--
Cl(%)	0.002	--	--	--	0.002	--	0.004	--	--	0.005
Cr	<6*	<10	19	<10	<10	<10	<8*	10	<10	<9*
Cs	4.0	--	--	--	4.3	--	3.8	--	--	3.4
F(%)	0.20	--	--	--	0.20	--	0.05	--	--	0.04
Ga	20	19	17	18	19	19	19	18	18	16
Hf	12.2	--	--	--	11.5	--	11.6	--	--	10.0
Mo	2	3	1	2	1	2	1	3	--	1
Nb	34	34	34	32	33	33	32	33	33	27
Ni	<5	<5	<5	<5	<5	<5	<5	<5	7	<5
Pb	17	30	14	19	22	20	18	14	9	10
Rb	355	355	305	363	274	360	268	342	4	288
Sb	0.2	--	--	--	0.3	--	0.2	--	--	0.2
Sc	5.4	--	--	--	4.5	--	4.4	--	--	4.2
Se	0.5	--	--	--	0.4	--	0.3	--	--	0.4
Sn	<5	<5	<5	5	<5	6	<5	6	5	<5
Sr	8	5	17	7	15	3	16	4	1	3
Ta	3.2	--	--	--	2.9	--	2.6	--	--	3.3
Th	21	28	24	29	28	78	34	21	21	21
U	8*	3	3	3	6*	3	7*	3	<3	5*
V	<3	<3	<3	<3	<3	<3	<3	<3	<3	<3
Y	104	97	74	86	114	173	111	76	30	65
Zn	38	64	74	65	108	81	74	17	8	14
Zr	349	343	348	344	348	353	343	352	362	285
La	14	--	--	--	89	--	128	--	--	20
Ce	34	--	--	--	180	--	289	--	--	51
Nd	18	--	--	--	86	--	167	--	--	25
Sm	4.2	--	--	--	17.7	--	23.0	--	--	4.6
Eu	0.38	--	--	--	0.87	--	1.15	--	--	0.38
Tb	1.3	--	--	--	2.9	--	2.6	--	--	1.0
Yb	11.0	--	--	--	10.8	--	11.0	--	--	7.2
Lu	1.53	--	--	--	1.52	--	1.56	--	--	0.78

SAMPLE	Trp	Trp	Trp	Tkn	Tkn	Tvp	Ttr	Ttr	Ttr	Thok
	245	244	246	243	242	247	237	241	239	180
SiO <sub>2</sub>	61.73	69.73	74.08	69.83	70.02	77.92	65.19	65.25	66.11	76.47
TiO <sub>2</sub>	0.54	0.50	0.29	0.43	0.44	0.13	0.44	0.46	0.44	0.16
Al <sub>2</sub> O <sub>3</sub>	17.34	15.70	13.22	15.03	14.47	11.29	17.15	16.99	16.36	11.98
Fe <sub>2</sub> O <sub>3</sub>	4.60	2.23	1.65	2.57	2.56	1.36	3.07	3.11	2.93	1.61
FeO	---	---	---	---	---	---	---	---	---	---
MnO	0.07	0.02	0.02	0.02	0.03	0.06	0.12	0.12	0.17	0.04
MgO	2.28	0.33	0.45	0.34	0.73	0.62	0.52	0.71	0.49	0.28
CaO	1.58	0.55	0.64	1.47	0.69	0.12	1.14	1.40	1.00	0.41
Na <sub>2</sub> O	4.60	2.99	3.78	3.44	1.02	1.67	6.09	6.16	5.86	3.11
K <sub>2</sub> O	4.79	6.76	5.38	5.79	6.67	7.87	5.56	5.19	5.66	4.96
P <sub>2</sub> O <sub>5</sub>	0.27	0.07	0.05	0.16	0.13	0.05	0.17	0.18	0.16	0.03
LOI <sup>5</sup>	3.30	0.49	1.18	0.51	3.91	0.27	0.46	0.55	0.64	0.87
TOTAL	101.10	99.37	100.74	99.59	100.67	101.36	99.90	100.12	99.82	99.92
As	---	---	---	---	---	---	<0.3	---	1.4	1.0
Ba	1484	1168	1338	919	751	89	2124	2656	1291	355
Br	---	---	---	---	---	---	---	---	0.8	1.1
Cl(%)	---	---	---	---	---	---	---	---	---	---
Cr	<10	<10	25	<10	<10	16	<1*	<10	<1*	<1*
Cs	---	---	---	---	---	---	0.5	---	0.7	5.2
F(%)	---	---	---	---	---	---	---	---	---	---
Ga	---	---	---	---	---	---	---	---	---	21
Hf	---	---	---	---	---	---	13.4	---	15.5	8.4
Mo	---	---	---	---	---	---	---	---	---	---
Nb	8	23	21	16	16	45	55	59	63	39
Ni	---	---	---	---	---	---	---	---	<12	<5
Pb	14	25	47	23	20	40	20	18	23	28
Rb	100	236	160	227	282	433	109	110	119	313
Sb	---	---	---	---	---	---	<0.1	---	<0.1	0.3
Sc	---	---	---	---	---	---	6.6	---	6.6	4.0
Se	---	---	---	---	---	---	<0.8	---	<0.2	<1.0
Sn	<5	<5	<5	<5	<5	<5	<5	<5	<5	11
Sr	635	110	140	242	86	6	97	195	60	92
Ta	---	---	---	---	---	---	3.0	---	3.5	3.7
Th	<3	30	31	22	25	38	16	16	18	41
U	<3	3	3	<3	<3	5	3*	<3	3*	9*
V	19	28	8	29	32	10	14	13	9	3
Y	19	47	62	34	32	87	46	51	56	103
Zn	---	---	---	---	---	---	---	---	---	51
Zr	155	526	311	185	175	303	601	569	706	200
La	---	---	---	---	---	---	85	---	99	55
Ce	---	---	---	---	---	---	168	---	187	140
Nd	---	---	---	---	---	---	66	---	77	59
Sm	---	---	---	---	---	---	10.6	---	12.0	12.3
Eu	---	---	---	---	---	---	2.9	---	2.7	0.65
Tb	---	---	---	---	---	---	1.4	---	1.6	2.2
Yb	---	---	---	---	---	---	4.4	---	5.5	11.1
Lu	---	---	---	---	---	---	0.73	---	0.89	1.75

SAMPLE	Thok 248	Thok 240	Tdike 249	Twsd 181	Twsd 117	Twsd 115	Twsd 122	Twsd 238	Twsd 120	Twsd 121
S <sub>10</sub> <sub>2</sub>	76.78	76.84	79.77	74.65	75.50	76.47	76.66	76.72	76.73	76.81
Ti <sub>10</sub> <sub>2</sub>	0.16	0.16	0.15	0.14	0.18	0.15	0.16	0.17	0.15	0.15
Al <sub>20</sub> <sub>3</sub>	11.70	11.68	10.88	11.54	12.60	12.28	12.12	11.68	11.85	12.10
Fe <sub>20</sub> <sub>3</sub>	1.58	1.53	0.50	1.51	1.28	1.12	1.21	1.14	1.18	1.21
Fe <sub>0</sub>	--	--	--	--	--	--	--	--	--	--
Mn <sub>0</sub>	0.12	0.08	<0.1	0.07	0.06	0.06	0.06	0.04	0.06	0.06
Mg <sub>0</sub>	0.34	0.34	0.41	0.42	0.25	0.21	0.48	0.24	0.26	0.23
Ca <sub>0</sub>	0.60	0.75	0.19	1.94	0.34	0.31	0.47	0.66	0.26	0.41
Na <sub>20</sub>	3.10	3.40	2.03	2.35	3.30	3.45	2.79	3.24	3.12	3.37
K <sub>20</sub>	5.38	4.74	6.27	2.93	5.36	5.16	5.00	5.10	5.22	5.10
P <sub>20</sub> <sub>5</sub>	0.03	0.03	0.04	0.03	0.02	0.02	0.02	0.06	0.02	0.02
LOI <sub>5</sub>	0.59	0.84	0.45	4.66	0.55	0.51	0.95	0.85	0.48	0.38
TOTAL	100.38	100.39	100.68	100.24	99.44	99.74	99.92	99.90	99.33	99.84
As	--	--	--	--	38.0	36.0	3.2	--	34.0	<1.4
Ba	275	223	188	205	103	85	87	103	67	73
Br	--	--	--	--	--	--	--	--	--	--
Cl(%)	--	--	--	--	0.003	0.004	0.005	--	--	0.001
Cr	14	20	21	<10	<10	<9*	<10	15	13*	23
Cs	--	--	--	--	6.1	4.2	4.0	--	6.7	13.1
F(%)	--	--	--	--	0.08	0.19	0.06	--	0.05	0.11
Ga	--	--	--	20	20	19	19	--	19	19
Hf	--	--	--	--	8.1	7.6	7.5	--	7.6	7.8
Mo	--	--	--	--	--	1	--	--	--	--
Nb	39	38	344	36	35	36	33	35	35	32
Ni	--	--	--	10	7	8	<5	--	<5	8
Pb	32	29	21	24	26	21	37	25	30	41
Rb	347	300	290	147	250	259	232	228	304	243
Sb	--	--	--	--	3.5	9.0	<0.1	--	0.4	7.8
Sc	--	--	--	--	3.7	3.3	3.1	--	3.1	3.2
Se	--	--	--	--	0.4	0.4	0.5	--	0.5	0.4
Sn	6	<5	<5	5	108	25	<5	<5	59	38
Sr	66	36	16	1151	16	16	18	14	12	13
Ta	--	--	--	--	3.4	3.5	3.7	--	3.2	2.9
Th	41	41	26	34	31	29	28	30	28	28
U	6	5	3	6	7*	8*	8*	4	8*	8*
V	5	5	<3	7	<3	<3	15	12	5	<3
Y	121	116	63	105	94	116	68	90	81	87
Zn	--	--	--	56	57	57	39	--	52	39
Zr	206	205	166	191	219	187	180	177	177	170
La	--	--	--	--	74	59	52	--	68	57
Ce	--	--	--	--	158	132	117	--	154	122
Nd	--	--	--	--	82	61	71	--	67	57
Sm	--	--	--	--	14.3	12.9	10.5	--	12.1	12.2
Eu	--	--	--	--	0.68	0.51	0.47	--	0.54	0.54
Tb	--	--	--	--	2.3	2.2	1.8	--	1.8	2.1
Yb	--	--	--	--	10.4	10.6	9.0	--	9.2	9.5
Lu	--	--	--	--	1.34	1.42	1.01	--	1.20	1.36



SAMPLE	Twsd	Iron	Iron	Iron	Iron	Iron	ore1	ore2	ore3	ore4
	116	197	200	201	198	199	270	271	272	273
SiO <sub>2</sub>	76.94	76.18	76.85	77.84	77.87	79.21	--	--	--	--
TiO <sub>2</sub>	0.15	0.07	0.08	0.02	0.07	0.07	--	--	--	--
Al <sub>2</sub> O <sub>3</sub>	12.09	12.48	12.25	11.76	11.98	11.01	--	--	--	--
Fe <sub>2</sub> O <sub>3</sub>	1.20	0.68	0.95	0.92	0.68	0.90	--	--	--	--
FeO	--	--	--	--	--	--	85.50	0.70*	2.50*	4.78*
MnO	0.06	0.04	0.07	0.03	0.03	0.04	--	--	--	--
MgO	0.20	0.05	0.04	<0.01	0.03	0.05	--	--	--	--
CaO	0.42	0.45	0.65	0.44	0.38	0.45	--	--	--	--
Na <sub>2</sub> O	3.20	3.97	3.89	4.12	4.15	3.82	0.02*	0.04*	0.19*	0.23*
K <sub>2</sub> O	5.18	5.23	5.16	4.71	4.53	4.15	--	--	--	--
P <sub>2</sub> O <sub>5</sub>	0.03	0.01	0.01	0.01	0.02	0.01	--	--	--	--
LOI	0.38	0.03	0.40	0.16	0.28	0.38	--	--	--	--
TOTAL	99.85	99.46	100.35	100.00	100.02	100.09	85.52	0.74	2.69	5.01
As	2.9	--	--	--	--	--	5.7	<0.1	37	2581
Ba	78	<16	23	35	44	58	<50*	480*	<200*	<100*
Br	--	--	--	--	--	--	<0.5	<0.5	<5.0	6.8
Cl(%)	0.003	0.01	--	0.002	0.003	--	--	--	--	--
Cr	<5*	<10	12	12	14	12	5*	22*	26*	21*
Cs	3.7	--	--	--	--	--	0.5	2.3	7.2	69.0
F(%)	0.08	0.20	--	0.18	0.24	--	--	--	--	--
Ga	17	27	26	26	28	24	--	0.5	0.8	0.2
Hf	7.3	--	--	--	--	--	4.7	--	--	--
Mo	--	--	--	--	--	--	--	--	--	--
Nb	34	73	76	68	82	66	--	<0.5*	<140*	<100*
Ni	<5	<5	<5	<5	<5	<5	120*	--	--	--
Pb	20	26	24	30	30	30	--	<15*	24*	29*
Rb	235	513	609	482	404	346	<30*	1830	2880	1262
Sb	0.1	--	--	--	--	--	15.5	0.9	1.1	0.9
Sc	3.1	--	--	--	--	--	74.2	<10	<9	<10
Se	0.4	--	--	--	--	--	<3.0	--	--	--
Sn	<5	<5	8	<5	<5	<5	--	--	--	--
Sr	16	1	3	3	8	10	--	0.9	<0.5	<0.3
Ta	3.3	--	--	--	--	--	22.3	3*	4*	8*
Th	29	--	--	--	--	--	2*	90*	20*	5*
U	8*	--	--	--	--	--	2*	--	--	--
V	4	<3	<3	<3	<3	<3	--	--	--	--
Y	84	107	156	112	89	94	--	--	--	--
Zn	47	22	26	27	23	39	--	--	--	--
Zr	178	148	154	147	134	135	--	--	--	--
La	52	--	--	--	--	--	2	5	7	8
Ce	123	--	--	--	--	--	5	27	<1	<20
Nd	55	--	--	--	--	--	<20	<1	<0.3	1.5
Sm	11.7	--	--	--	--	--	0.7	<0.1	<0.5	0.16
Eu	0.46	--	--	--	--	--	0.06	<0.2	<0.3	0.3
Tb	2.1	--	--	--	--	--	0.1	4.0	3.4	2.1
Yb	9.4	--	--	--	--	--	2.9	0.35	0.16	0.18
Lu	1.28	--	--	--	--	--	0.37	--	--	--
Co							17	<0.1	0.7	0.8
W							8	400	410	6

SAMPLE	ore5 274
SiO <sub>2</sub>	---
TiO <sub>2</sub>	---
Al <sub>2</sub> O <sub>3</sub>	---
Fe <sub>2</sub> O <sub>3</sub>	---
FeO	21.46*
MnO	---
MgO	---
CaO	---
Na <sub>2</sub> O	0.22*
K <sub>2</sub> O	---
P <sub>2</sub> O <sub>5</sub>	---
LOI	---
TOTAL	21.68

As	111
Ba	<90*
Br	1.8
Cl(%)	---
Cr	12*
Cs	41.2
F(%)	---
Hf	0.9
Mo	---
Nb	---
Ni	<160
Pb	---
Rb	35*
Sb	836
Sc	2.3
Se	<7
Sn	---
Sr	---
Ta	0.8
Th	17*
U	9*
V	---
Y	---
Zn	---
Zr	---

La	17
Ce	48
Nd	30
Sm	6.2
Eu	0.26
Tb	1.4
Yb	5.9
Lu	.0.80
Co	3.2
W	51



## APPENDIX 1C Oxygen isotopic data. Values reported relative to SMOW.

SAMPLE	MINERAL*	$\delta^{18}O$	Loc. #	REMARKS <sup>@</sup>
1	WR	8.01	TC	Mild VPC rhyolite
9	WR	8.78	TC	Mild VPC rhyolite
57	WR	15.90	PP	Mild VPC ignimbrite
78	WR	19.05	PP	Altered ignimbrite
88	WR	10.33	PP	Intensely altered ignimbrite
91	QTZ	24.27	CP	Quartz replacing ignimbrite
95	WR	18.94	CP	Intensely altered ignimbrite
109	WR	16.81	KP	Alunitized ignimbrite
115	WR	9.94	MC	Mild VPC rhyolite
116	WR	7.57	MC	Very mild VPC rhyolite
	QTZ	7.74		Quartz separate from 116
	SAN	6.79		Sanidine separate from 116
122	WR	9.32	MC	Intense VPC rhyolite
126	WR	9.32	KP	Mild VPC rhyolite intrusive
127	WR	12.72	KP	Silicified rhyolite intrusive
131	WR	6.13	PC	Lithophysal rhyolite
	QTZ	7.49		Quartz from lithophysae in 131
136	WR	7.33	NG	Mild VPC rhyolite
	QTZ	7.65		Quartz separate from 136
	SAN	7.04		Sanidine separate from 136
	MGT	2.40		Magnetite separate from 136
138	WR	19.44	NG	Silica replacement of rhyolite
140	WR	7.56	NG	Intense VPC rhyolite
141	WR	7.27	NG	Intense VPC rhyolite
146	WR	17.17	NG	Silicified selvage on Sn vein
149	WR	8.82	PC	Rhyolite vitrophyre
	QTZ	7.54		Quartz separate from 149
	SAN	6.7		Sanidine separate from 149
152	WR	7.48	PC	Intense VPC rhyolite
157	QTZ	5.79	TC	Vein quartz
158	WR	7.59	TC	Intense VPC rhyolite (vein wall)
	QTZ	11.0		Vein quartz
	CLAY	10.63		Vein Clays
163	QTZ	8.72	TC	Vein quartz
165	WR	7.97	TC	Intense VPC rhyolite
167	WR	9.03	KM	Mild VPC rhyolite
	QTZ	7.82		Quartz separate from 167
	SAN	7.65		Sanidine separate from 167
168	WR	8.41	KM	Intense VPC rhyolite

\*WR-WHOLE ROCK SAMPLE  
 QTZ-QUARTZ SEPARATE  
 SAN-SANIDINE SEPARATE  
 MGT-MAGNETITE SEPARATE  
 CLAY-CLAY MINERALS  
 @VPC-Vapor phase  
 crystallization

#TC-Taylor Creek  
 PC-Paramount Canyon  
 NG-Nugget Gulch  
 KM-Kemp Mesa  
 KP-Kline Mountain  
 CP-Clay Pits (upper Poverty Cr.)  
 PP-Poverty Creek

APPENDIX 1D Sr ISOTOPIC ANALYSES					
Sample	Rb	Sr	87Rb/86Sr	87Sr/86Sr	+2 Sigma#
Taylor Creek Rhyolite					
Boiler Peak Dome					
131	416*	3.830	318.15	0.83411	21
132	464*	2.407	569.70	0.92672	21
149	347.7	2.716	376.04	0.86338	1
150	393.8	2.474	469.27	0.90139	6
152	420.2	2.162	574.42	0.92573	30
190	366.7	16.10	66.07	0.73452	29
221	357.9	5.275	197.88	0.78940	1
226	376.3	5.635	194.74	0.78811	2
227	360.0	3.641	289.42	0.82724	9
Alexander Cienega dome					
213	364.3	4.79	213.83	0.79187	2
214	352.8	3.235	319.56	0.83799	2
215	340.1	5.982	165.62	0.77761	1
Nugget Gulch dome					
140	290*	7.143	118.06	0.75959	11
141	288.5	6.885	121.86	0.76040	18
142	288*	10.18	82.13	0.74259	15
196	8.03	199.6	0.116	0.70880	10
Round Mountain dome					
134	463*	1.871	736.31	0.99791	12
135	451.6	1.694	797.80	1.07262	1
North Paramount Canyon dome					
223	287.0	6.231	134.19	0.77874	1
North Nugget Gulch dome					
136	365.6	3.104	345.65	0.85374	1
Squaw Creek dome					
30	470*	75*	18.15	0.71770	20
31	676*	47*	41.69	0.71770	26
33	617*	174*	10.27	0.71470	18
Taylor Creek dome					
10	262.6	13.11	58.12	0.73654	9
155	281.3	22.01	37.05	0.72653	9
161	293*	65*	13.06	0.71987	11
165	261.5	9.222	82.38	0.74793	17
Kemp Mesa dome					
2	274.0	9.638	82.56	0.74601	15
3	326.0	15.82	59.79	0.78566	11
4	285.9	11.24	73.86	0.74165	14
167	292.2	19.24	44.03	0.72918	13
168	306.5	10.20	87.28	0.74710	10
268	264.3	11.01	69.68	0.74015	5
Indian Peaks dome					
205	272.9	6.356	180.67	0.80918	16
207	368.39	4.087	363.69	0.82106	18
208	300.2	10.09	86.43	0.74505	23
211	300.7	7.973	110.26	0.75529	10
Rhyolite of Dolan Peak					
219	223.1	8.48	76.43	0.74925	1
220	288.9	8.647	97.07	0.75049	1

## Appendix 1D cont.

## Rhyolite of Willow Springs Draw

115	259*	15.28	49.17	0.73403	25
116	235*	13.49	50.53	0.73423	15
117	250*	16.33	44.40	0.73198	19
121	235.9	13.08	52.27	0.72561	98
122	232*	16.66	40.39	0.72561	24

## Granite of Iron Mountain

197	495.2	2.743	516.06	0.95312	3
198	395.6	9.576	120.09	0.75567	1
199	359.6	11.70	89.25	0.74182	1
200	601.1	4.416	399.96	0.86676	2
201	469.5	4.49	306.16	0.83009	12

#- sigma=0.000XX

\* = analysis by XRF rather than isotope dilution

## APPENDIX 2--SAMPLE DESCRIPTIONS

The following sample descriptions are arranged in numerical order. The format is as follows: sample number; field number; formation; quadrangle; nearby geographic feature; location by section, township, range; location by latitude (deg.-min.-sec.), longitude (deg.-min.-sec.); sample description. This format is followed throughout so that the length of each entry is minimized. Vapor phase crystallization is abbreviated VPC throughout.

- 1 7-14-1; Taylor Creek Rhyolite; Wall Lake; Kemp Mesa; S6,T11S,R12W; 33-22-08, 108-07-06; Mildly VPC rhyolite containing about 30% phenocrysts of quartz and sanidine. Some iridescent sanidine. About equal quartz and sanidine. This sample is from the least VPC portions of the dome. The sample is pink to white, but very dense.
- 2 7-14-2; Taylor Creek Rhyolite; Wall Lake; Kemp Mesa; S6,T11S,R12W; 33-21-57, 108-07-04; Mildly VPC rhyolite lava. The sample is white and quite dense. Judging by the color and density, this sample has undergone a bit more VPC than #1.
- 3 7-14-3; Taylor Creek Rhyolite; Wall Lake; Kemp Mesa; S5,T11S,R12W; 33-21-53, 108-06-40; Intensely VPC rhyolite lava. The sample is white and quite porous, evidence of intense VPC. This sample was taken to investigate the possibility of disseminated Sn in the wall rocks 1 to 1.5 m from a Sn-bearing veinlet.
- 4 7-14-4; Taylor Creek Rhyolite; Wall Lake; Kemp Mesa; S5,T11S,R12W; 33-21-54, 108-06-35; This sample has an intermediate density and is white, suggesting an intermediate intensity of VPC. Collected to investigate the chemical variation due to VPC.
- 5 7-14-5; Hematite-cassiterite mineralization; Wall Lake; Kemp Mesa; S5,T11S,R12W; 33-21-48, 108-06-40; Hematite-cassiterite mineralization from a shallow prospect pit at the Kemp Mesa prospect. The veinlet is bounded by rhyolite lava (#3 above).
- 6 7-14-6; Taylor Creek Rhyolite; Wall Lake; Indian Creek; S32,T10S,R12W; 33-24-16, 108-05-30; Moderately VPC crystal-rich lava containing 30% phenocrysts of quartz and sanidine in subequal proportions. Some smokey quartz.
- 7 7-14-7; Taylor Creek Rhyolite; Wall Lake; Indian Creek; S3,T11S,R12W; 33-23-25, 108-04-33; Brecciated Taylor Creek Rhyolite with coarse calcite breccia filling. May be related to a fault.
- 8 7-14-8; Taylor Creek Rhyolite; Wall Lake; Indian Creek; S4,T11S,R12W; 33-22-57, 108-05-20; Rhyolite lava with about 30% phenocrysts of smokey quartz and sanidine in subequal proportions. Moderate VPC.
- 9 7-15-1; Taylor Creek Rhyolite; Wall Lake; Wall Lake; S2,T11S,R12W; 33-21-40, 108-03-35; Crystal-rich Taylor Creek Rhyolite lava. Moderate VPC.
- 10 7-15-2; Taylor Creek Rhyolite; Wall Lake; Wall Lake; S2,T11S,R12W; 33-21-55, 108-03-30; White, flow banded,

- crystal-rich rhyolite lava. Moderate to intense VPC.
- 11 7-20-1; Taylor Creek Rhyolite; Wall Lake; Wall Lake; S2,T11S,R12W; 33-22-28, 108-03-29; Crystal-rich rhyolite lava immediately below the carapace breccia found north of the Dawson Mine. Moderate to intense VPC.
  - 12 7-20-2; Tt10; Wall Lake; Wall Lake; S2,T11S,R12W; 33-22-30, 108-03-32; Crystal-rich, nonwelded, and intensely zeolitized ignimbrite.
  - 13 7-20-3; Tt10; Wall Lake; Wall Lake; S2,T11S,R12W; 33-22-31, 108-03-37; Crystal-rich, nonwelded, white to buff ignimbrite. Lithic fragments common at the top are rare in this sample from the base of the unit. The mineralogy and stratigraphic position is consistent with this unit originating from eruptions of the North Taylor Creek dome.
  - 14 7-20-4; Tt10; Wall Lake; Wall Lake; S2,T11S,R12W; 33-22-34, 108-03-38; Sample from near the top of Tt10 which is a thin, nonwelded ignimbrite. Contains 5 to 10% lithic fragments.
  - 15 7-20-5; Bloodgood Canyon Tuff; Wall Lake; Wall Lake; S2,T11S,R12W; 33-22-34, 108-03-38; Pink to lavender, moderately crystal-rich, poorly welded ignimbrite. About 5% quartz and 6-8% sanidine. Sphene is common. Intensely zeolitized. Collected near the base of the unit.
  - 16 7-20-6; Bloodgood Canyon Tuff; Wall Lake; Wall Lake; S2,T11S,R12W; 33-22-34, 108-03-38; Sample from about 7 m above the base of the Bloodgood Canyon Section.
  - 17 7-20-7; Bloodgood Canyon Tuff; Wall Lake; Wall Lake; S2,T11S,R12W; 33-22-34, 108-03-38; Sample from about 20 m above the base of the Bloodgood Canyon Tuff.
  - 18 7-20-8; Bloodgood Canyon Tuff; Wall Lake; Wall Lake; S2,T11S,R12W; 33-22-34, 108-03-38; Bloodgood Canyon Tuff about 40 m above the base and 10 m below the top of the unit.
  - 19 7-22-1; Kneeling Nun Tuff; Sawmill Peak; Koko Well; S6,T10S,R9W; 33-28-05, 107-48-13; Densely welded, crystal-rich, tan to buff ignimbrite. About 30% phenocrysts in a vitroclastic groundmass.
  - 20 7-22-2; Rubio Peak Formation; Sawmill Peak; Poverty Creek Store; S6,T10S,R9W; 33-28-13, 107-48-07; Andesite to basaltic andesite lava flow from the top of the Rubio Peak Formation. The sample is fine grained and contains about 5% iddingsite after olivine (?).
  - 21 8-4-1; rhyolite of Sawmill Peak; Sawmill Peak; Mud Hole; S1,T10S,R10W; 33-27-54, 107-49-47 Red, flow banded, lithoidal rhyolite lava with about 7% feldspar phenocrysts. Feldspars as much as 8 mm in length. Fractures are filled with chalcedonic quartz.
  - 22 8-4-2; rhyolite of Sawmill Peak; Sawmill Peak; Mud Hole; S1,T10S,R10W; 33-27-51, 107-49-50; Red, lithoidal, flow banded rhyolite lava with about 10% feldspar phenocrysts. Collected near the center of the flow.
  - 23 8-4-3; tuff of Stiver Canyon; Sawmill Peak; Mud Hole; S1,T10S,R10W; 33-27-50, 107-49-50; Poorly welded, crystal-poor, multiple flow ignimbrite. The unit is



- pink to buff to light gray and contains abundant flow banded rhyolite lava lithic fragments. Sanidine is sparse as is coppery biotite. Rare quartz.
- 24 8-4-4; tuff of Stiver Canyon; Sawmill Peak; Mud Hole; S1,T10S,R10W; 33-27-46, 107-49-50; Poorly welded, crystal-poor ignimbrite with about 3% phenocrysts (2% sanidine, 1% quartz, trace coppery biotite).
- 25 8-4-5; basaltic andesite of Poverty Creek; Sawmill Peak; Mud Hole; S1,T10S,R10W; 33-27-45, 107-49,50; Gray to black, flow banded andesite lava flow. The gray color may be due to incipient propylitic alteration. Very fine grained with about 0.5% iddingsite after olivine (?). Collected from the center of a 0.75 m boulder to avoid the possible alteration and weathering.
- 26 8-4-6a; Taylor Creek Rhyolite; Taylor Peak; Squaw Creek; S34,T9S,R11W; 33-28-41, 107-57-54; Samples 26 through 29 were cut from a single boulder and represent 1 cm thick samples cut parallel to a quartz vein. The samples were prepared to investigate the chemical effects of silicification on the Taylor Creek Rhyolite. Sample 26 is a sample of the vein quartz. Samples 27, 28, and 29 are progressively farther from the vein and thus represent progressively less altered material.
- 27 8-4-6b; Taylor Creek Rhyolite; Taylor Peak; Squaw Creek; S34,T9S,R11W; 33-28-41, 107-57-54; See #26 above.
- 28 8-4-6c; Taylor Creek Rhyolite; Taylor Peak; Squaw Creek; S34,T9S,R11W; 33-28-41, 107-57-54; See # 26 above.
- 29 8-4-6d; Taylor Creek Rhyolite; Taylor Peak; Squaw Creek; S34,T9S,R11W; 33-28-41, 107-57-54; very mildly silicified Taylor Creek Rhyolite. See #26 above.
- 30 8-4-7; Taylor Creek Rhyolite; Taylor Peak; Squaw Creek; S34,T9S,R11W; 33-28-53, 107-57-38; Crystal-rich, white, porous rhyolite lava containing two intersection hematite-cassiterite veinlets.
- 31 8-4-8; Taylor Creek Rhyolite; Taylor Peak; Squaw Creek; S34,T9S,R11W; 33-28-53, 107-57-38; White, porous, crystal-rich rhyolite lava with attached Sn mineralization. The geochemical sample avoided the veinlets. Collected to evaluate the possibility of disseminated mineralization between the Sn-bearing veinlets. Two veinlets are present, one consists of hematite and cassiterite, the other of zeolites.
- 32 8-4-9; Taylor Creek Rhyolite; Taylor Peak; Squaw Creek; S34,T9S,R11W; 33-28-53, 107-57-38; White, porous rhyolite lava with an attached veinlet of small, equant crystals, possibly zeolites. VPC is intense.
- 33 8-4-10; Taylor Creek Rhyolite; Taylor Peak; Squaw Creek; S34,T9S,R11W; 33-28-53, 107-57-38; White, porous, crystal-rich rhyolite lava with an attached Hematite-cassiterite-zeolite veinlet.
- 34 8-4-11; Wood tin; Taylor Peak; Squaw Creek; S34,T9S,R11W; 33-28-54, 107-57-38; Wood tin (?) from a veinlet at the Squaw Creek prospect.
- 35 8-4-12; Hematite; Taylor Peak, Squaw Creek; S34,T9S,R11W; 33-28-54, 107-57-38; Hematite from the upper adit at the Squaw Creek prospect.

- 36 8-4-13; Cassiterite; Taylor Peak; Squaw Creek; S34,T9S,R11W; 33-28-54, 107-57-38; Cassiterite from a nearly pure cassiterite veinlet. This veinlet is the richest tin ore in the Taylor Creek tin district.
- 37 8-4-14a; Taylor Creek Rhyolite; Taylor Peak; Squaw Creek; S34,T9S,R11W; 33-28-53, 107-57-38; White, porous rhyolite lava with an attached Sn-bearing veinlet. Sample 37 consists of material about 6 cm from the veinlet. Sample 38 includes the rhyolite as well as the veinlet itself. VPC is moderate to intense.
- 38 8-4-14b; Taylor Creek Rhyolite; Taylor Peak; Squaw Creek; S34,T9S,R11W; 33-28-53, 107-57-38; See #37 above.
- 39 8-4-15; basaltic andesite of Poverty Creek; Sawmill Peak; Mud Hole; S12,T10S,R10W; 33-27-30, 107-49-50; Mildly propylitized basaltic andesite flow. Minor bleaching along fracture surfaces. The rock is gray with light gray streaks due to the alteration.
- 40 8-4-16; basaltic andesite of Poverty Creek; Sawmill Peak; Mud Hole; S11,T10S,R10W; 33-27-26, 107-49-54; Gray to dark gray, fine grained basaltic andesite lava flow. Slight color changes along fracture surfaces suggest incipient propylitic alteration.
- 41 8-4-17; basaltic andesite of Poverty Creek; Sawmill Peak; Koko Well; S1,T10S,R10W; 33-27-44, 107-48-53; Dark gray, relatively fresh basaltic andesite lava with about 10% ferromagnesian minerals. Bowlingite suggests olivine may have been present. About 5% opaque minerals.
- 42 8-4-18; basaltic andesite of Poverty Creek; Sawmill Peak; Koko Well; S12,T10S,R10W; 33-27-36, 107-49-07; Gray basaltic andesite lava flow. Color suggests mild alteration.
- 43 8-4-19; rhyolite of Sawmill Peak; Sawmill Peak; Mud Hole; S2,T10S,R10W; 33-27-43, 107-50-34; Red, lithoidal rhyolite lava with about 10% sanidine and a trace of biotite. The sanidine is as large as 1.5 cm in length. This sample is believed to be outside the influence of the propylitic alteration associated with the rhyolite porphyry of Kline Mountain.
- 44 8-4-20; tuff of Stiver Canyon; Sawmill Peak; Mud Hole; S2,T10S,R10W; 33-27-41, 107-50-32; Poorly welded, crystal-poor ignimbrite containing 1% quartz, and 1% sanidine with a trace of biotite and opaque minerals. 1 to 2% lithic fragments, most of which are flow banded rhyolite lava. Collected near the top of the unit.
- 45 8-4-21; tuff of Stiver Canyon; Sawmill Peak; Mud Hole; S2,T10S,R10W; 33-27-40, 107-50-32; Crystal-poor, poorly welded ignimbrite from near the base of the unit with 1% sanidine, some of which is iridescent, about 1% quartz, and a trace of biotite. 1 to 2% lithic fragments which are dominantly rhyolite with numerous <1 cm diameter andesitic lithic fragments.
- 46 8-4-22; basaltic andesite of Poverty Creek; Sawmill Peak; Mud Hole; S11,T10S,R10W; 33-27-35, 107-50-35; Mildly propylitized basaltic andesite lava flow. The only evidence of alteration is the slightly bleached

- appearance of the rock. Consists of about 1% iddingsite believed to be an after olivine.
- 47 8-5-1; rhyolite of Sawmill Peak; Sawmill Peak; Mud Hole; S2,T10S,R10W; 33-27-46, 107-50-13; Red, lithoidal rhyolite lava. Bits of vitric groundmass remain and mild bleaching along flow bands is probably due to VPC. The presence of secondary quartz and clays along fractures and the few feldspars that are chalky in appearance suggest mild propylitic alteration.
- 48 8-5-2; tuff of Stiver Canyon; Sawmill Peak; Mud Hole; S2,T10S,R10W; 33-27-45, 107-50-10; White, poorly welded ignimbrite with 1 to 2% phenocrysts of quartz and sanidine and 1 to 2% of very small lithic fragments. Collected near the top of the unit.
- 49 8-5-3; tuff of Stiver Canyon; Sawmill Peak; Mud Hole; S2,T10S,R10W; 33-27-45, 107-50-10; White, poorly welded ignimbrite from near the middle of the unit.
- 50 8-5-4; tuff of Stiver Canyon; Sawmill Peak; Mud Hole; S2,T10S,R10W; 33-27-42, 107-50-13; White, poorly welded ignimbrite. Collected in the lower middle portion of the unit. Crystal-poor with about 2% quartz and sanidine phenocrysts.
- 51 8-5-5; tuff of Stiver Canyon; Sawmill Peak; Mud Hole; S11,T10S,R10W; 33-27-40, 107-50-13; Pumiceous, crystal-poor ignimbrite collected near the base of the unit. Here the unit has few lithic fragments. Pumice fragments to several cm.
- 52 8-5-6; basaltic andesite of Poverty Creek; Sawmill Peak; Mud Hole; S11,T10S,R10W; 33-27-40, 107-50-11; Gray, propylitically altered basaltic andesite lava flow. The rock is jointed every few cm and a truly fresh sample is impossible to obtain. The rock is somewhat bleached and the ferromagnesian minerals are no longer present.
- 53 8-5-7; rhyolite of Sawmill Peak; Sawmill Peak; Mud Hole; S2,T10S,R10W; 33-27-49, 107-50-43; Red, lithoidal rhyolite lava with about 10% phenocrysts of sanidine. Mildly propylitized, the few feldspars are chalky and some are skeletal.
- 54 8-5-8; rhyolite of Dolan Peak; Sawmill Peak; Mud Hole; S2,T10S,R10W; 33-25-51, 107-50-58; Gray, lithoidal rhyolite lava with 2% quartz, 7% sanidine, and a trace of biotite. The feldspars are mildly altered and the rock is mildly silicified. A few lithic fragments are present and are intensely altered.
- 55 8-5-9; rhyolite of Dolan Peak; Sawmill Peak; Mud Hole; S2,T10S,R10W; 33-27-51, 107-51-01; Flow banded, gray to lavender rhyolite lava. 5% sanidine and about 2% quartz with a trace of opaque minerals.
- 56 8-5-10; rhyolite of Dolan Peak; Sawmill Peak; Mud Hole; S2,T10S,R10W; 33-27-50, 107-51-00; Hydrated vitrophyre from the base of the Dolan Peak. 1% quartz, 7% sanidine, and a trace of amphibole (?) as phenocrysts.
- 57 8-5-11; tuff of Kline Mountain; Sawmill Peak; Mud Hole; S2,T10S,R10W; 33-27-45, 107-50-58; Nonwelded, white, moderately crystal-rich rhyolite ignimbrite. About 8% quartz, 12% sanidine, and a trace each of plagioclase,



- biotite, and zircon. Small vitric lithic fragments are identical to the overlying rhyolite of Dolan Peak. The abundant pumice fragments are rounded. Collected near the top of the unit.
- 58 8-5-12; tuff of Kline Mountain; Sawmill Peak; Mud Hole; S2,T10S,R10W; 33-27-45, 107-50-52; Nonwelded, white, pumiceous, moderately crystal-rich rhyolite ignimbrite from near the center of the unit. The rounded pumice are very large (2-4 cm).
- 59 8-5-13; tuff of Kline Mountain; Sawmill Peak; Mud Hole; S2,T10S,R10W; 33-27-44, 107-50-55; Nonwelded, tan, moderately crystal-rich rhyolite ignimbrite. Collected near the base of the unit.
- 60 8-5-14; tuff of Stiver Canyon; Sawmill Peak; Mud Hole; S2,T10S,R10W; 33-27-43, 107-50-53; Pink, poorly welded, crystal-poor ignimbrite collected near the top of the unit. Little hydrothermal alteration.
- 61 8-5-15; tuff of Stiver Canyon; Sawmill Peak; Mud Hole; S11,T10S,R10W; 33-27-35, 107-50-50; Pale pink, crystal-poor, poorly welded rhyolite ignimbrite. The feldspars are fresh, but the groundmass is locally altered to clay minerals.
- 62 8-5-16; tuff of Stiver Canyon; Sawmill Peak; Mud Hole; S11,T10S,R10W; 33-27-35, 107-50-50; Crystal-poor, poorly welded ignimbrite. Manganese oxide coatings on the joint surfaces suggest that this sample is within the alteration halo of the rhyolite porphyry of Kline Mountain.
- 63 8-5-17; tuff of Stiver Canyon; Sawmill Peak; Mud Hole; S11,T10S,R10W; 33-27-32, 107-50-54; Pink, poorly welded, crystal-poor rhyolite ignimbrite. Trace of coppery biotite. The lithic fragments and feldspars are fresh, but the groundmass is locally altered to clay minerals.
- 64 8-5-18; basaltic andesite of Poverty Creek; Sawmill Peak; Mud Hole; S11,T10S,R10W; 33-27-30, 107-50-45; Gray to "purplish" basaltic andesite lava. Dark brown veinlets of Fe and/or Mn oxides. The rock has been mildly propylitized.
- 65 8-5-19; La Jencia Tuff; Sawmill Peak; Mud Hole; S10,T10S,R10W; 33-27-40, 107-51-22; Densely Welded, crystal-poor rhyolite ignimbrite. The rock is various shades of pink, purple, and yellow because of intense argillic alteration. The normally dense rock is here punky and the original textures have been destroyed. The feldspars are relatively fresh.
- 66 8-5-20; La Jencia Tuff; Sawmill Peak; Mud Hole; S10,T10S,R10W; 33-27-40, 107-51-24; Densely welded, crystal-poor rhyolite ignimbrite altered to a punky, clay-rich rock. The original texture has been destroyed, but most of the feldspar phenocrysts are relatively fresh.
- 67 8-5-21; tuff of Kline Mountain; Sawmill Peak; Mud Hole; S10,T10S,R10W; 33-27-36, 107-51-22; White, poorly welded, moderately crystal-rich rhyolite ignimbrite with dark red nodules to 6 cm (#68). The original texture of the rock has been destroyed by alteration and the

- nodules are probably the result of alteration.
- 68 8-5-22; tuff of Kline Mountain; Sawmill Peak; Mud Hole; S10,T10S,R10W; 33-27-35, 107-51-21; Brick-red nodules from within the poorly welded, white, moderately crystal-rich rhyolite ignimbrite. The nodules consist of altered tuff in an iron-rich matrix. #67 above is the ignimbrite surrounding the nodules.
- 69 8-5-23; tuff of Kline Mountain; Sawmill Peak; Mud Hole; S10,T10S,R10W; 33-27-34, 107-51-21; Pink to red, poorly welded ignimbrite that has been mildly altered. The groundmass is dominantly clay. The edges of the pumice fragments and the sanidine phenocrysts are altered to clay minerals. The plagioclase and biotite are completely altered. The vitroclastic texture is obscured, but still recognizable.
- 70 8-5-24; tuff of Stiver Canyon; Sawmill Peak; Mud Hole; S10,T10S,R10W; 33-27-26, 107-51-26; Tan, poorly welded rhyolite ignimbrite with dark brown pumice and lithic fragments. An unidentified, dark brown, sooty material commonly coats joint surfaces.
- 71 8-6-1; La Jencia Tuff; Sawmill Peak; upper Poverty Creek; S3,T10S,R10W; 33-27-44, 107-51-38; Moderately to densely welded, crystal-poor, gray rhyolite ignimbrite. Mild VPC and little if any hydrothermal alteration. Contains about 7% sanidine and a trace of quartz and coppery biotite.
- 72 8-6-2; La Jencia Tuff; Sawmill Peak; upper Poverty Creek; S3,T10S,R10W; 33-27-50, 107-51-25; Densely welded, crystal-poor rhyolite ignimbrite. Similar to #71 above except that VPC is very mild.
- 73 8-6-3; La Jencia Tuff; Sawmill Peak; upper Poverty Creek; S3,T10S,R10W; 33-27-55, 107-51-16; Densely welded, crystal-poor rhyolite ignimbrite that is mildly altered, probably by hydrothermal solutions rather than VPC.
- 74 8-6-4a; La Jencia Tuff; Sawmill Peak; upper Poverty Creek; S3,T10S,R10W; 33-28-08, 107-51-09; Densely welded, crystal-poor rhyolite ignimbrite that is now punky due to hydrothermal alteration. This sample is white. #75 was collected about 5 cm away and is brown. The two samples were collected to investigate the cause of the color difference.
- 75 8-6-4b; La Jencia Tuff; Sawmill Peak; upper Poverty Creek; S3,T10S,R10W; 33-28-08, 107-51-09; See #74.
- 76 8-6-5; La Jencia Tuff; Sawmill Peak; upper Poverty Creek; S10,T10S,R10W; 33-27-36, 107-51-42; Densely welded, crystal-poor rhyolite ignimbrite with minor red stains along fractures and within the sample, suggesting that the rock has undergone mild hydrothermal alteration.
- 77 8-6-6; La Jencia Tuff; Sawmill Peak; upper poverty Creek; S10,T10S,R10W; 33-27-34, 107-51-41; Densely welded, crystal-poor rhyolite ignimbrite that is now punky due to hydrothermal alteration. The sanidine phenocrysts are fresh.
- 78 8-6-7; tuff of Kline Mountain; Sawmill Peak; upper

- Poverty Creek; S10,T10S,R10W; 33-27-35, 107-51-39; White, punky rhyolite ignimbrite with abundant clay minerals in the groundmass. As much as 30% pumice and about 1% lithic fragments. The feldspars are relatively fresh, but the biotite is altered to opaque minerals. Secondary hematite is abundant.
- 79 8-6-8; tuff of Kline Mountain; Sawmill Peak; upper Poverty Creek; S10,T10S,R10W; 33-27-34, 107-51-37; Pink, poorly welded rhyolite ignimbrite. The abundant pumice is white. The sample was collected near vertical features that may be fossil fumaroles (#80). Brown nodules found nearby are ignimbrite cemented with Mn oxides.
- 80 8-6-9; tuff of Kline Mountain; Sawmill Peak; upper Poverty Creek; S10,T10S,R10W; 33-27-33, 107-51-37; Sample of the vertical pipe-like features believed to be fossil fumaroles. The pipe-like features contain pumice and lithic material similar to the surrounding ignimbrite, but lack the fine material which is believed to have been winnowed out.
- 81 8-6-10; tuff of Kline Mountain; Sawmill Peak; upper Poverty Creek; S10,T10S,R10W; 33-27-34, 107-50-32; Mn cemented nodules in the tuff of Kline Mountain.
- 82 8-6-11; La Jencia Tuff; Sawmill Peak; upper Poverty Creek; S10,T10S,R10W; 33-27-18, 107-51-49; Silicified, densely welded, crystal-poor ignimbrite. The feldspar phenocrysts are fresh.
- 83 8-6-12; La Jencia Tuff; Sawmill Peak; upper Poverty Creek; S10,T10S,R10W; 33-27-18, 107-51-47; Densely welded, crystal-poor rhyolite ignimbrite that is now punky due to hydrothermal alteration. The rock is white with pale brown spots. Collected near the base of the unit.
- 84 8-6-13; tuff of Kline Mountain; Sawmill Peak; upper Poverty Creek; S10,T10S,R10W; 33-27-46, 107-51-16; Pink to white, poorly welded, moderately crystal-rich rhyolite ignimbrite. The pumice are nearly all totally kaolinized and all are altered. The feldspars are relatively fresh.
- 85 8-6-14; tuff of Kline Mountain; Sawmill Peak; upper Poverty Creek; S10,T10S,R10W; 33-27-16, 107-51-44; Poorly welded, moderately crystal-rich rhyolite ignimbrite that has been intensely altered. The pumice fragments have been altered to clay minerals and the weathered surfaces are now vuggy where the clay minerals have been eroded. "Fresh" surfaces show the pumice totally altered to white clay minerals. The feldspar phenocrysts are still fresh.
- 86 8-6-15; tuff of Stiver Canyon; Sawmill Peak; upper Poverty Creek; S10,T10S,R10W; 33-27-15, 107-51-40; Intensely kaolinized ignimbrite. The rock is punky due to the intense kaolinization of the groundmass and pumice fragments. Local pods of chalcedonic quartz may be replacements of pumice fragments. Sparse veinlets of opaline silica. The feldspar phenocrysts have been moderately altered to clay minerals.



- 87 8-6-16; tuff of Stiver Canyon; Sawmill Peak; upper Poverty Creek; S10,T10S,R10W; 33-27-15, 107-51-40; Quartz crystals from veinlets that crosscut the ignimbrite collected for possible fluid inclusion work.
- 88 8-6-17; tuff of Kline Mountain; Sawmill Peak; upper Poverty Creek; S9,T10S,R10W; 33-26-47, 107-52-06; Intensely kaolinized, poorly welded ignimbrite. The sample is >95% clay minerals with 2 to 5% relict quartz phenocrysts. The original texture has been totally obscured. No feldspar phenocrysts remain.
- 89 8-6-18; tuff of Kline Mountain; Sawmill Peak; upper Poverty Creek; S9,T10S,R10W; 33-26-49, 107-52-09; Intensely kaolinized ignimbrite. The feldspar phenocrysts and pumice fragments are all altered to clay minerals. On weathered surfaces, the original texture may locally be discerned.
- 90 8-6-19; tuff of Kline Mountain; Sawmill Peak; upper Poverty Creek; S16,T10S,R10W; 33-26-39, 107-52-10; Totally kaolinized ignimbrite. On weathered surfaces, relict texture is obvious.
- 91 8-6-20; tuff of Kline Mountain; Sawmill Peak; Clay pits; S16,T10S,R10W; 33-26-37, 107-52-09; Red, brown, and white chalcedonic quartz replacement of the tuff of Kline Mountain. This material is the end stage of the advanced argillic alteration in the area.
- 92 8-6-21; tuff of Kline Mountain; Sawmill Peak; Clay pits; S16,T10S,R10W; 33-26-44, 107-52-12; Kaolinized and partially silicified tuff of Kline Mountain.
- 93 8-6-22; tuff of Kline Mountain; Sawmill Peak; Clay Pits; S16,T10S,R10W; 33-26-42, 107-52-10; Sample of the silica replacement (#92) above that contains tiny, euhedral quartz crystals useful for fluid inclusion study.
- 94 8-6-23; tuff of Kline Mountain; Sawmill Peak; Clay Pits; S10,T10S,R10W; 33-27-03, 102-52-02; Very pumiceous ignimbrite that has been kaolinized and silicified. On weathered surfaces, the relict texture is obvious.
- 95 8-6-24; tuff of Kline Mountain; Sawmill Peak; Clay Pits; S10,T10S,R10W; 33-27-02, 107-51-56; Intensely kaolinized pumiceous ignimbrite.
- 96 8-6-25; tuff of Stiver Canyon; Sawmill Peak; Clay pits; S10,T10S,R10W; 33-27-03, 107-51-52; Mildly kaolinized and silicified crystal-poor ignimbrite. Vugs are produced where the clay minerals are eroded.
- 97 8-10-1; Taylor Creek Rhyolite; Wall Lake; Wall Lake; S2,T11S,R12W; 33-21-53, 108-03-47; Crystal-rich, white rhyolite lava with a hematite-cassiterite veinlet attached.
- 98 8-10-2; wood tin; Taylor Peak; Nugget Gulch; S2,T9S,R10W; 33-29-34, 107-52-34; Placer wood tin from Nugget Gulch.
- 99 8-10-3; ore; Wall Lake; Wall Lake; S2,T11S,R12W; 33-21-53, 108-03-47; Hematite-cassiterite vein material from the Dawson Mine.
- 100 9-14-1; tuff of Kline Mountain; Sawmill Peak; Clay pits; S16,T10S,R10W; 33-26-34, 107-52-06; Sample of the silica replacement of the tuff of Kline Mountain collected

- about 200 m south of the main kaolin pit. The sample is brecciated and contains abundant Fe oxides and quartz crystals. For fluid inclusion work.
- 101 9-16-1; rhyolite porphyry of Kline Mountain; Kline Mountain; S23,T10S,R10W; 33-25-25, 107-50-31; Intensely argillized and silicified rhyolite porphyry intrusive. The rock contains abundant quartz-pyrite stockwork veinlets. Some fractures are coated by pyrite. Disseminated pyrite to about 0.25%. The rock is gray with clear, subhedral quartz and pyrite. The feldspars are altered to clay minerals.
- 102 10-4-1; rhyolite porphyry of Kline Mountain; Sawmill Peak; Kline Mountain; S23,T10S,R10W; 33-25-10, 107-50-10; Argillized rhyolite porphyry intrusive that contains about 5% euhedral quartz and 5% sanidine which is in various stages of alteration to clay minerals. The altered sanidine frequently has a satin sheen. Joint surfaces are locally coated with as much as 3 mm of a vitreous, black mineral reminiscent of tenorite, but which is probable a Mn oxide.
- 103 10-4-2; rhyolite porphyry of Kline Mountain; Sawmill Peak; Kline Mountain; S23,T10S,R10W; 33-25-10, 107-50-12; Gray to brown rhyolite porphyry that contains about 3% quartz and 5% sanidine phenocrysts. The rock is intensely argillized and silicified. The feldspars are all altered to clay minerals.
- 104 10-4-3; rhyolite porphyry of Kline Mountain; Sawmill Peak; Kline Mountain; S23,T10S,R10W; 33-25-15, 107-50-38; Flow banded rhyolite porphyry with about 7% sanidine and 3% quartz phenocrysts. The quartz occurs as rounded to euhedral grains to 3 mm diameter. The feldspar is generally euhedral with cloudy rims.
- 105 10-4-4; rhyolite porphyry of Kline Mountain; Sawmill Peak; Kline Mountain; S23,T10S,R10W; 33-25-15, 107-50-21; Gray rhyolite porphyry that is only mildly argillized.
- 106 10-4-5a; rhyolite porphyry of Kline Mountain; Sawmill Peak; Kline Mountain; S23,T10S,R10W; 33-25-23, 107-50-31; Brecciated rhyolite porphyry with quartz breccia filling and stockworks.
- 107 10-4-5b; rhyolite porphyry of Kline Mountain; Sawmill Peak; Kline Mountain; S23,T10S,R10W; 33-25-23, 107-50-31; Rhyolite porphyry that has had all the feldspar and pyrite leached out.
- 108 10-4-5c; rhyolite porphyry of Kline Mountain; Sawmill Peak; Kline Mountain; S23,T10S,R10W; 33-25-23, 107-50-31; Intensely silicified rhyolite porphyry with minor secondary pyrite euhedra.
- 109 10-5-1; tuff of Kline Mountain; Sawmill Peak; Kline Mountain; S23,T10S,R10W; 33-25-43, 107-50-47; Intensely alunitized and kaolinized ignimbrite. Primary textures are totally obscured, but weathered surfaces suggest that this rock was an ignimbrite prior to alteration. It now consists of >60% alunite. Collected for dating (alunite).
- 110 no sample

- 111 10-6-1; breccia; Sawmill Peak; Bear Creek; S36,T10S,R10W; 33-23-32, 107-49-26; Green, propylitically altered breccia consisting of andesite and rhyolite fragments in a matrix of rhyolite similar to the rhyolite porphyry of Kline Mountain. The breccia is near the contact of rhyolite porphyry of Kline Mountain and the tuff of Stiver Canyon.
- 112 10-7-1; tuff of Stiver Canyon, Sawmill Peak, Whiskey Spring; S34,T10S,R10W; 33-24-02, 107-51-30; Argillized tuff of Stiver Canyon. Most of the feldspars are altered to clay minerals.
- 113 10-8-1; hematite-cassiterite vein material; Chise; Monticello Cutoff; S31,T11S,R6W; 33-18-54, 107-30-13; Hematite-cassiterite vein material collected from near the adit immediately east of the Monticello cutoff road in Willow Springs Draw.
- 114 10-8-2; vein material; Chise; Monticello Cutoff; S31,T11S,R6W; 33-18-54, 107-30-13; Quartz crystals from the quartz-calcite veins that occur with the hematite-cassiterite veinlets.
- 115 10-8-3; rhyolite of Willow Springs Draw; Chise; Monticello Cutoff; S31,T11S,R6W; 33-18-54, 107-30-13; Crystal-rich, flow banded lava similar to the Taylor Creek Rhyolite in the Black Range to the west. The rock contains about 11% quartz, 18% sanidine, and traces each of plagioclase and biotite as phenocrysts. The rock is relatively unaffected by VPC.
- 116 10-8-4; rhyolite of Willow Springs Draw; Chise; Monticello Cutoff; S31,T11S,R6W; 33-18-55, 107-30-14; Crystal-rich rhyolite lava that is little affected by VPC. This is probably the freshest sample collected in this unit.
- 117 10-8-5; rhyolite of Willow Springs Draw; Chise; Monticello Cutoff; S31,T11S,R6W; 33-18-54, 107-30-13; Crystal-rich rhyolite lava boulder with attached hematite-cassiterite veinlet.
- 118 10-8-6; vein material; Chise; Monticello Cutoff; S31,T11S,R6W; 33-18-33, 107-29-25; Dominantly hematite with minor cassiterite.
- 119 10-8-7; vein material; Chise; Monticello Cutoff; S31,T11S,R6W; 33-18-33, 107-29-25; Quartz crystals with minor hematite coatings associated with the hematite-cassiterite veinlets.
- 120 10-8-8; rhyolite of Willow Springs Draw; Chise; Monticello Cutoff; S31,T11S,R6W; 33-18-33, 107-29-25; Crystal-rich rhyolite lava with attached hematite-cassiterite veinlet. Intense VPC.
- 121 10-8-9; rhyolite of Willow Springs Draw; Chise; Monticello Cutoff; S31,T11S,R6W; 33-18-33, 107-29-25; Crystal-rich rhyolite lava little affected by VPC.
- 122 10-8-10; rhyolite of Willow Springs Draw; Chise; Monticello Cutoff; S31,T11S,R6W; 33-18-30, 107-29-24; Crystal-rich rhyolite lava. Moderate to intense VPC.
- 123 10-19-1; tuff of Koko Well; Sawmill Peak; Turkey Creek; S19,T10S,R9W; 33-25-50, 107-48-25; Crystal-poor ignimbrite. About 5% sanidine, 3% plagioclase, 1%



- biotite and a trace each of pyroxene and opaque minerals as phenocrysts. Chlorite is present along fractures suggesting minor propylitic alteration. This sample is from the thin, discontinuous, moderately welded ignimbrite at the base of the thick, poorly welded main body of the tuff of Koko Well.
- 124 10-19-2; rhyolite porphyry of Kline Mountain; Sawmill Peak; Kline Mountain; S23,T10S,R10W; 33-25-21, 107-50-31; Intensely argillized rhyolite porphyry intrusive.
- 125 10-19-3; rhyolite porphyry of Kline Mountain; Sawmill Peak; Kline Mountain; S35,T10S,R10W; 33-23-49, 107-50-41; Relatively fresh rhyolite porphyry. The rock is pink with slightly cloudy feldspars. Collected near the south contact of the intrusive.
- 126 10-19-4; rhyolite porphyry of Kline Mountain; Sawmill Peak; S35,T10S,R10W; 33-23-47, 107-50-41; Mildly silicified rhyolite porphyry intrusive. The feldspars are locally cloudy.
- 127 10-19-5; rhyolite porphyry of Kline Mountain; Sawmill Peak; S23,T10S,R10W; 33-25-26, 107-50-34; Mildly silicified and argillized rhyolite porphyry. The feldspars all consist dominantly of clay minerals with minor skeletal remains. Minor disseminated pyrite.
- 128 10-20-1; Taylor Creek Rhyolite; Taylor Peak; Squaw Creek; S34,T9S,R11W; 33-28-54, 107-57-38; Flow banded, crystal-rich rhyolite lava collected near the tin occurrence in Squaw Creek. The joints bounding the boulder are coated with a clear mineral, possibly zeolite.
- 129 10-20-2; vein material; Taylor Peak; Squaw Creek; S34,T9S,R11W; 33-28-53, 107-57-38; This sample consists of a boulder of Taylor Creek with attached hematite-cassiterite veinlets. Some of the hematite has been etched.
- 130 10-20-3; vein material; Taylor Peak; Squaw Creek; S34,T9S,R11W; 33-28-53, 107-57-38; Taylor Creek Rhyolite boulder with attached hematite-cassiterite mineralization.
- 131 10-21-1; Taylor Creek Rhyolite; Taylor Peak; Paramount Canyon; S22,T10S,R11W; 33-25-15, 107-57-29; Crystal-rich, flow banded rhyolite lava. The lava is lithophysal and the lithophysae contain drusy linings of quartz crystals with minor pseudobrookite, hematite, and rare red beryl and bixbyite. Collected about 150 m east of the Paramount Canyon tin occurrence.
- 132 10-21-2; Taylor Creek Rhyolite; Taylor Peak; Paramount Canyon; S27,T10S,R11W; 33-25-11, 107-57-30; Crystal-rich, flow banded, white rhyolite lava. The sample was collected about 0.5 m from the tin-bearing veinlet at the Paramount Canyon tin occurrence. The rock contains lithophysae with drusy linings of quartz, hematite, pseudobrookite, bixbyite, and possibly topaz. Moderate VPC.
- 133 10-21-3; vein material; Taylor Peak; Paramount Canyon; S27,T10S,R11W; 33-25-11, 107-57-30; Hematite-cassiterite vein material collected from the dumps at the Paramount

- Canyon tin occurrence.
- 134 11-1-1; Taylor Creek Rhyolite; Bailey Points; Round Mountain; S30,T11S,R10W; 33-18-43, 107-54-48; Crystal-rich flow banded, white rhyolite lava. The rock contains about 12% quartz and 18% sanidine phenocrysts in a gray to lavender groundmass. The phenocrysts rarely exceed 2 mm diameter. Intense VPC.
- 135 11-1-2; Taylor Creek Rhyolite; Bailey Points; Round Mountain; S30,T11S,R10W; 33-18-38, 107-54-49; Lithophysal, crystal-rich rhyolite lava. Each lithophysae contain a single, large (to 3 cm) topaz crystal. The topaz crystals contain numerous inclusions of quartz, hematite, and possibly pseudobrookite and bixbyite. Intense VPC.
- 136 11-15-1; Taylor Creek Rhyolite; Taylor Creek Rhyolite; Nugget Gulch; S29,T9S,R10W; 33-29-33, 107-53-31; Crystal-rich, flow banded, white to lavender rhyolite lava. The sample is little affected by VPC. The sample contains about 8% quartz, 9% sanidine and traces each of biotite and zircon. The quartz are <4 mm and the sanidine <2 mm.
- 137 11-15-2; Taylor Creek Rhyolite; Taylor Creek, Nugget Gulch; S28,T9S,R10W; 33-29-46, 107-52-45; Black, perlitic vitrophyre from the carapace breccia in Nugget Gulch. The feldspars are chalky, but the rest of the rock is apparently unaltered. XRD patterns of the feldspar indicate that it is opal rather than feldspar.
- 138 11-15-3; Taylor Creek Rhyolite; Taylor Peak; Nugget Gulch; S28,T9S,R10W; 33-29-45, 107-52-43; Siliceous sinter resulting from replacement of crystal-rich rhyolite lava by chalcedonic quartz.
- 139 11-15-4; Taylor Creek Rhyolite; Taylor Peak; Nugget Gulch; S28,T9S,R10W; 33-29-40, 107-52-40; Silicified Taylor Creek Rhyolite with attached wood tin.
- 140 11-15-5; Taylor Creek Rhyolite; Taylor Peak; Nugget Gulch; S33,T9S,R10W; 33-29-03, 107-52-34; Punky, crystal-rich rhyolite lava. The punky nature of the rock is due to intense VPC. The phenocrysts of sanidine are fresh as are the biotite phenocrysts, indicating that this is not an hydrothermal alteration. The rock consists of about 10% quartz, 14% sanidine, and a trace each of biotite and opaque minerals.
- 141 11-15-6; Taylor Creek Rhyolite; Taylor Peak; Nugget Gulch; S33,T9S,R10W; 33-29-16, 107-52-32; Punky, crystal-rich rhyolite lava. Intense VPC. This is about the most intense VPC found in the region.
- 142 11-15-7; Taylor Creek Rhyolite; Taylor Peak; Nugget Gulch; S28,T9S,R10W; 33-29-30, 107-52-35; Crystal-rich, white rhyolite lava. Moderate VPC.
- 143 11-15-8; Taylor Creek Rhyolite; Taylor Peak; Nugget Gulch; S28,T9S,R10W; 33-29-39, 107-52-43; White, flow banded, crystal-rich rhyolite lava. Moderate VPC.
- 144 11-15-9; Taylor Creek Rhyolite; Taylor Peak; Nugget Gulch; S28,T9S,R10W; 33-29-41, 107-52-46; Red, punky, clay-rich rhyolite lava. This sample has undergone intense hydrothermal alteration.



- 145 11-15-10; Taylor Creek Rhyolite; Taylor Peak; Nugget Gulch; S28,T9S,R10W; 33-29-43, 107-52-42; Intensely altered rhyolite lava. The sample consists of relict quartz and sanidine phenocrysts in a clay matrix.
- 146 11-15-11a; Taylor Creek Rhyolite; Taylor Peak; Nugget Gulch; S28,T9S,R10W; 33-29-37, 107-52-50; Intensely silicified Taylor Creek Rhyolite from adjacent to an hematite-cassiterite veinlet.
- 147 11-15-11b; Taylor Creek Rhyolite; Taylor Peak; Nugget Gulch; S28,T9S,R10W; 33-29-37, 107-52-50; Silicified Taylor Creek Rhyolite about 10 cm from an hematite-cassiterite-bearing veinlet.
- 148 11-15-12; Taylor Creek Rhyolite; Taylor Peak; Nugget Gulch; S28,T9S,R10W; 33-29-33, 107-52-54; Taylor Creek Rhyolite with attached tin mineralization from the exploration adit south of Nugget Gulch.
- 149 11-16-1; Taylor Creek Rhyolite; Taylor Peak; Paramount Canyon; S27,T1S,R11W; 33-25-02, 107-57-44; Vitrophyre of crystal-rich, flow banded rhyolite lava. The glass is green. Collected from the carapace breccia on top of the Boiler Peak dome. Contains about 7% quartz, 8% sanidine, 1% plagioclase, and a trace of biotite and green hornblende as phenocrysts. Minor spherulitic devitrification and abundant perlitic cracks.
- 150 11-16-2; Taylor Creek Rhyolite; Taylor Peak; Paramount Canyon; S27,T10S,R11W; 33-24-56, 107-57-26; White, crystal-rich rhyolite lava. Intense VPC.
- 151 11-16-3; Taylor Creek Rhyolite; Taylor Peak; Paramount Canyon; S27,T10S,R11W; 33-25-05, 107-57-25; White, Crystal-rich rhyolite lava. Mild to moderate VPC. The feldspars are fresh with cloudy rims.
- 152 11-16-4; Taylor Creek Rhyolite; Taylor Peak; Paramount Canyon; S27,T10S,R11W; 33-25-05, 107-57-30; Punky, crystal-rich rhyolite lava. Intense VPC. The groundmass contains minor clay minerals. VPC, weathering, or hydrothermal alteration may be the source of the clays. The feldspars are very fresh. The biotite and plagioclase are mildly to intensely altered. Large overgrowths on the quartz.
- 153 11-16-5; Taylor Creek Rhyolite; Taylor Peak; Paramount Canyon; S21,T10S,R11W; 33-25-36, 107-56-47; Crystal-rich, brown rhyolite lava. Lithic fragments to 3 cm diameter are common in this rock which is at the base of the flow that overlies the Boiler Peak dome. The rock consists of about 7% quartz, 9% sanidine, and a trace of biotite and green hornblende as phenocrysts in a vitric, flow banded groundmass.
- 154 11-16-6; Tt5; Taylor Peak; Paramount Canyon; S21,T10S,R11W; 33-25-52, 107-56-25; Crystal-rich, lithic-rich, white, poorly welded ignimbrite. Associated with thin sedimentary and pyroclastic rocks above the Boiler Peak dome.
- 155 11-17-1; Taylor Creek Rhyolite; Wall Lake; Wall Lake; S2,T11S,R12W; 33-21-39, 108-03-45; Red-brown, crystal-rich rhyolite lava. No VPC. Collected in the Tin Co. adit on Taylor Creek. The rock consists of 17% quartz,

- 14% sanidine, 1% plagioclase, 1% biotite, and traces each of zircon and sphene in a spherulitically devitrified groundmass.
- 156 11-17-2; vein material; Wall Lake; Wall Lake; S2,T11S,R12W; 33-21-39, 108-03-45; Chalcedony-quartz-fluorite vein attached to rhyolite host rock from the Tin Co. adit on Taylor Creek.
- 157 11-17-3; vein material; Wall Lake; Wall Lake; S2,T11S,R2W; 33-21-39, 108-03-45; Vein quartz from the Tin Co. adit on Taylor Creek.
- 158 11-17-4a; vein material; Wall Lake; Wall Lake; S2,T11S,R12W; 33-21-51, 108-03-49; Vein quartz and chalcedony with disseminated purple fluorite. The main vein consists of chalcedonic quartz with drusy quartz lining open space.
- 159 11-17-4b; Taylor Creek Rhyolite; Wall Lake; Wall Lake; S2,T11S,R12W; 33-21-51, 108-03-49; Intensely altered Taylor Creek Rhyolite at the margins of a quartz-fluorite vein (#158 above).
- 160 11-17-4c; clay minerals(?); Wall Lake; Wall Lake; S2,T11S,R12W; 33-21-51, 108-03-49; Clays that surround the quartz-fluorite vein in #158 above. The clays form a selvage between the quartz-fluorite vein and the wallrock.
- 161 11-17-5; vein material; Wall Lake; Wall Lake; S2,T11S,R12W; 33-21-51, 108-03-49; Intensely altered (probably VPC) rhyolite with as much as 10% disseminated hematite and minor cassiterite from a vein-like structure in the Tin Co. adit on Taylor Creek.
- 162 11-17-6; Hematite; Wall Lake; Wall Lake; S2,T11S,R12W; 33-21-51, 108-03-48; Hematite with very minor cassiterite mineralization from a veinlet cut by the Tin Co. adit on Taylor Creek.
- 163 11-17-7; vein material; Wall Lake; Wall Lake; S2,T11S,R12W; 33-21-51, 108-03-49; Vein quartz that has little of the fluorite found in most of the vein quartz in the area. Vein dips 40 degrees.
- 164 11-17-8; Taylor Creek Rhyolite; Wall Lake; Wall Lake; S2,T11S,R12W; 33-21-51, 108-03-49; Porous, intensely VPC rhyolite lava that contains abundant zeolites(?).
- 165 11-17-9; Taylor Creek Rhyolite; Wall Lake; Wall Lake; S2,T11S,R12W; 33-21-53, 108-03-45; White, somewhat punky rhyolite lava. Intense VPC. Collected near the main tin prospects at the Dawson Mine.
- 166 11-17-10; vein material; Wall Lake; Wall Lake; S2,T11S,R12W; 33-21-52, 108-03-47; Hematite-cassiterite mineralization from float around the main Dawson Mine.
- 167 11-17-11; Taylor Creek Rhyolite; Wall Lake; Wall Lake; S2,T11S,R12W; 33-21-35, 108-03-57; Crystal-rich rhyolite lava from the fringes of the Kemp Mesa Dome.
- 168 11-18-1; Taylor Creek Rhyolite; Wall Lake; Kemp Mesa; S5,T11S,R12W; 33-21-53, 108-06-40; Crystal-rich rhyolite lava. Intense VPC. From the prospects on Kemp Mesa.
- 169 11-18-2; vein material; Wall Lake; Kemp Mesa; S5,T11S,R12W; 33-21-48, 108-06-40; Hematite-cassiterite mineralization attached to a boulder of crystal-rich

- rhyolite lava.
- 170 11-18-3; vein material; Wall Lake; Kemp Mesa; S5,T11S,R12W; 33-21-48, 108-06-40; Hematite-cassiterite mineralization from the dumps around the prospect pits on Kemp Mesa.
- 171 83-6-1; Hematite breccia; Sawmill Peak; Kline Mountain; S28,T10S,R10W; 33-24-52, 107-52-11; Brecciated rhyolite porphyry cemented by hematite. Several float samples were collected, the material was never found in place. The sample consists of 70 to 80% hematite surrounding rhyolite fragments. May be a gossan.
- 172 83-6-2; Vein quartz; Taylor Peak; Kline Mountain; S28,T10S,R10W; 33-24-15; 107-52-43; Vein quartz crosscutting the tuff of Stiver Canyon. Collected for possible fluid inclusion work.
- 173 83-6-3; rhyolite porphyry of Kline Mountain; Sawmill Peak; Kline Mountain; S27,T10S,R10W; 33-24-44, 107-51-01; Quartz-pyrite stockworks in intrusive rhyolite porphyry. The pyrite forms selvages bounding the quartz veinlets. Advanced argillic alteration.
- 174 83-6-4; rhyolite porphyry of Kline Mountain; Sawmill Peak; Kline Mountain; S27,T10S,R10W; 33-25-16, 107-51-02; Intensely alunited and kaolinized rhyolite porphyry. The rock is >60% alunite so the original rock type is obscure.
- 175 83-6-5; basaltic andesite of Poverty Creek; Sawmill Peak; Kline Mountain; S27,T10S,R10W; 33-24-58, 107-51-52; Mildly propylitized gray to green basaltic andesite lava.
- 176 83-6-6; La Jencia Tuff; Taylor Peak; Scales Canyon; S28,T10S,R10W; 33-25-00, 107-52-53; Dark green vitrophyre of moderately to densely welded, crystal-poor ignimbrite. Collected near the base of the unit.
- 177 83-6-7; La Jencia Tuff; Taylor Peak; Scales Canyon; S21,T10S,R10W; 33-25-03, 107-52-53; Moderately to densely welded, crystal-poor ignimbrite. Devitrified, 7 to 10% sanidine, trace quartz. Black pumice imparts a pronounced foliation.
- 178 83-6-8; Tt5; Taylor Peak; Scales Canyon; S29,T10S,R10W; 33-24-25, 107-53-16; Sample of vesiculated block from the coarse breccia found at the top of the nonwelded pyroclastic section in Scales Canyon.
- 179 83-6-9; crystal-rich rhyolite lava; Taylor Peak; Scales Canyon; S29,T10S,R10W; 33-24-47, 107-53-52; Clast from the sandstone of Inman Ranch. The clast is mildly silicified, lithoidal, crystal-rich rhyolite lava that may have originated from the Boiler Peak dome.
- 180 83-6-10; rhyolite of HOK Ranch; Chise; Willow Springs Draw; S25,T11S,R7W; 33-19-12, 107-31-12; Two feldspar, crystal-rich rhyolite lava. 7% quartz, 7% sanidine, 2% plagioclase, and 2% biotite as phenocrysts. Plagioclase is milky, sanidine is clear.
- 181 83-6-11; rhyolite of Willow Springs Draw; Chise; Monticello Cutoff road; S36,T11S,R7W; 33-18-58, 107-30-39; Vesicular, brecciated, crystal-rich rhyolite lava from the carapace breccia of the rhyolite of Willow



- Springs Draw. Intense deuteric alteration.
- 182 83-6-12; La Jencia Tuff; Taylor Peak; Stiver Canyon; S32,T10S,R10W; 33-23-30, 107-52-55; Moderate to densely welded, crystal-poor ignimbrite. 5% sanidine and a trace each of quartz, biotite, brown hornblende, and lithic fragments. Mild VPC.
- 183 83-6-13; silica sinter; Taylor Peak; Nugget Gulch; S28,T9S,R10W; 33-29-45, 107-52-45; Silica sinter(?) from Nugget Gulch. The sample is entirely chalcedonic quartz with relict quartz phenocrysts suggesting that the rock may be due to replacement of the Taylor Creek Rhyolite. Small drusy quartz crystals in vugs may be amenable to fluid inclusion study.
- 184 83-6-14; wood tin; Taylor Peak; Nugget Gulch; S28,T9S,R10W; 33-29-45, 107-52-45; Fluid inclusion sample.
- 185 83-6-15; vein material; Taylor Peak; Scales Canyon; S30,T10S,R10W; 33-24-23, 107-54-53; Quartz with hematite but little cassiterite. Fluid inclusion sample.
- 186 83-6-16; vein material; Taylor Peak; Squaw Creek; S34,T9S,R11W; 33-28-53, 107-57-38; Hematite-cassiterite vein material from the Squaw Creek tin prospect.
- 187 83-6-17; Tt5; Taylor Peak; Scales Canyon; S29,T10S,R10W; 33-24-46, 107-53-17; Pumice fragments from the coarse air-fall deposit below the breccia in Scales Canyon. May be a Plinian deposit.
- 188 83-6-18; Tt5; Taylor Peak; Scales Canyon; S29,T10S,R10W; 33-24-45, 107-53-17; Pumice fragments from the thin air-fall(?) deposits above the thick air-fall and below the breccia in Scales Canyon.
- 189 83-6-19a; Tt5; Taylor Peak; Scales Canyon; S29,T10S,R10W; 33-24-46, 107-53-17; Block from the breccia at the top of the nonwelded pyroclastic section in Scales Canyon. The blocks consist of mildly vesiculated, crystal-rich rhyolite lava. Very mild VPC. This sample is a mildly vesiculated block with mild VPC. Collected from the poorly indurated base of the unit.
- 190 83-6-19b; Tt5; Taylor Peak; Scales Canyon; S29,T10S,R10W; 33-24-46, 107-53-17; Vitric block from the breccia in #189 above.
- 191 83-6-19c; Tt5; Taylor Peak; Scales Canyon; S29,T10S,R10W; 33-24-46, 107-53-17; Mildly vesiculated, lithoidal block from the breccia in #189 above.
- 192 83-6-20; Tt5; Taylor Peak; Scales Canyon; S19,T10S,R10W; 33-25-04, 107-54-15; Pumice fragments from a thin ignimbrite that laps onto the Boiler Peak dome. The deposit is nonwelded and quite easily disaggregated. This particular ignimbrite is only 0.5 to 0.75 m thick, but the entire sequence of pyroclastic material may be as much as 30 m thick.
- 193 83-6-21; La Jencia Tuff(?); Taylor Peak; Scales Canyon; S30,T10S,R10W; 33-24-38, 107-54-29; Pre-Taylor Creek Rhyolite crystal-poor rhyolite ignimbrite that dips under the Taylor Creek. Consists of only a few percent of sanidine phenocrysts in a tan to gray groundmass. Pumice fragments are gray to black. Though poorly

- welded, this unit may correlate with the nearby densely welded La Jencia Tuff.
- 194 83-6-22; quartz; Taylor Peak; Jct. of Scales and Stiver Canyons; S31,T10S,R10W; 33-23-55, 107-54-56; Lithophysal quartz handpicked from the lithophysae in Taylor Creek Rhyolite. Collected for fluid inclusion study.
- 195 83-6-23; rhyolite of Dolan Peak; Bailey Points; Near Lookout Mountain; approx. S3,T11S,R10W; Crystal-rich rhyolite lava. Mild VPC. About 7% sanidine and 1% quartz phenocrysts with a trace of biotite and zircon.
- 196 83-7-1; fluorite; Taylor Peak; Nugget Gulch; S28,T9S,R10W; 33-29-45, 107-52-45; Massive fluorite from the tin prospects at Nugget Gulch. Found only in float, the block

- 197 83-11-1; granite of Iron Mountain; Iron Mountain; Iron Mountain; S35,T9S,R8W; 33-32-40, 107-37-17; Fine grained, aplitic granite with abundant secondary(?) biotite.
- 198 83-11-2; granite of Iron Mountain; Iron Mountain; Iron Mountain; S35,T9S,R8W; 33-32-40, 107-37-17; Aplitic granite with as much as 5% secondary biotite.
- 199 83-11-3; granite of Iron Mountain; Iron Mountain; Iron Mountain; S35,T9S,R8W; 33-32-40, 107-37-17; Aplitic granite with stockworks of quartz-fluorite mineralization. Abundant secondary biotite. Some fluorite is disseminated and may be primary, phenocrystic fluorite.
- 200 83-11-4; granite of Iron Mountain; Iron Mountain; Iron Mountain; S35,T9S,R8W; 33-32-40, 107-37-17; Aplitic granite with quartz-fluorite stockworks and minor "phenocrystic" fluorite.
- 201 KAIM-1; granite of Iron Mountain; Iron Mountain; Iron Mountain; approx. S35,T9S,R8W; Aplitic granite. Dated by Charles Chapin. Sample courtesy of Charles Chapin, New Mexico Bureau of Mines and Mineral Resources.
- 202 83-11-5; Bloodgood Canyon Tuff; Indian Peaks West; Railroad Canyon; S22,T8S,R12W; 33-36-06, 108-03-14; Base of the Bloodgood Canyon Tuff, a crystal-poor, moderately welded regional ignimbrite.
- 203 83-11-6; Bloodgood Canyon Tuff; Indian Peaks West; Railroad Canyon; S22,T8S,R12W; 33-36-06, 108-03-14; Middle of the Bloodgood Canyon Tuff.
- 204 83-11-7; Bloodgood Canyon Tuff; Indian Peaks West; Railroad Canyon; S22,T8S,R12W; 33-36-06, 108-03-14; Top of the Bloodgood Canyon Tuff.
- 205 84-6-12-1; Taylor Creek Rhyolite; Indian Peaks East; S33,T8S,R11W; 33-34-18, 107-59-26; Fine grained, crystal-rich rhyolite lava. About 8% quartz, 8% sanidine, 1% plagioclase, and 0.5% biotite phenocrysts with a trace each of zircon and opaque minerals. Mild VPC.
- 206 84-6-12-2; Taylor Creek Rhyolite; Indian Peaks West; Indian Peaks; S6,T9S,R11W; 33-33-16, 108-00-38; Crystal-rich rhyolite lava similar to #205.
- 207 84-6-12-3; Taylor Creek Rhyolite; Indian Peaks West; Indian Peaks; S33,T8S,R11W; 33-33-49, 108-00-07; Flow banded, crystal-rich rhyolite lava with about 10% quartz, 10% sanidine, and a trace of plagioclase and opaque minerals as phenocrysts. Very minor VPC.
- 208 84-6-12-4; Taylor Creek Rhyolite; Indian Peaks West; Indian Peaks; S31,T8S,R11W; 33-34-14, 108-00-26; Crystal-rich rhyolite lava with moderate VPC.
- 209 84-6-12-5; tuff of Garcia Camp; Indian Peaks West; Indian Peaks; S25,T8S,R12W; 33-36-03, 108-02-53; Nonwelded, crystal-rich, rhyolite ignimbrite. Intense VPC. About 10% quartz, 6% sanidine, 1% biotite, and a trace of plagioclase and zircon as phenocrysts in a vitroclastic groundmass.
- 210 84-6-12-6; unnamed rhyolite lava; Indian Peaks West; Indian Peaks; S33,T8S,R11W; 33-36-27, 108-00-26;

- Spherulitic, crystal-poor rhyolite lava beneath the Taylor Creek Rhyolite north of Indian Peaks. Intense deuteric(?) alteration.
- 211 84-6-12-7; Taylor Creek Rhyolite; Indian Peaks West; Indian Peaks; S19,T8S,R11W; 33-36-21, 108-01-37; Crystal-rich rhyolite lava. Moderate VPC. From the breccia at the base of the flow.
- 212 84-6-12-8; wood tin; Indian Peaks West; Indian Peaks; S36,T8S,R12W; Wood tin float from the piedmont slope surface south of Indian Peaks.
- 213 84-6-13-1; Taylor Creek Rhyolite; Taylor Peak; Alexander Cienega; S34,T10S,R11W; 33-23-41, 107-57-07; White, medium grained, crystal-rich rhyolite lava. About 8% quartz, 13% sanidine, and a trace each of plagioclase, zircon, and opaque minerals as phenocrysts. Moderate VPC.
- 214 84-6-13-2; Taylor Creek Rhyolite; Taylor Peak; Alexander Cienega; S1,T11S,R11W; 33-23-12, 107-56-20; Crystal-rich rhyolite lava similar to #213 above except intense VPC.
- 215 84-6-13-3; Taylor Creek Rhyolite; Taylor Peak; Alexander Cienega; S1,T11S,R11W; 33-22-50, 107-55-55; Crystal-rich rhyolite lava from the carapace breccia of the Alexander Cienega Dome. Relatively fresh with about 6% quartz, 11% sanidine, and a trace of plagioclase, biotite, and possibly hornblende as phenocrysts. Very mild VPC.
- 216 84-6-13-4; Taylor Creek Rhyolite; Taylor Peak; Alexander Cienega; S1,T11S,R11W; 33-22-48, 107-55-54; Crystal-rich, hydrated rhyolite lava vitrophyre from the carapace breccia of the Alexander Cienega Dome. Contains about 9% quartz, 8% sanidine, and a trace each of plagioclase, hornblende, zircon, and opaque minerals as phenocrysts. Minor spherulitic devitrification.
- 217 84-6-13-5; Bearwallow Mountain Formation; Bailey Points; Alexander Cienega; S1,T11S,R11W; 33-22-26, 107-56-07; Black, vesicular basaltic andesite. Trace zeolites in vugs.
- 218 84-6-13-6; rhyolite of Keith Tank; Taylor Peak; Keith Tank; S3,T11S,R11W; 33-22-30, 107-58-20; Black rhyolite vitrophyre containing about 1% quartz, 1% plagioclase, and a trace each of sanidine, biotite, hornblende, zircon, and possibly pyroxene. About 5 to 10% lithic fragments, some of which are gabbroic(?).
- 219 84-6-13-7; rhyolite of Dolan Peak; Bailey Points; Seventyfour Draw; S4,T11S,R10W; 33-21-33, 107-53-26; Crystal-rich rhyolite lava with about 2% quartz, 15% sanidine, and a trace each of biotite and sphene as phenocrysts in a white groundmass. Minor VPC.
- 220 84-6-13-8; rhyolite of Dolan Peak; Bailey Points; Seventyfour Draw; S4,T11S,R10W; 33-21-33, 107-53-26; Rhyolite lava similar to #219 above with minor VPC.
- 221 84-6-14-1; Taylor Creek Rhyolite; Taylor Peak; Boiler Peak; S17,T10S,R10W; 33-26-10, 107-53-53; Fine grained, white rhyolite lava consisting of about 7% quartz, 7% sanidine, and a trace each of plagioclase, biotite, and green hornblende in a granophyric groundmass with relict spherulites.



- 222 84-6-14-2; Taylor Creek Rhyolite; Taylor Peak; Paramount Canyon; S23,T10S,R11W; 33-25-36, 107-57-14; White, crystal-rich rhyolite lava. Mild VPC.
- 223 84-6-14-3; Taylor Creek Rhyolite; Taylor Peak; Paramount Canyon; S12,T10S,R11W; 33-26-57, 107-56-19; White, crystal-rich rhyolite lava. Intense VPC.
- 224 84-6-14-4; Taylor Creek Rhyolite; Taylor Peak; Boiler Peak; S18,T10S,R11W; 33-26-23, 107-54-46; White, crystal-rich rhyolite lava. Moderate VPC.
- 225 84-6-15-1; Taylor Creek Rhyolite; Taylor Peak; Inman Ranch; S31,T10S,R10W; 33-23-59, 107-55-06; White, crystal-rich rhyolite lava block from a block of carapace breccia caught up and preserved inside the rhyolite dome.
- 226 84-6-15-2; Taylor Creek Rhyolite; Taylor Peak; Boiler Peak; S19,T10S,R10W; 33-25-30, 107-54-20; Lithoidal rhyolite lava from a clast in the carapace breccia on the dome. Little VPC.
- 227 84-6-15-3; Taylor Creek Rhyolite; Taylor Peak; Boiler Peak; S19,T10S,R10W; 33-25-27, 107-54-24; Pinkish, lithoidal rhyolite lava. Incipient VPC along flow bands.
- 228 84-6-15-4; Tt5; Taylor Peak; Boiler Peak; S19,T10S,R10W; 33-25-29, 107-54-20; Well sorted, 1 to 2 mm pumice bed. Possibly a Plinian deposit.
- 229 84-6-15-5; vein material; Taylor Peak; Boiler Peak; S19,T10S,R10W; 33-25-27, 107-54-27; Hematite-cassiterite mineralization from the exposed veinlets in the old placer digs locally known as the "Clearing".
- 230 84-7-1; rhyolite of Dolan Peak; Sawmill Peak; Straight Creek; S36,T9S,R10W; 33-29-00; 107-49-45; poorly welded, massive ignimbrite with about 6% sanidine, 4% quartz and 5% lithic fragments in a pinkish groundmass.
- 231 84-7-2; rhyolite of Hoyt Creek; Wall Lake; Whitetail Canyon; S5,T11S,R11W; 33-22-18; 108-00-17; Vitric, massive, locally brecciated rhyolite lava. Nearly aphyric, but perlitic cracks are obvious. In thin section, the texture is microtrachytic.
- 232 84-7-3; rhyolite of Whitetail Canyon; Wall Lake; Whitetail Canyon; S5,T11S,R11W; 33-22-21; 108-00-30; Finely flowbanded rhyolite lava with about 5% plagioclase, 1% pyroxene and a trace of biotite, hornblende, and opaque minerals as phenocrysts in a microtrachytic groundmass.
- 233 84-7-3; Taylor Creek Rhyolite; Wall Lake; Whitetail Canyon; S6,T11S,R11W; 33-21-59, 108-01-15; Crystal-rich rhyolite lava. Moderate VPC.
- 234 84-7-5; Bloodgood Canyon Tuff; Wall Lake; Whitetail Canyon; S6,T11S,R11W; 33-21-43, 108-01-35; Multiple flow, poorly welded, crystal-poor ignimbrite. About 4% quartz, 6% sanidine, and a trace each of biotite, pyroxene, zircon, and sphene. The sphene is quite large, frequently as much as 0.5 mm across.
- 235 84-8-1; Tt3; Taylor Peak; Burnt Cabin Flats; S9,T10S,R10W; 33-27-17, 107-52-35; Red, moderately crystal-rich, lithic-rich, ignimbrite immediately below

- the tuff of Garcia Camp.
- 236 84-8-2; Tt2; Taylor Peak; Nugget Gulch; S28,T9S,R10W; 33-29-50, 107-52-53; Sample of a rhyolite clot from the ignimbrite that overlies the Nugget Gulch dome. The material is vitric and is a magma clot or extremely collapsed pumice surrounded by a vitroclastic groundmass.
- 237 84-8-3; unnamed dacite; Priest Tank; Monticello Cutoff road; S6,T12S,R6W; 33-18-06, 107-29-27; Brown, vitric dacite lava with 5 to 8% feldspar and a trace of biotite as phenocrysts.
- 238 84-8-4; rhyolite of Willow Springs Draw; Priest Tank; Monticello Cutoff road; S31,T11S,R6W; 33-18-08, 107-29-42; Crystal-rich rhyolite lava similar to the Taylor Creek Rhyolite.
- 239 84-8-5; unnamed dacite; Priest Tank, Monticello Cutoff road; S31,T11S,R6W; 33-18-13; 107-29-47; Aphyric dacite lava.
- 240 84-8-6; rhyolite of HOK Ranch; Chise; HOK Ranch; S25,T11S,R7W; 33-19-06, 107-30-45; Two-feldspar rhyolite lava containing about 9% quartz, 6% sanidine, 3% plagioclase, and 2% biotite as phenocrysts in a granophyric groundmass.
- 241 84-8-7; dacite; Chise; HOK Ranch; S36,T11S,R7W; 33-18-27, 107-30-30; Dacite lava flow with about 10% sanidine, 5% plagioclase, and 2% hornblende and a trace of biotite as phenocrysts in a pilotaxitic groundmass.
- 242 84-8-8; Kneeling Nun Tuff; Chise; HOK Ranch; S26,T11S,R7W; 33-19-35, 107-31-48; Densely welded, crystal-rich rhyolite ignimbrite. As much as 30% phenocrysts of sanidine, quartz, and plagioclase. The plagioclase is chalky, suggesting that the region has undergone potassium metasomatism.
- 243 84-8-9; Kneeling Nun Tuff; Chise; HOK Ranch; S26,T11S,R7W; 33-19-33, 107-31-47; Fine grained example of #242 above. The plagioclase is fresh.
- 244 84-8-10; unnamed ignimbrite; Chise; HOK Ranch; S26,T11S,R7W; 33-19-31, 107-31-59; 10 to 15 m of rhyolite ignimbrite below the Kneeling Nun Tuff. About 15% sanidine, 5% plagioclase, and a trace of quartz, biotite, pyroxene, and zircon as phenocrysts.
- 245 84-8-11; unnamed andesite; Chise; HOK Ranch; S26,T11S,R7W; 33-19-27; 107-31-03; Lavender to gray andesite lava. Probably correlates with the Rubio Peak Formation.
- 246 84-8-12; unnamed ignimbrite; Chise; HOK Ranch; S26,T11S,R7W; 33-19-41, 107-32-20; Fine Grained, densely welded, lineated, crystal-poor rhyolite ignimbrite similar to the La Jencia Tuff. Collected immediately above the tan basal vitrophyre.
- 247 84-8-13; Vicks Peak Tuff; Chise; HOK Ranch; S23,T11S,R7W; 33-20-04, 107-31-37; Crystal-poor, densely welded, tan to pale red-brown rhyolite ignimbrite.
- 248 84-8-14; rhyolite of HOK Ranch; Chise; HOK Ranch; S23,T11S,R7W; 33-20-05; 107-31-35; Crystal-rich, two feldspar rhyolite lava (see #240 above).

- 249 84-8-15; dike; Chise; HOK Ranch; S23,T11S,R7W; 33-20-28, 107-31-52; Sample of dike rock that is identical to the rhyolite of HOK Ranch lavas (#240 and 248 above).
- 250 84-8-16; dike; HOK Ranch; S23,T11S,R7W; 33-20-23, 107-32-02; Dike rock similar to #249 above.
- 251 84-8-17; Taylor Creek Rhyolite; Alexander Cienega; S27,T10S,R11W; 33-24-38, 107-57-41; Crystal-rich rhyolite lava. Mild to moderate VPC.
- 252 84-8-18; vein material; Wall Lake; Wall Lake; S2,T11S,R12W; 33-21-39, 108-03-45; Clear Calcite from a vein in the Tin Co. adit for fluid inclusion study.
- 253 84-8-19; Taylor Creek Rhyolite; Wall Lake; Wall Lake; S2,T11S,R12W; 33-21-39, 108-03-45; Punky wall rock to one on the many tin occurrences in the area. The sample was collected to determine the clay mineralogy in the groundmass.
- 254 84-8-20; Taylor Creek Rhyolite; Wall Lake; Wall Lake; S3,T11S,R12W; 33-21-33, 108-04-30; Crystal-rich rhyolite lava. Intense VPC.
- 255 84-8-21; Taylor Creek Rhyolite; Wall Lake; Wall Lake; S10,T11S,R12W; 33-20-57, 108-04-57; Crystal-rich rhyolite lava. Intense VPC.
- 256 84-8-22; Bearwallow Mountain Formation; Wall Lake; Wall Lake; S10,T11S,R12W; 33-20-59, 108-04-48; Andesite flow from the spillway at Wall Lake. About 7% plagioclase and 3% pyroxene.
- 257 84-8-23; Bearwallow Mountain Formation; Wall Lake; Kemp Mesa; S3,T11S,R12W; 33-22-08, 108-04-38; Black, Coarse grained, andesite flow.
- 258 84-8-24; Bearwallow Mountain Formation; Wall Lake; Kemp Mesa; S3,T11S,R12W; 33-22-10, 108-04-38; Black, coarse grained andesite flow.
- 259 84-ARH-20; rhyolite of Hoyt Creek; Wall Lake; Hoyt Creek; S20,T11S,R11W; 33-19-37, 108-00-54; Hydrated vitrophyre of an aphyric rhyolite lava. Sample courtesy of Don Richter, U.S.G.S.
- 260 84-ARH-35; rhyolite of White Tail Canyon; Wall Lake; Whitetail Canyon; S5,T11S,R11W; 33-21-47, 108-00-35; Crystal-poor rhyolite lava. Sample courtesy of Don Richter, U.S.G.S.
- 261 850101; Tt2; Taylor Peak; Nugget Gulch; S28,T9S,R10W; 33-29-52, 107-52-37; Coarse, densely welded, pyroclastic flow that overlies the Nugget Gulch Dome.
- 262-268 KM-50, -74, -118, -147, -191, -270, and -302; Taylor Creek Rhyolite; Wall Lake; Kemp Mesa; S5,T11S,R12W; 33-21-54, 108-06-42; These seven samples are from a diamond drill hole in the Kemp Mesa prospect drilled by Danny Fowler. The hole was a total of 302 feet deep. The field sample numbers above correspond to the footage from which the sample was taken. The hole was entirely in Taylor Creek Rhyolite. No mineralization was intersected.
- 269 Ash Peak Az; exact location unknown; The sample is a tin-bearing rhyolite lava from a dome called Ash Peak in eastern Arizona.
- 270 Hematite; Taylor Peak; Boiler Peak; S20,T10S,R10W; 33-

- 25-51, 107-54-12; Hematite crystals handpicked from concentrate left at the old placer mill near the "Clearing" tin prospect.
- 271 Cassiterite; Taylor Peak; Boiler Peak; S20,T10S,R10W; 33-25-51, 107-54-12; Cassiterite crystals handpicked from concentrate left at the old placer mill near the "Clearing" tin prospect.
- 272 Cassiterite; Taylor Peak; Miners Tanks; S33,T9S,R11W; 33-28-47, 107-59-02; Cassiterite crystals handpicked from concentrate left at the old placer mill in Grogan Canyon.
- 273 Wood tin; Taylor Peak; Nugget Gulch; S28,T9S,R10W; 33-29-34, 107-52-34; Wood tin from the bottom of Nugget Gulch.
- 274 Ore; Taylor Peak; Squaw Creek: S34,T9S,R11W; 33-28-53, 107-57-38; Hematite-cassiterite vein material carefully broken from fluid inclusion sample #130. Contains only minor wall rock contamination.

## APPENDIX 2B. Point count data for various units in the Black Range.

SAMPLE UNIT(1)	1 Ttc9	10 Ttc7	21 Tsp	56 Tdp	115 Twd	116 Twd	128 Ttc1	136 Ttc2	140 Ttc2
quartz	15.5	11.8	tr	1.1	10.6	14.6	9.6	8.4	10.4
sanidine	14.7	14.8	5.3	5.4	18.0	17.4	11.5	8.9	14.0
plag.	0.9	0.7	--	--	0.2	0.2	--	--	--
biotite	0.3	0.6	0.3	--	0.2	0.4	0.1	0.2	0.4
amphibole	--	--	--	0.1	--	--	--	--	--
pyroxene	--	--	--	--	--	--	--	--	--
opaques	tr	tr	tr	tr	tr	tr	tr	tr	tr
zircon	tr	tr	tr	tr	tr	tr	tr	tr	tr
sphene	tr	--	--	--	--	--	--	--	--
TOTAL PHENOS lithics	31.4	27.9	5.6	6.7	29.0	32.6	21.2	17.5	24.8
n	2000	2000	2000	1787	500	500	2000	2000	2000
Q/S(2)	1.05	0.80	--	0.22	0.59	0.84	0.83	0.94	0.74
SAMPLE UNIT(1)	149 Ttc5	153 Ttc4	155 Ttc7	167 Ttc9	180 Thr	205 Ttcip	207 Ttcip	209 Tgc	213 Ttc6
quartz	7.4	6.5	17.3	18.9	6.8	7.7	9.7	10.0	8.0
sanidine	8.0	9.3	13.9	16.0	6.4	8.3	10.0	6.2	13.0
plag.	0.8	--	0.8	0.7	2.0	0.6	0.3	--	0.1
biotite	0.2	0.1	1.0	0.5	1.8	0.5	--	0.6	0.2
amphibole	--	tr	--	--	--	--	--	--	--
pyroxene	--	--	--	--	--	--	--	--	--
opaques	tr	tr	tr	tr	tr	tr	tr	tr	0.2
zircon	tr	tr	tr	tr	--	tr	tr	tr	tr
sphene	--	--	tr	--	--	--	--	--	--
TOTAL PHENOS lithics	16.4	15.9	33.0	36.1	17.0	17.1	20.0	16.8	21.3
n	2000	1000	2000	2000	500	2000	2000	2000	500
Q/S(2)	0.93	0.69	1.24	1.18	1.06	0.93	0.97	1.61	0.62



SAMPLE UNIT(1)	215 Ttc6	216 Ttc6	218 Tkt	220 Tdp	221 Ttc5	232 Twc	243 Tkn	248 Thr
quartz	6.3	9.1	1.0	5.2	7.2	--	4.2	8.6
sanidine	11.1	8.1	0.2	15.2	6.6	--	5.2	6.1
plag.	0.3	0.7	0.8	--	0.2	5.2	11.8	2.8
biotite	--	--	0.4	0.4	0.2	0.2	3.8	2.4
amphibole	--	--	tr	--	--	tr	--	--
pyroxene	--	--	tr	--	--	1.0	--	--
opaques	tr	tr	tr	tr	tr	tr	tr	tr
zircon	tr	tr	tr	tr	tr	--	tr	tr
sphene	--	--	--	--	--	--	--	--
TOTAL								
PHENOS	17.7	17.9	2.4	20.8	14.2	6.4	25.0	19.9
lithics	--	--	12.4	--	--	tr	--	--
n	2000	1500	500	5000	1000	500	500	2000
Q/S(2)	0.57	1.02	5.0	0.34	1.09	--	0.81	1.41

1 The units are as follows:

Black Range section

Tsp-rhyolite of Sawmill Peak

Tdp-rhyolite of Dolan Peak

Tkt-rhyolite of Kieth Tank

Twc-rhyolite of Whitetail Canyon

Ttc1-Taylor Creek Rhyolite-Squaw Creek dome

Ttc2-Taylor Creek Rhyolite-Nugget Gulch dome

Ttc4-Taylor Creek Rhyolite-North Paramount Canyon Dome

Ttc5-Taylor Creek Rhyolite-Boiler Peak-Paramount Canyon dome

Ttc7-Taylor Creek Rhyolite-Taylor Creek dome

Ttc9-Taylor Creek Rhyolite-Kemp Mesa dome

Ttcip-Taylor Creek Rhyolite-Indian Peaks dome

Tgc-tuff of Garcia Camp

Sierra Cuchillo section

Tkn-Kneeling Nun Tuff

Thr-rhyolite of HOK Ranch

Twd-rhyolite of Willow Springs Draw

2 Q/S=quartz/sanidine ratio

## APPENDIX 3. Instrumental settings for INAA and XRF analyses.

Procedures for analyses by instrumental neutron activation (INAA) are as follows. Approximately 100 milligrams of sample was sealed in high purity quartz vials (Jacobs and others, 1977). The vials were packed in aluminum foil and then sealed in a 3.5 in diameter irradiation container and irradiated at the research reactor at the University of Missouri, Columbia, MO. The container was then rotated in a flux of about  $1.3 \times 10^{13}$  n cm<sup>-2</sup> sec<sup>-1</sup> for about 36 to 40 hours. The samples were then counted with high purity Ge detectors. Data was reduced with software from Nuclear Data and with TEABAGS, a program developed at the Washington University, St. Louis, MO (Lindstrom and Korotev, 1982).

The following instrumental settings are for a Rigaku automated XRF spectrometer which utilizes a Rh x-ray tube. Two theta angles and pulse height distribution were checked prior to each calibration and were adjusted accordingly. The change in 2 theta was on the order of 0.0X degrees. The trace elements are divided into four groups, each of which consist of a number of elements that have similar analytical properties. Groups 1, 2, and 3 utilize the Rh K-alpha Compton peak to correct for mass absorbtion. Group 4 utilizes mass absorbtion coefficients calculated from the major element compositions. Group 3 elements with the exception of Ga need to be corrected for peaks generated in the x-ray tube. This correction used the Rh K-alpha line to calculate an interference factor.

For all elements except tin, the instrument was calibrated using a number of reference materials. The compilations of Abbey (1983) and Govindaraju (1984) were used to estimate the content of each analyte in each reference material for the calibrations. Examples of the calibration lines and the reference material used for calibrations are available from the senior author. Tin was calibrated using a single reference material, MA-N, assuming that MA-N contains 1050 ppm tin.



Major elements

tube settings 35kv, 75ma

Element	time	angle	crystal	window	slit	detector
SiO2	40	109.00	PET	1-1	coarse	f-pc
TiO2	20	86.14	LIF220	2-1	coarse	scint
Fe2O3	40	57.52	LIF220	1-1	fine	scint
Al2O3	80	144.74	PET	1-1	coarse	f-pc
MnO	20	62.93	LIF220	1-1	coarse	scint
MgO	200	45.19	TAP	1-3	coarse	f-pc
CaO	20	113.08	LIF220	2-1	coarse	scint
Na2O	200	55.10	TAP	2-2	coarse	f-pc
K2O	20	136.67	LIF220	1-1	coarse	scint
P2O5	40	140.96	LIF220	2-2	coarse	scint

Trace elements

Group 1

tube settings 60kv, 40ma

Element	time	angle	crystal	window	slit	detector
Bkg1	40	23.08	LIF200	1-1	coarse	f-pc
Y	100	23.68	LIF200	1-1	coarse	f-pc
Bkg2	40	24.54	LIF200	1-1	coarse	f-pc
Sr	100	25.02	LIF200	1-1	coarse	f-pc
Bkg3	40	25.62	LIF200	1-1	coarse	f-pc
RHC	100	26.36	LIF220	1-1	coarse	f-pc
Bkg4	100	27.71	LIF220	1-1	coarse	f-pc
Nb	200	30.26	LIF220	1-1	coarse	f-pc
Zr	100	31.94	LIF220	1-1	coarse	f-pc
Bkg5	100	32.85	LIF220	1-1	coarse	f-pc
Bkg6	100	36.68	LIF220	1-1	coarse	f-pc
U	200	37.14	LIF220	1-1	coarse	f-pc
Rb	100	37.85	LIF220	1-1	coarse	f-pc
Th	200	39.11	LIF220	1-1	coarse	f-pc
Pb	200	40.26	LIF220	1-1	coarse	f-pc
Bkg7	100	40.98	LIF220	1-1	coarse	f-pc

## Group 2

Tube setting 45kv, 60ma

Element	time	angle	crystal	window	slit	detector
Bkg1	100	13.50	LIF200	1-1	coarse	scint
Sn	200	14.04	LIF200	1-1	coarse	scint
Bkg2	100	14.45	LIF200	1-1	coarse	scint
RHC	40	18.52	LIF200	1-1	coarse	scint

## Group 3

tube setting 40kv, 60ma

Element	time	angle	crystal	window	slit	detector
RHKA	40	17.52	LIF200	1-1	fine	f-pc
RHC	40	18.52	LIF200	1-1	fine	f-pc
Ga	100	38.86	LIF200	2-2	fine	f-pc
Bkg1	40	39.50	LIF200	2-2	fine	f-pc
Zn	100	41.74	LIF200	2-2	fine	f-pc
Cu	100	44.98	LIF200	2-2	fine	f-pc
Bkg2	40	46.80	LIF200	2-2	fine	f-pc
Ni	100	48.61	LIF200	2-2	fine	f-pc
Bkg3	40	50.00	LIF200	2-2	fine	f-pc

## Group 4

tube settings 50kv, 60ma

Element	time	angle	crystal	window	slit	detector
Bkg6	40	88.71	LIF220	3-2	fine	scint
Ba	100	87.22	LIF220	3-2	fine	scint
Ti	20	86.16	LIF220	3-2	fine	scint
Bkg4	40	80.48	LIF220	3-2	fine	scint
V	100	76.94	LIF220	3-2	fine	scint
Bkg3	40	75.98	LIF220	3-2	fine	scint
Bkg2	40	70.73	LIF220	3-2	fine	scint
Cr	100	69.34	LIF220	3-2	fine	scint
Bkg1	40	68.23	LIF220	3-2	fine	scint

## Appendix 4

The following tables consist of analyses of three internal standards used throughout the course of this study. The TTC material consists of Taylor Creek Rhyolite. A sample consisting of about 5 kg was ground in a tungsten carbide tema mill, split, recombined, and reground in the tema mill. At least one aliquot of this sample was prepared during each sample preparation session to monitor both the sample preparation procedures and analyses. Sample NMR is an internal standard used in the x-ray analytical laboratory of New Mexico Bureau of Mines and Mineral Resources. No details of the sample preparation are available. Sample CZB is a basalt from the malpais near Carrizozo, New Mexico. This sample was prepared similar to TTC, but about 2 kg were processed. NMR and CZB were run to check precision at concentration levels other than those represented by TTC.

Appendix 4A, 4B, and 4C consist of major element analyses for the internal standards. The number following the symbol is the aliquot number, the number beneath the aliquot number is the number of times that aliquot was analyzed (n). The tables are arranged as follows:

average for n runs  
estimated standard deviation (s)  
coefficient of variation (s/average)

the coefficient of variation for each aliquot represents an estimate of the instrumental precision for that run. The totals row at the bottom of each table are ordered identically to the individual aliquots. The analyses for the aliquots is reported, assuming that the average for each aliquot is a single analysis. The coefficient of variation in this case estimates the precision of the entire analytical process, including sample preparation. This precision estimate changes with the amount of a component in the sample, that is, precision increases with increasing content of a component.

Appendix 4D consists of precision estimates for loss on ignition (LOI) for the internal standards. LOI was determined by fusing an aliquot of dry sample for 2 hours at 1010 degrees C.

Appendix 4E and 4F are trace element analyses for the internal standards TTC and CZB. The order for the tables and the interpretation of the results is similar to the major element analyses with the exception that the number of analyses of each aliquot is the bottom number in each case. Dashes indicate that no analysis was performed. Sn is not included in this table. TTC has a tin content of about 6 ppm which is the detection limit and precision is probably on the order of +/- 100% at that level.

Appendix 4G consists of the mean, estimated standard

deviation (s), and coefficient of variation (CV) for triplicate analyses in two INAA irradiations and a single analysis from a third irradiation. Irradiation K5M15 had two triplicate samples. The sample is the TTC internal standard.

Appendix 4H are representative analyses of G-2 and BCR-1, U. S. Geological Survey reference materials compared to analyses from Abbey (1983). These tables can be used to evaluate accuracy.

## Appendix 4A Major element precision estimates; TTC internal Standard.

SAMPLE	SiO2	TiO2	Al2O3	Fe2O3	MNO	MGO	CAO	NA2O	K2O	P2O5
TTC-1	77.10	0.05	12.20	1.15	0.05	0.17	0.19	3.72	4.85	0.02
21	0.15	0.01	0.05	0.007	0.003	0.012	0.003	0.049	0.021	0.001
	0.19	25.55	0.40	0.57	5.78	6.99	1.44	1.32	0.43	5.0
TTC-2	76.77	0.05	12.73	1.13	0.05	0.17	0.19	4.12	4.91	0.02
21	0.28	0.02	0.08	0.008	0.003	0.016	0.003	0.101	0.038	0.002
	0.3	30.94	0.69	0.71	5.38	9.35	1.73	2.45	0.78	9.04
TTC-3	77.03	0.05	12.13	1.14	0.05	0.16	0.19	3.70	4.86	0.02
20	0.18	0.08	0.06	0.006	0.002	0.014	0.003	0.077	0.016	0.001
	0.24	16.08	0.45	0.56	4.78	8.48	1.48	2.07	0.33	6.23
TTC-4	77.17	0.05	12.28	1.14	0.05	0.17	0.19	3.7	4.89	0.02
20	0.18	0.01	0.06	0.008	0.003	0.015	0.003	0.039	0.021	0.001
	0.23	17.39	0.46	0.66	4.86	8.77	1.48	1.05	0.42	7.49
TTC-5	77.38	0.05	12.25	1.17	0.05	0.17	0.19	3.64	4.84	0.02
20	0.15	0.01	0.07	0.008	0.002	0.020	0.003	0.045	0.014	0.004
	0.19	17.44	0.55	0.69	3.55	11.97	1.51	1.24	0.28	18.71
TTC-6	77.38	0.11	12.19	1.06	0.05	0.27	0.19	3.57	4.83	0.02
3	0.22	0.006	0.038	0.006	--	0.010	0.012	--	0.01	0.001
	0.28	5.41	0.31	0.54	--	3.70	6.19	--	0.21	5.59
TTC-14	76.74	0.01	12.26	1.07	0.05	0.14	0.19	3.59	4.8	0.04
10	0.14	0.01	0.02	0.008	0.002	0.018	0.002	0.032	0.014	0.001
	0.18	4.5	0.13	0.74	3.73	12.69	1.10	0.9	0.29	2.8
TTC-15	77.18	0.10	12.10	1.17	0.05	0.26	0.20	3.69	4.80	0.02
15	0.26	0.004	0.046	0.009	0.003	0.073	0.002	0.087	0.024	0.002
	0.34	4.1	0.38	0.79	5.9	28.31	1.20	2.36	0.49	9.80
TTC-16	77.62	0.10	12.15	1.06	0.05	0.14	0.19	3.72	4.82	0.02
15	0.08	0.003	0.056	0.005	0.002	0.04	0.002	0.095	0.014	0.002
	0.10	3.2	0.46	0.48	4.10	29.10	1.00	2.54	0.29	9.10
TTC-17	77.95	0.11	12.16	1.16	0.06	0.52	0.21	3.71	4.86	0.02
10	0.10	0.003	0.024	0.005	0.002	0.003	0.002	0.078	0.011	0.002
	0.13	2.8	0.20	0.41	4.20	6.40	0.90	2.11	0.22	7.4
TOTALS	77.23	0.07	12.21	1.12	0.05	0.22	0.19	3.72	4.85	0.02
10	0.37	0.034	0.056	0.044	0.003	0.116	0.007	0.152	0.036	0.006
CV=	0.48	48.93	0.46	3.93	6.32	53.73	3.55	4.08	0.74	31.60

## APPENDIX 4B Major element precision estimates:NMRI internal standard.

SAMPLE	SiO2	TiO2	Al2O3	Fe2O3	MNO	MGO	CAO	NA2O	K2O	P2O5
NMRI-8	72.72	0.44	14.32	2.55	0.06	0.43	1.60	3.16	4.83	0.13
40	0.18	0.01	0.03	0.01	0.003	0.019	0.007	0.029	0.009	0.002
	0.24	1.30	0.20	0.40	4.90	4.40	0.46	0.90	0.20	1.22
NMRI-9	72.75	0.43	14.33	2.67	0.05	0.47	1.60	3.12	4.83	0.13
40	0.17	0.01	0.03	0.01	0.003	0.018	0.008	0.037	0.016	0.002
	0.24	1.34	0.17	0.42	5.05	3.86	0.52	0.52	0.33	1.57
NMRI-10	72.39	0.43	14.26	2.64	0.06	0.42	1.60	3.13	4.78	0.14
40	0.20	0.01	0.03	0.01	0.003	0.018	0.011	0.038	0.017	0.003
	0.28	1.45	0.24	0.48	5.7	3.86	0.66	1.22	0.35	1.83
NMRI-11	72.43	0.43	14.29	2.66	0.06	0.42	1.60	3.13	4.78	0.14
40	0.21	0.01	0.02	0.01	0.003	0.018	0.008	0.025	0.02	0.002
	0.29	1.36	0.28	0.47	5.48	4.92	0.49	0.80	0.41	1.36
NMRI-12	72.76	0.43	14.34	2.69	0.06	0.45	1.60	3.14	4.83	0.13
40	0.19	0.01	0.04	0.01	0.002	0.023	0.008	0.027	0.017	0.002
	0.26	1.38	0.26	0.45	4.26	5.26	0.57	0.87	0.36	1.53

---

TOTALS	72.61	0.43	14.31	2.64	0.06	0.44	1.60	3.14	4.82	0.13
5	0.19	0.01	0.03	0.05	0.004	0.022	0.008	0.015	0.022	0.002
CV=	0.25	1.00	0.23	2.06	7.47	4.95	0.52	0.47	0.45	1.74

---

## APPENDIX 4C Major element precision estimates; CZB internal standard.

SAMPLE	SiO2	TiO2	Al2O3	Fe2O3	MNO	MGO	CAO	NA2O	K2O	P2O5
CZB-1	58.56	0.98	16.39	9.52	0.23	0.98	3.61	6.03	3.87	0.29
15	0.12	0.01	0.08	0.01	0.005	0.068	0.007	0.131	0.008	0.007
	0.21	0.61	0.46	0.10	2.00	6.92	0.21	2.17	0.21	2.55
CZB-2	59.63	0.98	16.37	9.42	0.23	1.07	3.61	6.10	3.89	0.29
15	0.08	0.01	0.04	0.023	0.005	0.067	0.012	0.139	0.009	0.005
	0.14	0.75	0.25	0.25	2.01	6.22	0.34	2.29	0.23	1.79
CZB-3	58.52	0.98	16.30	9.62	0.23	0.91	3.63	6.06	3.90	0.29
5	0.05	0.002	0.06	0.025	0.003	0.077	0.011	0.097	0.007	0.004
	0.09	0.19	0.10	0.26	1.20	8.40	0.30	1.59	0.18	0.19

---

TOTALS	58.57	0.98	16.35	9.52	0.23	0.99	3.62	6.06	3.89	0.29
3	0.06	0.002	0.05	0.10	0.002	0.080	0.012	0.035	0.015	0.001
CV=	0.10	0.24	0.29	1.05	0.67	8.13	0.32	0.58	0.39	0.20

## APPENDIX 4D Precision of loss on ignition determinations.

SAMPLE	n	MAX	MIN	AVG.	S	CV
TTC	14	0.38	0.17	0.27	0.08	29.7
NMR1	3	0.74	0.72	0.73	0.01	1.4
CZB	6	-0.32	-0.23	-0.30	0.035	11.9



## APPENDIX 4E Trace element precision estimates; TTC internal standard.

SAMPLE	Y	Sr	Nb	Zr	U	Rb	Th	Pb	Ga	Zn	Ni	Ba	Cr
TTC-1	74	2.5	44.1	151	4	372	37	28	22.5	46	6.3	14.5	4.1
	--	--	--	--	--	--	--	--	0.5	0.7	0.6	5.6	1.7
	--	--	--	--	--	--	--	--	2.2	1.5	9.8	38.5	41.1
	1	1	1	1	1	1	1	1	12	12	12	6	6
TTC-2	76	2.0	44	157	3	373	37	28	21.9	46.9	6.5	16.5	5.8
	--	--	--	--	--	--	--	--	1.7	1.4	0.8	4.0	1.4
	--	--	--	--	--	--	--	--	7.5	1.8	14.8	25.5	24.7
	1	1	1	1	1	1	1	1	12	12	12	6	6
TTC-3	76	2.1	45	155	2	375	36	26	22.6	46.7	6.4	21.6	4.6
	--	--	--	--	--	--	--	--	0.5	1.4	0.8	12.8	0.7
	--	--	--	--	--	--	--	--	2.3	3.0	11.6	59.2	15.1
	1	1	1	1	1	1	1	1	12	12	12	6	6
TTC-3A	--	--	--	--	--	--	--	--	--	--	--	18.8	7.9
	--	--	--	--	--	--	--	--	--	--	--	1.5	0.9
	--	--	--	--	--	--	--	--	--	--	--	7.8	11.6
	--	--	--	--	--	--	--	--	--	--	--	6	6
TTC-4	--	--	--	--	--	--	--	--	22.4	45.8	6.2	16.8	10.0
	--	--	--	--	--	--	--	--	0.5	0.8	0.7	2.7	0.6
	--	--	--	--	--	--	--	--	2.2	1.7	11.0	16.2	6.0
	--	--	--	--	--	--	--	--	11	11	11	6	6
TTC-5	--	--	--	--	--	--	--	--	22.6	46.4	6.8	20.0	8.9
	--	--	--	--	--	--	--	--	0.8	0.8	0.9	4.1	2.0
	--	--	--	--	--	--	--	--	3.5	1.8	13.8	20.6	22.4
	--	--	--	--	--	--	--	--	11	11	11	9	9
TTC-6	--	--	--	--	--	--	--	--	--	--	--	18.8	15.5
	--	--	--	--	--	--	--	--	--	--	--	2.7	1.4
	--	--	--	--	--	--	--	--	--	--	--	14.2	9.1
	--	--	--	--	--	--	--	--	--	--	--	9	9
TTC-7	78	1.7	45.5	175	--	375	--	28	--	--	--	--	--
	0.6	0.3	0.5	1.0	--	1	--	1.3	--	--	--	--	--
	0.8	16.8	1.2	0.6	--	0.3	--	3.1	--	--	--	--	--
	6	6	6	6	--	6	--	6	--	--	--	--	--
TTC-8	78	1.7	45.2	170	--	374	--	27	--	--	--	--	--
	0.6	0.3	0.4	1.1	--	0.8	--	0.8	--	--	--	--	--
	0.7	17.6	0.9	0.6	--	0.2	--	3.1	--	--	--	--	--
	6	6	6	6	--	6	--	6	--	--	--	--	--
TTC-9	77	1.5	45.3	170	--	374	--	27	--	--	--	--	--
	0.4	0.3	0.5	--	--	1.2	--	0.5	--	--	--	--	--
	0.5	18.4	1.1	--	--	0.3	--	1.9	--	--	--	--	--
	6	6	6	6	--	6	--	6	--	--	--	--	--

## APPENDIX 4E (cont)

SAMPLE	Y	Sr	Nb	Zr	U	Rb	Th	Pb	Ga	Zn	Ni	Ba	Cr
TTC-10	76	2.0	47.3	160	3.9	370	41	28	---	---	---	---	---
	1.0	0.6	0.6	8.4	0.4	4.1	0.8	1.6	---	---	---	---	---
	1.3	30.0	1.2	5.2	9.8	1.1	1.8	5.7	---	---	---	---	---
	16	16	16	16	7	16	7	16	---	---	---	---	---
TTC-11	77	2.0	45.3	160	3.9	370	40	28	---	---	---	---	---
	0.6	0.8	0.6	9.0	1.1	4.8	0.7	1.6	---	---	---	---	---
	0.8	41.5	1.3	5.5	28.0	1.3	1.7	5.6	---	---	---	---	---
	16	16	16	16	7	16	7	16	---	---	---	---	---
TTC-12	76	3.4	45.7	149	3.9	362	40	28	---	---	---	---	---
	0.6	0.7	0.5	1.1	0.4	2.8	1.1	1.2	---	---	---	---	---
	0.8	20.3	1.1	0.7	9.8	0.8	2.8	4.1	---	---	---	---	---
	7	7	7	7	7	7	7	7	---	---	---	---	---
TTC-13	77	3.1	45.7	150	3.9	363	41	28	---	---	---	---	---
	1.3	0.4	0.5	1.3	0.7	1.7	0.5	1.2	---	---	---	---	---
	1.6	13.4	1.1	0.9	17.9	0.5	1.3	4.1	---	---	---	---	---
	7	7	7	7	7	7	7	7	---	---	---	---	---
TTC-14	76	2.9	46.1	152	4.0	362	39	29	---	---	---	---	---
	1.2	0.6	0.4	2.6	0.8	4.4	1.1	1.8	---	---	---	---	---
	1.6	20.4	0.8	1.7	20.4	1.2	2.9	6.3	---	---	---	---	---
	7	7	7	7	7	7	7	7	---	---	---	---	---
-----													
TOTALS	77	2.2	45.4	159	3.6	370	39	28	22	46	6.4	18	11.2
	1.1	0.6	0.9	9.1	0.7	5.2	2.0	0.8	0.3	0.6	0.2	2.2	6.8
	1.5	29.1	2.0	5.7	20.0	1.4	5.0	2.9	1.3	1.2	3.6	12.2	61.2
	8	8	8	8	5	8	5	8	5	5	5	10	10



APPENDIX 4G Precision estimates for instrumental neutron activation analysis.

ELE.	K3M3	K4M4			K5M15		
		MEAN n=3	S	CV	MEAN n=3	S	CV
La	31.5	30.5	0.13	0.43	28.8	0.25	0.8
Ce	96.6	101.2	0.52	0.52	110.7	0.79	0.78
Nd	26.7	29.2	1.33	4.55	27.3	0.95	0.7
Sm	7.82	7.98	0.012	0.15	7.36	0.1	1.3
Eu	0.195	0.196	0.021	10.7	0.223	0.007	3.1
Tb	1.35	1.50	0.066	4.4	1.63	0.035	2.2
Yb	9.89	10.44	0.56	5.36	8.32	0.04	0.5
Lu	1.27	1.339	0.024	1.79	1.32	0.027	2.0
As	--	--	--	--	0.75	0.11	14.0
Br	--	--	--	--	0.19	0.07	35.0
Co	--	--	--	--	0.27	0.09	31.9
Cs	4.72	5.87	0.107	1.82	5.17	0.11	1.40
Hf	7.4	8.13	0.18	2.1	8.14	0.11	1.4
Rb	372	397	6.5	1.64	371	6.81	1.80
Sb	--	--	--	--	1.07	0.27	22.8
Sc	2.56	2.6	0.10	3.85	2.05	0.04	2.0
Se	0.6	0.58	0.012	2.07	--	--	--
Ta	4.61	4.91	0.06	1.22	3.82	0.11	3.0
Th	36.6	38	1.0	2.63	34.1	0.42	1.20
U	7.24	8.33	0.21	2.50	6.3	--	--
W	--	--	--	--	2.9	0.25	8.7
Na20	3.62	6.66	0.07	1.91	3.87	0.06	1.5
Fe203	1.12	1.10	0.02	1.82	--	--	--
FeO	--	--	--	--	1.03	0.006	0.6

## APPENDIX 4H. Accuracy estimates, instrumental neutron activation analysis.

ELE.	G-2 NAA				BCR-1	
	K3M3	K4M4	K5M15	ABBEY	K5M15	ABBEY
La	88.8	87.3	82.9	92	24.3	27
Ce	163	162	164	160	53	53
Nd	55.7	58.2	54.6	58	30	26
Sm	7.5	7.1	7.2	7.2	6.6	6.5
Eu	1.32	1.30	1.27	1.4	1.92	2.0
Tb	0.34	0.37	0.45	0.5	1.1	1.0
Yb	0.88	0.59	0.83	0.86	3.28	3.4
Lu	0.112	0.078	0.096	0.1	0.526	0.5
Ba	1949	1914	1820	1900	647	680
Co	4.4	4.4	4.3	5	37	36
Cr	9.7	13.0	6.9	8	11.2	15
Cs	1.5	1.7	1.3	1.4	0.99	0.96
Hf	8.2	8.4	8.5	8	4.97	5
Rb	196	180	163	170	50	47
Sb	0.09	0.09	0.05	0.06	0.54	0.6
Sc	3.7	3.5	3.3	3.5	31.99	33
Se	0.09	0.12	--	--	--	0.1
Ta	0.83	0.86	0.75	0.8	0.72	0.8
Th	26	26	23	25	5.7	6.1
U	2.6	2.1	1.6	2.1	1.6	1.7
W	--	--	2.6	0.1	--	0.4
Na20	4.25	4.05	3.87	4.06	--	3.3
Fe203	2.84	2.76	2.60	2.69	13.51	13.41